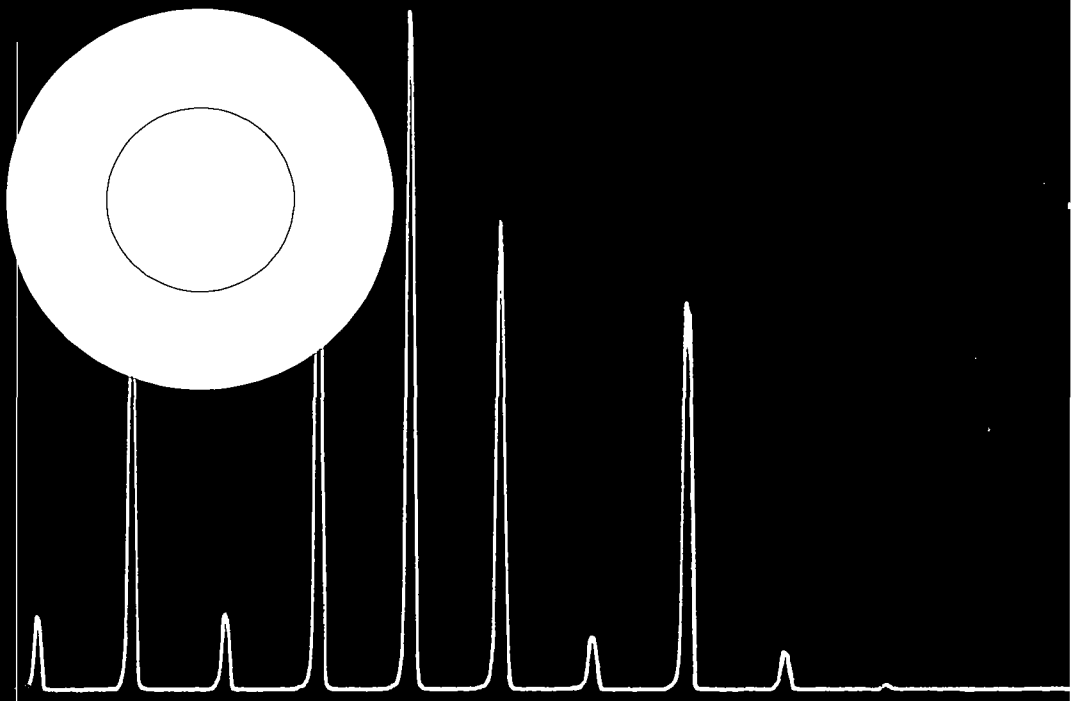

Eighteenth Annual Conference on Mass Spectrometry and Allied Topics

Eighteenth Annual Conference on Mass Spectrometry and Allied Topics

June 14-19, 1970
San Francisco, California

Arranged by the
American Society for Mass Spectrometry
in cooperation with ASTM Committee E-14

Table of Contents

Introduction

This volume is a collection of papers presented at the Eighteenth Annual Conference on Mass Spectrometry and Allied Topics, held in San Francisco, California, June 14-19, 1970. It is intended that this volume be distributed only to members of ASMS, and registrants of the Conference, and therefore should not be considered as a publication.

It is suggested that any future references to individual reports be cited in the form: author(s), presented at the Eighteenth Annual Conference on Mass Spectrometry and Allied Topics, San Francisco, California, June 1970.

R. E. Honig, Program Chairman

Arranged by the American Society for Mass Spectrometry (ASMS), in cooperation with ASTM Committee E-14.

ASMS

President: J. L. FRANKLIN, Department of Chemistry, Rice University, Houston, Texas 77001

Vice-President (Program): R. E. HONIG, RCA Laboratories, Princeton, New Jersey 08540

Vice-President (Arrangements): C. E. JOHANNSEN, Bell & Howell Analytical Instruments Division, 1500 S. Shamrock, Monrovia, California 91016

Vice-President (Data & Standards): H. R. HARLESS, Union Carbide Technical Center, South Charleston, West Virginia 25303

Secretary: J. M. McCREA, Applied Research Lab. (73), United States Steel Corp., Monroeville, Pennsylvania 15146

Treasurer: H. D. COOK, Westinghouse Bettis Atomic Power Lab., Box 79, West Mifflin, Pennsylvania 15122

Past President: H. M. ROSENSTOCK, National Bureau of Standards, Washington, D. C. 20234

Directors-at-Large:

J. T. HERRON, National Bureau of Standards, Washington, D. C. 20234

R. F. PORTER, Department of Chemistry, Cornell University, Ithaca, New York 14850

ASTM COMMITTEE E-14

Chairman: H. R. HARLESS, Union Carbide Technical Center, South Charleston, West Virginia 25303

Vice-Chairman: H. E. LUMPKIN, Esso Research & Engineering Co., P. O. Box 4255, Baytown, Texas 77520

Secretary-Treasurer: W. F. KUHN, Philip Morris, Inc., Richmond, Virginia 23206

ASMS COMMITTEES AND ASTM E-14 SUBCOMMITTEES

ASMS Com. II - "Fundamental Aspects", W. A. Chupka, Argonne National Laboratory, 9700 South Cass Avenue, Argonne, Illinois 60439.

Joint (Sub) Com. III - "Computer and Data Processing", M. C. Hamming, Continental Oil Company, P.O. Drawer 1267, Ponca City, Oklahoma 74601.

ASTM E-14 Subcom. IV - "Data and Information Problems", Paul W. Shearer, Hercules, Inc., Wilmington, Delaware 19899.

ASMS Com. V - "New Instruments and Techniques", H. J. Svec, Department of Chemistry, Iowa State University, Ames, Iowa 50010.

ASTM E-14 Subcom. VI - "Standards and Procedures", J. R. Roboz, Mt. Sinai School of Medicine, New York, New York.

ASMS Com. VII - "Study of Solids", A. J. Ahearn, 9621 E. Bexhill Drive, Kensington, Maryland 20795.

ASMS Com. VIII - "High Resolution Studies", K. Biemann, Department of Chemistry, Massachusetts Institute of Technology, Cambridge, Massachusetts 02139.

ASMS Com. IX - "Aids to Education", D. C. Damoth, Bendix Corporation, Rochester, New York 14603.

ASTM E-14 Subcom. X - "Definitions and Terms", G. L. Cook, U. S. Bureau of Mines, Box 3395, University Station, Laramie, Wyoming 82070.

ASTM E-14 Subcom. XI - "Evaluation of Critical Data", A. J. Sharkey, U. S. Bureau of Mines, 4800 Forbes Avenue, Pittsburgh, Pennsylvania 15213.

In The Court of Common Pleas

Of Allegheny County, Pennsylvania

James F. Clarke,
Prothonotary

To All To Whom These Presents Shall Come, Greetings:

Whereas *on the* 28th *day of* July *in the year of our Lord, One Thousand Nine Hundred* Sixty-nine *at No.* 650 October *Term, 19*69.

R. V. FRITZEL — NORMAN D. GOGGESHALL — JOHN J. McGOVERN
V. BRUCE KING — JOHN M. McCREA — WILLIAM M. HICKAM

filed in this Court their application for a Charter, and

Whereas *Certificate of Registration from the Secretary of the Commonwealth and Proofs of Publication of Notice of this Application as required by Law and by the Rule of this Court have been filed, and*

Whereas *in compliance with the provisions of the Non-Profit Corporation Law of Pennsylvania approved May 5, 1933, P. L. 289, the Court having found that the purpose or purposes set forth in said Article lawful and not injurious to the Community.*

Now Therefore, Be It Remembered *that on the* 4th *day of* August *in the year of our Lord, One Thousand Nine Hundred* Sixty-nine *, on motion of* WILLIAM R. McKEE *Attorney for Petitioner the Court by his Honor* DAVID R. MAGEE, JR., *did Order and Decree that*

Articles of Incorporation

are approved, and that upon recording of said Articles of Incorporation, together with this Order, that the subscribers thereto named and their associates and successors shall be and are a Non-Profit Corporation by the name and title of

THE AMERICAN SOCIETY FOR MASS SPECTROMETRY

Said Non-Profit Corporation shall exist perpetually,

and shall be invested with and have and enjoy all the powers, privileges and franchises incident to a non-profit corporation and be subject to all the duties and requirements and restrictions specified and enjoined in and by the Non-profit Corporation law and all other applicable laws of this Commonwealth.

Witness *THE Honorable* HENRY X. [illegible]
President Judge of our said Court at Pittsburgh, this 7th *day of* August *1969.*

From the Record,

James F. Clarke
Prothonotary

*Record*ed August 4, 1969 *Charter Book* *Vol.* 72 *Page* 519

THE AMERICAN SOCIETY FOR
MASS SPECTROMETRY
CONSTITUTION AND BYLAWS
CONSTITUTION

ARTICLE I. Name

The name of this society shall be "The American Society for Mass Spectrometry".

ARTICLE II. Aims and Purpose

It is the aim and purpose of this society to promote and disseminate knowledge of mass spectrometry and allied subjects.

ARTICLE III. Membership

Membership in the American Society for Mass Spectrometry shall be open to any individual or with approval of the Board of Directors any corporate entity with a bona-fide interest in mass spectrometry.

ARTICLE IV. Management

The management of the society shall be vested in the Board of Directors which shall consist of the following voting members: the officers of the society hereafter listed, two elected members at large, and the immediate past President; of the following non-voting members: the duly appointed chairmen of such committees that may be duly appointed within the society.

The Officers of the Society shall be:

President
Vice-President for Programs, who shall be President Elect of the Society
Vice-President for Arrangements
Vice-President for Standards and Procedures, who shall be the Chairman of ASTM Committee E-14 on Mass Spectrometry and shall serve, ex-officio, as an Officer of the Society.
Secretary
Treasurer

ARTICLE V. Duties of Officers

Section 1. The President shall be the chief executive officer of this society; he shall preside at all meetings of the members and directors; he shall have general and active management of the business of this society; he shall see that all orders and resolutions of the Board of Directors are carried out; he shall execute all bonds, mortgages, and all contracts of this society and cause or direct the affixing of the corporate seal thereto; he shall have general superintendence and direction of all other officers of this society and see that their duties are properly performed; he shall submit a report of the operations of the society for the fiscal year to the Board of Directors and members at their annual meeting, and from time to time shall report to the Board of Directors all matters within his knowledge that may affect this society; he shall be ex-officio a member of all committees and shall have the power and duties and management usually vested in the Office of President in a corporation; he shall appoint all committees except as herein otherwise provided. He may individually send or cause to be sent by the Secretary notices of any meetings of the Board of Directors.

Section 2. The Vice-President for Programs shall be vested with all the powers and shall perform all the duties of the President during the absence of the latter and shall have such other duties as may, from time to time, be determined by the Board of Directors. The same shall be true of the Vice-President for Arrangements who shall be next in the line of succession. In the event that the President shall be absent at any meeting, the Vice-President for Programs shall preside, and if neither is present at a meeting, then the Vice President for Arrangements shall preside.

Section 3. The Secretary shall attend all sessions of the Board of Directors and all meetings of members and act as a clerk thereof; and shall record all votes and minutes of all proceedings in a book to be kept for that purpose as directed; he shall send notices of all meetings to the members of the Board of Directors; and shall perform such other duties as may be prescribed by the Board of Directors or the President under whose supervision he shall be; and he shall be the custodian of the corporate seal and all of the books and records of this society, except as may be otherwise provided.

Section 4. The Treasurer, under the direction of the Board of Directors, shall have charge of the funds of this society and shall deposit the same in the name of this society in depositories designated by the Board of Directors; he shall arrange for the payment of all vouchers or orders properly attested by the President and Secretary from said society funds, and shall make a complete and accurate report of the finances of this society at each annual meeting of the members, or at any time upon request, to the Board of Directors.

ARTICLE VI. Duties and Powers of the Board of Directors

1. The property and business of this society shall be managed by the Board of Directors.

2. In addition to the general powers of the Board of Directors by virtue of their office, the powers and authority expressly given by law, by terms of the charter of this society, and elsewhere in these by-laws, the following specific powers are expressly conferred on the Board of Directors.

To purchase or otherwise acquire for the society any property, right or privilege which it is authorized to acquire at such price or consideration, and upon such terms as they deem expedient; to appoint, to remove or suspend subordinate agents or servants, to determine their duties and affix their salaries; to confer by resolution upon any officer or agent of this society the power of permanently removing or suspending any subordinate officer or servants; to determine who shall be authorized, on behalf of this society, to sign bills, notices, receipts, acceptances, endorsements, checks, releases, contracts and any other instruments; to delegate any of the powers of the Board to any standing committee, special committee, or to any officer or agent of the society, with such powers as the Board may deem fit and proper to grant; generally to do all such lawful acts and things as are not by law, or by charter, or by these by-law directed or required to be done by members of the Board of Directors.

3. Any action which may be taken at a meeting of the Directors, may be taken without a meeting, if consent in writing setting forth the action so taken be signed by all the Directors and filed with the Secretary of the society.

4. In the event that the office of any elected officer or member of the board of directors shall become vacant, the board of directors shall immediately fill the vacancy for the remainder of the unexpired term; however, no member who thus fills a vacancy in the

office of Vice-President for programs shall automatically succeed to the presidency, but the society shall in such event elect its next President. The provision of Article IV which pertains to the immediate past president shall not apply to a president who vacates office.

5. The ballot for the election to membership on the Board of Directors of this society shall be by a closed, written ballot.

6. Any member in good standing shall be eligible to hold office in this society either as an officer or a member of the Board of Directors.

ARTICLE VII. Fidelity Bonds.

Section 1. The Board of Directors may require such officers or agents to be bonded as it shall deem necessary; for any amount or amounts as it may deem requisite, at the expense of the Society.

ARTICLE VIII. Location.

The principal office of this society shall be located in the City of Pittsburgh, Commonwealth of Pennsylvania.

ARTICLE IX. Dissolution.

In the event of either voluntary or involuntary dissolution of the Society, the funds or assets of the Society, remaining after discharging all just debts of the society or its officers in the name of the society, shall be distributed without encumbrances to a non-profit group, organization or institution of learning engaged in the field of spectroscopy within the contemplation of Section 170 (c) (2) of the Internal Revenue Code (1954). The selection of the recipient or recipients shall be made by the majority vote of the Board of Directors or Governing Board in office at the time of dissolution but in no event shall the assets be distributed to any member or members of the society.

ARTICLE X. Society Seal.

This society shall have a seal, upon which shall be inscribed the name of the society, the year of its creation, and the words "Incorporated Commonwealth of Pennsylvania."

ARTICLE XI. Amendments.

Section 1. Proposed amendments to this Constitution and the Bylaws of the society, signed by at least three members of the Board of Directors or by twenty members of the society must be submitted to the Secretary at least fifteen weeks before the regular business meeting of the society at which meeting the proposed amendments may be discussed and amended. The Secretary shall send or cause to be sent the proposed amendments to each member within a reasonable time and at least before or with the notice of the next regular meeting thereafter. A two-thirds vote of the members present shall authorize a letter ballot on the proposed amendments (as amended in meeting) and if two-thirds of the votes obtained by letter ballot are in favor of the proposed amendments, they shall be adopted.

Section 2. The Board of Directors shall also have the power to amend the bylaws by a two-thirds vote of the Board of Directors by letter ballot of all the members or a like majority at a meeting where all the Board members are present and voting.

Section 3. The Board of Directors is authorized to renumber articles and sections of the Constitution and Bylaws to correspond with any changes that may be made.

ARTICLE XII. Relations with A.S.T.M.

Section 1. This Society shall cooperate with A.S.T.M. and its appropriate committees in matters concerned with standards and procedures relevant to Mass Spectrometry.

Section 2. This society shall make appropriate arrangements for joint meetings with A.S.T.M. Committee E-14. Other A.S.T.M. groups interested in mass spectrometry as applied to specific materials are invited to schedule their meetings in conjunction with meetings of the society.

ARTICLE XIII. Constitution and Bylaws

Section 1. The Constitution and Bylaws shall be adopted by a majority vote of the members present and voting at the time of their proposal to the members for the ratification.

Section 2. The Constitution and Bylaws shall be in full force and effect immediately upon their adoption as set forth in Section 1.

BYLAWS

1. Membership

1.1 Application for membership shall be made in writing, on a form to be specified by the Board of Directors. The membership year shall commence October 1 and end September 30.

1.2 Applicants shall be admitted by the action of the Board of Directors and membership thereafter becomes effective upon receipt of dues by the Treasurer.

1.3 Failure to pay dues for six months shall automatically terminate membership. Payment of arrears and current dues shall suffice for reinstatement.

1.4 Membership may be terminated without prejudice by written notice to the Secretary, with the requirement that dues up to and including the year of written notice be paid.

1.5 A voting member of A.S.T.M. Committee E-14 shall automatically be admitted to membership upon submission of an application for membership and payment of dues to the Treasurer.

1.6 Every member in good standing shall have the right to vote at the general membership meetings and to hold office.

1.7 Any member not in good standing shall lose the right to vote or hold office.

1.8 The books, accounts and records of this society shall be open for inspection to any member of the Board of Directors at any time. Members of this society may upon written request to the Board of Directors, inspect such books, accounts and records of this society at such reasonable times as the Board of Directors may by resolution designate.

2. Collections and Disbursements

2.1 Membership classes and dues within such classes shall be determined by the Board of Directors.

2.2 The Board of Directors is authorized to determine separately a registration fee for each general meeting to cover the expenses of holding the meeting. Payment of this fee is a requirement for attendance.

2.3 Disbursements shall be made in accord with an adopted budget or by approval of a majority of the Board of Directors and the fiscal year of the corporation shall be from October 1 to September 30.

2.4 The Secretary will prepare or cause to be prepared at least one annual financial and membership report to the Board of Directors.

2.5 The Treasurer will prepare or cause to be prepared an annual financial report to the Board of Directors.

2.6 The report of the Secretary on membership and the financial report of the Treasurer shall be made available for inspection for any reasonable purpose by any member of the society on written request to the Secretary or Treasurer.

3. Terms of Office and Election

3.1 The elected officers and directors at large shall hold office for a term of two (2) years, except as otherwise provided in Article IV and VI of the Constitution with their term year commencing on July 1 and ending on June 30.

3.2 The President shall appoint a nominating committee of not less than three members on or before October 1 of his second year in office. He shall not be a member of this committee. The committee shall nominate a slate of candidates and report in writing to the Board of Directors no later than the first day of the following February. The Secretary shall prepare or cause to be prepared a letter ballot to be mailed to the membership at the time of the sending of the final meeting notice and requesting return no later than two weeks preceding the annual meeting. Election will be by majority of votes cast. Write-in votes shall be accepted. The election results shall be made known at the next annual business meeting and the new officers shall assume office at the beginning of the next term year as specified in paragraph 3.1 of the Bylaws.

4. Committees

4.1 The President shall appoint such committees as are necessary for the carrying out of the aims and purposes of the society. Membership and chairmanship of such committees shall not exceed the term of office of the President. He may terminate a committee at any time. Members and chairmen may be reappointed by the incoming President.

5. Meetings

5.1 The society shall meet at least once a year in order to present scientific papers and conduct business. Twenty members shall constitute a quorum for the transaction of business.

5.2 The time and place of the general meeting shall be determined by the Board of Directors.

5.3 Meetings of the Board of Directors may be called by the President or, in his absence, by the Vice-President for Programs. Alternatively, two thirds of the Board of Directors may call a meeting by written request to the President. Five directors, including at least three voting members shall constitute a quorum of the Board of Directors.

5.4 A simple majority shall be required to pass any motion at any meeting of the members or Board of Directors, unless otherwise provided. Any member in arrears six months or more shall not have the right to vote or hold office.

5.5 Each director shall be entitled to two weeks' notice of any meeting of the Board of Directors.

5.6 Notices of all meetings, regular or special, shall be in writing and sent through the United States mails to each member or director on the Board of Directors as the case may be; at his latest address recorded on the books of this society.

5.7 Each member shall be entitled to thirty days' notice of the annual general meeting.

5.8 The President shall, in response to a petition bearing the signatures of not fewer than twenty members and requesting that the Board of Directors consider a specified question, place this item on the agenda of the first meeting of the Board of Directors which is scheduled to convene on a date not preceding the thirtieth day following receipt of the petition. The member whose signature appears first on the petition shall be entitled to two weeks' notice of such meeting, and the same member or a member designated by him shall be entitled to attend such meeting and discuss the specified question with the Board of Directors.

5.9 Unless otherwise provided by law, whenever any notice is required to be given, by the provisions of the Bylaws, a waiver thereof in writing, signed by the person or persons entitled to such notices, whether before or after the time stated therein, shall be equivalent thereto.

6. Compensation

6.1 No officers of the society shall receive salaries or fees for their services.

6.2 Officers of the society shall be reimbursed for all reasonable expenses not otherwise covered, except transportation, incurred in connection with their official duties. Reimbursement for transportation expenses imperative to the business of the society may be authorized by unanimous vote of the Board of Directors.

*Invited Paper

Author Index

Author Index

Author Index

Author Index

MASS SPECTROMETRY BIBLIOGRAPHIES

Bibliographies based on computer and manual searches of the literature in mass spectrometry comprising publications in open journals and government research reports have been prepared and published as AEC reports. To date reports are available at $3.00 per copy from the

Clearing House for Federal Scientific and Technical Information
National Bureau of Standards, U. S. Dept. of Commerce
Springfield, Virginia 22151

	No. of References
IS 1335 (1965) published Mar. 1966	1591
IS 1611 (1966) published July 1967	2907
IS 1829 (1st half 1967) published Apr. 1968	3569
IS 2058 (2nd half 1967) published June 1970	4674
IS 2059* (1st half 1968) expected publication; Fall 1970	4589
IS 2327* (2nd half 1968) expected publication; Winter 1970	5290
IS 2356* (1969) expected publication; Winter 1970	~4800
A report covering 1970; expected publication, Spring 1971	~4500

From these statistics, the literature of mass spectrometry is expected to contain > 32000 references for the last six years. There is no doubt that some references have been missed, especially those containing no reference to mass spectrometry in their titles, those whose authors are not yet on our computer search profile or those published in journals not listed by journal-contents publishers.

*The assistance of ASTM E-14 and ASMS in the form of stenographic support is acknowledged for these issues.

Harry J. Svec

Mass Spectrometrists, 1969-70

The membership records of the American Society for Mass Spectrometry contain a wealth of information about mass spectrometrists and their interests during 1969-70. The average year of birth coincides with the median year of 1931; but the mode of the distribution is 1936. Over 97% of the members are male and over 97% have a college degree. Of the degree holders, 55% have earned a doctors at one of 109 institutions. Massachusetts Institute of Technology, the University of California (Berkeley), the University of Illinois and Cornell University rank in the order given for doctor's degrees granted, but collectively account for just over 15% of the doctorates. The top four for junior degrees are Pennsylvania State University, University of California (Berkeley), Iowa State University and Ohio State University, but collectively account for under 10% of those without the doctorate. About 3.5% of the members are students still enrolled at colleges, and 23% are employed in academic institutions. Another 19% work for the government or not-for-profit institutes, and nearly 54% work in industry. Two members were not employed when they joined the Society.

The members were asked to give their selection of fields of interest on their application forms. The condensed results on this selection are shown in Table I. The compilation was done by assigning weights of 1, 1/2, 1/3, etc. to first, second and third etc. choices, and expressing the final "interest spectrum" on a percentage basis.

The geographical distribution of the members' addresses can be compiled in detail from the list of members given elsewhere in this book. The ASMS as of June 22, 1970 had members from 41 states, the District of Columbia and 19 other countries. The states leading in number of members are California with 89, New York and Pennsylvania each with 59, New Jersey with 52 and Texas with 49. Countries with a relatively large number of ASMS members include Canada with 24, France with 10, Great Britain and Japan each with 9 and Germany with 7.

Compiled June 22, 1970
J. M. McCrea, Sect., ASMS

Table I
Members' Interests and Applications, 1969-70

Topic	%
Analysis, qual/struc.	11.8
Instrument, single focus	9.4
Instrument, double focus	7.4
Analysis, MS+GC/DTA, etc	7.4
Analysis, isotopic	7.3
Analysis, quant chem	6.7
Analysis, solids (spark etc)	5.7
Computer, calculations	5.1
Ionization, electron,energetics	4.8
Instruments, quadrupole	4.2
Beams, collision reactions	4.1
Special studies, kinetics	3.6
Computer, interface systems	3.4
Computer, data compilation	2.9
Ion rearrangements	2.8
Thermodynamics	2.7
Instruments, time of flight	2.5
Ionization, surface, thermal	2.3
Ionization, chem, field	2.0
Theory	1.4
Physical Constants	0.7
Other Interests	1.8

Discipline	%
Chemistry, phys/inorg	32.5
Chemistry, organic	31.8
Physics	14.5
Biochemistry, Medicine	13.4
Geology, geophysics	7.8

Type of Application	%
Basic Properties	20.4
Instrument Development	19.7
Materials Research	13.8
Chemicals	11.5
Space Research	7.3
Petroleum	6.7
Nuclear Science	6.5
Surfaces	5.2
Instrument prodn, sales	5.1
Other	3.8

Members of The American Society for Mass Spectrometry

June 22, 1970 (*signifies charter member)

A

R M	Abernathey	Idaho Falls, Id
S	Abrahamsson	Goteborg, Sweden
F P	Abramson	Monrovia, Ca
*T	Aczel	Baytown, Tx
*A J	Ahearn	Kensington, Md
J E	Ahnell	Baltimore, Md
C A	Alexander	Columbus, Oh
E D	Alford	Louisville, Ky
M B	Alice	Southfield, Mi
*J G	Allard	Washington, DC
*H R	Almond, Jr.	Fort Washington, Pa
R L	Altman	Moffet Field, Ca
*A R	Anderson, Jr	Ames, Ia
W A	Anderson	Danvers, Ma
*W R	Anderson, Jr	Portland, Or
R J	Anthony	Hemlock, Mi
*W	Arnold	Monrovia, Ca
*G P	Arsenault	Lexington, Ma
*W B	Askew	Wilmington, De

B

*D A	Bafus	Houston, Tx
*D K	Bakale	Monroeville, Pa
J A	Baker	Hemlock, Mi
C R	Baldock	Oak Ridge, Tn
V S	Ban	Cranbury, NJ
M	Baril	Quebec, PQ Canada
F B	Barker	Bethel Park, Pa
D F	Barofsky	Portland, Or
C W	Barrick	Golden, Co
*R P	Barron	Washington, DC
*R P	Bastide	Burlington, Ma
D S	Baugher	Houston, Tx
J E	Beachey	Kansas City, Mo
*J L	Beck	Rahway, NJ
H D	Beckey	Bonn, Germany
V E	Bedwell	Chatsworth, Ca
C E	Beers	Bethlehem, Pa
D P	Beggs	Linden, NJ
J F	Below	Berkeley, Ca
*J G	Bendoraitis	Paulsboro, NJ
S L	Bennett	Kansas City, Mo
*W	Benz	Nutley, NJ
*E	Berkey	Pittsburgh, Pa
*J	Berkowitz	Argonne, Il
R H	Bernas	Orsay, France
R J	Berndt	Wilmington, De
*T E	Beukelman	Wilmington, De
*J H	Beynon	Buxton, Derby, England
*D R	Bidinosti	London, Ont Canada
K	Biemann	Cambridge, Ma
F J	Biros	Perrine, Fl
*T A	Blazer	Gibbstown, NJ
*E R	Blosser	Columbus, Oh
T	Blumenstock	Arlington, Va
G D	Blue	Columbus, Oh
*J R	Boal	Pittsburgh, Pa
R D	Board	Palo Alto, Ca
*H G	Boettger	La Canada, Ca
R D	Boies	Needham Heights, Ma
P H	Bommer	Nutley, NJ
*L I	Bone	Commerce, Tx
R N	Botter	Gif-sur-Yvette, France
H H	Bovee	Seattle, Wa
M T	Bowers	Santa Barbara, Ca
P B	Bowman	Kalamazoo, Mi
*R T	Brackmann	Pittsburgh, Pa
D K	Brain	Cincinnati, Oh
*E R	Braswell	Cranbury, NJ
*D A	Brent	Vaellingby, Sweden
D	Briglia	Palo Alto, Ca
C E	Brion	Vancouver, BC, Canada
P	Brown	Tempe, Az
*W M	Brubaker	Arcadia, Ca
C	Brunnee	Bremen, Germany
R M	Bryndza	Palo Alto, Ca
A P	Buchs	Geneva, Switzerland
*S N	Bulusu	Succasunna, NJ
J D	Burden	Palo Alto, NJ
*R R	Burke	Princeton, NJ
W H	Burke	Dallas, Tx
M M	Bursey	Chapel Hill, NC
A S	Butterfield	Oakland, Ca
S E	Buttrill	Minneapolis, Mn

C

*R B	Callen	Paulsboro, NJ
*L A	Cambey	Monrovia, Ca
A E	Cameron	Oak Ridge, Tn
*J M	Capellen	Ames, Ia
*H S	Carden	Kettering, Oh
*E G	Carlson	Pasadena, Tx
R R	Carlton	Rochester, NY
J P	Carrico	Southfield, Mi
*S R	Carroll	Colorado Spgs, Co
V	Cermak	Prague, Czechoslovakia
*E M	Chait	Wilmington, De
W S	Chamberlin	Littleton, Co
*T L	Chang	Stamford, Ct
P J	Chantry	Pittsburgh, Pa
P	Chastagner	Aiken, SC
C T	Chen	Houston, Tx
*W H	Christie	Oak Ridge, Tn

N F Christopher	Piketon, Oh	
W A Chupka	Argonne, Il	
S J Clark	Boston, Ma	
S K Clemans	Rensselaer, NY	
R P Clow	Salt Lake City, Ut	
N G Coggeshall	Pittsburgh, Pa	
A I Cohen	New Brunswick, NJ	
*H A Cohen	Framingham, Ma	
M J Cohen	West Palm Beach, Fl	
S N Cohz	Northridge, Ca	
K H Colberg	Barrington, Il	
J E Collin	Sart-Tilman par Liege, Belgium	
*J G Collins	Houston, Tx	
C M Combs	Evansville, In	
R N Compton	Oak Ridge, Tn	
*C Cone	Austin, Tx	
*D C Conway	College Station Tx	
*R J Conzemius	Ames, Ia	
*G L Cook	Laramie, Wy	
*H D Cook	West Mifflin, Pa	
*J C Cook, Jr	Urbana, Il	
*R G Cooks	Manhattan, Ks	
R A Coombs	Hanover, NJ	
A F Cornu	Grenoble, France	
J E Coutant	Ithaca, NY	
L W Cramer	Tulsa, Ok	
C K Crawford	Wilton, NH	
R W Crawford	Livermore, Ca	
R F Cree	Liverpool, NY	
*I H Crocker	Chalk River, Ont. Canada	
*E P Crowell	Princeton, NJ	
*H M Curtis, Jr	Ponca City, Ok	

D

R A Daly	Chicago, Il	
S S Daly	Golden, Co	
*J N Damico	Washington, DC	
*D C Damoth	Rochester, NY	
H S Danaceau	Arlington, Va	
A J Darby	Washington, DC	
K G Das	Poona, India	
*C E Davis	Deer Park, Tx	
P H Dawson	Quebec, PQ, Canada	
J R Dean	Edmonton, Alta Canada	
B A DeBarbieri	Nutley, NJ	
P J De Bievre	Kasterlee, Belgium	
G H DeBus	Geel, Belgium	
*A W Decora	Laramie, Wy	
F J DeGreve	Voreppe, France	
D C DeJongh	Detroit, Mi	
E B Delaney	Ridgefield, Ct	
*J E Delmore	Idaho Falls, Id	
B Dewey	Maynard, Ma	
*V H Dibeler	Rockville, Md	
D M Desiderio	Houston, Tx	
*L A Dietz	Schenectady, NY	
*J G Dillard	Blacksburg, Va	
C Djerassi	Stanford, Ca	
A S Doan	Greenbelt, Md	
J E Dooley	Bartlesville, Ok	
J R Dooley, Jr	Denver, Co	
F G Doolittle	Laramie, Wy	
*R C Dougherty	Tallahassee, Fl	
J H Duncan	Baltimore, Md	
A M Duffield	Stanford, Ca	
W E Duffy	Boise, Id	
J V Dugan	Cleveland, Oh	
*D L Dugger	Dallas, Tx	
R J Dupzyk	Livermore, Ca	

E

D P Easter	Washington, DC	
A A Ebert	Wilmington, De	
*R E Eby	Oak Ridge, Tn	
T R Edwards	Huntsville, Al	
T C Ehlert	Milwaukee, Wi	
*R M Elliott	Sale, Cheshire England	
*W H Elliott	St. Louis, Mo	
*T A Elwood	Chapel Hill, NC	
D E Emerson	Amarillo, Tx	
*E M Emery	Piscataway, NJ	
G G Engerholm	Cincinnati, Oh	
S Enomoto	Medford, Ma	
*E E Escher	Monrovia, Ca	
T J Eskew	State College, Pa	
B E Evans	Palo Alto, Ca	
*C A Evans, Jr	Lexington, Ma	
*D L Evans	Webster, NY	
J W Ewing	Lynchburg, Va	

F

I S Fagerson	Amherst, Ma	
F C Fehsenfeld	Boulder, Co	
H M Fales	Bethesda, Md	
*H Farrar	Woodland Hills, Ca	
R P Fedchenko	Monrovia, Ca	
*T P Fehlner	Notre Dame, In	
N Fein	New York, NY	
M H Feller	Toledo, Oh	
D C Fenimore	Houston, Tx	
P F Fennessey	Denver, Co	
*C C Fenselau	Baltimore, Md	
*F H Field	Linden, NJ	

Members of The American Society for Mass Spectrometry

June 22, 1970 (*signifies charter member)

*H O Finley	Cresent, Ok
*R E Finnigan	Palo Alto, Ca
I P Fisher	Sheridan Park, Ont. Canada
W L Fite	Pittsburgh, Pa.
M. E. Fitzgerald,	Philadelphia, Pa
*G D Flesch	Ames, Ia
R A Fluegge	Buffalo, NY
T L Folk	Akron, Oh
*R L Foltz	Columbus, Oh
*H T Ford	Ponca City, Ok
K D Foster	Quebec, PQ Canada
*N G Foster	Denton, Tx
*R E Fraas	Lexington, Ky
*J C Franklin	Oak Ridge, Tn
*J L Franklin	Houston, Tx
D S Franks	Enfield, Ct
J Franzen	Dortmund, Germany
*H Friedman	Philadelphia, Pa
L Friedman	Upton, NY
*M A Frisch	Yorktown Heights NY
G J Frisone	Piscataway, NJ
*P T Funke	Hoboken, NJ
R J Furr	Dallas, Tx
*J H Futrell	Salt Lake City, Ut

G

*E J Gallegos	Richmond, Ca
M A Garofalo	Rochester, NY
E L Garner	Washington, DC
*A W Garrison	Athens, Ga
D L Geiger	Dayton, Oh
E Gelpi	Berkeley, Ca
L H Gevantman	Washington, DC
J M Gibert	Houston, Tx
H C Gibson, Jr	West Palm Beach Fl
*B G Giessner	Houston, Tx
E J Gilbert	Bethesda, Md
P W Gilles	Lawrence, Ks
D E Gilmartin	Los Angeles, Ca,
K A Gingerich	College Station, Tx
T A Giorgi	Milan, Italy
R E Glick	Tallahassee, Fl
L C Glover	Menlo Park, Ca
S M Gordon	Pretoria, South Africa
B B Goshgarian	Edwards, Ca
M A Grayson	Ballwin, Mo
J H Green	Ridgefield, Ct
M M Green	Ann Arbor, Mi
F T Greene	Kansas City, Mo
*R C Greenough	Morris Plains, NJ
*R D Grigsby	College Station. Tx
*R T Grimley	Lafayette, In
M F Grostic	Kalamazoo, Mi
S L Grotch	Pasadena, Ca
*J B Grutka	Riverside, Il
S R Gryczuk	State College, Pa
*J G Guerrera	Matawan, NJ
*R J Guidoboni	Lexington, Ma
S K Gupta	Cleveland, Oh
M A Gusinow	Albuquerque, NM
*J W Guthrie	Albuquerque, NM

H

W F Haddon	Albany, Ca
*L G Hall	Pomona, Ca
*F O Halliday	Pleasanton, Ca
*J S Halliday	Sale, Cheshire England
R M Halverson	Essex Junction, Vt
M Hamell	Tarrytown, NY
N E Hamilton	Lexington, Ma
*M C Hamming	Ponca City, Ok
C F Hammer	Washington, DC
R J Hanrahan	Gainesville, Fl
E R Hansen	Golden, Co
G P Happ	Rochester, NY
W J Harchak	State College, Pa
A L Harkness	Elmhurst, Il
*H R Harless	So Charleston, WVa
D B Harrington	Palo Alto, Ca
*W L Harrington	Princeton, NJ
W W Harrison	Charlottesville, Va
*B F Hartenstein	Midland, Mi
J R Hass	Chapel Hill, NC
D D Hatler	Palo Alto, Ca
S E Hattox	Houston, Tx
*R M Haynes	Sheridan Park, Ont Canada
P L Haug	Houston, Tx
J M Hayes	Bloomington, In
*N D Heitkamp	Louisville, Ky
*R J Hellmann	Cincinnati, Oh
D Henneberg	Mulheim, Germany
*J T Herron	Washington, DC
G R Hertel	Orlando, Fl
*L F Herzog	State College, Pa
R F Herzog	Lexington, Ma
*E A Hetherington	Dallas, Tx
G Heyden	London, England
*W M Hickam	Pittsburgh, Pa
D L Hildenbrand	Huntington Beach, Ca
H Hintenberger	Mainz, Germany
J A Hipple	New York, NY
R A Hites	Cambridge, Ma
E W Hobart	Teaneck, NJ

Members of The American Society for Mass Spectrometry

June 22, 1970 (*signifies charter member)

D C Hobbs	Groton, Ct	
H D Hoberecht	New Haven, Ct	
D L Hobrock	Centerville, Oh	
*J H Hoffman	Dallas, Tx	
H E Hoda	Bayside, NY	
*A M Hogg	Edmonton, Alta, Canada	
J M Hollerbach	Hopewell Jct, NY	
*P K Hon	Hong Kong, Brit. Crown Colony	
*R E Honig	Princeton, NJ	
B A Hopper	Tulsa, Ok	
J C Horton	Oak Ridge, Tn	
*H E Howard	Brea, Ca	
O H Howard	Oak Ridge, Tn	
*J D Hribar	Ithaca, NY	
W K Huber	Balzers, Liechtenstein	
F G Hudda	Latham, NY	
J E Hudson	Baltimore, Md	
B M Hughes	Wright-Patterson AFB, Oh	
*R E Huie	Washington, DC	
M H Hunt	Bedford, Ma	
*R H Hunt	Deer Park, Tx	
W W Hunt	Chelmsford, Ma	
D I Hunter	Golden, Co	
W T Huntress, Jr	Pasadena, Ca	

I,J

P J Ihrig	Whiting, In	
A P Irsa	Upton, NY	
D M Jackson	Phoenix, Az	
D W Jarosz	State College, Pa	
*D Jerolamon	Morristown, NJ	
K R Jennings	Sheffield, England	
A Johannin	Brest, France	
*C E Johannsen	Monrovia, Ca	
R H Johnsen	Tallahassee, Fl	
P G Johnson	Livermore, Ca	
H C Jones	Oak Ridge, Tn	
*J W Jones	Alexandria, Va	
*T E Joyce	Dayton, Oh	
*C M Judson	Altadena, Ca	
*G A Junk	Ames, Ia	

K

J R Kalasky	State College, Pa	
G J Kallos	Midland, Mi	
M S Kaminsky	Argonne, Il	
*A Kant	Watertown, Ma	
*F W Karasek	Waterloo, Ont Canada	
*J Karliner	Ardsley, NY	
A T Kashuba	Pittsburgh, Pa	
E O Kazimir	Hightstown, NJ	
*G L Kearns	White Plains, NY	
P Kebarle	Edmonton, Alta Canada	
G W Keen	Ponca City, Ok	
*B R Kendall	University Park Pa	
*P R Kennicott	Scotia, NY	
R A Kent	Los Alamos, NM	
*D P Kilinski	Elmhurst, Il	
W E Killinger	Clarksville, Md	
*J F Kinder	Harvey, Il	
D G Kingston	Albany, NY	
*K F Kinneberg	Stillwater, Ok	
*T H Kinstle	Ames, Ia	
W E Kirby	Lafayette, Ca	
*M C Kirk	Birmingham, Al	
S Kisaka	Osaka, Japan	
*R W Kiser	Lexington, Ky	
*F G Kitson	Wilmington, De	
F S Klein	Rehovoth, Israel	
W Kneen	Pasadena, Ca	
T C Knight	Ann Arbor, Mi	
B E Knox	University Park Pa	
K Kodera	Sakyo, Kyoto, Japan	
*F C Kohout	Pennington, NJ	
*C W Koch	Berkeley, Ca	
R M Kolb	Albuquerque, NM	
*M G Kolor	Tarrytown, NY	
R A Kornfeld	Ithaca, NY	
H Kramer	Dover, NJ	
G J Krige	Pretoria, South Africa	
R E Kugel	Port Chester, NY	
*W F Kuhn	Richmond, Va	

L

B Lacy	Dugway, Ut	
*C R Lagergren	Richland, Wa	
C La Lau	Amsterdam, Netherlands	
F W Lampe	University Park Pa	
W R Landis	Bethesda, Md	
J Lang	Piketon, Oh	
*A Langdon	Oak Ridge, Tn	
W J Lange	Pittsburgh, Pa	
*H G Langer	Wayland, Ma	
R C Lao	Ottawa, Canada	
*M T Laug	Idaho Falls, Id	
W R Lankenau	Horseheads, NY	
J A Lawless	Moffet Field, Ca	
*J R Leger	Houston, Tx	
*R B Lehotsky	Pomona, Ca	

Members of The American Society for Mass Spectrometry

June 22, 1970 (*signifies charter member)

*F D Leipziger	Lexington, Ma	
H K Lembersky	Columbia, SC	
I Lengyel	Jamaica, NY	
*D F Lesher	Allentown, Pa	
*J E Leta	Elmhurst, Il	
*M I Levenberg	North Chicago, Il	
*P L Levins	Cambridge, Ma	
E J Levy	Oxford, Pa	
C I Lewis	Greensboro, NC	
J S Lewis	Kingsport, Tn	
*J W Lewis	Bound Brook, NJ	
H Y Li	Dallas, Tx	
L M Libbey	Corvallis, Or	
*J F Light	Clarksville, Md	
D A Lightner	Los Angeles, Ca	
W Lijinsky	Omaha, Nb	
*K A Lincoln	Redwood City, Ca	
*L P Lindeman	Richmond, Ca	
E Lindholm	Stockholm, Sweden	
J Linett	Monrovia, Ca	
*R H Littmann	Riverside, Il	
J A Llewellyn	Tallahassee, Fl	
P M Llewellyn	Palo Alto, Ca	
G D Lominac	Chapel Hill, NC	
F P Lossing	Ottawa, Ont. Canada	
E D Loughran	Los Alamos, NM	
*M Lounsbury	Chalk River, Ont Canada	
R E Lovins	Athens, Ga	
*M D Lubin	Sacramento, Ca	
A J Luchte	Rochester, NY	
*H E Lumpkin	Baytown, Tx	

M

A Maccoll	London, W C 1 England
D B Maclean	Hamilton, Ont. Canada
J K Macleod	Canberra, A.C.T. Australia
J M Madson	St Louis, Mo
K Maeda	Tanashi, Tokyo Japan
D P Maier	Rochester, NY
G J Mains	Detroit, Mi
T Makita	Sakyo, Kyoto, Japan
D L Malm	Murray Hill, NJ
A Mandelbaum	Haifa, Israel
J P Mannaerts	State Gollege, Pa
*G W Mappes	St. Louis, Mo
*A B Marcus	Pittsburgh, Pa
J L Margrave	Houston, Tx
*S P Markey	Denver, Co
D L Marks	Nampa, Id
P M Marmet	Quebec, P Q Canada
T W Martin	Nashville, Tn
*J Maruska, Jr	League City, Tx
E M Masumoto	Pasadena, Ca
H Matsuda	Toyonka, Osaka Japan
*R K Mauldin	Charlotte, NC
D J McAdoo	Ithaca, NY
T L McClaskey	Huntington, WV
U McCleary, Jr	Monrovia, Ca
J A McCloskey	Houston, Tx
*J M McCrea	Monroeville, Pa
*K E McCulloh	Washington, DC
C A McDowell	Vancouver, BC Canada
W H McFadden	Union Beach, NJ
J McGlotten	Bloomfield, NJ
J J McGovern	Pittsburgh, Pa
*C R McKinney	Monrovia, Ca
*H S McKown	Oak Ridge, Tn
*F W McLafferty	Ithaca, NY
D A McMillan	South Euclid,Oh
W J McMurray	New Haven, Ct
J McSorley	Youngwood, Pa
T E Mead	Stamford, Ct
H H Mehnert	Denver, Co
*G G Meisels	Houston, Tx
*C E Melton	Hull, Ga
R Menendez	Pau, France
*C. Merritt	Natick, Ma
M C Mertes	Atlanta, Ga
*R A Meyer	Thousand Oaks, Ca
R T Meyer	Albuquerque, NM
*S Meyerson	Whiting, In
J P Mieure	St. Louis, Mo
J M Miller	St. Catharines, Ont. Canada
W J Miller	Princeton, NJ
N Milleron	Berkeley, Ca
R M Mills	Rockville, Md
G W Milne	Bethesda, Md
T A Milne	Kansas City, Mo
R F Miner	Arcadia, Ca
J Momigny	Sart-Tilman par Liege, Belgium
A Moore	Littleton, Co
P E Moreland	Wheaton, Il
J E Morgan	Montreal, PQ Canada
*T D Morgan	Bartlesville, Ok
R N Morris	Arvada, Co
*G H Morrison	Ithaca, NY

Members of The American Society for Mass Spectrometry

June 22, 1970 (*signifies charter member)

*J D Morrison		Bundoora, Vic. Australia
*M	Mosharrafa	Minneapolis, Mn
C E	Muller	Houston, Tx
M A	Munroe	Nutley, NJ
*B	Munson	Newark, De
*E	Murad	Bedford, Ma
E E	Muschlitz	Gainesville, Fl
*W G	Myers	Troy, NY

N

M	Nalbantoglu	Neuilly/Seine France
Y	Nakagawa	Fukushimaku, Osaka, Japan
*J C	Neerman	Dearborn, Mi
G G	Nelson	Palo Alto, Ca
W R	Nes	Philadelphia, Pa
J E	Neuzil	Chicago, Il
*A S	Newton	Berkeley, Ca
T H	Nicholls	Charlotte, NC
A J	Nicholson	Clayton, Vic Australia
J B	Nicholson	Glendale, Ca
A O	Nier	Minneapolis, Mn
T	Noda	Katsuta, Ibabaki Japan
T A	Norris	Beacon, NY
P	Nounou	Chatou, France

O

*D W	Oblas	Bayside, NY
R T	OConnor	New Orleans, La
J T	ODonovan	Rockville, Md
J S	Ogden	Columbus, Oh
*R D	Ohlinger	Cincinnati, Oh
R A	Okerholm	Boston, Ma
*W R	Oliver	Cincinnati, Oh
J	Oro	Houston, Tx
J C	Orr	Boston, Ma
S F	Osman	Philadelphia, Pa
A I	Ossinger	Denver, Co
*E B	Owens	Lexington, Ma

P,Q

C F	Pachucki	Schenectady, NY
*F G	Padrta	Des Plaines, Il
*R P	Page	Oak Forest, Il
J L	Painter	New Brunswick, NJ
*R J	Pancirov	Linden, NJ
E H	Parkison	Baltimore, Md
N H	Parsons	St. Petersburg, Fl
R D	Partridge	Worcester, Ma
*P J	Paulsen	Washington, DC
*J F	Paulson	Claymont, De
*J F	Paulson	Bedford, Ma
J N	Pawloski	Houston, Tx
A R	Pebler	Pittsburgh, Pa
*J A	Peden	Pittsburgh, Pa
T C	Peng	St Louis, Mo
E G	Perkins	Urbana, Il
B	Perovic	Belgrade, Yugoslavia
*R E	Perrin	Tulsa, Ok
I G	Peters	Brooks AFB, Tx
R L	Peterson	Golden, Co
J K	Phillips	Akron, Oh
R W	Phillips	Golden, Co
W C	Phillips	Urbana, Il
J L	Pinkus	Brookline, Ma
A J	Pirone	Claymont, De
H O	Pitts	Boulder, Co
*B E	Plashko	Fargo, ND
R F	Porter	Ithaca, NY
R F	Pottie	Ottawa, Ont. Canada
*P	Powers	Cheadle Hulme, England
G A	Pressley	Evanston, Il
D W	Priddle	Toronto, Ont Canada
*R T	Puckett	Summit, NJ
*T L	Pugh	Wilmington, De
J W	Pyper	Livermore, Ca
*D L	Quick	Glendora, Ca

R

*T	Radford	Atlanta, Ga
H H	Raddatz	Menlo Park, Ca
W T	Rainey	Oak Ridge, Tn
E S	Ramey	Corpus Christi, Tx
*R B	Randall	Madison, Wi
P C	Rankin	Beltsville, Md
*J R	Rec	North Highlands, Ca
R I	Reed	Glasgow, Scotland
*W V	Reeds	Beacon, NY
*J R	Reeher	Ames, Ia
N M	Reid	Huntsville, Al
V N	Reinhold	Cambridge, Ma
R W	Reiser	Wilmington, De
E J	Renshaw	West Mifflin, Pa
A A	Repucci	Woodside, NY
*F L	Reynolds	Berkeley, Ca
W E	Reynolds	Stanford, Ca
*R E	Rhodes	West Point, Pa
T C	Rhyne	Blacksburg, Va
*W W	Rice	Oak Ridge, Tn
W J	Richter	Berkeley, Ca
W	Riepe	Dortmund, Germany
K L	Rinehart,	Urbana, Il
*C F	Robinson	Goleta, Ca

Members of The American Society for Mass Spectrometry

June 22, 1970 (*signifies charter member)

*C J Robinson	Whiting, In	
*R J Robinson	Midland, Mi	
J Roboz	Cresskill, NJ	
R J Roenigk	Houston, Tx	
*P F Rogerson	Chapel Hill, NC	
W K Rohwedder	Peoria, Il	
D J Rokop	Argonne, Il	
M P Romiez	Moffett Field, Ca	
*T L Rose	College Station, Tx	
*D D Rosebrook	Kansas City, Mo	
*H M Rosenstock	Washington, DC	
*F M Rourke	Cohoes, NY	
*L H Rovner	San Diego, Ca	
R W Rozett	Bronx, NY	
*M R Ruecker	Pomona, Ca	
F G Ruedenauer	Cambridge, Ma	
R E Rummel	Nashville, Tx	
*J D Rusk	Golden, Co	
D S Russell	Ottawa, Ont. Canada	
*M E Russell	DeKalb, Il	
*J M Ruth	College Park, Md	
K R Ryan	Camden, NSW Austrailia	
A L Ryland	Wilmington, De	

S

*F E Saalfeld	Washington, DC	
P C Samson	Elkgrove, Il	
J M Sanders	Painesville, Oh	
*A Sanderson	Union Beach, NJ	
G Sanzone	Blacksburg, Va	
J H Sayer	Syracuse, NY	
G P Schacher	Schenectady, NY	
G Schaden	Darmstadt, Germany	
R Schafranek	Somerset, NJ	
F Schaub	Rockville, Md	
S E Scheppele	Stillwater, Ok	
*S M Schildcrout	Youngstown, Oh	
P O Schissel	Chappaqua, NY	
D M Schoengold	Claymont, De	
*J L Schornick	Houston, Tx	
J M Schroeer	Normal, Il	
M F Schulman	Springfield, NJ	
D D Scott	Tulsa, Ok	
*W M Scott	Tucson, Az	
*S K Searles	Washington, DC	
*D E Seizinger	Bartlesville, Ok	
*L A Shadoff	Midland, Mi	
*M M Shahin	Rochester, NY	
*T W Shannon	Wayland, Ma	
R Shapiro	Barrington, Il	
R H Shapiro	Boulder, Co	
*A G Sharkey, Jr	Pittsburgh, Pa	
T E Sharp	Dearborn, Mi	
*P W Shearer	Wilmington, De	
W R Sherman	St Louis, Mo	
*R M Sherwood	Philadelphia, Pa	
*S R Shrader	Philadelphia, Pa	
*R J Shuba	Philadelphia, Pa	
J L Shultz	Pittsburgh, Pa	
B R Simoneit	Berkeley, Ca	
J R Sites	Oak Ridge, Tn	
A J Smith	State College, Pa	
D A Smith	State College, Pa	
J S Smith	Morristown, NJ	
L A Smith	Oak Ridge, Tn	
*R F Smith	Paducah, Ky	
L D Smithson	Wright-Patterson AFB, Oh	
*G W Snow	Doraville, Ga	
A J Socha	Pasadena, Ca	
*G R Sparrow	St. Paul, Mn	
R L Sperling	Hopkins, Mn	
*J A Sphon	Wayne, Mi	
E J Spitzer	Oak Ridge, Tn	
K F Sporek	Toledo, Oh	
R A St Hilaire	Dallas, Tx	
F E Stafford	Evanston, Il	
*S W Staley	College Park, Md	
*J L Stauffer	Lexington, Ma	
J S Stacey	Denver, Co	
J B Stanley	New Orleans, La	
C A Stearns	Cleveland, Oh	
*S J Steck	Houston, Tx	
W C Steele	Lowell, Ma	
E Stenhagen	Goteborg, Sweden	
A J Steikunas	Arvada, Co	
J D Stein	San Jose, Ca	
R P Stein	Pleasant Gap, Pa	
D W Stewart	Rochester, NY	
R N Stillwell	Houston, Tx	
W I Stillwell	Houston, Tx	
J J Stoffels	Richland, Wa	
*M S Story	Sunnyvale, Ca	
*R N Stover	State College, Pa	
D S Stratouly	Medford, Ma	
*W K Stuckey	Los Angeles, Ca	
C Sulfridge	Oak Ridge, Tn	
C L Sullivan	Cleveland, Oh	
*R E Sullivan	Piscataway, NJ	
R W Supple	Palo Alto, Ca	
*H J Svec	Ames, Ia	
W A Svec	Argonne, Il	
A R Swanson	Minneapolis, Mn	
C C Sweeley	E Lansing, Mi	
G G Sweeney	Pittsburgh, Pa	
B N Swiners	Chatou, France	

Members of The American Society for Mass Spectrometry

June 22, 1970 (*signifies charter member)

T

C D Tabor		Piketon, Oh
*C E Taylor		Irwin, Pa
E E Taylor		Dallas, Tx
J W Taylor		Madison, Wi
L W Taylor		Wood River, Il
*R M Teeter		Richmond, Ca
M K Testerman		Little Rock, Ar
*T O Tiernan		Wright-Patterson AFB, Oh
B	Tiffany	Aiken, SC
L	Tokes	Palo Alto, Ca
K B Tomer		Boulder, Co
S C Tong		Corning, NY
F L Torney, Jr		Cambridge, Ma
J R Turbett		Boulder, Co
J	Turk	Boulder, Co
W R Turner		Palo Alto, Ca

U,V

B W Ullmann		Menlo Park, Ca
*W S Updegrove		Houston, Tx
*P P Vallon		Brooklyn, NY
*R W Vander Haar		Whiting, In
F M Vane		Nutley, NJ
G E Van Lear		Pearl River, NY
M J Vasile		Murray Hill, NJ
F J Vastola		University Park Pa
R	Venkataraghavan	Ithaca, NY
M L Vestal		Baltimore, Md
*G P Vidal		Chatillon-Sous-Bagneux, France
F P Viehbock		Seibersdorf, Austria
C E V n Sydow		Goteborg, Sweden
P	Vouros	Houston, Tx

W

F M Wachi		Long Beach, Ca
*M E Wacks		Tucson, Az
Y	Wada	Tokyo, Japan
P A Wadsworth		Emeryville, Ca
*L C Wagner		Lafayette, In
*A L Wahrhaftig		Salt Lake City, Ut
J D Waldron		Manchester, England
*G R Waller		Stillwater, Ok
J A Walker		Washington, DC
*B C Walsh		West Mifflin, Pa
D C Walters		Columbus, Oh
*J R Walton		Oak Ridge, Tn
V L Warren		Los Alamos, NM
H W Washburn		Long Beach, Ca
S	Wisniewski	Salt Lake City, Ut
E	Watanabe	Akishima, Tokyo Japan
J T Watson		Nashville, Tn
K F Watterson		Bethlehem, Pa
J C Webber		Hopewell Junction NY
E R Weiner		Denver, Co
C R Weisenberger		Columbus, Oh
*T J Weismann		Pittsburgh, Pa
H W Werner		Eindhoven, Netherlands
R	Wertzler	Harvey, Il
*A R West		Sunbury on Thames England
T A Whatley		Sunland, Ca
G V Wheeler		Idaho Falls, Id
N R Whetten		Schenectady, NY
E	White	Houston, Tx
F A White		Troy, NY
*G W Widdicombe		Allentown, Pa
J R Wieland		Teaneck, NJ
*F B Wiens		Denver, Co
H U Wiesendanger		Los Altos, Ca
J J Wijtvliet		Eindhoven, Netherlands
*G W Wilcox		Ferndale, Mi
*H F Wiley		Altadena, Ca
R H Wiley		New York, NY
P	Williams	Winnipeg, Man. Canada
M P Williamson		Niagara Falls, NY
C R Winkelman		Los Alamos, NM
*D L Winter		Ponca City, Ok
*C H Williams		Albuquerque, NM
*L H Wojcik		Salt Lake City, Ut
R L Wolfgang		New Haven, Ct
C G Woll		Honey Brook, Pa
W A Wolstenholme		White Plains, NY
*G M Wood, Jr		Newport News, Va
*D R Woods		Ashland, Ky
J W Woods		Newton, Ma
J R Woodyard		Bayside, NY
*J R Woolston		Princeton, NJ
A A Wroblewski		West Mifflin, Pa

XYZ

R H Yarbrough		Sunnyvale, Ca
D Y Yee		Little Falls, NJ
*A L Yergey		Linden, NJ
L R Yetter		Apalachin, NY
C F Yu		Nutley, NJ
*R G Zaylskie		Fargo, ND
*F	Zitomer	Summit, NJ
*B Y Zwolinski		College Station, Tx

ELEMENTAL ABUNDANCES IN LUNAR MATERIALS BY SPARK SOURCE MASS SPECTROSCOPY

G. H. Morrison, A. T. Kashuba, and A. M. Rothenberg
Department of Chemistry
Cornell University
Ithaca, N. Y. 14850

Among the most important types of information desired from the lunar materials returned to earth by the Apollo missions is the characterization of their chemical composition. Of the various multielement techniques for the survey analysis of solids, spark source mass spectrography provides the greatest scope and sensitivity. The approach is particularly helpful in obtaining maximum elemental abundance data on limited sample sizes of lunar materials. A method is described for the analysis of lunar material and results are presented for the analysis of lunar soil and rocks returned by the Apollo 11 and 12 missions.

According to the Surveyor results (1,2,3), the lunar surface materials near the site of the landings resemble basalts in their major element abundances. Therefore, a general technique for basalt analysis was devised. U.S. Geological Survey basaltic standards W-1 and BCR-1 were selected respectively as "standard" and "unknown."

Electrode shape, composition, magnet current, electrostatic analyzer voltage, duty cycle and proportionality settings were studied to optimize sensitivity (4). The last three, being continuous functions, were subjected to a standard analysis of variance experiment, which quickly elucidated the optimal values. Magnet settings were altered to accomplish two purposes:

1. A low magnet setting, together with relatively low charge collections ($\lesssim$ 30 ncoul.) and a narrow slit (0.0005") effectively spread out the spectrum under study, elements with masses below the rare earths, in order to obtain data on the major elements and those trace elements normally obscured by halation caused by the majors and conducting matrix, graphite powder.
2. A high magnetic setting with higher charge collections (1000 ncoul.) and a wider slit (0.0025") sharpened and intensified the high-mass trace elements, eliminated $^{12}C^+$ and $^{13}C^+$ from the spectrum. Halation effects were minimized by increasing the spacing between the larger exposures.

For use with terrestrial basalts, In was used as the internal standard. For subsequent work with lunar materials, the small amounts of sample available precluded the doping of an internal standard. The existing trace Zr was used, and neutron activation analysis (5) was used to ascertain the Zr concentration in the samples. Sensitivity factors were obtained from the analysis of W-1.

Because of the complex nature of the lunar materials with attendant serious interference problems, the use of mass spectroscopy alone would have precluded the determination of many elements of geochemical interest. Therefore, the mass spectrographic analysis was combined with neutron activation analysis of the same samples resulting in the determination of 67 elements (6) (7).

Figure 1. Apollo 11 average lunar composition. Values in parentheses represent limited number of analyses.

Average Lunar Composition
Apollo 11
(ppm)

H																	He
Li	Be											B	C	N	O	F	Ne
12	2.5											3.8	130	94	40.1%	140	
Na	Mg											Al	Si	P	S	Cl	A
.35%	4.50%											5.87%	19.34%	.057%	.17%	15	
K	Ca	Sc	Ti	V	Cr	Mn	Fe	Co	Ni	Cu	Zn	Ga	Ge	As	Se	Br	Kr
.14%	8.18%	75	5.62%	60	.21%	.19%	13.47%	26.1	.02%	14	20	4.4	.7	.05	(.5)	.15	
Rb	Sr	Y	Zr	Nb	Mo	Tc	Ru	Rh	Pd	Ag	Cd	In	Sn	Sb	Te	I	Xe
3.2	162	131	.04%	25	.4		—	—	(.005)	(.03)	(.06)	(.2)	(.6)	(.007)	—	(.7)	
Cs	Ba	La	Hf	Ta	W	Re	Os	Ir	Pt	Au	Hg	Tl	Pb	Bi	Po	At	Rn
.12	198	19.9	12.1	1.8	.29	—	(.3)	(.003)	—	(.002)	(.004)	(.001)	2.5	(.001)			
Fa	Ra	Ac															

Ce	Pr	Nd	Pm	Sm	Eu	Gd	Tb	Dy	Ho	Er	Tm	Yb	Lu
58.4	12.8	45.3		15.2	2.0	21.0	3.9	24.9	5.8	15.0	1.9	13.4	1.9
Th	Pa	U	Np	Pu	Am	Cm	Bk	Cf	E	Fm	Mv		
2.2		.47											

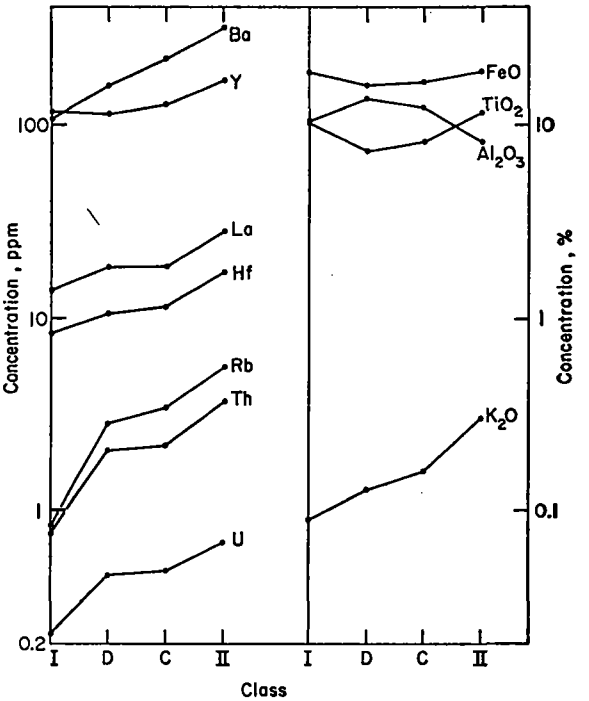

Figure 2. Classification of Apollo 11 igneous rocks into groups I and II based on large variation in elemental abundances. D represents soil and C represents breccias.

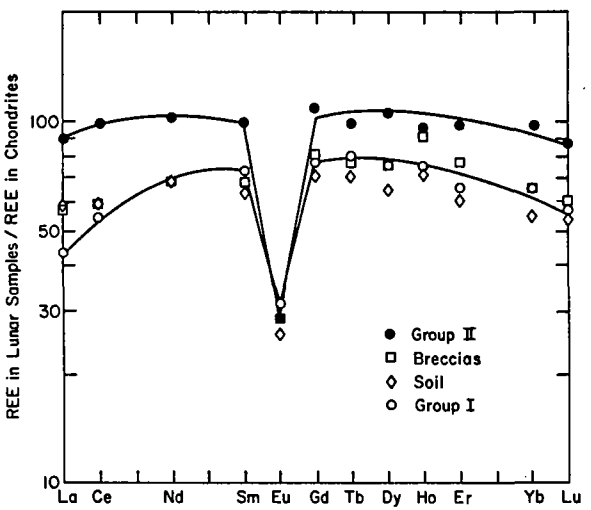

Figure 3. Chondrite normalized rare earth abundance patterns for Apollo 11 igneous rock groups I and II and soil and breccias.

Comparison of the results of our laboratory for the analysis of seven rocks and soil from Apollo 11 shows good agreement with the results of other investigators presented at the Lunar Science Conference (8).

The average composition of Apollo 11 lunar material is given in Figure 1. It includes the average of 17 igneous rocks, 11 breccias and the soil representing all of the data published by all investigators at the Lunar Science Conference using a variety of methods. The values in parentheses are based on limited numbers of analyses, in some cases only one analysis was available.

All rocks have unusually high concentrations of Ti, Sc, Zr, Hf, Y, and trivalent rare earth elements and low concentrations of Na. Some of the more volatile elements, i.e. Bi, Hg, Zn, Cd, Tl, Pb, Ge, Cl and Br are signficantly depleted with respect to their presumed abundance in the primitive solar system.

The chemical composition of all of the igneous rocks are similar except for the concentrations of K, Ti, Ba, Y, La, Hf, Rb, Th and U. See Figure 2. These trace elements, which normally do not enter the major mineral phases, distinguish two groups of igneous rocks. The composition of the soils (D) and breccias (C) is similar to but distinguishable from the igneous rocks and fall between the groups I and II igneous rocks. The igneous rocks also exhibit a depletion of Eu relative to the other rare earth elements as shown in Figure 3 where the abundances are normalized to those in chondrites. Groups I and II igneous rocks are distinguishable with soil and breccia clustering around group I.

Based on the limited data so far, the Apollo 12 lunar materials are chemically similar to those of Apollo 11 but with a number of interesting differences including lower concentrations of Ti, K, Rb, Zr, Y and Ba in Apollo 12 samples. Further details on the Apollo 12 results and a comparison of both Apollo 11 and 12 basalts with terrestrial and achondrite basalts will be published later.

References

1. A. L. Turkevich, E. J. Franzgrate and J. H. Patterson, Science 158, 635 (1967).
2. _____, ibid. 160, 1108 (1968).
3. _____, ibid. 162, 117 (1968).
4. G. H. Morrison and A. T. Kashuba, Anal. Chem. 41, 1842 (1969).
5. G. H. Morrison, J. T. Gerard, A. Travesi, R. L. Currie, S. F. Peterson and N. M. Potter, Anal. Chem. 41, 1633 (1969).
6. G. H. Morrison, J. T. Gerard, A. T. Kashuba, E. V. Gangadharam, A. M. Rothenberg, N. M. Potter, and G. B. Miller, Science 167, 505 (1970).
7. _____, ibid., Geochem. et Cosmoschim. Acta, 34, April, 1970.
8. Summary of Apollo 11 Lunar Science Conference, Science 167, Jan. 30, 1970.

HEAVY ELEMENTS IN LUNAR SAMPLES*

C. M. Stevens, Donald J. Rokop, Parker E. Moreland, Jr.,
Paul R, Fields, Herbert Diamond, and Donald N. Metta,
Chemistry Division Argonne National Laboratory

Mass spectrometric and radiochemical analysis methods were used to determine concentrations by isotopic dilution of thorium and uranium in Apollo 11 and 12 soil samples, isotopic abundance of uranium, and to search for transuranic and super heavy elements.[1] Preliminary results are: Apollo 11 soil sample 10084, Th = 2.24 ppm, U = 0.59 ppm, $^{235}U/^{238}$ = 0.007241 ± 0.000012, $^{236}U/^{238}$ = 3 ± 3 ppb; Apollo 12 soil sample 12070, Th = 6.47 ppm, U = 1.75 ppm, $^{235}U/^{238}$ = 0.007248 ± 0.000018. No ^{244}Pu or ^{247}Cm were found to the limit of about 10^{-16} gm/gm in the Apollo 11 sample. The limit for ^{239}Pu is 10^{-15} gm/gm. Special chemical procedures were used to prevent contamination and blanks were run in all cases. The mass spectrometry was done using multiple filament surface ionization with a 12" radius single-stage routine instrument, a two-stage mass spectrometer with ion retarding lens, and the high sensitivity 100" radius instrument. Except for the members of the Th and U series no radioactivity has been dedected. Analytical work is still in progress.

---

*Work performed under the auspices of the U. S. Atomic Energy Commission and NASA Contract T-76536.

[1]Paul R. Fields, Herbert Diamond, Donald N. Metta, C. M. Stevens, Donald J. Rokop, and Parker E. Moreland, Science 167, 499 (1970).

Ion Microprobe Analysis of the Apollo 11 Samples

C. A. ANDERSEN and J. R. HINTHORNE, Hasler Research Center,
Applied Research Laboratories, Goleta, California 93017

The ion microprobe mass analyzer has been used to study the trace element chemistry of lunar rocks returned from the Apollo 11 mission. Quantitative mass analyses were made in situ on the major and trace element contents of individual mineral grains and glasses. Five polished thin sections of 1 to 5 mm. fragments of lunar breccia, types A and B basalts and an anorthosite-like rock were studied. The data are compared to similar analyses made on a basaltic achondrite (Cachari) and young terrestrial basalts from the Mojave Desert and the Mid-Atlantic Ridge.

A 100 μm thick crust glass partially coating a breccia fragment was found to have major and trace element abundances nearly identical to the bulk chemistry of the breccia and dust reported by other investigators. P, Zr and Y are slightly depleted in the crust glass, suggesting that these elements might be present in refractory phases in the lunar rocks. A vein glass in Cachari also has a composition very similar to its bulk rock analysis. Compared to the lunar glass Cachari appears to contain more Fe, Na, Mn, Cr, Ni, B and V, and less Ti, K, P, Sr, Zr, Ba, Y and Co.

A comparison of the trace element abundances in lunar, terrestrial and meteoritic silicate phenocrysts shows that Ti and Cr are enriched in the lunar silicates while Ni, K, Na and Pb are depleted. Mn, Al and V tend to group closely in phenocrysts from all the basalts analyzed. Table 1. gives representative analyses of the major lunar mineral phases. The data are from the centers of phenocrysts.

Partitioning studies indicate that Li is concentrated in lunar plagioclase, rather than in clinopyroxene and olivine as in all the terrestrial samples so far analyzed. The other trace elements studied are distributed approximately the same in lunar and terrestrial silicates. Zoning studies of individual olivine crystals in a lunar Type B basalt show that the outer edges of the crystals are enriched relative to the centers in Al, Ca, Mn and Co, and depleted in Na, K, P, Ti, V, and Cr.

In an attempt to compare the trace element contents of all the basaltic rocks measured we have plotted the abundances in the major silicate phases versus the Fe/Na+K ratio for the same mineral grains. When this is done, the "incompatible" elements, Ringwood (1966), are found to decrease regularly with increasing Fe/Na+K and the "compatible" elements to increase with increasing values of Fe/Na+K. This ratio, even in individual phases appears to be a measure of the degree of partial melting which produced a given basalt, and suggests that the lunar and meteoritic basalts are products of more extensive partial melting than terrestrial basalts. On a plot such as this Ti appears to be even more enriched in Apollo 11 rocks than a simple comparison of abundances would suggest.

Th and U and the resulting radiogenic Pb were found to be concentrated in minor mineral phases such as ZrO_2, apatite, and a Ti, Zr, Y, R.E. oxide. The Th/U and $^{208}Pb/^{206}Pb$ ratios differ by more than a factor of 10 among these phases, but the $^{207}Pb/^{206}Pb$ ratios in the two Zr-rich phases are nearly the same (0.45 ± 5%).

10085/17	Olivine -28	Clinopyroxene -26	Plagioclase -25	Ilmenite -28	Crust Glass -17
Li	< 3	12	17	9	31
B	< 12	11	12	< 1	26
Na	24	312	3000	18	3800
Mg	M	M	988	18000	M
Al	390	15200	M	1600	M
Si	M	M	M	852	M
P	43	33	32	1.5	130
K	9	14	108	3.5	666
Ca	1230	M	M	< 475	M
Ti	475	5200	498	M	M
V	19	69	< 0.5	120	45
Cr	680	1340	< 2	3300	858
Mn	980	505	42	1600	795
Fe	M	M	1450	M	M
Ni	< 45	< 1	n.a.	< 2	15
Co	17	7	n.a.	11	16
Sr	1.2	4	68	< 4	70
Y	0.9	8	< 1	5	21
Zr	< 1.0	4	< 1	36	61
Ba	< 0.9	< 0.4	< 1	n.a.	29
Pb	< 1.0	< 0.7	< 0.5	< 1.0	< 0.8

M = Major Element n.a. = not analyzed

Table 1. Representative trace element abundances in the major mineral phases and a glass in the Apollo 11 fines material (ppm atomic). 10085/17-28, 26, 25 and 17 indicate rock fragments analyzed.

Paper to be submitted to Geochimica et Cosmochimica Acta.

References:

Ringwood, A.E. (1966), Advances in Earth Science, P.M. Hurley, ed., MIT Press Boston, p. 287-356.

MASS SPECTRAL REARRANGEMENT IN ORGANO-PHOSPHORUS PESTICIDES

by

William A. Laurie and Morton E. Wacks
Department of Nuclear Engineering
The University of Arizona
Tucson, Arizona

and

Robert W. Anderson, James F. Dietz, Bennie Lacy
and James E. Snowden, Jr.
Chemical Division
Dugway Proving Ground
Dugway, Utah

Several investigators [1,2,3,4] have studied the mass spectra of phosphorus containing pesticides in order to find structural correlations which can be used to identify pesticidal residues. Although it has been shown, for example, that dimethoxy and diethoxy phosphorothionates have characteristic fragmentation pathways, it is difficult to differentiate phosphorothionates from phosphorothiolates. This is important since isomerizations of this type can occur readily under the action of heat or moisture, and it has been shown that such changes can have a large effect on the toxicity of the compound [5].

The difficulty in differentiating such isomers by mass spectrometric techniques lies mainly in the fact that such isomerizations also take place in the mass spectrometer. Jorg *et al.* [2] have attributed this to thermal rearrangement prior to ionization, whereas a study on related phosphorus compounds [6] has suggested the rearrangements are electron impact induced.

The study described here encompasses 14 organo-phosphorus pesticides, several of which have been examined before. The general fragmentation of the dimethoxy phosphorothionates examined is illustrated in Figure 1 (abundances given are for methyl parathion). In all cases the R group is a substituted phenyl ring. In this and other diagrams, transitions marked with an asterisk are those for which a metastable ion has been observed in the normal spectrum. The relative intensity of each ion with respect to the most abundant peak is given in brackets after the mass number.

The ion at m/e 125 can be formed by at least two pathways, as shown. One involves cleavage of a phosphorus-oxygen bond prior to rearrangement of the molecular ion, and the other involves a similar cleavage after alkyl migration to sulphur to form ion a. Evidence for the loss of CH_2S from m/e 125. The most likely mode of formation of m/e 109 is aryl migration to given ion b followed by a similar phosphorus-oxygen bond cleavage. Investigation of the temperature dependence of the intensities of these two ions indicated that the observed isomerizations are electron impact induced. The ion intensity ratio was constant over source temperature range of 50° to 250°C.

Although the normal spectrum had no metastable ions for the formation of m/e 125 and m/e 109, the use of the instrument to detect metastable transitions taking place in the first field free region [7] by variation of the ion acceleration voltage allowed detection of such metastable peaks. For example, methyl parathion had metastable transitions which indicated three precursors for both m/e 109 and m/e 125. These were the molecular ion, $(M - OH)^+$, and $(M - NO)^+$.

This technique was of greater importance in the interpretation of the spectrum of fenthion. In contrast to the other dimethoxy compounds studied, fenthion has two important ions corresponding to charge retention on the aromatic substituent. These ions have both been shown by examination of metastable spectra to give m/e 125 (Figure 2). The probable precursors for m/e 109 are shown in Figure 3, and this suggests that m/e 153 as well as m/e 125 and m/e 109 are doublets. Hence the use of the metastable detector has pre-empted the need for mass measurement in this case.

The only phosphorothiolate studied (Meta-Systox) showed evidence of isomerization although to a lesser extent. This may have been due to the greater propensity for migrations to sulphur rather than oxygen which has been observed in mass spectrometry or to the fact that all three substituents were alkyl in nature (aryl migration is favored). It

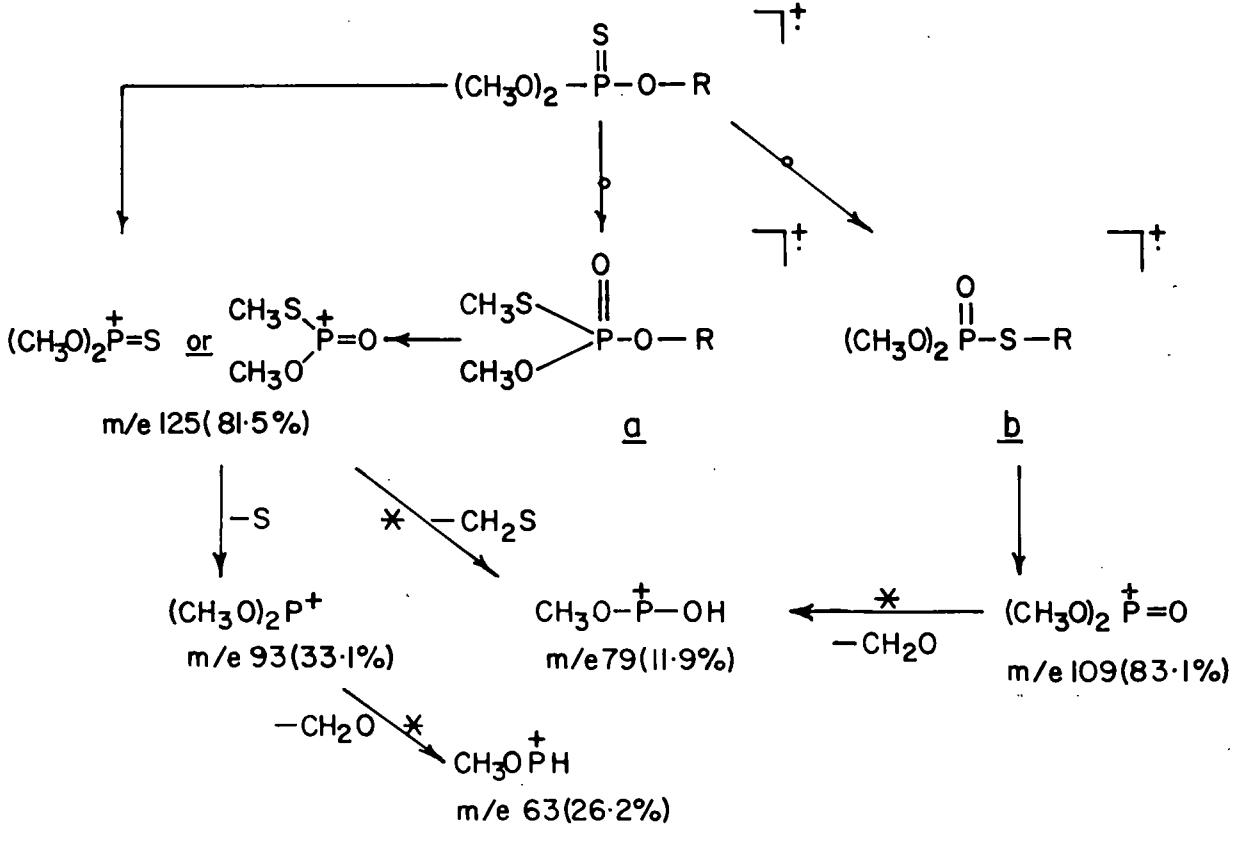

FIG.1 Fragmentation of Dimethoxy Phosphorothionates

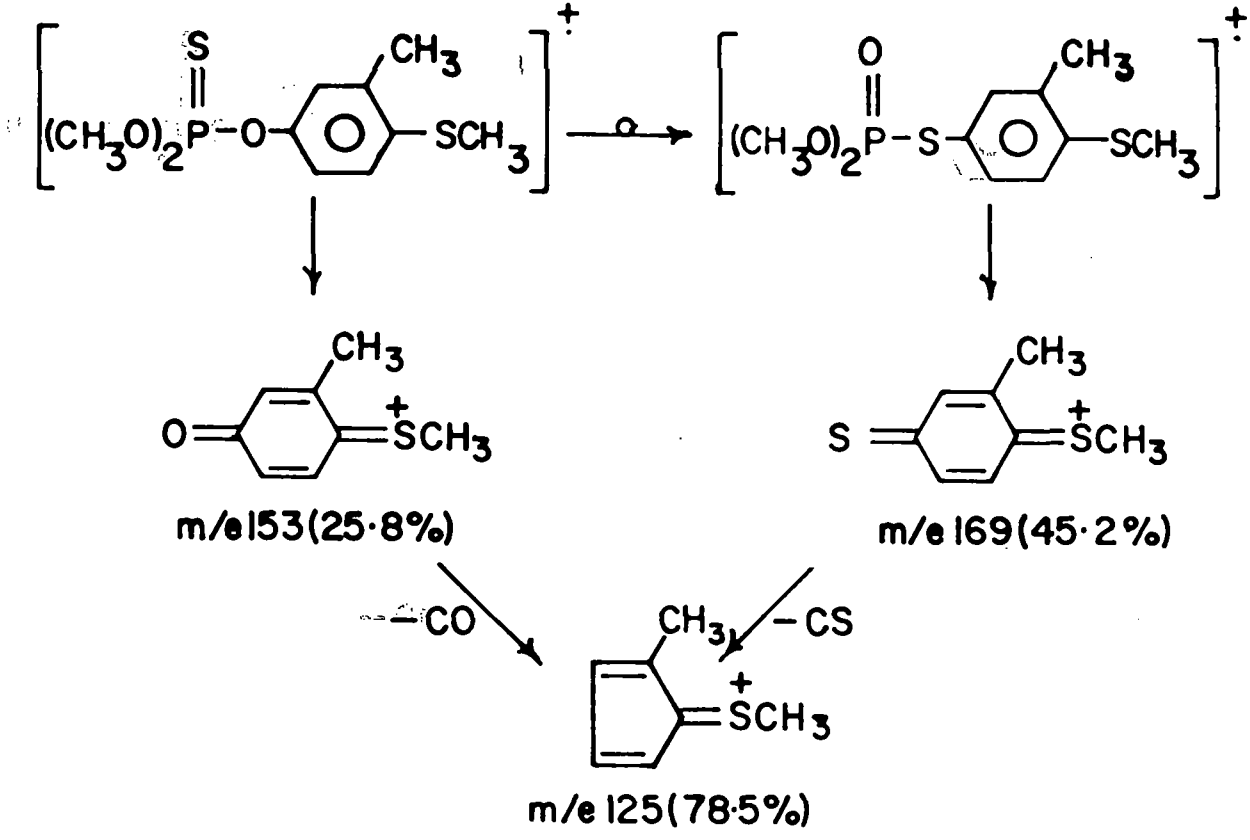

Fig.2. Transitions observed for Fenthion using defocussing technique

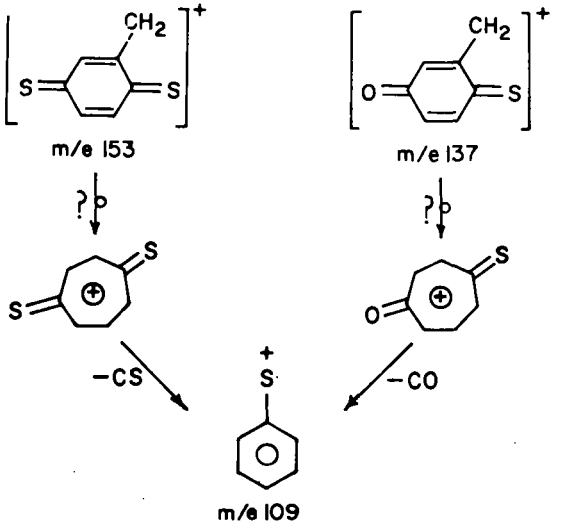

Fig 3. Transitions observed for Fenthion using defocussing technique

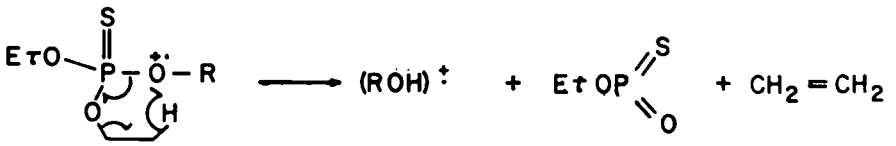

FIG. 4 Rearrangement of diethoxy substituted phosphorothionates.

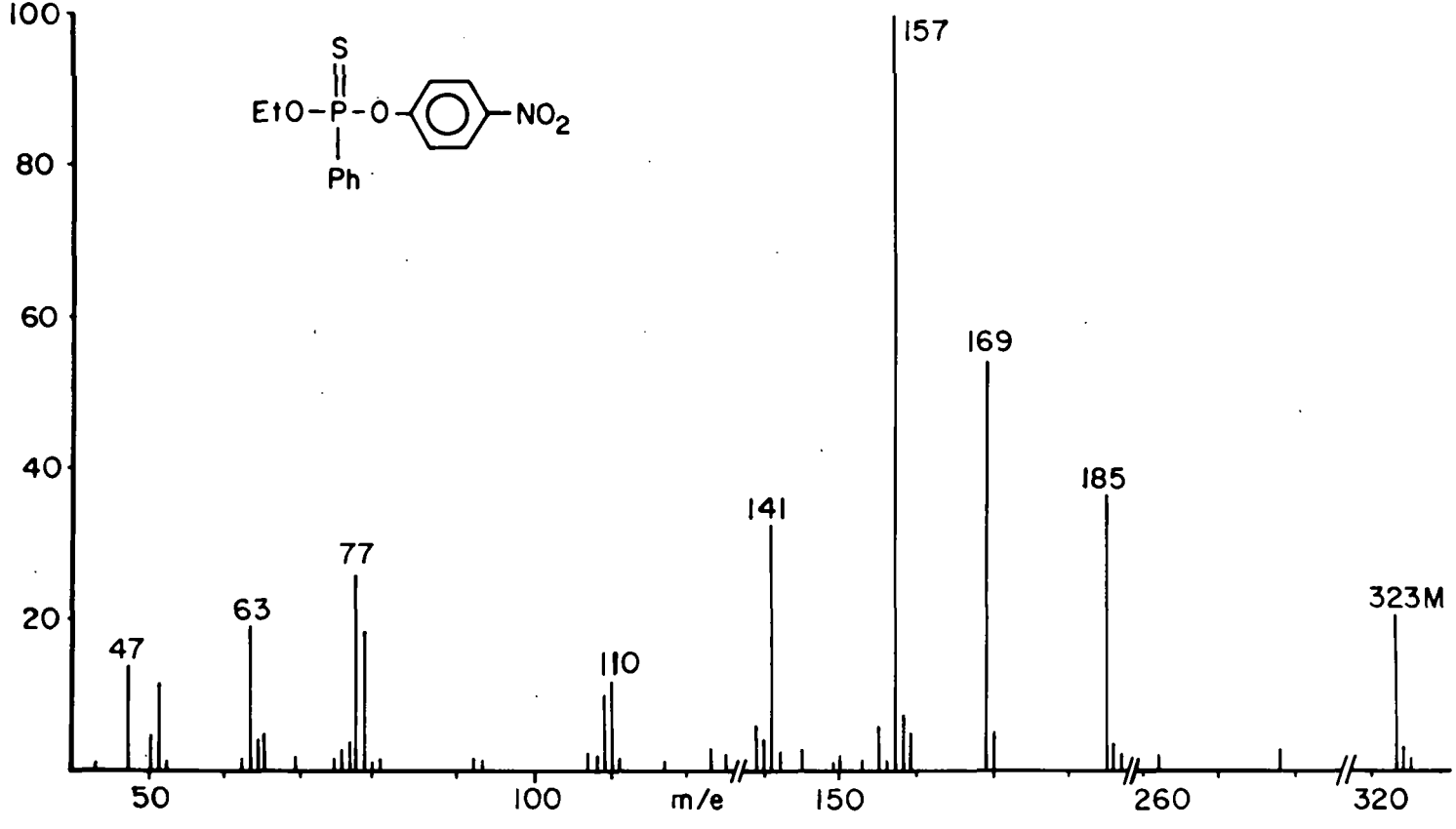

Fig 5 Mass spectrum of O-ethyl O-p-nitrophenyl phenylphosphonothioate

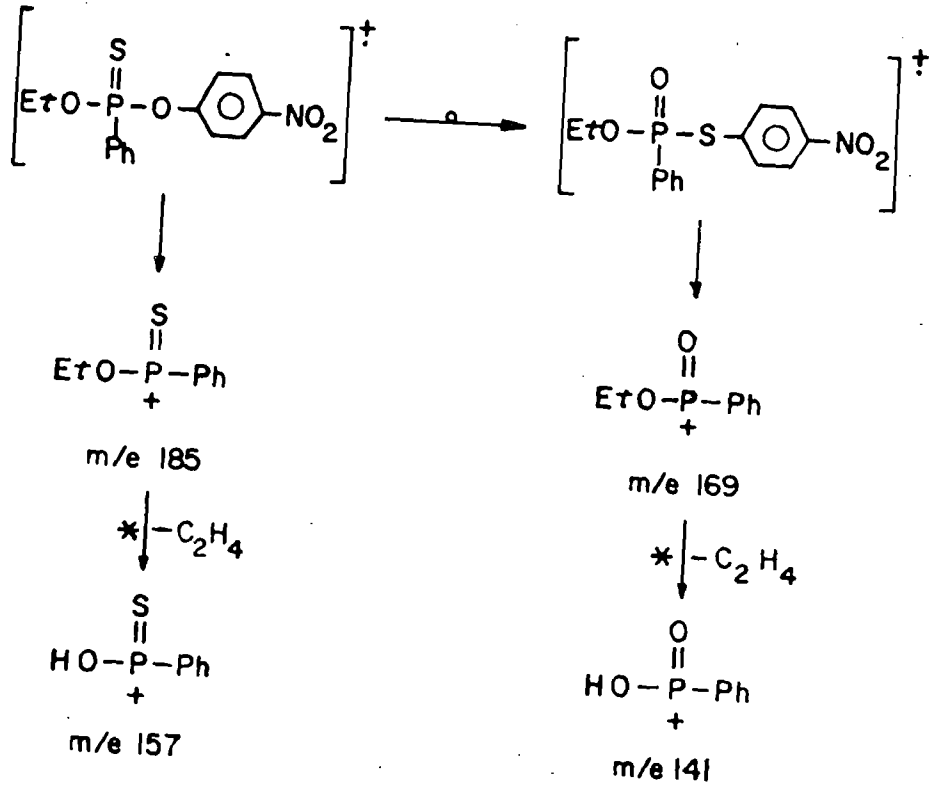

FIG. 6 Fragmentation of O-ethyl O-p-nitrophenyl phenylphosphonothioate.

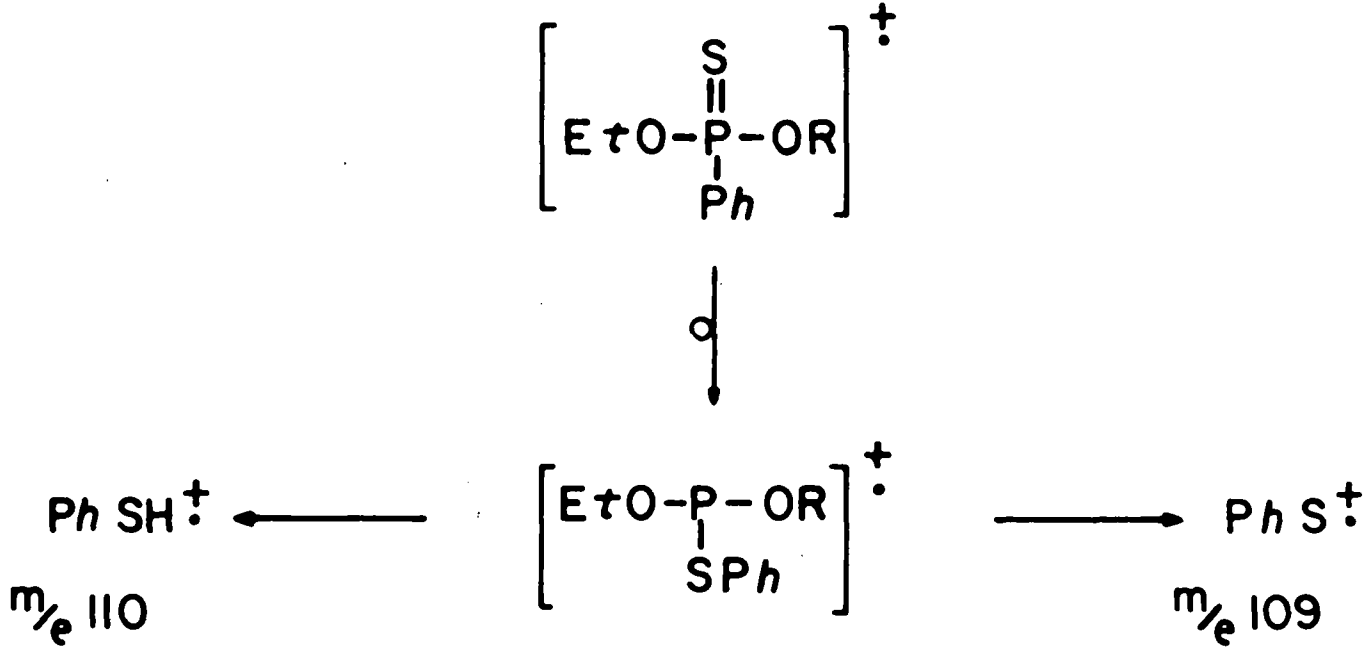

FIG. 7 Rearrangement of phenylphosphonothioates.

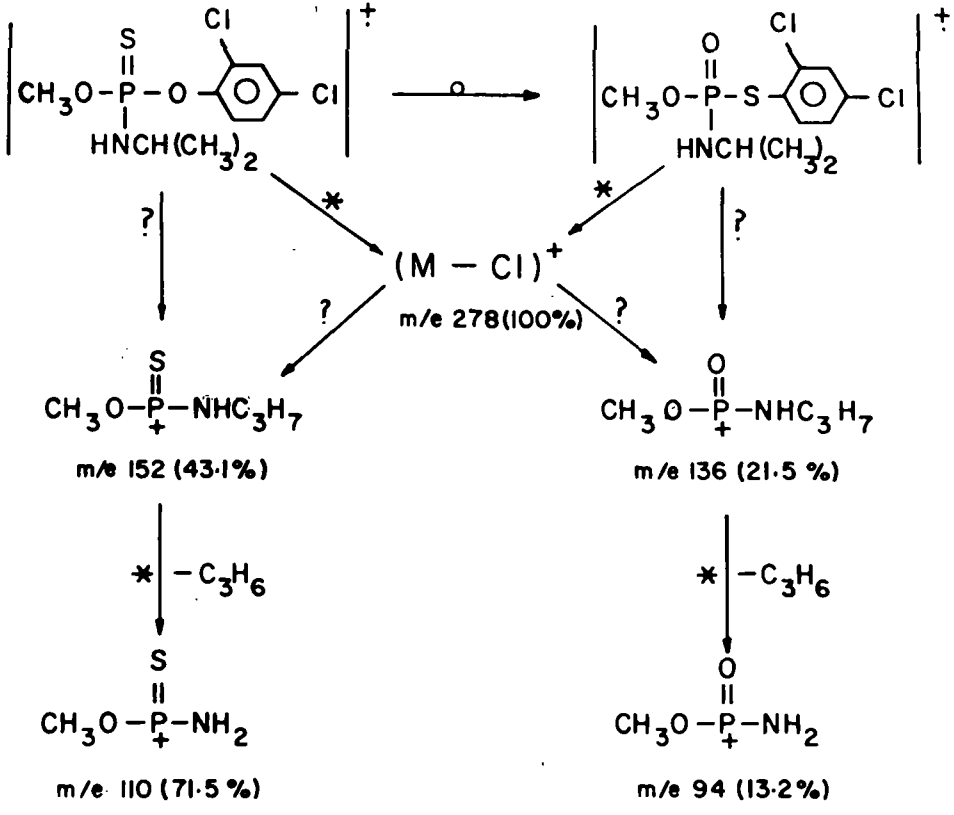

FIG. 8 Fragmentation of Dowco 118.

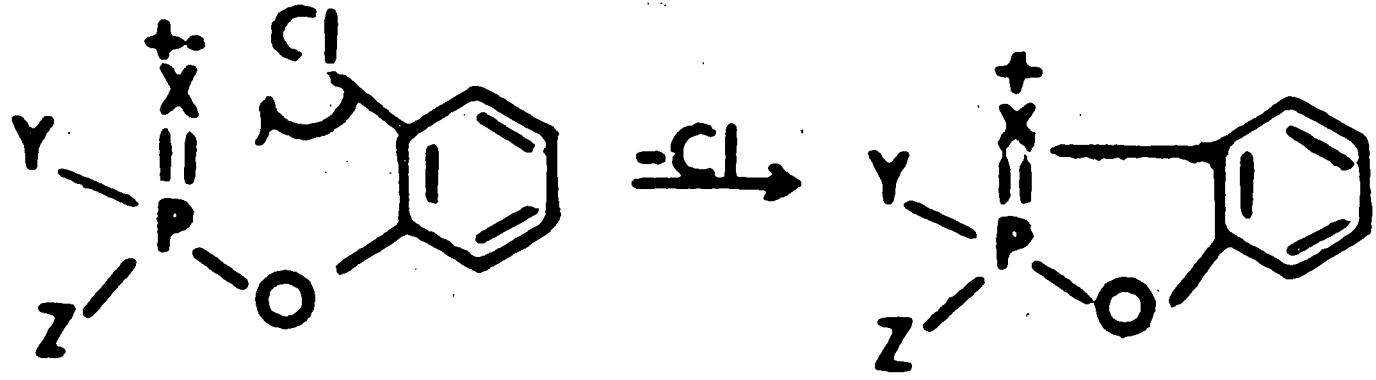

X = O, S

Fig. 9 Chlorine loss from o-chlorophenyl substituents.

was noted that temperature had little effect on the abundance of m/e 109 and m/e 125, again suggesting the isomerization was not thermal. The absence of a metastable transition in the normal mass spectrum for the loss of CH_2S from m/e 79 (even though this pathway was evident in the metastable spectrum) may provide a diagnostic tool for differentiating between thiolate and thionate isomers.

The three diethoxy compounds studied gave predictable results - a similar fragmentation to the dimethoxy compounds with subsequent elimination of two molecules of ethylene. However with these compounds an increased proportion of the observed ion current corresponded to the aromatic substituent plus one hydrogen. This could be attributed to the rearrangement in Figure 4 which is obviously impossible for the dimethoxy substituted compounds.

The spectra for three previously unreported phosphonothioates have been determined. The O-ethyl O-p-nitrophenyl phenylphosphonothioate spectrum (Figure 5) is seen to be fairly simple. The aryl migration to sulphur observed for the phosphorothionates is also important for these compounds and explains two of the four most important ions in the spectrum (Figure 6). Ions at m/e 109 and m/e 110 also indicate migration of the phenyl group directly bonded to phosphorus as shown in Figure 7. Surecide (O-p-cyanophenyl O-ethyl phenylphosphonothioate) behaves in a similar manner. The nature of these peaks is confirmed by their absence from the spectrum of Agritox (O-ethyl O-2,4,5 trichlorophenyl ethylphosphonothioate) which exhibits a fragmentation pathway similar to that shown in Figure 6 but does not have a molecular ion peak (M-Cl being the highest mass peak observed).

The introduction of an isopropylamino function in Dowco 118 (Zytron) leads to the fragmentation shown (Figure 8) which still exhibits the aryl migration to sulphur as for all the other compounds discussed. In these compounds containing an o-chloro substituent on the -R moiety loss of this chlorine was a dominant process, and this ion (Figure 9) could be used to indicate the presence of an ortho rather than a meta or para chloro substituent.

All the organo-phosphorus compounds examined above showed evidence of rearrangements which could lead to difficulties in the interpretation of unknown spectra. Further work on pure compounds of the phosphorothiolate type may yield results which will allow unambiguous *a priori* structure determination of pesticidal residues.

Acknowledgments

The authors wish to thank the Army Research Office, Durham, North Carolina (Contract DAHC04-70-C-0021); Deseret Test Center, Salt Lake City, Utah; and the National Science Foundation for funding this research. In addition, we are indebted to Mr. John Drake, Department of Entomology, University of Arizona, for supplying the pure compounds used in this research.

References

[1] J. N. Damico, *JAOAC* 49, 1027 (1966).

[2] J. Jörg, R. Houriet, and G. Spiteller, *Monatsh. Chem.* 97, 1064 (1966).

[3] J. N. Damico, R. P. Barron, and J. A. Sphon, *Int'l. J. Mass Spec.* 2, 161 (1969).

[4] R. E. Lovins, *J. Agr. Food Chem.* 17, 663 (1969).

[5] R. D. O'Brien, *Insecticides: Action and Metabolism*, Chap. 3, Academic Press, New York (1967).

[6] R. G. Cooks and A. F. Gerrard, *J. Chem. Soc. (B)* 1327 (1968).

[7] J. H. Beynon, *Analyt. Chem.* 42, 97A (1970).

HYDROGEN SCRAMBLING IN THE METHYL ACETATE MOLECULE-ION

B2

P. R. Briggs and T. W. Shannon

The Dow Chemical Company
Eastern Research Laboratory
Wayland, Massachusetts 01778

During the course of investigating collision-induced dissociations (CID), it was noted that wo similar molecules behaved in entirely different manners. Acetone loses a methyl radical to give the acetyl ion while the same ion is formed from methyl acetate by the loss of the methoxy radical. Under CID conditions, namely a high analyser tube pressure, the transition in acetone is almost entirely collision induced, while the loss of methoxy from methyl acetate remains a unimolecular decomposition. Further, using labelled compounds, CD_3COOCH_3 and CH_3COOCD_3, the observed metastable peak now becomes a triplet. Since the metastable peak corresponds to α-cleavage with loss of a methoxy radical the hydrogens and deuteriums have partially exchanged prior to α-cleavage. The relative abundance of the three metastable peaks varies with changing accelerating voltage indicating that ion lifetimes have a decided effect on the observed metastable abundances. This effect was investigated as a possible means of obtaining a value for the rate of exchange of the hydrogens prior to fragmentation.

Experimental:

Variation of ion lifetimes was accomplished by changing the accelerating potential of the MS-12 mass spectrometer used. The ion source was modified by the insertion of an extra slit plate, P1, in the electron gun assembly. The plate was electrically insulated from both the ion source block and the filament. Under pulsing operation P1 is initially at filament potential. The mass spectrometer is then focussed on an ion beam of interest and the electron beam is arrested by applying a bias, negative with respect to the filament, to the electron beam control plate. Complete stoppage of the electron beam is indicated by the disappearance of the focussed ion beam. A positive pulse, supplied by a Hewlett-Packard Model 214A pulse generator was applied to P1 to provide a pulsing electron beam.

The pulsing electron beam provides bursts of ions which are accelerated out of the ion chamber by the positive potential applied to the repeller and by penetration of the accelerating field through the ion exit plate P_2 into the ion chamber. The main acceleration occurs between the beam centering and earth plates after which the ions travel at constant velocity past the y-deflection plate, through the field-free region of the analyser tube and into the magnetic field where they suffer a deflection according to their momentum. The observed metastable peaks are the result of ionic decompositions occurring during flight from the earth plate to the entrance to the magnetic field.

The passage of ions through the ion gun may be detected by the use of a second pulse applied to either the beam centering or y-deflection plates. The second pulse (approximately 75 volts, 0.05 μ sec. width) is triggered after a variable time delay by the electron beam pulse. If the pulse on the y-deflection plate coincides with the arrival of a burst of ions at that electrode, the ions will suffer a deflection and thus not reach the collector. The result is a decrease in a recorded peak intensity. By varying the time between the ionizing and deflecting pulses, a time profile of the ions passing the plate may be obtained. The ion flight times may then be measured directly as the time between the center of the two pulses at which the deflection is a maximum.

The arrival time at the y-deflection plate, τ_y, for the m/e 77 ion from methyl acetate-d_2 was determined as a function of the accelerating potential. These potentials were measured accurately using a calibrated high-voltage probe and a digital voltmeter. The final velocity of the ion is calculated from the total potential drop suffered by the accelerated ion and this in turn may be used to calculate the ion flight time from the earth plate to the y-deflection plate. Subtracting this value from the observed τ_y values gives T_1, the arrival time of the ion in the field-free drift region. The drift-region flight time may be calculated from

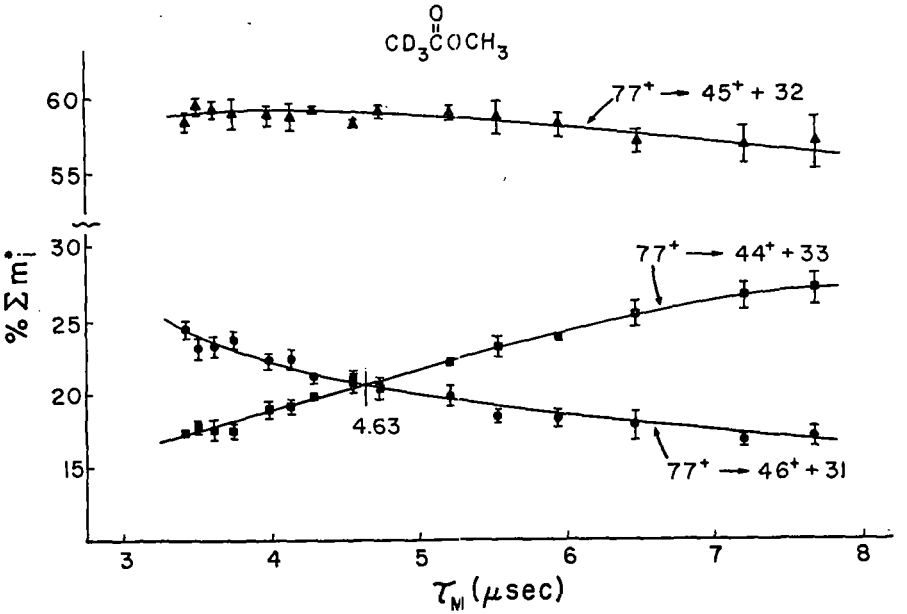

Figure 1. Variation of metastable peak abundances with ion flight time - α -cleavage process in $CD_3CO_2CH_3$.

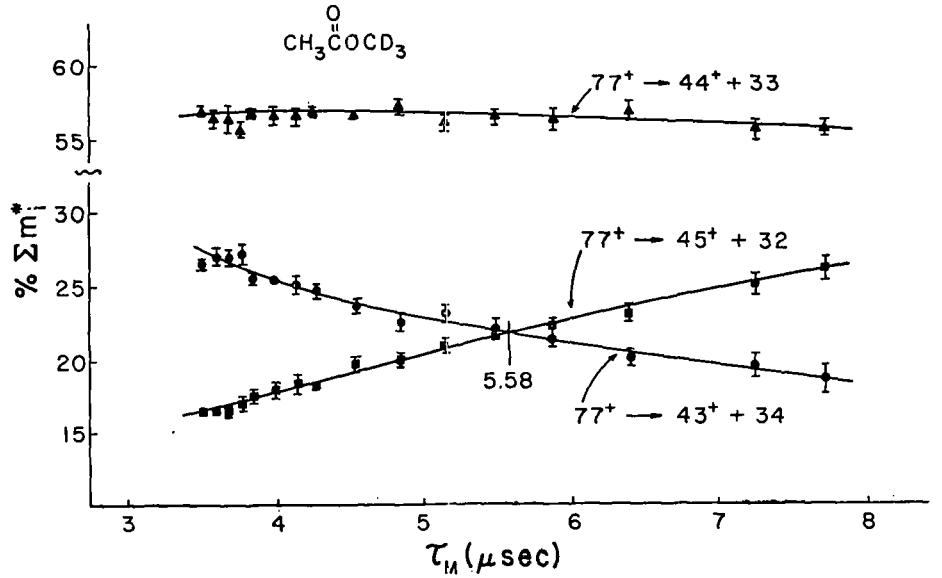

Figure 2. Variation of metastable peak abundances with ion flight time- α -cleavage process in $CH_3CO_2CD_3$.

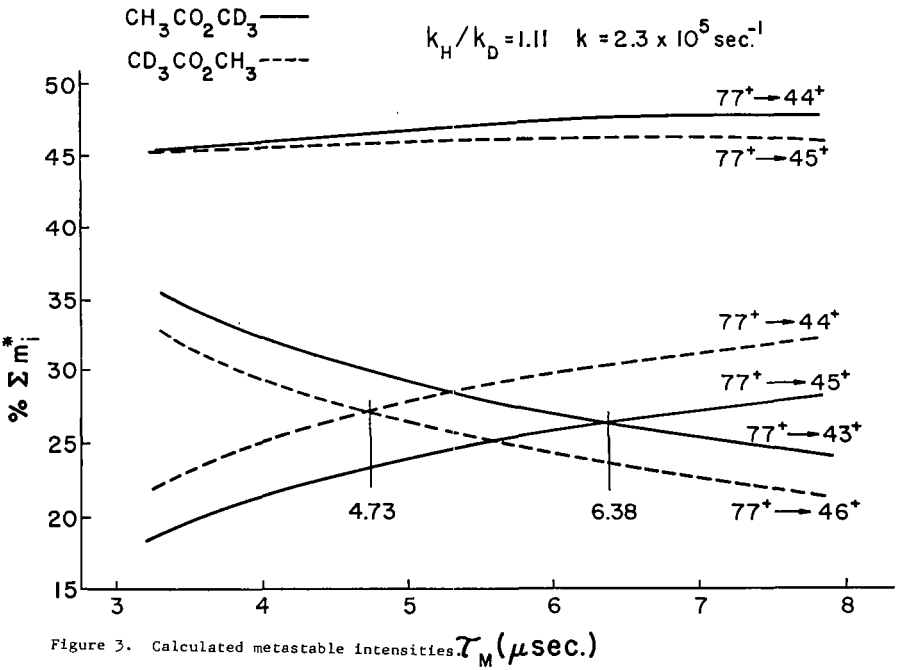

Figure 3. Calculated metastable intensities.

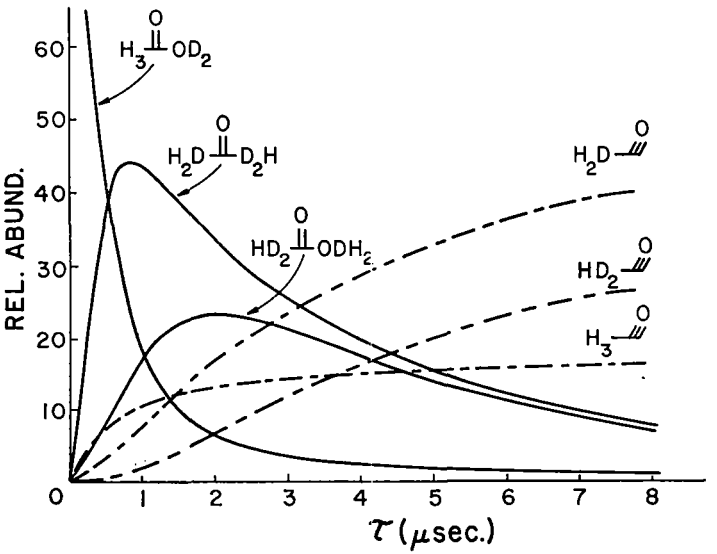

Figure 4. Variation of ion abundances in the drift tube with lifetime.

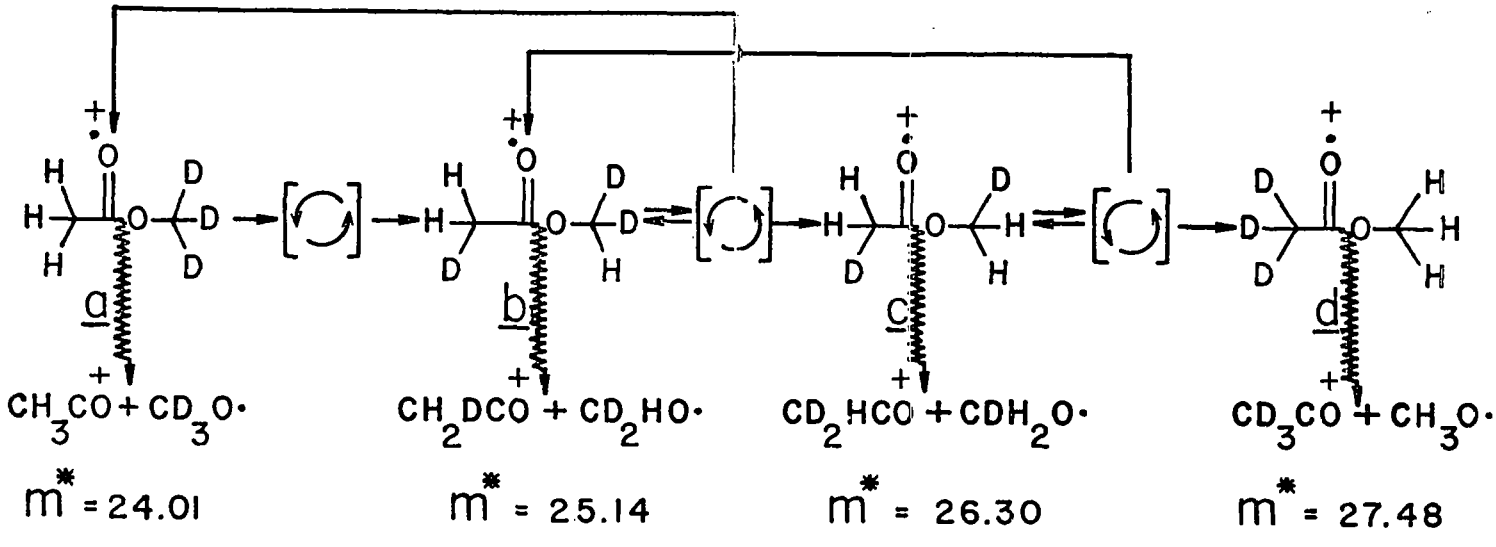

REACTION SCHEME

the known drift-region length and ion velocity. The ion arrival time at the entrance to the magnetic field τ_m, is the sum of T_1 and the drift-region flight time and is the total elapsed time during which metastable decompositions may be observed.

Results and Discussion:

Unlabelled methyl acetate shows a metastable peak at m/e 24.99 corresponding to the transition $74^+ \longrightarrow 43^+ + 31$ resulting from α-cleavage of the parent ion. For labelled methyl acetate, namely CD_3COOCH_3, the parent ion moves up to m/e 77 and instead of a single metastable peak at m/e 27.48, three metastable peaks are observed at m/e 25.14, 26.30, 27.48 corresponding to the transitions m/e 77 $\longrightarrow$ m/e 44, 45, 46. Similarly in CH_3COOCD_3 three metastable peaks are observed for the transitions m/e $\longrightarrow$ m/e 43, 44, 45. Since the fragmentation occurs via α-cleavage some exchange of the hydrogens and deuteriums between the two methyl groups has occurred prior to scission of the C-O bond.

Similar isotopic mixing has been observed in the mass spectra of specifically labelled ketones.[1-3] For example in deuterated octan-3-one H/D scrambling occurs in the alkyl chain prior to a loss of an ethyl radical by α-cleavage. However, this scrambling process is only evident at low electron energies. Similarly in other deuterated ketones[2,3] the *metastable peaks corresponding to α-cleavage preceded by scrambling show* significant variation between the first and second drift region of a double-focusing mass spectrometer. Thus the lifetime of the scrambling process is long and suggests that a variation of the ion residence time in the drift region may result in significant variations in the observed metastable abundances.

Such an effect is indeed evident as shown in Figures 1 and 2 in which the observed relative metastable abundance is plotted vs. the parent ion lifetime to the magnetic field. The error bars associated with each data point are the standard deviation of at least four measurements. Obviously, interpretation of deuterium labelling experiments in which the relative retention of the label is evidenced from metastable peak intensities must be treated with caution unless demonstrated that such variations as shown in Figures 1 and 2 do not occur.

To account for the scrambling, a multi-step process may be envisioned in which the reaction is initiated by the presence of a free radical. Such a process is illustrated in Scheme 1.

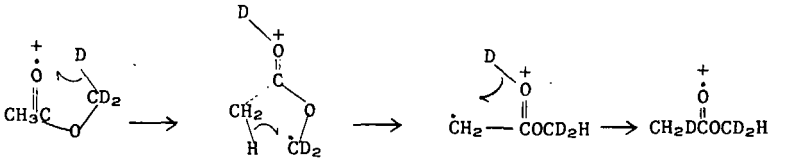

Scheme 1

The application of this type of mechanism to the case of labelled methyl acetate is shown in scheme 2. The metastable decomposition of d resulting in a peak at m/e = 27.48 is observed but is of such low intensity that accurate data concerning its intensity variation could not be collected. Since all hydrogens on both the methyl groups have equal probabilities of attaining the appropriate transition state configuration reverse reactions are therefore possible. If it is assumed that once the transition state is reached transfer will occur and that there is no isotope effect in the transfer of an H or a D, scheme 2 condenses to the following;

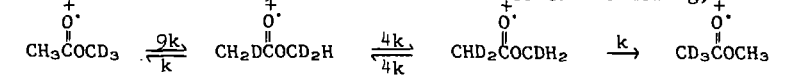

a b c d

The relative ordering of the rate constants is determined by the number of ways in which the reaction may occur and setting the rate for a single possibility equal to k. The rate of decomposition of a, b, and c by

α-cleavage is assumed to be identical and equal to k*.

Since the scheme is based on the assumption of no primary isotope effect, the plots of $I(m_1^*)$ vs. τ_2 for both CH_3COOCD_3 and CD_3COOCH_3 should be identical. Inspection of figures 1 and 2 reveal that this is not the case. The cross-over point, $I(m_1^*)=I(m_3^*)$, occurs at a longer time for CH_3COOCD_3. As the process of exchange of H and D occurs by three steps in the postulated mechanism then the reaction sequence can be depicted schematically as follows;

$$D_3\text{-}OH_3 \underset{DHD}{\overset{HDH}{\rightleftharpoons}} D_2H\text{-}OH_2D \underset{DHD}{\overset{HDH}{\rightleftharpoons}} DH_2\text{-}OHD_2$$

$$H_3\text{-}OD_3 \underset{HDH}{\overset{DHD}{\rightleftharpoons}} H_2D\text{-}OD_2H \underset{HDH}{\overset{DHD}{\rightleftharpoons}} HD_2\text{-}ODH_2$$

where DHD for example indicates the sequential transfer of deuterium, hydrogen and deuterium. Assuming an equal isotope effect (of $y = k_D/k_H$) for each intermediate step in the process then we have HDH = yk and DHD = y^2k where k is the rate constant for no primary isotope effect.

Figure 3 shows the calculated metastable intensities for y = 0.90 as a function of the flight time to the magnet. The difference in cross-over times of 1.65 μsec. is longer than the observed difference of 0.95 μ sec. Other calculations indicate that decreasing y causes an increase in the time separation of the cross-over points. Thus it appears that an isotope effect of 0.90 to 0.95 is operative in the present example.

The relative abundance of the ion species in the drift tube change as a function of time for the reaction sequence outlined in scheme 2. This is illustrated in figure 4 for $CH_3CO_2CD_3$ using k* = 1k and k = 0.230 X 10^6 $sec.^{-1}$ The concentration of $CH_3CO_2CD_3$, decreases rapidly, with $CH_2DCO_2CD_2H$ and then $CHD_2CO_2CDH_2$ increasing to a maximum and then falling off with the concurrent production of CD_3CO^+ etc. ions. These ions are not directly observed as metastable peaks, rather the sum of all such ions produced in the drift region is collected as the metastable peak. Under such circumstances the matching of the calculated curves (Fig. 3) to the experimental data (Figs. 1 and 2) is basically a trial and error process in which we have two unknowns k* and k. Although the agreement between the calculated and observed relative abundances is not good, the change in intensity as a function of time is qualitatively reproduced. Other simpler mechanisms were calculated but would not reproduce the changes in abundance as well as the full mechanism.

Although the original objective of determining the rate of exchange of the hydrogens prior to fragmentation has not been achieved, it was possible to determine the primary isotope effect for the intramolecular transfer of deuterium atoms in the molecule-ion. Further, the substantial variation of the metastable ion abundances with lifetime illustrates the need for caution when applying such data as evidence for ionic structures.

References:

1. W. Carpenter, A. M. Duffield and C. Djerassi, J. Am. Chem. Soc., 90, 160 (1968).
2. A. N. H. Yeo, R. G. Cooks and D. H. Williams, Chem. Comm. 1269 (1968).
3. A. N. H. Yeo and D. H. Williams, J. Am. Chem. Soc., 91 (1969).

THE DYNAMIC STEREOCHEMISTRY OF THE ELIMINATION OF ACETIC ACID UNDER ELECTRON IMPACT

This work has now appeared in the literature: Mark. M. Green, J. Michael Moldowan, David J. Hart, and Jeffrey M. Krakower, J. Amer. Chem. Soc., 92, 3491 (1970).

Anchimeric Assistance in the Loss of Bromine from 5-Bromo-2-Phenyl-2-Pentene

K. B. Tomer and R. H. Shapiro

Department of Chemistry, University of Colorado, Boulder, Colo. 80302

The molecular ions of ring-substituted 5-bromo-2-phenyl-2-pentenes undergo two major competing reactions: 1) The loss of $\cdot CH_2Br$ through a simple cleavage reaction and 2) the expulsion of Br· (Figure 1).

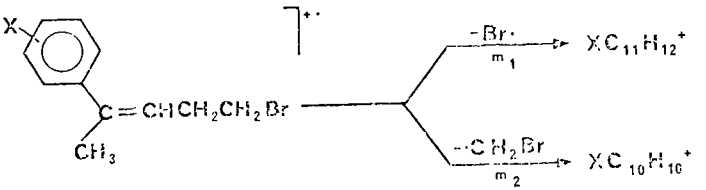

Figure 1

Chupka[1] in 1959 and recently McLafferty and Fairweather[2] have shown that a rearrangement process will show a more intense metastable peak than will a competing simple cleavage process.

Chupka[1] and recently Williams and Cooks[3] reported another method for determining the occurrence of a rearrangement process based on the simplified form of the basic rate equation of the quasi-equilibrium theory (equation 1).

$$K(E) = \nu \left[\frac{E - \epsilon}{E}\right]^{S-1} \qquad \text{(equation 1)}$$

For two competing reactions, one being a simple cleavage and the other a rearrangement process, the terms E and S-1 are constant for the two reactions. The frequency factor (ν_r) for a rearrangement reaction is lower than the frequency factor (ν_s) for a simple cleavage, and it has been experimentally determined that the activation energy (ϵ_r) for many rearrangement processes is lower than the activation energy (ϵ_s) for a competing simple cleavage. At high ionizing energies the simple cleavage is expected to occur to the greatest extent, since the large difference between E and ϵ allows the frequency factor to rule the rate expression. As the ionizing energy is decreased, the activation energies begin to control the rates of the competing reactions, and the rearrangement process should become progressively more important.

We employed these two methods to determine whether the expulsion of bromine proceeds via a rearrangement reaction or a simple cleavage. Our results for the relative abundances of the competing reactions as a function of energy are presented in Figure 2 and our results on the relative abundances of the metastable are presented in Figure 3.

Effect of Ionizing Energy on the Relative Abundance of $(M-Br)^+$ and $(M-CH_2Br)^+$

$$\frac{(M-Br^+)}{(M-Br^+)+(M-CH_2Br^+)}$$

Substituent	30 eV	20 eV	18 eV	16 eV	14 eV
m-CH_3O	.807	.834	.849	.894	.948
m-NO_2	.694	.70	.709	.714	.752
p-CF_3	.583	.629	.6615	.738	.839
m-CF_3	.559	.6175	.6525	.725	.835
m-F	.5635	.61	.639	.70	.807
m-Cl	.573	.5975	.6275	.695	.7845
m-CH_3	.513	.556	.5835	.637	.741
H	.501	.539	.564	.625	.725
p-Cl	.45	.483	.509	.556	.685
p-F	.432	.459	.49	.5435	.643
p-CH_3	.4785	.476	.50	.5625	.680
p-CH_3O	.311	.335	.3525	.3825	.483

Figure 2

Metastable Ratios at 30 eV $\frac{M_1^*}{M_2^*}$

H	p-OCH_3	m-OCH_3	p-CF_3	m-CF_3	p-CH_3	m-CH_3	p-F	m-F	p-Cl	m-Cl	m-NO_2
3.25	0.9	7.65	7.87	7.60	2.66	4.33	3.33	9.0	4.67	1.85	2.4

Figure 3

The data indicate that, with the possible exception of the nitro substituted compound, the expulsion of bromine proceeds through a 'rearrangement-like' transition state.

The substituent effects are best explained on the basis of two mechanisms for participation as shown in Figure 4 and Figure 5.

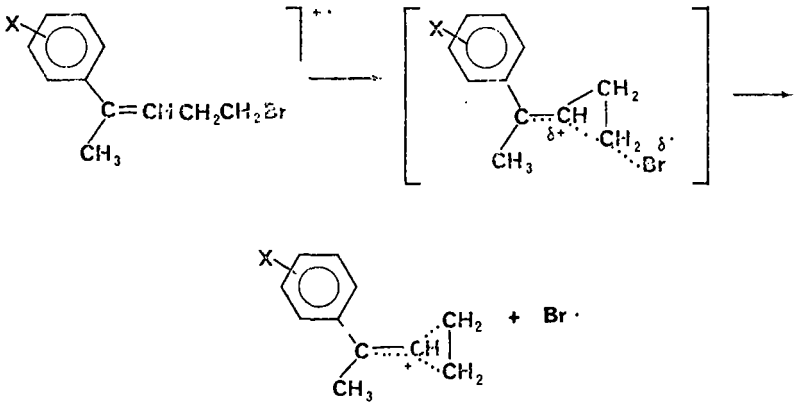

Figure 4

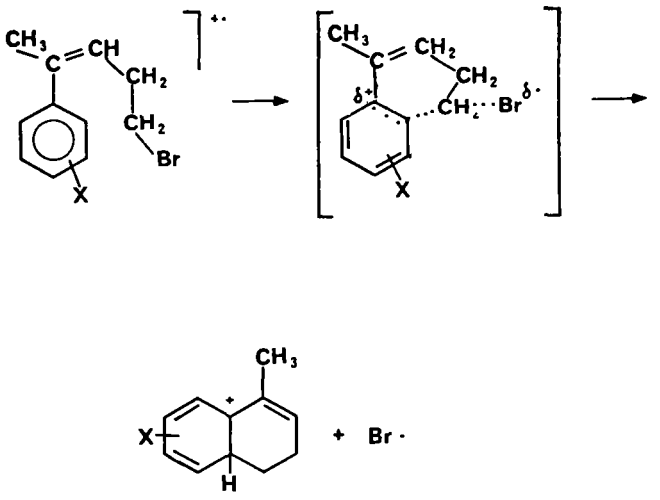

Figure 5

References

1. W. A. Chupka, J. Chem. Phys., 30, 191 (1959).
2. F. W. McLafferty and R. B. Fairweather, J. Am. Chem. Soc., 90, 5915 (1968).
3. D. H. Williams and R. G. Cooks, Chem. Comm., 663 (1968).

Mass Spectra and Pyrolysis of Cyclic Sulfites and Carbonates of Aromatic Diols. **B6**

D. C. DEJONGH, R. Y. VANFOSSEN BRAVO, and D. A. BRENT, Department of Chemistry, Wayne State University, Detroit, Michigan 48202.

ABSTRACT -- A variety of cyclic sulfites of aromatic diols have been prepared and their mass spectra obtained. The compounds have been passed over a glowing Nichrome coil in a stream of nitrogen and the products of pyrolysis trapped. For example, o-phenylene sulfite shows a loss of SO, followed by CO, from its molecular ion:

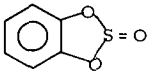

M^+	$(C_6H_4O_3S)$
M-SO	$(C_6H_4O_2)$
M-SO-CO	(C_5H_4O) (base peak, 70eV)
M-SO-2CO	(C_4H_4)

Upon pyrolysis, a 80% yield of the dimer of cyclopentadienone is formed:

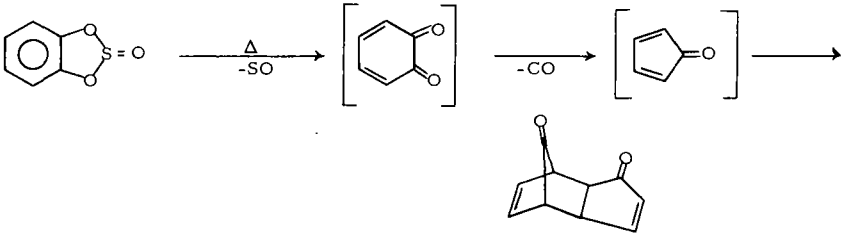

Thus, the same neutral molecules, SO and CO, are eliminated in each case. Several substituted sulfites have been studied, also. On the other hand, 2,2'-biphenylene sulfite shows competing losses of SO and SO_2 from the molecular ion. Upon pyrolysis, a 22% yield of dibenzofuran and a 52% yield of hydroxydibenzofuran are obtained:

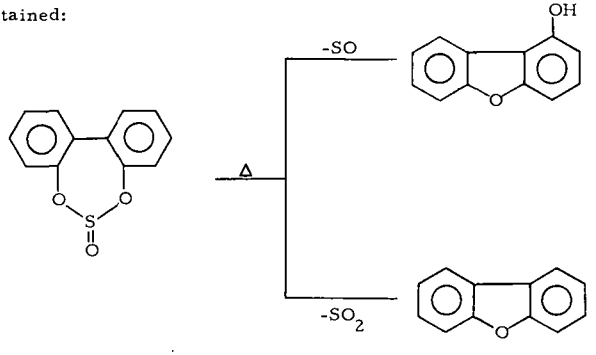

These competing losses upon electron-impact have been studied at various electron energies, and metastable peak characteristics have been noted.

The corresponding cyclic carbonates have been studied and their mass spectra and pyrolysis products have been compared to those of the sulfites. For

example, o-phenylene carbonate loses CO_2, rather than CO which would be analogous to the loss of SO from o-phenylene sulfite:

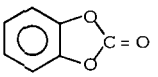

M^+	$(C_7H_4O_3)$
$M-CO_2$	(C_6H_4O)
$M-CO_2-CO$	(C_5H_4) (base peak, 70eV)

Pyrolysis in a 12 in. hollow quartz tube with a nitrogen flow rate of 0.8 ℓ/min and with methanol as a trapping agent gives a 44% yield of the dimer of cyclopentadiene-1-carboxylate:

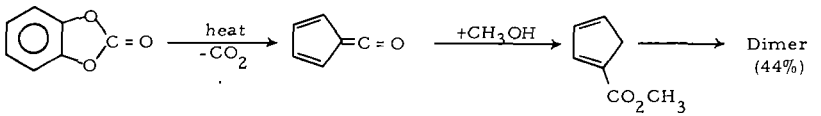

2,2'-Biphenylene carbonate eliminates CO_2 upon electron impact and pyrolsis. Dibenzofuran is formed in 80% yield upon pyrolysis in the quartz tube.

Factors such as product-ion stability, stability of the neutrals eliminated, and possible intermediates from rearrangement are being considered to explain the differences observed in comparison of the behavior of the sulfites and carbonates.

(This work will be published in Journal of Organic Chemistry.)

MASS SPECTRA OF THE KETALIZATION PRODUCTS OF ACENAPHTHENEQUINONE

Allen I. Cohen, Ingeborg T. Harper and Seymour D. Levine
The Squibb Institute for Medical Research
New Brunswick, New Jersey 08903

High-resolution mass spectrometry generally produces reliable structural assignments. In some cases, however, the determination of structure also requires information about fragmentation pathways. Fragmentation pathways can be established by utilizing the defocusing technique of Barber and Elliott[1] and electric-sector techniques[2].

EXPERIMENTAL

The acid-catalyzed reaction of acenaphthenequinone with ethylene glycol in refluxing benzene afforded three products, which were isolated by preparative thick-layer chromatography. The mass spectra were obtained with an AEI MS-902 double-focusing mass spectrometer equipped with a manually operated accelerating voltage defocusing attachment and for high-resolution data acquisition a Honeywell 7600 frequency modulated analog tape recorder. The ion block temperature was maintained at 180°C. In high-resolution mode, the dynamic resolution was one part in 13000 and the spectra were scanned at a rate of 16 seconds per decade. The analog tape was processed on an IBM 1800 computer, using Squibb programs. The accuracy of high-resolution mass measurements was better than 10 ppm, while that of metastable ion defocusing was ±1 amu. Chemical ionization spectra were obtained by Dr. H. Fales on a modified AEI MS-902, with methane at 0.5 mm pressure at 220°C.

RESULTS AND DISCUSSION

The low-resolution mass spectrum of the monoketal is shown in Figure 1. The composition of the M+ at m/e 226 was confirmed by high-resolution techniques as $C_{14}H_{10}O_3$. The odd-electron ion at m/e 198, arising from the loss of the ketonic carbonyl as carbon monoxide, is ten times more abundant than the ion at m/e 198 resulting from the elimination of ethylene. The m/e 170 ion has the molecular composition $C_{11}H_6O_2$. The m/e 198 ion eliminates C_2H_4O to form the m/e 154 ion. Defocusing experiments confirm that the m/e 182 ion is also a precursor of the m/e 154 ion, although the precursor ion is present in only very small abundance. However, doubly charged ions at m/e 182, 154, and 126 are present. While the elimination of carbon dioxide from the m/e 170 ion is expected, the double decarbonylation to form the m/e 142 and 114 ions is unexpected, especially since the loss of a nuclear carbon is involved. To explain this finding, we postulate that the ion resulting from the elimination of ethylene from the m/e 198 ion rearranges, in part, to 1,8-naphtholactone, which in turn decarbonylates in two steps to form the m/e 114 ion. Recently, Seibl[3] described the fragmentation of 1,8-naphtholactone by a double decarbonylation in a similar manner.

The other two ketalization products of acenaphthenequinone were non-ketonic isomers. The mass spectrum of the low-melting isomer is shown in Figure 2. Below m/e 200, the mass spectrum is very similar to that of the ketonic product. The doubly charged ions at m/e 182, 154 and 126 are, however, more prominent. As in the monoketal, it is believed that the m/e 170 ion exists as the 1,8-naphtholactone ion, from which two CO groups are eliminated successively. The m/e 198 ion may be formed in three different ways: 1) by loss of ethylene, followed by the elimination of carbon dioxide; 2) by loss of $C_3H_4O_2$; and 3) by ring-cleavage, with successive losses of $C_2H_3O\cdot$ and $CHO\cdot$.

The chemical ionization spectrum of the low-melting isomer is shown in Figure 3. The base ion at m/e 183 is probably protonated acenaphthenequinone, which is formed through the consecutive elimination of two C_2H_4O moieties from the Q+ at m/e 271.

Although the mass spectral data for the low-melting isomer are consistent with the normal ethylene diketal structure, the corresponding data for the high-melting isomer are consistent only with the structure shown in Figure 4. The base ion of the latter is 16 amu lower (m/e 154) than in the low-melting isomer (m/e 170), while a prominent m/e 182 ion is observed. The m/e 182 ion is formed either through the elimination of $C_2H_4O_2$ and then of ethylene or by the reverse process; like the acenaphthenequinone ion (cf. Figure 5), it loses carbon monoxide in two steps. The fragmentation pathway that demonstrates the bis-dioxane structure, however, is the elimination of $C_2H_4O_2$ from the molecular ion to form the stabilized unsaturated ion of m/e 210, which further eliminates ethylene to form the m/e 182 ion. The M-58 ion is formed by the stepwise elimination of ethylene and formaldehyde from the M+. The ions at m/e 198, 170, 142 and 114 are formed in the same manner as in the low-melting isomer, i.e. by the elimination of carbon dioxide from the m/e 242 ion. The loss of formaldehyde and $C_2H_4O_2$ could occur from a m/e 242 ion that had been formed from the elimination of ethylene, while the loss of carbon dioxide from the m/e 242 ion would require rearrangement to the m/e 198 ion present in the low-melting isomer. Although no ion is found for the loss of C_4H_8O, there are two ions at m/e 199, one corresponding to the ^{13}C isotope peak of the m/e 198 ion and the other to the loss of C_4H_7O from the M+. In contrast to the electron impact mass spectrum of the high-melting isomer, the chemical ionization mass spectrum (cf. Figure 6) shows a very intense m/e 199 ion. No metastable ion is detected for its formation and, unfortunately, the exact mass for this ion was not measured nor was it determined by metastable

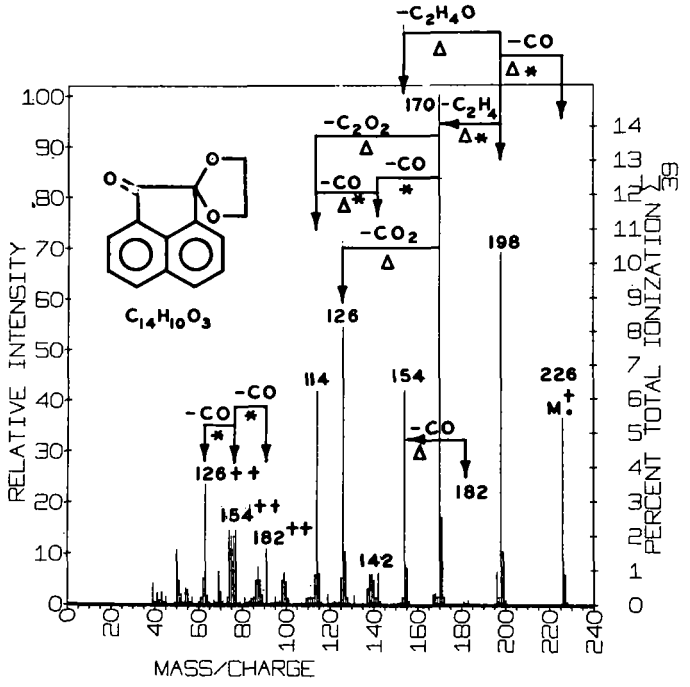

FIGURE 1 Electron Impact Mass Spectrum of the Monoketal of Acenaphthenequinone
*Metastable Transition Δ Defocused Ion Transition

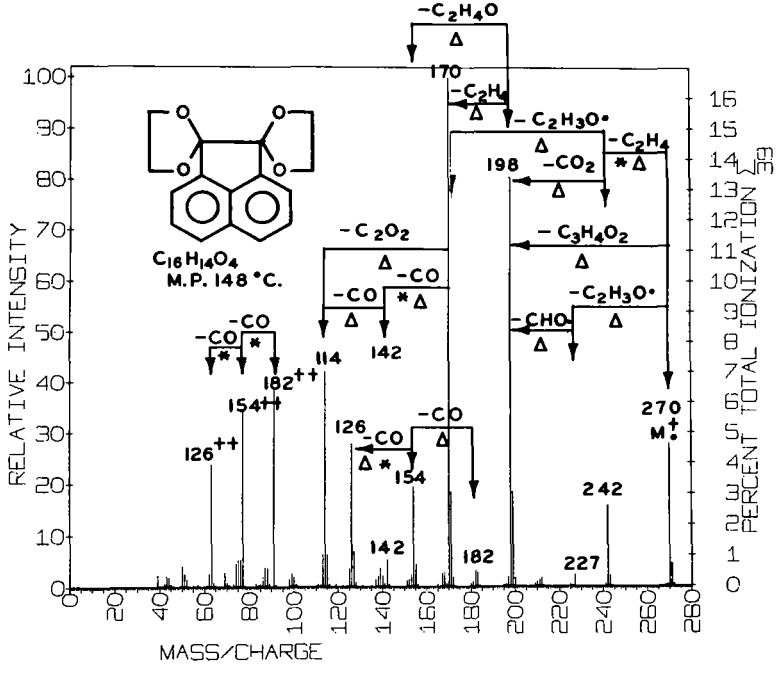

FIGURE 2 Electron Impact Mass Spectrum of the Diketal of Acenaphthenequinone

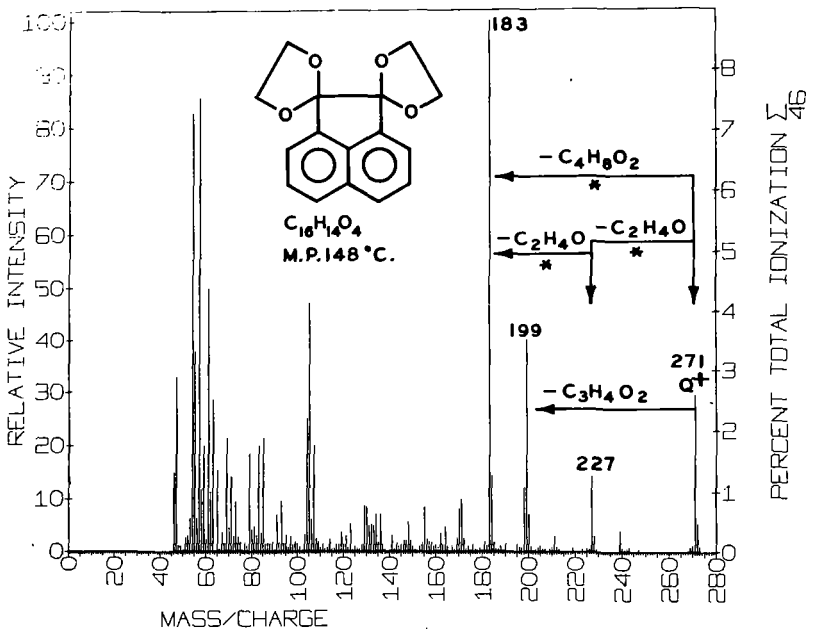

FIGURE 3 Chemical Ionization Mass Spectrum of the Diketal of Acenaphthenequinone

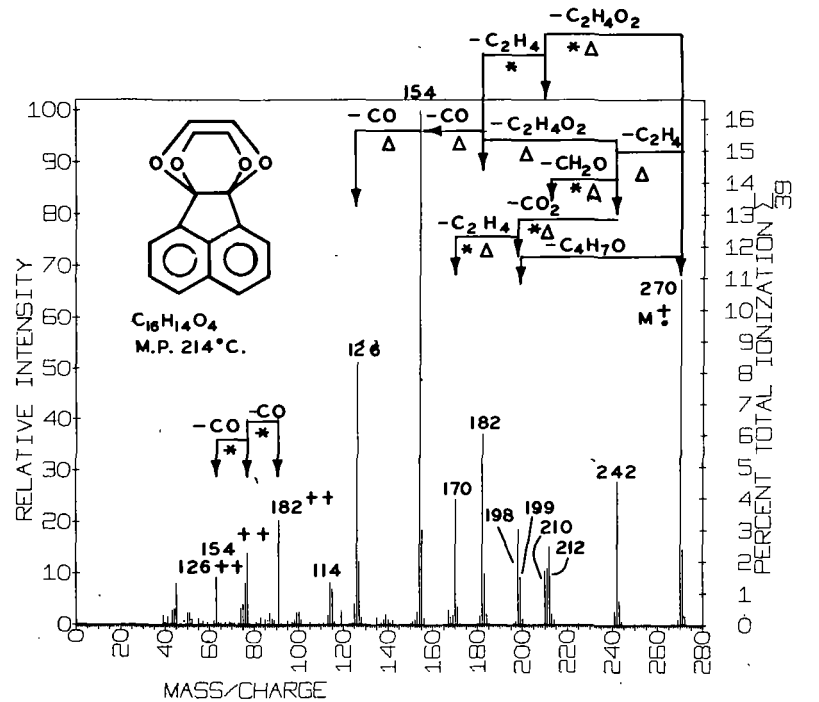

FIGURE 4 Electron Impact Mass Spectrum of the Bis-Dioxane of Acenaphthenequinone

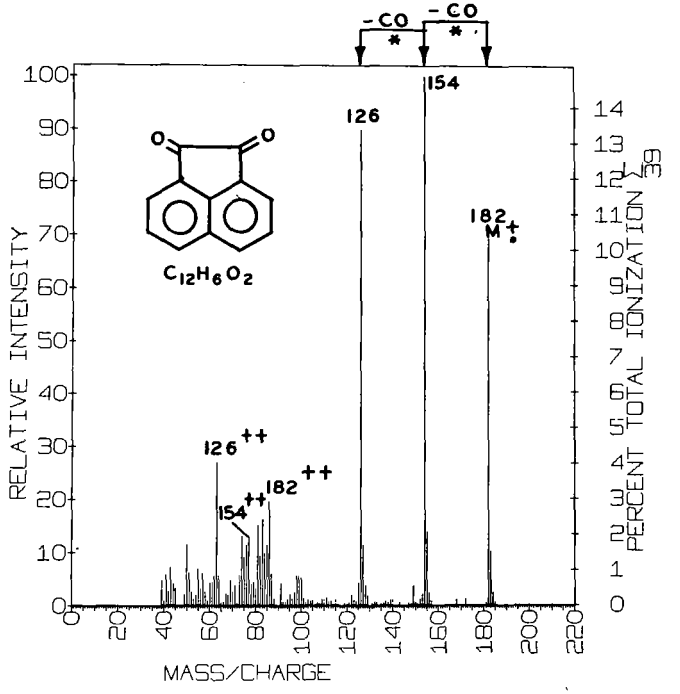

FIGURE 5 Electron Impact Mass Spectrum of Acenaphthenequinone

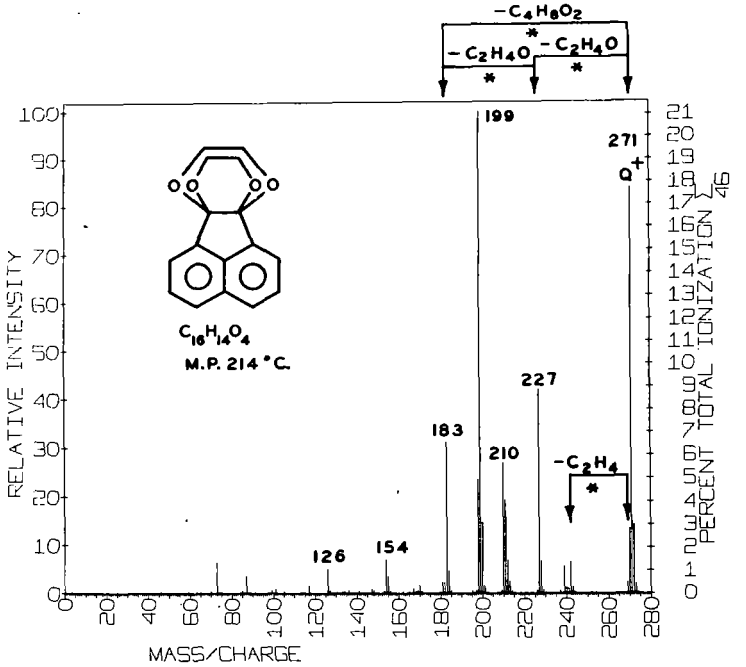

FIGURE 6 Chemical Ionization Mass Spectrum of the Bis-Dioxane of Acenaphthenequinone

defocusing experiments. Assuming that rearrangement is not favored in chemical ionization, C_4H_8O should be lost from the quasimolecular ion to form the m/e 199 ion. Metastable ion transitions are observed for the consecutive losses of two C_2H_4O moieties from the quasimolecular ion. Finally, a m/e 210 ion is present, resulting from the elimination of $C_2H_4O_2$ and a proton to form the unsaturated ion; the ion corresponding to loss of the elements of ethylene and formaldehyde is not observed.

Ketalization of cyclohexane-1,2-dione gives the normal diketal as the major product plus a small amount (ca. 2%) of tetraoxapropellane[4,5]. The mass spectrum of this compound is shown in Figure 7. The characteristic peak for the elimination of $C_2H_4O_2$ from the M+ is observed, accompanied by both metastable and defocused ions. In addition, the M-58 ion also illustrates that C_3H_6O is lost from the M+. Russell and Ochrymowycz[6] reported that the mass spectrum of the ketalization product of phenylglyoxal favors the normal product, although they found a small M-60 ion that would be consistent with the bis-dioxane structure.

ACKNOWLEDGEMENTS

We would like to thank Dr. Henry Fales (NIH) for obtaining the chemical ionization spectra and Dr. T.D.J. D'Silva (Union Carbide) for a sample of tetraoxapropellane.

REFERENCES

1. M. Barber and R.M. Elliott, ASTM E-14 Conference on Mass Spectrometry, Montreal, Canada, May, 1964.
2. J.H. Beynon, *Anal. Chem.*, *42*, No. 1, A97 (1970).
3. J. Seibl, *Experientia*, *25*, 1009 (1969).
4. T.D.J. D'Silva, *Chem. Ind.*, 202 (1970).
5. R.H. Jaeger and H. Smith, *J. Chem. Soc.*, 160 (1955).
6. G.A. Russell and L.A. Ochrymowycz, *J. Org. Chem.*, *34*, 3618 (1969).

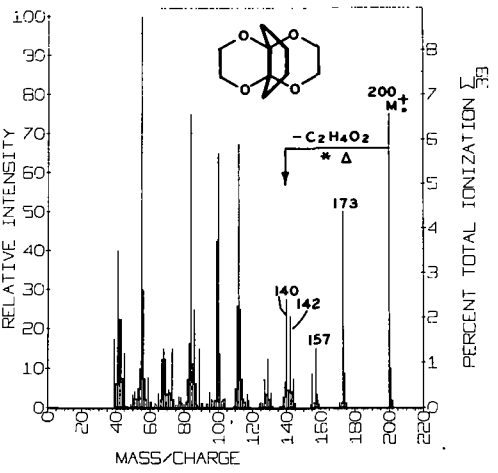

FIGURE 7 Electron Impact Mass Spectrum of Tetraoxapropellane

ENERGY EFFECTS IN THE MASS SPECTRA OF AROMATIC COMPOUNDS

Noel Einolf and Burnaby Munson
Department of Chemistry
University of Delaware
Newark, Delaware

The effect of substituents on particular fragmentation pathways was studied by an energy variation technique. These competing reactions in the benzophenone series were chosen:

$$YC_6H_4COC_6H_5^{+\cdot} \xrightarrow{k_1} YC_6H_4CO^+ + C_6H_5\cdot \qquad (1)$$
$$\xrightarrow{k_2} C_6H_5CO^+ + YC_6H_4\cdot$$

$$YC_6H_4COC_6H_5^{+\cdot} \xrightarrow{k_1} YC_6H_4^+ + C_6H_5CO\cdot$$
$$\xrightarrow{k_2} C_6H_5^+ + YC_6H_4CO\cdot \qquad (2)$$

For a decomposition of molecular ion to fragment ion, the dependence of k is given by quasi-equilibrium theory as

$$k = \nu \left(\frac{E - E_0}{E} \right)^{N - 1} \qquad (3)$$

A comparison of rate constants for reactions in equations (1) and (2) will take the logarithmic form

$$\log k_1/k_2 = \log \nu_1/\nu_2 + (N - 1) \log \left(\frac{E - E_0{}^1}{E - E_0{}^2} \right) \qquad (4)$$

Equation (4) predicts a dependence of rate constant ratio on a frequency factor term and an energy term.

The mass spectra of 12 substituted benzophenones were evaluated at electron energies ranging from less than 15 eV to 70 eV. A plot of log $YC_6H_4CO^+/C_6H_5CO^+$ vs. E_{el} gives smooth, regular curves, as shown by representative substituents in the figure. This ratio is greater than one at 70 eV for electron donating groups and increases with decreasing E_{el}. For electron withdrawing groups the ratio $Y\phi CO^+/\phi CO^+$ is less than one with 70 ev electrons and decreases with decreasing E_{el}. There is a good correlation of the quantity log $YC_6H_4CO^+/C_6H_5CO^+$ with σ^+.

Results for the phenyl ions (equation 2) were not as good, probably due to multiple pathways for the formation of these ions.

Charge exchange spectra show a similar dependence of log $YC_6H_4CO^+/C_6H_5CO^+$ on internal energy of the molecular ion, E. Internal energy is determined by the recombination energy of the reactant ions, Xe^+, Kr^+, Ar^+. Also apparent in the charge exchange spectra is a drastic decrease in intensity of the molecular ion as E is increased.

By extending this preliminary work on charge exchange, we hope to clarify the effects of substituents and electron energy on the rate constants for decomposition of these ions and on the resultant mass spectra of the neutral compounds.

(To be submitted to Organic Mass Spectrometry)

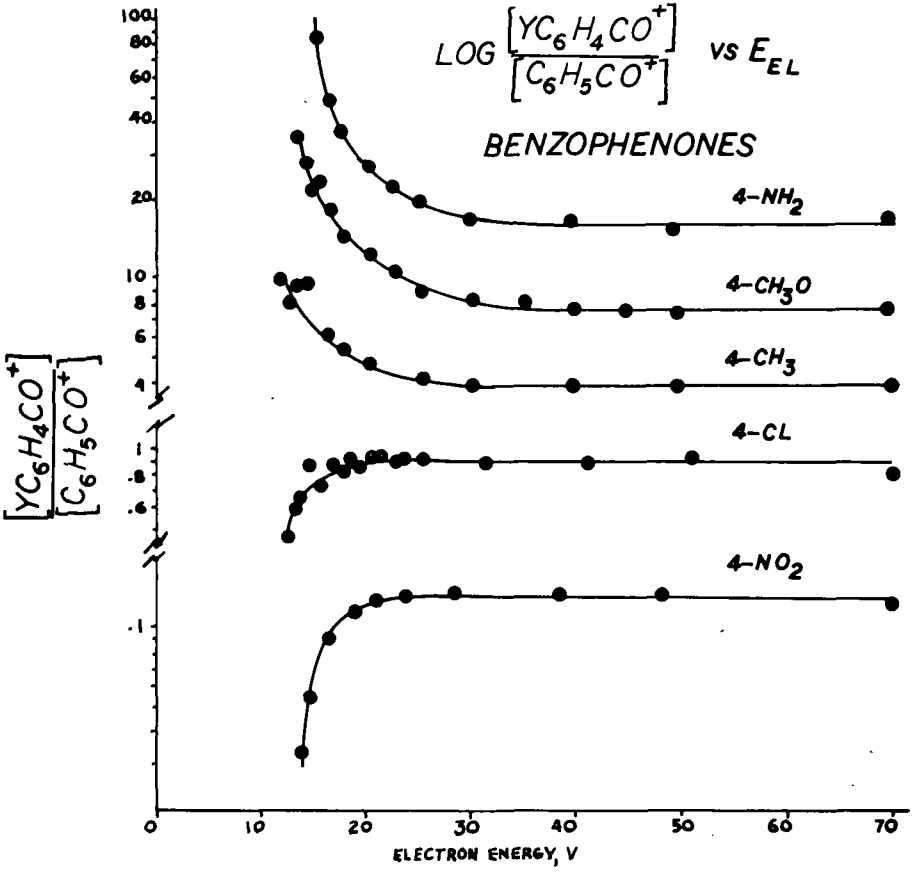
LOG [YC6H4CO+] / [C6H5CO+] VS EEL
BENZOPHENONES
4-NH2
4-CH3O
4-CH3
4-CL
4-NO2
[YC6H4CO+] / [C6H5CO+]
100
80
60
40
20
10
8
6
4
.8
.6
.1
0
10
20
30
40
50
60
70
ELECTRON ENERGY, V

SIMULATED DISTILLATION BY HIGH RESOLUTION LOW VOLTAGE MASS SPECTROMETRY

B9

Thomas Aczel and H. E. Lumpkin

Analytical Research Laboratory
Esso Research and Engineering Company
Baytown, Texas 77520

The detailed characterization of complex aromatic mixtures obtained through high resolution low voltage analysis(1) is now being used to predict the distillation characteristics of the material analyzed.

The approach is based on the determination of the concentration of each component and sorting according to boiling points. The concentrations of all the components with boiling points within each five degree Fahrenheit range interval, from 170 to 1230°F, are summed to obtain a distillation curve. The occasional nonvolatile portion of the sample is determined by weighing the residue remaining in the solid sample inlet system(2) after the analysis.

The experimental procedures and the mass spectrometric and computer equipment used are those described previously(1). The distillation curve is printed by the computer at each 5°F. The data are normalized both on a total volatiles and on a total sample basis, taking into consideration the nonvolatile residue. A summary table, giving these values at each 50°F interval, is also printed.

The most important step in the procedure is securing a set of boiling points for the up to 2900 components included in the analysis. Two main approaches are used for this purpose: 1) use of true boiling points from the literature; 2) calculation of empirical boiling points from the high resolution low voltage mass spectral analysis of narrow conventional or gas chromatographic distillation cuts.

Data from the literature were obtained using various sources(3,4). As structural isomers, such as anthracene and phenanthrene, cannot be distinguished by low voltage mass spectrometry, average boiling point values were used in these cases. The boiling points of many of the higher molecular weight components could not be found in the literature; therefore, extrapolated data based on those available were used for the heavier components.

The boiling points of aromatic hydrocarbon nuclei were extrapolated using a plot of boiling points versus molecular weight. The boiling points of hydroxyaromatic nuclei were extrapolated from a plot of the ratio of the available boiling points of corresponding aromatic and hydroxyaromatic nuclei (benzene and phenol, for example) versus the carbon number of the compounds involved. As expected, the boiling point ratios between hydroxyaromatic and aromatic structures were higher for the low carbon number structures where the contribution of the hydroxyl group is great with respect to the rest of the molecule. Boiling points for aromatic sulfur nuclei were also based on those of the aromatic nuclei. One S atom has approximately the same effect on boiling point as two C atoms; for example, benzothiophene has a boiling point close to that of naphthalene, dibenzothiophene to that of phenanthrene, etc.

Finally, the curves used to extrapolate the effect of alkyl substitution on the 58 aromatic hydrocarbon, aromatic oxygen, and aromatic sulfur nuclei were based on the changes in boiling points observed for n-paraffins of increasing chain length.

The other approach mentioned, not yet in use in the computerized procedure, is based on the observed fact(5) that plots of the average carbon number determined by the high resolution low voltage analysis for a series of narrow distillate cuts are reasonably linear for all homologous series with respect to the median boiling points of the same fractions. These plots can thus furnish empirical boiling point data for each carbon number in a given series for a given type of sample.

In addition to furnishing empirical boiling point data, the study of narrow distillation fractions has shown that in a practical distillation each component is described better by a boiling range rather than by an ideal, unique boiling point. For example, a single compound such as naphthalene is found in several narrow distillate fractions, covering a range of up to 100-150°F. Plots of concentration of a given compound versus the median boiling points of the distillation fractions in which they are present are essentially Gaussian. We are now in the process of adding a so-called sloppy distillation curve to our computer output which will be based on boiling range intervals rather than on unique boiling points.

The precision of the mass spectral distillation is acceptable as shown by the values tabulated below, obtained on five replicate analyses in a period of two months on a coal liquefaction product.

Temperature, °F	Weight Percent Off	
	Average	Standard Deviation
400	3.49	0.78
500	40.68	1.75
600	60.67	2.25
700	72.03	2.29
800	76.39	1.78
900	78.01	1.36
1000	78.75	1.30
Total volatiles	79.42	1.26

A large number of data has shown that the amount of nonvolatiles by MS corresponds to the 1000°F+ bottoms for coal liquefaction samples.

An example of the accuracy, that is the ability to predict conventional data, is given by the figure shown below in which MS data are compared to those obtained from a conventional glass spiral distillation for coal liquefaction products.

COMPARISON OF MS, GS DISTILLATIONS

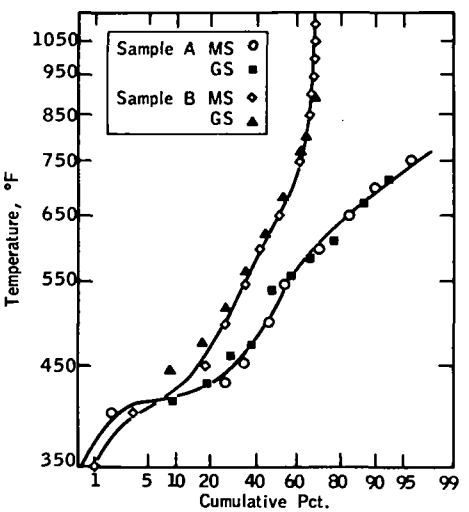

In some cases we have observed considerable deviations between MS and conventional data. These were due to some extent to the MS calibration coefficients, now being revised, but mostly to the use of ideal boiling points in the MS procedure. Even in these cases, however, the MS data were consistent and sufficient to predict the variations in the distillation curve resulting from changed processing parameters.

The MS simulated distillation provides rapid, precise data at a negligible marginal cost for samples analyzed by the mass spectrometer. It requires a minimum of sample, furnishes extremely detailed data and avoids polymerization in the still. Its possible disadvantages are the reliance on extrapolated calibration data both for sensitivity and boiling point values, the restriction to volatile aromatics, and the impossibility of furnishing physical cuts.

This latter disadvantage is partially compensated by predicting the composition of narrow distillate cuts from the composition of the total fraction, using the boiling point data in the program. This is a very promising approach, as shown by the partial data reported below.

Component	Wide Boiling Sample 400-700°F. Found	Cuts 400-530°F Found	400-530°F Predicted	530-700°F Found	530-700°F Predicted
$C_{10}H_8$	6.7	14.7	12.5	0.0	0.0
$C_{12}H_{12}$	2.8	4.8	5.3	0.9	0.0
$C_{14}H_{16}$	1.1	-	-	2.4	1.9
Avg. MW, Naphthalenes	147	138	138	186	190
C_nH_{2n-6}	1.3	2.3	2.7	0.1	0.0
C_nH_{2n-10}	8.5	6.6	6.3	10.6	11.0
C_nH_{2n-14}	14.2	5.0	3.8	24.7	23.7
C_nH_{2n-18}	8.2	0.0	0.0	17.6	15.0
C_nH_{2n-22}	1.6	0.0	0.0	3.5	3.3
Avg. MW	164	144	144	192	189
Avg. Z No.	11.9	9.4	9.2	14.7	14.9
Percent off at 500°F	45.0	83.3	84.2	1.2	0.0
Percent off at 600°F	71.2	99.9	100.0	37.2	38.2

Simulated distillation by high resolution mass spectrometry to predict the distillation characteristics of aromatic mixtures has been used in our laboratories with good success for the past year. It has been applied mainly to the prevalently aromatic coal liquefaction products, but is also useful for the aromatic portion of petroleum streams and, integrated with data from the gas chromatographic distillation of the saturates, for total petroleum streams.

We plan to submit an extended version of this paper to Analytical Chemistry.

---

(1) Thomas Aczel, E. E. Allan, J. H. Harding and E. A. Knipp, Anal. Chem., 42, 341(1970).
(2) H. E. Lumpkin and G. R. Taylor, Anal. Chem., 33, 476(1961).
(3) S. W. Ferris, Handbook of Hydrocarbons, Academic Press, New York, N.Y.(1955).
(4) H. C. Anderson and W. R. K. Wu, Properties of Compounds in Coal Carbonization Products, Bulletin 606, Bureau of Mines, The Department of Interior.
(5) Thomas Aczel and B. H. Johnson, 153rd National Meeting of the American Chemical Society, Miami Beach, Florida, April 9-13, 1967, Preprints of Symposia, Vol. 12, No. 2, page B-83.

High Resolution Mass Spectrometry of Nucleic Acid Hydrolysates

W. A. Koenig, A. M. Lawson, L. C. Smith, P. F. Crain and James A. McCloskey

Institute for Lipid Research and Department of Biochemistry
Baylor College of Medicine
Houston, Texas

High resolution mass spectrometry has been applied to the identification of modified nucleosides in ribonucleic acid (RNA), based on the identification of structurally diagnostic predetermined sets of exact masses. This approach has the principal advantage that it can often clearly distinguish and identify closely related compounds with similar physical and chromatographic properties.

Transfer RNA was chosen as a model system, since pure (isoaccepting) tRNAs of known sequence yield hydrolysates of known nucleoside content which include modified forms of the four major nucleosides occurring in RNA. Also, since tRNAs contain about 80 nucleotide residues they provide an extreme test for identification of minor components, most of which occur only one time per molecule.

Experimental methods. tRNA (100-300 μg) was enzymatically degraded to nucleosides, and the hydrolysate passed through a micro DEAE Sephadex column, dried over P_2O_5, then converted to either trimethylsilyl (TMS) (1, 2) or trifluoroacetate (TFA) derivatives. A sample of approximately 50 μg of derivatives was placed in the direct probe of a CEC 21-110B mass spectrometer. This amount of sample is equivalent to 30 μg tRNA or 22 μg of free nucleosides, assuming quantitative hydrolysis and derivatization. A single mass spectrum was photographically recorded over a 3 minute period while the sample temperature was raised from 220° to 260°. Since the photographic plate integrates the ion current over the period of exposure, varying rates of evaporation of different components from the probe are of no consequence. At a magnetic field strength of 11.2 kilogauss and 8 KV accelerating voltage, the region from m/e 28 to ~ 706 is recorded, which is sufficient for virtually all known nucleosides. Reduction of the accelerating voltage to 6 KV extends the mass range to over m/e 900 but with an approximately two-fold decrease in sensitivity. Resolution of 18.000 - 20,000, was found to provide a suitable compromise between resolution of multiplets (often over 8 lines per a.m.u.) and sensitivity. Studies with nucleoside-TMS standards using Ilford C2 plates indicated that sample quantities equivalent to 20-50 ng gave signal/noise ratios of > 30:1 for major ions at resolution 20,000.

Mass spectra were recorded on either Ilford C2 photoplates, or Technical Operations evaporated silver bromide plates, the latter of which gave excellent sensitivity at high mass values and negligiable background.

The high resolution mass spectrum of a typical tRNA hydrolysate contains approximately 900 lines (exclusive of mass standards), and consequently yields the same number of exact mass values. These data represent the 8-14 nucleosides of varying concentrations usually present in a transfer RNA, plus small amounts of impurities. The reduction of high resolution data and the search for characteristic exact mass values are carried out using a time-sharing system of an IBM 360/50 computer.

Results. Tyrosine transfer RNA from yeast (3) having a known nucleotide sequence of 78 residues (4) yields the following nucleoside composition on hydrolysis: guanosine (20), cytidine (19), adenosine (15), uridine (8), dihydrouridine (6), pseudouridine (3), N^2-methylguanosine (1), 2'-O-methylguanosine (1), N^2, N^2-dimethylguanosine (1), N^6-(3-methyl-2-butenyl)adenosine (1), 5-methylcytidine (1), thymine riboside (1), 1-methyladenosine (1). As TMS derivatives 11 of the 13 components were identified in a single high resolution spectrum. 5-Methylcytidine $(TMS)_4$ and 2-O-methylguanosine $(TMS)_4$ were not found. 1-Methyladenosine was observed as the $(TMS)_3$ derivative (including the M, M-15 ions) but could not be distinguished from N^6-methyladenosine, to which it can rearrange during isolation (5). Using trifluoroacetyl derivatives, all nucleosides except 2'-O-methylguanosine $(TFA)_3$ were identified in a single spectrum.

As an alternative to the recording of spectra of mixtures at high resolving power,

prior separation of components by a gas chromatograph directly coupled to a mass spectrometer is feasable, and is under investigation in our laboratory as a possible approach.

References

1. Y. Sasaki and T. Hashizume, Anal. Biochem., 16, 1 (1966).

2. J. A. McCloskey, A. M. Lawson, K. Tsuboyama, P. M. Krueger and R. N. Stillwell, J. Amer. Chem. Soc., 90, 4182 (1968).

3. We are indebted to Dr. J. T. Madison for a sample of this compound.

4. (a) J. T. Madison, G. A. Everett and H. Kung, Science, 153, 531 (1966); (b) J. T. Madison and H. Kung, J. Biol. Chem., 242, 1324 (1967).

5. J. T. Madison, G. A. Everett and H. Kung, J. Biol. Chem., 242, 1318 (1967).

Applications of Ultra-High Resolution Mass Spectrometry and Direct Data Reduction in Labeling and Tracer Studies

J. R. Chapman,* S. Evans* and W. A. Wolstenholme+

*AEI Scientific Apparatus Ltd., Manchester, England
+AEI Scientific Apparatus Inc., White Plains, N.Y. 10604

INTRODUCTION

The use of high resolution mass spectrometers in conjunction with computer-based data processing systems is becoming more widespread. An increasing number of laboratories is using complete high resolution spectra in conjunction with low resolution and limited high resolution studies. In the authors' laboratory a data system based on a small computer (DEC PDP8/I) is used routinely to record complete high resolution spectra and has been applied to variety of chemical problems.(1) The data system is normally connected on line to the mass spectrometer and, typically, the resolving power of the instrument is set to 10-15,000.

One of the interesting applications of ultra-high resolution studies (say 30,000 to 100,000) is in the study of isotopically labelled molecules. The interest in these compounds is frequently to determine how much label is present and also at what point in the structure has the incorporation taken place.

The advantage of ultra-high resolution studies for this work is that it enables one to study uniquely the peaks containing the label. It removes any ambiguity from the data and thus increases greatly the reliability of the data.

The use of a mass spectrometer at ultra-high resolution involves, of course, a considerable decrease in sensitivity compared with low resolution operation. This condition is further aggravated when studying isotopically labelled molecules since ideally one would like to study and record the peak containing the label at the molecular ion. Thus, not only is high resolution required but also one is studying isotope peaks, the intensity of which is typically a few percent of the unlabelled peak.

In the authors' laboratory,work has recently been carried out which enables much higher sensitivity to be achieved at high resolution (about a factor 30 increase at a resolution of 40,000). These results are described in a paper by Evans and Hallas presented at this meeting.

In this paper we wish to present the first results obtained using the ion optical modifications.

EXPERIMENTAL

The experimental work was carried out on an AEI MS902 high resolution mass spectrometer connected on-line to a DS-20 data system based on a DEC PDP8/I computer with a 4k working store and 64k disc back-up. The compound used for these initial studies was ^{15}N enriched gliotoxin:

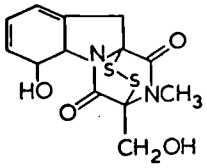

Gliotoxin

The sample used was prepared using a substrate to which ^{15}N-glycine had been added. Previous work by Bose et al had shown that under these conditions both nitrogens are labelled although to unequal extents.(2) The doublets requiring separation for unambiguous study of labeled peaks are thus:

$^{14}NH - {}^{15}N \qquad \Delta M = 0.0108$

$^{13}C^{14}N - {}^{12}C^{15}N \qquad \Delta M = 0.0063$

Thus, at the molecular ion minus S_2 region of gliotoxin (M/e 263), the required resolution is 41,000 and at typical indole fragment (M/e 145) a resolution of 23,000 is required.

Initially, a routine complete high resolution (10,000) spectrum was recorded for gliotoxin and this element listing data used to select peaks for further study at higher resolution.

RESULTS

Table I shows the compositions of some of the ions in the gliotoxin spectrum determined from the scan at resolution 10,000 on-line to the data system.

TABLE I

COMPOSITION OF IONS IN GLIOTOXIN SPECTRUM OBTAINED FROM COMPLETE HIGH RESOLUTION SCAN

M/e	Composition
326	$C_{13}H_{14}N_2O_4S_2$ (molecular ion)
262	$C_{13}H_{14}N_2O_4$
144	C_9H_6NO
143	C_9H_5NO
116	C_8H_6N
115	C_8H_5N

Gliotoxin very readily loses the sulphur even when admitted to the mass spectrometer by direct insertion and the peak at $(M-S_2)$ was chosen to obtain a measure of the total ^{15}N incorporation. The fragment ions in the M/e 143 region are due to the indole moiety and, therefore, give a measure of the incorporation at the indole nitrogen.

In order to separate the doublets of interest, a complete spectrum was recorded at a resolution of 30,000. The relative intensities of the isotope peaks at M/e 263, 145, 144 and 117 were measured from the chart and the results are summarized in Table II in terms of the measured enrichment.

TABLE II

GLIOTOXIN (^{15}N GLYCINE SUBSTRATE)
^{15}N ENRICHMENT LEVELS MEASURED FROM COMPLETE SCAN AT R.P. 30,000

Composition of Ions Measured	^{15}N enrichment level
$C_{13}H_{14}{}^{15}NNO_4$) $C_{13}H_{14}N_2O_4$)	4.8%
$C_9H_6{}^{15}NO$) C_9H_6NO)	1.8%
$C_9H_5{}^{15}NO$) $C_9H_5\ NO$)	2.0%
$C_8H_6{}^{15}N$) $C_8H_6\ N$)	1.9%

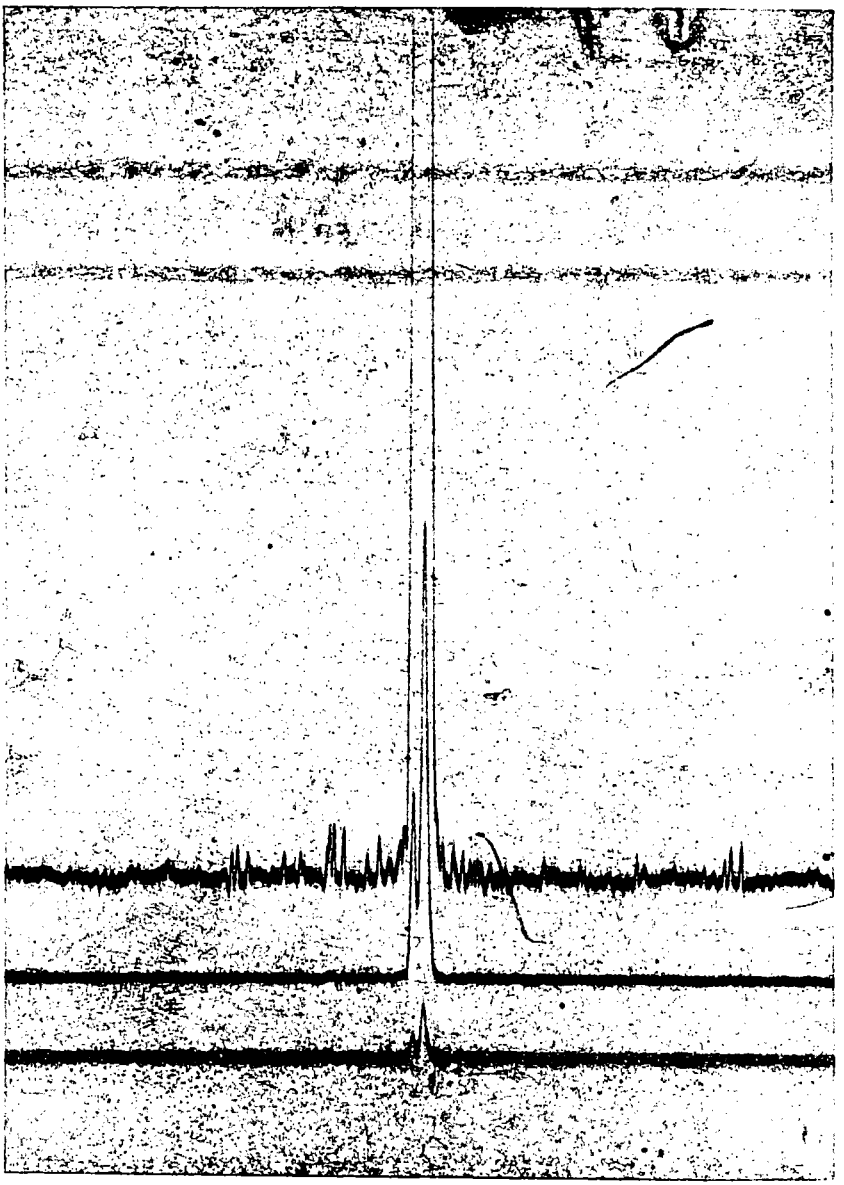

Figure 1. Gliotoxin, M/e 263 due to $C_{12}{}^{13}CH_{14}N_2O_4$- $C_{13}H_{14}{}^{14}NNO_4$

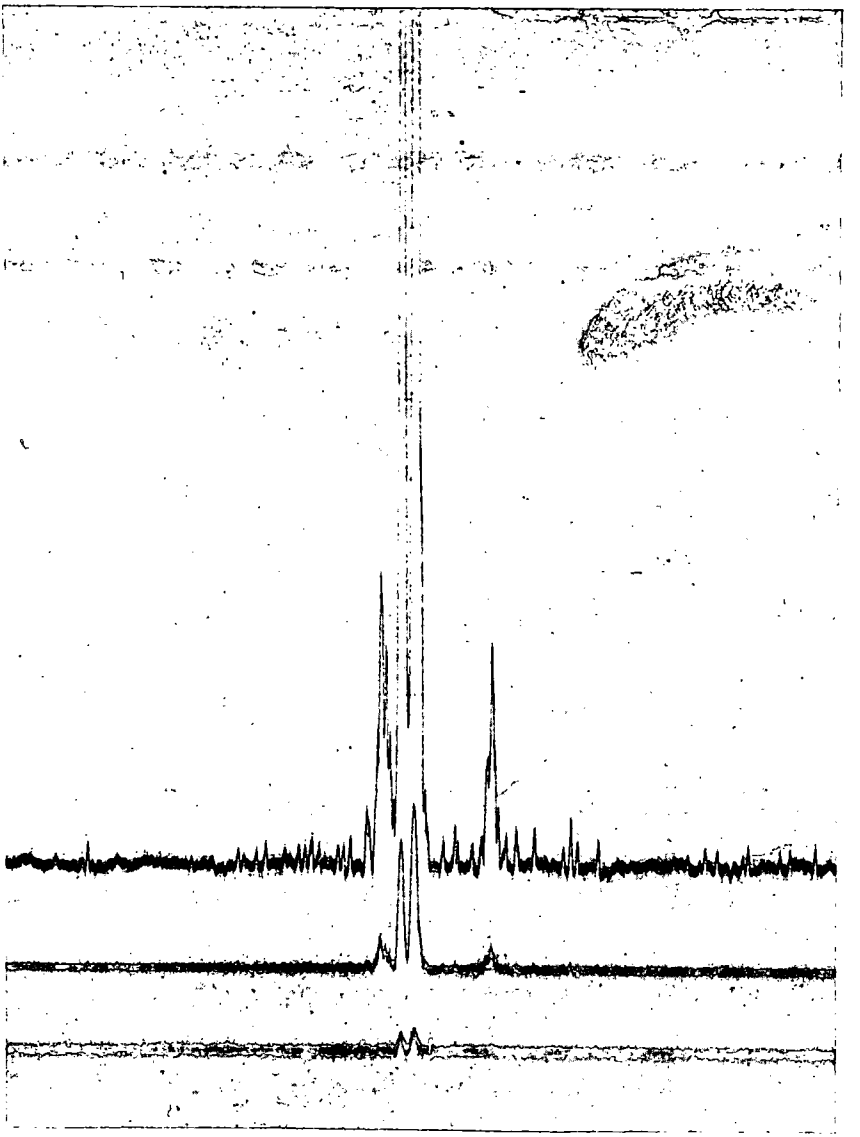

Figure 2. Gliotoxin, M/e 145 triplet. $C_9H_6{}^{15}NO$, $^{13}CC_8H_6NO$, & C_9H_7NO

Figure 3. Part of Data System Print Out at 40,000 Resolution.

PART OF SCAN ON ^{15}N ENRICHED GLIOTOXIN (RP 40.000).

MEASURED MASS	ERR	C12/13	H	N	O	NX
145.0527	- .42	8/0	6	2	0	1
	.00	*9/0	7	1	1	0
145.0480	- .61	7/1	5	2	0	1
	- .18	*8/1	6	1	1	0
145.0418	- .06	*9/0	6	0	1	1
144.0439	-1.40	8/0	5	2	0	1
	- .97	*9/0	6	1	1	0
	1.28	5/0	7	1	3	1
144.0339	- .18	*9/0	5	0	1	1
143.0369	- .51	8/0	4	2	0	1
	- .12	*9/0	5	1	1	0

Figure 1 shows the doublet recorded at M/e 263 due to $C_{12}{}^{13}CH_{14}N_2O_4$ and $C_{13}H_{14}{}^{15}NNO_4$. Figure 2 shows a triplet at M/e 145 due to $C_9H_6{}^{15}NO$, $^{13}CC_8H_6NO$, and C_9H_7NO. It can be seen that the resolving power and sensitivity are quite adequate for unambiguous identification of the specific isotope peak of interest and also for the reliable measurement of relative intensity.

The results obtained show that 4.8% of molecules which would normally contain ^{14}N, contain one ^{15}N atom. Also, the values in Table I show the percentage of molecules which contain ^{15}N in the indole moiety instead of natural ^{14}N.

Finally, Figure 3 shows part of the computer output from a complete high resolution scan recorded at 40,000 resolution. At mass 145, the triplet due to the CH, ^{13}C and ^{15}N containing components is resolved and each component identified. The correct assignments have been marked manually with an asterisk.

CONCLUSIONS

It has been shown that ultra-high resolution mass spectrometry can be successfully applied to the study of isotopically labelled molecules. The sensitivity which can be obtained with focusing modifications described by Evans and Hallas enabled good *relative intensity data to be obtained for isotope peaks recorded at resolutions* in excess of 30,000. Thus, total incorporation of, say, ^{15}N can be measured directly and unambiguously at the molecular ion peak, certainly up to mass 300. The further advantage of the complete high resolution spectrum is that it affords an opportunity to check the level of incorporation several times by using several fragment ion peaks arising from the same part of the molecule.

An interesting and important extension of this work will be the application of the techniques described to double-labeled molecules. It is planned, in fact to next study gliotoxin labelled both with ^{15}N and ^{13}C. These studies will probably be carried out with dethiodehydrogliotoxin which is more easily admitted to a mass spectrometer.

REFERENCES

1. A. J. Geddes, G. N. Graham, H. R. Morris, F. Lucas, M. Barber and W. A. Wolstenholme, Biochem. J. (1969) 114, 695.

2. A. K. Bose et al Abs. 4th International Symposium on Chemistry of Natural Products, Stockholm, 1966, p. 150; J. Amer. Chem. Soc., 90, 1968.

ACKNOWLEDGEMENTS

The authors are indebted to Dr. Ajay K. Bose of the Stevens Institute of Technology, Hoboken, New Jersey for the gliotoxin sample. They would also like to thank Dr. J. D. Waldron, Managing Director, AEI Scientific Apparatus Ltd. for permission to publish this paper.

Solar Wind Gases, Cosmic-Ray Spallation Products and the Irradiation History of Lunar Material

C3

K. Marti

Department of Chemistry
University of California at San Diego
La Jolla, California 92037

Abstract:

All 23 stable isotopes of the noble gases He to Xe and 2.1 x 10^5y Kr^{81} have been measured by mass spectrometry in the soil and in four rocks from the Apollo 11 mission. The soil contains large amounts of trapped solar wind gases which almost completely mask other components. In the crystalline rocks, on the other hand, cosmic-ray induced spallation and radiogenic gases are predominant. The isotopic abundances of the rare gases in the fines are found to be similar to those previously reported for gas-rich meteorites. Relative to the heavy gases, Ne and He are depleted by factors of 2.5 and 10 respectively. Kr-Kr^{81} ages of rocks # 10017, 10047, 10057, 10071 and of the soil cover a range of from 47 to 509 million years. K-Ar ages of type A rocks lie between 2.3 and 2.9 billion years, that of a type B rock (#47) is 3.5 billion years. Varying relative production rates of the Kr and Xe isotopes in the rocks are due to differences in chemical composition as well as irradiation conditions. A complex history for at least some of the rocks is indicated and will be discussed. First results from the Apollo 12 samples were reported.

Abstract

Neutron Capture Effects in Lunar Material

G. W. Lugmair

Department of Chemistry, University of
California at San Diego, La Jolla,
California 92037

Because of its high capture cross section, Gadolinium is a sensitive indicator for integrated thermal neutron fluxes. Gd was separated to a very high degree of purity from 50 to 100 mg of several lunar rock and soil samples brought back by Apollo 11 by ion-exchange techniques. The isotopic ratios of GdO^+ were measured on a programmable 12" radius magnetic mass spectrometer with an accuracy of better than 2 parts in 10^4. The sample sizes analyzed were approximately 1×10^{-7} g Gd. Two detection modes, ion counting and current integration, were applied. The anomalies of the isotopic ratio $^{158}GdO/^{157}GdO$ relative to terrestrial standards vary from below detection limit up to 0.72 percent. They correspond to integrated thermal neutron fluxes of $(17.4, 4.8, 1.04) \times 10^{15} n/cm^2$ for rocks 10017, 10071 and 10057 respectively, and of $9.5 \times 10^{15} n/cm^2$ for the soil. These results, together with theoretical calculations of the lunar neutron flux carried out by Lingenfelter et al. in 1961, and radiation ages as well as spallation spectra obtained from rare gas analyses, permit to design a model for the average depth at which a rock was located for most of the time of its irradiation.

MASS SPECTRA OF MITOMYCIN ANTIBIOTICS

G. E. Van Lear

Lederle Laboratories, American Cyanamid Company,
Pearl River, New York 10965

ABSTRACT

The mass spectra of the four known mitomycin antibiotics, mitomycin A, mitomycin B, mitomycin C, porfiromycin[1,2] and four related compounds have been obtained.[3] These compounds are the first naturally occurring compounds containing an aziridine ring. A structure for mitiromycin,[1] a compound in the mitomycin class of antibiotics, has been determined by spectroscopic methods.[4]

1. D. V. Lefemine, M. Dann, F. Barbatschi, W. K. Hausmann, V. Zbinovsky, P. Monnikendam, J. Adam and N. Bohonos, J. Amer. Chem. Soc., 84, 3184 (1962).
2. J. S. Webb, D. B. Cosulich, J. H. Mowat, J. B. Patrick, R. W. Broschard, W. E. Meyer, R. P. Williams, C. F. Wolf, W. Fulmor, C. Pidacks, and J. E. Lancaster, J. Amer. Chem. Soc., 84, 3185 (1962).
3. G. E. Van Lear, Tetrahedron, 26 (1970).
4. G. O. Morton, G. E. Van Lear, and W. Fulmor, J. Amer. Chem. Soc., 92, 2588 (1970.

D2

Techniques for Mass Spectrometry of Drug Metabolites Without Extensive Purification

Donald C. Hobbs
Pfizer, Inc., Groton, Conn.

The mass spectrometer has proven to be an extremely useful tool in the determination of structures of drug metabolites because it requires only very small quantities of material and because it usually permits one to make a complete structure determination without any additional information. To function effectively however it is usually necessary that the sample, as presented to the instrument, be pure. Drug metabolites, because of their origin from complex biological systems, are contaminated with innumerable extraneous materials which must first be removed. Gas chromatography has been used with great success in the separation of drugs and drug metabolites when the substances, or their derivatives, are sufficiently volatile. A combination of gas-chromatography and mass spectrometry has recently been employed in numerous laboratories with great success in the elucidation of metabolite structures. To be as exhaustive as possible, it is important that the sample be subjected to combined gas chromatography-mass spectrometry prior to any preliminary purification, since some metabolites might be lost during such purification. However, samples obtained in such a manner generally contain a multitude of substances of natural origin which are not drug-related but which yield significant peaks in the gas chromatogram and whose mass spectra must receive partial interpretation to ensure that they are not drug-related.

A group of commercially available components has been assembled in order to rapidly determine which of the many components emerging from the gas chromatographic column are drug-related. By means of a group of unions and valves located within the oven of an LKB 9000 combined gas chromatograph mass spectrometer, the effluent is directed to a Barber-Colman radioactivity detector and a flame detector, or to a Tracor flame photometric detector, or to the mass spectrometer. Where radioactive (carbon 14 or tritium) or sulfur-containing drug has been administered, these specific detectors will establish which of the substances being eluted is of interest. In a subsequent run the effluent is directed to the mass spectrometer and spectra of the desired compounds obtained. For example, the figure shows the tracings obtained on chromatography of a silylated extract of urine from an animal which had received carbon-14 labeled o-nitroaniline. The flame and radioactivity traces, obtained simultaneously, clearly indicate which of the many substances being eluted are labeled. Only those are of interest. The total ion monitor trace in the subsequent sample injection corresponds well with the flame tracing and permits appropriate spectra to be obtained to deduce the structures of the labeled substances (A is disilylated phenylenediamine, B is silylated nitroaniline, C and D are monosilylated hydroxylated nitroaniline and E is disilylated hydroxylated nitroaniline). Similar results have been obtained with tritium-labeled and sulfur-containing drugs.

As newer derivatizing techniques become available to volatilize polar drug metabolites this approach to their rapid identification and structure elucidation should become increasingly valuable. A full account of this work is being submitted to Analytical Chemistry.

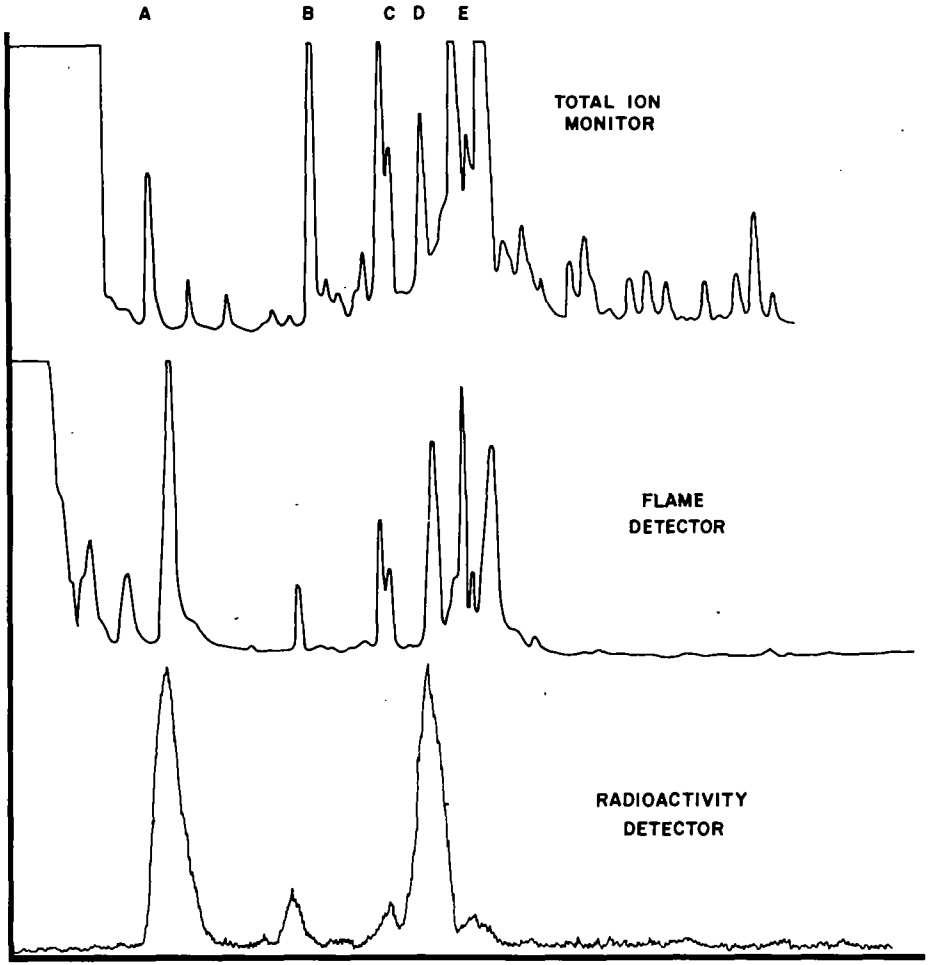
A
B
C
D
E
TOTAL ION MONITOR
FLAME DETECTOR
RADIOACTIVITY DETECTOR

MASS SPECTRA OF ORGANIC COMPOUNDS III. FRAGMENTATION STUDIES OF PHOSPHOLIPIDS AND RELATED COMPOUNDS BY HIGH RESOLUTION MASS SPECTROMETRY[++]

H. G. Boettger and A. M. Kelly

Space Sciences Division
Jet Propulsion Laboratory
Pasadena, California

During the course of our work on the identification of biologically important compounds in geochemical and cosmochemical samples, the question of identifying complex lipids arose. A search of the applicable literature revealed many excellent studies related to the mass spectrometry of fatty acids (1-4), steroids (5), and simple glycerides (6). In contrast, nothing was found on the mass spectrometry of the more complex glycerides and phospholipids. Therefore, we decided to investigate the possibility of using mass spectrometry for the direct structural analysis of the more complex lipids. The results of the first phase of the investigation are reported in this presentation.

Experimental Conditions

High and low resolution spectra of 25 lipids and related compounds were recorded on a modified MS-902. The samples were introduced via a direct probe introduction system (7) at probe temperatures of 35°C to 150°C and an ion source temperature of 180°C. Perfluorokerosine was used as a reference compound. Precise masses and elemental compositions were determined using our previously described automatic data system (8). Low voltage spectra were obtained for some of the compounds and typical examples are shown in Figs. 1 and 2. Since the results showed no advantages over 70 e-Volt spectra, only the latter were used in the rest of our work.

Results

As an inspection of the spectra (Figs. 3-6) shows, the most intense and structurally most significant peaks occur at high mass. They are due to fragmentation at the phosphorous atom and can be assigned to the formula

$$\begin{array}{l} R_1 - COO - CH_2 \\ R_2 - COO - CH \\ \qquad\qquad\quad CH_2 - O \end{array}^{+}$$

where R_1 and R_2 are C_{16} and/or C_{18} fatty acids. Occasionally, less intense groups of peaks approximately 28 and 56 mass units higher are found. They are due to the presence of one or two C-20 acids. Another series of peaks is found 16 and 17 lower.

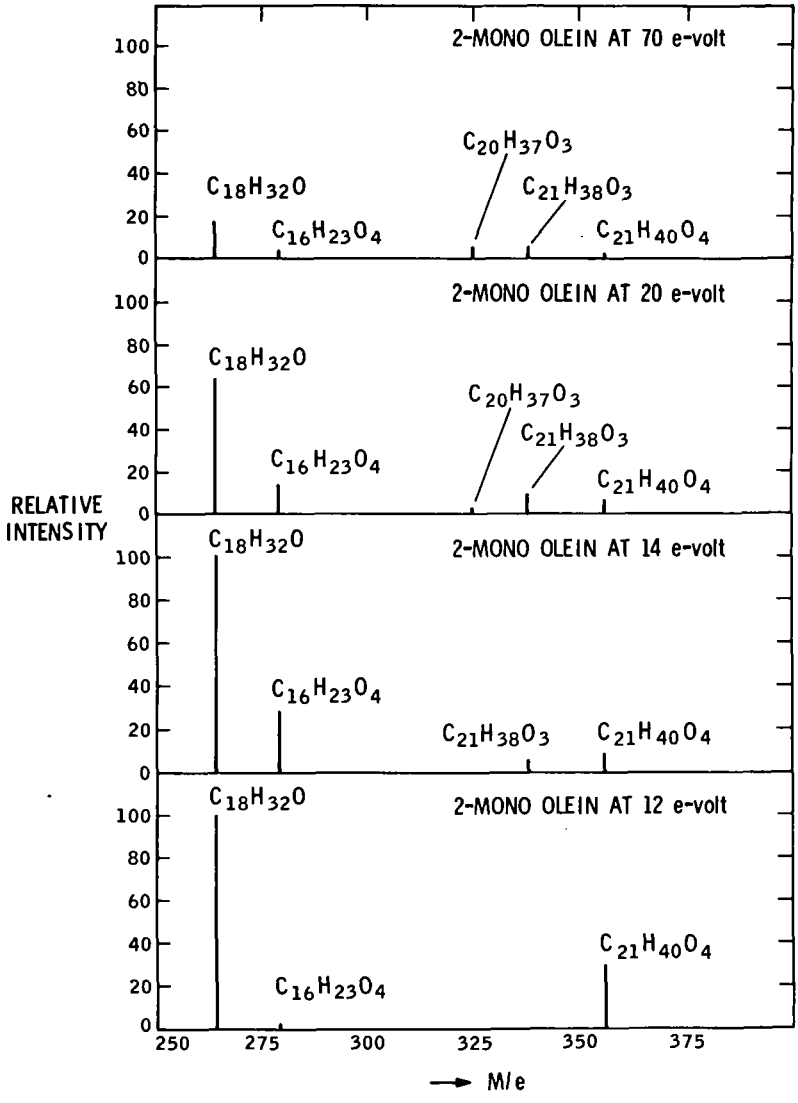

Figure 1

Line Drawing Of High Mass End Of Low Resolution Spectrum Of 2-Mono Olein At Different Ionizing Voltages

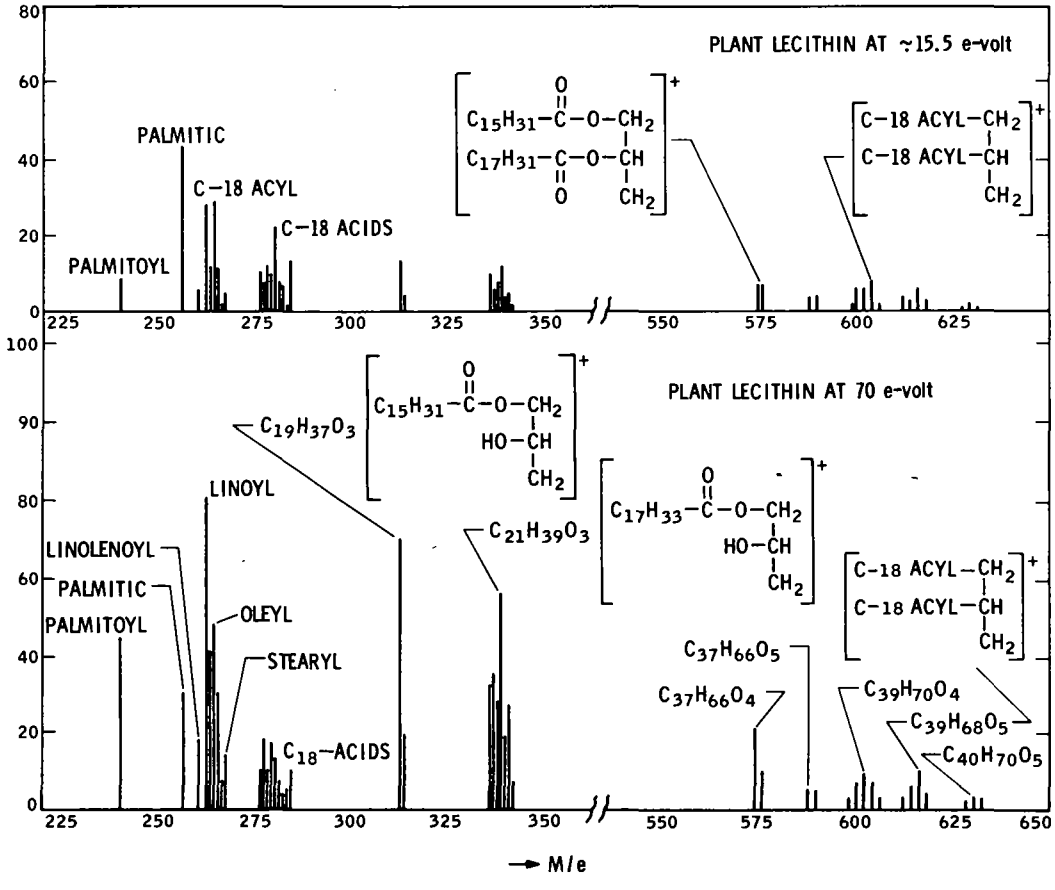

Figure 2
Line Drawing of Low Resolution Spectrum of Plant Lecithin at 15 and 70 eV.

PALMITOYL-LYSO-PHOSPHATIDYL CHOLINE C24.H50.N.07.P.

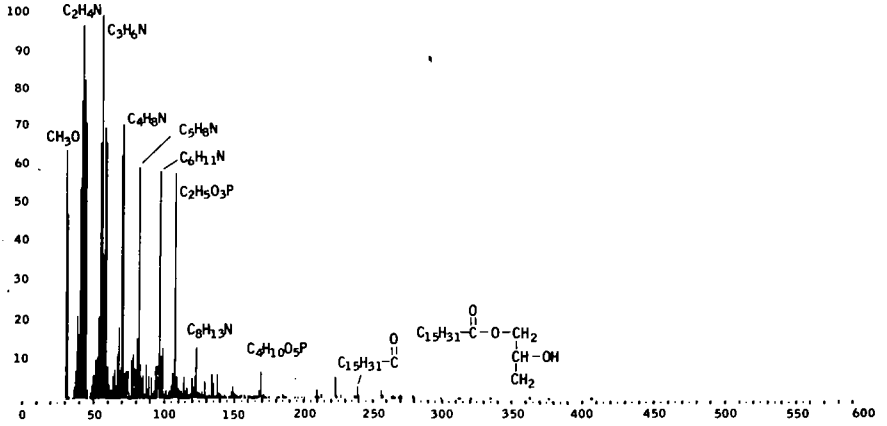

PALMITOYL-LYSO-PHOSPHATIDYL ETHANOLAMINE C21.H44.N.07.P.

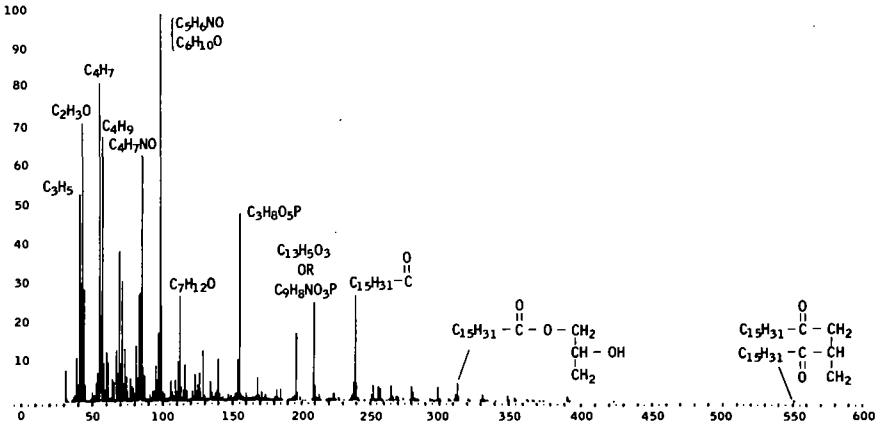

Figure 3

1-MONO-PALMITIN C19.H38.04.

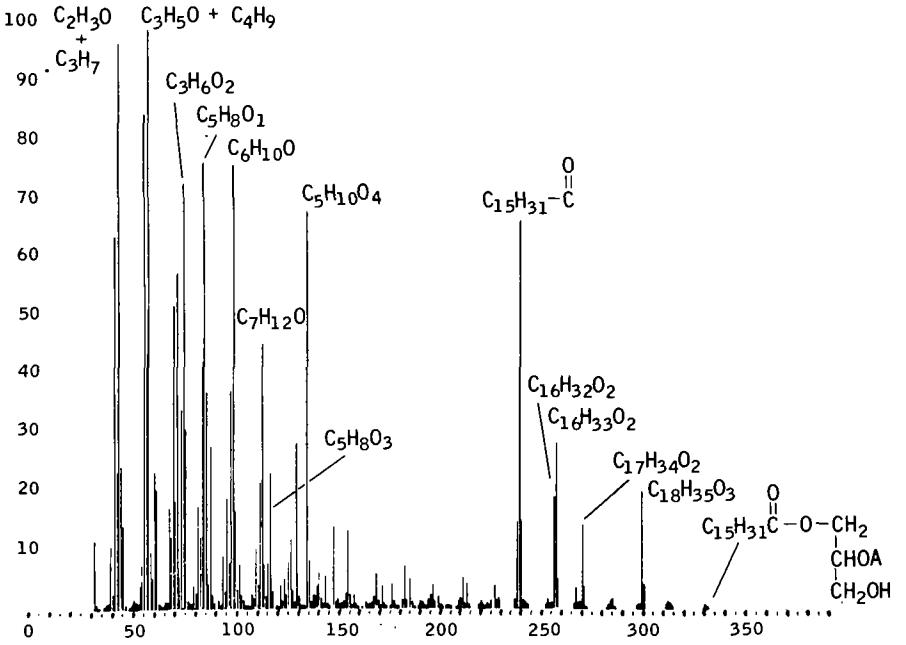

2-MONO-PALMITIN C19.H38.04.

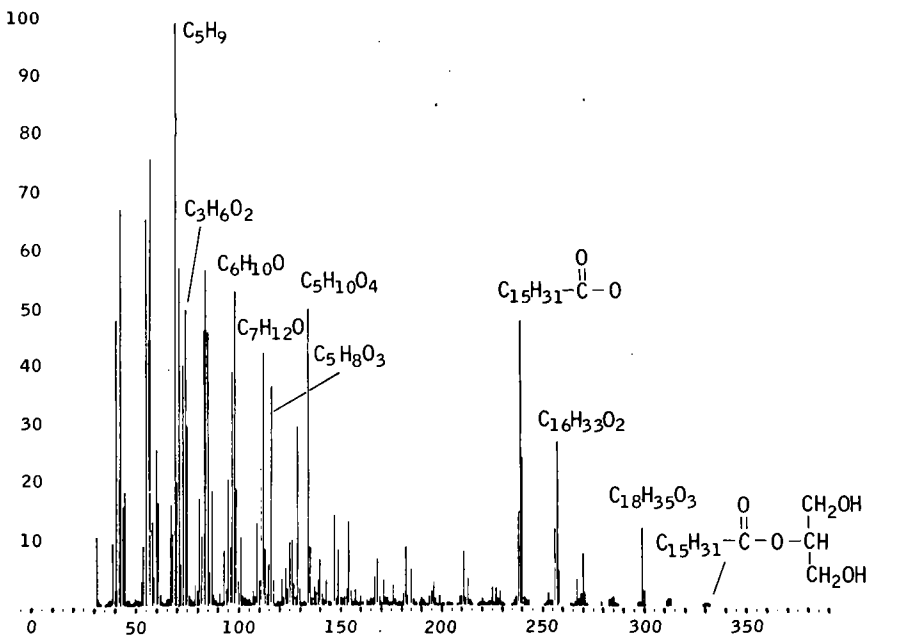

Figure 4

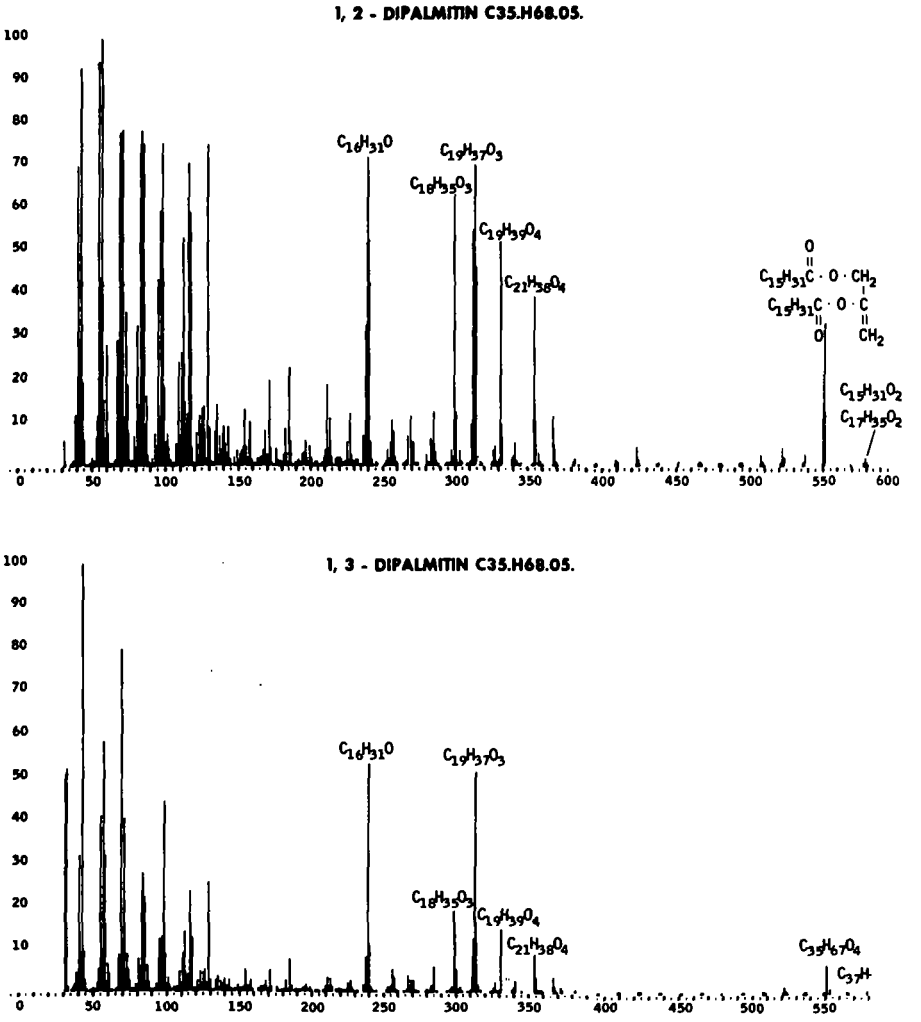
1, 2 - DIPALMITIN C35.H68.05.
100
90
80
70
60
50
40
30
20
10
0
50
100
150
200
250
300
350
400
450
500
550
600
$C_{16}H_{31}O$
$C_{19}H_{37}O_3$
$C_{18}H_{35}O_3$
$C_{19}H_{39}O_4$
$C_{21}H_{38}O_4$
$C_{15}H_{31}C \cdot O \cdot CH_2$
$C_{15}H_{31}C \cdot O \cdot C$
CH_2
$C_{15}H_{31}O_2$
$C_{17}H_{35}O_2$
1, 3 - DIPALMITIN C35.H68.05.
100
90
80
70
60
50
40
30
20
10
0
50
100
150
200
250
300
350
400
450
500
550
$C_{16}H_{31}O$
$C_{19}H_{37}O_3$
$C_{18}H_{35}O_3$
$C_{19}H_{39}O_4$
$C_{21}H_{38}O_4$
$C_{35}H_{67}O_4$
$C_{37}H$

Figure 5

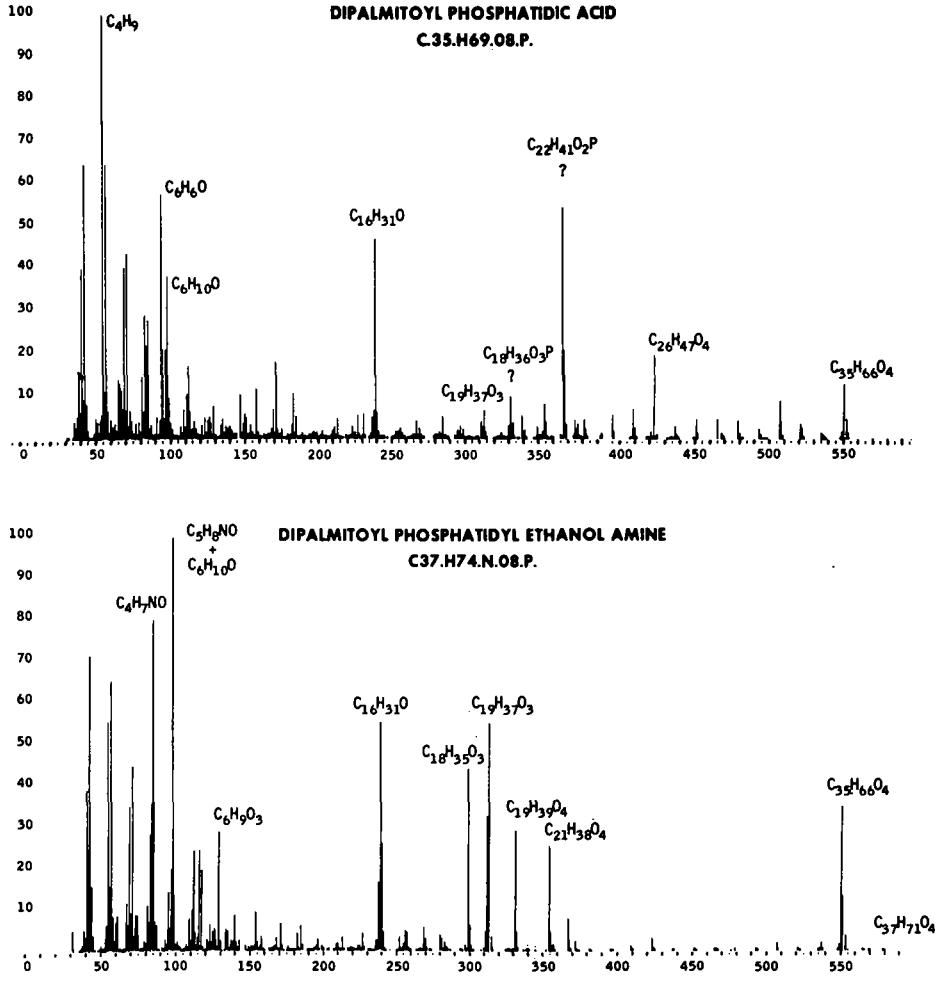
DIPALMITOYL PHOSPHATIDIC ACID
C.35.H69.08.P.
C_4H_9
C_6H_6O
$C_6H_{10}O$
$C_{16}H_{31}O$
$C_{22}H_{41}O_2P$
?
$C_{18}H_{36}O_3P$
?
$C_{19}H_{37}O_3$
$C_{26}H_{47}O_4$
$C_{35}H_{66}O_4$
DIPALMITOYL PHOSPHATIDYL ETHANOL AMINE
C37.H74.N.08.P.
C_5H_8NO
+
$C_6H_{10}O$
C_4H_7NO
$C_{16}H_{31}O$
$C_{19}H_{37}O_3$
$C_{18}H_{35}O_3$
$C_6H_9O_3$
$C_{19}H_{39}O_4$
$C_{21}H_{38}O_4$
$C_{35}H_{66}O_4$
$C_{37}H_{71}O_4$

Figure 6

SAMPLE \ M/e / COMPOSITION OF ION	605 $C_{39}H_{73}O_4$	603 $C_{39}H_{71}O_4$	601 $C_{39}H_{69}O_4$	579 $C_{37}H_{71}O_4$	577 $C_{37}H_{69}O_4$	575 $C_{37}H_{67}O_4$	573 $C_{37}H_{65}O_4$	551 $C_{35}H_{67}O_4$	549 $C_{35}H_{65}O_4$	547 $C_{35}H_{63}O_4$	545 $C_{35}H_{61}O_4$
DIOLEYL PHOSHATIDIC ACID	32.7	100	16.9	7.1	40.8	42.3	14.3	16.5	35.6	24.4	9.4
DIOLEYL PHOSPHATIDYL CHOLINE	30.2	100	16.0		34.3	37.7					
DIOLEYL PHOSPHATIDYL ETHANOL AMINE	16.8	100			47.5	74.3			50.4	40.9	
DIPALMITOYL PHOSPHATIDYL ETHANOL AMINE				1.0				100	9.5		
DIPALMITOYL PHOSPHATIDIC ACID				10.6				100	37.7		
LYSO PHOSPHATIDYL ETHANOL AMINE				20.0	75.0			100	5.0		
PALMITOYL LYSO PHOSPHATIDYL ETHANOL AMINE				3.4	54.7	7.9		100	5.2		
LYSO LECITHIN											
LECITHIN	32.9	37.4	50.6		36.9	100	20.4				
1,2-DIOLEIN	8.4	100	15.4		23.0	35.6			16.7	11.8	2.2
1,3-DIOLEIN	23.4	100	10.1	2.8	41.3	4.5		6.0	41.4	20.4	4.0
1,2-DIPALMITIN				6.3				100	12.7		
1,3-DIPALMITIN				9.6				100	12.2		
PHOSPHATIDYL ETHANOL AMINE		6.2	13.0	8.7	100	11.8		12.8	39.1	9.8	1.5
	STEARYL-OLEYL	DIOLEYL	OLEYL-LINOLEYL	PALMITOYL-STEARYL	PALMITOYL-OLEYL	PALMITOYL-LINOLEYL	PALMITOYL-LINOLENEYL	DIPALMITOYL	PALMITOYL-PALMITOLEYL		

Figure 7
Relative
Intensity of
Diacyl-Glyceride
Ions in Complex
Lipids.

SAMPLE \ M/e / COMPOSITION OF ION	341	339	337	335	313	285	257
	$C_{21}H_{41}O_3$	$C_{21}H_{39}O_3$	$C_{21}H_{37}O_3$	$C_{21}H_{35}O_3$	$C_{19}H_{37}O_3$	$C_{17}H_{33}O_3$	$C_{15}H_{29}O_3$
DIOLEYL PHOSPHATIDIC ACID	29.6	100	12.3	.6	30.2	23.2	1.3
DIOLEYL PHOSPHATIDYL CHOLINE	69.9	100	42.2	–	63.1	47.0	3.2
DIOLEYL PHOSPHATIDYL ETHANOL AMINE	17.2	100	7.0	–	29.2	26.6	1.8
DIPALMITOYL PHOSPATIDYL ETHANOL AMINE	.5	–	–	–	100	1.2	.3
DIPALMITOYL PHOSPHATIDIC ACID	17.0	5.8	–	–	100	5.1	–
PALMITOYL LYSO PHOSPHATIDYL CHOLINE	–	–	–	–	100	–	–
LYSO PHOSPHATIDYL ETHANOL AMINE	8.3	16.7	9.1	5.6	100	–	–
LYSO LECITHIN	–	–	–	–	100	2.4	–
LECITHIN	–	–	–	–	100	26.2	–
1-MONO OLEIN	25.5	75.9	100	–	16.4	.3	.1
2-MONO OLEIN	–	100	15.5	–	23.0	–	–
1,2-DIOLEIN	–	100	13.2	–	27.5	–	–
1,3-DIOLEIN	30.7	100	22.3	.8	52.0	35.0	1.9
1-MONO PALMITIN	31.4	100	10.1	.5	44.6	7.7	1.7
2-MONO PALMITIN	–	–	–	–	100	49.4	21.0
1,2-DIPALMITIN	8.9	–	–	–	100	25.8	21.6
1,3-DIPALMITIN	6.8	.5	.2	–	100	17.3	.5
CEPHALIN	5.4	–	–	–	100	11.1	.2
PHOSHATIDYL ETHANOL AMINE	–	36.6	1.7	–	100	4.9	.3
PHOSPHATIDYL ETHANOL AMINE	5.1	31.6	1.6	–	100	3.9	.3
	STEARIC	OLEIC	LINOLEIC	LINOLEIC	PALMITIC	MYRISTIC	LAURIC

Figure 8
Relative Intensity
of Monoacyl Glyceride
Ions in Complex Lipids

It is due to ions of the general formula

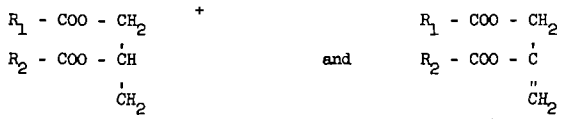

As we progress further down the mass scale we find another family of peaks in the 310-340 mass region. These ions correspond to a mono-glyceride and are formed through loss of an acyl group from the primary diglyceride fragment. Furthermore, we find a number of intense peaks between m/e = 239 and m/e = 294 which are due to the acyl group. In the low mass region we see a variety of intense ions resulting from the amino-terminal of the molecule as well as ions which retained the phosphate group. These are in addition to the alkyl ions from the acid moieties.

If we summarize these results we come to the following general conclusions:

1. No parent ions are found when a free phospholipid is analyzed by the direct insertion probe technique.
2. It is not clear at this point whether the primary fragmentation of the molecules is caused by electron impact or thermally or both.
3. If one studies the mass spectrum of a typical phospholipid, then one can recognize several series of fragments which are always related to each other by either a common origin or a common mechanism of creation. These are:
   (a) Fragments derived from the glyceride moiety of the molecule.
   (b) Fragments derived from the amine part of the molecule.
   (c) Fragments retaining the phosphorous atom.
   (d) Fragments resulting from rearrangement reactions.

A more detailed investigation of the various fragment groups proved quite revealing from the standpoint of the composition of a complex lipid. The structurally most interesting portion of the molecule appears to be the glyceride moiety. Here fragmentation proceeds exactly along the lines of a free diglyceride or, in the case of a lysophospholipid, along the lines of a mono-glyceride. In other words, we find a "Parent"-ion of the glyceride moiety and ions due to the loss of R-COO, R-COOH, and R-COO-CH_2. Furthermore, there are always intense acyl ions, as well as acyl plus 128 and acyl plus 74 AMU. Thus it is relatively simple to determine the fatty acid content of a phospholipid by mass spectrometry.

Next, it would be of interest to determine the relative position of the various

acyl groups in mixed lipids. Mass spectrometric determination of the position of a specific acyl group in the glyceride molecule has been demonstrated previously (6) for triglycerides. Our investigations confirmed these results, but showed also that the situation is much more complicated in the case of the mono- and diglycerides and complex phospholipids. It can be seen, that even though there are quantitative differences, qualitatively the spectra of positional isomers are the same. At this time we are unable to say whether the similarity is due to acyl migration under electron impact or because we did not have the pure isomer to start with. Probably there is a combination of these factors at work. This prevents us from clearly distinguishing positional isomers. Efforts are under way to resolve the question. These efforts involve more vigorous purification of the samples and chemical labelling of the free hydroxyl groups.

The second major group of primary fragments is produced by fragmentation on the other side of the central phosphate group. In case of the samples which we have investigated this involves either ethanolamine or choline. In either case, the spectrum of the amine portion can be readily recognized.

The third group of peaks involves those fragments that have retained the phosphorous atom. This group usually includes a few intense peaks of phosphorous oxides, e.g., PO_2, PO_3, etc., and a few peaks due to short chain alkyl-phosphates. This type of ion loses intensity rapidly as the chain length increases. The most intense peaks are usually CH_4PO_2 and $C_2H_5PO_3$. Neither fragment has much structural significance beyond the indication that we are dealing with a phosphorous compound in case of a total unknown.

The situation changes drastically when we are dealing with a free phosphatidic acid. In this case, we have the glyceride moiety attached to the phosphoric acid but no amine or carbohydrate group. Under these circumstances one of the acyl groups seems to migrate to the phosphate group. We get intense ions of the composition: $C_{19}H_{36}O_5P$ or $C_{21}H_{38}O_5P$ for palmitoyl and oleyl phosphatidic acids respectively. The proposed structure for these fragments is

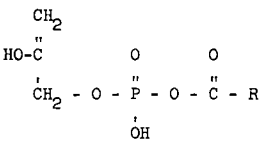

The primary fragment is followed in each case by several series of secondary fragmentation products of the general composition $C_nH_{2n-2}O_5P$ and $C_2H_{2n+1}O_4P$, etc. Our conclusion, that we are dealing with a rearrangement process rather than simple cleavage, is based solely upon the facts that:

1. We do not find ions of this nature when the phosphate group is occupied.
2. If we were seeing straight cleavage fragments, then one would expect fragments of the general composition:

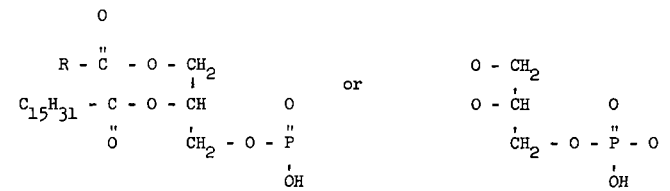

However, we have found no evidence of ions of this type.

The last series of ions which are found in certain phospholipids must also be due to a rearrangement process. Ethanolamine phospholipids show an intense series of peaks which are derived from acyl migration to the amine group, e.g., $C_{15}H_{31} - \overset{O}{\overset{\|}{C}} - NH - CH = CH_2$ (m/e = 280) etc. from palmitoyl phosphatidyl ethanol amines. In each case the entire series of

$$C_nH_{2n-2}NO$$

is found. Ions of this type are not found when the amino group is alkylated as in choline.

Conclusions

The preliminary investigation has shown that mass spectrometry is quite suitable for the characterization of complex phospholipids, regardless of the fact that a parent ion of the intact molecule is not found without chemical modification. This is clearly demonstrated in Figs. 7 and 8. Mixtures of lipids, mixed lipids ($R_1 \neq R_2$) and lyso-lipids (R_1 = H) can easily be recognized in the presence of each other.

Further work is required to enable us to determine the position of R_1 and R_2 in mixed lipids, to produce a parent ion and to make the method more quantitative. This work is now in progress and will be reported later.

References

1. G. P. Happ and D. W. Stewart. SACS 74, 4404 (1952).

2. N. C. Rol. Rev. Trav. Chim. 84, 413 (1965).

3. H. Budzikiewicz, C. Djerassi and D. H. Williams. "Mass Spectrometry of Org. Compounds", Holden-Day 1967, 174-205.

4. R. Ryhage and E. Stenhagen. "Mass Spectrometry of Long Chain Esters in Mass Spectrometry of Organic Ions", F. W. McLafferty (Editor), Academic Press 1963.

5. H. Budzikiewicz, C. Djerassi and D. H. Williams. "Structure Elucidation of Natural Products by Mass Spectrometry", Vol. II, Holden-Day, 1964.

6. M. Barber, T. O. Merren and W. Kelly. Tetrahedron Letters 18, 1063 (1964).

7. H. G. Boettger and A. M. Kelly. 17th Annual Conference on Mass Spectrometry and Allied Topics, Dallas, Texas, 1969.

8. H. G. Boettger. 15th Annual Conference on Mass Spectrometry and Allied Topics, Denver, Colorado, 1967.

++ This paper presents the results of one phase of research carried out at the Jet Propulsion Laboratory, California Institute of Technology, under Contract NAS 7-100, sponsored by the National Aeronautics and Space Administration.

Applications of Mass Spectrometry to Studies of Polyene Antibiotics. RAMESH C. PANDEY AND KENNETH L. RINEHART, JR., University of Illinois, Urbana, Ill. 61801

A very useful method for the study of polyene antibiotics' structures involves reduction of the antibiotic to a saturated hydrocarbon[1] or to a methyl ester[2] for study of its fragmentation pattern. Trimethylsilyl derivatives have occasionally been employed for molecular weights.[3] We have now developed an alternative mass spectral method for structure studies of polyene antibiotics, involving acetylation, both of the intact antibiotic and of its perhydrogenated derivative. We have applied both the older and the newer techniques in assigning structures to a tetraene antibiotic, tetrin A,[4] and also to several pentaene antibiotics, including chainin[5] and a number of minor components of the filipin complex.[5]

[1]A. C. Cope, et al., J. Am. Chem. Soc. 84, 2170 (1962).

[2]O. Ceder, J. M. Waisvisz, M. G. Van der Hoeven, and R. Ryhage, Acta Chem. Scand. 18, 83 (1964).

[3]B. T. Golding, R. W. Rickards, and M. Barber, Tetrahedron Lett., 2615 (1964).

[4]R. C. Pandey and K. L. Rinehart, Jr., Abstr. (Org) 155, Am. Chem. Soc., 157th Meeting, Minneapolis, April 1969.

[5]R. C. Pandey, K. L. Rinehart, Jr., and N. Narasimhachari, to be presented at the 7th International Symposium on the Chemistry of Natural Products, Riga, Latvia, June 1970.

The Elucidation of the Primary Structure of the Hypothalamic Thyroid Stimulating Hormone Releasing Factor of Ovine Origin by Means of Mass Spectrometry

D. M. Desiderio - Institute for Lipid Research and the Department of Biochemistry, Baylor College of Medicine, Houston, Texas 77025

R. Burgus, T. F. Dunn, W. Vale, and R. Guillemin - Salk Institute, San Diego, California 92112

D. N. Ward - Department of Biochemistry, University of Texas, M.D. Anderson Hospital and Tumor Institute, Houston, Texas 77025

The hypothalamus releases various neurohumoral substances to the vascular system of the adenohypophysis, which, in turn, releases hormones which stimulate the activity of specific target organs. The six known adenohypophyseal hormones are adrenocorticotropic, luteinizing, follicle, thyrotropic, growth, and prolactin stimulating hormones (1). Each hormone has its own corresponding releasing (or in the case of prolactin, inhibiting) factor. The object of this paper is to illustrate the role that mass spectrometry played in the elucidation of the thyroid stimulating hormone releasing factor (TRF).

About one nanogram of TRF is isolated from each sheep hypothalamus so that it is necessary to obtain about a million hypothalami to produce one milligram of natural TRF. (2) The biological assay for TRF has been published (3). Employing purification techniques developed over a decade, one milligram of TRF was finally isolated and structural work was begun. Hydrolysis with 6N HCl afforded three amino acids - His, Pro, and Glu- in equimolar quantities. These amino acids accounted for all of the weight in the monoacetate form of a tripeptide. Carboxy-peptidase did not detect a free C-terminus. As a dansyl derivative could not be formed, there was no free N-terminus.

In collaboration with Hoffman-La Roche, the six isomeric tripeptides that could be made from His, Pro, and Glu were synthesized (4). None showed activity. In order to protect the N-terminus, as presumably occurred with TRF, all peptides were acetylated. Only the product from Glu-His-Pro-OH showed

activity (5,6). This particular reaction product was shown to be L-2 pyrrolidone-5-carboxylyl-L-histidyl-L-proline-OH, or, in abbreviated form, PCA-His-Pro-OH, by means of its mass and infrared spectra. This product had ten units of activity (Natural TRF has 55,000 units of activity. For activity definition see 7). As many brain peptides have a C-terminal amide, the methyl ester was prepared in order to form the amide by ammonolysis. The PCA-His-Pro-OMe had a drastic increase of activity to 28,000 units. After ammonolysis, the amide had an activity qualitatively similar and statistically indistinguishable from natural TRF activity.

The mass spectrum of the final ammonolysis product proved to be essentially identical to the spectrum of natural TRF (8). It was necessary to methylate the two substances with diazomethane in order to increase the volatility. No molecular ion was observed, but the high and low resolution spectra both showed that TRF had the structure PCA-His-Pro-NH_2, which was substantiated by the mass spectra of the synthetic material.

This mass spectral work was corroborated by the following six techniques (9); TLC mobility, IR, NMR, nitrogen analyses, PCA peptidase, and the biological assay and specificity.

Acknowledgment - Financial support from NIH (GM-13901, GM-16216) and the Robert A. Welch Foundation (Q-125) is gratefully acknowledged. Computer facilities were provided by the Common Research Computer Facility, supported by USPHS RR 254.

This work has been submitted to Organic Mass Spectrometry for publication.

References

1. Campbell, H.J., Ch. 3 in "The Biological Basis of Medicine," E. Bittar and N. Bittar, Eds., Academic Press, New York, 1968.
2. Burgus, R., and Guillemin, R., Ann. Rev. Biochem., 39, 1970.
3. Yamazaki, E., Sakiz, E., and Guillemin, R., Experentia, 19, 1, 1963.
4. Burgus, R., Dunn, T.F., Desiderio, D. M., Ward, D. N., Vale, W., Guillemin, R., Felix, A. M., Gillessen, D., and Stüder, R.O., Endocrinology 86, p. 573, March, 1970.

5. Burgus, R., Dunn, T. F., Ward, D. N., Vale, W., Amoss, M., and Guillemin, R., C. R. Acad. Sc. Paris, 268, 2116-8, April, 1969.

6. Burgus, R., Dunn, T. F., Desiderio, D. M., Vale, W., and Guillemin, R., C. R. Acad. Sci., Paris, Vol. 269, p. 226, July, 1969.

7. Guillemin, R. and Sakiz, E., Nature 207, 297, July, 1965.

8. Burgus, R., Dunn, T.F., Desiderio, D. M., Ward, D. N., Vale, W. and Guillemin, R., Nature 226, p. 321, April, 1970.

9. Burgus, R., Dunn, T. F., Desiderio, D. M., Guillemin, R., C. R. Acad. Sci., Paris, Vol. 269, p. 1870, Nov. 1969.

Applications of GC-MS to Metabolic Research Problems. Sanford P. Markey, Keith B. Hammond, and James R. Plattner, B. F. Stolinsky Research Laboratories, Department of Pediatrics, University of Colorado Medical Center, Denver, Colorado 80220.

In certain disorders relating to mental retardation, abnormal quantities of metabolites are excreted in urine. In support of a routine screening program for inborn errors of metabolism, instrumentation has been developed to identify the structures of these metabolites. Structure elucidation is necessary to determine the site of the metabolic lesion - usually the absence or decreased activity of an enzyme. Compounds must be identified rapidly in order to initiate treatment before irreversible damage has occurred. Because of the quantities excreted, gas chromatography is used for initial screening, and combined gas chromatography - mass spectrometry (gc-ms) is utilized for compound identification. On-line computer recording is currently being developed for automated identification of known metabolites. The combined system is described below, along with several illustrations of its applicability to common problems.

An analytical gas chromatograph is coupled to a medium resolution mass spectrometer through an all-glass system, including magnetically operated glass valves and a fritted interface.[1] The fritted interface has recently been modified to accept a one cm length of porous ceramic tubing (8 mm o.d., 6 mm i.d.), rated to have a pore size of one micron.[2] The porous ceramic replaces a 2.5 cm length of ultrafine porosity fritted glass tubing previously used, and found to be unsatisfactory because of widely varying wall thickness and pore size. Ceramic frit has resulted in the construction of a more compact separator, the characteristics of which can be duplicated without extensive calibration of the particular section being used. Due to the thinner wall (higher conductance) of the ceramic, it is possible to use shorter lengths for enrichments similar to those obtained with glass frits. Smaller pore sizes are being tested to see if it is possible to substantially improve enrichment characteristics. As with a glass frit, silanizing eliminates thermal decomposition of polar compounds in the separator.

The mass spectrometer is interfaced to a small digital computer (4 K core), which has two 32 K disks for data and program storage. Peripheral equipment includes a teletype, high speed paper tape reader and punch, and digital plotter. Synchronization of the start of a magnetic scan and computer sampling is accomplished by a double throw relay in the repetitive scan circuit. Although time - to - mass conversion routines are incomplete, several programs have been written which utilize the reporducibility of repetitive scanning.

Signal enhancement resulting from point by point addition of repetitive scans effectively increases the dynamic range and sensitivity of electical detection mass spectrometers, in a manner similar to that described recently by Biros.[3] Figure 1 illustrates the integrative capability of signal addition. In a case where only noise spikes are visable after one scann, real peaks can be discerned after addition of forty scans. Resolution is not significantly degraded by scan addition as shown in Figure 2. A single scan was recorded at high sensitivity; the multiplier gain was reduced, and the doublet was scanned and added ten times. Further reducing the multiplier gain, and scanning over the doublet 100 times shows little loss in resolution. Thus signal enhancement by scan addition may be used at high m/e values with confidence. Figure 3 shows a portion of a spectrum of a molecule for which no measurable peaks could be observed above m/e 1100 with conventional oscillograph recording.

Signal enhancement by scan addition is of particular value for detecting weak ions and measuring isotope ratios for compounds emerging from the gas chromatograph. Maximum chromatographic resolution results in broadened peaks - i.e., low concentrations of sample entering the ion source over a period of time. Scan addition allows the chromatographer to take advantage of maximum resolution, without losing the sensitivity which results from having a high concentration of sample in the ion source over a short period of time. The use of stable isotopes to label ingested compounds will become the major method for human metabolism studies as carbon-13 enriched compounds become available at reasonable prices. In addition to cost, most investigators have been deterred from the usage of stable isotopes by the difficulty of detecting and accurately measuring them, particularly when compared to the ease of using carbon-14. Safety and the desirability of a macro-quantity tracer will make carbon-13 more popular, if adequate methods of detection and quantitation are available. Gc-ms is useful for metabolite separation and identification, but not for accurate isotope measurement. Signal integration produces more accurate intensity data, particularly for weak peaks. For major ions, the signal may be averaged with respect to the number of scans. Results of a point-by-point averaging routine applied to two ions in a chloroform spectrum run at constant sample pressure are shown in Table I. It is apparent that the larger the number of averaged scans, the more precisely peak intensities will be determined. The degree of accuracy will depend to a large extent upon conditions employed for chromatographic introduction of the sample, mass range to be scanned, scan rate, and the parameters used to define a peak. Programming efforts are being continued to enable automatic determination of isotope content in a labeled molecule as it emerges from the gas chromatograph.

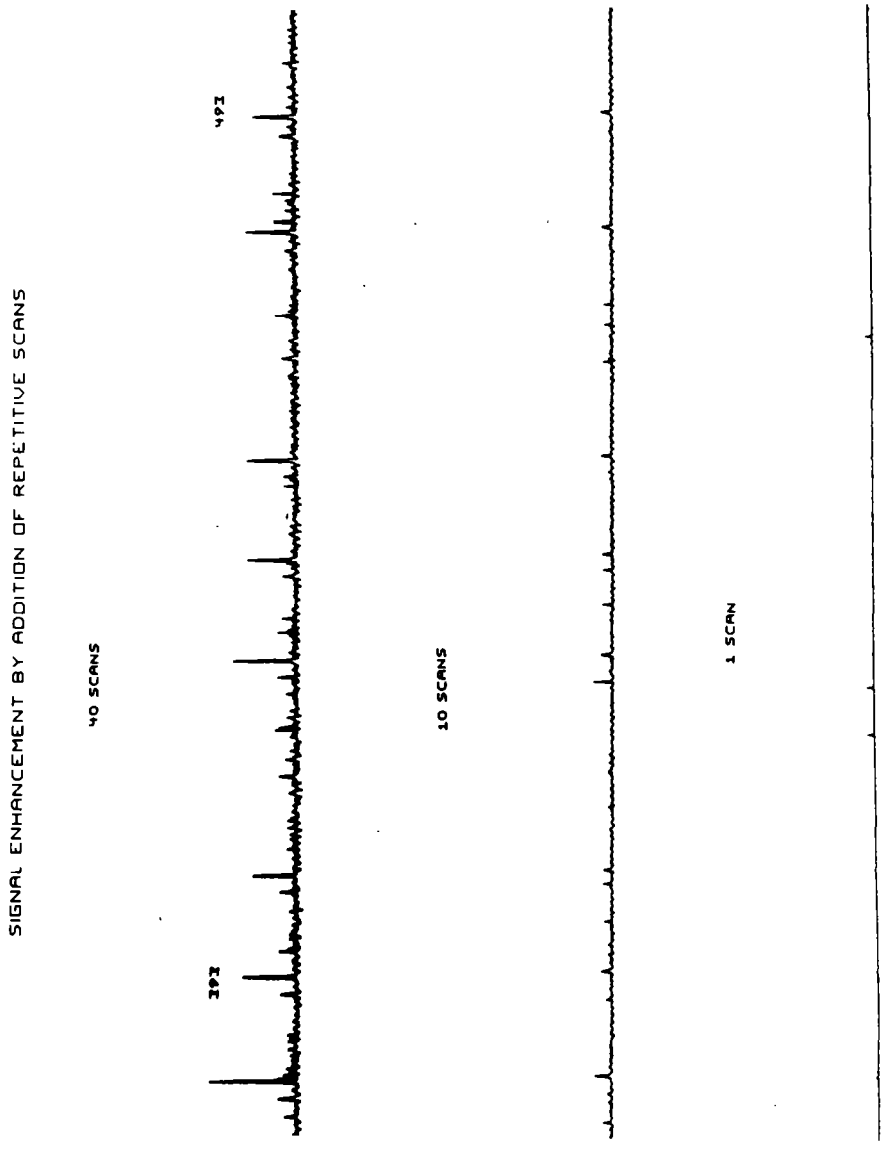

Figure 1.

Signal ENHANCEMENT By Addition of Repetitive Scans.

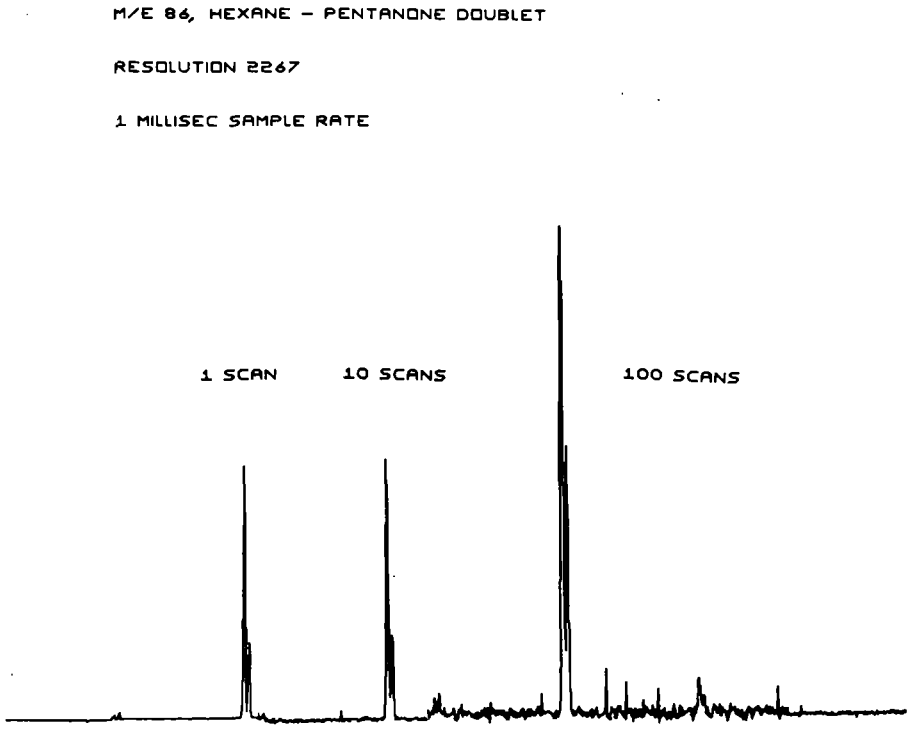

Figure 2.

Retention of Resolution During Repetitive Scanning.

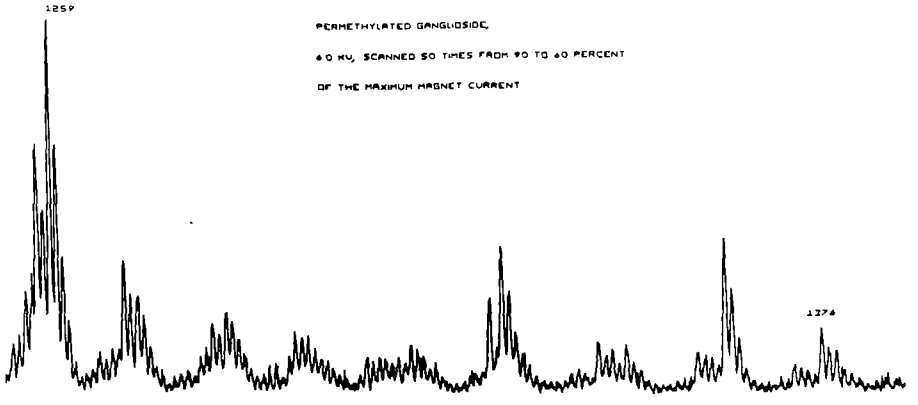

Figure 3.

Repetitive Scanning At High m/e Values For A Compound Showing No Peaks Above m/e 1000 By Conventional Recording.

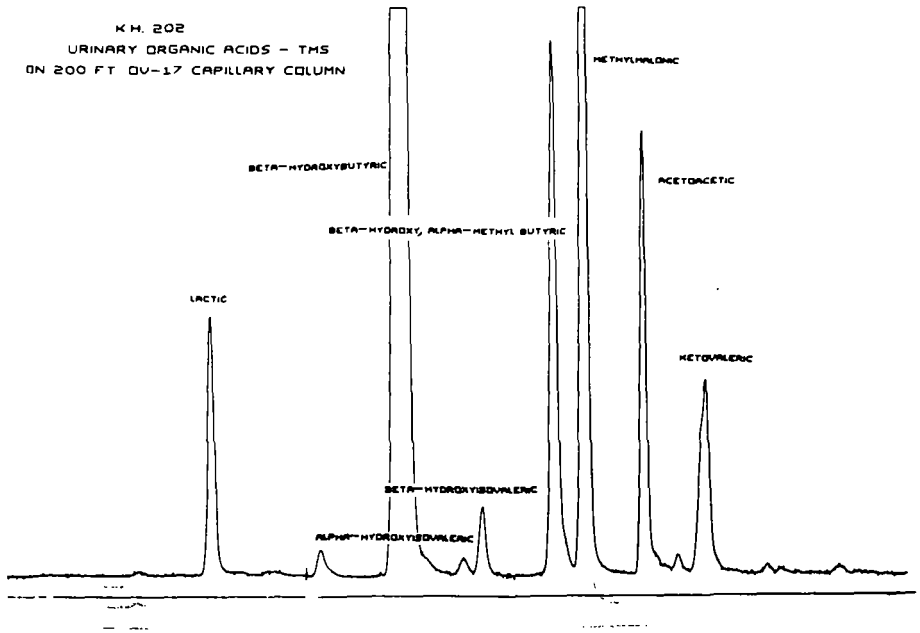

Figure 4.

Tentative Identifications Of Urinary Organic Acids From A Methylmalonic Aciduria Patient.

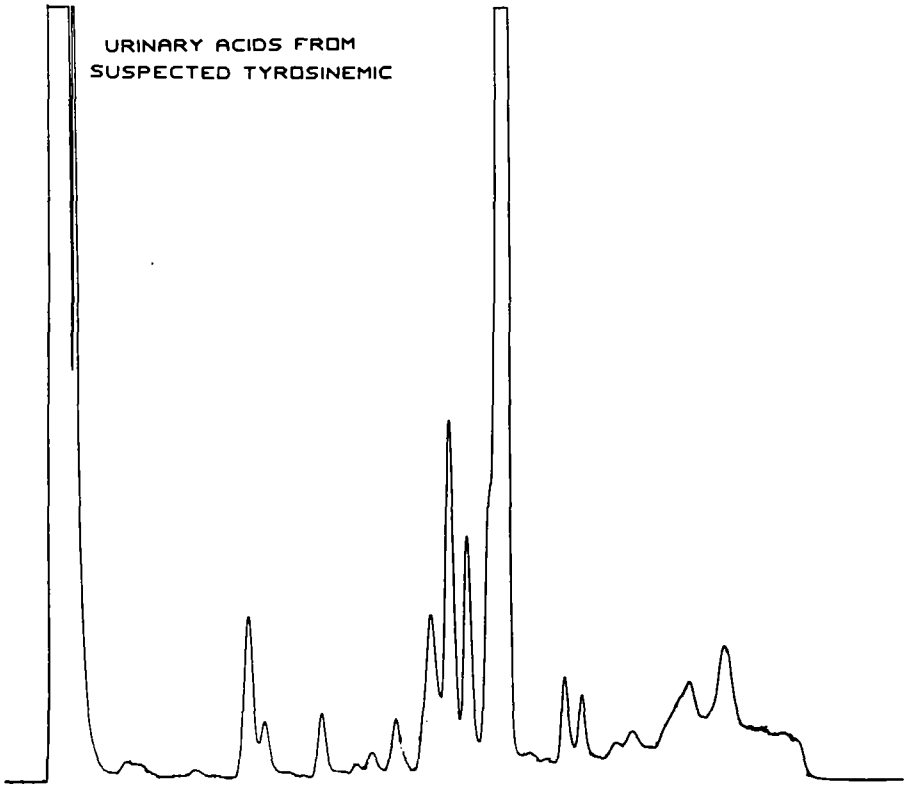

Figure 5.

Chromatogram Of Urinary Organic Acids From A Suspected Tyrosinemic.

Table 1. Increased Reproducibility of Intensity Data by Scan Averaging

No. Scans (3 trials)	Mean Ratio of Intensities m/e 117/119	Standard Deviation
1	.99415	.0894
10	1.0237	.0425
20	.9935	.0277

The metabolic research problems encountered using the above instrumentation differ with respect to the clinical information sought. It may be important to identify minor as well as major components; to establish the absence of certain compounds; to confirm identifications based upon gc data alone; or to identify a previously unreported compound.

The first example deals with the identification of minor components. In methymalonic aciduria, excessive amounts of methymalonic acid are excreted by children who presumably lack the means to convert it to succinate. Several cases have been found by our screening program. Some patients appear to respond to large doses of Vitamin B_{12}, co-factor for the isomerase which converts methylmalonyl-CoA to succinyl-CoA. Other patients grow weaker and die, although their levels of methylmalonic acid decrease. Initially, the analytical problem was to identify methylmalonic acid; then the question arose as to the identity of other organic acids present in higher than normal amounts. Mass spectra of the acids (TMS derivatives) as they emerged from packed columns showed imcomplete resolution. The spectra obtained as they emerged from a 200 ft OV-17 capillary column permitted the identifications shown in Figure 4 to be made. Of particular interest are the presence of alpha and beta-hydroxyisovaleric, and alpha-methyl, beta-hydroxybutyric (tentative), which could arise from a block in the metabolism of leucine and isoleucine. This suggests a generalized metabolic lesion, affecting several enzymes.

A second example is that of a premature infant, who was thought to have tyrosinemia - an inborn error of tyrosine metabolism associated with the lack of para-hydroxyphenylpyruvic acid oxidase. The chromatogram of extracted organic acids (TMS derivatives) is shown in Figure 5. Metabolites of tyrosine (para-hydroxyphenyllactic, phenylacetic, etc.) were expected, and the observed peaks had suitable retention times. Mass spectra revealed the major component was not a metabolite of tyrosine, but was an aromatic compound which could only arise from drug metabolism. The patient was found to be on heavy doses of anticonvulsents (phenobarbital, dilantin) which adequately accounted for the other excreted organic acids. In this case, mass spectra clarified a confusing situation. Supplying positive results within a few hours can save days of misdirected efforts as well as help in diagnoses.

The third example is an identification of an abnormal metabolite, previously unreported. The patient was observed in hematology clinic to have an unusual odor, particularly noticeable during an illness. A fishy smell was present in urine, but became imperceptable upon standing. A mass spectrum of the volatile components of raw urine (liquid inlet system) led to a tentative identification of trimethylamine. This was substantiated by gc-ms using a column suitable for the separation of low molecular weight amines. Trimethylamine is a metabolite of choline, normally excreted as its N-oxide. Enzyme assays are in progress to confirm this patient's inability to oxidize trimethylamine.

The cited examples and description of instrumentation indicate the current role and anticipated applicability of gc-ms to clinical research problems.

References
1. S. P. Markey, Anal. Chem., 42:306, 1970.
2. Landay Scientific Glass, Inc., Boulder, Colorado.
3. F. J. Biros, Anal. Chem., 42:537, 1970.

Analyzing Breath and Air (10^{-6} to 10^{-12} sensitivity) by Counting Ions Through A Quadrupole and Searching a Library of Spectra Regressively. NORMAN MILLERON, University of California Lawrence Radiation Laboratory, Berkeley, California 94720

Neither the principle metabolite (CO_2) nor the other gases abundant in breath[1] and air are central here. Rather, this paper reports work in progress aimed at exploration of metabolites in breath and substances in air in the two sensitivity ranges $1\text{-}10^{-6}$ and 10^{-6} to 10^{-12}. The equipment and techniques used are as follows: 1) A commercial quadrupole mass filter (E.A.1.200) modified to count each and every ion striking an E.M.I. 20 stage electron multiplier[2] during time intervals set by the steps of a D.C. staircase, each step corresponding to an M/e in the range 45-145; 2) a liquid helium cryopump around the ionization stage of the quadrupole; 3) a molecular beam sample inlet; 4) analysis of the ion counts using a stepwise regression code[3] to search a library of unknown or known spectra; 5) a 200°C ultraclean vacuum system for drawing off the original sample; 6) a membrane filter[4] to discriminate against abundant gases; 7) alternatively, a quadrupole lens in series with the E.A.1.200 permitting exclusion of all M/e below some number, i.e., 45.

The rationale behind the choice of these equipments and techniques is as follows: The modified commercial quadrupole was already in house; thus a least cost feasibility step is made possible to answer the question, "Should a second step be undertaken." In our second step program, we plan to develop a quadrupole instrument along the trail blazing lines demonstrated by J. M. Nitschke in his on-line isotope separator.[5] Nitschke's accomplishments[5] that are of especially great importance in our breath and air studies are: his magnetron ionizer having 1% efficiency and operating on a large cross sectional area molecular beam; and his rf only first quadrupole lens (related to W. Brubaker's[6] segmented rod idea) that serves two important functions: 1) it acts as a high pass filter splitting off all M/e $\leq$ some number, say 45; and II) reduces the large loss of ions due to their deflection by the fringe field at the entrance to the high resolution mass filter lens.

Naturally occurring (pure) air contains a number of gases made up of isotopes. From molecular weight 45 and up these are as follows: carbon dioxide, nitrous oxide, nitrogen dioxide, ozone, krypton, xenon, uranium hexaflouride and radon (these two latter are present in concentrations too small for us to anticipate seeing in our first step).

Splitting of the sample, in our first step, will be done electrically within the E.A.I. quadrupole mass filter lens. Splitting the sample in this manner (after ionization within the high resolution lens) limits the number of molecules that can be analyzed per unit time, because the maximum amount of electrical charge that can pass into the mass filter lens per unit time is fixed by space charge effects. Note: J. M. Nitschke's tandem lens system and ionizer increases the number of molecules that can be ionized and processed per unit time from about 10^{12}/sec to about 10^{16}/sec. Scanning can continue without accumulating undue noise for times up to 10 minutes. As a step for the future, it may be straightforward to program Nitschke's high pass lens and thus cast out the giant size peaks and their fragments (less than 15 in number in the range M/e 1 to 49) while keeping all the little peaks (at least 35 in number).

We propose to test the feasibility of analyzing air, breath and skin respiration at a combination of sensitivity and short time rate never before reported. Our case rests upon engineering rather than invention, for probably nothing we propose to do is patentable. By consensus of mass spectrometer experts at L.R.L., the problems presented by our gas sampling system offer perhaps the most technical challenge, the other necessary technical art having been already demonstrated.

It is worth remarking that the total number of all organic compounds known that have molecular weights less than or equal to 500, present in or derived from any of the living plants or animals (including microorganisms) probably is not much greater than 3000.[8] This number is interestingly small compared to the millions of organic compounds know to be possible. Life forms are apparently economical. Conceivably then, one could handle all of the metabolites associated with living things by establishing twenty libraries of spectra.

Stuff found in air is far more complex, however. This is because machines make more complex garbage than do living systems. For example, upwards of 12,000 chemical compounds have been found in the atmosphere inside a nuclear submarine.[9]

1. K. T. Fowler, Phys. Med. Biol. 14, 2, 185-199, 1969.
2. N. Milleron, R. Wolgast, J. M. Nitschke, Proc. 4th Intl. Vac. Cong., 1968.
3. D. D. Tunnicliff, P. A. Wadsworth, Anal. Chem. 37, 1082-5, 1965.
4. D. E. Green, Western Pharmacology Society, Vol. 12, 69 pp. 50-54, San Francisco.
5. J. Nitschke, Nucl. Inst. and Methods, Feb. 1, 1970.
6. W. M. Brubaker (private communication).
7. M. W. Miller (private communication, 1970).
8. H. J. Morowitz, Energy Flow in Biology, 1968, Academic Press.
9. F. E. Saalfeld and R. A. Saunders, Invited paper, I2, 18th Annual Conf. on Mass. Spectrometry, June 14-19, 1970, San Francisco, California.

Applications of GC-MS in Drug Metabolism Studies

S.R. Shrader, C. Hetzel
Wyeth Laboratories Inc., Philadelphia, Pa. 19101

and K. Fotherby
Postgraduate Medical School, London, England

Urine extracts from humans receiving the progestational agent (racemic 13β-ethyl-17α-ethynyl-17β-hydroxygon-4-en-3-one) I were examined by the combined gc-ms technique. Though a large number of endogenous steroids, and other material, was found in the extracts, drug-related compounds were easily recognized by the fragmentation behavior. In all cases, the extracts were silylated before injection onto the gc column.

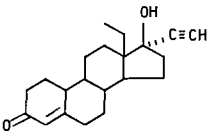

I

The fragmentation of I and its derivatives is characteristic, with a large M-C_2H_5 ion occurring in all cases. Endogenous steroids, containing only angular methyl groups, exhibit no such ion. In addition, fragmentation of the D-ring leads to characteristic ions at the appropriate masses.

The major metabolite of I is the reduced derivative II. In addition, we have identified the 3β-5β, 3α-5α, and 3β-5α isomers of this compound. Other metabolites include hydroxylated derivatives of both I and II.

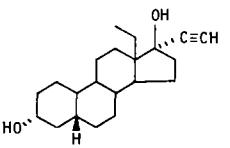

II

STRUCTURAL INVESTIGATION OF GLYCOPROTEINS USING A GAS CHROMATOGRAPH-MASS SPECTROMETER-COMPUTER SYSTEM;

Neuraminic Acid and Linkage Studies

V. N. Reinhold, J. Biller, and K. Biemann
Department of Chemistry
Massachusetts Institute of Technology
Cambridge, Massachusetts 02139

The application of gas chromatography-mass spectrometry-computer assisted analysis to structural problems in glycoproteins was introduced earlier (1). This quantitative and qualitative work on a number of glycoproteins from diverse sources allowed structural assignment to a wide variety of carbohydrate monomers derived from methanolyzed, silylated glycoproteins.

In the present work we have given additional attention to the neuraminic acid components found in glycoproteins in order to fully understand the gas-chromatography-mass spectrometry of these derivatives. This work was carried out with the analytical system shown in figure 1 (2).

Of the five acetylated and glycolated neuraminic acid derivatives, di- and triacetylated species and permutations of these are found in biological sources (3). Studies with 10-15 crystalline neuraminic acid derivatives has indicated that all appear to follow a fragmentation shown in figure 2; exemplified here with methyl N-acetyl neuraminate methyl ester.

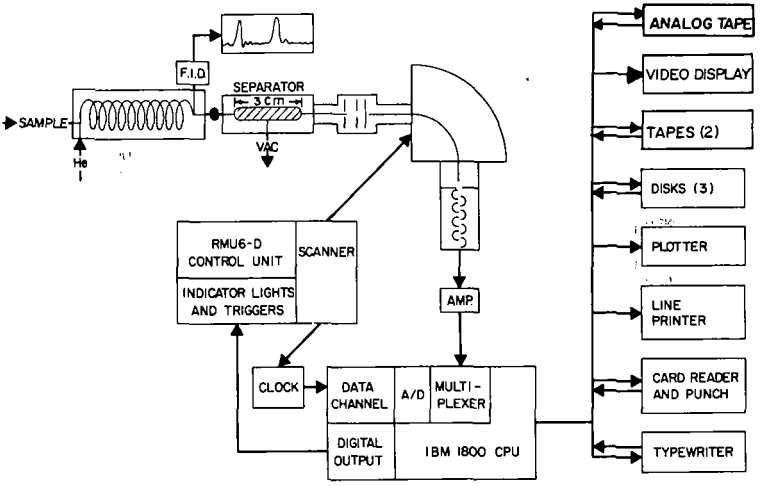

FIGURE 1

By observation of masses following the fragmentation pathways A, B, and C, one can quickly ascertain the degree of acetylation and/or glycolylation. By noting the appearance of peaks consistant with fragmentations following pathway D and E an assignment can be given to any of the possibilities observed in natural products.

The utility of this understanding is presented in figure 3 with results obtained from a study of the glycoprotein-rich fraction of

porcine blood serum. The top two "mass chromatograms" (2) of 508 and 420 readily show that the peaks at spectrum index number 170 and 190 in the total-ionization plot must be due to the N-acetyl and the N-glycolyl neuraminate derivatives, respectively, following cleavage analogous to D as indicated in figure 2. This assessment of "mass chromatograms" yielding "ion retention times" has provided a unique parameter to quickly ascertain the types of neuraminic acid derivatives obtained from enzymatic, hydrolytic or methanolically treated glycoproteins.

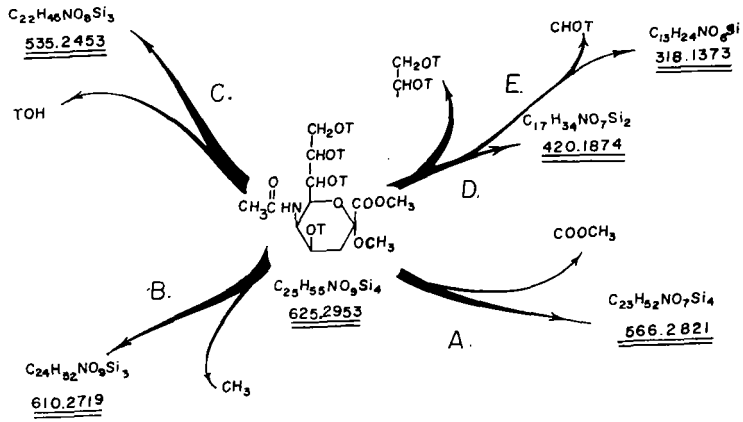

NEURAMINIC FRAGMENTATION

FIGURE 2

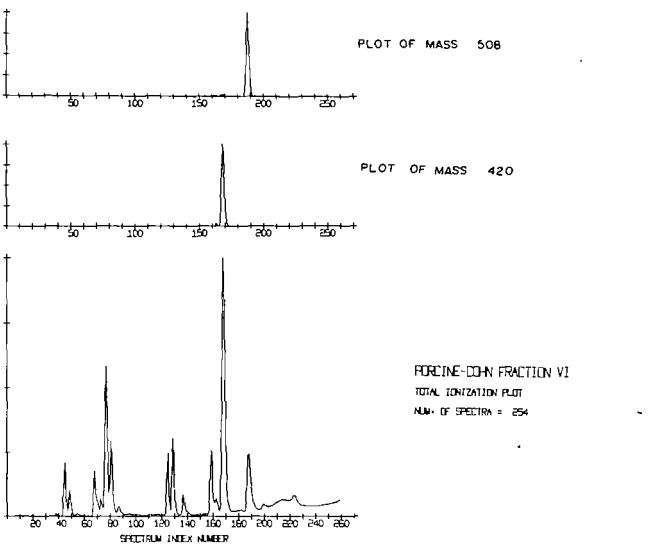

FIGURE 3

A very characteristic structural feature of a glycoprotein is the manner to which the carbohydrate side chain is linked to the protein core. At present there appears to be only three types of linkages involving the amino acids asparagine, serine and/or threonine and hydroxylysine. In this study we have been concerned with the first and third class, that is, the asparagine-glucosamine series found in the blood glycoproteins, and the hydroxylysine-galactose linkage found in connective tissue. The actual structures investigated in this work included mono- and disaccharides, linked to the above amino acids with variations in the linkage between the component moieties. All compounds were characterized by conventional techniques and this work has allowed us to study the limits of mass spectral intrepretation of ring size, amino acid present, linkage type and sequence arrangement.

All compounds were analyzed as their trimethylsilylated analogs and their molecular weights ranged from 695 to 1206 amu. The derivatives were gas-chromatographed on lightly loaded silicon coated non-porous glass beads. Compounds of greater than 700 amu exceeded the present low-resolution mass spectral-computer assisted calibration limit and thus higher-mass ions along with their resultant exact mass values, were obtained from a high resolution mass spectrometer.

The spectrograms of aspartyl glucosamine showed the presence of the molecular ion along with the fragments indicating methyl, trimethylsilyl, carboxyl, and trimethylsilanol loss from the molecular ion. Glycosidic cleavage and the ions characteristic of a 2-acetamido-2-deoxy-hexopyranose were easily identifiable. Analysis of a similar compound but with an additional glucosamine residue linked β(1-4) to the amino hexose again yielded the molecular ion along with ions indicating loss of the asparaginyl and asparagine-glucosaminyl residue, see figure 4. Comparison of this compound with a similar derivative, only linked B(1-6), resulted in an ion characteristic of this linkage and not observed in the B(1-4) compound.

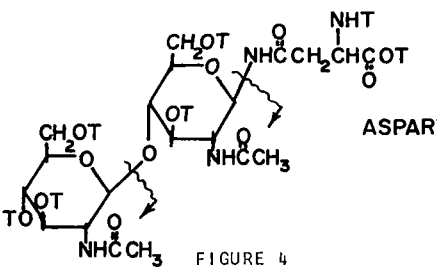

FIGURE 4

Analysis of the glucosyl-galactosyl-hydroxylysine, see figure 5, linkage compound yielded the expected fragment ions for the hexose, and hexose disaccharide along with the smaller ions of further fragment-ion arising from each component moiety. The molecular ion was not observed with this derivative but the exact mass ion of M^{+} -73 and the M^{+} -90 indicated the expected composition. The sequence information indicated a (1-2) hexopyranoside disaccharide linked to hydroxylysine.

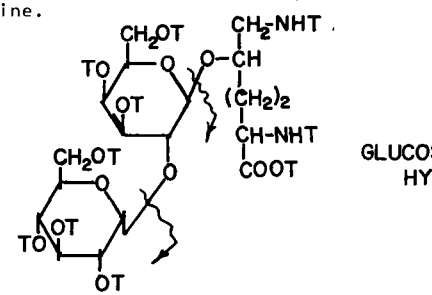

FIGURE 5

The known sequence of glucosyl-galactose could not be assigned by this analysis and the derivative galactosyl-glucose may well yield identical spectra.

Results presently indicate that using this analytical approach would provide a facile method to characterize glycoprotein linkage regions along with considerable detail into carbohydrate fine structure. The degree of fine structural information available from a mass spectra will be further pursued by comparison with other carbohydrate derivatives.

Acknowledgement

The authors would like to acknowledge the assistance of Dr. Charles Hignite for high resolution analysis.

Many samples used in this work have been kindly provided by Dr.R. Jeanoz, Harvard Medical School, Boston, Mass.

This work was supported by NASA Research Grant No. NGR 22-009-005.

References

1. V. Reinhold and K. Biemann, Proceedings of the 17th Annual Conference on Mass Spectrometry and Allied Topics, Dallas, Texas, May, 1969.
2. Ronald A. Hites and K. Biemann, Anal. Chem. 42, 855 (1970).
3. Von Roland Schauer and Hans Faillard, Hoppe-Seyler's Z. Physiol. Chem., 349, 961 (1968).

Mass Spectra of some germacranolides and furanogermacranolides

K.G.Das, M.S.B.Nayar, V.H.Kulkarni and S.K.Kelkar
National Chemical Laboratory, Poona-8, India.

With a view to correlate the fragmentation modes and structural features a comparative study of the mass spectra of some germacranolides and furanogermacranolides has been made.

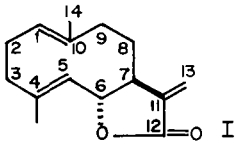

I

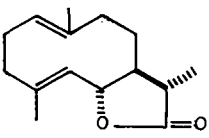

II

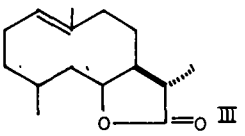

III

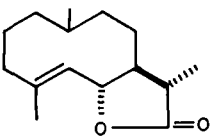

IV

The general fragmentation modes operating in these compounds were established from high resolution data and metastable transitions. Deuterium labelling technique was employed wherever feasible for further confirmation of the postulated mechanisms. To support the fragmentation modes induced by the lactone ring, a comparative study was made with the mass spectra of C8-desoxy esters prepared from these lactones.

Some of the characteristic features in the spectra of these lactones are (i) a significant parent ion (ii) fragments corresponding to the direct and successive loss of a methyl radical and a molecule of carbon monoxide from the molecular ion. The general fragmentation modes observed in the mass spectra of these lactones are: loss of 44 (CO_2), 55 (C_4H_7, C_3H_3O), 57 (C_4H_9, C_3H_5O, C_2HO_2), 59 ($C_2H_3O_2$), 71 (C_5H_{11}, C_4H_7O, $C_3H_3C_2$), 73 ($C_3H_5O_2$) and 83 (C_6H_{11}, C_5H_7O) mass units from the parent ion.

The C8-desoxy esters show a preferred loss of the side chain ($C_4H_7O_2$). The general fragmentation modes observed in the lactones appear to operate from the M-$C_4H_7O_2$ ion in these esters.

The furanogermacranolides studied are shown below.

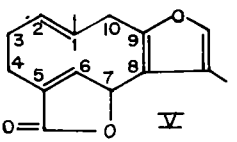

V

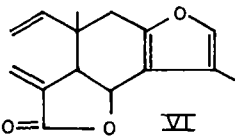

VI

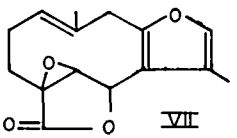

VII

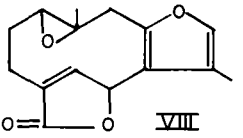

VIII

The main fragmentation modes of linderalactone are (i) loss of CO_2H, (ii) elimination of C_4H_7 (iii) formation of m/e 148, m/e 121 and m/e 93 fragments.

To study the effect of epoxidation of the Δ 1-2 and Δ 5-6 double bonds on the fragmentation processes, the mass spectra of linderane, neolinderane, zeylinicine and zeylinicine were examined.

These epoxides appear to rearrange to the ketones under electron impact. This is supported by the further fragmentation modes of these supposed intermediate ketones.

References:

1. K.N.Sathe, S.H.Kulkarni, G.R.Kelkar and K.G.Das, Org.Mass Spectrom. 2, 935 (1969)

2. L.Tsai, R.J.Highet and W.Hertz, J.Org.Chem. 34, 945(1969) and references sited therein

3. S.M.Kupchan, Ayuchchi, J.M.Cassady, H.K.Schnoes and A.L. Burlingame, J.Org.Chem. 34, 3867 (1969).

E1

DECONVOLUTION OF IONIZATION EFFICIENCY DATA AS A MEANS OF DETERMINING FRAGMENTATION MECHANISMS IN THE MASS SPECTROMETER*

Harry J. Svec and Gerald D. Flesch

Institute for Atomic Research and Department of Chemistry
Iowa State University, Ames, Iowa

As a result of the interactions between electrons and molecules in the ion source of a mass spectrometer, positive and negative ions and neutral fragments of molecules are formed. If chemists are to understand fully the reactions involved they must be able to observe and measure the characteristics of all these particles. As you know from past presentations we have made here, we have successfully built a mass spectrometer which simultaneously detects positive and negative ions and another which detects neutral fragments. Aside from detection and mass measurement, these instruments also are capable of characterizing the various types of particles according to the energy required to form them and whether or not they possess excess translational energy when they are formed. One measures ionization efficiency curves to obtain data about the first and retarding potentials to obtain information about the second. However, these data are not always interpretable in a simple way. Indeed, even for simple molecules, one cannot always assume simple ion source chemistry, especially where fragment ions are concerned. What we have been attempting to do about this is the subject of this paper.

Our initial development was based upon data from two methane-like molecules, CrO_2F_2 and CrO_2Cl_2. They were chosen because the compounds are quite volatile and the various possible fragments uniquely characterizable. Furthermore, the possible neutral fragments which are formed when either positive or negative ions dissociate have easily observable energy requirements. Despite the fact that we have worked with both positive and negative ions (Int. J. Mass Spectrometry Ion Phys. 3 339 (1969)) we will consider only positive ions today. Figure 1 shows the ionization efficiency (IE) curves for all of the possible positive ions from chromyl chloride (A) and chromyl fluoride (B). Noteworthy about these data is that they are recorded automatically and thus the solid lines represent an "infinity" of data points. Furthermore, the shape of the IE curves for the fragments indicate complex origins for these ions. One origin depends upon the fact that different chemical reactions are occurring as a function of the electron energy. Figure 2 shows an example of this for the fragment ions CrF^+ and $CrCl^+$. Ionization efficiency curves for these ions have been simply deconvoluted to account for the reactions:

*Work was performed in the Ames Laboratory of the U. S. Atomic Energy Commission.

$$CrO_2F_2^+ \rightarrow CrF^+ + O_2 + F, \text{ a low energy process}$$

and

$$CrO_2F_2^+ \rightarrow CrF^+ + 2O + F$$

on the left and:

$$CrO_2Cl_2^+ \rightarrow CrCl^+ 2O + Cl,$$
$$CrO_2Cl_2^+ \rightarrow CrCl^+ OCl + O$$

and

$$CrO_2Cl_2^+ \rightarrow CrCl^+ + O_2 + Cl$$

on the right. Although the energy differences are difficult to discern from the figure, determination of the onset potentials corresponding to each chemical process by the extrapolated difference method, yields values corresponding to the bond dissociation energies of O_2 and OCl within the experimental uncertainties. The molecule OF is not observed because it has at best only an emphemeral existence, doubted by some.

Such treatment of IE data is however insufficient to account for all possible precursors of fragment ions. Since a knowledge of precursors of fragment ions is the essence of this symposium, we now turn to a description of a scheme we have developed for deconvoluting IE data in order to account for all possible reaction paths.

During this symposium you will be hearing of a variety of methods for obtaining information about ion fragmentation paths in the mass spectrometer. The principal direct evidence that a reaction may occur is the observation of metastable ions, but these are limited generally to reactions with lifetimes > 10^{-6} seconds, and do not necessarily account for the majority of very much faster reactions taking place in ion sources. Isotope labelling may also give information about reaction paths although it is not always possible to do labelling experiments and labelled compounds can be difficult to make. Clastograms sometime give an insight into possible reactant-product ion pairs but they are useful only if the product-ion abundance represents a large fraction of the reactant-ion abundance. Appearance potentials of fragment ions can be useful but generally they give no information concerning which of several possible paths is most probable. Lifshitz and Long (J. Chem. Phys. 41 2468 (1964)) and Cantone, Grasso and Pignataro (J. Chem. Phys. 44 3115 (1966)) have used the changes in slopes of favorable fragment ion IE curves to assign fragmentation paths for simple molecules. We have extended this idea to the deconvolution of IE data as a means of observing changes in slope. Although we will be citing data from the chromyl halides representing work done during the development of the method, it has already been applied to the Group VI A hexacarbonyls, some substituted ferrocenes and most recently we have begun on some esters of acetic acid.

The IE data in our experiments were obtained with an ionizing electron beam of 2 μa collimated by a ~125 gauss magnetic field. The energy spread of the electrons was 0.7 eV at half height. Ion source residence times for the ions of interest were 1-5 μsec. As stated earlier, the IE data were automatically plotted with an XY recorder

and the data were recorded over the 18 volt energy range immediately above the ionization potential of the molecule under study. Onset potentials were obtained by the extrapolated difference method.

The deconvolution procedure is based upon several assumptions which are similar to those of Lorquet (Ninth ASTME-14 Conference on Mass Spectrometry, Chicago, June 1961) in his non-statistical approach to mass spectra. These are given in Table 1.

Table 1. Assumptions

1. The parent ion is the direct or indirect presursor for all the fragment ions.
2. Fragmentation reactions proceed independently of each other.
3. The total-ions IE curve shape is that for the parent ionization and each fragmentation reaction.
4. The experimental IE curve observed for an ion is the sum of the individual IE curves for reactions related to that ion.

The first assumption is widely accepted. The second assumption is the key to the method. Since the conditions attained in the mass spectrometer ion source essentially prevent interactions between the various ions, each decomposition proceeds independently and is determined by the particular energy state to which the molecule-ion is excited.

The third assumption is required so that a reference IE curve shape for the deconvolution procedure can be determined experimentally. This *total ions IE curve, or more simply, total ionization (TI) curve, is* the sum of the observed IE curves for all of the ions of the compound in the 18 volt energy range above the molecular IP. In order for this to be valid, the detection efficiency of all ions should be equal and their kinetic energy zero or negligible. Direct measurement of the detection efficiency indicates that the ions from molecules we have studied are indeed very nearly equal and even in cases where they are different, the difference is ~5% or less. Direct measurements of excess kinetic energies indicate values of a few-hundreths of an eV or less in the (IP +18) volt energy range even for highly fragmented ions. The last assumption is a consequence of assumption 2 and is required in order to be able to correct the data for subsequent decompositions of the product ions.

An example of how a deconvolution proceeds is illustrated with Figure 3 which treats the IE data for $CrOCl^+$ from chromyl chloride. In Figure 3A the open circles represent the observed IE data. The TI curve, which is the sum of all the IE curves, is translated along the energy axis and its amplitude adjusted until a good fit is obtained at the foot of the observed curve. (That this is proper is given in Figure 4 which shows the IE data for all of the fragment ions from the chromyl halides. The amplitudes are normalized at 2.0 volts above the onset potentials and plotted on a single graph. There is little doubt about the similarity of the shape of these curves in this onset region. Similar data exists for rare gases and ions from many other types of molecules.)

Returning to Figure 3A; after the fit is obtained, the modified TI curve is projected to the energy boundary and this projection appears as "Calculated I" in 3A. The shaded area between the curves represents $CrOCl^+$ ions produced by an additional, independent fragmentation process. The differences between the curves are calculated and plotted as "Deviation I", the open circles in 3B. Again the TI curve is fit to the foot of "Deviation I" by translational and adjustment of its amplitude. The TI curve is again projected to the energy boundary, and the result is shown as "Calculated II", closed circles, on Figure 3B. This time there is a negative deviation between the data indicating that $CrOCl^+$ formed at the higher electron energies is disappearing due to decomposition into some other species. The negative deviation (difference between the two curves) indicated by the shaded area is calculated and plotted as "Deviation II" in Figure 3C. Again the TI curve is translated and its amplitude adjusted so that there is a fit in the region of the foot. This time the factor used to adjust the amplitude has a negative sign. The adjusted curve is again projected to the energy boundary and appears as "Calculated III". The difference between these two curves is another negative deviation indicating still another path by which $CrOCl^+$ can be lost. Presumably in this case, this occurs by the simultaneous loss of both O and Cl. In Figure 3D, no differences are evident thus indicating no other processes are occurring. In the processes discerned by the data on the figure, $CrOCl^+$ was formed from the parent ion, $CrO_2Cl_2^+$ and from CrO_2Cl^+ and $CrOCl_2^+$. The energ etics indicate it decomposed by losing O to form $CrCl^+$ or by losing both O and Cl to form Cr^+.

In our handling of the deconvolution procedure the TI curve was translated in 0.25 eV steps. Thus, the best possible precision in determining an onset potential should be expected to be ± 0.25 eV. However, because of the arithmetic involved in obtaining onset potentials above the lowest value for each ion, the accuracy becomes less certain for each succeeding step. This must be kept in mind when comparing product and reactant ion onset potentials. Another important point is the low energy resolution of the method. Processes whose onsets differ by less than ~1.5 eV may not be separable and the deconvolution result may suggest a single process occurring at an average onset potential.

The IE data for all of the ions from CrO_2F_2 and CrO_2Cl_2 were deconvoluted and in each case the onset potential for each process and the ion abundance projected at the energy boundary was recorded. If our assumptions are correct, there should be a one-to-one correspondence between a negative deviation observed in the deconvolution of the IE data for one ion with a positive deviation in another. A partial listing of some of the results for chromyl chloride are shown in Figure 5. As you can see, the abundances of various reactant ions going to product ions is in good agreement. It is patently apparent that reactant ions are related to more than a single product ion and product ions related to more than a single reactant ion.

Once the pairings are made, a critical test of their validity is to be able to convolute IE curves on the basis of the ion-pairings and the projected abundances at the energy boundary. The convoluted curves are then compared with the experimental IE curves and ion abundances are calculated. We have done such calculations on the basis of a total abundance of 10000 units. Table 2 shows a comparison of abundances calculated on the basis of convolution, which in turn was based on the deconvolution results, with the observed experimental abundances. A measure of the fit between the convoluted and experimental data is the RMS-percent deviation between the two. We were pleased with the results given in column 4. When viewed as a single set of data the agreement between the two is within 3%.

Let us now examine some of the fragmentation schemes which we have derived for simple molecules. Figure 6 shows the fragmentation of CrO_2F_2 which is fairly simple. The algebraic sum of the relative abundances associated with each symbol gives the experimentally observed abundance. For example, we calculate that 21% of the parent ions decompose to form $CrOF_2^+$ but 6 of these 21 subsequently decompose further to give CrF_2^+II. This leaves a net observed ion current for $CrOF_2^+$ of 15% of the total ions. An interesting observation indicated on the figure shows that two metal-oxygen bonds, one metal-oxygen bond or one metal-oxygen and metal-fluorine bond are broken more often than one metal-fluorine bond. The data indicate that in some cases, although a molecule apparently has absorbed enough energy to eject either an oxygen or a fluorine, it does not do so unless both are ejected. Thus the total excitational energy may not always be accessible to a particular bond. Not only must the total energy be sufficient to break a bond, but also the energy must be properly distributed. This is a plausible reason why many bond dissociation energies calculated from fragment ion IE data are higher than those obtained by other means. On the other hand, some bond dissociation energies from fragment ion data may be too low because of unknown low energy reactions forming a fragment ion.

The fragmentation map for chromyl fluoride contains only 14 reaction-product pairs. That of chromyl chloride shown in Figure 7 is more complicated with 24 reactions taking place. Note that there are many ions specially designated with Roman numerals. These are apparently specific excited states of ions which are due to unique reactions occurring at different energies.

Figure 8 contains fragmentation maps for the hexacarbonyls of the Group VI A metals. The encircled numbers on the figure correspond to the number of carbonyl groups left attached to the metal atom. Thus (4)$^+$ refers to the $M(CO)_4^+$ ion. These data indicate that only $W(CO)_6$ decomposes by the stepwise loss of CO. However there is also a non-stepwise loss of CO. There is no direct decomposition of $Cr(CO)_5^+$ and $Mo(CO)_5^+$ to the $M(CO)_4^+$ ion. Also, in the case of $Mo(CO)_6$, there is no significant stepwise loss of CO to form $Mo(CO)^+$ and Mo^+.

The fragmentation of ferrocene, Figure 9, is interesting. The deconvolution not only indicates the direct stepwise loss of a cyclopentadienyl moiety but also a relatively minor path corresponding to the simultaneous loss of two cyclopentadienyl groups. The energetics of the reaction indicates that these are lost not as two separate cyclopentadienyl groups but as dicyclopentadienyl. This would be an interesting neutral fragment to observe directly!

In this presentation we have attempted to outline briefly a method for deconvoluting IE data. The method is an empirical one which is based upon reasonable assumptions. Its application gives reasonable answers to questions which have plagued us and others concerning why some ionization efficiency data give bond dissociation energies in good agreement with those obtained by other methods while other data give poor agreement. At present the procedure is somewhat crude because it lacks sufficient energy resolution. However, in spite of this, its use can give insights into the complexity of ion source chemical reactions which may not be amenable to the application of other techniques. Thus it can serve as a means of defining and giving supporting evidence for ion source reaction mechanisms. A detailed manuscript is being prepared describing more fully the method and the implications of results.

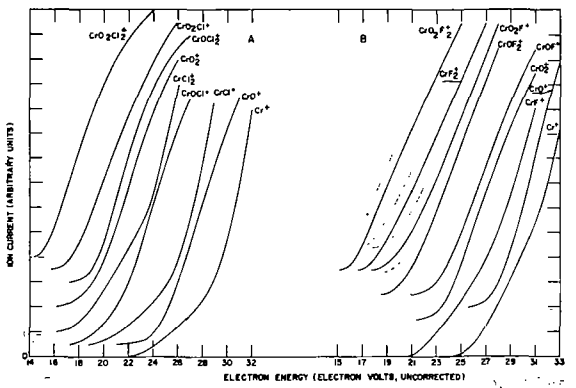

Figure 1. Ionization efficiency curves for the positive ions of CrO_2X_2. Base lines are offset for clarity.

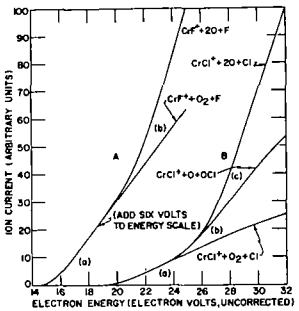

Figure 2. Deconvolution of IE curves for CrX^+.

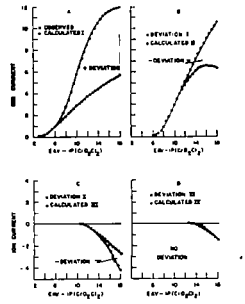

Figure 3. Deconvolution of $CrOCl^+$ (CrO_2Cl_2) ionization.

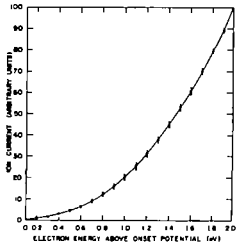

Figure 4. Average IE curve for the positive and molecular ions from CrO_2Cl_2 and CrO_2F_2. The indicated limits are one standard direction.

REPRESENTATIVE TABULATION OF ONSET POTENTIALS AND RELATIVE ION ABUNDANCES DETERMINED BY DECONVOLUTION OF IE DATA OF CrO_2Cl_2

Onset Energy Above	Reactants Ion	Reactants Abundance	Products Ion	Products Abundance
4.50			CrO_2^+	595
5.00	$CrO_2Cl_2^+$	865		
5.00			$CrCl^+$	106
5.50	CrO_2Cl^+	510		
6.00			$CrOCl^+$	905
6.75	$CrO_2Cl_2^+$	234		
6.75	$CrOCl_2^+$	12		
		1631		1606

Figure 5. Representative tabulation of Results from CrO_2Cl_2.

A COMPARISON OF CALCULATED AND EXPERIMENTAL DATA FOR THE IONS OF CrO_2Cl_2 AT THE ELECTRON ENERGY (IP + 18)eV

Ion	Calc Ions	Obs Ions	RMS % Dev
$CrO_2Cl_2^+$	4851	4828	0.6
$CrOCl_2^+$	187	189	3.8
$CrCl_2^+$	173	173	1.1
CrO_2Cl^+	2131	2138	1.0
$CrOCl^+$	1249	1193	2.3
$CrCl^+$	361	353	1.1
CrO_2^+	660	668	1.5
CrO^+	620	584	2.4
Cr^+	220	224	2.7

Table 2. A comparison of calculated and experimental data for the ions of CrO_2Cl_2 at the electron energy (IP^2+ 18) eV.

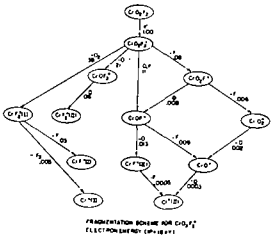

Figure 6. Fragmentation map of CrO_2F_2.

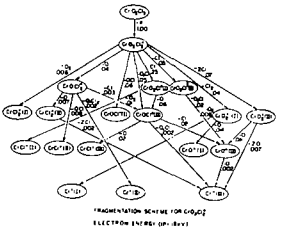

Figure 7. Fragmentation map of CrO_2Cl_2.

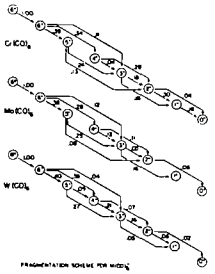

Figure 8. Fragmentation map of the group VI-A hexacarbonyls.

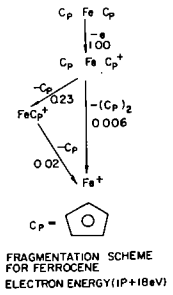

Figure 9. Fragmentation map of ferrocene.

SUBSTITUENT EFFECTS ON COMPETING CLEAVAGE AND REARRANGEMENT PROCESSES IN MOLECULAR ION DECOMPOSITION REACTIONS

Peter Brown

Department of Chemistry

Arizona State University

Tempe, Arizona 85281

Abstract

Ionization and appearance potentials have been determined for apparently competing M-CH_3 cleavage and M-CH_2O rearrangement reactions in a series of m- and p-X substituted anisoles, and for M-NO_2 cleavage and M-NO rearrangement processes in substituted nitrobenzenes. Approximate activation energies AP-IP have been found to give reasonably linear correlations when plotted against substituent constants (e.g., σ, σ^+). For the two reactions in the anisoles, the slopes of the plots AP-IP vs. σ^+ are positive; for the two reactions in the nitrobenzenes, the corresponding plots display negative slopes. It has been concluded from these data that in the M-CH_3 and M-CH_2O anisole reactions an additional degree of positive charge is developed at the reaction site, while conversely in the M-NO_2 and M-NO processes in the nitrobenzenes a degree of positive charge is dissipated at the reaction site. Reaction mechanisms are proposed for these reactions consistent with these energetic requirements.

The merits of AP-IP as a parameter that reflects rate are discussed, and compared with peak relative abundance methods (such as Z-values). The limitations of AP-IP are also discussed. Plots of log (Z/Z_o) and log $[A_o]/[M_o]$ (1-f) vs. substituent constants are reproduced and discussed also.

Submitted for publication in Organic Mass Spectrometry.

E5

Energetics and Metastable Ion Intensities in the Determination of Ionic Structure

J. L. Occolowitz
Eli Lilly and Company, Indianapolis, Indiana, U.S.A.

Introduction

The determination of the energetics of ionic reactions and the relative intensities of metastable ions have been used to deduce and compare the structure of ions produced in mass spectrometers. Usually the energetic method is used to find the heat of formation of an ion at the threshold or with just sufficient energy to undergo a reaction, and structural assignments are made by comparing this quantity with the heat of formation of an isomeric ion derived from another source. The determination of the abundance of metastable ions gives a measure of the kinetic behavior of reactingions.

Because of the isolated nature of ionic reactions, it is not valid to extrapolate results obtained for reacting ions to isomeric ions produced at the threshold. The energy difference of these ions (say, ~60 Kcal.mol.$^{-1}$) can allow for the participation of ionic structures having ground state energies intermediate between that of the ions produced at threshold and those having sufficient energy to react. Also, it can usually be shown that the structures of intermediate energy undergo the same reactions when excited to the appropriate internal energy.

Energetics

The heat of formation of an ion F^+ formed in the reaction

$$M - e \longrightarrow F^+ + N_1 + N_2 + \text{----} \qquad \text{——— 1}$$

can be calculated by the equation

$$\Delta H_f(F^+) = \Delta H_f(M) + A.P.\ (F^+) - \Sigma\Delta H_f(N) - E \qquad \text{——— 2}$$

where E includes such terms as relative translational energy, vibrational energy, and reverse activation energy. The uncertainty in $\Delta H_f(F^+)$ arises from the possible inability to determine the appearance potential of F^+ and E with sufficient accuracy. In assessing the method, it is necessary to discuss each of the possible errors in some detail.

1) Reverse Activation Energy. This is the energy required to initiate the reaction between F^+ and N when they are initially in their ground states. Its existence in ionic reactions has been queried on the basis that many ionic reactions occur without evidence of excess energy.[1] However, there are many ionic reactions in which considerable excess energy is involved; and this excess energy may include a reverse activation energy component. Further information may be obtained by studying the temperature dependence of ion-molecule reactions. In this context it has been stated that no activation energy has been found for any ion-molecule reaction studied. However, it transpires that the temperature independence of ion-molecule reactions is inferred implicitly from the experimental details and that often no temperature study was made.[2]

   It would seem that presently there is little evidence for or against the widespread occurrence of reverse activation energy in ionic reactions.

2) Kinetic Shift. Unless metastable species are being studied, critical potentials are determined on ions produced in the ion source. For fragment ions ion source residence times of ~1×10^{-6} sec. require a minimum reaction rate for observation of a particular species at the collector. Consequently, appearance potentials will be too high by the excess energy required to achieve this minimum reaction rate. Generally this reaction rate is taken to be ~10^5 sec^{-1}, because,[3] the maximum point in derivative ionization efficiency curves occurs at this rate and it is thought that the usual methods for determining appearance potentials give results

corresponding roughly to the maximum on the derivative ionization efficiency curves. However, rate constants of $5 \times 10^2 sec.^{-1}$ will give rise to an observable current at the collector (less than 1/1000 of the 50 ev current). Whether methods of extrapolation using electron-impact derived ionization efficiency curves, which have a super-imposed electron energy distribution, can give appearance potentials corresponding to rate constants of ~500sec.$^{-1}$ is a question still unanswered.

Lower limits for kinetic shifts have been deduced by measuring appearance potentials for normal and metastable ions resulting for a given ionic reaction. For some reactions of disubstituted benzenes the appearance potential for the metastable ion is ~0.5ev lower than for the normal ion.[4]

3) Vibrational Energy. There is general agreement that many ionic reactions at the threshold result in vibrationally excited product ions and neutrals. However, methods to detect this vibrational energy are either of limited applicability[1] or based on doubtful premises.[5]

For reacting ions of less than about ten atoms, it has been shown[1] that the vibrational energy is related to the translational energy released by the equation

$$E = \alpha NT \qquad \text{——— } 3$$

where T= translational energy release, N= number of degrees of freedom in the reacting ion, α= an empirical constant (~0.45), and E= total vibrational energy. T was determined from the peak shape of the product ion using a time-of-flight mass spectrometer. Using this approach a number of heats of formation have been successfully determined.[6] One puzzling aspect of this method is that translational energies derived from the T.O.F. instrument are considerably greater, for randomely selected cases, than those determined from metastable peak widths on a magnetic sector instrument.[7] Also, application of equation 3 to more complex molecules seems doubtful, e.g. in the reactions

$$\rightarrow C_5H_6^{+\cdot} + \begin{cases} CO, & R=OH \\ HCN, & R=NH_2 \end{cases} \qquad \text{——— } 4$$

the kinetic energy release for the reaction of aniline is zero and for phenol 5 Kcal.mol.$^{-1}$ (both determined from metastable peaks[8]). Assuming that both reactions give rise to C_5H_6 ions of similar structure, then similar heats of formation are to be expected. Correction of the heats of formation using equation 2 results in values of 278 Kcal.mol.$^{-1}$ and 216 Kcal.mol.$^{-1}$ for the heats of formation of the C_5H_6 fragment ions from aniline and phenol respectively. Not only are these values considerably different but the value for phenol is 21 Kcal.mol.$^{-1}$ lower than that for the C_5H_6 ion derived from cyclopentadiene, the lowest energy structure likely to be formed.

A method has been devised[5] to qualitatively demonstrate excess energy in one pair of ions having the same structure. For the reactions

$$M^{+\cdot} \longrightarrow A^{+\cdot} \xrightarrow{m^*} B^+ \qquad \text{——— } 5 \text{ Indirect}$$

$$A^{+\cdot} \xrightarrow{m^*} B^+ \qquad \text{——— } 6 \text{ Direct}$$

$A^{+\cdot}$ in reaction 5 is said to be formed with excess energy if the relations

$$\frac{[A]}{[B]}_{\text{Direct}} > \frac{[A]}{[B]}_{\text{Indirect}}$$

$$\frac{[A]}{[m^*]}_{\text{Direct}} > \frac{[A]}{[m^*]}_{\text{Indirect}}$$

$$\frac{[B]}{[m^*]}_{\text{Direct}} < \frac{[B]}{[m^*]}_{\text{Indirect}}$$

are observed. The figure below (Fig. 1) shows a hypothetical situation where $A^{+\cdot}$ in the indirect reaction is formed with no excess energy but where the molecular ion energy distributions are somewhat different.

FIGURE 1

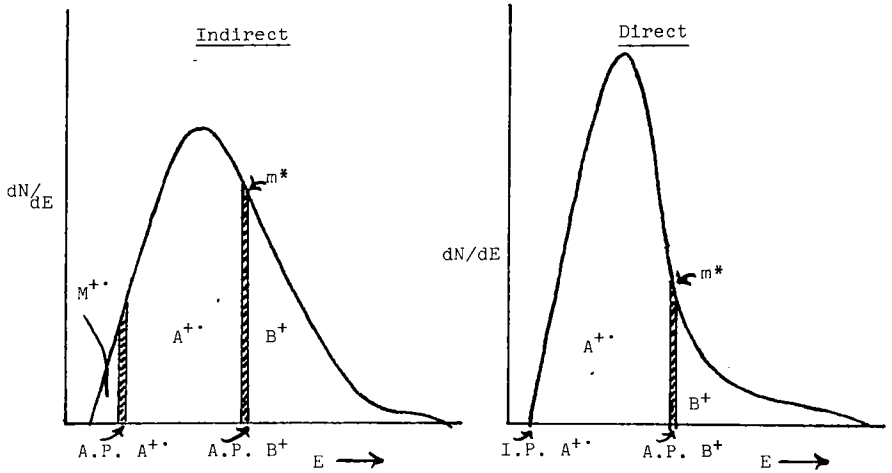

For simplicity it is assumed that the k(E) vs. E curves for the reactions are steep so that the relative abundances of $A^{+\cdot}$ and B^{+} are represented by the appropriate unshaded areas under the curves; and also that the abundance of m* can be estimated from the distance between the E axis and the point on the curve vertically above the appropriate appearance potential. For this system the inequalities which indicate excess energy in $A^{+\cdot}$ formed indirectly are observed, but in fact it is formed with no excess energy.

It is doubtful, in most cases, whether the inequalities give any indication of excess energy in a fragment. They most likely measure differences in molecular ion energy distributions and the position of critical potentials on these curves. The positions of these critical potentials will depend not only on whether excess energy is involved but also on the enthalpies of the reactant molecule and the neutral product expelled.

4) Errors Due to Temperature. The vibrational energy acquired by a molecule prior to ionization can be utilized in the subsequent fragmentation of the molecular ion. Hence the appearance potential will be lower than would be observed using a less thermally excited molecule. In the calculation of the heats of formation of fragment ions, this error would be lowered if the heat of formation for the molecule at the temperature of ionization was used in equation 2. Usually such information is not available and a value for a lower temperature is substituted. In these instances the calculated heat of formation of the fragment will be lowered, perhaps cancelling out any error arising from kinetic shift. Of all the errors discussed here, this is the only one which lowers the observed heat of formation.

5) Multiplicity of Reaction Pathways. It is possible, especially in the ionic reactions of alkanes, that a fragment ion can arise by more than one pathway. If the energy requirements of these pathways are

different, the appearance potential for the lower energy process can be in error.

Assuming that the appearance potential can be obtained from the ionizing voltage difference required to have the calibration gas ion and the fragment ion reach 0.1% of their abundance at 50ev,[9] the error can be estimated when the slope of the linear part of the semi-log ionization efficiency curve is known.[7] For two processes having appearance potentials separated by 1ev the error ranges from zero when all of the 50ev current is due to the lower energy process to +13 Kcal.mol.$^{-1}$ when only 1/10 of the ion current at 50ev is due to the lower energy process. The figures are applicable to an Atlas CH_4 instrument. For ionizing sources with less energy spread the errors will be less.

6) General Considerations. Although the considerations above might indicate the contrary, many heats of formation obtained from electron impact data appear to be reasonably accurate, e.g., heats of formation for the C_8H_8 ion derived from seven different sources are shown in Table 1.

TABLE 1

Heats of Formation[10] of $[C_8H_8]^{+\cdot}$

Source	ΔH_f (Kcal.mol^{-1})	Neutral Products
$Ph(CH_2)_3CHO$	232	CH_2CHOH
$Ph(CH_2)_3COCH_3$	232	$CH_2C(CH_3)OH$
$Ph(CH_2)_2COOH$	236	HCOOH
$Ph(CH_2)_3COOH$	231	$H_2O + CH_2CO$
$Ph(CH_2)_2COOCH_3$	234	$HCOOCH_3$
$Ph(CH_2)_3COOCH_3$	227	$CH_3OH + CH_2CO$
$PhCH = CH_2$	231 (Photoionization)	- - - -

The results agree quite well and indicate that all ions have the same structure as that of the styrene molecular ion. Although all of the reactions result from rearrangements, which would imply a relatively low K(E) vs. E. slope, there is no evidence of a marked error due to kinetic shift. Also in the case of C_8H_8 ions resulting from multiple reactions,no greater error is evident as would be the case if the excess energies enumerated before were of importance. Lastly, in those reactions where stable neutral particles are formed there is no evidence of appreciable reverse activation energy.

For the reactions[11]

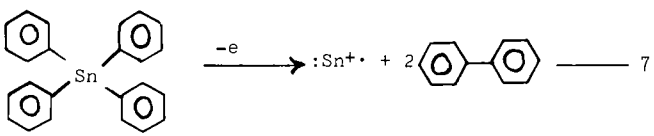

7

and

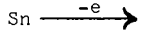

8

the heat of formation of $:Sn^{+\cdot}$ derived from 7 is 241 Kcal.mol.$^{-1}$, and from reaction 8, 243 Kcal.mol.$^{-1}$. For these reactions the monoatomic nature of the product ion allows no ambiguity due to different possible structures. Again, although considerable rearrangement is involved, there is no significant error in the experimental heat of formation of the fragment ion. It should be noted however that the $:Sn^{+\cdot}$ ion derived from $SnMe_4$ is formed with excess energy.[11]

To sum up, the values of thermodynamic quantities derived from electron impact measurement are subject to errors whose magnitude is not known with any reliability. However, for many complex ionic reactions, the sum of these errors appears to be small. There is presently no simple way of predicting whether large errors are to be expected by considering the structures of reactants and products.

It is reasonable to question structures derived from energetic

considerations because of the uncertainties involved in the measurements. In particular in those reactions where a molecule is expelled from a cyclic ion, it is intuitively attractive to postulate that the product ion is cyclic, even though energetic measurements indicate an acyclic product with a higher ground state energy. The question arises whether the sum of the errors are sufficient to account for the ~30 Kcal.mol.$^{-1}$ difference in energies of the cyclic and acyclic structures. Fig. 2 illustrates graphically the experimentally determined energy levels for postulated cyclic and acyclic structures (horizontal lines) and the values obtained for fragment ions (crosses) derived for a number of ionic reactions involving expulsion from acyclic precursor.[8]

FIGURE 2

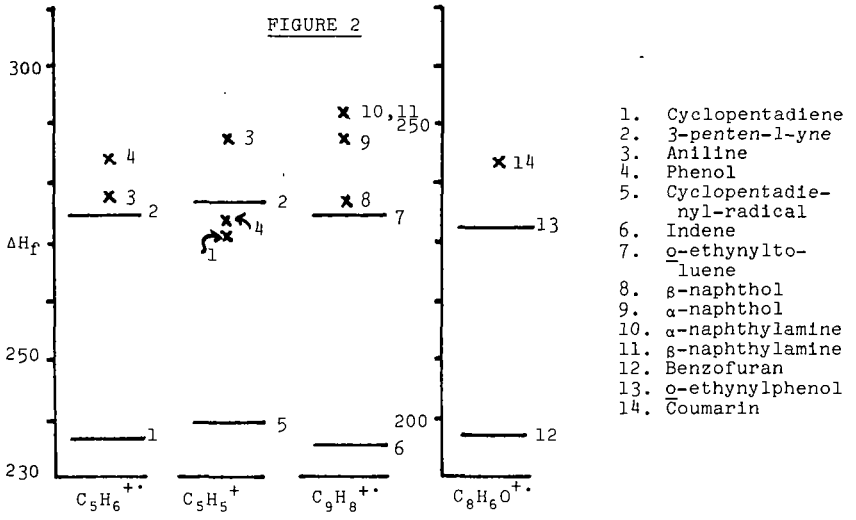

In all cases the heat of formation for the fragment is not significantly less than for the acyclic structure. It seems unlikely that the uncertainties in the determination of these energy levels would always be sufficient to account for the difference in energy between the two possible structures.

Abundance of Metastable Ions in Structure Determination

Two approaches are used here, to determine the abundance of one metastable ion for a given reaction and compare it with the abundance of a reactant or product ion involved in the same reaction; or to compare two metastable abundances for two reactions of the ion in question. The comparison of ionic structure for ions derived from different precursors by the first of these approaches is likely to be unreliable because of reasons outlined previously (Section 3). Unless there is evidence to indicate that the molecular ion energy distributions and energetics are similar, e.g., as is probably the case for some disubstituted benzenes,[4] it is better to use the second approach. In the system

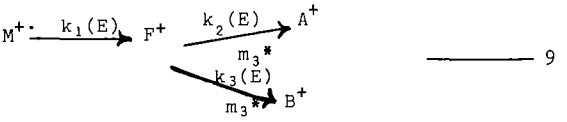

where $[m_2^*]/[m_3^*]$ is used to characterize F^+ certain conditions must be met[12] for this ratio to be independent of the nature of $M^{+\cdot}$. The conditions are:

1) The reactions to give $A^{+\cdot}$ and B^+ must arise from the same state of F^+ for the ratio $[m_3^*]/[m_2^*]$ to be independent of the energy distribution of $M^{+\cdot}$. If different abundance ratios are obtained for F^+ derived from different molecular ions, then, if possible, the determination of a second abundance ratio using a third reaction of F^+ will be useful in detecting the presence of different reacting states.[12]

2) $k_1(E) \gg k_2(E) + k_3(E)$ in the range of energy for which $k_2(E) + k_3(E) < 10^6$.

3) There are no marked changes in the energy distribution of $M^{+\cdot}$ in the energy range for which $10^2 < k_2(E) + k_3(E) < 10^6$.

In practice the failure of some systems to conform to these criteria will lead to variations in the metastable abundance ratio for the same F^+ derived from different molecular ions. Some judgement may have to be used to determine whether the variation is due to differences in the structure of F^+ in each system or whether it is due to the initial preparation effects outlined above.

In some instances there may be evidence, e.g., from energetic determinations or from spectral similarities, to show that reacting ions of the same composition derived from different molecules have the same structure. In these instances it is possible to draw inferences about molecular ion energy distributions and/or rates of isomerization of molecular ions by measurement of metastable abundance ratios. For the system

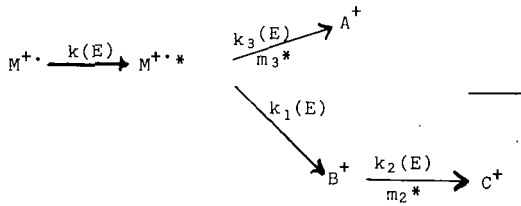

10

It can be shown[7] that

$$\frac{[m_3^*]}{[m_2^*]} = \frac{\int_0^E f[k(E),\ k_1(E),\ k_3(E)]\ \frac{dN}{dE}\ dE}{\int_0^E g[k(E),\ k_1(E),\ k_2(E),\ k_3(E)]\ \frac{dN}{dE}\ dE} \qquad 11$$

If k(E), the rate of isomerization of ground state molecular ions to the common reacting state $M^{+\cdot}*$, is fast compared to its rate of decomposition in the energy ranges for which the integrands of equation 11 are significant then $[m_3^*]/[m_2^*]$ can be shown to be independent of k(E). In this case, for common $M^{+\cdot}*$ species derived from different precursors, the ratio $[m_3^*]/[m_2^*]$ will vary only because of changes in dN/dE, the molecular ion energy distributions near the appearance potentials of A^+ and C^+.

Table 2 lists metastable abundance ratios for some simultaneous and consecutive reactions of ions derived from C_7H_{12} isomers. In attempting to interpret this data, it must be born in mind that the analysis of the systems represented by equations 9 and 10 shows that even if all of the reacting states are common to all of the eight compounds the abundance ratios will be influenced by the rate of isomerization of $M^{+\cdot}$ ($M^{+\cdot}* \equiv F^+$ in equation 9), and in those cases where the appearance potentials of the product ions are not the same the ratio will be influenced by the energy distribution of the molecular ions. Previously determined energetic measurements[13] on the first five compounds in Table 2 showed that the ions m/e 81, 68 and 67 have appearance potentials in a range of ~0.4ev, consequently the metastable

TABLE 2

96→81	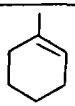			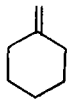				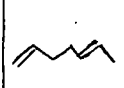
96→68	372±29	418±20	364±50	126±20	54±4	14±2	477±31	290±31
96→55	133±9	164±14	214±26	171±39	2045±208	65±9	508±46	722±107
94→79	23±5	46±10	34±4	51±2	261±27	35±3	231±7	339±38
95→67	15±1	16±1	20±1	17±2	37±7	7.8±0.9	48±6	48±6
95→80	400±18	375±56	597±128	491±47	758±95	250±33	726±98	937±46

abundance ratios [96→81]/[96→68] and [96→81]/[95→67] are not likely to be much influenced by differences in molecular ion energy distributions. Differences in these ratios will reflect differences in molecular isomerization rates, or differences in reacting states, or both. However, it is not possible, using this data, to determine the relative magnitude of these effects. If one assumes common reacting states, then the differences are explainable by differences in molecular ion isomerization rates.

The appearance potentials of m/e 81 and m/e 55 for the first five compounds in Table 2 differ by about 1.2ev, and it is to be expected that differences in molecular ion distributions in this range will change the ratio [96→81]/[96→55] even if similar reacting states are involved. For the first four compounds, assuming similar reacting states, it appears that differences in isomerization rates and energy distributions have a relative small effect (about 60%) on the ratio. The much different ratio for the fifth compound can be attributed to one or more of the following, different reacting states, different rates of isomerization, and, probably less likely, difference in molecular ion energy distribution.

It can be seen that for a study of these ionic reactions determination of metastable abundance ratios are of limited use only because of a lack of knowledge of the magnitudes of the factors which may influence them. Their utility would be increased if some of these variables, e.g., molecular ion energy distributions, could be determined by another means.

An estimate of the effect of isomerization rates can be gauged from Table 3 in which equation 11 was integrated, by computer, for a hypothetical set of rate constants.

TABLE 3

Variation of Metastable Ratio ($[m_3^*]/[m_2^*]$) with Rate of Molecular Ion Isomerization (k) and Rate of Decomposition (k_1+k_3)

k	$[m_3^*]/[m_2^*]$
0.1 (k_1+k_3)	18.3
0.6 (k_1+k_3)	82.9
10 (k_1+k_3)	220
100 (k_1+k_3)	236

For the calculation $k_1+k_3 = 2\times10^{12}(1-\frac{3.00}{E})^{.6}$ and $k_1 = 10^{10}(1-\frac{5.00}{E})^{.5}$ The mass spectrometer time scale derived by Chupka[3] was used.

REFERENCES

1. Haney, Max. A. and Franklin, J. L., J. Chem. Phys., 48, 4093 (1968).
2. Field, F. H., J.A.C.S., 91, 2827 (1969).
3. Chupka, W. A., J. Chem. Phys., 30, 191 (1959).
4. Brown, P., Org. Mass Spectrom., 3, 639 (1970).
5. Williams, Dudley H., Cooks, Graham, R., and Howe, Ian, J.A.C.S., 90, 6759 (1968).
6. Haney, Max A. and Franklin, J. L., Trans. Faraday Soc., 65, 1794 (1969).
7. Occolowitz, J. L., Unpublished results.
8. Occolowitz, J. L. and White, G. L., Austral. J. Chem., 21, 997 (1968).
9. Kiser, R. W. and Gallegos, E. J., J. Phys. Chem., 66, 947 (1962).
10. Occolowitz, J. L., Austral. J. Chem., 20, 2387 (1967).
11. Occolowitz, J. L., Tetrahedron Lett., No. 43, 5921 (1966).
12. Occolowitz, J. L., J.A.C.S., 91, 5202 (1969).
13. Winters, Robert E. and Collins, Jerome H., J.A.C.S., 90, 1235 (1968).

NEIGHBORING GROUP PARTICIPATION IN THE MASS SPECTRAL FRAGMENTATION OF SOME AZULENES*

R. G. Cooks, N. L. Wolfe, J. R. Curtis, H. E. Petty, and R. N. McDonald

Department of Chemistry
Kansas State University
Manhattan, Kansas 66502

Participation by phenyl groups, acting as neighboring groups, has been observed in two previous studies on gaseous ions.[1,2] The nature of the systems studied meant that the evidence for participation was necessarily indirect, involving mainly a demonstration that the reaction in question possesses the energy/rate characteristics typical of a rearrangement not those of a simple cleavage. The non-benzenoid azulene system has the advantage that participation is isomer dependent.

In a series of isomeric azulenes being the substituents $-(CH_2)_2OH$, $-(CH_2)_2OAc$, $-(CH_2)_2OTs$, $-CH_2CO_2CH_3$, and CH_2CO_2H, it was found that the 4-substituted isomers, and only those isomers, exhibited abundant ions due to several highly unusual cleavages (Table I).

TABLE I

Ion Abundances in Azulene Tosylate Spectra

Tosylate	M^+	M^+-Ts·	M^+-TsO·	M^+-TsOH	M^+-$TsOCH_2$·
1-Azulyl	20	≤ 0.5	0	58	100
4-Azulyl	56	100	5	32	17
6-Azulyl	64	0	≤ 1	100	18
1-Naphthyl	8	0.1	≤ 3	100	33

Evidence that these unusual processes are not simple cleavages but in fact involve bond formation, was obtained from their metastable and rate characteristics. A detailed interpretation of the mechanism of some of the participation processes was attempted using energetic data. It is suggested that in the form of molecular ion undergoing these reactions, the charge is "localized" in the substituent leaving the C_3-ring position, with its characteristic high electron density, to participate in the loss of the radical. Such a mechanism, if general, helps to reconcile earlier work[1] with recent criticism.[3]

The p-toluene sulfonates studied undergo neighboring group participation in solution. This is only seen in the 1-substituted compounds and probably involves intermediacy of the azulonium ion (cf. "phenonium" ion). The striking difference between participation processes occurring in solution and those observed in the gaseous ion derives from the marked facility with which the 1-substituted azulenes undergo β-cleavage. Moreover, it leads us to predict that solvolysis of the 4-substituted propanol derivatives should exhibit a participation process analogous to that observed in the ethanol derivatives in the gas phase.

This study also allowed some conclusions regarding ion structures. In particular, the structures of the substituted azulenes appear to be retained upon ionization; neither ring opening, nor substituent random-

* A full account of this work has been submitted for publication in the Journal of the American Chemical Society.

ization, nor isomerization to the naphthalene structure occurs. There is evidence, however, that β-cleavage is followed by structural isomerization.

REFERENCES

1. R. H. Shapiro and T. F. Jenkins, Org. Mass Spectrom., 2, 771 (1969).

2. W. J. Richter and W. Vetter, Org. Mass Spectrom., 2, 781 (1969).

3. H. F. Grützmacher, Org. Mass Spectrom., 3, 131 (1970).

Charge-Exchange Spectra of Some Substituted Benzophenones and N-Substituted Phenyl Benzamides

Robert H. Shapiro and Jonathan Turk

Department of Chemistry, University of Colorado, Boulder, Colo. 80302

Using 10 charge-exchange (CE) ions with recombination energies ranging from 10.5 to 24.6 eV, we measured the intensities of the ions produced by interaction of three benzophenones (I) and three N-phenyl benzamides (II) with the CE reagents.

$C_6H_5COC_6H_4X$ (I) $C_6H_5CONHC_6H_4X$ (II)

As with electron-impact (EI) excitation, the CE spectra of I (X = H, p-NO_2 or p-OCH_3) contain peaks corresponding to I^+, $C_6H_5CO^+$, $C_6H_5^+$, $XC_6H_4CO^+$ and decomposition products from the latter species. The CE spectra of II (X = H, p-NO_2 or p-OCH_3) contain peaks corresponding only to $II^{+\cdot}$, $C_6H_5CO^+$ and $C_6H_5^+$.

We measured the molecular ion abundances ($I^{+\cdot}$ and $II^{+\cdot}$) as a function of ionizing energy and our results (Table 1) indicate that certain high energy molecular ions appear to have relatively long lifetimes on the mass spectrometry time-scale. That is, instead of molecular ion abundance falling off steadily with increasing ionizing energy, at some point the molecular ion abundance increases.

A second important set of results was obtained in measuring the abundance of $C_6H_5^+$ ions relative to the abundance $C_6H_5CO^+$ (i.e. $(77^+)/(105^+)$) in the CE spectra of the six compounds. We determined these ratios as a measure of the relative amounts of internal energies, and hence their secondary reaction rates, of the primary benzyl ions. The results for two values of ionizing energy are shown in Table 2. These values typify the results of high energy behavior (24.6 eV) and low energy behavior (15.8 eV). The $(77^+)/(105^+)$ ratio obtained from the spectra of the benzophenones (I) follows the order of $NO_2 < H < OCH_3$ at both 24.6 and 15.8 eV, indicating that electron-donating groups attached to I lead to more energetic benzoyl ions, consistent with the previous findings and conclusions by Gross and McLafferty.[1] Since electron-donating substituents tend to lead to a favorable formation of $XC_6H_4CO^+$, making formation of $C_6H_5CO^+$ the higher energy process, perhaps McLafferty's "competitive shift"[2] explains the effect of the substituent. The benzamides (II), however, behave rather differently at 24.6 eV, since the $(77^+)/(105^+)$ ratio follows the order $NO_2 > H > OCH_3$ indicating that in the absence of a competing reaction electron-withdrawing groups attached to II lead to more energetic benzoyl ions. At 15.8 eV (and lower ionizing energies as well),

however, the opposite order of $(77^+)/(105^+)$ ratios is observed. Combining these data with those in Table 1 we are led to propose the following argument.

Upon charge-exchange a molecular ion is produced with a descrete amount of excess internal energy. These ions undergo a series of competing reactions as follows: (1) Simple cleavage of hot molecular ions to give hot benzoyl ions which decompose to $C_6H_5^+$, (2) emission of low energy photons to yield semi-hot molecular ions which undergo cleavage to yield semi-hot or cold benzoyl ions and (3) emission of higher energy photons to yield cold molecular ions.

Therefore the observed ion abundances will be determined by the relative rates of the competing cleavages and emissions.

Further work is in progress to determine whether emission actually occurs from the generated ions.

Table 1

$M^{+\cdot}$ Relative Abundances

Ionizing Energy (CE)	I, X=H	I, X=p-OCH_3	I, X=p-NO_2	II, X=H	II, X=p-OCH_3	II, X=p-NO_2
10.5	68	70	57	39	42	13
11.4	28	26	23	--	--	--
12.4	48	34	18	27	26	8
12.7	12	15	14	--	12	--
13.8	14	11	8	8	10	0
14.0	6	10	8	10	6	0
15.3	26	26	7	16	13	5
15.8	10	28	14	20	6	10
21.6	22	19	10	6	1	0
24.6	21	16	8	14	2	0

Table 2

Relative Abundances of $(105)^+$, $(77)^+$ and (56.5*) in the Spectra of Substituted Benzophenones and N-Substituted-Phenyl Benzamides

	X = $(77^+)/(105^+)$	Y = $(56.5^*)/(105^+)$
Substituent	X at 15.8 eV (CE)	X at 24.6 eV (CE)
I, X=p-NO_2	0.21	1.1
I, X=H	0.58	1.2
I, X=p-OCH_3	0.80	2.7

Substituent	X at 15.8 eV (CE)	X at 24.6 eV (CE)
II, X=p-NO_2	0.29	1.5
II, X=H	0.36	1.1
II, X=p-OCH_3	0.57	0.6

References

1. M. L. Gross and F. W. McLafferty, Chem. Commun. 254 (1968).
2. F. W. McLafferty, Timothy Wachs, Chava Lifshitz, Guiseppa Innorta, and Philip Irving, General Factors Determining Ion Abundances in Mass Spectra, Reported at Eighteenth Annual Conference on Mass Spectrometry and Allied Topics; June 1970.

MASS AND PHASE SPECTROMETRY OF HOT SF_6*

R. T. Brackmann, W. L. Fite and W. M. Jackson

Department of Physics
University of Pittsburgh
Pittsburgh, Pa. 15213

One of the principal attractions of introducing gas into a mass spectrometer in the form of a molecular beam running in high vacuum is that the gas source is thermally decoupled from the ionizer and it becomes routine to study hot gases and gases containing free radicals.[1] A problem with molecular beams is that the gas density decreases with distance from the source, and at reasonable distances the density in the beam becomes comparable with the density in the residual gas in the vacuum, thus making it difficult to distinguish between signals from the beam and signals from the residual gas. This problem is solved by modulating the molecular beam while operating the ionizing electron current dc. Under these circumstances, the ions coming from the beam produce ac signals at the modulation frequency and in specified phase while ions from the background gas give dc signals; the two can be separated electronically and lock-in detection circuitry can be used to bring the signal-to-noise level to a satisfactory point.

Fig. 1 shows a schematic of the modulated beam mass spectrometer used in the present studies, the EMBA-II, manufactured by Extranuclear Laboratories, Inc. Gas from a source enters through an aperture into the first of two differentially pumped vacuum chambers. The aperture size is chosen such that the pressure in the first chamber is approximately 10^{-4} Torr under the gas load from the source. At this pressure those molecules traveling along the axis of the instrument can reach the second aperture without suffering collisions and enter the second differentially pumped vacuum chamber as a molecular beam traveling in high vacuum. Shortly after entering the second chamber, in which the pressure is approximately 10^{-7} Torr, the beam is interrupted periodically at an audio-frequency by a rotating toothed chopper wheel. The beam then travels a distance, L, before entering an ionizer in which dc electron beams cross the modulated neutral beam at right angles, ionizing a portion of the neutrals in the modulated beam. Both the ions and neutrals travel into the mass filter. Upon emergence from the mass filter the ions are deflected into an electron multiplier, which is set off the axis, while the neutrals (and any accompanying photons and metastable neutrals) travel on to the back wall of the chamber. Since the neutrals travel as a beam in high vacuum and strike no surfaces, the identities of the species in the beam are preserved. The ionizer is separated from the actual gas source by high vacuum, so there is complete thermal decoupling and the only limitations on gas temperature come from the materials of which the gas source is constructed.

As with any mass spectrometer, a modulated beam instrument provides both signal strengths and appearance potential information. Additional important information is carried on the phase of the ac signals observed. In particular, from the phase of a signal one can often identify the parent neutral from which an observed ion comes, and determine whether a signal that increases with gas temperature is due to a free radical being formed or to an enhancement of a dissociative ionization cross section with internal energy of a neutral. It is the phase information obtained in experiments on heated SF_6 that is of principal interest here.

The phase lag at which an ion signal appears consists of two separate contributing phase lags. The first, ϕ_n, arises because of the time taken for a neutral to pass between

* This research was supported by the Advanced Research Projects Agency, The Department of Defense, and was monitored by the U. S. Army Research Office - Durham, Box CM, Duke Station, Durham, North Carolina 27706, under Contract No. DA-ARO-D-31-124-G1085.

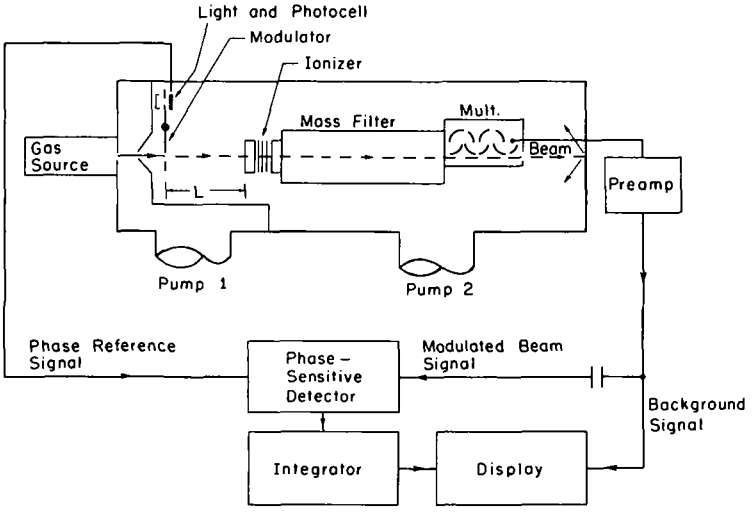

Figure 1. Simplified schematic of EMBA-II.

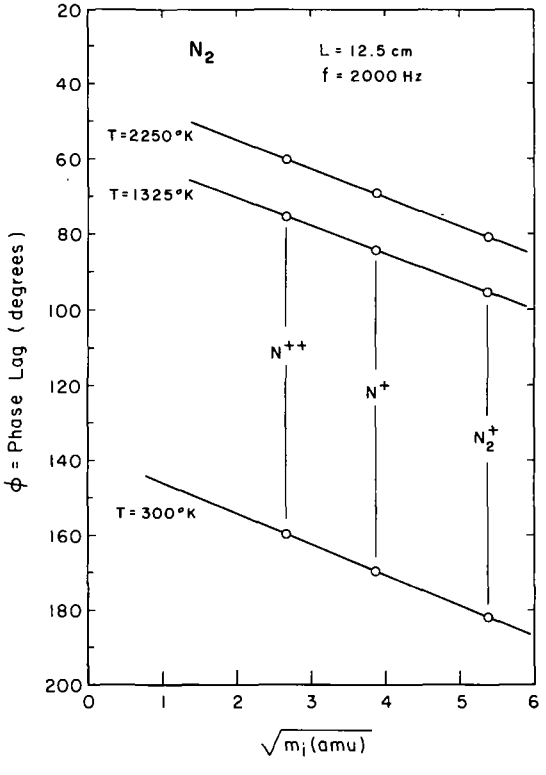

Figure 2. Phases of ion signals from heated N_2.

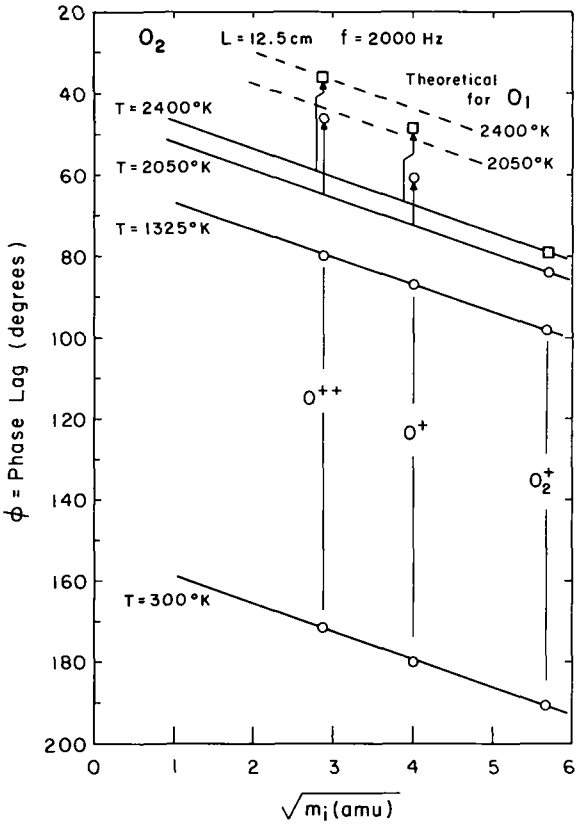

Figure 3. Phases of ion signals from heated O_2.

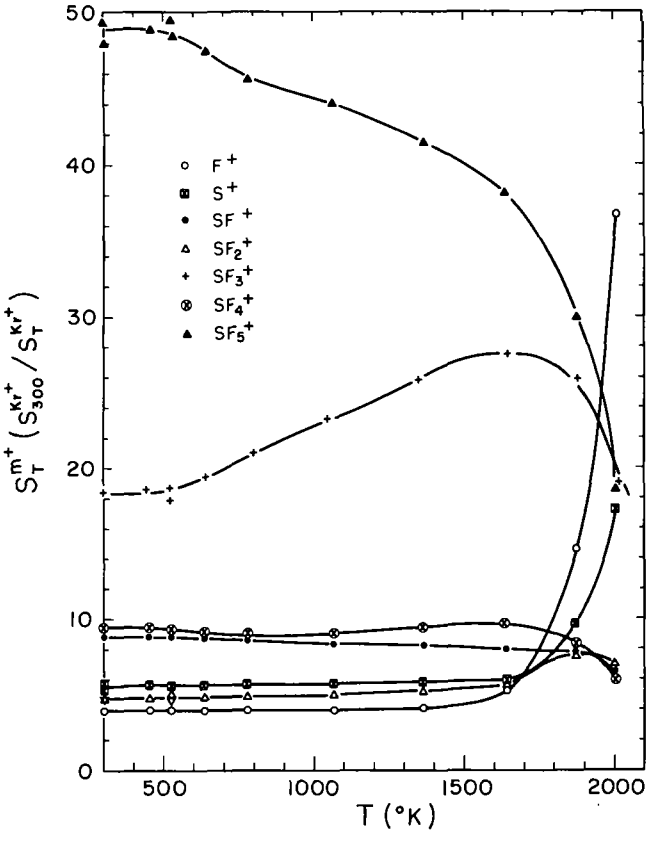

Figure 4. Amplitudes of ions from SF_6 as a function of gas temperature.

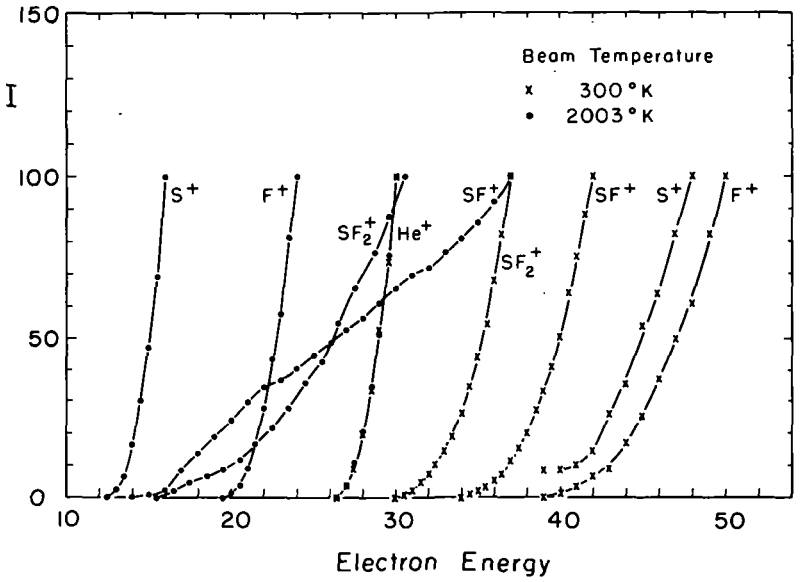

Figure 5. Appearance potential curves for light ion fragments from SF_6. The electron energy scale is uncorrected for contact potentials.

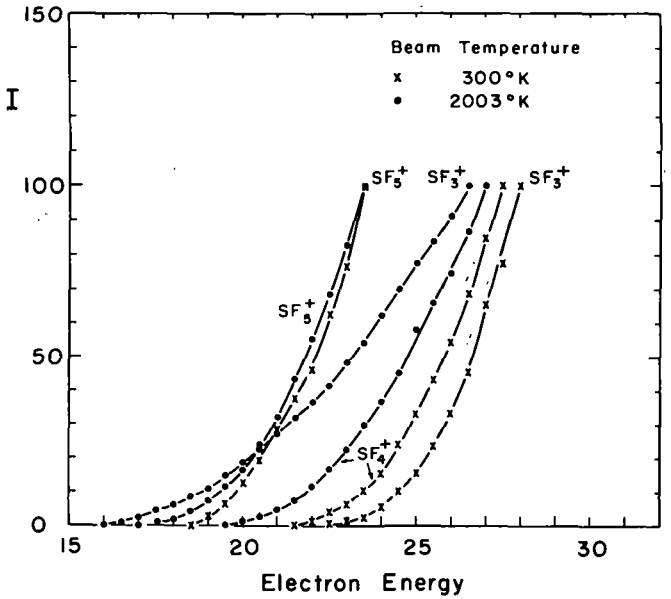

Figure 6. Appearance potential curves for heavier ion fragments from SF_6. The electron energy scale is uncorrected for contact potentials.

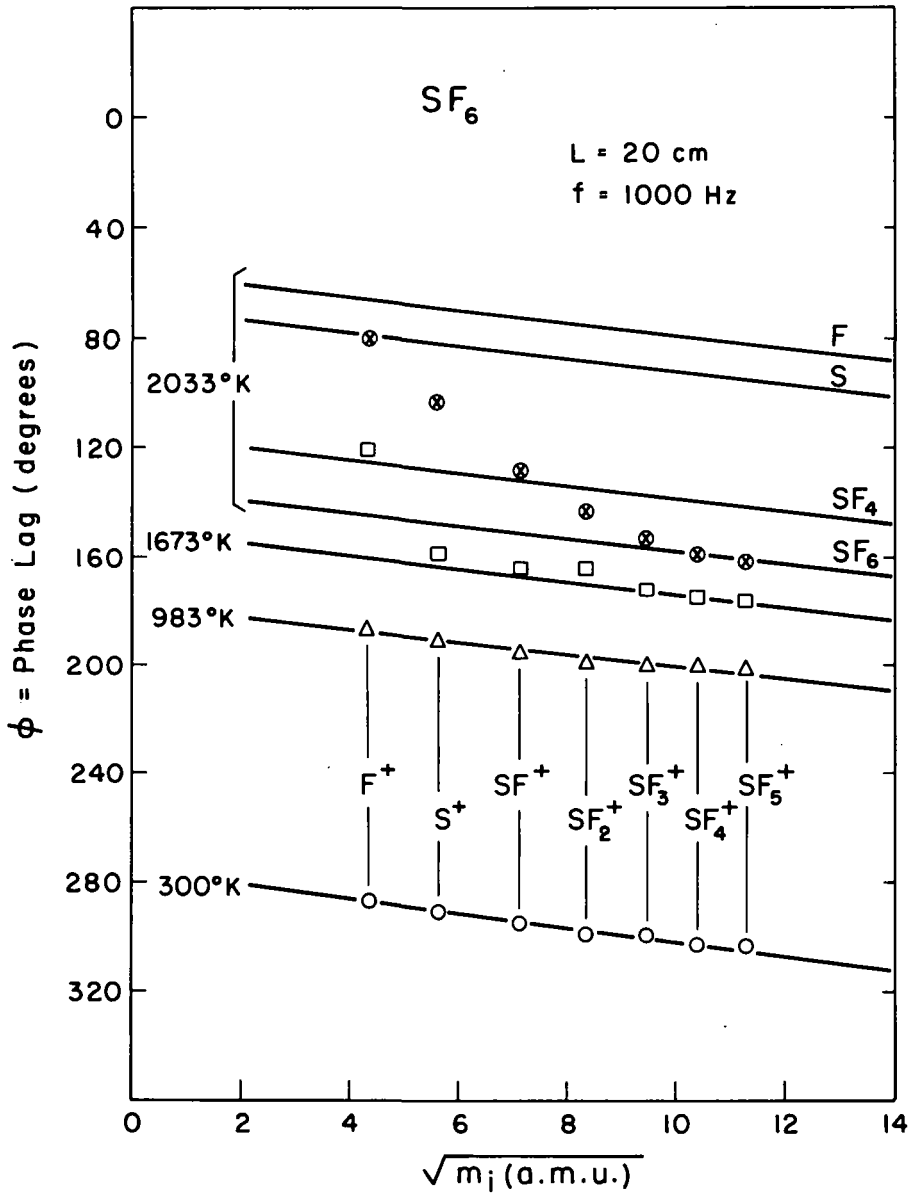

Figure 7. Phases of ion signals from heated SF_6.

the modulator and the ionizer. This time, t_n, is given by L/v_n, where L is the distance traveled and v_n is the molecular velocity. In the simplest instance

$$\phi_n = \omega t_n = \omega L/v_n \propto \omega L(M_n/T)^{1/2} \quad (1)$$

where $\omega = 2\pi f$ where f is the modulation frequency, M_n is the mass of the neutral molecule and T is the gas temperature. This expression is modified somewhat for square-chopped Maxwellian beams at high values of ϕ_n, the actual phases having been worked out by Harrison, Hummer and Fite.[2]

The second contribution to phase lag of a signal is due to the time of flight of the ion through the mass filter. This ion phase shift is given by

$$\phi_i = \omega t_i = \omega L_i/v_i \propto \omega L_i(m_i/V)^{1/2} \quad (2)$$

where L_i is the distance through the mass filter from the ionizer to the ion detector, m_i is the ion mass and V is the energy given the ion for passage through the mass filter. The total phase shift is the sum of ϕ_n and ϕ_i.

The effects of these phase shifts can be seen in Fig. 2, which plots the signal phases of ions formed from heated N_2 gas. Increasing phase lag is plotted in the downward direction. At room temperature, the phases are linear with $m_i^{1/2}$ as predicted from Eq. (2). As the gas temperature is increased, the phase lags diminish in accordance with Eq. (1), but the $m_i^{1/2}$ relationship still holds. The latter attests to all signals coming from N_2 at all temperatures, i.e., indicating that N_2 does not thermally dissociate.

This situation is to be contrasted to the case of oxygen that is heated in a tubular iridium source, for which the phases are shown in Fig. 3. At room temperature the phases of the various ions again lie on a straight line on a ϕ vs. $m_i^{1/2}$ plot, again indicating that all observed ions come from O_2. At 1325°K the ions still lie along a parallel straight line. At 2050°K, however, the mass 8 and 16 ions have shifted away from the line associated with the O_2 parent, corresponding to the onset of dissociation. At the highest temperature, the shift from the line of the O_2 parent is quite pronounced and the phase of the O^{++} indicates that this ion came almost entirely from neutral atomic oxygen, which is confirmed from observation of the signal strengths and appearance potentials.

While in simple cases, such as diatomic molecules, phase information is largely redundant, in more complicated molecules the phase information gives an added dimension of knowledge.

Our interest in SF_6 arose because of questions of attachment in electron scavenging experiments at elevated temperatures performed by Dr. Peter Chantry of the Westinghouse Research Laboratories. The point to be examined was the validity of the calculations of Wilkins[3] on thermal dissociation of SF_6.

In the experiments, SF_6 gas was admitted to a tubular iridium furnace source which had an aperture in the side. The dimensions of the source and the aperture size were such as to give a residence time in the source of approximately 10^{-2} seconds. The pressures used were normally in the range 50 to 100 μHg, which implied that gas-gas collisions were less important than gas-wall collisions. The mean number of wall collisions of a molecule before emerging in the beam was approximately 1000.

Fig. 4 shows the amplitudes of the various ions observed as a function of temperature. Particularly to be noted is the persistence to high temperature of the SF_5^+ ion, the heaviest and most prominent ion produced in electron impact on SF_6.

Fig. 5 shows appearance potential curves for the lighter ions observed at both room temperature and in the vicinity of 2000°K. The control ion He^+ shows the shape of the appearance potential from a simple ionization process in the instrument, and the shapes of

both the F^+ and S^+ curves, as well as their appearance potentials, indicate the presence of both atomic F and S in the heated gas.

Fig. 6 shows appearance potential curves on the heavier observed ions. The progression of appearance potentials at room temperature is as expected. At higher temperatures the fact that SF_3^+ has a lower appearance potential than SF_4^+ indicates the presence of free neutral SF_3 in the heated gas.

While the rise of the SF_3^+ signal with temperature (Fig. 4) and the knowledge of the presence of SF_3 (Fig. 6) might suggest appreciable dissociation to SF_3, the phase information indicates that this is not the case. In Fig. 7, the phases show that the SF_3^+ signal, even at the highest temperatures, continues to lie very close to the straight line associated with ions coming from SF_6, and suggests that something in excess of 80% of the SF_3^+ still comes from SF_6. The enhancement of the SF_3^+ signal relative to the SF_5^+ signal evidently must be attributed to the cross section for dissociative ionization of SF_6 to SF_3^+ becoming enhanced with internal energy in the SF_6. Analysis of the signal strengths indicates that this dissociative ionization cross section is increased by at least 50% at the higher temperatures.

It is also to be noted in Fig. 7 that at the highest temperatures the phase of SF^+ lies above the line associated with ions coming from SF_4. Evidently the SF^+ comes primarily from lighter dissociation products. The fact that F^+ lies below the line for F suggests that a significant fraction of F^+ is produced from heavier radicals than F at 2033°K.

The seemingly inescapable conclusion of these studies is that, for reasons unknown, the SF_6 is very slow to achieve dissociative equilibrium in an iridium furnace. The amount of SF_6 remaining at the highest temperatures exceeds by orders of magnitude the amount expected from the calculations of Wilkins.

It seems unlikely that SF_6 would not approach equilibrium during the approximately 1000 wall collisions each molecule has while in the furnace; it seems equally unlikely that surface reactions which are known to remove F atoms would produce an overabundance of SF_6 rather than an underabundance. Noting that the furnace source used in these experiments is a form of what Benson and Spokes[4] refer to as a "very low pressure pyrolysis" reactor, one can apply their formulas to obtain a rate coefficient for unimolecular dissociation of excited SF_6, but given the known binding energy of an F atom to SF_6, the deduced pre-exponential factor is far less than what seems reasonable.

It is hoped that further experiments will clarify the question of why dissociative equilibrium is not achieved in a furnace such as was used in these experiments. In the meantime, it seems clear that peculiarities in electron attachment to heated SF_6 should be attributed to changes in attachment cross sections to internally excited SF_6 rather than to attachment of electrons to dissociation fragments.

1. S. N. Foner and R. L. Hudson, J. Chem. Phys. 21, 1374 (1953).

2. H. Harrison, D. G. Hummer, and W. L. Fite, J. Chem. Phys. 41, 2567 (1964).

3. K. L. Wilkins, J. Chem. Phys. 51, 853 (1969).

4. S. W. Benson and G. N. Spokes, Proceedings of the XIth International Symposium on Combustion, pp. 95-103, The Combustion Institute, Pittsburgh, Pa., 1967.

Dissociation energies of gaseous GaAg, Ga_2, InAg, and In_2

Karl A. Gingerich
Department of Chemistry
Texas A&M University
College Station, Texas 77843
and
Gary D. Blue
Department of Chemistry
The Ohio State University
Columbus, Ohio 43210

Preliminary studies of the dissociation energies of gaseous GaAg and InAg[1] appeared to establish a correlation between the bond energies of the homonuclear diatomic molecules of the constituent atoms and their electronegativity difference in terms of the Pauling model.[2] The results of further investigations of these molecules and the simultaneous reinvestigations of the symmetric diatomic molecules of the constituent atoms are reported here.

The Knudsen cell mass spectometric method was used to investigate a number of gaseous equilibria involving these molecules. The enthalpies of reaction were evaluated by the third law method and where possible, by the second law method. In the case of the gallium-silver system, the pure metals were placed in a graphite cell together with tungsten phosphide. The tungsten phosphide decomposed in the course of the investigations into gaseous phosphorus-containing species and solid tungsten. For the indium-silver system high purity indium and silver were simultaneously evaporated from a boron nitride Knudsen cell that was surrounded by a molybdenum cell. The Knudsen cells were heated by radiation from a tungsten - mesh resistance heater. The neutral precursors of the observed ions were identified by their mass to charge ratio, isotopic abundance distribution, ionization efficiency curves, and shutter profile measurements. Pressure calibration was made by total vaporization of a known mass of both metals. Temperatures were measured with a calibrated optical pyrometer sighted on a black-body hole in the bottom of the effusion cell after correcting for the prism and window transmission, or with a chromel alumel thermocouple fitted into a hole in the bottom of the cell.

The treatment of the third law data was similar to that used previously,[3] except that measured multiplier gains and experimental ionization cross sections for Ga and In relative to Ag[4] were used.

For the Ga-Ag system the thermochemical data obtained from the measurement of several gaseous equilibria and the derived dissociation energies of the corresponding diatomic molecules are summarized in the first table. The second table contains the corresponding data for the In-Ag system.

Summary of Reaction Enthalpies in the Ga-Ag System

Reaction	Method	ΔH°_0 kcal/mole	D°_0(AB) kcal/mole	AB
GaAg(g)=Ga(g) + Ag(g)	2nd Law	40.8	40.8	GaAg
	3rd Law	42.4	42.4	
GaAg(g) + Ag(g)=Ag_2(g) + Ga(g)	3rd Law	5.7	43.3[a]	GaAg
GaAg(g) + Ga(g)=Ga_2(g) + Ag(g)	3rd Law	9.4	33.0[b]	Ga_2
Ga_2(g)=2Ga(g)	2nd Law	32.3	32.3	Ga_2
	3rd Law	33.6	33.6	

a) Using $D^\circ_0(Ag_2)$=37.6 kcal/mole: Drowart, Reference(5)

b) Using D°_0(GaAg)=42.4 kcal/mole: this work

Summary of Reaction Enthalpies in the In-Ag System

Reaction	Method	ΔH_o° kcal/mole	$D_o^\circ(AB)$ kcal/mole	AB
$InAg(g)=Ag(g)+In(g)$	2nd Law	38.9	38.9	InAg
	3rd Law	39.1	39.1	
$InAg(g)+Ag(g)=Ag_2(g)+In(g)$	2nd Law	1.7	39.3[a]	InAg
	3rd Law	1.9	39.5[a]	
$InAg(g)+In(g)=In_2(g)+Ag(g)$	2nd Law	14.5	36.9[b]	InAg
	3rd Law	13.1	35.5[b]	
$In_2(g)=2In(g)$	2nd Law	23.0	23.0	In_2
	3rd Law	25.2	25.2	
$Ag_2(g)=2Ag(g)$	3rd Law	37.4	37.4	Ag_2

a) Using $D_o^\circ(Ag_2)$=37.6 kcal/mole: Drowart, Reference (5)

b) Using $D_o^\circ(In_2)$=22.4 kcal/mole: DeMaria et al., Reference (7)

Weighted average experimental values for the dissociation energies, in kcal/mole are: $D_o(Ga_2)$=33.5, $D_o(In_2)$=24.5, $D_o(GaAg)$=42.5 and $D_o(InAg)$=39.0. The 3rd law value, $D_o(Ag_2)$=37.4 kcal/mole is in close agreement with literature values reviewed by Drowart.[5] The value for $D_o(Ga_2)$ is consistent with that found by Chupka et al. of 32 kcal/mole.[6] Within the accuracy of determination, our value also agrees with the literature value, $D_o(In_2)$=22.4 kcal/mole.[7]

From previous investigations with gaseous intermetalic compounds, it appears that the Pauling model of a polar bond[2] has a wide applicability.[1,5,8] The values in kcal/mole for the dissociation energies of GaAg and InAg calculated by either the geometric mean or the arithmetic mean versions of this method are 43.9 or 40.9 for GaAg and 35.1 or 34.8 for InAg. In these calculations our values for the dissociation energies of Ga_2 and In_2 and Drowart's value for Ag_2[5] were used. The Pauling electronegativities[2] for Ga and In were taken as 1.4 and 1.5, respectively, after correction to a common valence state with silver.[9] A closer agreement for InAg could be obtained by assuming an electronegativity difference between monovalent In and Ag of 0.5 on the Pauling scale. The calculated values by geometric and arithmetic mean methods then become 38.3 and 36.3 kcal/mole, respectively. As has been previously shown for the Al-group IB compounds,[1] the values calculated with the geometric mean method agree best with the experimental values.

Because the Pauling model can be applied to these compounds, we expect it to also apply to other diatomic intermetallic compounds of gallium and indium. Future investigations of such compounds would in addition, be expected to lead to a refinement of electronegativity values for these elements.

References

(1) G. D. Blue and K. A. Gingerich, Proceedings of the 16th Annual conference on Mass Spectrometry and Allied Topics, May 1968, Pittsburgh, ASTM-Committee E-14, paper 129, 383-387.
(2) L. Pauling, "The Nature of the Chemical Bond," (Cornell University Press, Ithaca, New York, 1960) 3rd ed., Chap 3.
(3) K. A. Gingerich and G. D. Blue, J. Chem. Phys. 47, 5447 (1967).
(4) K. A. Gingerich and G. D. Blue, to be published.
(5) J. Drowart, "Phase Stability in Metals and Alloys," P. S. Rudman, J. Stringer and R. I. Jaffee, Eds, McGraw-Hill(1967) pp 305-317.

(6) W. A. Chupka, J. Berkowitz, C. F. Giese, and M. G. Inghram, J. Phys. Chem. 62, 611 (1968).
(7) G. DeMaria, J. Drowart and M. G. Inghram, J. Chem. Phys. 31, 1076(1959)
(8) K. A. Gingerich and H. C. Finkbeiner, J. Chem. Phys. 52, 2964 (1970).
(9) W. Gordy and W. J. O. Thomas, J. Chem. Phys. 24, 439 (1955).

DISSOCIATION ENERGY OF F_2

F3

J. J. De Corpo, Ronald P. Steiger, J. L. Franklin and J. L. Margrave

Department of Chemistry
Rice University
Houston, Texas 77001

The dissociation energy of F_2 has been determined mass spectrometrically. The heat of formation of fluorine, $\Delta H_f^\circ(F)$, was determined from measurements of both the appearance potentials and translational energies of the products resulting from electron impact, including both positive and negative ions. One can derive a value for the dissociation energy from each of the possible processes, namely: 1) dissociative electron attachment, 2) ion-pair formation, and 3) dissociative ionization. The three values are in excellent agreement and establish $D^\circ(F_2) = 37.5 \pm 2.3$ kcal/mole.

A complete paper has been submitted for publication to the Journal of Chemical Physics.

F4

Electron Impact Measurement of Bond Strengths in Some Transition Metal Chlorides

D. L. Hildenbrand

Douglas Advanced Research Laboratories
McDonnell Douglas Corporation
Huntington Beach, California 92647

Very little is known about the dissociation energies of the diatomic transition metal halides, although these quantities are of some interest from both theoretical and practical standpoints. The most reliable information of this sort generally is obtained from third-law treatment of equilibrium data, but the lack of knowledge about the configurations and energies of the low-lying electronic states of many of these molecules introduces serious uncertainties into the derived results. As an alternative, the possibility of obtaining definitive dissociation energy data from electron impact measurements was explored, after earlier work on the IIA metal chlorides indicated that such an approach would be feasible.

Measurements were made with a Nuclide Corp. Model 12-60 HT direction focusing mass spectrometer equipped with a Nier-type electron impact ion source. The repeller and the electron trap were kept at ionization box potential, but otherwise no special changes were made in the ion source. Ionization efficiency curves were plotted continuously with an X-Y recorder using an ionizing current of about 1 μA in all instances. Threshold appearance potentials of the various positive ions were determined by means of the extrapolated voltage difference (EVD) method, using xenon, argon and the appropriate metal atoms as reference standards; only that portion of the IE curve within 2 eV of threshold was considered. Beams of the metal dichlorides were produced by vaporizing the corresponding solids from graphite Knudsen cells, while vaporization in the presence of a metal reducing agent yielded a small amount of the diatomic metal chloride along with the dichloride.

A series of threshold measurements on the parent molecular ions NO^+, H_2O^+, HCl^+ and Ar^+, using the EVD method with Xe^+ as standard, yielded highly reproducible results, which in all cases agreed with the known ionization potentials to 0.07 eV or better, the average error being 0.03 eV. It is tentatively concluded that the accuracy of the method as applied here is on the order of 0.10 eV.

Table I gives the ionization and appearance potentials determined by the EVD method for the iron, cobalt and nickel chlorides. The MCl^+ fragment ions are assumed to arise from the process $MCl_2 + e \rightarrow MCl^+ + Cl + 2e$, while the atomic fragment ions M^+ come from $MCl_2 + e \rightarrow M^+ + 2Cl + 2e$. For $Ni^+/NiCl_2$ the IE curve shows two thresholds; the lower one (given in Table I) presumably originating from $NiCl_2 + e \rightarrow Ni^+ + Cl_2 + 2e$. On this basis, the dissociation energies D(ClM-Cl) and $D(MCl_2)$ were derived from the measured electron impact (EI) threshold values and are shown in Table II; implicit in these calculations is the assumption that any excess energy carried away by the dissociation products is negligibly small. Also shown in Table II are thermochemical (TC) values of $D(MCl_2)$, obtained from vaporization and calorimetric data, and which are seen to be in fair agreement with the electron impact data. The thermochemical values of $D(MCl_2)$ are believed to be the more reliable, and these were combined with D(ClM-Cl) to yield the diatomic dissociation energies D(MCl).

The method appears promising, as judged by the nature and consistency of the results, and should be especially useful for studying effusion beam species where "monoenergetic" techniques are difficult to apply. More work needs to be done, however, on ascertaining the threshold excess energies of the various dissociation processes, as well as on assessing the effects of internal thermal excitation on the measured ionization thresholds.

Table I

IONIZATION AND APPEARANCE POTENTIALS
OF M-Cl SPECIES, eV

	IP(MCl)	IP(MCl_2)	AP(MCl^+/MCl_2)	AP(M^+/MCl_2)
Fe	8.08	10.63	12.58	16.24
Co	8.71	10.75	12.70	15.82
Ni	9.28	11.38	12.88	12.65

ESTIMATED ACCURACY ± 0.10 eV
EVD METHOD

Table II

DERIVED BOND DISSOCIATION ENERGIES, IN eV

	$D_o(ClM-Cl)_{EI}$	$D_o^\circ(MCl_2)_{EI}$	$D_o^\circ(MCl_2)_{TC}$	$D_o^\circ(MCl)$
Fe	4.50	8.37	8.17	3.67
Co	3.99	7.96	7.81	3.82
Ni	3.60	7.50	7.70	4.10

ESTIMATED ACCURACY ± 0.15 eV

Interpretation of Ion Yield Curves for Positive and Negative Ions from Carbon Vapor*†

C. Herndon Williams
Sandia Laboratories
Albuquerque, N. M. 87115

Ion yields ($I^{\pm}/e^{-}$) for some of the positive and negative ions produced by electron impact on carbon vapor from zero through 30 eV have been obtained using an automated signal averaging data acquisition system.[1] The objective was to determine the ionization/fragmentation energetics by means of structure in the ion yield curves and to interpret these energetics in terms of electronic levels in the (0, ±) potential energy diagrams for these systems, where possible.

The carbon molecular beam effused from a Ta tube furnace at 3000°K and contained the species C_1 - C_5(v). The electron beam was emitted by a hot W filament and was not energy selected. The studies were done in the ion source of a Bendix 3015 TOF mass spectrometer. The ion yield of Xe^+ was compared with the ionization cross section measured by D. Rapp and P. Englander-Golden[2] to calibrate the positive ion EE scale; SF_6(g) was used to calibrate the negative ion EE scale. The ionization potentials (IP) were determined by the semilog plot method; appearance potentials were located by the linear break method. Some averaged values of the IP and AP measured in this work are given below:

Ion	Ionization Potentials (eV)	Appearance Potential(s) (eV)
C_1^+	11.32 ± 0.15	17.7 ± 0.1 19.5 ± 0.2
C_2^+	12.30 ± 0.15	19.8 ± 0.1 21.7 ± 0.2
C_3^+	12.25 ± 0.15	13.8 ± 0.2 16.8 ± 0.4
C_4^+	11.10 ± 0.25	13.2 ± 0.2
C_5^+	11.20 ± 0.25	13.3 ± 0.3
C_2^-	-----	5.0 ± 0.5

These energy terms were interpreted as thresholds for the ionization, fragmentation and electronic excitation of the molecular ions in the Franck-Condon region of the neutral. Some approximate KE measurements for the ions C_1^+ and C_2^+ were made as a function of EE. From these interpretations it was possible to tentatively locate several electronic energy levels in the $C_2^{o,\pm}$, $C_3^{o,+}$ and C_4^+-C_5^+ systems and to derive two additional thermochemical quantities: (1) the heat of formation of C_3(g) at 3000°K, 190 ± 5 kcal/mole, and (2) the electron affinity of C_2(g), 3.1 ± 0.5 eV.

* This work was supported by the United States Atomic Energy Commission.

† This material is being prepared for submission to the Journal of Chemical Physics.

1. C. Herndon Williams and Arthur W. Lynch, another paper at this conference, Session T.

2. D. Rapp and P. Englander-Golden, J. Chem. Phys. 43, 1464 (1965).

MASS SPECTROMETRY OF A CHEMICALLY QUENCHED HIGH TEMPERATURE RF PLASMA*

J. M. Madson, J. H. Mullen and T. C. Peng
McDonnell Douglas Research Laboratories
St. Louis, Missouri 63166

The processes which govern the production and loss of electrons together with reactions between ions and neutrals play an important role in determining the plasma environment of a vehicle during planetary reentry. In many instances it would be desirable to be able to control the composition of this plasma, in particular the plasma electron number density. However, this requires the knowledge of the dominant electron production and loss processes together with their reaction rates at temperatures in the range encountered during reentry (2000 - 4000 K). Some measurements have been made on the temperature dependence of the electron dissociative attachment cross section for N_2O up to 1000 K[1] and for O_2 up to 2000 K[2]. These measurements show the electron dissociative attachment cross section to be strongly dependent on gas temperature. In addition, studies made on SF_6 at temperatures up to 1200 K[3] indicate a change in the dominant negative ion formed as the temperature increases.

The experimental apparatus shown in block diagram form in Fig. 1 has been developed to investigate the chemical reactions occurring when target molecules interact with a hot plasma. Details of the apparatus will be given elsewhere[4]. The plasma source is operable from 1 to 760 Torr and up to 69 kW input power to the generator on argon and up to 600 Torr and 100 kW input power on air. Measurements to be reported here were obtained at 165 Torr argon and 57 kW input power. The plasma tube housing is a Teflon water jacket with access ports for an X-band radiometer and an optical spectrometer for electron temperature determinations. The plasma flows from the discharge tube through a 4 mm diameter reaction channel at sonic velocity. The local pressure in the reaction channel is about half the discharge pressure (87 Torr for these measurements). The channel length is variable to permit the determination of an effective reaction time. Target gas molecules are supersonically injected into the channel through orifices which range from 35 to 200 μm in diameter. Light pipes are provided near both ends of the channel for spectroscopic measurements.

Spectroscopic measurements of the ArI intensities in the plasma source and at two places along the reaction channel were made with a one meter (Jarrell Ash Model 78-466) spectrograph. For the measurements presented here, the electron temperature in the source was 8500 K and in the channel 5300 K.

Local gas temperatures are measured in the reaction channel with a high temperature tungsten - rhenium thermocouple. These measurements are in good agreement with calculations of the temperature in the plasma source and reaction channel based on gas dynamic considerations. For a plasma source pressure of 165 Torr the thermocouple measurements gave a reaction channel gas temperature of 3000 K which leads to a gas temperature of 4000 K in the plasma source assuming an isentropic expansion.

The plasma leaving the reaction channel undergoes a free jet expansion into a vacuum chamber at 0.26 Torr. The rapid expansion occurring in the free jet essentially preserves the reaction products formed in the channel. The centerline core flow of the expanded plasma is sampled by an extractor nozzle with a 250 μm orifice for analysis by a quadrupole mass spectrometer. An interferometer operating at 34.48 GHz is used to measure the electron density just ahead of the mass sampling orifice. The extractor nozzle was designed so as to minimize boundary layer effects near the sampling orifice and gas particle scattering back into the expansion plume ahead of the orifice. A commercial EAI 150A quadrupole analyzer and ionizer is used in the present experiments. Ion currents from the analyzer are collected with a Faraday cage and measured by an electrometer. Biasing on the input electrodes to the analyzer and the Faraday cage is adjusted to optimize the positive or negative ion signal. Neutral specie detection is accomplished by activating the internal filament and biasing supplies of the quadrupole control unit. The background pressure in the analyzer region is about 2×10^{-6} Torr. Simultaneous determination of the change in intensity of the positive and/or negative ion signal and the electron density as a function of the amount of target gas injected aids in determining the reaction processes and their associated reaction rates.

Preliminary measurements have been made using various target gases to determine their relative effectiveness in reducing the electron density at a gas temperature of 3000 K. Figure 2 shows the behavior of the electron density, F^- and SF_5^- signals with the addition of SF_6. As SF_6 is injected, the F^- signal builds up first. An estimated

*This research was conducted under McDonnell Douglas Independent Research and Development Program.

production rate for F^- from the initial slope of the F^- curve gives a value of $k(F^-) = 1.4 \times 10^{-9}$ cm^3 molecule^{-1} sec^{-1}. The estimated rate for SF_5^- production from the initial slope of the SF_5^- curve is also $k(SF_5^-) = 1.4 \times 10^{-9}$ cm^3 molecule^{-1} sec^{-1}. At this point the exact process involved in the negative ion production has not been determined. The production is probably due to a combination of

$$e + SF_6 \longrightarrow SF_5 + F^- \quad \text{Dissociative Attachment}$$
$$\longrightarrow SF_5^- + F$$

and

$$e + SF_6 \longrightarrow (SF_6^*)^- \longrightarrow SF_5^- + F \quad \text{Temporary Excited Negative Ion}$$
$$SF_5 + F^-$$

with the former dominating in the F^- production and the latter in the SF_5^- production. An explanation for the decrease in the negative ion signals is not available at the present time. Also, the appearance of positive ions of the SF_6 dissociation products together with the increase in the lighter SF_6 dissociation product negative ion species have not as yet been evaluated.

Production of O^- from N_2O is shown in Fig. 3. The estimated rate constant for O^- production from the ion intensity curve is $k(O^-) = 1.8 \times 10^{-10}$ cm^3 molecule^{-1} sec^{-1}. This presumably is the rate for the dissociative attachment reaction

$$e + N_2O \longrightarrow O^- + N_2.$$

More recent data where the O^- buildup is linear over a larger range of signal intensity is in general agreement with this rate.

An attempt was made to determine the quenching effectiveness of bromine. A small sample of bromine was heated in a boiler and injected through a hot calibrated orifice. The results are shown in Fig. 4. The ion intensity plotted here is the sum of the Br^{79} (50.5%) and Br^{81} (49.5%) isotopes. The estimated rate constant from the Br^- ion signal is $k(Br^-) = 1.3 \times 10^{-10}$ cm^3 molecule^{-1} sec^{-1} presumably for the dissociative reaction

$$e + Br_2 \longrightarrow Br^- + Br.$$

Injection of O_2 and CO_2 into the reaction channel produced no negative ion signals in the range of detection sensitivity used for the other measurements presented here.

Figure 5 shows the ion signals obtained with H_2 injection. Again, within the range of sensitivity being used, no negative ions were observed. However, the normal positive ions seen in an Ar-H_2 mixture were present. Using the linear portion of the Ar^+ decay to estimate the reaction rate for

$$Ar^+ + H_2 \longrightarrow ArH^+ + H$$

gives an approximate rate constant of $k(ArH^+) = 6.3 \times 10^{-11}$ cm^3 molecule^{-1} sec^{-1}. Reaction rates for the production of the other ions have not been determined. No H_2^+ signal was detected within the sensitivity of these measurements. It is possible that H_2^+ is produced by $Ar^+ + H_2 \longrightarrow Ar + H_2^+$ and then rapidly lost be the reactions

$$H_2^+ + H_2 \longrightarrow H_3^+ + H$$

and

$$H_2^+ + Ar \longrightarrow ArH^+ + H.$$

In summary, an experimental apparatus has been assembled for the study of attachment reactions as well as ion-molecule reactions at temperatures in the range of 1000 - 3500 K. The goal of these studies is to determine the relative effectiveness of various chemical additives in controlling the electron density in a high temperature plasma and to investigate the reaction processes involved. Initial measurements on N_2O, SF_6, O_2, CO_2, Br_2 and H_2 indicate that of these, SF_6 is still the best electron attacher at 3000 K.

References:

1. P. J. Chantry, J. Chem. Phys. 51, 3369 (1969).
2. W. R. Henderson, W. L. Fite, and R. T. Brackman, Phys. Rev., 183, 157 (1969).
3. C. L. Chen and P. J. Chantry, Bull. Am. Phys. Soc. 15, 418 (1970).
4. J. H. Mullen, J. M. Madson, L. N. Medgyesi-Mitschang, T. C. Peng, P. M. Doane, Rev. Sci. Instr. (to be submitted).

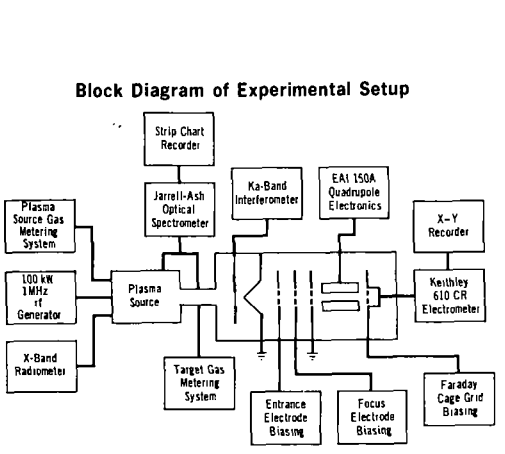

Fig. 1 Block Diagram of Experimental Setup

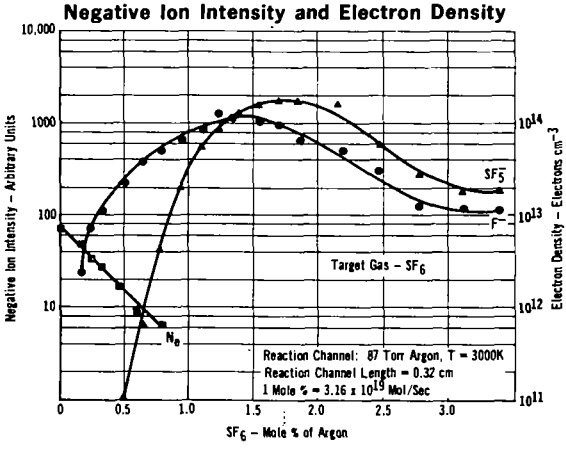

Fig. 2 Negative Ion Intensity and Electron Density for SF_6 in Argon

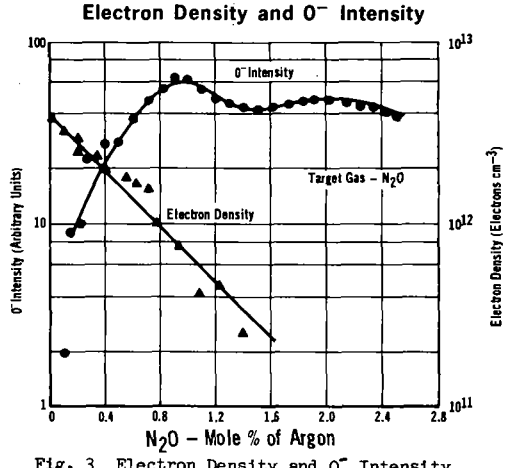

Fig. 3 Electron Density and O^- Intensity for N_2O in Argon

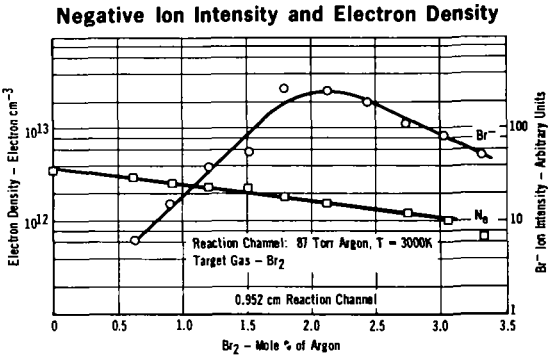

Fig. 4 Negative Ion Intensity and Electron Density for Br_2 in Argon

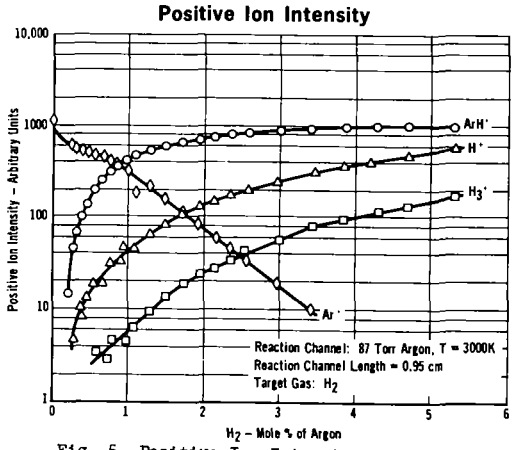

Fig. 5 Positive Ion Intensity for H_2 in Argon

MASS SPECTROMETRIC STUDY OF VAPOR TRANSPORT REACTIONS*

Vladimir S. Ban

RCA Laboratories
Princeton, New Jersey

In vapor transport reactions a substance in the condensed state reacts with a transporting gas to form a gaseous product. Reactions of the resulting gaseous product with other constituents of the vapor phase lead in certain systems to the deposition of a new condensed phase; crystal growth from the vapor phase is based on processes of this type.

The MA-1 Bendix time-of-flight (TOF) mass spectrometer was coupled to a vapor phase crystal growth apparatus[1] and the composition of the vapor phase (total pressure 1 atm) was monitored as a function of the temperature, flow rates and concentrations of the reacting gases. The gas sampling was accomplished by means of a quartz capillary 1 inch long, which was maintained at the temperature of the sampled gas phase. The collimated molecular beam emanating from the capillary entered the TOF ionizing region, which was positioned at 5 inches from the capillary.

The described experimental set-up was used to study a transport of $Ga_{(l)}$ and $In_{(l)}$ with $HCl_{(g)}$. It was found that the following reaction occurs:

$$M_{(l)} + HCl_{(g)} \rightarrow x\ MCl_{(g)} + (1-x)\ HCl_{(g)} + \frac{x}{2} H_{2(g)}$$

where

M = In or Ga; and

X = mole fraction of $HCl_{(g)}$ participating in reaction.

At T = 750°C the value of x was determined to be 0.70 - 0.75 and 0.80 - 0.85 for indium and gallium, respectively. These results indicate a deviation from chemical equilibrium; the equilibrium value of x would be above 0.99 in both cases. The observed deviation increased with increasing gas flow velocity in the crystal growth system.

The thermal decomposition of AsH_3 and PH_3 was also studied. These gases decompose according to the following reaction:

$$MH_{3(g)} \rightarrow (1-x)\ MH_{3(g)} + (1-\alpha)\ \frac{x}{4} M_{4(g)} + \alpha\ \frac{x}{2} M_{2(g)} + \frac{3}{2} x\ H_{2(g)}$$

where

$MH_3 = PH_3$ or AsH_3;
$M_4 = P_4$ or As_4;
$M_2 = P_2$ or As_2;
x = mole fraction of MH_3 decomposing; and
α = degree of dissociation of M_4 molecules.

---

* It is expected that a more complete version of this work will appear in J. Electrochem. Soc.

At T = 850°C the values of x = 0.90 and α = 0.40 were obtained for the case of PH_3; in the case of AsH_3 the corresponding numbers were 0.99 and 0.35.

From these results one concludes that the thermal decomposition of MH_3 gases in the growth system is incomplete. Furthermore, the ratio of abundances M_2/M_4 was found to be larger than the ratio predicted from the thermodynamical calculations.

A study of the thermal decomposition of a 1:1 mixture of AsH_3 and PH_3 revealed the existence of various mixed species, such as AsP, As_3P, As_2P_2 and AsP_3, in abundances comparable to those of the M_4 and M_2 molecules.

Finally, a reaction leading to the deposition of crystalline GaAs was studied. It was determined that the reaction responsible for the deposition is

$$GaCl_{(g)} + \frac{1}{4}\,As_{4(g)} + \frac{1}{2}\,H_{2(g)} \rightleftarrows GaAs_{(s)} + HCl_{(g)}.$$

This result is in contradiction with the common assumption that GaAs is deposited via the reaction

$$3GaCl_{(g)} + \frac{1}{2}\,As_{4(g)} \leftarrow 2GaAs_{(s)} + GaCl_{3(g)}.$$

In conclusion, the application of the mass spectrometer to a study of processes occuring in a vapor phase yielded the following results:

1) Significant deviations from chemical equilibrium occur in vapor growth systems, mainly due to kinetic effects.
2) Indium and gallium are transported as monochlorides, but the conversion of HCl is incomplete.
3) AsH_3 is 99% decomposed at 850°C; PH_3 is 90% decomposed at 850°C.
4) Mixed species (AsP and As_xP_y, where x + y = 4) have been detected in the AsH_3-PH_3 system.
5) A new reaction leading to the deposition of GaAs crystals has been established.

---

[1] J. J. Tietjen and J. A. Amick, J. Electrochem. Soc. 113, 724 (1966).

High Temperature Equilibria Involving Bonding by Platinum--A Most Reactive Noble Metal

GARY D. BLUE
Chemistry Department, The Ohio State University, Columbus, Ohio 43210 and
R. S. CARBONARA and C. A. ALEXANDER
Columbus Laboratories, Battelle Memorial Institute, Columbus, Ohio 43201

The high temperature mass spectrometric technique has been applied to the determination of activities of components in reaction systems containing Pt and $ZrPt_3$ during studies directed toward quantitative confirmation of the Brewer-Engel theory and its prediction of some extremely stable intermetallic compounds formed by certain transition metals. Pure Pt in a BeO cell was studied over 5 decades of vapor pressure at 1725-2383°K with resultant excellent agreement for 2nd and 3rd law ΔH vapor values calculated employing Margrave's recent enthalpy measurements for liquid Pt. A provisional value of $D_0^\circ(Pt_2)$ is ca. 4 ev. For $ZrPt_3$ in beryllia from 1800-2600°K, Pt(g) was readily observable, but Zr activity values were determined from ZrO(g), Be(g), BeO(g) and known properties of BeO(s). Activities and partial molar heats of vaporization of the component metals give free energy and heat of formation values in accord with Brewer's predictions and lend support to vital aspects of the theory. Numerous interesting reactions were encountered in preliminary studies of Pt and $ZrPt_3$ in graphite and zirconia cells.

Thermodynamic Characterization of Intermetallic Compounds of High Stability: NiAl

C. A. ALEXANDER, J. S. OGDEN, W. M. PARDUE
Columbus Laboratories, Battelle Memorial Institute,
Columbus, Ohio 43201 and
GARY D. BLUE
Chemistry Department, The Ohio State University, 43210*

Of considerable importance in chemical thermodynamics is the ability to predict the stability of possible compounds or compositions, hence, the Engel-Brewer correlation[1] holds considerable promise as a means of estimation of thermodynamic properties of materials. The correlation has generally been used to relate structures of metals to electronic configurations. The correlation, however, that in a mixture of two types of metals an electron transfer will occur from the metal with the surplus of electrons to the metal with low-lying vacant orbitals. This charge transfer would then result in a salt-like reaction with a significant enthalpy of formation.

As an example of an intermetallic compound where such forces might be operative NiAl was chosen. Its melting point of 1910°K is considerably above either Ni (1728°K) or Al (932°K) hence it exhibits considerable thermal stability. Also the material has been previously characterized as to structure and enthalpy of formation. The structure of NiAl is body center cubic while both Ni and Al are face centered cubic. The Engel postulates would require for the b.c.c. structure one (s + p) electron per atom while originally Ni and Al would have three (s + p) electrons per atom, hence, in the compound some of the electrons must increase the charge density between Ni and Al. As a first estimate it would be expected that the strongest bonding in the compound would be Ni-Ni, or Al-Ni because the high melting point would certainly indicate that the bonding was not predominantly Al-Al in nature. Goldfinger and co-workers[2] have established that for similar compounds $D(AB)/\Delta H_{atom}(AB) = k$ where k is a characteristic constant for each type of compound, and ΔH_{atom} (AB) is the energy change between the compound and its gaseous elements.

In an effort to determine if the mass spectrometric approach could contribute to an understanding of the energy changes accompanying charge transfer a series of determinations were performed on NiAl. The Nuclide 12-90-HT was used for the mass spectrometric determinations and an Ainsworth recording vacuum balance coupled to a tungsten resistance furnace was used for the weight-loss effusion determinations. The results of the investigation are shown in Figure 1. It can be seen from the slopes of the vapor pressure curves that the change in the heat of vaporization of nickel has been very small (if at all) while about a 30 kcal/mole change occurred for Al. Also, the activity of nickel has not been lowered significantly while aluminum has been lowered considerably. This lends credence to the concept of charge transfer and increased bonding strength between constituent metal atoms.

In the course of the investigation gaseous NiAl was observed and its dissociation energy was determined to be 61 kcal/mole. If the bonding then between Ni-Ni is about the same as Al-Ni then

$$\frac{D^\circ\ (NiAl)}{\Delta H_{atom}\ (NiAl)} = \frac{D^\circ\ (Ni_2)}{2\Delta H_{atom}\ (Ni_{bcc})}$$

using

ΔH_{atom} Al = 77 kcal/mole

ΔH_{atom} Ni = 98 kcal/mole (for bcc)

D° (NiAl) = 61 kcal/mole

D° Ni_2 = 58 kcal/mole

Then ΔH_{atom} (NiAl) = 206 kcal/mole.

Since $\Delta H_{atom} = -\Delta H_f$ (NiAl) + ΔH_{atom} (Al) + ΔH_{atom} (Ni) = 206 kcal/mole

ΔH_f (NiAl) = -31 kcal/mole

as compared to a literature value[3] ΔH_f (NiAl) = -28 kcal/mole

Although the first experiments look promising and ab initio calculations of other aluminum-transition metal compounds have shown a good correlation it is still considered an open matter as to whether this is a fruitful method for calculating the energy changes which occur during charge transfer in intermetallic compounds.

* Work performed in part under AEC Contract W-7405-eng-92

REFERENCES

(1) Brewer, L., Chapter 2 of High Strength Materials, V. F. Zackay, New York, John Wiley (1965).

(2) G. Verhaegen, F. E. Stafford, P. Goldfinger, and M. Ackerman, Trans. Faraday Soc., 58, 1926 (1962); R. Colin and P. Goldfinger in Condensation and Evaporation of Solids, Gordon and Breach, New York, 1964, p. 165.

(3) Metallurgical Thermochemistry, O. Kubaschewski, E. Evans, and C. B. Alcock, Pergammon Press (1967).

FIGURE 1

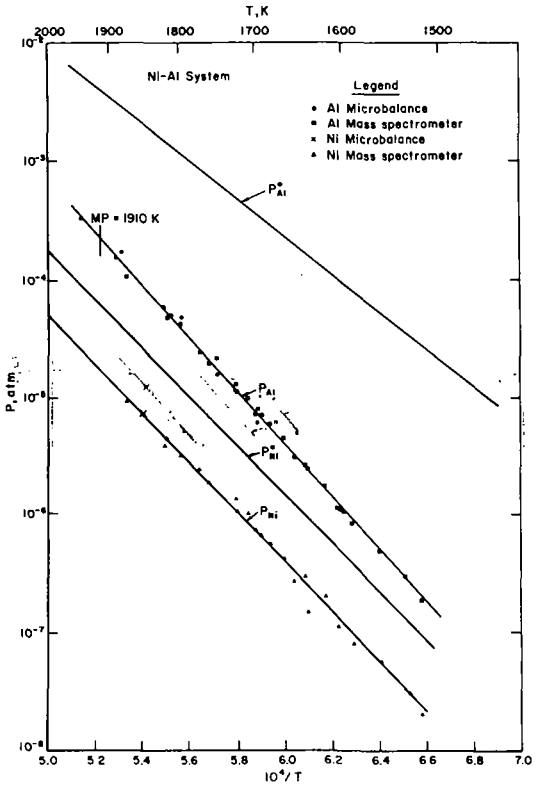

NITROGEN THERMOCHEMISTRY IN HIGH TEMPERATURE REACTIONS OF ZIRCONIUM DROPLETS*

R. T. Meyer
Sandia Laboratories
Albuquerque, New Mexico 87115

ABSTRACT

Recent experiments have yielded new information pertinent to the physicochemical mechanism of microbubble formation and explosion of liquid zirconium droplets which are burned in N_2/O_2 mixtures at 3000-4000°K. Extensive application of a mass spectrometry technique for picomole gas analyses has provided N_2(g) evolution data as a function of reaction time, N_2/O_2 reactant ratio, and degree of prenitridation. Prenitridation with $^{15}N_2$ or $^{15}N_2 + {}^{14}N_2$ mixtures has proven conclusively the origin of the evolved N_2(g) and has indicated the presence of atomic nitrogen in the bubble nucleation process. The results demonstrate the equivalence of the reaction mechanisms for Zr burned in N_2/O_2 and for prenitrided Zr burned in pure O_2. Studies of the physical structure and internal color of the solidified reaction product as a function of N_2/O_2 reactant ratio and of reaction time have revealed the transitional progression of the reaction from slow oxidation to explosive combustion and the existence of concentration gradients within the reacting zirconium droplet prior to bubble formation.

The present results are combined with previously published data[1-3] on surface temperature versus time, ZrO(g) emission spectra and zirconium droplet oxidation kinetics to suggest a thermochemical mechanism for the explosion phenomenon. The proposed mechanism is a thermal, self-accelerating decomposition of a ternary alloy of zirconium, oxygen and nitrogen, in which N-atom recombination provides a localized source of energy for bubble nucleation and ZrO vaporization supports the growth and explosion of the gas bubble.

---

* This work was supported by the U.S. Atomic Energy Commission.

1 R. T. Meyer and L. S. Nelson, High Temperature Science, 2, 35 (1970).

2 R. T. Meyer and W. G. Breiland, High Temperature Science, 2, 000 (1970).

3 L. S. Nelson, D. E. Rosner, S. C. Kurzius and H. S. Levine, in "Twelfth Symposium (International) on Combustion, 1968," p. 59, Combustion Institute, Pittsburgh, 1969.

THERMOCHEMISTRY OF THE Eu-Se SYSTEM FROM MASS SPECTROMETRIC MEASUREMENTS

by

Margaret Frisch

IBM Thomas J. Watson Research Center, Yorktown Heights, N. Y. 10598

Abstract

An apparatus for mass spectrometric measurements of high temperature gaseous species has been constructed which incorporates several unique features:

1. The mass effusion rate from a Knudsen cell can be measured simultaneously with the ion current by means of a Cahn electrobalance, thus permitting direct calibration of ion current in terms of pressure.

2. Both furnace and mass spectrometer chambers are ion pumped which yields a very low count rate for organic ions.

3. The molecular beam is modulated in the furnace one cm from the orifice which eliminates any contribution to a peak due to re-evaporation from the shields.

4. Ion counting via a bidirectional scaler is employed which greatly increases the signal-to-noise ratio of low pressure constituents.

This system has been applied to the study of the vapor species over EuSe single crystals in a tantalum Knudsen cell over the temperature range 1550°K to 1927°K. The primary reaction is the decomposition to the elements. However, the molecular species EuSe(g) and Se_2(g) were observed both at about 0.5% of the total vapor. The experimental and derived data for the study are given in the accompanying Table. The experimental uncertainties reported are from statistical scatter of the data while those associated with the derived quantities are the accumulated errors including the temperature and the thermodynamic data for Eu(g)[1] and Se(g).[2]

C. Bergman, P. Coppens, J. Drowart, and S. Smoes[3] have just recently published values for the dissociation energies of the gaseous rare earth monoselenides, based on mass spectrometric measurements. Their result of 71.1 ± 3.6 kcal/mole for D_0° of EuSe(g) is in excellent agreement with the value of 71.4 ± 2.0 kcal/mole, derived from our data.

References

1. R. Hultgren, Selected Values of Thermodynamic Properties of Metals and Alloys (John Wiley & Sons, New York, 1963).

2. D. R. Stull and G. C. Sinke, Thermodynamic Properties of the Elements (American Chemical Society, Washington, D. C., 1956).

3. C. Bergman, P. Coppens, J. Drowart, and S. Smoes, Trans. Faraday Soc. 66, 800 (1970).

TABLE I.

THERMODYNAMIC PROPERTIES OF THE Eu-Se SYSTEM.

	Experimental Data			Derived Data			
Reaction Studied	Temperature Range °K	ΔH°_r kcal/mole	ΔS°_r Gibbs/mole	Species	T_{av} °K	ΔH°_f kcal/mole	S° Gibbs/mole
Eu(g) + Se(g) = EuSe(g)	1686-1927	-74.4 ± 0.3	-25.8 ± 0.2	EuSe(g)	1800	-6.0 ± 2.0	80.0 ± 2.0
Eu(g) + Se(g) = EuSe(s)	1550-1800	-196.0 ± 2.3	-55.7 ± 2.3	EuSe(s)	1670	-127.1 ± 4.0	49.1 ± 3.0

Unimolecular Decomposition of Desoxybenzoin Azine Induced by Electron Impact. Stuart E. Scheppele and Ronald K. Mitchum, Department of Chemistry, Oklahoma State University, Stillwater, Oklahoma 74074 and Ronald D. Grigsby, Department of Biochemistry and Biophysics, Texas A and M University, College Station, Texas 77843.

Mass spectra of desoxybenzoin azine(I), desoxybenzoin azine d_4, and desoxybenzoin azine -d_{10} (α-ring deuterated) have been obtained. The preliminary results are as follows. Although the fragmentation mechanisms for I fit the general pattern observed for acetophenone[1](II) and benzaldehyde[2](III) azines, the intensities of a number of the fragmentation and rearrangement-fragmentation pathways are altered by change in α substituent from methyl(II) and hydrogen(III) to benzyl(I). For example, percent ionizations for α cleavage in the molecular ions with loss of methyl(II), hydrogen(III) and benzyl(I) are 18, ca. 2, and 26. Percent ionizations for loss of C_6H_5 from the molecular ions of I, II, and III are 0.1, 4, and 17 respectively. A specific 1,3 migration of benzyl (0.2% Σ) and hydrogen (ca. 1% Σ) is observed for the molecular ions of I and III. However, the corresponding migration of methyl is not observed in the spectrum of II. The ion at m/e 194 in the spectrum of I appears to be formed via simple nitrogen-nitrogen bond rupture in the molecular ion and loss of benzonitrile from the M-91 ion. A 1,4 migration of a benzylic hydrogen to nitrogen in the molecular ion of I followed by cleavage of the nitrogen-nitrogen bond appears to lead to m/e 193 and 195. Formation of the C_7H_7 ion in the spectrum of I appears to specifically involve one of the original benzyl groups of I.

References

1. (a) S. E. Scheppele, R. D. Grigsby, E. D. Mitchell, and G. R. Waller, J. Amer. Chem. Soc., 90 3521 (1968).

(b) S. E. Scheppele, R. D. Grigsby, D. W. Whitaker, S. Hinds, K. F. Kinneberg, and R. K. Mitchum, Org. Mass Spec. 3, 571 (1970).

2. (a) R. G. Cooks and S. W. Tam, ibid, 1 583 (1968).

(b) B. Zeek and R. Beutler, ibid, 1, 791 (1968).

(c) S. E. Scheppele, R. D. Grigsby, K. F. Kinneberg, E. D. Mitchell, and C. A. Mannan, ibid, 3, 557 (1970).

COMPUTER INTERPRETATION OF AMINE MASS SPECTRA

A. M. Duffield, A. Buchs,* Allan B. Delfino and Carl Djerassi
Department of Chemistry, Stanford University
Stanford, California 94305

The scope of the computer program Heuristic DENDRAL has been extended[1,2] to the interpretation of the low resolution mass spectra of aliphatic amines. To accomplish this result it was found necessary to develop an irredundant notational system for the representation of saturated aliphatic amine structures. This was done using the symbols T, S, P and M to define the degree(s) of substitution of the carbon atom(s) attached to nitrogen in saturated aliphatic amines. Thus the symbols T, S, P and M are defined as follows:

$$T = -\overset{|}{\underset{|}{C}}-; \quad S = -\overset{|}{C}H-; \quad P = -CH_2- \text{ and } M = CH_3$$

The canonical order in this convention is defined as T>S>P>M and the following superatoms are presented as examples of this notation.

$$TP = -\overset{|}{\underset{|}{C}}-N-CH_2- \qquad TSM = -\overset{|}{\underset{|}{C}}-\overset{|}{N}-CH-$$
$$\qquad\qquad\quad H \qquad\qquad\qquad\qquad\quad CH_3$$

A total of 31 superatoms can be constructed from all possible combinations of T, S, P and M in addition to the three special cases of M, MM and MMM which translate to methyl amine, dimethyl amine and trimethyl amine respectively.

Figure 1 is a schematic representation of the Heuristic DENDRAL program as applied to aliphatic saturated amines. The right hand section of Figure 1, which is enclosed in dotted lines, is an optional NMR subsection and is only utilized if NMR experimental data are available. This NMR sub-routine uses the position of the NMR signal, its integral value and multiplicity. From these data the program identifies the number of carbon and nitrogen bound methyl groups and if possible the number of hydrogen atoms situated on a carbon atom itself joined to nitrogen.

The sub-routine SIZE (Figure 1) is used by the program to determine whether a particular superatom, plus the minimum number of methyl groups to saturate all its free valences, can be built within the limits of the empirical composition. If insufficient carbon atoms are available for the construction of a superatom (for example TTT which requires a minimum of 12 carbon atoms) then that superatom is discarded from future consideration.

The mass spectrometric bound conditions are represented diagramatically in Figure 1 and begin with the well documented α-cleavage process of aliphatic amines.[3] Additional theory is incorporated in the heuristic decisions represented by MAXINTENS etc. through the sub-routine called REARRANGEMENT. The theoretical basis and the implications of these decisions are described in our forthcoming publication.[4]

The presence of all the 31 superatoms which can be constructed for saturated aliphatic amines from combination of the symbols T, S, P and M on the initial GOODLIST requires that the program consider all possible answers to a given problem. When a superatom fails any one of the heuristic decisions described in Figure 1 it is removed from GOODLIST and hence eliminated as a potential solution to the problem at hand. The program then computes the number of possible isomers consistent with all entries remaining on GOODLIST and this number represents the number of solutions to any given problem. If the structure of each of the isomers is required then this can be obtained from the optional STRUCTURE GENERATOR portion of the program.

Using a library of 93 saturated amine mass spectra the computer program (Heuristic DENDRAL) always presented the correct answer in its final output. A brief summary of the results obtained using the program are listed in Table 1. It is evident that an impressive degree of truncation is achieved by the program when only mass spectrometric input is used while if this is supplemented by NMR data in general only one answer (the correct one) results.

Acknowledgements. Financial support from the Advanced Research Projects Agency (Contract SD-183), the National Aeronautics and Space Administration (Grant NGR-05-020-004) and the National Institutes of Health (Grant AM 04257) is gratefully acknowledged.

* Present Address: University of Geneva, Geneva, Switzerland.

Figure 1

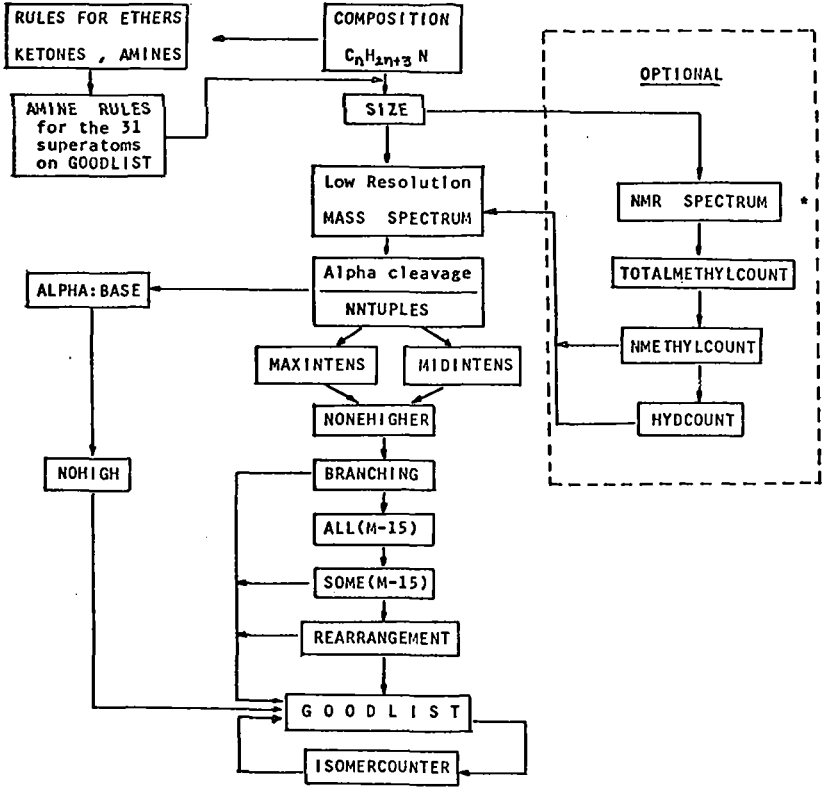
RULES FOR ETHERS
KETONES , AMINES
COMPOSITION
$C_nH_{2n+3}N$
AMINE RULES for the 31 superatoms on GOODLIST
SIZE
OPTIONAL
Low Resolution MASS SPECTRUM
NMR SPECTRUM
TOTALMETHYLCOUNT
NMETHYLCOUNT
HYDCOUNT
Alpha cleavage
NNTUPLES
ALPHA:BASE
MAXINTENS
MIDINTENS
NONEHIGHER
NOHIGH
BRANCHING
ALL(M-15)
SOME(M-15)
REARRANGEMENT
G O O D L I S T
ISOMERCOUNTER

Table 1

Amine	Number of amine isomers	Mass spectra alone: Number of superatoms on GOODLIST	Mass spectra alone: Number of possible isomers	Mass spectra + NMR spectra: Number of superatoms on GOODLIST	Mass spectra + NMR spectra: Number of possible isomers
3-hexyl	39	1	2	1	1
1,3-dimethylbutyl	39	2	8	1	2
2,2-dimethyl-3-butyl	39	2	8	1	1
N-methyl-ethyl-n-propyl	39	8	15	2	2
N,N-dimethyl-2-butyl	39	6	6	1	1
2-heptyl	89	2	16	1	1
n-propyl-n-butyl	89	5	10	1	1
1,3-dimethylpentyl	89	2	16	1	4
1,5-dimethylhexyl	211	2	34	1	9
N,N-dimethyl-3-hexyl	211	3	6	1	1
N-methyl-n-butyl-isopropyl	211	10	31	1	1
Di-isopropyl-ethyl	211	6	18	1	1
N-methyl-n-propyl-n-butyl	211	5	24	1	1
n-propyl-n-hexyl	507	7	42	1	1
3,3,5-trimethylhexyl	507	1	89	- *	-
N-methyl-isopropyl-n-amyl	507	5	20	-	-
N-methyl-n-propyl-n-hexyl	1238	10	46	1	1
N,N-dimethyl-3-octyl	1238	8	36	1	1
n-butyl-n-hexyl	1238	3	48	1	1
N,N-dimethyl-2-ethylhexyl	1238	4	156	-	-
n-amyl-n-hexyl	3057	9	112	-	-
Tri-n-butyl	7639	2	8	-	-
Di-n-heptyl	48865	6	510	-	-
Tri-isoamyl	124906	2	40	1	9
N-methyl-8-hexadecyl	321198	1	3471	-	-
n-octyl-n-nonyl	830219	2	6942	1	1
N,N-dimeth-8-hexadecyl	2156010	4	14418	1	1
Tri-n-hexyl	2156010	2	240	1	1
Tri-n-heptyl	38649142	2	1938	-	-

* Blanks in columns 5 and 6 indicate that no NMR spectrum was available.

REFERENCES

1. A. M. Duffield, A. V. Robertson, C. Djerassi, B. G. Buchanan, G. L. Sutherland, E. A. Feigenbaum and J. Lederberg, J. Amer. Chem. Soc., 91, 2977 (1969).

2. G. Schroll, A. M. Duffield, C. Djerassi, B. G. Buchanan, G. L. Sutherland, E. A. Feigenbaum and J. Lederberg, J. Amer. Chem. Soc., 91, 7440 (1969).

3. H. Budzikiewicz, C. Djerassi and D. H. Williams, Mass Spectrometry of Organic Compounds, Holden-Day Inc., San Francisco, 1967, pp. 297-303.

4. A. Buchs, A. B. Delfino, A. M. Duffield, C. Djerassi, B. G. Buchanan, G. L. Sutherland, E. A. Feigenbaum and J. Lederberg, J. Amer. Chem. Soc., submitted for publication.

Fragmentation Processes in the Mass Spectra of Trialkyl Phosphates, Phosphorothionates, Phosphorothiolates, and Phosphorodithioates.

Francis J. Biros and Ralph T. Ross
Perrine Primate Research Branch, Division of Pesticide Chemistry and Toxicology, Food and Drug Administration, Perrine, Florida 33157.

Abstract: The low resolution mass spectra of four trialkyl phosphates, two trialkyl phosphorothiolates, four trialkyl phosphorothionates, and three trialkyl phosphorodithioates (derivatized metabolic and hydrolytic products of organophosphorus pesticidal compounds) have been recorded. Fragmentation-structure correlations have been outlined and some pathways to prominent ions established by means of metastable ion data and accurate mass measurements. Important initial reactions of the molecular ions of the phosphates included replacement of an ethyl group by a hydrogen atom. Secondary processes involved double rearrangements and cleavage at the phosphorus atom with the latter reaction predominating in the case of the trimethyl substituted compounds. Similar dissociative processes involving elimination of alkyl, alkoxyl, and thioalkoxyl groups were observed for the phosphorothionates in addition to internal electron impact induced P(:S)-OR to P(:O)-SR rearrangements and significant fragments due to abstraction of either a sulfur atom or ·SH radical. The trialkyl phosphorodithioates exhibited fragmentation schemes involving combinations of those observed for the phosphorothionates and phosphorothiolates.

Introduction: The mass spectral properties of several classes of organic pesticidal compounds have received recent attention. Electron impact induced dissociative processes have been discussed for chlorinated hydrocarbon (1-3), carbamate (4,5) and organophosphorus (6) pesticides. In addition, reports are available for a number of miscellaneous groups of compounds used as pesticides including uracils (7), triazines (3), and phenoxyalkanoic acids (3). Mass spectral studies of this type have been found to be of invaluable assistance in the interpretation of data obtained for unknown pesticidal transformation products isolated during the course of animal and plant metabolism and photochemical decomposition studies. In fact, the unimolecular reactions of ions produced in the mass spectrometer may bear a mechanistic relationship to the photochemical behavior of certain classes of compounds including pesticides (5,14). In addition, mass spectral data of standard materials are required for comparative purposes when the mass spectrometric method is employed as an individual technique or combined with gas chromatography for the purpose of confirmation of pesticide residues isolated from human, animal and environmental media.

During the course of method development studies directed toward the determination of the metabolic and hydrolytic products of organophosphorus insecticides in human and animal blood and urine (12,13), the mass spectra of a series of trialkyl substituted phosphorus compounds were required. These compounds may be considered to be derivatized (methylated or ethylated) hydrolysis products of organophosphorus pesticides and consist of four classes or compound types including phosphates, phosphorothionates, phosphorothiolates, and phosphorodithioates. This report presents a summary discussion of the chemical fragmentation processes observed for several compounds of each structural type. A detailed, inclusive discussion will be presented elsewhere. Dissociative schemes have been proposed on the basis of low resolution mass spectral studies coupled with metastable ion data and accurate mass measurements.

Results and Discussion: - Trialkyl Phosphates -

The mode of fragmentation of the four trialkyl phosphate compounds examined are very similar to that reported for triethyl phosphate and other alkyl and aryl substituted phosphate compounds (8-11) which have been discussed previously by other authors. For dimethyl monoethyl phosphate (DMMEP) and diethyl monomethyl phosphate (DEMMP), the initial process observed to occur was the very favorable elimination of one ethyl substituent with back transfer of two hydrogen atoms to form a tetra-covalent phosphorus species, m/e 141 for DEMMP and m/e 127 for DMMEP. In both cases, the tetra-covalent phosphorus ion formed in this fashion accounted for the base peak in the mass spectrum. Metastable ions were observed for both these transitions.

For DEMMP, an elimination of a neutral ethylene molecule from the base peak followed which led to the formation of a fragment of m/e 113 with a metastable ion observed at m/e 90.56. Subsequent loss of water from this fragment was observed to occur with the formation of intense ion current at m/e 95, $[CH_3OP(O)OH]+$.

The base peak in the mass spectrum of DMMEP of m/e 127, undergoes facile loss of a molecule of water to form the m/e 109 ion corresponding to the $[(CH_3O)_2P{=}O+]$ species or dissociation can occur at the phosphorus atom, with hydrogen rearrangement to form the ion at m/e 79, $[CH_3OPOH+]$. Elimination of a methoxyl group from an intense m/e 95 ion results in the formation of the m/e 65 $[P(OH)_2+]$ fragment with single hydrogen rearrangement and the m/e 66, $[PH(OH)_2+]$, fragment with double hydrogen rearrangement.

Trimethyl phosphate (TMP) exhibited a relatively simple mass spectrum with intense

peaks at m/e 110, $[(CH_3O)_2POH]+\cdot$; m/e 109 $[(CH_3O)_2P{=}O]+$; m/e 95, $[CH_3OP(O)OH]+$; m/e 80, $[CH_3OP(H)OH]+\cdot$; and m/e 79, $[CH_3OPOH]+$. Metastable ions were observed for the transitions m/e 140 ⟶ m/e 110 (m/e 86.43), m/e 110 ⟶ m/e 109 (m/e 108.01), m/e 110 ⟶ m/e 80 (M/e 58.20), and m/e 109 ⟶ m/e 79 (m/e 57.25). A more detailed discussion of the mass spectrum of TMP has been presented by other investigators (10).

- Trialkyl Phosphorothionates -

The fragmentation pattern for this class of organophosphorus compounds is characterized by a competition of decomposition modes involving either elimination of an ethyl substituent with hydrogen rearrangement or fission of the phosphorus oxygen bond, with or without an associated hydrogen rearrangement. In addition, significant processes involved the elimination of a sulfur atom or ·SH radical and electron impact induced thiono to thiolo rearrangements leading to the formation of relatively intense fragment ions (15).

The molecular ions produced in the mass spectra of the phosphorothionates were quite intense ranging from 53% relative intensity for trimethyl phosphorothionate (TMTP) to 100% relative intensity for dimethyl monoethyl phosphorothionate (DMMETP). For TMTP the predominant initial process involves elimination of a methoxyl substituent coupled with back transfer of a hydrogen atom to form the fragment ion m/e 126, $(CH_3O)_2PSH^+$, or without hydrogen rearrangement to form an ion of m/e 125, $(CH_3O)_2PS+$. Subsequent elimination of an ·SH radical leads to the formation of the base peak ion of m/e 93 corresponding to the $(CH_3O)_2P+$ ion. A metastable ion at m/e 68.64 was observed for this transition. Elimination of the CH_2O species from the base peak generates the m/e 63 fragment of CH_3OPH composition.

An entirely analogous dual decomposition scheme may be postulated to explain the significant fragment ions in the mass spectrum of triethyl phosphorothionate (TETP). As was noted in the mass spectrum of trimethyl phosphorothionate, fragment ions of m/e 137, $(CH_3CH_2O)_2P{=}O+$, m/e 109, $CH_3CH_2OPO(OH)+$, and m/e 81, $(HO)_2P{=}O+$, may be formed from a rearranged, electron impact produced triethyl phosphorothiolate molecular ion species.

A similar dissociation scheme for DMMETP may be postulated assuming the occurrence of a dual decomposition pathway. Thus, the molecular ion of m/e 170 undergoes fragmentation with loss of a C_2H_4O species to yield the m/e 126 $(CH_3O)_2PSH^+\cdot$ radical ion which may then eliminate a ·SH radical to form the base peak at m/e 93, $(CH_3O)_2P+$. Decomposition involving elimination of an ethyl substituent with back transfer of one or two hydrogen atoms results in the generation of m/e 142 and m/e 143 fragment ions. Loss of water from the m/e 143 ion of $(CH_3O)_2P(OH)SH+$ composition results in a $(CH_3O)_2P{=}S$ species at m/e 125. Elimination of a CH_2O molecule from the m/e 142 fragment yields the m/e 112, $CH_3OP(OH)SH^+\cdot$ species. The m/e 125 fragment may also be formed by elimination of a CH_3CHO molecule from the rearranged S-methyl-O-ethyl-O-methyl phosphorothiolate molecular ion. Fragment ions resulting from the dissociation of another rearranged molecular species (S-ethyl-O,O-dimethyl phosphorothiolate) occur at m/e 109 and m/e 110.

- Trialkyl Phosphorothiolates -

Three dissociative pathways for the molecular ion are observed in the fragmentation scheme of the phosphorothiolate class of compounds. For the compound O,O-diethyl-S-ethyl phosphorothioate (TEPTh), these include elimination of a molecule of ethylene from either a sulfur atom or an oxygen atom to form the m/e 170 fragment ion, and cleavage with hydrogen rearrangement of either an ethoxyl or thioethoxyl substituent to form the $(CH_3CH_2O)_2P{-}OH^+\cdot$ ion. Further loss of an ethoxyl group from this fragment accompanied by back transfer of one or two hydrogen atoms accounts for the base peak of m/e 111 with a $CH_3CH_2OP(H)(OH)_2+$ structure and a significant fragment of m/e 110, corresponding to a $CH_3CH_2OP(OH)_2^+$ species. Subsequent loss of a molecule of water from the m/e 111 ion results in the formation of the m/e 93, CH_3CH_2OPOH+ fragment.

The pathway resulting from elimination of an ethoxyl group from the molecular ion leads to the m/e 154, $CH_3CH_2OP(OH)SCH_2CH_3^+\cdot$ species which in turn may eliminate a molecule of ethylene to yield a fragment of either S-ethyl or O-ethyl structure with $C_3H_7PO_2S$ composition at m/e 126. Multiple pathways may also be postulated for the decomposition of the molecular ion by elimination of ethylene. Thus the fragment ion of m/e 170 most probably consists of contributions from structures such as $(CH_3CH_2O)_2P(O){-}SH^+\cdot$ and $CH_3CH_2O{-}\overset{OH}{P}(O){-}SCH_2CH_3^+\cdot$.

- Trialkyl Phosphorodithioates -

The mass spectra for the phosphorodithioate class of organophosphorus compounds studied present a complex dissociative scheme due to the possibility of formation of fragment ions with several isomeric structures. Decomposition processes involve the generation of fragment ions by elimination of alkoxyl and thioalkoxyl substituents accompanied in some cases by hydrogen rearrangement. For the compounds containing ethyl substituents, significant alkyl fragmentation occurs with loss of an ethylene molecule.

The simplest decomposition scheme is afforded by the compound O,O-dimethyl-S-methyl phosphorodithioate (TMDTP). The molecular ion (m/e 172) may fragment by elimination of a methoxyl group or a thiomethoxyl group with hydrogen rearrangement yielding ions of m/e 142 and m/e 126, respectively. These fragments have been assigned structures of $CH_3SP(SH)OCH_3^+\cdot$, and $(CH_3O)_2PSH^+\cdot$. The subsequent decomposition is identical in both cases

and involves the abstraction of a ·SH radical producing the base peak m/e 93, $(CH_3O)_2P^+$ fragment from m/e 126, and the m/e 109, $CH_3SPOCH_3^+$ fragment from m/e 142. Metastable ions were observed for the m/e 142 ⟶ m/e 109 transition at m/e 83.66 and for the m/e 126 ⟶ m/e 93 decomposition at m/e 68.64. Further loss of methoxyl substituents from these two ions produces relatively intense peaks at m/e 95, m/e 63, and m/e 79. Also observed was the initial decomposition of the molecular ion to form a m/e 125 fragment by elimination of a thiomethoxyl group.

The mode of fragmentation of 0,0-diethyl-S-ethyl phosphorodithioate (TEDTP) was noted to be somewhat more complex due to the possibility of formation of isomeric ion fragments with identical elemental composition. Thus, elimination of ethylene from the molecular ion results in the generation of the m/e 186 fragment undoubtedly consisting of contributions from the structures $CH_3CH_2OP(S)(OH)SCH_2CH_3^+$ and $(CH_3CH_2O)_2P(S)SH^+$. If a dithiolo rearrangement species is initially formed, the m/e 186 ion may consist of contributions from additional structures such as $(CH_3CH_2S)_2P(O)OH^+$ and $CH_3CH_2SP(O)(SH)$—$OCH_2CH_3^+$.

An alternate decomposition pathway results from initial elimination of a thioethoxyl substituent from the parent species, m/e 214 radical ion. Subsequent processes include sulfur abstraction and ethylene elimination to yield significant fragments at m/e 121, m/e 125, m/e 97, m/e 93, and m/e 65. Additionally, the molecular ion may decompose with loss of an ethoxyl group and hydrogen rearrangement to the m/e 170, $CH_3CH_2OP(SH)SCH_2CH_3^+$ species which in turn may lose a ·SH radical to form the m/e 137, $CH_3CH_2OPSCH_2CH_3^+$ ion. Further decomposition by elimination of ethylene results in the m/e 109, $CH_3CH_2OPSH^+$, or $CH_3CH_2SPOH^+$ species with a metastable peak observed at m/e 86.72. The m/e 109 fragment may also conceivably be produced by elimination of C_2H_4S from a m/e 170, $(CH_3CH_2S)_2POH^+$ ion if one assumes the existence of a dithiolo molecular ion species.

Experimental: The low resolution 80 eV mass spectra reported here were obtained on a Perkin Elmer Model 270 combined gas chromatograph-mass spectrometer using direct probe introduction techniques. Only ion fragments greater than m/e 40 are considered in the mass spectra of the trialkyl phosphates. Both the sample probe and ion source were maintained at ambient temp. (approx. 35°C). To avoid sample degradation as much as possible, no external heat was applied to the target. However, the target temperature averaged 145°C due to the heat of the source filament (100 μa emission). Electrostatic sector and ion source potentials were adjusted for maximum ion beam current at 2.6 kV accelerating voltage.

High resolution accurate mass measurements were made by peak matching techniques employing an AEI MS-9 double focusing mass spectrometer by Prof. R. C. Dougherty of the Department of Chemistry, Florida State University.

References:

(1) J. N. Damico, R. P. Barron, and J. M. Ruth, Org. Mass Spectrom. 1, 331 (1968).
(2) J. A. Sphon, and J. N. Damico, Org. Mass Spectrom. 3. 51 (1970).
(3) J. Jörg, R. Houriet, and G. Spiteller, Monatsh. Chem. 97, 1064 (1966).
(4) J. N. Damico, and W. R. Benson, J. Assoc. Offic. Anal. Chemists. 48, 344 (1965).
(5) W. R. Benson, and J. N. Damico, J. Assoc. Offic. Anal. Chemists. 51, 347 (1968).
(6) J. N. Damico, J. Assoc. Offic. Anal. Chemists. 49, 1027 (1966).
(7) R. W. Reiser, Org. Mass Spectrom. 2, 467 (1969).
(8) F. W. McLafferty, Anal. Chem. 23, 306 (1959).
(9) A. Quayle, Advan. Mass Spectry. 365 (1959).
(10) D. A. Bafus, E. J. Gallegos, and R. W. Kiser, J. Phys. Chem. 70, 2614 (1966).
(11) H. Budzikiewicz, C. Djerassi, and D. H. Williams, Mass Spectrometry of Organic Compounds. Holden Day, Inc., San Francisco. 1967, p. 645 ff.
(12) M. T. Shafik, and H. F. Enos, J. Agr. Food Chem. 17, 1186 (1969).
(13) M. T. Shafik, and D. Bradway, Abstracts CIC/ACS International Meeting, Toronto, Canada, May 24-29, 1970, #PEST 054.
(14) N. J. Turro, D. C. Necker, P. A. Leermaker, D. Seldner, and P.D'Angelo, J. Amer. Chem. Soc., 87, 4097 (1965).
(15) R. G. Cooks and A. F. Gerrard, J. Chem. Soc. B 1968, 1327.

HYDROGEN TRANSFER IN ALKYLAROMATICS

David A. Lightner
Department of Chemistry, University of California
Los Angeles, California 90024

The hydrogen transfer rearrangement of alkylbenzenes has been investigated by a number of workers.[1-4] The source of the hydrogen transferred in n-butylbenzene was shown to be largely (95%) from the γ-carbon by single deuterium labelling studies.[1,5] In this same work,[1,5] it was also shown that 5% of the hydrogen transferred originated from the δ-carbon. Our data, shown in Table 1, also clearly point to the γ-carbon as the major site of transferred hydrogen (deuterium) regardless whether the hydrogen (deuterium) is primary (1°), secondary (2°) or tertiary (3°). Recent data[4] on more extensively deuterated alkylbenzenes, viz., a given chain carbon fully deuterated, indicates that H-D exchange occurs between the ortho positions of the aromatic ring and the alkyl hydrogens (deuteriums). Exchange processes (Scheme 1) of this type have been noted in N-alkylpyrrole[6] and γ-phenylpropyl bromide[7], and 1-phenylheptene[8] mass spectra. The presence of an ion at m/e 94, which may be found when more than one γ-deuterium atom is present in the molecule, is rationalized in terms of the exchange

Scheme 1

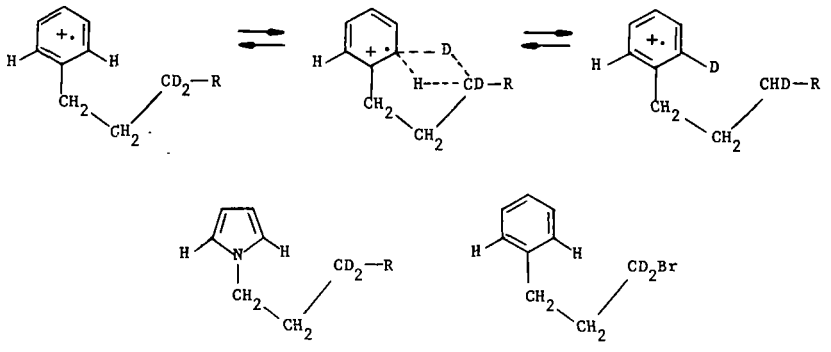

Table 1

Percent Ionization at 14 eV for the Region m/e 95-91 of Alkylbenzenes

			95	94	93	92	91
Isobutyl	(1°)	d_0				58	42
		γ-d_6		2	50	6	43
n-Butyl	(2°)	d_0				59	41
		γ-d_2		6	42	6	42
Neopentyl	(1°)	d_0				98	2
		γ-d_9		1	84	12	3
Isoamyl	(3°)	d_0				87	13
		γ-d_1			37	60	3

Table 2

Substituent Effect on the m/e 92 and 91 Fragment Ions of $C_6H_5CH_2CH_2CH_2X$

	Percent Ionization (70 eV) at m/e:		
X	M^+	92	91
H	8	2	41
CH_3	5	14	31
OH	5	9	20
OC_2H_5	0.7	7	15
Br	9	6	48
CN	10	4	40
NO_2	0.7	0.4	23

depicted in Scheme 2. A critical evaluation of extensively deuterium labelled n-alkyl-

Scheme 2

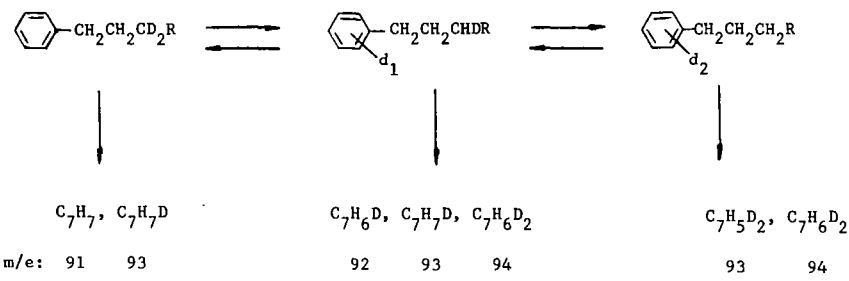

benzenes[4] suggests that in the non-deuterated examples m/e 91 arises essentially exclusively from the parent ion at all ionizing voltages and that although exchange does occur between the ortho positions on the ring and β,γ,δ,ε etc positions in the alkyl chain, only transfer from the γ-carbon leads directly to formation of m/e 92. The data of Table 1 appear also to suggest that H-D exchange between the ring and side chain proceeds to the greatest extent in the life-time of the fragmenting parent ion for 3° hydrogen (deuterium) transfer (3° > 2° > 1°).

The relative importance of the type of hydrogen (3°, 2°, *or* 1°) *transferred and the* stability of the neutral fragment may be seen in Figures 1 and 2 which depict a McLafferty rearrangement mechanism. Thus, Figure 1 shows a correlation in which hydrogen is transferred most easily (intensity of m/e 92) if it is 3° and least easily if it is 1°. This finding is in agreement with the work of Budzikiewicz, Fenselau and Djerassi[9] who found a 10:1 preference of 2° H over 1° H transferred in the mass spectra of ketones. We also note however, in Figure 1, that the greater m/e 92 intensity is associated with the more stable (more highly substituted) olefin. This type of correlation can be seen

Figure 1

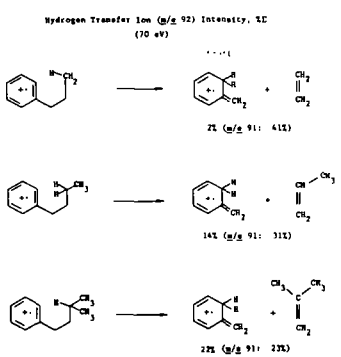

Figure 2

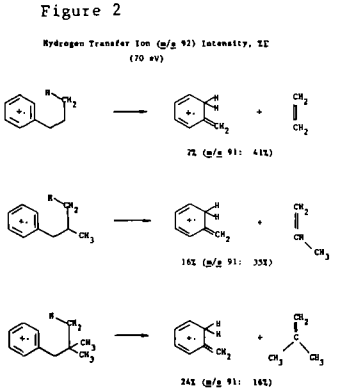

more easily in Figure 2 which depicts 1° H transfer in all cases leading to m/e 92 ions whose intensity correlated one-for-one with the neutral fragment stability. A comparison of the data in Figures 1 and 2 finds the m/e 92 intensities roughly equal (14% vs 16%) when the neutral fragment is propylene (cf. n-butylbenzene, 2° H and isobutylbenzene, 1° H) and also nearly equal (22% vs 24%) when the neutral fragment is isobutylene (cf. isoamylbenzene, 3° H and neopentylbenzene, 1° H). It would appear from these data that the transition state for the transfer mechanism resembles products more closely than reactants as is predicted for an endothermic reaction.[10,11]

As a further probe of the parameters affecting the McLafferty rearrangement, the data of Table 2 indicate the effect of a substituent located on the γ-carbon. In keeping with the results of free radical hydrogen abstraction,[12] the NO_2, CN and Br substituents retard the formation of m/e 92 relative to CH_3, OH and OC_2H_5 substituents. Moreover, both steric and electronic effects explain the influence of ortho-methyl groups of the McLafferty rearrangement ion of n-butyl- and neopentylbenzene (Table 3). Thus, for n-butylbenzene, the effect of one o-CH_3 lowers the m/e 106 ion intensity approximately to the same extent as does a p-CH_3 (but greatly different from that of m-CH_3). On the other hand, two o-CH_3 groups drop the m/e 120 ion intensity to zero. Whether this second effect is a steric or an electronic effect is difficult to ascertain; however, the steric requirements of the transition state leading to m/e 106 are sufficiently disturbed by one o-CH_3 in neopentylbenzene to give a very low intensity (cf. the effect of p-CH_3).

The nature of the hydrogen transfer transition has been further investigated in molecular orbital calculations. Some results of a calculation of benzylic bond orders (a) for the ground and excited states of radical cations, using a modified Extended Huckel program[13], are shown in Table 4. An extremely small bond order is found for both concerted (A) and stepwise (B) mechanisms (X = H); however, the stepwise (B) mechanism is a lower energy pathway by 0.5 eV [see state (m.o.s.) 5 in A and 6 in B] than the concerted (A) route. Furthermore, correlation is found with experimental data on aminobutylbenzenes[3] for which the energy of the corresponding low bond order state of m-NH_2 (14.3 eV) is close to that of unsubstituted butylbenzene (14.4 eV) and the normalized hydrogen-transfer ion intensities are nearly equal. On the other hand,

Table 3

Influence of Methyl Substituents on the McLafferty Rearrangement Ion

Intensities (M^+ - 100%) at	70 eV	12 eV
	236	34
p-CH_3	40	6
m-CH_3	190	25
o-CH_3	75	5
2,6-di-CH_3	0	0
	681	267
p-CH_3	984	376
m-CH_3	1440	659
o-CH_3	15	2

Table 4

Energetics of Alkylbenzene Fragmentation

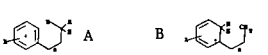

State	Bond Order	ΔE (eV)	State	Bond Order	ΔE (eV)
ground*	0.87	0.0	ground*	0.64	0.0
1	0.68	3.7	1	0.65	0.9
2	0.66	4.3	2	0.64	2.7
3	0.65	7.5	3	0.63	3.0
4	0.60	13.9	4	0.58	12.7
5	0.18	14.9	5	0.64	13.3
6	0.70	15.3	6	0.05	14.4
7	0.42	18.1	7	0.64	15.4
8	0.73	18.5	8	0.74	16.3
9	0.60	18.9	9	0.48	18.8

m-NH_2 corresponding state 14.3

p-NH_2 corresponding state 14.8

the normalized hydrogen-transfer ion intensity of the p-NH_2 isomer is considerably less than that of butylbenzene (cf. 14.8 eV vs 14.4 eV).

REFERENCES

1. H.M. Grubb and S. Meyerson, in "Mass Spectrometry of Organic Ions," F.W. McLafferty, Ed., Academic Press, Inc., New York, N.Y., 1963, chapter 10.
2. For leading references see H. Budzikiewicz, C. Djerassi and D.H. Williams, "Mass Spectrometry of Organic Compounds," Holden-Day, Inc., San Francisco, Calif., 1967, pp 73-85.
3. R. Nicoletti and D.A. Lightner, J. Am. Chem. Soc., 90, 2997 (1968).
4. D.A. Lightner, unpublished data.
5. J.D. McCollum and S. Meyerson, J. Am. Chem. Soc., 81, 4116 (1959).
6. A.M. Duffield, R. Beugelmans, H. Budzikiewicz, D.A. Lightner, D.H. Williams, and C. Djerassi, J. Am. Chem. Soc., 87, 805 (1965).
7. N.M.M. Nibbering, PhD Thesis. Amsterdam; University of Amsterdam (1968).
8. A.F. Gerrard and C. Djerassi, J. Am. Chem. Soc., 91, 6808 (1969).
9. H. Budzikiewicz, C. Fenselau, and C. Djerassi, Tetrahedron, 22, 1391 (1966).
10. F.H. Field and J.L. Franklin, Electron Impact Phenomena, Academic Press, New York, 1957, chapter 4.
11. G.S. Hammond, J. Am. Chem. Soc., 77, 334 (1955).
12. For leading references see E.S. Gould, Mechanism and Structure in Organic Chemistry, H. Holt and Co., New York, 1959, chapter 16, part II.
13. W.A. Beavers, unpublished data, this laboratory. We recognize the errors inherent in this type of calculation for open shell configurations and for neglecting configuration interaction for spectroscopic quantities. We feel, however, that the orbital energy differences between corresponding transition states in the models are significant.

The hydrogen transfer reaction will be discussed in detail in papers submitted to Organic Mass Spectrometry.

ABSTRACT

ELECTRON IMPACT STUDIES OF GROUP IV-A ORGANOMETALLIC ACETYLIDES

D.I. MacLean and R.E. Sacher, Boston College,
Chestnut Hill, Massachusetts 02167

INTRODUCTION

The purpose of this project was to measure the mass spectral patterns, ionization potentials and appearance potentials for as many compounds as possible of the carbon, silicon, germanium and tin methylacetylides, most of which have never been studied by mass spectrometry. Complete mass spectral schemes have been postulated and related to bonding and structure.

EXPERIMENTAL

The compounds studied are:

$(CH_3)_3CC{\equiv}CH$

$(CH_3)_nSi(C{\equiv}CH)_{4-n}$, n = 3, 2, 1, 0

$(CH_3)_nGe(C{\equiv}CH)_{4-n}$, n = 3, 2, 1, 0

$(CH_3)_nSn(C{\equiv}CH)_{4-n}$, n = 3, 2

All compounds except the solid tetraacetylides were purified on an aerograph autoprep A-700 gas chromatograph using a QF-1 fluorosilicon column.

Experimental conditions were: electron voltage - 70 ev, electron trap current - 0.125 microamperes, temperature of inlet system - 293±2°K, temperature of ion source - approx. 325°K.

The experimental apparatus consisted of a homemade, all glass inlet system leading into a Bendix Model 2012 Time-Of-Flight Mass Spectrometer.

RESULTS AND DISCUSSION

Correlations of the results of the experimentally determined monoisotopic spectra will be presented in tables and graphs. Contributions from the metal isotopes and C-13 were summed to give total ion abundances. The abundance of each species is expressed as the percentage of the sum of the abundances of all the metal-containing ions, since the hydrocarbon abundances are negligible.

I. General Features

1. Consider the series $(CH_3)_nM(C{\equiv}CH)_{4-n}$ where M=C, Si, Ge, Sn. The abundance of the molecular ion increases from carbon to silicon and decreases to germanium. For the tin analog, one finds a decrease in abundance in the monoacetylide series and an increase in the diacetylides. As each methyl group is replaced by an acetylene group the molecular ion intensity increases in the silicon series to methyl-silicon-triacetylide and then decreases to silicon-tetraacetylide. In the germanium series it increases from tetramethylgermanium- to trimethylgermaniumacetylide, then decreases to methylgermaniumtriacetylide and increases again going to the tetraacetylide of germanium. The ion abundance increases as acetylene groups are added in the tin series.

2. The most abundant ion in all compounds except for $CH_3Si(C{\equiv}CH)_3$ and $M(C{\equiv}CH)_3$ is the trivalent ion (loss of methyl radical). This is due to the fact that ionization is accomplished by removing one of the bonding electrons of the M-C bond, thus weakening the bonding power.
3. The metal-containing ions are responsible for the major part of the ion current. This is due to the difference in electronegativity between carbon and the metals. The positive charge will reside on the metal-containing fragment.
4. The abundance of rearrangement ions decreases with the increasing size of the metal atom. This is caused by an increase in polarization or a decrease in the M-C bond energy.
5. Only a few metastable ions were found in the mass spectra.
6. There is an absence of C-H fission from $M-CH_3$ groups. The lower stability of the M-C bonds explains this effect.
7. The decomposition of the molecular (odd electron) ion occurs mainly by elimination of an odd electron (radical) fragment giving even electrons.

II. Individual Groups of Compounds

The effect of central atom on the fragmentation patterns of the individual groups of compounds is treated first, and then the replacement of methyl groups by acetylene groups is studied. In general, the amount of the molecular ion formed increases with the number of acetylene groups. The initial cleavage step, the elimination of the CH_3 radical, increases in importance as each acetylene replaces a methyl group.

III. Ionization and Appearance Potentials

Ionization potentials of the carbon, silicon and germanium members of the organometallic acetylides are presented. No ionization potential of the methylgermanium triacetylide could be measured since its parent peak is too small.

Appearance potentials for the monomethyl metal ion of each member of the silicon and germanium series are reported. As the number of acetylene groups is increased the energy needed to fragment and ionize is also increased.

ACKNOWLEDGMENT

This project was supported in part by the U.S. Army Materials and Mechanics Research Center, Watertown, Massachusetts. Special gratitude is due Dr. W. Davidsohn for donating the majority of the compounds studied.

ELECTRON IMPACT FRAGMENTATION PATHWAYS OF HALOACETONES

By: Edward R. McCarthy and J. S. Smith, Allied Chemical Corporation, Morristown, N.J. 07960

We have examined spectra of sixteen fluorine and chlorine containing acetones over a wide range of ionizing voltages. We evaluated the influence of halogen substitution on the fragmentation pathways of these small compounds. Hopefully, this study would provide information to assist in the interpretation of the spectra from more complex molecules. Also we thought it would be of interest to compare the behavior of the haloacetones with that of the aliphatic ketones.

The molecular ion of an aliphatic ketone decomposes by two competing pathways. These processes correspond to the formation of an acyl ion. The lower activation energy process corresponds to loss of the smaller alkyl radical as evidenced by an increase in the value of the ratio $R_L\text{-}C{\equiv}O^+/R_S\text{-}C{\equiv}O^+$ as the ionizing voltage is decreased. The formation of the alkyl ions, R_S^+ and R_L^+, resulted from subsequent fragmentation of the acyl ions which is discriminated against at lower electron energies.

Two perhaloacetones were examined in this study, CF_3COCF_3 and CCl_3COCCl_3. The results are similar to acetone. The major process is the cleavage of the carbon-carbon bond. However, the major ion in the 70eV.spectrum is CX_3^+. An increase in the value of the ratio $CX_3\text{-}C{\equiv}O^+/CX_3^+$ with decreasing electron energy is observed. The formation of the acyl ion is the lower activation energy process. The fluorine and chlorine derivatives differ from each other. The abundance of $CF_3\text{-}C{\equiv}O^+$ exceeds that of CF_3^+ at 15eV.whereas, the abundance of $CCl_3\text{-}C{\equiv}O^+$ does not become greater than that of CCl_3^+ until 11eV. This may indicate that some CCl_3^+ is formed directly from the molecular ion at higher voltage.

Nine hydrogen containing haloacetones have been examined. The lowest activation energy process is the formation of $R_H\text{-}C{\equiv}O^+$ where R_H is the methyl group containing the maximum number of hydrogen atoms. We again observe an increase in the value of the ratio $R_H\text{-}C{\equiv}O^+/R_H^+$ with decreasing electron energy suggesting that R_H^+ is formed by subsequent fragmentation of the $R_H\text{-}C{\equiv}O^+$ ion. The value of the ratio $R_H\text{-}C{\equiv}O^+/R_H^+$ is always greater than one at low electron voltages. However, the reverse is true at 70eV. when R_H contains only one hydrogen atom.

Two major fragmentation pathways are discerned for the molecular ion of haloacetones containing only fluorine and chlorine. They correspond to the formation of $R\text{-}C{\equiv}O^+$ and R^+. The major fragment at 70eV. is always R_{Cl}^+ where R_{Cl} is the methyl group containing the more chlorine atoms. The formation of R_{Cl}^+ is the major decomposition pathway for unsymmetrical chlorofluoroacetones. A rapid increase in the abundance of this ion as the electron energy is decreased occurs. The acyl ion is of greater importance in the symmetricl chlorofluoroacetones where we observe an increase in the value of the ratio $R_{Cl}\text{-}C{\equiv}O^+/R_{Cl}^+$ as the electron energies are decreased.

Summarizing the fragmentation modes of chlorofluoroacetones, it can be seen that chlorine exerts a strong influence on the course of fragmentation. We propose the following rule to describe the effect of chlorine at threshold electron energies. The carbon-carbon bond is broken with charge retention favoring the group containing the more chlorine atoms. This rule changes when hydrogen is added to the haloacetone. In those cases the acyl ion containing the more hydrogen atoms is the major decomposition reaction product at low electron energies. We feel these data can be rationalized by considering the inductive and resonance effect of the halogen atom on the product ion

stability. The stability of the acyl ion is decreased with the addition of electron withdrawing groups, thus giving an order of stability of $R_H\text{-}C{\equiv}O^+ > R_{Cl}\text{-}C{\equiv}O^+ > R_F\text{-}C{\equiv}O^+$. On the other hand, the stability of the methyl cation would be increased by the electron donating resonance effect of chlorine. The inductive effect of fluorine outweighs any electron-donating effect. Therefore, order of stability of the methyl ion is $R_{Cl}^+ > RH^+ > R_F^+$. At this stage of the study some bromine containing compounds would be interesting.

It must be noted no cross-over of the value of the ratio $R_1\text{-}C{\equiv}O^+/R_2\text{-}C{\equiv}O^+$ was observed with electron voltage change.This is distinctly different from the behavior of aliphatic ketones.

There are some minor fragmentations of the molecular ion of these haloacetones. One very interesting rearrangement reaction is the loss of carbon monoxide. In symmetrical chlorofluoroacetones the $[M\text{-}CO]^+$ ion is small at 70eV. (<2% $\lesssim_{28}$ however, the value increases to approximately 20% $\lesssim_{28}$ at threshold electron energy. Since this curve almost coincides with that of $R\text{-}C{\equiv}O^+$ ion, we concluded that there is competition between two separate mechanistic pathways.

The formation of rearranged halomethyl ions is not an important fragmentation pathway. However, we observed two such ions at 70eV. which persisted at lower voltages (i.e., the formation of CCl_3^+, 3% $\lesssim_{28}$, from $CFCl_2COCFCl_2$). In these cases we feel that this ion is not derived from a sample impurity.

The hydrogen and chlorine containing ketones, $CHCl_2COCHCl_2$ and $CH_2ClCOCH_2Cl$ are characterized by the formation of ketenes, $[CHCl{=}C{=}O]^+$ and $[CH_2{=}C{=}O]^+$ ions respectively. These ions are major fragments at 70eV. and they are present at threshold electron energies. Although most of this fragment ion probably arises from the loss of a halogen atom from the acetyl ion, some might come directly from the molecular ion.

Haloethyl ions corresponding to the loss of COX from the molecular ion are observed to a varying degree in most of the haloketones. Only in the chlorofluoroacetones (with the exception of CF_3COCF_2Cl) did the $[M\text{-}X]^+$ ion persist at lower eV. values.

It may be possible to link these minor fragmentation pathways mechanistically to a molecular ion rearrangement before decomposition occurs. We propose the following intermediate molecular ion structure as a guide to future experiments. We feel that this halogen bridge ion is an extension of previously proposed five membered ring chloro and bromonium ion structures.

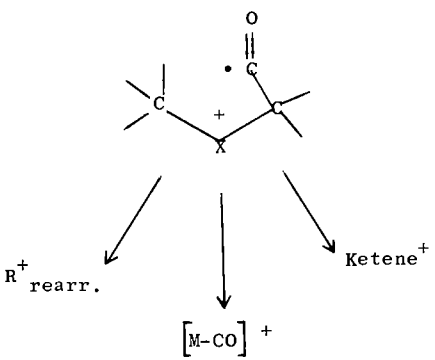

Mass Spectral Fragmentation Mechanisms of Some Dibenzo[c,f][1,2]diazepines

Adria C. Casey, James H. Green
and Michael Mautner

New England Institute
Ridgefield, Connecticut 06877

Abstract

The fragmentation mechanisms of 11H-dibenzo[c,f][1,2]diazepine (I), its 3,8-dichloro derivative (II), 3,8-dichlorodibenzo[c,f]-[1,2]diazepin-11-one (III) and 3,8-dichloro-11H-dibenzo[c,f][1,2]-diazepin-N-oxide (IV) are discussed. The initial loss of molecular nitrogen is characteristic of I, II and III. IV has a strong molecular ion, that competitively eliminates either NO or $Cl\cdot$ and N_2O. The common radical ion, $\frac{m}{e}$ 166, present in the mass spectra of I, fluorene, 2-methyl-9,10-anthraquinone and 2-methylbenzo[c]cinnoline, appears to be formed in different states.

In Press for J. Heterocyclic Chem.

The Class Approach to Fragmentation Mechanisms--The Mass Spectra of Alpha and Beta-Naphthylthiaalkanes. NORMAN G. FOSTER, ROBERT W. HIGGINS*, Texas Woman's University, Denton, Texas 76204, and MYNARD C. HAMMING, Continental Oil Company, Ponca City, Oklahoma 74601.

The mass spectra of fifteen alpha and beta substituted naphthylthiaalkanes are reported and used to illustrate the process of correlation and delineation of fragmentation routes in a class of compounds. Spectra from low, intermediate and high resolution instruments are used to demonstrate the process where, 1) by human inspection the correlations are made; 2) the additional value of data from intermediate resolution finds important use; 3) the need remains for high resolution to solve some problems. The application of data from metastable ions and low-voltage spectra are integrated into the process at places where the computer can be substituted for human inspection. Additional benefits from the class approach are explained. Isotopic labeling can be applied to proposed mechanisms with the preliminary class approach assisting in selecting species to be labeled by syntheses. For unknown structures, the intercomparison of the observed spectra and fragmentations predicted from bond orders obtained from M.O. calculations may prove fruitful.

(To be submitted to "Organic Mass Spectrometry").

*Deceased.

Fragmentation of Amino Acids and their Esters Containing a Sulfur, Phenyl or Hydroxyl Group

Kozo Hirota and Mitsuo Saito

Faculty of Science
Osaka University
Toyonaka, Osaka 560, Japan

The base peak of the important amino acid esters contains an amino group in their usual MS ("amine-fragment").[1] However, esters of tyrosine and methionine offer rare exceptions, because their base peak does not contain amino group.

This paper attempts to show that the base peak of these abnormal esters can be explained as well as that of the others by our MO-theory,[2] which is based on the assumption that "the initial scission probability of the skeletal bond of the bombarded compounds is proportional to the charge density of the HO-MO allotted at the bonds of their excited parent ion". To calculate the charge density at each bond, the LCGO approximation of Franklin[3] was adopted, regarding CH_2, CH, CO_2, NH_2 etc. as united atoms, and the electron density of the neutral molecules is calculated, because in the present approximation it equals to the charge density of the parent ion. The new parameters used in the calculation are shown in Appendix, where that of S is the new one determined from the recent data of photo-ionization potential. The charge density at each bond in the HO-MO is approximated to be the mean of two groups forming the bond. However, charge density at the CN bond, even though generally large, is excluded from discussion on the scission probability, because the value is mostly due to lone pair electrons at the N atom. Actually, this bond is hardly rupturable, so that its contribution can be neglected in experiment. This presumption was justified to be plausible on alkylamines.[2b]

Distribution of the charge density of some ethyl esters, which contain no special group, is shown in Table 1, where the left C-C bond adjacent to the CN bond always becomes the largest in the charge density. This finding corresponds to the experiment that the base peak is produced by scission of this bond, denoted by the virtical dotted line, and thus the amine-fragment is charged. Similar results can be obtained on the esters of Ala, nor-Val, nor-Leu and i-Leu. The above theoretical assumption is supported.

Table 1

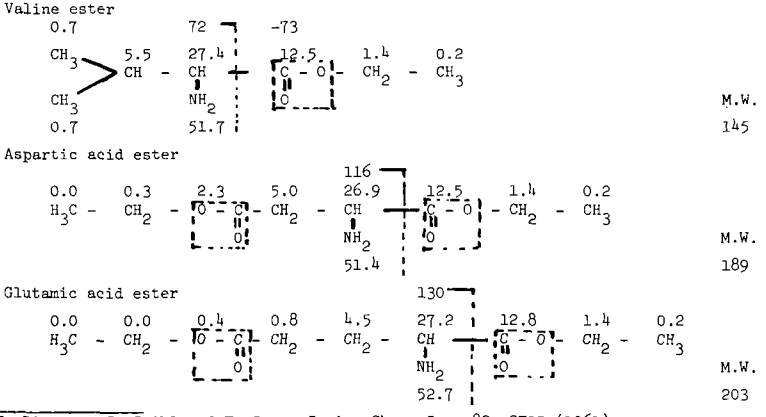

1) K. Biemann, J. Seibl and F. Gapp, J. Am. Chem. Soc. 83, 2795 (1961).
2) (a) K. Hirota and Y. Niwa, J. Phys. Chem. 72, 5 (1968); (b) K. Hirota, I. Fujita, M. Yamamoto and Y. Niwa, ibid. 74, 410 (1970).
3) J. L. Franklin, J. Chem. Phys. 22, 1304 (1954).

Amine-fragment becomes also the base peak in some esters, which contain -OH, -S- or C_6H_5- group. Hereby, charge density at the C_6H_5-CH_2 bond may be expected to be lower than the mean value of the two groups, because the charge at the C_6H_5 group localizes at the ring. It is noteworthy that rupture of the left bond adjacent to the CN bond produces the next highest peak (m/e 91), and correspondingly the charge density at the bond is also large. The ester of lysine or δ-amino norleucine can be classified into this category, though the base peak m/e 84 is produced by a successive unimolecular separation of NH_3 from m/e 101, as explained by Biemann et al.[1)]

Table 2

Serine ester

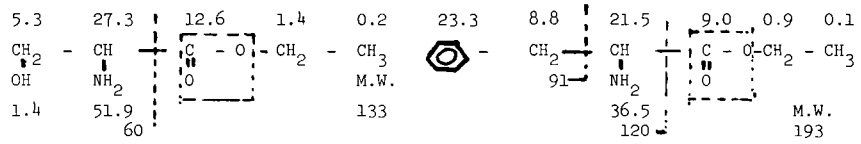

Phenylalanine ester

Cystein ester

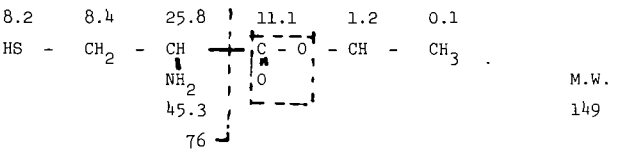

Lysine ester

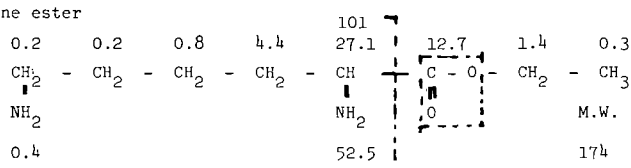

However, the amine-fragment is not the base peak in the esters of methionine and tyrosine, because their base peaks are m/e 61 ($CH_3SCH_2^+$) and m/e 107 (HO-C_6H_4-CH_2^+), respectively, as the dotted lines in Table 3 show. The above irregularity is, however, of apparent nature.

Table 3

Methionine ester

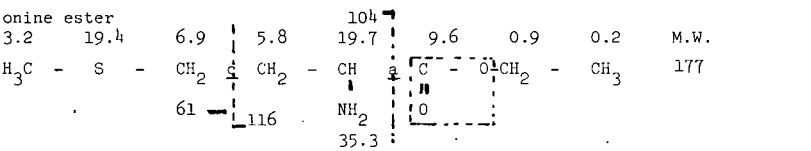

Tyrosine ester

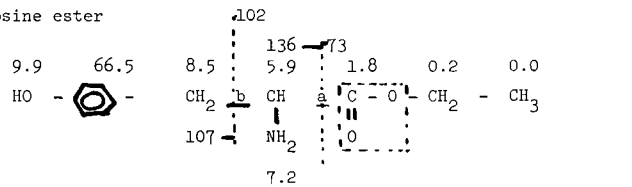

In this latter case, the charge density at the b-bond is larger than at the a-bond, so that this finding is concordant with our theory. In the former case, however, the same explanation is not applicable, because despite the small charge density

at the c-bond the peak at m/e 61 becomes the highest.*) This finding may be brought about by the successive unimolecular fragmentation of the ion of m/e 104. This possibility can be shown by alternation of both ions as the base peak if the ionization voltage is decreased lower than the usual one. The MS measured using a high resolution apparatus of Hitachi RMU-7HR confirms the tendency. (Cf. Table 4 (1°)).

Table 4 Important Peaks in the MS of Esters of Methionine (1°) and Tyrosine (2°) vs. Ionizing voltage in Volts

	m/e	Assigned Ion	V_i = 80	20	15	10
(1°)	56	$H_2C{=}CH\text{-}{}^{+}CH\text{-}NH_2$	116	71	51	12
	61	$H_3C\text{-}S\text{-}CH_2^{+}$	171	96	57	12
	104	$H_3C\text{-}S\text{-}CH_2\text{-}CH_2\text{-}{}^{+}CH\text{-}NH_2$	100	100	100	100
	116	${}^{+}CH_2\text{-}\underset{\underset{NH_2}{|}}{CH}\text{-}\overset{\overset{O}{\|}}{C}\text{-}O\text{-}C_2H_5$	10	10	10	11

	m/e	Assigned Ion	V_i = 70	20	15	10
(2°)	102	${}^{+}CH(NH_2)\text{-}COO\text{-}C_2H_5$	55	35	42	55
	107	$HO\text{-}C_6H_4\text{-}CH_2^{+}$	100	100	100	100
	136	$HO\text{-}C_6H_4\text{-}CH_2\text{-}{}^{+}CH(NH_2)$	52	84	101	115
	74	$(COOC_2H_5)\text{-}H^{+}$?	41	12	9	9

Similar experiment is carried out (by one of the authors (M.S.)) on tyrosine ester. In this case, the probability of scission at the b-bond does not become less than that at the a-bond, considering that sum of the height of m/e 107 and m/e 102 is always larger than the height of m/e 136 even if the ionizing voltage is decreased. (Cf. Table 4 (2°)).

Lastly, the MO-theory is extended, so as to predict which fragment of the two has the charge after the bond-scission. As a working assumption, Stevenson's rule[4] is applied; viz., "relative probability to be given the charge is larger for the fragment whose total charge density is larger, if the ionizing voltage is larger than the ionization potential plus bond energy". As an example, the assumption will be tested on valine ester. Total charge density at the left amine fragment is 86.0 (%), while that at the right non-amine-fragment is 14.1 (%), so that the markedly large height of amine fragment (m/e 72) as compared to that of its complemental one (m/e 73) can be explained.

Similarly, this assumption may be shown applicable for the base peak of other esters (Asp, Glu, Ser, Phe, Cys, Lys, and Tyr). Nevertheless, if the assumption be applied to methionine ester, the peak at m/e 116 would become very high instead of m/e 61, in the case when scission at the c-bond occurs initially, because their total charge is 71.5% and 29.5 %, respectively. This deviation from the expectation indicates again that the initial scission occurs at the a-bond, but not at the c-bond. The same treatment is applicable, but the details will be reported elsewhere in future.

*) Since charge density at -S- may localize at its lone pair, scission at the C-S bond is difficult in the mass spectra.

4) D. P. Stevenson, Discussion Faraday Soc., 10, 35 (1951).

Appendix The Parameters Used in the Calculation (e.V.)

Groups	New parameters		Franklin's parameters	
	coulomb integral	resonance integral	coulomb integral	resonance integral
$-CH_3$, $=CH_2$, -CH	13.31	1.65	13.31	1.55
$-NH_2$	10.154[a,d]	2.264	10.52	2.08
-S-	10.46[a,c,d]	1.986	10.47[b]	1.73[b]
C_6H_5-, $-C_6H_4$-	9.245[a,c]	1.379	9.52	1.09
-COO-	11.05[a,c]	1.413	11.51	1.46
-OH	12.59[c]	2.065	12.76	2.06

a) K. Watanabe et al., "Final Report on I. P. of molecules by a Photoionization Method", Dec. 1959, Dept. of Army #5B99-01-004, ORD-#TB2-001-00R-#1624. b) H. J. Svec and G. A. Junk, J. Am. Chem. Soc. 89, 790 (1967). c) K. Watanabe, J. Chem. Phys. 26, 542 (1957). d) K. Watanabe, J. R. Mottle, J. Chem. Phys. 26, 1773 (1957).

NOVEL SKELETAL REARRANGEMENTS IN DIFUNCTIONAL BROMOAMIDES

István Lengyel, David B. Uliss, and Robert V. Mark

Department of Chemistry, St. John's University
Jamaica, New York 11432

Within the framework of a broader program undertaken to investigate effects of stereochemistry on mass spectra, especially in remote group interactions and skeletal rearrangements in polyfunctional organic compounds subsequent to electron impact, we had occasion to record the mass spectra of some bis-α-bromoamides. Model compounds of two types were synthesized: bis-N-t-alkyl- and cycloalkyl-bromoamides with (i) skeletal or conformational flexibility to permit interaction of the functionalities through space and (ii) with a skeletally rigid connecting link precluding steric interaction of functional groups. Representatives of these two types are N,N'-p-menth-1,8-ylenebis [2-bromo-3,3-dimethylbutyramide] (Ia, m.p. 233°), derived from 1,8-diamino-p-menthane, and 2,2'-(1,3-adamantylene)bis[2-bromo-N-t-butylacetamide] (IIIa, m.p. 259°) derived from 1,3-adamantanediacetic acid, respectively.

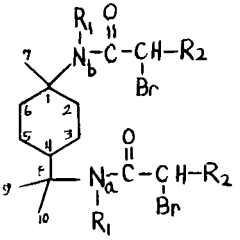

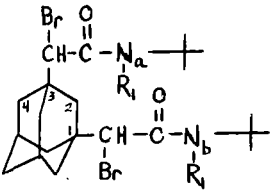

Ia, R_1 = H; R_2 = t-C_4H_9

Ib, R_1 = D; R_2 = t-C_4H_9

II, R_1 = H; R_2 = 1-Adamantyl($C_{10}H_{15}$)

IIIa, R_1 = H

IIIb, R_1 = D

Due to the second functionality, the 70eV mass spectrum[1] of compound Ia shows some unexpected fragmentation processes. Our interest was especially kindled by an abundant (20% rel.int.) singlet at m/e 210. High resolution measurement revealed an elemental composition of $C_{13}H_{24}NO$. Deuterium labeling of both N-H groups (Ib) caused a 90% shift to m/e 212. Exchange of the N-t-butyl groups for N-adamantyl (II) resulted

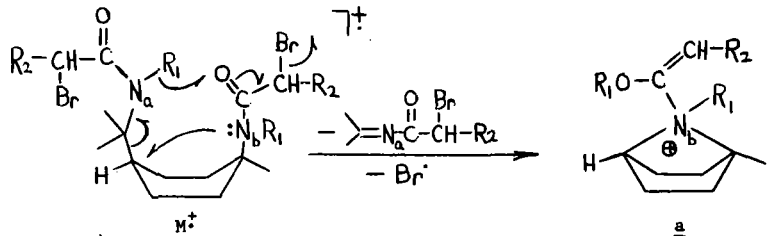

M·+ a

Ia, m/e 522/524/526($C_{22}H_{40}N_2O_2Br_2$)

Ib, m/e 524/526/528

II, m/e 678/680/682

Ia, m/e 210($C_{13}H_{24}NO$)

Ib, m/e 212

II, m/e 288

in a shift of the corresponding bromine-free even-electron ion to m/e 288. Thus, the fragmentation process leading to this ion involves elimination of carbon atoms 8, 9 and 10 of the terpene skeleton together with the 8-substituent and the second bromine atom, accompanied by transfer of the N_a-hydrogen. A mechanism consistent with the isotopic and substituent labeling and high resolution data, involving an anchimerically assisted multicentered rearrangement ($M^{+\cdot} \rightarrow a$) with a 10-membered ring transition state can be rationalized for the cis isomer (1-CH_3 equatorial) with the cyclohexane ring in the boat conformation[2]. Formation of ion a from the trans isomer (axial 1-methyl, equatorial 1-amino group) would require ring C-C bond fission.

While - predictably - no evidence for a similar remote-group interaction was found in the spectrum of the skeletally and conformationally rigid bis-amide III, the latter compound nevertheless showed a number of other interesting features. As attested to by the appropriate metastables and accurate mass determinations, bis-bromoamide IIIa undergoes the following unexpected major 3-step fragmentation sequence:

$$M^{+\cdot} \xrightarrow{-C_5H_9NO} b \xrightarrow{-C_4H_8} c \xrightarrow{-C_6H_9\cdot} d$$

Ion d still contains both bromine atoms. As the particles eliminated in succession originate from three different distant parts of the molecule, fragmentation steps b → c and c → d require charge migration (or charge redistribution). In the mass spectrum of the N_aN'-dideutero analogue (IIIb), ions b and c are shifted by two mass units but d by only one. These labeling data indicate that the hydrogen originally attached to the nitrogen lost in the first step (N_a) rearranges to a carbon atom that is eliminated together with five others in the third step. After the loss of nine carbon atoms, elimination c → d must necessarily involve the adamantane nucleus. Although at first glance not immediately obvious, closer scrutiny reveals that there is only one possible set of six carbon atoms (marked with asterisk) that can be ejected so as to take the deuterium atom originally attached to N_a. Initial fission of the 3-4 bond in adamantane and elimination of C_4H_8-N=C=O with saturation of the primary radical followed by McLafferty rearrangement in the remaining amide function with ejection of C_4H_8 from the N-t-butyl group leads to odd-electron ion c which probably rearranges to c' by allylic C-C bond cleavage and multiple hydrogen migrations. Ion c' eliminates the conjugated allylic radical $C_6H_9\cdot$ to afford the abundant triplet d (m/e 282/284/286).

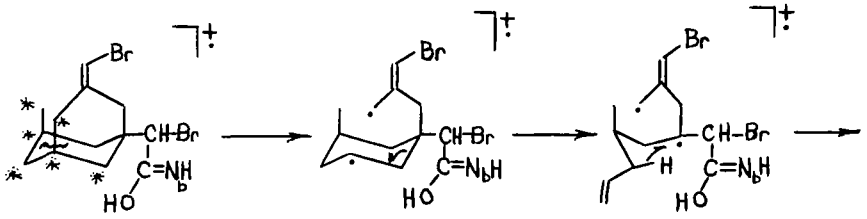

c

IIIa, m/e 363/365/367
IIIb, m/e 365/367/369

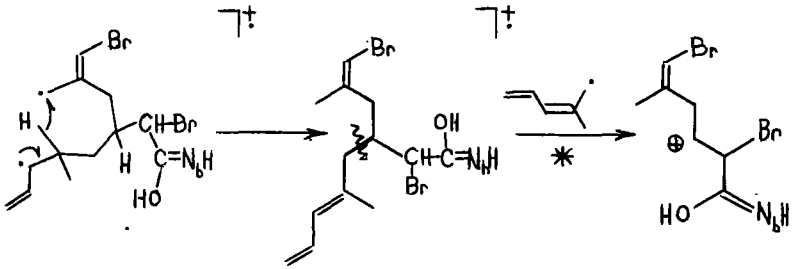

c'

d

IIIa, m/e 282/284/286
IIIb, m/e 283/285/287

ACKNOWLEDGEMENT

We thank Professor K. Biemann, Department of Chemistry, Massachusetts Institute of Technology, for the high resolution mass spectra.

FOOTNOTES

1. The low resolution mass spectra were recorded on a Hitachi-Perkin Elmer RMU 6D instrument at Morgan-Schaffer Corp., Montreal, Canada. The high resolution data, in the form of "element maps" were obtained on a CEC 21-110B doubly focusing mass spectrometer in conjunction with an IBM 1801 computer system.

2. A predistilled sample of the 1,8-diamino-*p*-menthane (Rohm-Haas Co., Philadelphia, Pa.) used in the preparation of I was gas chromatographically homogeneous. The thermodynamically more stable isomer, in analogy with 1,8-terpin and 1,8-dihalo-*p*-menthanes [R. M. Carman and H. C. Deeth, Aust. J. Chem., 22, 2651 (1969).] is assumed to be the cis (equatorial methyl, axial amino group in position 1). Work to synthesize the thermodynamically less stable trans 1,8-diamino-*p*-menthane is in progress.

Site Specific Hydrogen Abstractions in Even Electron Ions. THOMAS H. KINSTLE, W. P. BRYANT, P. J. IHRIG AND E. J. GOETTERT, Iowa State University, Ames, Iowa 50010.

The transfer of a γ-hydrogen atom in the McLafferty rearrangement is a thoroughly studied example of a site-specific hydrogen abstraction reaction. Various workers have pointed out the importance of the non-filled orbital with regard to facility and specificity in this reaction. Many examples of hydrogen migration in even-electron ions are known, but the reactions are non-site specific. We have documented essentially complete site specificity in a β-hydrogen transfer-olefin elimination reaction of the even electron silyl cations 1 (R=H,CH_3) and 2 (R=CH_3, n-Bu) [Kinstle, Ihrig and Goettert, J. Am. Chem. Soc., 92, 1780 (1970)].

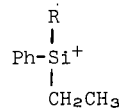

1

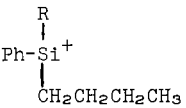

2

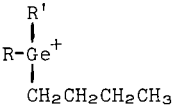

3

We have extended this study to a series of organogermanium compounds 3 (a, R=Ph, R' = n-Bu; b, R=R'=n-Bu; c, R=Ge(n-Bu)$_3$, R'=n-Bu) and their deuterated analogs. We again find an extremely site specific (even more so than with ions 1 and 2) hydrogen transfer from the β-position accompanying the loss of butene in these compounds. Even more striking was the high degree (>80%) of β-hydrogen transfer which occurred during the sequential loss of a second butene molecule, presumably from a structure such as 4. This contrasts with analagous silyl cations in

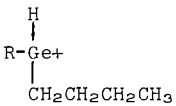

4

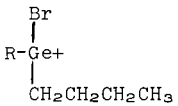

5

which the second olefin elimination is accompanied by a clearly non-specific hydrogen transfer. Germanium cation 5 shows a lessened degree of site specificity, possibly due to an inductive withdrawal of electron density from the germanium cationic site by the electronegative bromine atom.

These results are discussed in terms of a size effect of the metalloidal abstracting atom. Silicon and Germanium are the largest atoms thus far investigated in this regard. Results with phosphorous and sulfur compounds are briefly presented.

MATSUDA TYPE VIRTUAL IMAGE DOUBLE FOCUSING MASS SPECTROMETER

H. Matsuda
Institute of Physics, College of General Education,
Osaka University

E. Watanabe, M. Naito and M. Nojiri
Japan Electron Optics Laboratory Co., Ltd.

Abstract

A double focusing mass spectrometer with an electrostatic field having the same divergence function as the concave lens has been brought to realization and commercialized. One of the features of this instrument is that due to the characteristics of its diverging electrostatic field, the instrument, despite compact size, can easily attain a resolution of 1000 to 2000, using a wide main slit. This instrument is named "the JMS-06 Mass Spectrometer," which has a diverging electrostatic field with a mean radius of 150 mm and deflection angle of 90°, and a homogeneous magnetic field with a mean radius of 120 mm and deflection angle of 60°. The JMS-06 is used mainly for GC-MS routine analysis. A resolution of 1000 (10 % valley) has been obtained by the use of a 100 μ main slit.

Introduction

A conventional double focusing mass spectrometer has an electrostatic and a magnetic field having the same focusing function as a convex lens. One of the authors predicted six years ago that the electrostatic field having the same divergence function as a concave lens would be possible and named it "the diverging electrostatic field."[1] This field only permits the formation of a virtual image, but not a real image. However, the formation of the latter image is also made possible if this field is combined with the magnetic field having the same focusing function as a convex lens. So, if a collector slit is provided at the position of real image, a double focusing mass spectrometer can be formed.

With a coordinate system such as shown in Fig. 1 (a), Newton's equation shown below applies to the diverging electrostatic field having a mean radius of (a) and deflection angle of (ϕ). [2]

$$(l' + g^*)(l''^* - g^*) = -f^{*2}$$

$$f^* = \frac{a}{k} \frac{1}{\sinh k\phi}$$

$$g^* = \frac{a}{k} \coth k\phi$$

where g* is the distance between the field boundary and virtual focus, and f* is the distance between the principal plane and virtual focus.

The relationship between these values is shown by an optical analogy in Fig. 1 (b).

Also, the image magnification X of the diverging electrostatic field and the dispersion D* at the virtual image are given respectively by:

$$X = \frac{g^* - l'^*}{f^*} = \frac{f^*}{l' + g^*}$$

TABLE I
COMPARISON OF So, Sc, R AND TOTAL ION PATH

		JMS – 06	ORDINAL NIER-JOHNSON TYPE
THEORETICAL RESOLUTION	FORMULA $R=\frac{\alpha m(1+Xm)}{2(XeXmSo+Sc)}$	αe = 150mm αm = 120mm ϕe = 90° ϕm = 60° Xe = 0.3 Xm = 0.6	αe = 150mm αm = 120mm ϕe = 90° ϕm = 60° Xe = 1 $Xm = \frac{2}{3}$
	So = 200 μ Sc = 50 μ	1100	545
	So = 100 μ Sc = 25 μ	2200	1090
MAIN SLIT WIDTH AT R = 1000 (Sc = Xe·Xm So)		266 μ	75 μ
TOTAL ION PATH		789 mm	906 mm

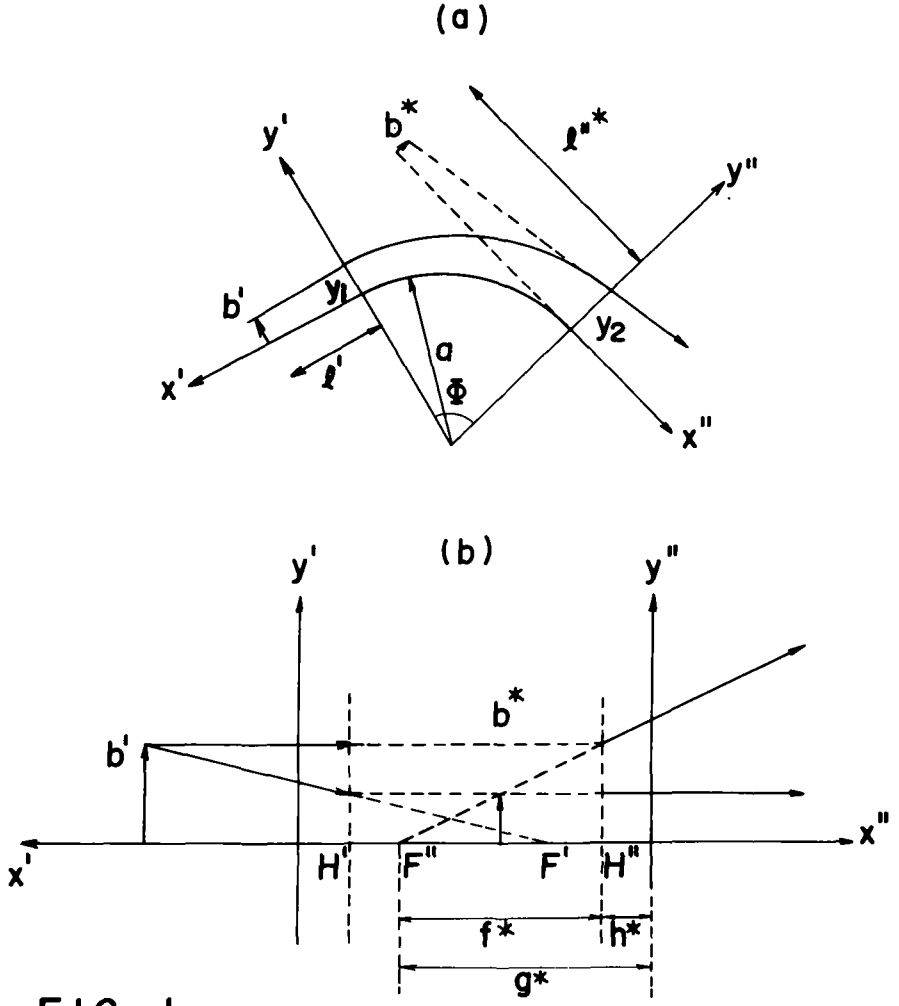

FIG. 1

(a) Coordinate system and virtual image formed by diverging electric field.

(b) Optical analogue

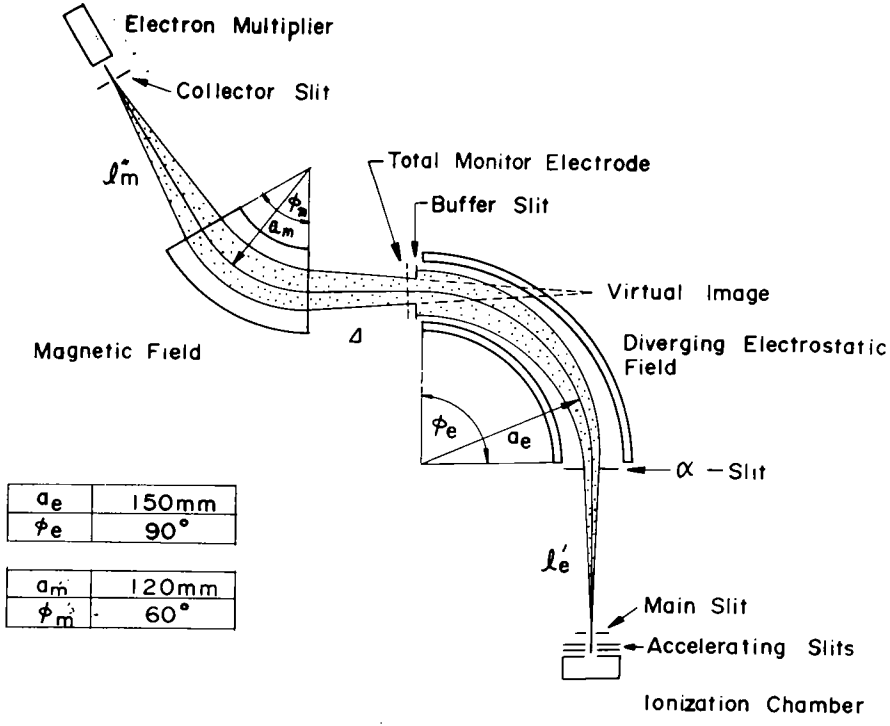

a_e	150mm
ϕ_e	90°

a_m	120mm
ϕ_m	60°

FIG. 2 PRINCIPLE OF JMS-06 MASS SPECTROMETER

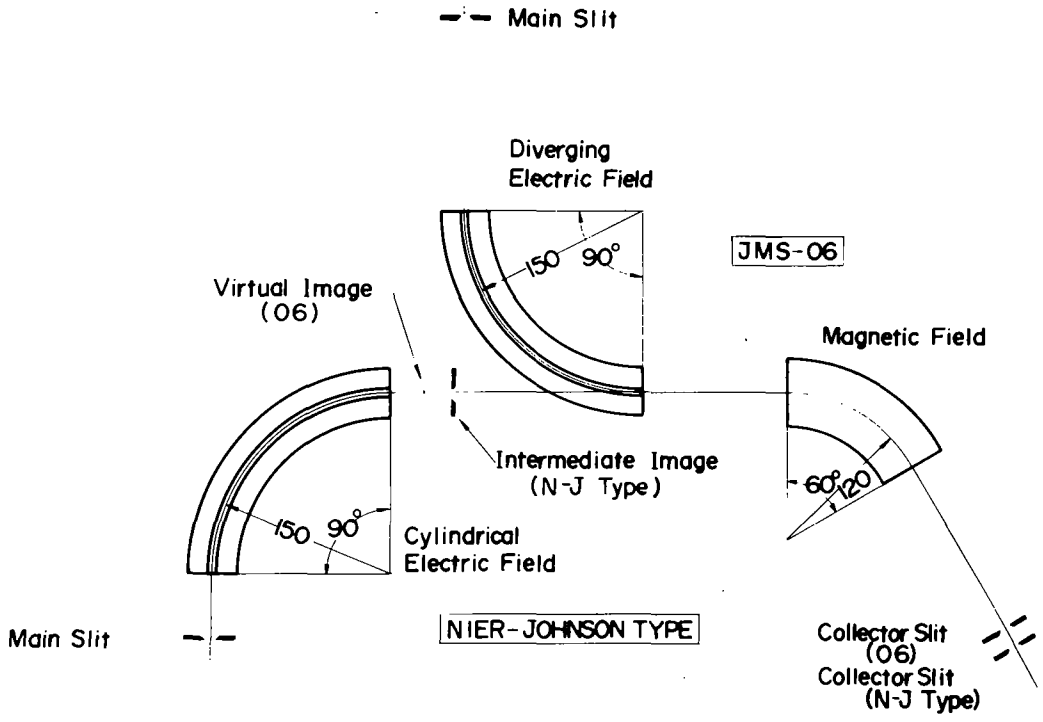

FIG. 3
COMPARISON OF JMS-06 AND ORDINARY NIER-JOHNSON TYPE

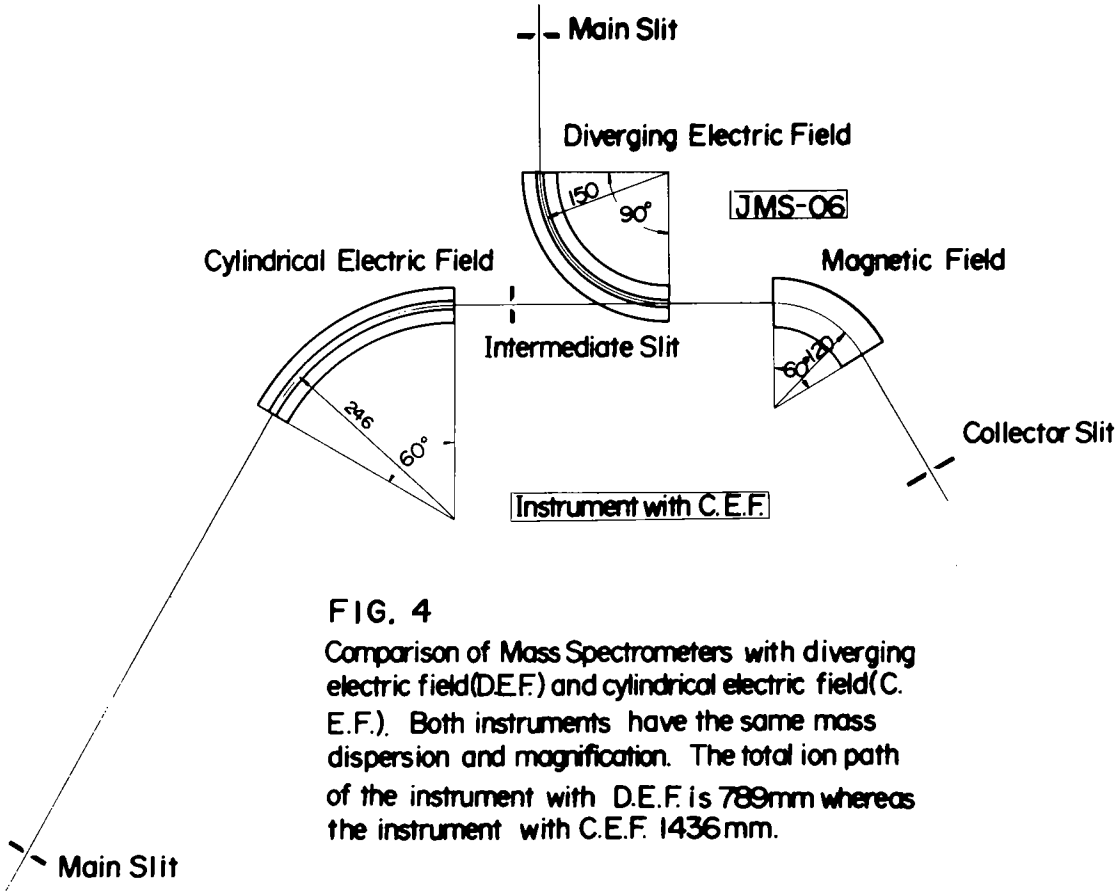

FIG. 4

Comparison of Mass Spectrometers with diverging electric field(D.E.F.) and cylindrical electric field(C. E.F.). Both instruments have the same mass dispersion and magnification. The total ion path of the instrument with D.E.F. is 789mm whereas the instrument with C.E.F. 1436mm.

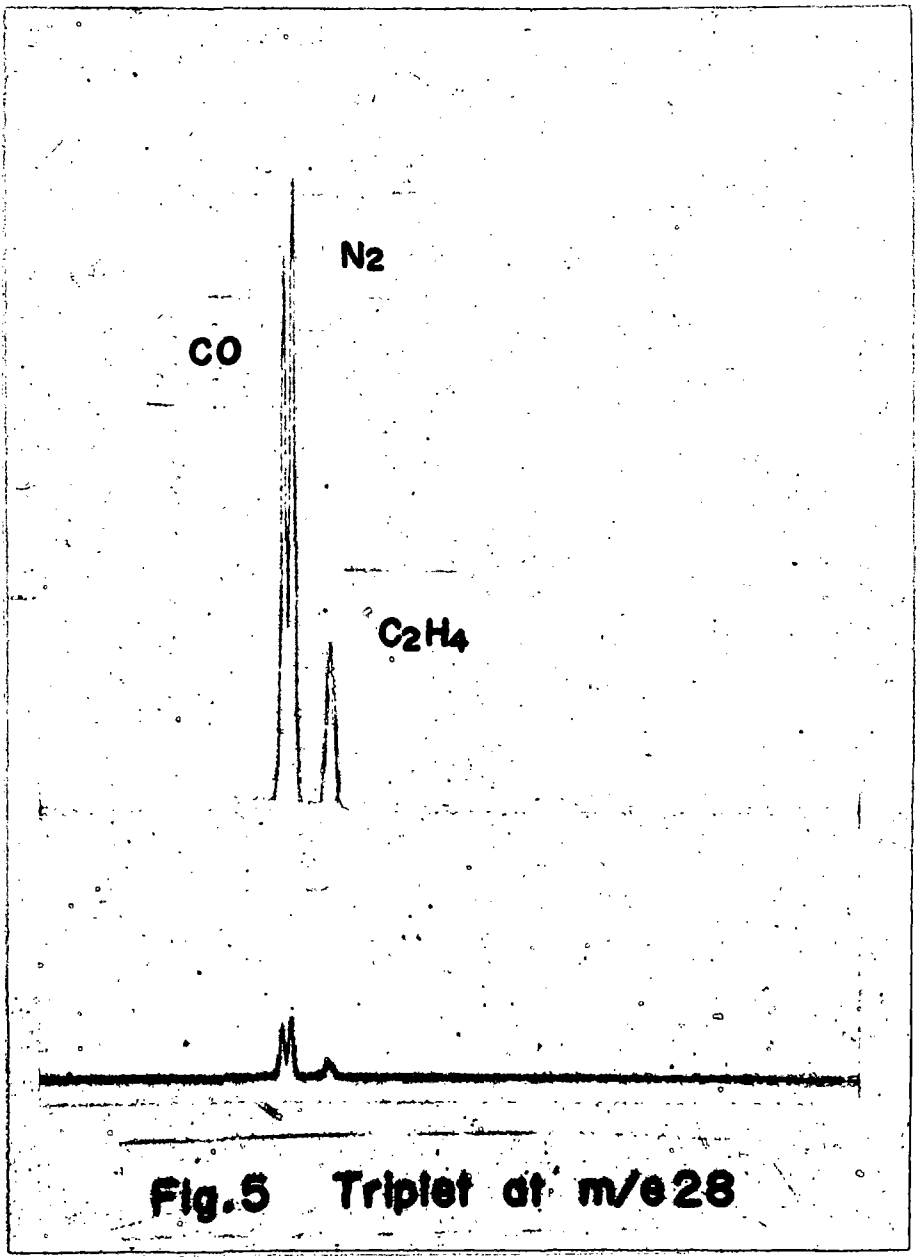

Fig.5 Triplet at m/e 28

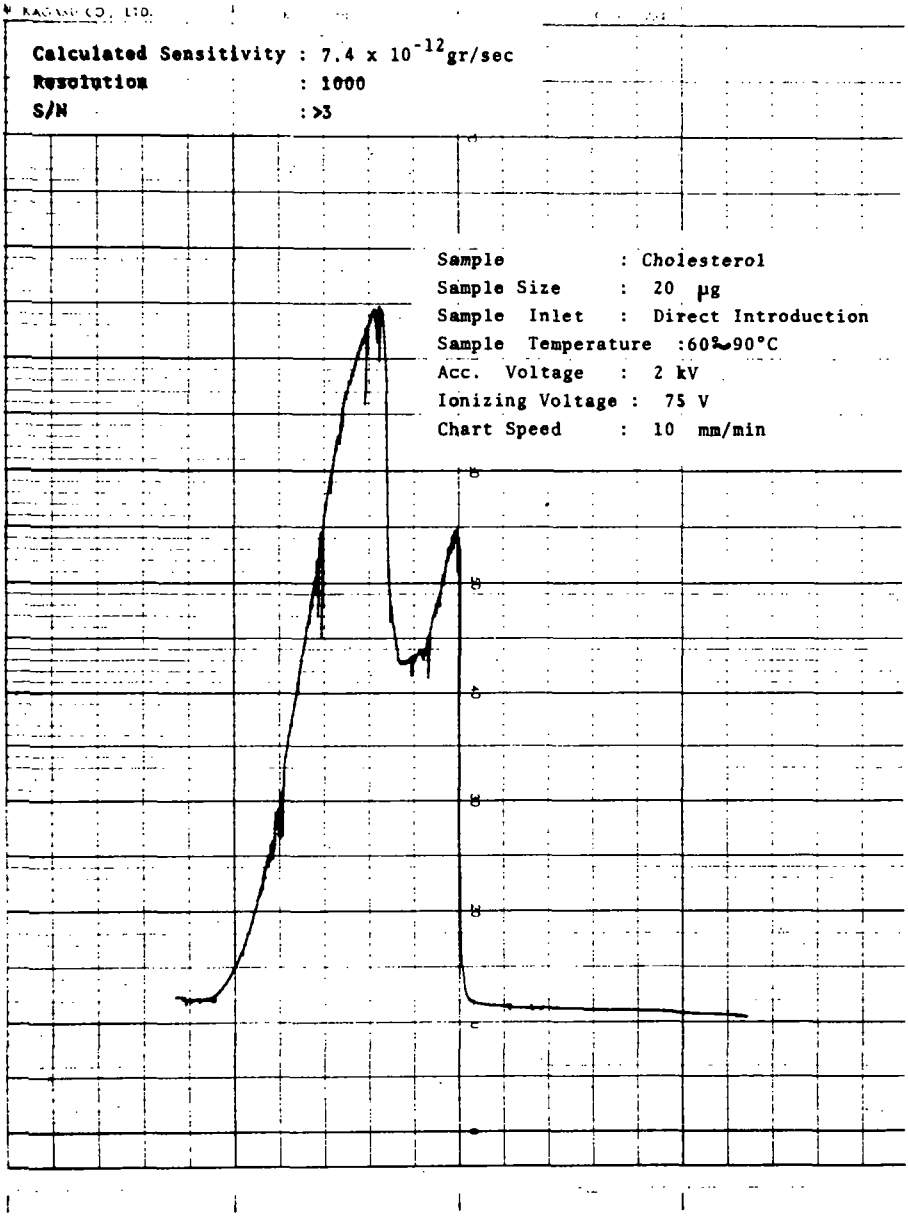

Fig. 6 Fragmentgram of cholesterol molecular peak

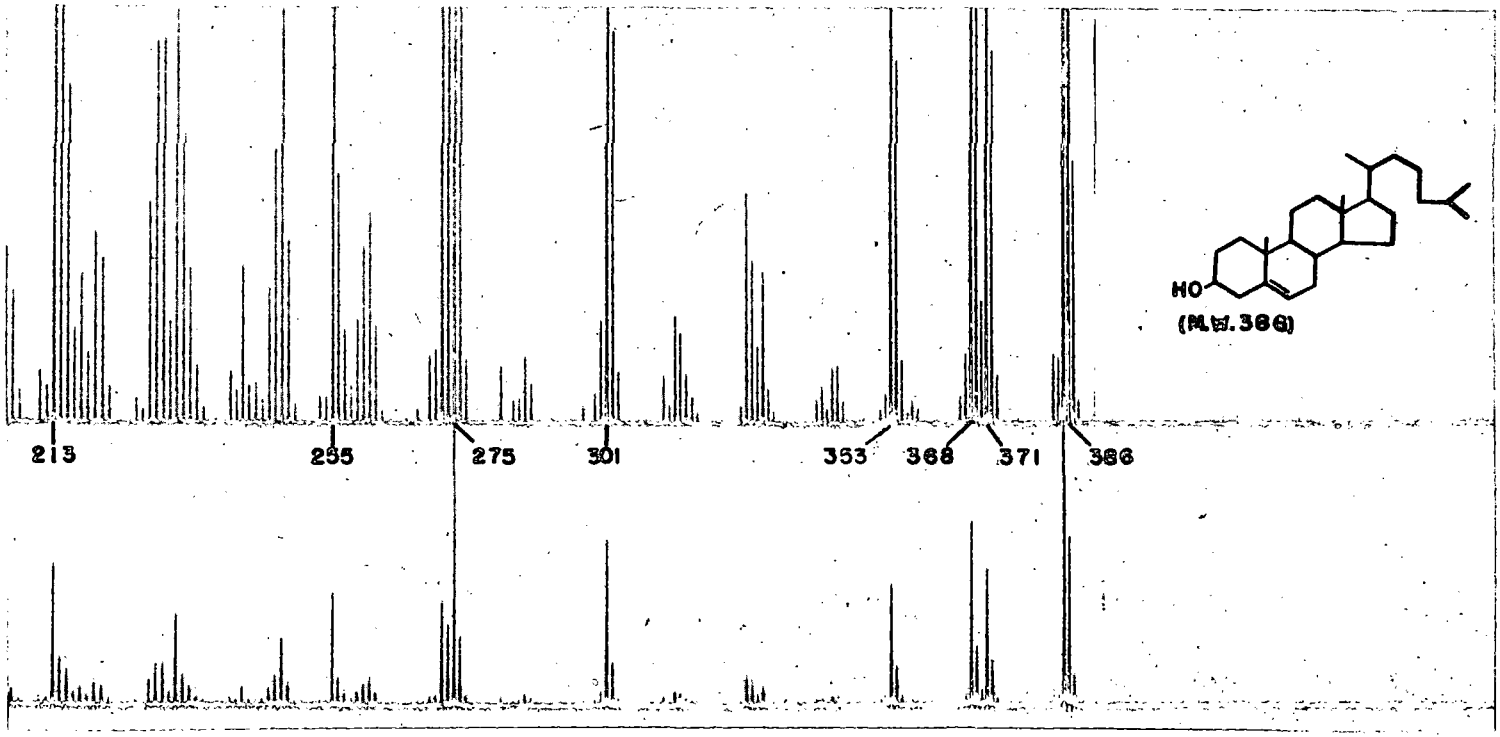

Fig. 7 Mass spectrum of cholesterol
Ionizing volt: 75v
Accel. volt. : 2kv

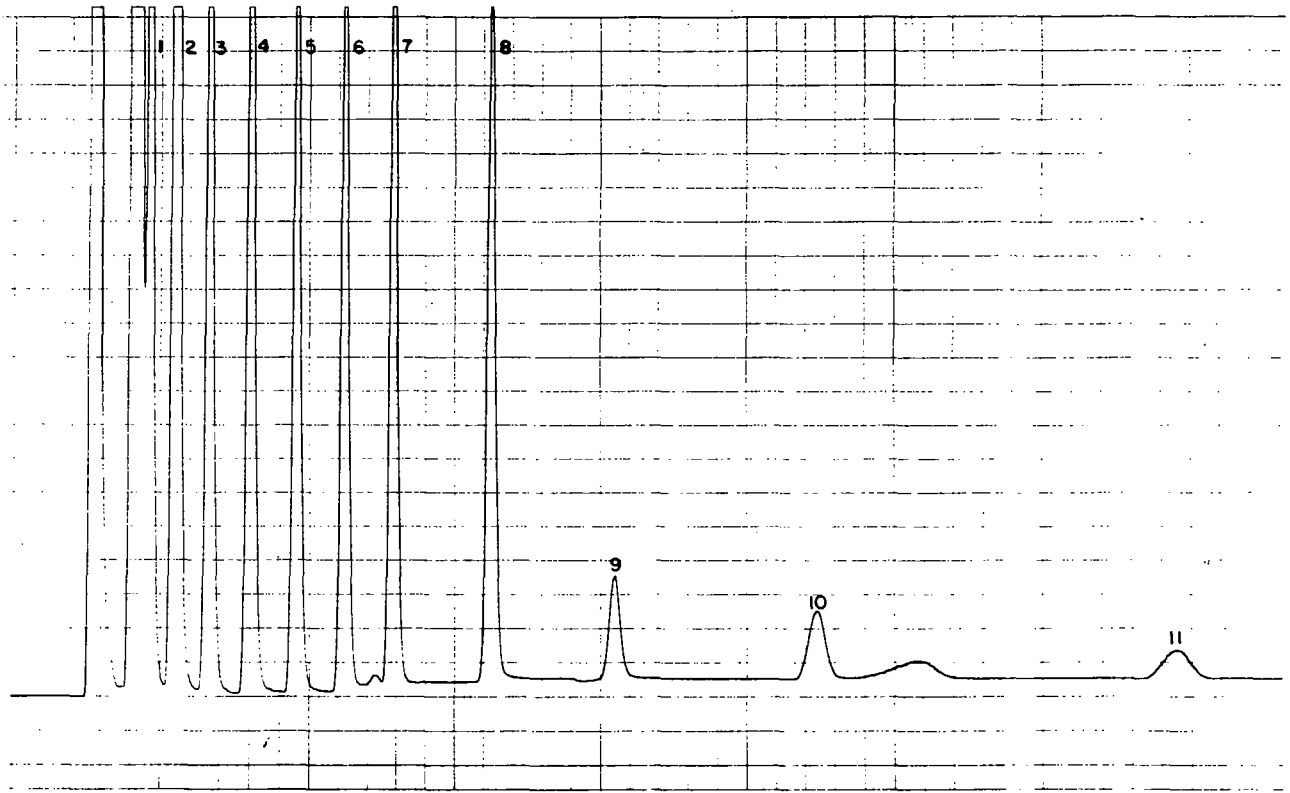

Fig. 8 Gas chromatogram of a mixture of fatty acid methyl esters

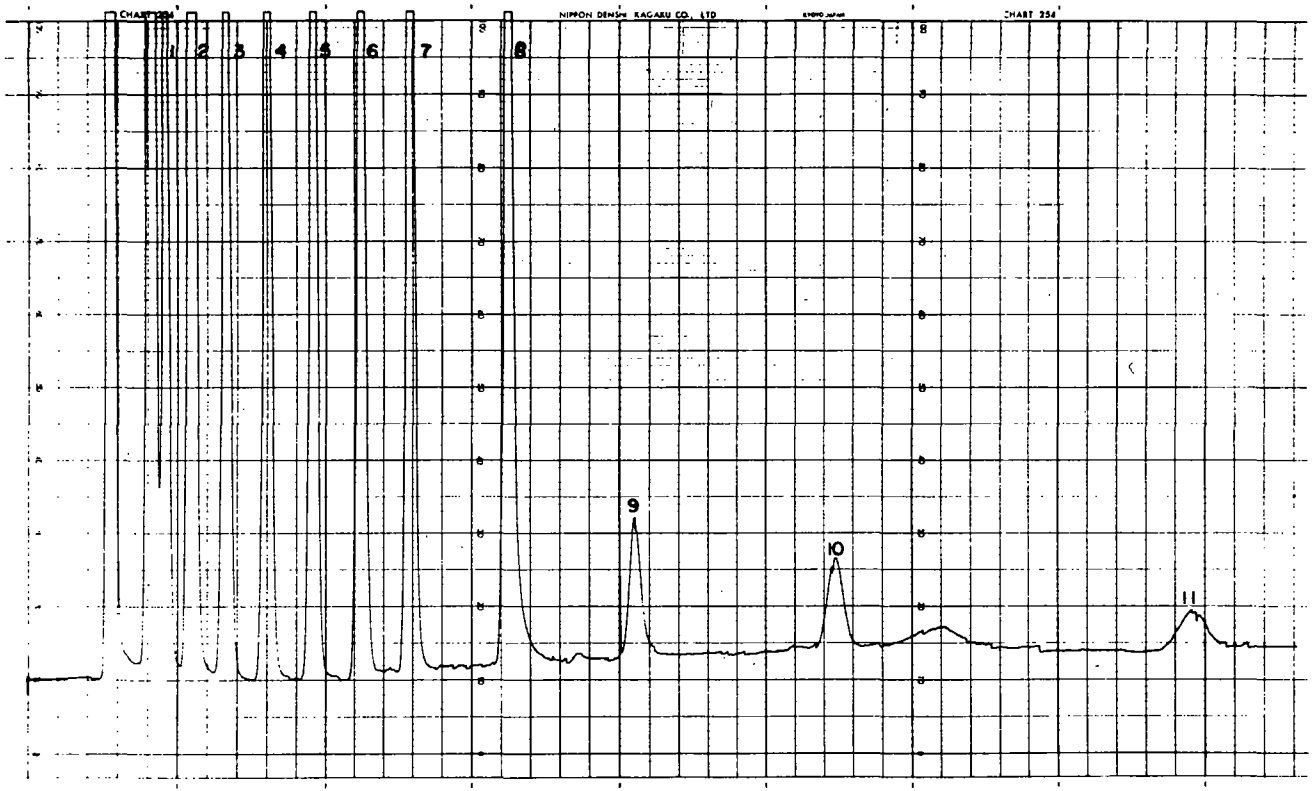

Fig. 9 T.I.M. chromatogram of a mixture of fatty acid methyl esters

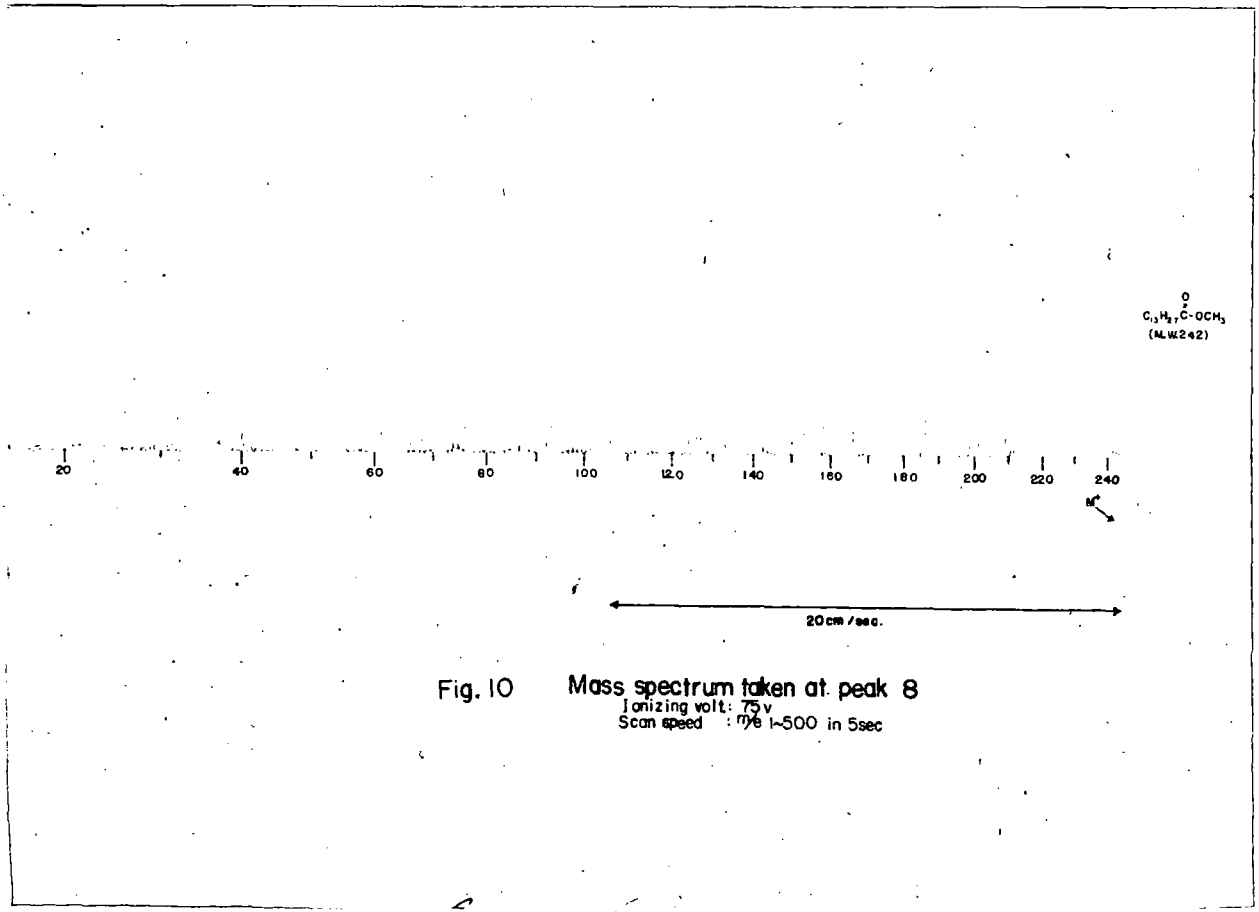

Fig. 10 Mass spectrum taken at peak 8
Ionizing volt: 75v
Scan speed : m/e 1~500 in 5sec

$$D^* = a\delta^*(X-1)$$

where $$\delta^* = \frac{\gamma + 2\beta}{k^2}$$

The diverging electrostatic field has a focusing function with respect to ion movement in the axial direction. The image position in the Z-direction is given by:

$$(\ell' - q_z)(\ell_z'' - q_z) = f_z^2$$

$$f_z = \frac{a}{\kappa_z} \frac{1}{\sin \kappa_z \phi}$$

$$q_z = \frac{a}{\kappa_z} \cot \kappa_z \phi \quad \text{where} \quad \kappa_z^2 = k^2 + 2$$

To make a double-focusing mass spectrometer by combining a diverging electrostatic field and a magnetic field, it is necessary to bring the virtual image at the electrostatic field into coincidence with the objective image at the magnetic field, and use the magnetic field to cancel out the energy dispersion caused by the electrostatic field.

Let us suffix e to values concerning the electrostatic field and m to values concerning the magnetic field. In the case of a homogeneous magnetic field, Newton's equation shown below applies to the image formation of the ions entering and leaving the field at a right angle.

$$(\ell_m' - q_m)(\ell'' - q_m) = f_m^2$$

$$f_m = \frac{a_m}{\sin \phi_m}$$

$$q_m = a_m \cot \phi_m$$

Also, the image magnification Xm by the magnetic field is given by:

$$X_m = \frac{\ell'' - q_m}{f_m} = \frac{f_m}{\ell_m' - q_m}$$

To satisfy the condition of directional focusing, the distance between the electrostatic and magnetic fields, Δ, should be made:

$$\Delta = \ell_m' - \ell_e''^*$$

As Δ must be a positive value, it is necessary that $\ell'm > \ell''e^*$. The condition of energy focusing is given by the following condition:

$$\frac{2a_e}{k^2}(1 - X_e) = a_m\left(1 + \frac{1}{X_m}\right)$$

A double focusing system is obtained if the instrument is designed so as to satisfy the above conditions.

The mass dispersion D at the final image position is given by:

$$D = \frac{a_m}{2}(1 + X_m)\gamma = \frac{a_e}{k^2}(1 - X_e)X_m\gamma$$

Instrument

The JMS-06 is a double focusing mass spectrometer combining a diverging electrostatic field and a homogeneous magnetic field. The diverging electrostatic field has a mean radius of 150 mm and a deflection angle of 90°; the homogeneous magnetic field 120 mm and 60°, respectively. The ion orbit of this instrument is shown in Fig. 2. Table 1 shows a comparison between the JMS-06 and the standard Nier-Johnson (N-J type) type mass spectrometer whose cylindrical electrostatic field and homogeneous magnetic field have the same mean radius as the JMS-06. Their ion orbits are shown in Fig. 3.

As is seen from Table 1, the JMS-06 exhibits twice the theoretical resolution of the N-J type instrument, in case they use the same main and collector slit widths. Furthermore, the JMS-06 can use a main slit about 3.5 times as wide, to obtain the same resolution as the N-J type instrument. This means that the JMS-06 offers a higher sensitivity than the N-J type instrument in measurement at the same resolution, because it can use a larger ion beam. Another factor that enhances the sensitivity of the JMS-06 is the focusing function of its diverging electrostatic field in the axial direction, which reduces ion beam divergence at the image point.

If an instrument offering the same magnification and mass dispersion as the JMS-06 is to be materialized by the use of a cylindrical electrostatic field with a deflection angle of 60°, that will be a medium-sized instrument with a mean radius 1.6 times and an ion path 1.8 times as large as the JMS-06, as shown in Fig. 4. In other words, the JMS-06 has a resolution as high as that of a medium-sized instrument. Also, the JMS-06 excels it in sensitivity, due to the focusing function in the axial direction.

The power supplies of the JMS-06 employ all solid-state circuitry, ensuring stability for a long period of time. Magnetic scan and mass number indication are made while the magnetic intensity is being measured by the Hall element. Furthermore, the JMS-06 incorporates a total ion monitor (T.I.M.), which permits a T.I.M. chromatogram to be easily recorded by plugging a pen recorder in the T.I.M. monitor. The connection between the JMS-06 and a gas chromatograph can be easily made by the stop valve located between them, and on-line connection with a computer is also possible.

Two operation panels —— one for push button control of the evacuation system and the other for electrical system control —— are provided on the front for ease of operation.

The main evacuation system consists of two 2.5" DPs —— one for the ion source and the other for the analyzer —— which are each fitted with a liquid nitrogen trap. The ultimate vacuum degree is 1×10^{-7} Torr. The sample can be introduced by three different systems—— the direct sample inlet, reservoir type inlet, or gas chromatograph. The vacuum system is operated by push buttons on the front graphic panel, and is provided with various interlocks intended for safe operation.

Results

Fig. 5 shows the multiplet at m/e = 28. Resolution is 3500 (10 % valley). Fig. 6 shows a fragmentgram of the molecular peak of cholesterol. When the molecular peak is detected at S/N = 5, with consideration given to the peak intensity and duration, and a reserve of sensitivity of the detection system (X1000), the sensitivity of the JMS-06 is calculated as 7.4×10^{-12} gr/sec. A spectrum of cholesterol obtained with the use of a direct sample inlet is shown in Fig. 7. Fig. 8, 9 and 10 show spectra obtained by a combination of a gas chromatograph and a JMS-06.
Fig. 8 shows a gas chromatogram, Fig. 9 a T.I.M. chromatogram and Fig. 10 a mass spectrum of the 8th peak of the T.I.M. chromatogram, obtained at a scan speed of 5 sec/m/e 1 ∿ 500.

Acknowledgement

The authors wish to express their thanks to Mr. Y. Wada, Director of JEOL for his encouragement in the accomplishment of this project, and Mr. E. Yamauchi for his devoted assistance.

References

1. Matsuda, H. "Mass Spectroscopy," 1964, 11, 127.
2. Matsuda, H. "Mass Spectroscopy," 1968, 16, 30.

A NEW ACHROMATIC MASS SPECTROMETER

H3

Marcel Baril

Centre de Recherche sur les atomes et les molécules,

Dept. de Physique, Université Laval, Québec, Qué., Canada.

The aim of this work was to build an achromatic mass spectrometer. Many energy dispersive elements could have been chosen, but the plane parallel condenser seemed to be the easiest to construct and align.

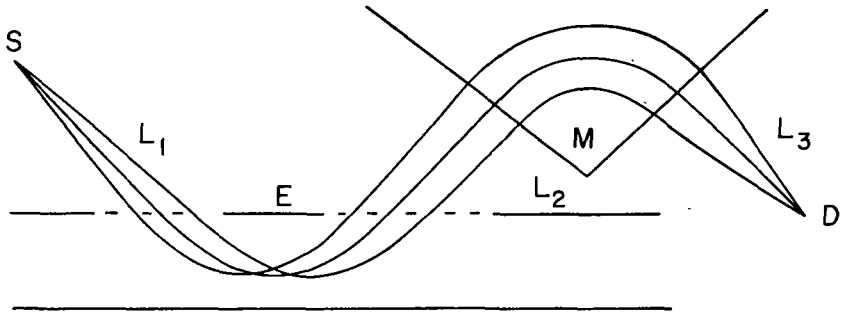

FIGURE 1

Figure 1 shows the system which was studied and constructed. There are three drift spaces called L_1, L_2 and L_3, a mirror called E and a magnetic prism called M. Optical properties of the system were calculated by matrix algebra, since each element can be represented by a matrix whose dimension varies with the order of the terms utilised. For the first order, only 4 x 4 matrices are needed. Second order needs 14 x 14 matrices, in which the 4 x 4 matrices are included.

The four variables utilised are:

x, the lateral displacement relative to the main path,

α, the angular displacement relative to the main path,

$\Delta E/E$, the relative difference in kinetic energy between the particle under study and another one which starts with no kinetic energy,

$\Delta m/m$, the relative difference in mass between the particle under study and another one which follows the main path in the magnetic field with a kinetic energy of E.

The four following equations with the coefficients taking appropriate values, can represent each element and also the complete system.

$$(1)\qquad x_q = Ax_p + B\alpha_p + C(\Delta E/E)_p + D(\Delta m/m)_p + Ex_p^2 + F\,x_p\alpha_p + Gx_p\,(\Delta E/E)_p + Hx_p\,(\Delta m/m)_p + I\alpha_p^2 + J\,\alpha_p\,(\Delta E/E)_p + K\alpha_p\,(\Delta m/m)_p + L\,(\Delta E/E)_p^2 + M\,(\Delta E/E)_p\,(\Delta m/m)_p + N\,(\Delta m/m)_p^2$$

$$(2)\qquad \alpha_q = ax_p + b\alpha_p + c(\Delta E/E)_p + d(\Delta m/m)_p + ex_p^2 + fx_p\,\alpha_p + gx_p\,(\Delta E/E)_p + hx_p\,(\Delta m/m)_p + i\alpha_p^2 + j\alpha_p\,(\Delta E/E)_p + k\alpha_p\,(\Delta m/m)_p + (\Delta E/E)_p^2 + m(\Delta E/E)\,(\Delta m/m)_p + n(\Delta m/m)_p^2$$

$$(3)\qquad (\Delta E/E)_q = (\Delta E/E)_p$$

$$(4)\qquad (\Delta m/m)_q = (\Delta m/m)_p$$

In the matrix representing the complete system B = 0 corresponds to an imaging system, and B = C = 0 corresponds to an achromatic imaging system. By imaging system we mean that the source slit is imaged at the detecting slit. The values of the parameters of the mirror, the prism and the drift spaces for which these relations are valid have been studied in ref. 1.

Aberrations can also be studied by the same procedure, and it is possible to correct α^2 and $\alpha(\Delta E/E)$ simultaneously for an achromatic imaging system. These results will be published soon. (ref. 2).

This type of system is being integrated with an ion bombardment source to study the secondary ions produced. Results obtained up to now are very encouraging.

---

1. Baril, Marcel. Can. Jour. Phys., vol. 47, no. 3, p. 331 (1969).

2. Baril, Marcel. To be published in Can. Jour. Phys.

ASTRONAUT BREATH ANALYZER*

WILSON M. BRUBAKER †

Earth Sciences, a Teledyne Co., Pasadena, Calif.

INTRODUCTION

A prototype of a miniature mass spectrometer for use by an astronaut has been developed. The entire vacuum system, including the ion pump and the mass analyzer, fits inside the helmet, under the chin. A small inlet tube conducts breath gas from the nose to the ion source of the mass spectrometer. A micro-sized needle valve admits the very small gas stream to the instrument. The mass spectrometer jump-scans mass peaks associated with the four main components of breath gas: water vapor, nitrogen, oxygen, and carbon dioxide. Most of the associated electronic apparatus is carried in a back-pack.

THE LEAK

The most difficult part of this project was the micro-leak. Size limitations result in an ion pump with a speed on the order of a tenth of a liter per second. Operation of the pump at a pressure of 10^{-6} torr results in a through-put of 10^{-7} torr-liters/second. The admission of gas at earth atmosphere pressure requires a leak with a conductance of about 10^{-10} liters/second.

The leak developed for this program consists of an electrically polished tungsten needle operating in a seat in a thin gold foil. The etched point is invisible to the naked eye. The laboratory version of this leak is operated by a combination of screws and levers to give the required mechanical advantage. The flight model which is designed but not assembled is operated by thermal expansions.

THE PUMP

The pump is a simple Penning Cell with a tantalum-tungsten wire sublimator on its axis. The self-contained magnetic field structure is in the form of a pillbox with ports for pumping conductances. The external dimensions are 1 inch in diameter by 1 inch long. The external magnetic field is so weak that it will not reverse a compass needle. This containment is essential, because the ion source of the mass spectrometer is placed adjacent to the ion pump.

THE MASS SPECTROMETER

Mass analyses are made by a small quadrupole mass filter. The rods are 2 inches long, and have hyperbolic field forming surfaces. Although the laboratory type quadrupole used four simple hyperbolic rods,[1] those on the flight unit will have insulated segments to provide a delayed dc ramp[2] mode of operation.

The desired fast response of the instrument is achieved through the use of an ion source of unusually small dimensions. Its total volume is only 0.3 cc. Differential pumping is achieved by causing the admitted gas to leave the ion source through the ion exit aperture. Rhenium filaments are used to minimize the chemical reaction of oxygen and water vapor with the hot surfaces.

* This research was supported in whole by the National Aeronautics and Space Administration under Contract No. NAS 98371 and monitored by Mr. Paul W. Schlottman.

† Present address: Analog Technology Corp., Pasadena, California.

INSTRUMENT PERFORMANCE

Operating at a sensitivity of about 5×10^{-6} amperes/torr the resolving power is sufficient to display flat-topped peaks, indicating essentially 100% ion transmission. The addition of segmented rods should improve the sensitivity appreciably.

The system responds to a step change in the composition of the breath gas (accomplished by an abrupt change from exhale to inhale while observing the carbon dioxide peak) with a time constant of 50 milliseconds.

The most critical portion of the device is the leak and pump combination. Laboratory versions of these have operated cooperatively for eleven weeks without a single failure. When the test was terminated voluntarily at the end of this period, the equipment was operating satisfactorily and showed every indication of continuing to do so indefinitely.

(1) "Theoretical and Experimental Comparisons of Quadrupole Mass Analyzers with Round and Hyperbolic Field-Forming Surfaces," W. M. Brubaker and W. S. Chamberlin, International Conference on Mass Spectrometry, 1969, Kyoto.

(2) "An Improved Quadrupole Mass Analyzer," W. M. Brubaker, Advances in Mass Spectrometry, Volume 4.

Influence of Ion Beam Energy and Density Distributions on Peak Shapes and Sensitivity of Quadrupole Mass Spectrometers*

by

M. Mosharrafa
Department of Physical Medicine and Rehabilitation
University of Minnesota
Minneapolis, Minnesota 55455

Abstract

The well-observed deterioration of mass peak shapes of quadrupole mass filters have been successfully related to imperfections in the geometry of the analyzing field by N.R. Whetten and T.H. Dawson.[1,2,3,4] This paper describes experimental evidence of an additional dependence of peak shapes (or transmission efficiency) on the cross-sectional density and energy distribution functions of the ion beam entering the quadrupole field. This dependence, which can be further influenced by field imperfections, is explained by identifying the portions of the ion beam cross-section responsible for the production of the corresponding portions of the mass peak, and initial transmission criteria from the stability diagram. The experimental data was obtained from a small quadrupole mass spectrometer (L = 5 cm, r_o = 2mm) designed and built for use in clinical and medical research. Variations in energy and density distributions of the ion beam entering the analyzing field was possible experimentally over a limited range by the use of a radial electron impact ion source. The experimental results emphasize the importance of controlling the inlet conditions of the ions in order to improve the overall performance of quadrupole-type mass spectrometers.

Introduction

In constructing quadrupole-type mass spectrometers, a large degree of emphasis is placed on the dimensional accuracy and electronic stability of the analyzing field. Practical limits of these parameters determine the maximum attainable resolving power of the instrument. Towards gaining a better understanding of the sensitivities of the instrument to the practical limitations in design parameters, it is necessary to study in detail, with the aid of a digital computer, the factors affecting ion transmission efficiency through the analyzing field. Several investigators[1,2,3,4,5,6] have successfully used the digital computer to describe and plot the trajectory of the ion as a function of the time which it spends in the analyzing field. Brubaker[6] has also investigated the effects of the fringe fields on the ion trajectories as well as the hyperbolic-to-circular geometry approximation. However, several experimental phenomena associated with the passage of an ion through the quadrupole analyzing field have not been fully explained. The most prominent of these is the observation of mass peak shape deterioration and loss of sensitivity in most quadrupole instruments. Von Busch and Paul[7] demonstrated analytically the existence of non-linear resonances in the trajectories of ions due to field errors in a quadrupole mass spectrometer. Dawson and Whetten[3,4] used the digital computer to gain information on peak shape deterioration in the three dimensional quadrupole ion trap. They have successfully correlated their findings to the existence of higher order fields which result from errors in electrode shape, spacing, or harmonics in the rf field.

It is surprising that very little work has been done to investigate the effects of density and energy distribution functions over the cross-section of the ion beam entering the quadrupole field upon peak shapes, and most important, upon transmission efficiency. Maximizing the coupling efficiency between the ion source and the analyzing field is a necessary step towards optimization of quadrupole mass spectrometer performance.

*This work was supported by Social Rehabilitation Service Grant RT-2.

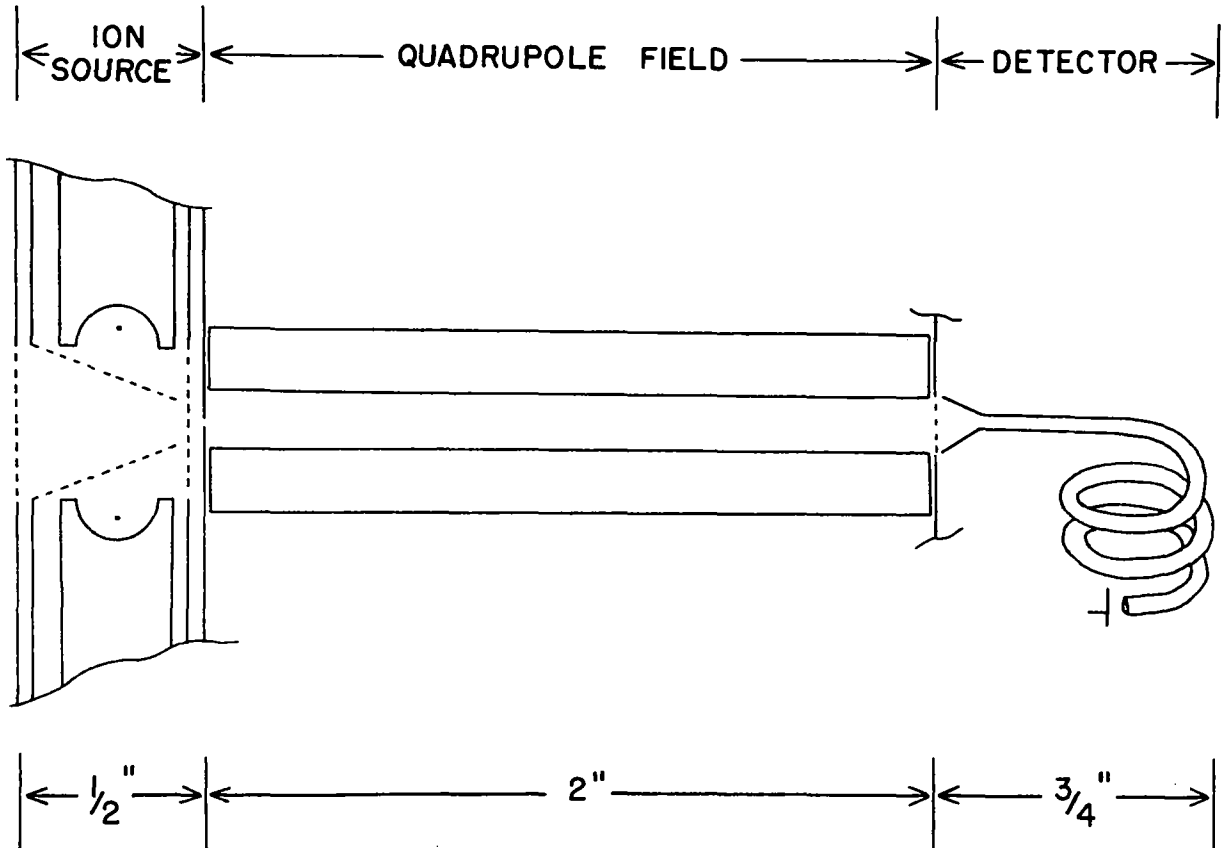

Fig. 1

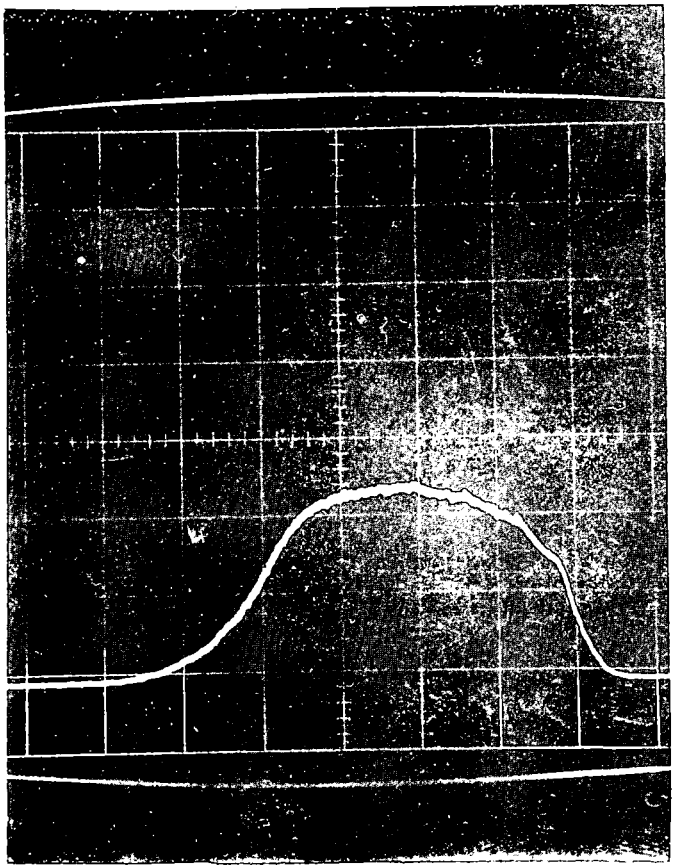

Fig. 3

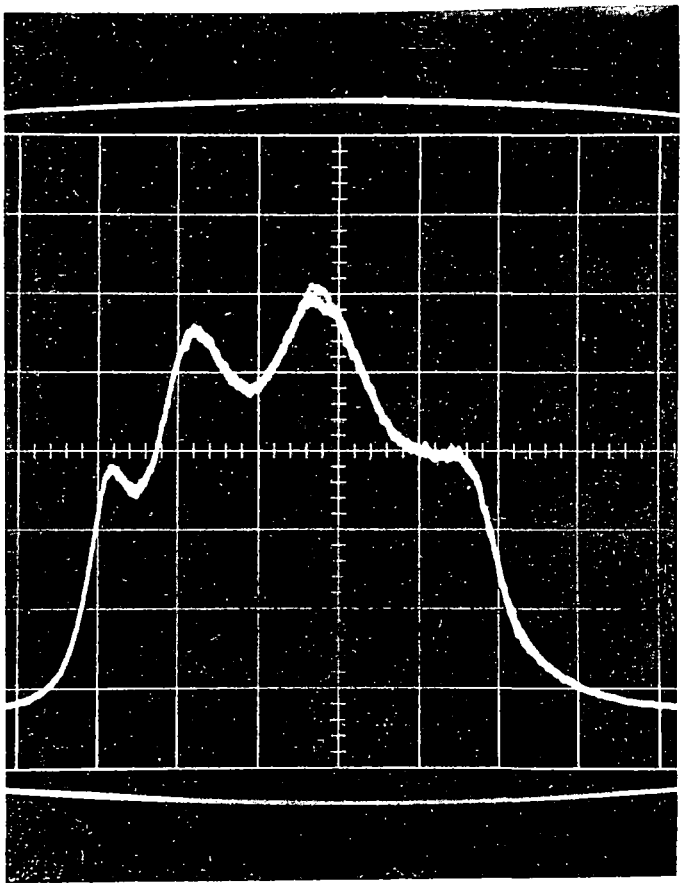

Fig. 4

$N(x,y) = k$ for $0 \leq (x^2 + y^2) \leq R^2$

$N(x,y) = 0$ for $(x^2 + y^2) > R^2$

$E(x,y) = 0$

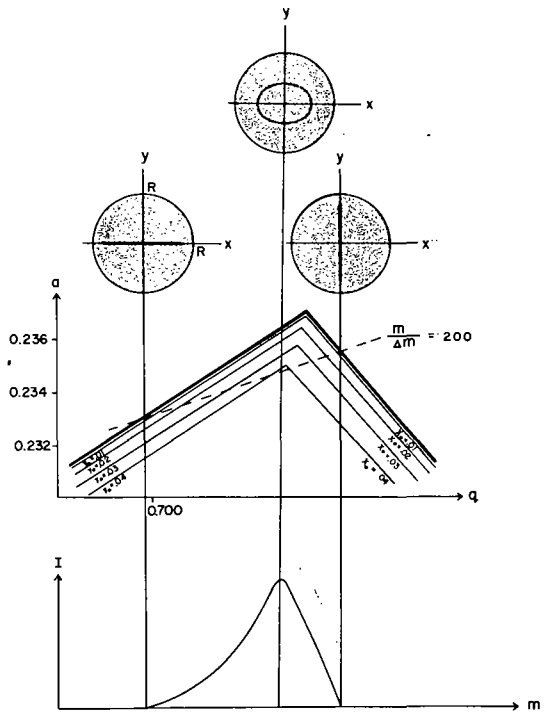

UNIFORM DENSITY DISTRIBUTION

Fig. 5

$N(x,y) = k_1$ $0 \leq (x^2 + y^2) \leq R_1^2$

$N(x,y) = k_2$ for $R_1^2 \leq (x^2 + y^2) \leq R_2^2$

$N(x,y) = 0$ for $(x^2 + y^2) > R^2$

$k_2 \gg k_1$

$E(x,y) = 0$

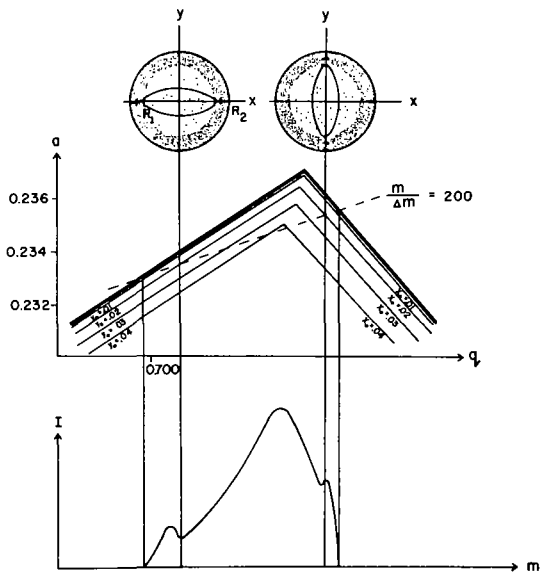

ANNULAR DENSITY DISTRIBUTION

Fig. 6

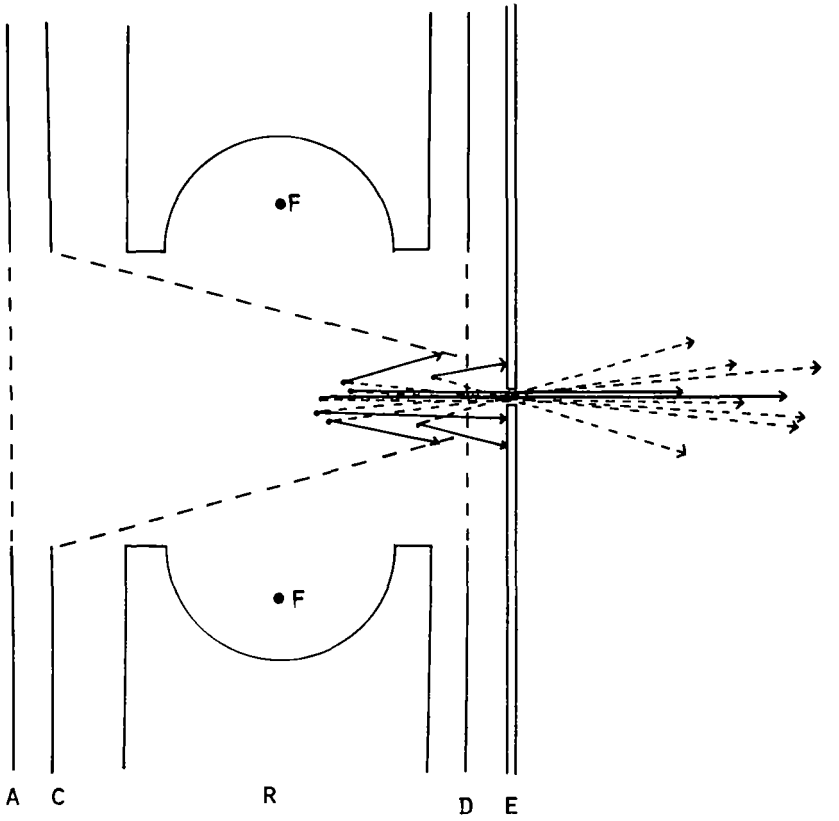

F - FILAMENT

A - ANODE

C - CONE-GRID ELECTRODE

R - ELECTRON REPELLER

D - DRAWOUT GRID

E - EXIT APERTURE

⟶ WEAK FOCUSING

⇢ STRONG FOCUSING

Figure 2 ION SOURCE CONFIGURATION

Experimental

The experimental data was obtained on a small quadrupole mass spectrometer which was designed and built in our laboratories for medical applications. The instrument, shown schematically in fig. 1, has an analyzing field length of 5 cm, and a field radius of 2 mm. The instrument is capable of operating in the mass range of 1-100 amu per/electron with a PWHM resolution of 150. The required dc and rf voltages applied to the quadrupole rods are generated using solid-state circuitry exclusively. The operating frequency of 3 MHz is generated by a crystal controlled oscillator for maintaining the desired frequency stability. Sweep linearity is maintained at better than ±.1% over the entire mass range with a very high degree of amplitude stability. A small radial electron bombardment source is used for production of the ion beam. The source shown schematically in fig. 2 is similar to that investigated by Brubaker[6] with an additional grid used for ion drawout from the ionizing region. The source features high ionization efficiency for the incoming gas sample with maximum ion production close to the axis of the quadrupole analyzer. The exit aperture diameter is 0.5 mm.

Using an ion source of this geometrical configuration, a large variation was observed in the shape of the mass peak pertaining to an ion species, depending upon the operational parameters of the ion source alone. The peak shape was found to be a strong function of the amplitude of the voltage applied to the cone-shaped grid electrode. With reference to fig. 2, two operating conditions can be deduced:

a) weak focusing: with small positive voltages applied to the cone (0 to 4v), only those ions formed in the ionization region very close to the quadrupole axis of symmetry are able to leave the source through the small exit aperture. These ions, therefore, possess little or no radial energies. Under such conditions, an almost ideal peak shape similar to that shown in fig. 3 is obtained.

b) strong focusing: increasing the amplitude of the positive voltage applied to the cone-shaped grid electrode focuses the ion beam, at, or near the pinhole exit aperture, with the resulting increased radial energy of the ions. In this case, despite the increased sensitivity resulting from the focusing effect, additional structure appears on the mass peak. This structure is a very strong function of the cone potential. At cone voltages slightly above 4v, a precursor peak appears on the low mass side. Increasing the cone voltage results in an increase in the number and prominence of the structural peaks. At 8v cone potential the peak shape deteriorates to that shown in Fig. 4. The peak shape is also dependent to a lesser extent on pressure, emission current, and resolution. Increasing the emission current to a point where the ion source is space-charge limited will improve the peak shape. Upon decreasing resolution additional oscillations appear on the peak, while increasing resolution will eliminate the oscillations starting at the high mass side of the peak; the precursor peak is least effected by resolution changes. The structure is, on the other hand, independent of accelerating potential, electron energy and sweep rate.

Discussion and Conclusions

These experimental observations indicate that the transmission efficiency and quality of mass spectra of quadrupole mass spectrometers is a strong function of energy and density distribution across the incoming ion beam cross-section as predicted from theoretical considerations. Furthermore, the influence of analyzing field geometry imperfections upon the performance of the instrument can be determined to a certain extent by the entrance conditions of the ions. This is evident when one considers the simple example of ions entering parallel to the quadrupole axis with no radial energy. Since the maximum amplitude of oscillation of the ions traversing the quadrupole field is proportional to their initial displacement, the analyzing field errors which are proportional to higher order powers of the distance from the field axis[3] will have an increasing influence upon the transmission efficiency with increasing amplitude of oscillation.

A qualitative interpretation of these experimental observations can be arrived at by identifying the segments of the ion beam cross-section responsible for the production of the corresponding portions of the mass peak, while taking into account initial transmission requirements from the stability diagram. We shall consider first the simplest case, that of an ion beam with a circular cross-section of radius R entering the quadrupole analyzing field with zero radial energy. Consider first the case of uniform density distribution; i.e., the number density of the ions is a constant over the cross-section of the beam. With reference to fig. 5 which shows the tip of the stability triangle together with the admissable initial conditions of the ions for injection parallel to the axis, one can readily see that the low mass side of the peak during the scan results from the transmission of those ions which enter the quadrupole analyzing field near the x-axis, while the high mass side of the peak results from ions entering close to the y-axis. With a uniform density distribution and no significant field distortions, the resultant mass peak would therefore be similar to that predicted by theory.

Considering next, as an example, the case of an annular density distribution function similar to that shown in fig. 6. In this case, similar reasoning illustrates how fine structure may appear on the mass peak. The mass spectrometer acts, therefore, during the scanning of the stability triangle pertaining to a specific ionic species, as a secondary profile scanner of the cross-section of the incoming ion beam in a unique manner starting with the x-axis and ending on the y-axis of the beam.

This simplified analysis has not taken into consideration the influence of the errors in field geometry and the initial radial energy of the incoming beam. It further assumes that the transmission efficiency of the ion is independent of the operating point within the stability boundary. This assumption is known to be incorrect, especially when imperfections in field geometry are present as reported by Dawson and Whetten[3,4] and Brubaker.[6] Additional structure may therefore appear on the mass peak during the traversing of the stability triangle. The influence of the initial conditions would therefore be to enhance the structure.

In conclusion, an attempt has been made to demonstrate in a qualitative preliminary manner that initial density distributions of ions can play an important role in the performance of the quadrupole mass spectrometer. It would be advantageous to study in detail, with the aid of a digital computer, the exact nature of the dependence of these parameters in order to arrive at a realizable density and energy distribution function for the ions for optimizing quadrupole mass spectrometer operation. The results of this study may lead to the design of a new ion source which will be compatible with quadrupole mass filters and enhance the quality of their performance.

Acknowledgements

The author is indebted to Mr. John Munsch for construction of the quadrupole analyzer and ion source.

References

1. P.H. Dawson and N.R. Whetten. G.E. Research & Dev. Center, Report #67-C-282 (1967).
2. P.H. Dawson and N.R. Whetten. G.E. Research & Dev. Center, Report #67-C-283 (1967).
3. P.H. Dawson and N.R. Whetten. G.E. Research & Dev. Center, Report #68-C-286 (1968).
4. N.R. Whetten and P.H. Dawson. G.E. Research & Dev. Center, Report #68-C-311 (1968).
5. R.F. Lever. IBM Journal, 26 (1966).
6. W.M. Brubaker, NASA Final Report Contract NASW-1298 (1967).
7. F. VonBusch and W. Paul. Z. Physik, 164, 588 (1961).
8. W. Paul, H.P. Reinhard and U. von Zahm. Z. Physik 152 (2), 143 (1958).

A NEW TIME-OF-FLIGHT MASS SPECTROMETER*

J.M.B. Bakker

Shell Research Limited,
Sittingbourne, Kent, England.

In the course of work on a helical path time-of-flight mass spectrometer (Bakker 1970) a straight path beam modulated time-of-flight mass spectrometer was constructed. The instrument consists of an ion source, drift tube and a collector. The ion source is constructed by combining a conventional ionization chamber with an electron gun structure from a cathode ray tube. The gun comprises a three element lens followed by an X-Y deflection system. The ion beam is modulated by applying to the X or Y plates a voltage varying in accordance with a step function. The advantages of using beam modulation are that continuous ionization improves sensitivity, and a continuous ion beam makes resolution independent of the position where the ions are generated. The mathematical analysis of the beam modulation process has shown that the theoretical resolving power of this instrument is inversely proportional to the beam plus collector slit width and proportional to the square of the flight path or:

$$R = \frac{VL^2}{2dU\ (B+S)} \quad , \quad \text{where}$$

R	=	resolving power
V	=	potential difference of the step function applied to the deflection plates
d	=	separation of the deflection plates
L	=	length of drift space
U	=	ion beam accelerating voltage
B	=	beam width
S	=	collector slit width

The validity of this equation was tested by varying the flight path from 60 cm to 150 cm. The resolution obtained for complete separation of adjacent masses was 120 and 700 respectively, giving an experimental increase of 5.8x versus a theoretical value of 6.25x.

No difference was observed between the resolving power for organic species and the resolving power for inorganic species.

* A more detailed account of this work will be submitted for publication in the Journal of Scientific Instruments.

Bakker, J.M.B. (1970). To be presented at the Triennial International Conference on Mass Spectrometry, Brussels, September 1970.

A NEW TIME OF FLIGHT MASS SPECTROMETER

J. P. Carrico, L. D. Ferguson, and R. K. Mueller
Bendix Research Laboratories

The possibility of using the measurement of the time of flight of ions in an inhomogeneous, oscillatory electric field to separate ions of different mass-to-charge (m/e) ratios is being investigated in this laboratory. Calculations and experiments have been performed using a field which is a linear function of position and has both static and oscillatory components. The equations of motion are of the form of the familiar Mathieu Equation.(1)

Ions are pulse injected into the oscillatory field at the position of zero field. For the appropriate choice of field parameters, ions having a limited range of m/e ratios can return to the source region where they are detected. The extent of this range and the associated m/e values are controlled by the field parameters.

Important properties of the arrival time of ions at the detector include: the arrival time depends only on the field parameters and m/e and does not depend on the ion's initial velocity; for fixed field parameters, the arrival times and the difference in arrival times of adjacent masses increase with increasing mass; and, depending on the field parameters and the phase of the oscillatory field at which injection occurs, the spread in arrival times of ions of a given m/e ratio can be less than the spread in their injection times.

(1) See, for example, W. Paul, J. P. Reinhard, and U. von Zahn, Zeit. fur Physik 152, 143 (1958).

A TOF MASS SPECTROMETER WITH MASS SCALE STABILITY

H8

Donald C. Damoth, A.J. Luchte, Patrick McGinnis

The Bendix Corporation
Scientific Instruments & Equipment Division
Rochester, New York

A stable mass scale is desirable in a mass spectrometer for many reasons. Typical cases where stability is very important are continuous measurement of several mass peaks simultaneously as in on-line process monitoring for respiratory gases, and obtaining the most efficient GC/MS analytical measurements. With a stable mass scale, it is possible to obtain better sensitivity and accuracy in simultaneous peak monitoring because the measurements can be taken on the tops of the peaks, eliminating time spent scanning where it serves no purpose. In gas chromatograph/mass spectrometer analyses, a stable mass scale permits assignment of mass numbers to unknown peaks by simple comparison of scans of the unknown to scans of known compounds such as perfluorokerosene. If the mass scale is not stable, direct comparison of scans is unreliable, causing inefficiency due to uncertainty. Therefore, mass scale stability is a most important parameter in a mass spectrometer.

The primary factors affecting the mass scale stability in a TOF mass spectrometer are the voltages on the electrodes and the relative timing of the pulses. These factors also affect the resolution and quantitative stability.

It was the development of solid-state electronic circuitry with its inherently superior stability that led to the design of a new generation of TOF instruments. In addition to design of power supplies with stability of $10^5/1$ or better, a time delay generating circuit was developed which has a stability in excess of $10^5/1$. This time delay generator is vital when resolution of 600 is obtained, because this is obtained with a 30 microsecond flight time and 5 nanosecond peak widths. So, if the peak location instability is greater than 2 nanoseconds, it is not possible to unequivocally assign the mass numbers.

The combination of parameters in the new TOF instruments yields a timing stability of better than one nanosecond over extended periods of time. This means the mass scale is stable to about ± 0.2 amu at mass 500. Consequently, it is feasible to set the analog gates on mass peaks and they will remain there indefinitely unless the basic timing conditions are changed. Similarly, the mass scale can be calibrated on an occasional basis with confidence that the calibration is holding.

The task of defining or testing the mass scale stability was considered and the technique of setting the gate on the side of a mass peak was determined to be the most definitive and clearest test. It is also easy to do.

The mass scale stability of the MA-3 Time-of-Flight Mass Spectrometer was tested by narrowing the scanning gate width to a narrow width which yields near maximum resolution, setting the gate on the side of a mass peak at the 75% of peak height level and observing the output level of the instrument as a function of time. Due to the steep slope of the mass peak, any mass scale instability is observed as an output change. A change of 10% in output level corresponds to a change of about 10% of a mass number at mass 500 by this technique.

Since the test was to be continued over a period of several weeks, a constant sample source was needed. Mass 28 due to nitrogen in air was chosen and a two-stage inlet comprised of a capillary followed by molecular leak was used to obtain most stable flow. The advantages of the nitrogen in air sample constancy outweighed the dramatic effects possible by performing the same experiment on a peak in the mass 500 range. Even pump fluid background abundance is not reliable for such long periods and no suitable high mass sampling means could be found.

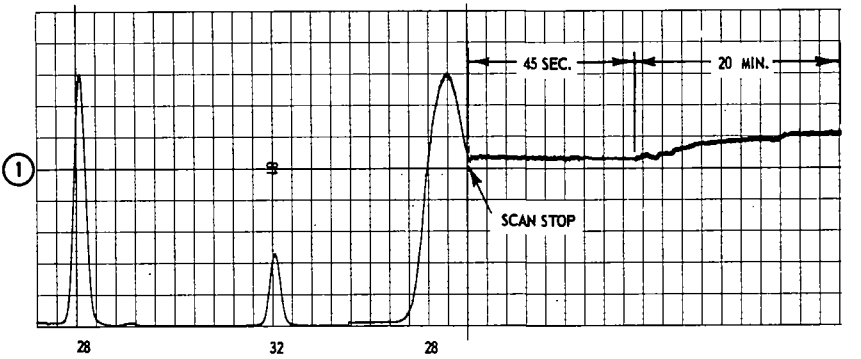

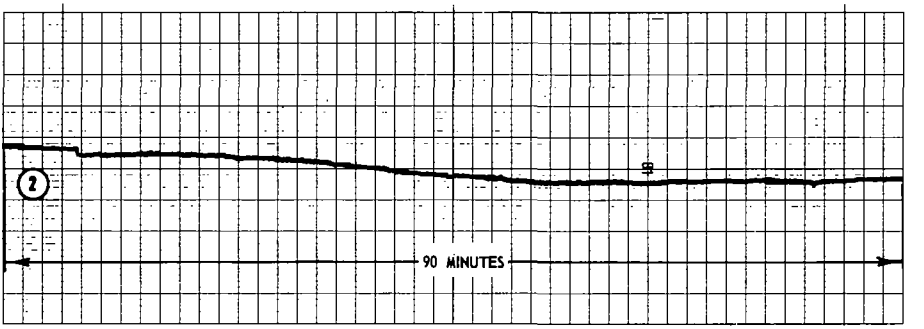

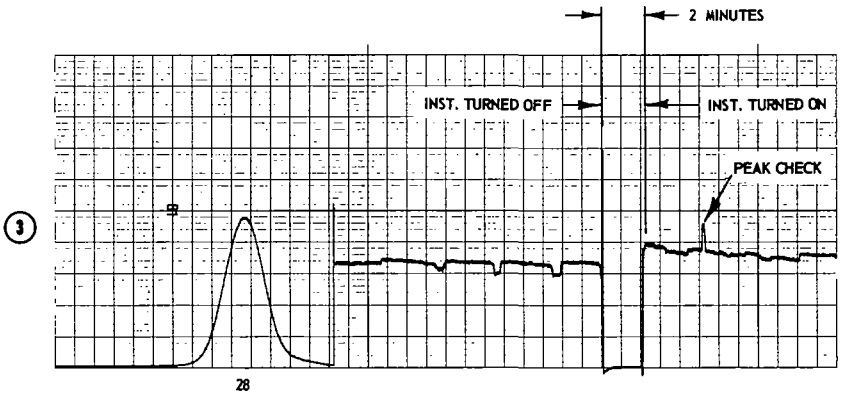

MA-3 MASS SCALE STABILITY

No attempt was made to stabilize input line voltage and consequently the 60-cycle voltage into the instrument varied from 115 to 130 volts during the experiments. A standard production MA-3 type instrument was used to insure typical results.

The experiment was performed by setting the gate on the side of the mass 28 peak, then simply recording the output. Figure 1 shows part of the actual data. In 1A, the 28 to 32 peaks were scanned, then the gate was stopped on the side of the 28 peak. The recorder speed was slowed after 45 seconds. In 1B, the trace is shown for a ninety-minute period. The complete electronic portion of the instrument was turned off at the end of the working day and turned on again the following work day without touching any controls except the single on-off button.

In 1C, the 28 peak was scanned, then the gate set on the side of the peak again. The whole instrument was turned off for two minutes, then turned on again. The gate returned to within 0.1 amu easily. The 28 maximum is shown again. We wish to reemphasize that these tests were conducted at near maximum resolution. That makes this procedure a most critical test.

The short-term mass scale stability appears to be better than 1/100th of a mass unit at m/e 28 and the largest excursion observed over a 30-day period was less than 1/10th of a mass unit even by turning the electronics off over a three-day weekend. The mass scale stabilized faster than the output stability, but by manually going from the side of the peak to the top to observe the position on the peak during the warm-up period, it was evident that the mass scale stabilized to these values in less than ten minutes. The variation of abundance sensitivity settled to about $\pm$ 1% short term within 30 minutes. This is consistent with a normal warm-up stabilization time for the electronics, ion source and glass strips in the magnetic electron multiplier.

Another measurement of this stability was obtained on an MA-2 by use of an Infotronic CRS-160 analog to digital converter and MDS high-speed printer. It took less than 15 minutes to hook the CRS-160 to the MA-2 and calibrate it to 0.2 amu at 500 amu. The calibration was observed to hold constant from day-to-day also, even with indiscriminate turning off and on.

It is clear that this degree of mass scale stability opens up new possibilities of scan function beyond the historical continuous sweep scans. It is now feasible to make the TOF mass spectrometer scan by means of computer control which allows complex scan functions in addition to the linear ramp so commonly used.

One of the most promising complex scan modes is the optimum-dwell jump scan wherein the analog jumps from peak-to-peak and stays on top of each peak just long enough to reach the required statistical level, then quickly moves on to the next peak of interest. This scan mode will yield much greater useable sensitivity in fast scanning GC effluent peaks.

The absence of any factors such as magnetic hysterisis or R.F. field instability in the TOF makes this type of programmed scan feasible.

To summarize, a production MA-3 TOF mass spectrometer has been shown to have better than 0.1 amu stability from week-to-week with line voltage changes of 15 volts and being turned off and on daily.

A TIME-OF-FLIGHT MASS SPECTROMETER FOR SPACE EXPLORATION H9

Tony C. D. Knight

Bendix Aerospace Systems Division, Ann Arbor, Michigan 48107

The Time-of-Flight mass spectrometer has many desirable features for space applications. Hitherto the resolution attained with a drift-tube length compatible with a flight constrained instrument has been inadequate for most applications and consequently few TOF instruments have been flown. However, recent improvements in certain mechanical components and the significant advances during the last few years in high speed electronics have led to an instrument fully compatible with the requirements and constraints of flight hardware. The characteristics of a flight instrument using the current state-of-the-art is shown in Figure 1.

In the past the major technical obstacle lay in the general area of electronics stability-particularly in stability of the timing delay. Figure 2 shows various timing relationships for the instrument and timing delay stabilities of about ± 2 nanoseconds are required in time delays up to about 8 microseconds in order to realize the full potential of the TOF spectrometer for the space application. This stability requirement can be approached using digital logic in the 300 megahertz range but this is precluded in a flight instrument due to the relatively high power requirement. After various investigations and trade-offs two reasonable approaches were identified. Both of these met the stability requirements and were generally compatible with flight hardware constraints. The first technique was to use acoustic delay lines-similar to those developed for phased radar arrays, and the second was to use electronic delays based on the circuit techniques used in the commercial range of instruments. Pertinent performance data is presented in Figure 3 for these two approaches.

The acoustic delay appears to provide the best performance but since the delay can not be varied the electronic delay approach was finally selected in view of its greater flexibility. The temperature coefficient of the electronic delay circuit is rather higher than ideal but it is a comparatively simple matter to design all of the circuits that have some effect on the required delay to effectively reduce the overall temperature coefficient by about one order of magnitude from that of the delay circuit alone. This being the case, then the temperature coefficient problem becomes insignificant. The configuration selected for the timing and data handling section of the flight instrument is shown in Figure 4. The delay obtained from the delay circuit varies approximately linearly with the level of the reference voltage applied. For the flight instrument this reference voltage is derived from a 12 bit D/A converter. This provides the capability for performing digital control either to scan through some, or all, of the mass range or to sit on a particular mass peak for as long as required. The 12 bit level provides an increment of about 2 nanoseconds per digital step, which provides a perfectly adequate timing resolution. The delay timing is initiated by the ion draw-out pulse and outputs from the delay timers are used to trigger the data collection channels (or can be used to trigger pre-dynode gating channels).

The output from the multiplier is amplified and fed into a linear fan-out, each output feeding separate identical data handling channels, so allowing monitoring of more than one mass peak or mass range at the same time. The linear fan-out feeds a fast gate and dual fan-out; the opening of the gate being triggered by the delay timer and the period during which the gate is open and accepts a signal, if present, either being pre-set and fixed or adjustable via up-link command.

One channel of the dual fan-out feeds an analogue electrometer channel and the other a digital counting channel. The electrometer channel is intended to handle the higher level signals and provides a logarithmic compression of the current. On read-out command the electrometer voltage output is sampled and held in a sample and hold circuit for later multiplexing into the data stream. As soon as the sampling is completed the channel is ready for the next measurement. This technique allows sampling many data channels at exactly the same time and yet still multiplexing the data into a serial data stream.

The digital channel is intended for the low signal levels. Its capability is to detect whether or not at least one ion is present in an instrument cycle and sum these over the period between readouts. On readout command the digital output is stored in a buffer store for multiplexing into the data stream. The expected noise level in a digital channel is about one count every 50 to 100 seconds so allowing the digital mode to provide an exceptional minimum detectable signal level. At low signal levels the statistical probability of there being more than one ion in any instrument cycle is very low and the count provided in the digital mode can be considered to be a true ion count. As the count rate increases then the probability of there being more than one ion detected in each cycle increases and an additional statistical error has to be added to the basic statistical error which varies as a function of count rate. The actual count in the digital register can be used to determine whether the analogue or digital output is multiplexed into the data as providing the most accurate output. An area of overlap, in which both the analogue and digital output are read, provides a means of obtaining a calibration of the analogue channel. If required one of the outputs from the fan-out can feed directly into a electrometer to provide a total ion current output.

Other aspects of the instrument design will not be considered here but the design is a straightforward application of flight design practice to relatively simple problems.

FIGURE 1
PROJECTED INSTRUMENT CHARACTERISTICS

WEIGHT:	12-16 POUNDS
SIZE:	~13" X 8" X 6" (~.36 CU FT)
POWER:	10 WATTS + 1 WATT PER OUTPUT CHANNEL
RESOLUTION:	BETTER THAN UNIT RESOLUTION AT MASS 150 AMU
USEFUL MASS RANGE:	1 THROUGH 250 AMU
SENSITIVITY:	TO ABOUT 10^{-15} TORR PARTIAL PRESSURE FOR NITROGEN
DYNAMIC RANGE:	TYPICALLY 10^6

FIGURE 2
INSTRUMENT TIMING RELATIONSHIPS

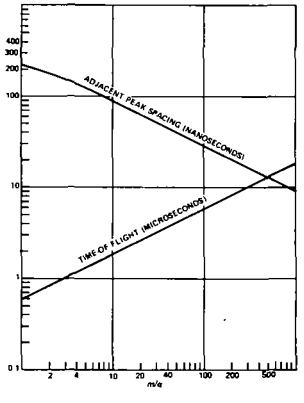

FIGURE 3
DELAY TIMING STABILITY

ACOUSTIC DELAY LINES:

- 8 MICROSECOND DELAY ± 0.25 NANOSECONDS
- TEMPERATURE COEFFICIENT 0.04 NANOSECONDS/°C

ELECTRONIC DELAY LINES:

- 9835 ± 0.5 (1 S.D.) NANOSECONDS DELAY
  SHORT TERM (10 MINUTE) STABILITY
- TEMPERATURE COEFFICIENT 0.20 NANOSECONDS/°C

FIGURE 4
DATA HANDLING—SIMPLIFIED BLOCK DIAGRAM

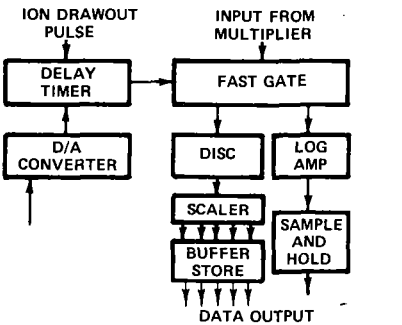

ENVIRONMENTAL ASSAY OF TRACE METALS

W. G. Myers and F. A. White

Department of Nuclear Science
Rensselaer Polytechnic Institute
Troy, New York 12181

INTRODUCTION

At this particular laboratory we are interested in environmental measurements of trace metals, especially those metals that relate to the nuclear industry. In many instances, techniques other than mass spectrometry may be employed and a useful comparison of sensitivity has been reported by Morrison and Skogerboe[1]. Nevertheless, mass spectrometry often exceeds, in sensitivity, neutron activation methods and it provides isotopic information that rarely can be obtained by other methods.

Inasmuch as this presentation is intended to provide preliminary information, rather than a complete report, we have chosen to make reference to three types of environmental measurements. First we shall discuss the utility of mass spectrometry in measuring transient phenomena - specifically, the assay of copper in rainfall. Secondly, we shall review recent measurements of uranium and rubidium concentrations in surface waters of New York State. Finally, we would like to call attention to the increasing importance that isotopic data is expected to provide in future environmental surveys, especially as the nuclear power industry in the United States will generate literally tons of material whose isotopic abundance will be significantly changed from the naturally occurring elements. Additional applications of mass spectrometry to trace metals analysis in environmental sciences have been suggested by one of the authors.[2]

ASSAY OF COPPER IN RAINFALL

The primary sources of metallic pollutants and their rate of introduction into the atmosphere is generally known. The natural forces and meteorological processes regulating their removal, however, are not as well defined, receiving comparatively little attention to date. The high sensitivity of thermal ionization, mass spectrometry to metal analysis was applied at this laboratory to observe the dynamic "washout" of copper from the atmosphere.

Figure 1 shows the copper content of fractionally collected rain samples taken during a shower in the Troy, New York area, June 1968. The samples were collected in plastic containers and spiked with an isotopically enriched nitric acid mixture. The analysis was performed on drop-sized (10 μl) portions of the precipitation whose total copper content amounted to only 1×10^{-10} gm in some cases. The results shown in Figure 1 were found to agree with theoretical models[3] describing contaminant wash-

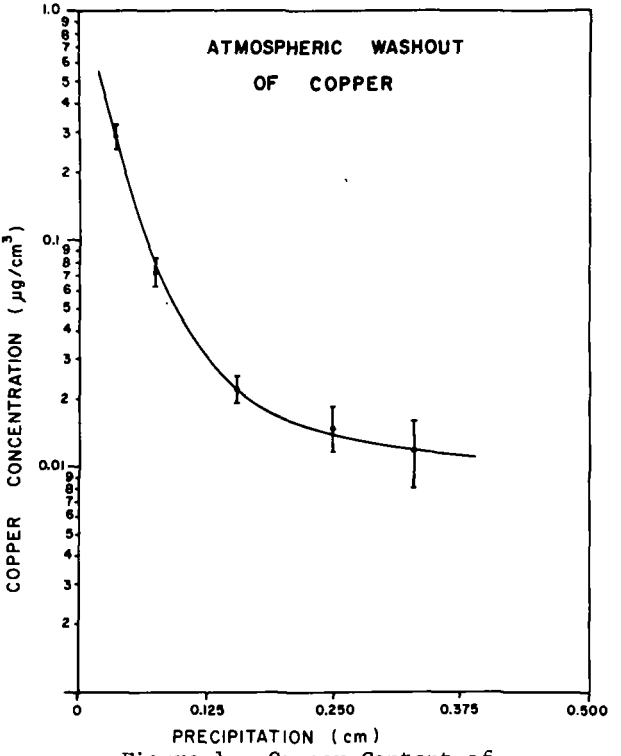

Figure 1. Copper Content of Fractionally Collected Rain Samples from the Troy, New York Area, June 1968.

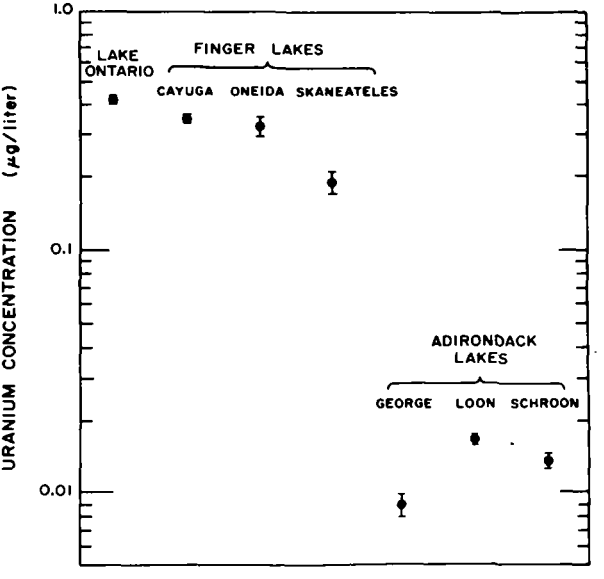

Figure 2. Uranium Concentrations in Seven New York State Lakes, 1966-67.

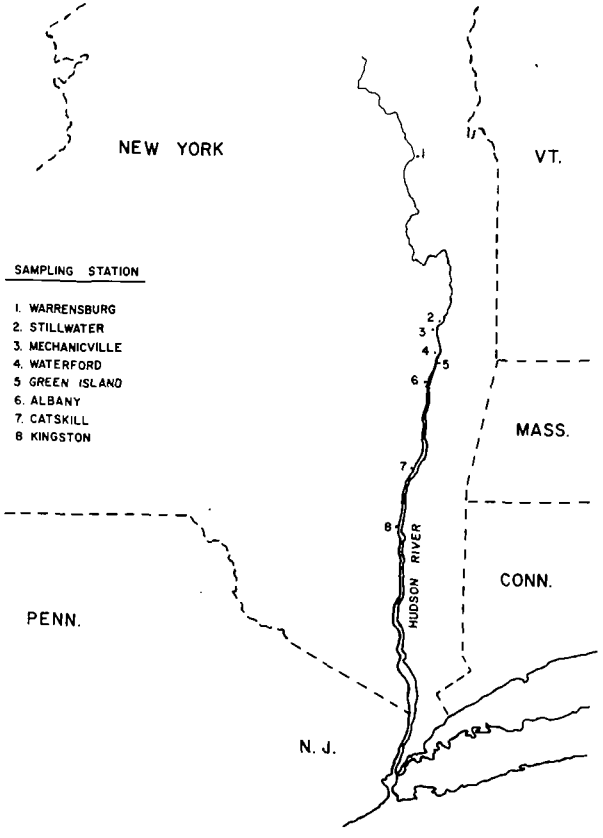

Figure 3. Water Sampling Stations along Hudson River for Rubidium Analysis.

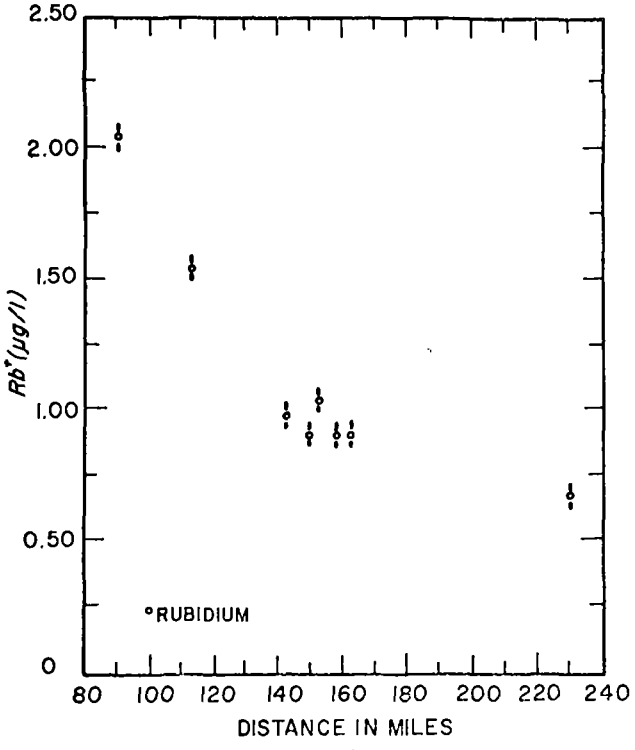

Figure 4. Rubidium Concentration versus Distance from the Mouth of the Hudson River, November 22 & 23, 1966.

METAL CONCENTRATIONS IN THE ATMOSPHERES OF U. S. CITIES, 1960 - 1965[a]

POLLUTANT	CONCENTRATIONS $\mu g/m^3$	
	AVERAGE	MAXIMUM
IRON	1.58	22.00
LEAD	0.79	8.60
ZINC	0.67	58.00
COPPER	0.09	10.00
TIN	0.04	1.10
URANIUM	0.000018[b]	—

[a] U. S. Dept. Health, Education & Welfare

[b] This laboratory, sample site - Albany, N.Y., 1969

Table I

out mechanisms. Graphical analysis of this data indicated the copper concentration in the precipitation follows the expression:

$$C\ (\mu g\ Cu/cm^3) = \frac{0.00275}{h}\ (1 - e^{-36.6h}) + \frac{0.0044}{h}\ (1 - e^{-1.66h})$$

where h is in terms of centimeters of rainfall. By estimating other parameters of each storm, one can calculate the approximate copper content in ambient air both prior to and during the period of precipitation. Such information, along with direct air sample analyses allows the determination of atmospheric self-cleansing rates, and provides a better understanding of the complex mechanisms which establish contaminant concentration levels.

ENVIRONMENTAL MONITORING OF URANIUM AND RUBIDIUM

The need for increasing numbers of nuclear power generating stations and their deployment adjacent to large bodies of water initiated two studies at this laboratory to establish base line concentrations of specific elements within the confines of New York State. In one study, [4] conducted in 1967, the determination of the uranium concentrations in seven New York lakes was made. The analytical procedure employed, involved collecting 100 ml water samples, followed by spiking with U^{235} enriched isotopes, evaporation and ether extraction at the laboratory, and the subsequent isotopic dilution analysis via thermal ionization mass spectrometry. Figure 2 lists the uranium concentrations. The significant difference in concentrations between the Adirondack Lakes and those of the Finger Lake and Lake Ontario grouping can be explained on the basis of the geological and agricultural history of these two distinct regions.

In another study [5] during the period 1966-67, the rubidium concentration over a 140 mile length of the Hudson River was determined. The interest in rubidium stems from it being a naturally occurring radioactive element whose chemical similarity to potassium allows it to play at least a passive role in biological processes. Rubidium is also a significant end-product of the nuclear fission of uranium. Figure 3 shows the stations along the Hudson River which were sampled. The observed rubidium concentrations ranged from 0.66 µg/l to 2.06 µ/l; Figure 4 showing the gradient as a function of distance from the mouth of the river. Other data indicated that domestic waste and some industrial sources have significant rubidium concentrations which would produce noticeable variation in hourly concentrations.

A current investigation at this laboratory is directed towards the analysis of trace elements in urban air environments. Although the National Air Surveillance Network is monitoring urban atmospheres for some 15 odd metals, the instrumental methods of analysis presently applied to these samples are not sensitive enough to detect those metals which exist in trace concentrations. One example of the sensitivity and value of mass spectrometric analysis to environmental surveillance has been demonstrated on air samples taken in June 1969 from downtown Albany, New York. These samples were analyzed for their uranium content by employing the isotopic dilution procedure, using thermal ionization source techniques [5] developed by the authors. The results of this particular analysis are listed in Table 1 along with the concentrations of a few other metals present in the atmospheres of U.S. cities as a means of comparison.

IMPORTANCE OF ISOTOPIC ASSAYS IN FUTURE STUDIES

We believe that within the near future, not only will the elemental "finger-print" of environmental systems be recorded and monitored, but also their isotopic composition. In addition to being ideal for biological and environmental tracer studies, stable isotopic analyses offers a very sensitive means of observing human induced changes to natural environmental systems. A change in the isotopic abundance of an element will not only provide a measure of the amount of contamination introduced, but possibly its source. This technique has already been demonstrated with the element lead [7,8].

Those interested in monitoring the impact of the nuclear industry on the environment will find the rare earth elements particularly useful for such purposes. The rare earth elements are attractive here because

of their relatively low abundance in nature and rather high yield from nuclear fission. Based upon a predicted power output of 10^6 MW (T) in the year 1990 from nuclear plants, the yearly production of stable fission product elements therefrom would be 110,000, 58,000, 28,000 and 24,000 pounds of neodynium, cerium, lanthanum and samarium, respectively. The introduction of a small portion of this material into the environment would be detectable due both to the low levels (i.e. 5×10^{-10} g Sm/l in seawater) presently existing there and the characteristic isotopic abundance difference between natural and fission product elements. As an example, the isotopic ratio of Ce^{140}/Ce^{142} in nature is 7.98, whereas that from the fission of uranium 235 is about 0.015. Given a body of water containing 12×10^{-10} g Ce/l (seawater), the input of only a small quantity of fission product cerium will produce a noticeable change in the natural isotopic ratio. In the case of a river with a flow rate of 26,000 ft^3/sec (Hudson River at Albany), a nuclear power plant leaking only 6×10^{-6} g/sec into the river would produce an isotopic ratio change from 7.98 to 7.5 downstream even after complete mixing.

The need for establishing background concentrations and isotopic analyses of these and other ecosystems is apparent. It is here that mass spectrometry can provide a unique contribution to environmental studies.

REFERENCES

1. G.H.Morrison and R.K. Skogerboe, Trace Analysis: Physical Methods, G.H.Morrison, Editor, Interscience Publishers, J.Wiley & Sons,N.Y., 1965, p.10.

2. F.A.White, Mass Spectrometry in Science and Technology, J. Wiley & Sons, N. Y., (1968) p. 278.

3. K.P.Makhon'ko, Tellus, 19, 3, 469, (1967).

4. A.A.Levin, Ph. D. Thesis, R.P.I., Troy, N.Y. (1967).

5. K.R.Murphy, Ph. D. Thesis, R.P.I., Troy, N.Y. (1969).

6. W.G.Myers, and F.A.White, Anal. Chem. 41, 1861, (1969).

7. T.J.Chow, and M.S. Johnston, Science, 147, 502, (1965).

8. W.V.Ault, R.G.Senechal, and W.E.Erlebach, Envir. Sci. & Tech., 4, 4, 305, (1970).

ANALYSES OF ATMOSPHERES OF ENCLOSED ENVIRONMENTS

F. E. Saalfeld and R. A. Saunders
Physical Chemistry Branch
Naval Research Laboratory, Washington, D. C. 20390

I. Introduction

Since the mid-1950's, the Naval Research Laboratory has analyzed a number of different kinds of closed environmental atmospheres from the point of view of determining their trace contaminant content in order to maintain a check on the viability of these atmospheres. These atmospheres have included aviators' and divers' breathing gases, high-pressure atmospheres for diving habitats such as the Sealab experiments and Tektite, various manned and unmanned spacecraft atmospheres, the atmospheres from a variety of environmental chambers, and, of course, nuclear submarine atmospheres. The importance of these contaminants is illustrated by the fact that the length of a submarine cruise is now limited by the purity of the atmosphere.

The number of organic trace contaminants in these closed atmospheres varies from as few as 50 to more than 12,000 in nuclear submarine atmospheres. Many of the seemingly harmless contaminants cannot be ignored because some of them can be decomposed to form toxic or corrosive materials by the catalytic burners installed in these atmosphere systems to oxidize CO. These contaminants exist in the atmosphere as gases, or as liquid or solid particulates. For the most part, our attention has been confined to the volatile contaminants. Because most of our experience has been with submarine atmospheres, it will be primarily these mixtures that will be discussed here.

This report will review some of the Navy's effort in this area from the following points of view:

(1) how are the atmospheres sampled?

(2) how are the contaminant mixtures analyzed?

(3) what are some of the current analytical problems?

(4) what are some of the mechanical and physiological problems caused by atmospheric contaminants?

II. Sampling Methods

The choice among the several methods of sampling an atmosphere depends on the purpose of the analysis. The most commonly used methods of sampling are:

(1) adsorption on activated charcoal[1];

(2) sampling of whole air;

(3) *in situ* sampling (and monitoring) of the atmosphere.

By far the most used method of these is the charcoal technique. It is thus the most important and will be described more fully than the other sampling methods.

In the nuclear submarines, the entire volume of the atmosphere of the submarine is passed through a charcoal bed every few minutes. When the bed becomes loaded with contaminants, it is replaced. The used adsorbant is sealed in plastic bags and returned to various laboratories for analysis.

Contaminants are recovered from charcoal in our laboratory by slowly heating the adsorbant in a vacuum to a temperature of 300°C and retaining the desorbate in cryogenic traps at various temperatures, the last trap being cooled with liquid nitrogen. The efficiency with which various contaminants are adsorbed on charcoal varies considerably, as does the efficiency with which they are desorbed. Low molecular weight or volatile compounds are recovered with ease, whereas many high-molecular-weight contaminants may not be recovered at all. Thus, for assay purposes, charcoal is not a good sampling method, but for qualitative identification it is the best method available.

Sampling of whole air is accomplished by two methods. An evacuated flask is opened at a given time or sometimes pressurized with a specially designed pump. This method of sampling the atmosphere has some major drawbacks, however. Only a relatively few of the more concentrated contaminants can be accurately assayed in an "as is" sample of the atmosphere. The identification of contaminants present at lower levels of concentration requires a sampling method which concentrates the contaminants. This can be accomplished

by adsorption on activated charcoal or by freeze-out in cryogenic traps. The former method has the problems just discussed, while the latter method greatly concentrates the CO_2 and H_2O in addition to the organic pollutants.

The last sampling method is perhaps the best of all the methods - in situ sampling. In this approach the sample is pumped from the various compartments of the enclosed environment to an analysis instrument. The major concern here is the prevention of contaminant condensation. The instruments will be briefly described in the next section. Obviously, the in situ approach eliminates the troublesome absorption-desorption or concentration steps of the previous two sampling methods. The more serious drawbacks of this method are associated with the instruments employed for the analysis and will be dealt with in the next section of this paper.

III. Analytical Methods

Before describing the techniques employed to analyze the contaminant mixtures, a brief description of the type of mixture being considered is in order. A typical submarine atmosphere contaminant profile is given in Table 1. Of the compounds present in submarine atmospheres, most are hydrocarbons. These may be analyzed as "types", denoted in Table 1 as aromatic and aliphatic hydrocarbons, rather than specific compounds. This greatly simplifies the analysis problem.

At present there are three types of instruments being employed in the submarines and diving habitats for atmosphere analysis. The oldest of these monitors several gases by different techniques; e.g., oxygen by a paramagnetic measurement, hydrogen by thermal conductivity, and carbon monoxide by infrared absorption. A newer approach, based on multicolumn chromatography, also monitors only a preselected number of components. The last technique, also based on chromatography, can measure the very volatile organic contaminants (methane and a few chlorinated compounds) individually and the bulk of the hydrocarbons in total, by a back-flush technique. Appropriately, this instrument is known as the Total Hydrocarbon Analyzer.

All of the above methods suffer from several major drawbacks, e.g., they will not detect a new deleterious component and they are not capable of distinguishing between aliphatic and aromatic hydrocarbons, which is now a requirement of submarine atmosphere analyzers.

Thus, if the Navy is to successfully monitor the contaminants a new in situ approach to the analysis is necessary. The one of immediate interest to the Navy is a combination of mass spectrometer/computer. It must be born in mind that such a system must be operated and maintained by sailors and therefore the combination must be rugged and automated both in its operation and in its data readout. The use of this combination should also enable the concentration of aromatic hydrocarbons to be assayed in the classical hydrocarbon "type" determination. This system is currently being investigated by the Naval Ship and Engineering Command.

As for the material returned to the laboratory for analysis, after the contaminants have been concentrated almost every technique possible is employed to aid in the identification of the pollutants. The most useful analytical system for analysis of these complex organic mixtures is the gas chromatograph/mass spectrometer combination. There are several excellent commercial combinations available. The particular system in use at NRL is an F&M 810 gas chromatograph coupled to an Atlas CH4 dual ion source mass spectrometer. We have employed many different types of interfaces between these two instruments, some obtained from commercial sources and others built at NRL, but with the tremendous concentration differences and the diverse nature of mixture components found in these atmospheres, none of the interfaces has been entirely satisfactory. We obtain the most satisfactory results when the entire effluent of the gas chromatograph is fed into the mass spectrometer. Therefore, the development of a gas chromatograph/mass spectrometer using a chemical ionization source is most exciting. In principle, one has only to record a mass spectrum of each component as it elutes from the column to make an identification. However, it is not quite that simple because even with the best column resolution, many of these peaks represent more than one component. By obtaining a mass spectrum on the leading side, at the peak maximum, and on the trailing side of a peak, it is often possible to identify unresolved components. In the case of the space cabin atmosphere, and some of the other simpler atmospheres, there may be no more than 50-100 contaminants and the gc/ms technique by itself is adequate to identify them. However, for more complicated atmospheres, such as those from nuclear submarines, where there are a great many sources of contaminants, more specialized techniques are required in order to identify the pollutants.

One of these specialized methods of analysis, which has not been adequately tested but appears promising, is the slow desorption of charcoal (a very small amount) directly

Table 1

A Typical Submarine Atmosphere Contaminant Profile

H_2
Methane
Nitric Oxide
Carbon Dioxide
Nitrogen Dioxide
Aliphatic Hydrocarbons
Vinylidine Chloride
Trichloroethylene
Aromatic Hydrocarbons
Methyl Chloroform
Freon 12
Freon 11
Freon 114
Freon 113
Freon 1143-2
Benzene
Mercury
N_2O
CO
Ozone

Table 2

Analysis of Tektite Carbon

Desorption Method	Direct Probe Method
Butane	Butane
n-Pentane	n-Pentane
Benzene	Benzene
Xylene	Xylene
Unidentified GC Peaks	*Ethanol*
	Isopropanol

in the ion source of a mass spectrometer. The sample is placed on the direct insertion probe which can be cooled to -150°C to retain very volatile components. To prevent condensation of H_2O and CO_2 during cooling, the probe is immersed in a stream of pure helium before being inserted into the vacuum lock; after insertion into the ion source, it is slowly heated. As the probe temperature rises, repeated mass spectra are recorded until all the volatile components have been desorbed. A comparison of the results obtained by the probe approach and a conventional desorption for a Tektite sample are shown in Table 2. The results are encouraging. We have also used this approach for a submarine desorbate, and while the results are not as satisfying, they are acceptable. The limitation of the technique is the minute concentration of some of the constituents of the mixture. If one only wishes to determine the major impurities, the probe approach is adequate. Its major advantages are a great savings in time (2 hours compared to 16 hours for the normal desorption analysis) and the capability to follow the various constituents as they proceed through the charcoal bed. The method is, of course, an extension of the technique first described by Amy, et al. (1) and Damico and co-workers (2) for the identification of chromatographic peaks.

IV. Current Analytical Problems

One of the most troublesome problems in these analyses is the selection of the chromatographic columns which will give the best resolution of the contaminant mixture. No single column is likely to give complete resolution. Therefore, the use of several columns is frequently required to separate the mixture. This is accomplished by the use of stop-flow chromatography. A problem to be considered in stop-flow chromatography is the mixing of components on the first column when the carrier gas column flow is halted. This occurs to a very limited extent if the column flow is not halted for too long a period. Assuming that it might take 20 minutes to investigate each of the components on a second column and that there are five or six different peaks on the first chromatogram being investigated, the total hold-up time on the first column might run to as much as three hours. Towards the end of this time some mixing does occur and ghosts of peaks are observed on the first column. But the problem is nonexistent, or only slightly troublesome for the first few peaks. Another technique, which is really essentially the same as stop-flow chromatography, involves collecting fractions as they are eluted from one column and reintroducing the fraction onto a different column or directly into the mass spectrometer with a direct insertion probe (1,2).

Another problem arises from the relative concentrations of the components in these contaminant mixtures. Some components are present at concentrations 1, 2 or 3 orders of magnitude lower than others. In the case of multiple components eluted from the chromatographic column at the same time, the concentration of one is usually very much higher than the others; thus, the mass spectrum of the abundant component tends to mask the presence of the minor components. It is helpful if the concentration of the major component can be reduced relative to the other components to enhance the identification of the minor components. When a sample is concentrated by cryogenic techniques, CO_2 is a major contaminant. The concentration of this component is usually 1 to 2 orders of magnitude greater than any of the other contaminants present in the mixture. The amount of sample which can be introduced onto the chromatographic column is limited and this, in turn, limits the quantities of the minor components which reach the mass spectrometer ion source. The CO_2 concentration may be greatly reduced by passing the sample through a lithium hydroxide trap, which does not adsorb any significant quantity of the remaining trace material. The relative concentration of the other components in the mixture is thus enhanced and a far greater number of contaminants can now be identified from the mass spectra.

V. Connections between Analysis Results and Environmental Problems

There is a fantastic number of components which contaminate a submarine atmosphere and, in spite of the sophisticated techniques available for identifying them, only a relatively small number have actually been identified. Once a component has been identified, the Navy is interested in determining its short- and long-range toxicity. This work is done at the Naval Toxicology Unit at Bethesda, Maryland. It is interesting that only a very few of the many contaminants in a submarine atmosphere have ever caused any obvious physiological or equipment problems. There have been a few incidents, of course. One particularly troublesome situation, which has occurred on a number of occasions, has involved the generation of strong lachrymators. The source of lachrymation in all cases has been traced to overheated lubricating oil. Surprisingly, the lachrymator formed is not acrolein, $H_2C{=}CH{-}CHO$, as one might think, but acetaldehyde. Another contaminant which has given a great deal of trouble in some environmental atmospheres, and whose existence in these atmospheres is quite surprising, is dichloroacetylene. According to the literature, this compound is spontaneously explosive in air, and was previously believed to be unstable in these atmospheres. The compound, however, can exist in air at low concentrations because it is stabilized by the presence of other contaminants,

notably trichloroethylene and methyl chloroform. Dichloroacetylene is not off-gassed from materials as are most contaminants, but is actually produced in the environmental control system designed to eliminate contaminants. It is generated when trichloroethylene (or methyl chloroform) reacts with lithium hydroxide, or any other alkaline material used to adsorb carbon dioxide. Dichloroacetylene is extremely toxic and concentrations of only a few tenths of a part per million can effectively incapacitate a man for normal activities after 7-8 days of continuous exposure.

VI. Summary

In summary, GC-mass spectrometry is an extremely apt technique for the resolution and identification of the many trace organic contaminants which develop in environmental atmospheres. The complexity of some of these contaminant mixtures, however, requires certain additional supporting techniques to identify the maximum number of components. These special techniques include special sampling methods and chromatographic tricks, such as "stop-flow" chromatography, fraction collection, and really any other technique available.

Finally, one must always be aware of the possibility of introducing new and perhaps deleterious compounds into an enclosed atmosphere from a seemingly harmless source; for example, the generation of dichloroacetylene from trichloroethylene, as mentioned previously. Another source of potential problems is the partial decomposition of materials in the catalytic burner (present in the atmosphere purification system to oxidize CO to CO_2) to toxic or corrosive materials. Since the presence of these materials can seldom be predicted, the need for a sensitive, universal atmosphere analyzer, such as a mass spectrometer/computer, which can be operated and maintained by nonscientific personnel, is apparent.

VII. References

1. J. W. Amy, E. M. Chait, W. E. Baitinger and F. W. McLafferty, Anal. Chem. 37, 1265 (1965).

2. J. N. Damico, N. P. Wong and J. A. Sphon, Anal. Chem. 39, 1045 (1967).

THE USE OF MASS SPECTROMETRY IN THE IDENTIFICATION OF ORGANIC CONTAMINANTS IN WATER FROM THE KRAFT PAPER MILL INDUSTRY

A. W. Garrison, L. H. Keith, M. M. Walker

Southeast Water Laboratory
Federal Water Quality Administration
U. S. Department of the Interior
Athens, Georgia 30601

Contaminants in Kraft Mill Effluents

A research project at the Southeast Water Laboratory is the identification of the chemical constituents that are present at the various stages of a kraft pulp mill's waste treatment system. Special attention is focused on the chemicals that remain after the final stage of waste treatment, at the point where the effluent enters the natural water system. Although many of the organic chemicals occurring naturally in the wood and some of those produced by the pulping process have been identified, little or nothing has been done to characterize the organics remaining in the process wastes after treatment.

Waste treatment processes are currently evaluated by the measurement of such gross pollution parameters as biochemical oxygen demand (BOD) and total organic carbon (TOC). Such determinations give useful information but may be misleading when effluents contain toxic or nonbiodegradable chemicals. BOD and TOC values do not specify which chemicals have been degraded. Many organics may have been only partially hydrolyzed, photolyzed, oxidized, or reduced, leaving derivatives that may be toxic or otherwise troublesome. The identification of the compounds that are resistant to present treatment processes is essential to the design of more efficient facilities; this information will also provide a basis for determining the effects of industrial effluents on the quality of our natural waters. A comprehensive analysis of the complex mixture of chemicals entering our waters from kraft pulp mills was practically impossible before the advent of the technique of tandem gas chromatography-mass spectrometry.

The treatment facilities of a modern kraft paper mill were chosen for our first study. These particular facilities are fairly advanced by today's standards and reduce substantially the BOD and TOC of the mill effluent. This is to be expected since the chemicals involved are of natural origin and are susceptible to secondary (biological) treatment. However, even in this case it will be shown that the treatments are not removing as many of the chemicals as BOD and TOC measurements are often interpreted to indicate.

The mill effluent is first pumped into a 225 ft. diameter storage tank where particulate material is allowed to settle or, in the case of wood fibers, to float to the top where they are continuously skimmed off. Next, the effluent is sprayed into a 100,000 cu. ft. trickling filter where it trickles over a lattice covered with a slime bacteria for biological degradation. It is collected in the basin of the trickling filter and passed through a secondary 160 ft. diameter clarifier before being discharged into a series of aerated lagoons with an area of 21.6 acres and a retention time of three days. At the end of the lagoons, approximately 13 million gallons per day of this treated effluent are discharged into the river.

Previous characterization efforts have relied almost exclusively on gas chromatographic analysis. We have developed a program that will, in general, employ the following outline:

1. An initial study to determine the best method of obtaining samples for analyses.

2. Identification of as many components of the sample extract as possible by gas chromatography/mass spectrometry.

3. Identification of compounds by NMR, IR, UV, and high resolution mass spectrometry/computer analysis when necessary.

Two methods of sampling were considered:

1. The first is that of collecting one or two gallons of "grab sample". This method has the advantages of being rapid and easy; the samples are also readily frozen and stored until used. However, relatively small amounts of material are available for analysis. Although GC-MS analysis requires only submicrogram quantities of each component, other methods such as NMR or infrared spectroscopy require 10 micrograms to a milligram of each pure compound, which must be isolated from the mixture by preparative gas chromatography or some other separation technique.

2. The second method involves the adsorption of the organics from several hundred gallons of water onto activated carbon, followed by drying and desorption with some suitable solvent. This method can supply enough material for preparative gas chromatographic separations. The disadvantages are: it is more complicated than the "grab sample" method, all of the compounds are not completely desorbed from the carbon, and some of the compounds present in the final extract may be the products of hydrolysis, oxidation, reduction, isomerization or some other chemical reaction of the original materials catalyzed by the large surface area of the activated carbon.

To obtain an evaluation of the first ("grab sample") method of sampling, 1 liter aliquots of the treated paper mill effluent were extracted with four different solvents. Each solvent extract was concentrated and analyzed by the same gas chromatographic procedure. Of the four solvents used -- petroleum ether, ethyl ether, chloroform, and ethyl acetate -- chloroform had the greatest extraction efficiency and was used for all further extractions.

In the second method, carbon filters were set up in two parallel banks of 4 filters each, and 900 gal. of the treated effluent, obtained at its point of discharge into the river, was passed through each bank for a total of 1800 gal. The carbon from the filters was then air dried at room temperature and extracted with chloroform in a Soxhlet apparatus for 24 hours. Concentration of the 8 gal. of extract solution to 300 ml was effected in a Kuderna Danish apparatus. The gas chromatogram of the carbon chloroform extract (CCE) was very similar to that of the grab sample chloroform extract, with minor differences in the intensities of the peaks.

Since an abundance of material was at hand from the CCE procedure, it was decided to characterize the compounds remaining after treatment using this extract. The sample was chromatographed on a 0.02 inch x 50 ft. support coated open tubular (S.C.O.T.) carbowax 20 M column, programmed from 85-220° @ 2.5°/min. The chromatograph was interfaced with the mass spectrometer via a heated capillary line and a Watson-Biemann separator. Peaks were scanned as they were eluted from the chromatograph and detected by the total ion current monitor. The GC was a Perkin-Elmer 900; the mass spectrometer a Hitachi Perkin-Elmer RMU-7.

It is beyond the time and intent of this paper to present a lengthy interpretation of all the mass spectra obtained from this research. A few examples will suffice.

The earliest eluting compound for which we could obtain mass spectra exhibits a parent ion at m/e 136, corresponding to an empirical formula of $C_{10}H_{16}$. The relatively intense parent ion suggested a cyclic structure and/or conjugated double bonds, and the empirical formula is characteristic of the monoterpene class of compounds. The fragment at m/e 121 (M - 15) indicates the presence of a methyl group. Most, if not all, of the other monocyclic monoterpenes, except limonene, have their base peak at m/e 93 or above; the unusual base peak at m/e 68 quickly led to the identification of this compound as limonene. Fragmentation of the molecule into two isoprene units is postulated to explain the base peak of limonene (1).

Two compounds, eluting after 12.5 and 18.0 minutes, both exhibited a parent ion at m/e 152. This, coupled with the long retention times, suggested oxygenated monoterpenes of empirical formula $C_{10}H_{16}O$. Lack of significant ions at m/e 134 (M - 18) further indicated them to be terpene ketones rather than alcohols or aldehydes since the latter would tend to lose water in the GC-MS system.

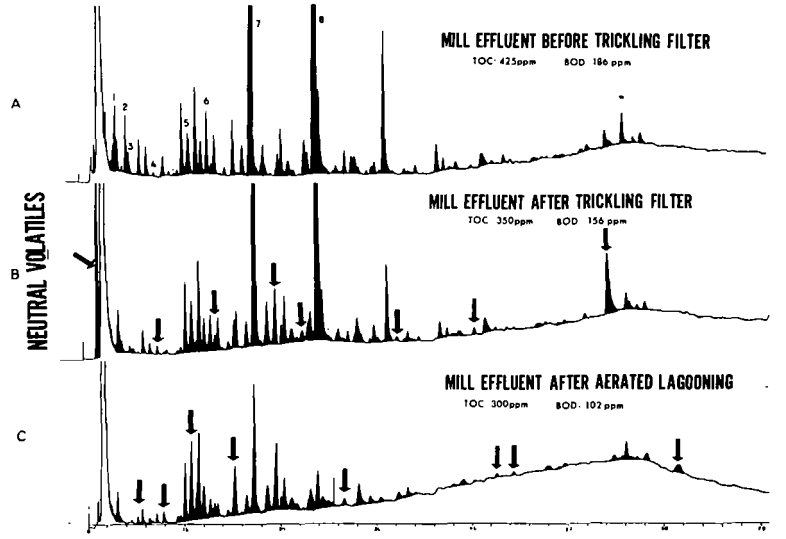

Figure 1. Gas chromatogram of kraft paper mill effluent at various stages of treatment. Arrows indicate peaks which increase at each stage of treatment. Numbered peaks correspond to: 1, limonene; 2, p-cymene; 3, terpinolene; 4, fenchone; 5, camphor; 6, fenchyl alcohol; 7, α-terpineol; and 8, guaiacol. GC conditions: 18' x 1/8" SS column packed with 6% SE-30 on Gas Chrom Q. Programmed at 70° for 4 min., then 6.5°/min. to 250°, then held for 25 min. Instrument was a PE-900 with flame ionization detector.

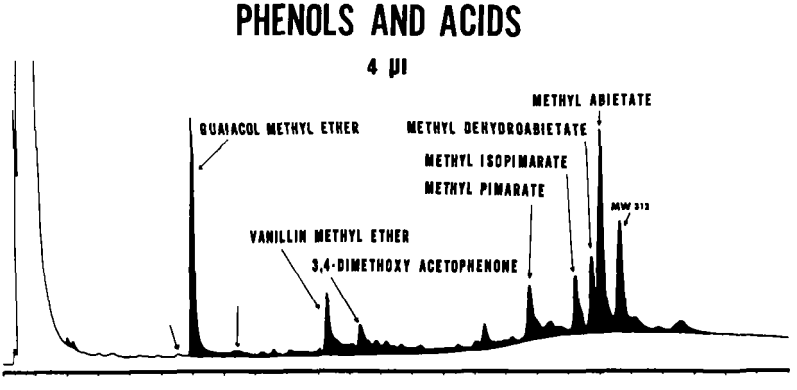

Figure 2. Gas chromatogram of acidic fraction of kraft paper mill effluent before treatment. GC conditions same as in Figure 1.

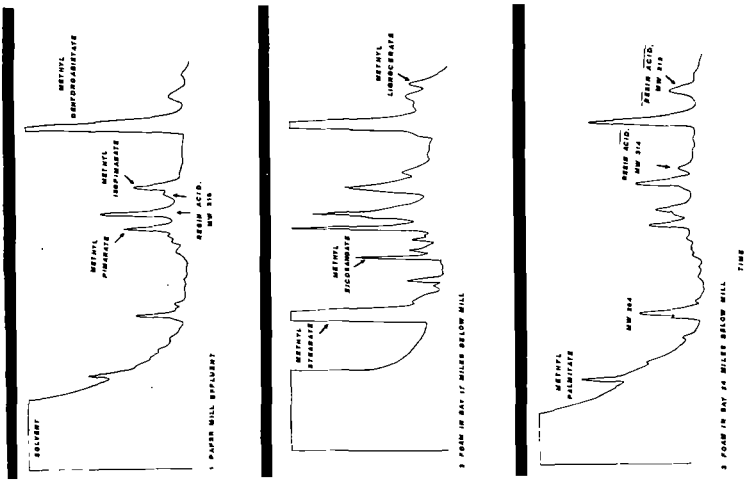

Figure 3. Methyl esters of resin acids and long-chain acids from Perdido Bay, Florida. GC conditions: 0.02" x 50' SCOT column with carbowax 20 M liquid phase. Programmed at 170° for 5 min., then 2.5°/min. to 210° and held. PE-900 GC with FID detector.

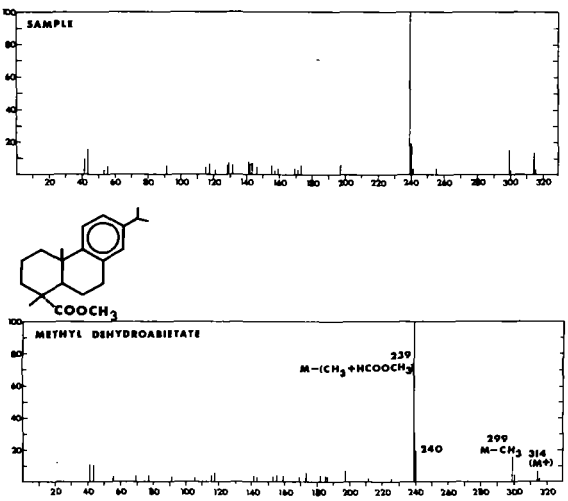

Figure 4. Mass spectrum of methyl dehydroabietate in Perdido Bay foam sample compared with a standard. Hitachi Perkin-Elmer RMU-7 mass spectrometer; 70 eV; introduced via gas chromatograph.

The literature (2) revealed that fenchone had the same base peak (m/e 81) as the earlier eluting compound, but there were major dissimilarities in the fragmentation patterns since the published spectrum was obtained from a different instrument and under different instrumental conditions. A standard fenchone spectrum obtained from our instrument under the same instrumental conditions used for the unknown sample from the mill was identical to the spectrum of the unknown.

The mass spectrum of the longer eluting compound closely matched the fragmentation pattern of camphor found in the literature (2), and comparison with the spectrum of an authentic sample confirmed the identification. The longer retention time of camphor results because enolization can occur in this isomer whereas it cannot occur in fenchone.

The mass spectrum of alpha-terpineol was considerably different from that appearing in the literature (3) because the fragmentation is dependent on source temperature and because we could not obtain complete gas chromatographic separation of this compound. No parent ion was observed; the fragment at mass 139 arises from loss of CH_3. The intense fragment at m/e 136 is produced by loss of H_2O, the peak at m/e 59 is the $C_3H_7O^+$ fragment, and the base peak arises from M-(18 + 43) (3).

In summary, we found compounds of the monoterpene class and their alcoholic and ketonic derivatives to be the primary contaminants being adsorbed on the carbon and desorbed by chloroform. In addition to the compounds previously mentioned, we also identified and confirmed p-cymene, terpinoline, fenchyl alcohol, and guaiacol.

To determine the source of various compounds, we collected grab samples of the effluent before and after the trickling filter and after the full treatment, which included aerated lagooning (Figure 1). The BOD and TOC values decrease during the two stages of the treatment. However, various chemical components vary greatly in their behavior in these waste treatment systems. Some are completely removed or effectively reduced by the trickling filter while others remain unchanged. Likewise, some compounds are completely removed or effectively reduced by the aerated lagooning. Many compounds, however, remain unchanged by either of these biological treatment systems, at least as employed at this mill; and, further, some compounds are actually produced!

For instance, fenchyl alcohol (peak #6, Figure 1) can be seen to decrease in intensity during both steps of the biological treatment while the peak corresponding to fenchone (peak #4) correspondingly increases in intensity. Thus, a simple oxidation of the alcohol to the ketone has occured. This process contributes to a lowering of the BOD, but, at the same time increases the concentration of a chemical that could potentially cause taste and odor problems in water. Camphor (peak #5) an isomer of fenchone, is also produced, undoubtedly from one or both of its alcoholic precursors, borneol and isoborneol. 2-Methylisobornoel was determined to be the cause of an earthy taste and odor problem in the water supply of Celina, Ohio. Although the latter was a separate problem and completely divorced from a paper mill source of pollution, it illustrates the point that these terpene derivatives are a potentially obnoxious class of water pollutants.

A similar approach was used to characterize the phenolic and acidic components of the effluent. Samples from the same three sites (before and after the trickling filter, and after lagooning) were extracted with chloroform to remove the terpenes and other neutral organics and were methylated with dimethylsulfate in sodium hydroxide solution. Comparison of the gas chromatograms again shows that most of the compounds are reduced in concentration by one or both phases of the biological treatment, a few are removed, and the concentrations of a few increased in the course of the treatment with at least one new chemical being produced by the lagooning.

A number of compounds have been identified in this fraction of the effluent by GC-MS (Figure 2). These include guaiacol, vanillin, pimaric and isopimaric acids, and abietic and dehydroabietic acids. Efforts are continuing to identify more of the constituents.

This chemical analysis of kraft mill wastes is an example of an approach to pollution control that may be applicable to many other industries. Specifically, when the final results of this work are made available to the kraft paper industry, one very important parameter of pollution can be considered that has been neglected previously -- the qualitative and quantitative identification of individual chemicals introduced into the ecosystem by this industry. Other mills will be able to use

these data to evaluate the effectiveness of their treatment systems. New types of treatments can be compared to the existing ones for a chemical evaluation of their efficiency.

We are currently comparing the chemical constituents in untreated effluents from several different kraft mills; preliminary analyses show that they are quite similar, at least qualitatively. Another extension of our current work will be the identification of products from several different treatment systems. Preliminary analyses show that very definite differences exist in the chemical composition of effluents that have undergone different treatments.

Contaminants in the Environment

The pollution of our aquatic environment from industrial wastes is so extensive today that the need for the analysis of organic pollutants in natural water arises often. In such cases, the concentration of pollutants is much less than in industrial effluents. The GC-MS has proven to be admirably applicable to such analytical problems.

For example, Perdido Bay, in Florida's Western Panhandle, has been plagued by a foam problem for several years. Foam floats to shore in brown masses and creates a nuisance to recreational and other water activities, as well as being esthetically unpleasant. The suspected source of this foam, or the chemicals causing it , was a kraft paper mill at the north end of the bay; the substance causing the foam was suspected to be tall oil from the mill.

To determine the presence of resin acids from tall oil in the water and foam, grab samples were collected, extracted with chloroform, esterified with diazomethane, and analyzed by flame ionization gas chromatography (4). At least three resin acids -- pimaric, isopimaric, and dehydroabietic -- were indicated to be present in all samples. Their structures were confirmed by GC-mass spectrometry.

A water sample was taken between one and two miles below the paper mill in a stream that is almost totally composed of the plant's effluent. The sample was collected just below the second of two sedimentation ponds formed as part of the stream. As shown by the gas chromatogram from the GC-MS analysis, several compounds other than pimaric, isopimaric, and dehydroabietic acids were present (Figure 3, top). Methyl esters of two different resin acids of molecular weight (MW) 318, one of MW 312, an unknown compound of MW 264, and methyl palmitate were also shown to be present by the mass spectrometer.

The second sample was of foam and scum collected at a point in Perdido Bay about 17 miles below the paper mill at a location where foam was in abundance (Figure 3, center). Methyl esters of pimaric, isopimaric, and dehydroabietic acids were identified, as were the long-chain stearic, eicosanoic and lignoceric acid esters. Unknown resin acids of MW 318, 314, and 312 were also found.

The last sample was of foam only and was collected at a point about 24 miles below the paper mill (Figure 3, bottom). Methyl esters of pimaric, isopimaric, dehydroabietic, and palmitic acids were identified. Esters of unidentified resin acids of MW 312, 314, and 318 were found as well as the unknown compound of MW 264.

The three mass spectra of the methyl esters of dehydroabietic, pimaric and isopimaric resin acids in the samples are distinctly different from each other, and each compares favorably with its standard spectrum. There is no ambiguity about their identification, especially since GC retention times also match with those of the standards.

The mass spectrum of methyl dehydroabietate is simple (Figure 4). The m/e 239 peak, due to loss of CH_3 and $HCOOCH_3$ from the molecular ion, is the most intense peak by far (5). The m/e 240 peak is due to loss of CH_3 and $COOCH_3$. There are medium intensity peaks due to the molecular ion at m/e 314 and due to loss of CH_3 at m/e 299.

The spectrum of methyl pimarate (Figure 5) is also relatively simple, the peak at m/e 121 constituting a large part of the total ionization. This peak is due to a fragment in which the A ring of the resin acid is still intact (6). The extended resonance possibilities of this ion may be one of the driving forces leading to its formation. The ion of m/e 181 is composed of this same ring with the carbomethoxy group still attached. Other imporatnt, but low intensity, ions in this spectrum are

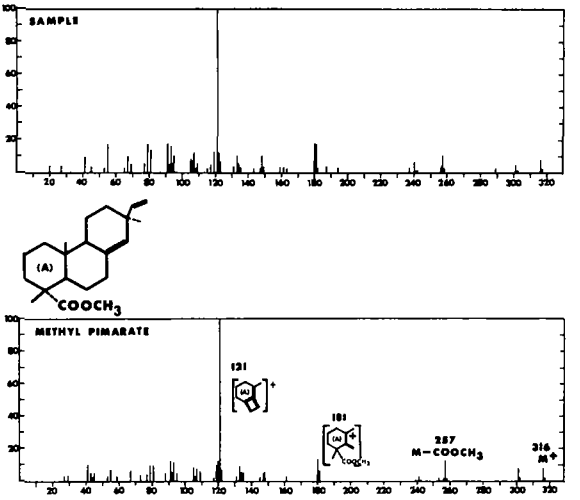

Figure 5. Mass spectrum of methyl pimarate in Perdido Bay foam sample compared with a standard.

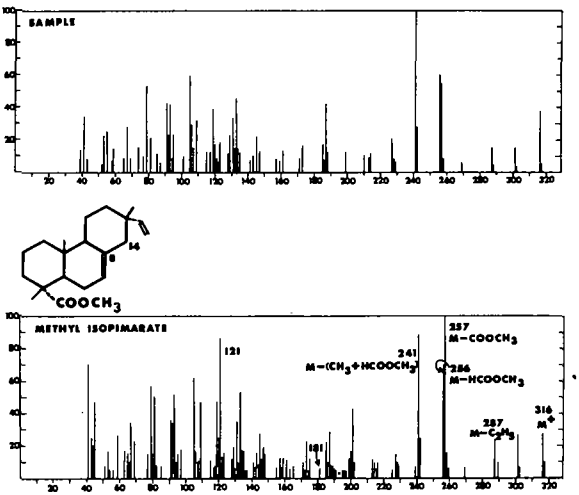

Figure 6. Mass spectrum of methyl isopimarate in Perdido Bay foam sample compared with a standard.

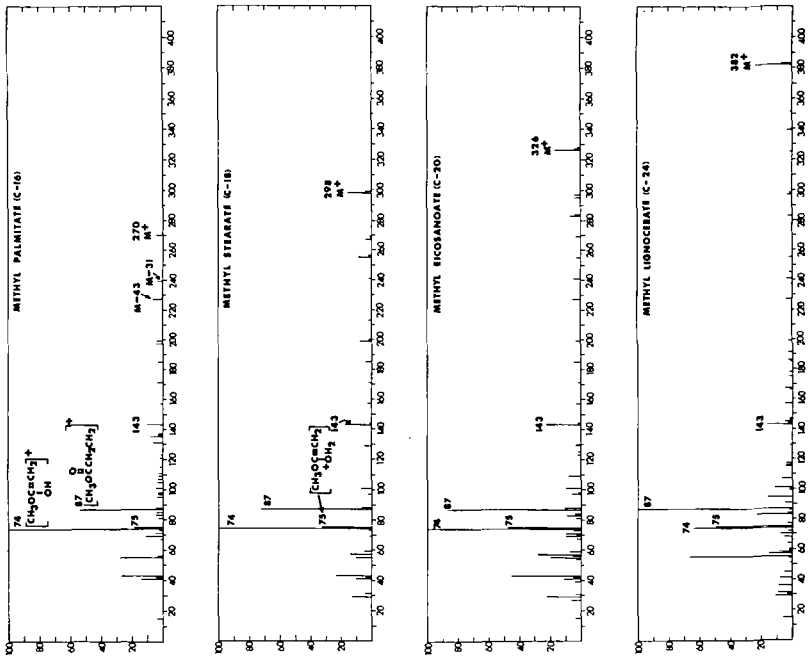

Figure 7. Mass spectra of methyl esters of long-chain acids in water and foam. Hitachi Perkin-Elmer RMU-7 mass spectrometer; 70 eV; introduced via gas chromatograph.

the molecular ion at m/e 316; and the M - CH_3 (m/e 301), M - $COOCH_3$ (m/e 257) and the M - (CH_3 + $HCOOCH_3$) (m/e 241) ions.

The mass spectrum of methyl isopimarate (Figure 6) is much more complex than those of the preceding resin acid esters. The m/e 257 peak, due to M - $COOCH_3$; the m/e 256 peak, due to M - $HCOOCH_3$; and the M - (CH_3 + $HCOOCH_3$) peak at m/e 241 are more intense. The relative intensities of these ions are reversed in the standard spectrum; however, the pattern in the sample spectrum closely matches that of several published spectra (6,7). Peaks at m/e 181 and 121 constitute a much smaller percentage of the total ionization than they did in the spectrum of methyl pimarate. This indicates the absence of a double bond between the C-8 and C-14 carbon atoms. Presence of this double bond, as in methyl pimarate, is apparently necessary for formation of high intensity ions at m/e 121 and 181 (6). Other important peaks in the spectrum of methyl isopimarate are those at m/e 316 (the molecular ion), m/e 301 (M - CH_3), m/e 287 (M - C_2H_5) and m/e 227 [M - (CH_3CH_2 + $HCOOCH_3$)].

Work is in progress to identify the four unknown resin acid esters found in the samples. The MS fragmentation patterns of these compounds are similar to those of the identified resin acid esters. The spectrum of the ester of MW 312, for example, is similar to that of methyl dehydroabietate except that the molecular ion peak (m/e 312) and one major peak (m/e 237) appear at 2 mass units lower, with the addition of a base peak at m/e 197. The spectrum of the unknown resin acid ester of MW 314 is similar to that of methyl isopimarate except that most major peaks are at 2 mass units lower. The spectrum of one of the unidentified MW 318 esters is similar to that of methyl isopimarate except that many of the important peaks are at 2 mass units higher.

Four long-chain acids were identified (Figure 7). The presence of palmitic, stearic, and eicosanoic acids in the samples was verified by matching GC retention times and mass spectra with those of standards. The presence of methyl lignocerate was deduced by interpretation of its mass spectrum.

Mass spectra of long-chain acid methyl esters are well documented (8); a detailed interpretation of their spectra is unnecessary here. All four esters show the molecular ion, M - 29 ion, M - 31 ion and M - 43 ion; all at low intensity. The peak at m/e 143, formed by 6,7-bond cleavage, is present in medium intensity in all these esters. Peaks at m/e 74, 75, and 87, characteristic of long-chain methyl esters, are the most intense peaks in all four spectra (Figure 7).

In conclusion, application of mass spectrometry, especially in tandem with gas chromatography, is essential to water contaminants characterization. No other tool presently available provides such definitive information on the constituents of small samples of complex mixtures.

References:

1. R. Ryhage and E. von Sydow, Acta Chem. Scand., 17 (7) 2025 (1963).

2. E. von Sydow, ibid., 18 (5), 1099 (1964).

3. E. von Sydow, ibid., 17 (9), 2504 (1963).

4. F. H. M. Nestler and D. F. Zinkel, Anal. Chem., 39, 1118 (1967).

5. C. A. Genge, Anal. Chem., 31, 1750 (1959).

6. K. Biemann, Mass Spectrometry, McGraw-Hill, New York, 1962, p. 335.

7. H. H. Bruun, R. Ryhage, and E. Stenhagen, Acta Chem. Scand., 12, 789 (1958).

8. R. Ryhage and E. Stenhagen in (F. W. McLafferty, ed.) Mass Spectrometry of Organic Ions, Academic Press, New York, 1963, Chapter 9.

DIESEL ODOR IDENTIFICATION

by
F. G. Padrta and P. C. Samson
Universal Oil Products Company
Des Plaines, Illinois

ABSTRACT

In order to develop an efficient means for eliminating the odorants from diesel exhaust, a thorough investigation was made into the identity of these components.

The diesel odor sample is condensed from the exhaust with a thermal gradient trap, extracted and separated by liquid-solid chromatography into two fractions, unburned diesel fuel and odorants. The odorants are further divided into different solubility classes, which are then analyzed by the mass spectrometer.

A unique mass spectrometer inlet system was used for in-situ reaction of samples with phenyl hydrazine or silylation agents for identification of compound types. A nominal ionizing voltage of 10 simplified interpretation of the spectra by reducing the intensity of the fragment ion peaks. Identification of 38 types of oxygen- and/or nitrogen-containing compounds are made. However, narrow chromatographic fractions taken of the odorants showed that no specific types could be associated with diesel odor confirming that the odor is due to a synergistic effect.

###

Chemical Identification of the Odor Components in Diesel Engine Exhaust. ALEGRIA B. CARAGAY, JOHN T. FUNKHOUSER, DAVID A. KENDALL, GREGORY LEONARDOS, PHILIP L. LEVINS, Arthur D. Little, Inc., Cambridge, Massachusetts 02140. Research sponsored jointly by the Coordinating Research Council and the National Air Pollution Control Association.

The chemical species responsible for the characteristic odor of diesel engine exhaust are being identified using the combined techniques of sensory characterization and identification through the use of high resolution mass spectrometry on well resolved fractions. Exhaust condensate is separated from the non-odorous components and resolved into specific odor fractions through solvent extraction and liquid column chromatography on silica gel to yield two primary odor fractions: oily-kerosene and smoky-burnt. These are further resolved by a two stage gas chromatography approach on a non-polar and a polar column. Odor profiles are obtained on the effluent from the gas chromatograph, and final identification of individual odor components is achieved through coupled gas chromatography - high resolution mass spectrometry. The oily-kerosene odor complex appears to have its origin at least in part in the unburned fuel and consists mainly of cycloparaffins and aromatics. The smoky-burnt odor complex is unique to the combustion process and contains a variety of oxygenated species.

SIMILARITIES OF ORGANIC CONTAMINANTS IN AIRBORNE PARTICULATES AND COAL TAR BY HIGH-RESOLUTION MASS SPECTROMETRY

by

A. G. Sharkey, Jr., J. L. Shultz, T. Kessler, and R. A. Friedel

INTRODUCTION

The purpose of this investigation was to compare mass spectral data for organic material extracted from airborne particulates with similar data for coal tars.

Sawicki et al.[1] reported extensive investigations of polynuclear aromatic hydrocarbons associated with particulate matter and other airborne contaminants. Hangebrauck, von Lehmden, and Meeker[2] reported determinations on several of the major polynuclear aromatics in emissions from potential sources of contaminants in the atmosphere.

A detailed high-resolution mass spectrometry study of coal-tar pitch was reported previously by the Pittsburgh Energy Research Center.[3] Preliminary data were also reported for polynuclear aromatics vaporized from airborne particulate matter.[4] In the present investigation additional data were obtained for the composition of organic material in airborne particulates, waste water, and products from treated municipal wastes.

EXPERIMENTAL PROCEDURE

A Consolidated Electrodynamics Model 21-110B double focusing mass spectrometer was used for this investigation. A resolving power of 1 in 12,000 was used for most of the determinations. Spectra were obtained at low and high ionizing voltages to determine parent ions. Thirteen fractions of organic material extracted from airborne particulates were obtained from Thomas Stanley, U.S. Public Health Service, Cincinnati, Ohio. A sample of airborne particulates collected in Pittsburgh, Pa., by Morton Corn, Graduate School of Public Health, University of Pittsburgh, was also investigated.

RESULTS AND DISCUSSION

The major oxygenated compounds detected in fractions of organic extracts from airborne particulates contained one and two oxygen atoms. Components with molecular weights over 400 were detected.

Mass spectral data for aromatic hydrocarbons in airborne particulates and coal tars from low- and high-temperature carbonization are compared in table 1, including the average molecular weights, the ratio of peri- to cata-condensed ring systems, the ratio of unsubstituted to alkyl substituted ring systems, and the mean structural unit. Aromatic components from the particulate sample collected in the Pittsburgh area showed a higher degree of condensation, that is, a higher ratio of peri- to cata-condensed structures, than the other samples investigated.

A major difference appears in the ratio of unsubstituted to alkyl substituted structures. The high ratio, 0.93, observed for the coal-tar pitch is typical of high-temperature carbonization, while the lower values of 0.34 and 0.39 obtained for the airborne particulates are typical of a lower temperature carbonization product. The mean structural units, indicating the average number of aromatic rings per molecule, varied only from 3.0 to 4.2 for the airborne particulates and the coal tar.

A distinctive series of peaks corresponding to fatty acids has been observed in spectra obtained from extracts of airborne particulates as well as material vaporized directly from the particulates. Fatty acids from airborne particulates and treated refuse show similar distributions.

Samples of secondary treated waste water, obtained from a municipal sewage disposal plant, were examined before and after treatment with activated carbon. Mass spectral data for polynuclear aromatics also indicated similarity between high-temperature carbonization products and organic material in waste water.

In a related investigation heavy oils from the destructive distillation of tires were examined. This type of incineration is another possible source of airborne contaminants. A minimum of 17 structural types were indicated. Alkyl benzenes in the 78-190 mass range and alkyl naphthalenes in the 128-212 mass range were the major components of the heavy oil.

Table 1.- Aromatic hydrocarbons in airborne particulates and coal tars from low- and high-temperature carbonization

	Aromatic fraction (Public Health)	Total sample, Pittsburgh	Low-temperature carbonization (total tar)	High-temperature carbonization (pitch)
Av. mol. wt.	229	195	208	242
Σ P/C[a]	2.9	3.6	2.6	2.8
Σ Unsub./Alk. Sub.	0.39	0.34	0.15	0.93
Mean structural unit	3.6	2.9	3.0	4.2
Percent of sample analyzed[b]	11	12	c/	50-70

a/ Ratio of peri-condensed to cata-condensed ring systems determined from 4-, 5-, 6-, and 7-ring compounds.
b/ Total sample for airborne particulates is considered to be the total organic fraction obtained by solvent extraction.
c/ Unknown.

CONCLUSIONS

Many similarities were observed in mass spectral data for polynuclear aromatic hydrocarbons in coal tars from high-temperature combustion and airborne particulates collected from urban areas:

1. Average molecular weights of material examined are in range 195 to 242.

2. Peri-condensed polynuclears are more prevalent than cata-condensed structures.

3. Aromatic ring systems contain alkyl substituents with up to four carbon atoms and show a progressive decrease in concentration for alkyl derivatives.

4. Aromatic ring systems contain from one to at least seven rings.

5. Mean structural units of the aromatic systems contain three to four rings.

Fatty acids derived from natural fats and oils show similar distributions for airborne particulates and products from hydrogenated refuse. Mass spectra of airborne particulates and extracts of waste water indicate many of the same aromatic compounds.

REFERENCES

1/ Sawicki, E., T. R. Houser, W. C. Elbert, F. T. Fox, and J. E. Meeker. Polynuclear Aromatic Hydrocarbon Composition of the Atmosphere in Some Large American Cities. Am. Ind. Hygiene Asso. J., v. 23, 1962, p. 137.

2/ Hangebrauck, R. P., D. J. von Lehmden, and J. E. Meeker. Sources of Polynuclear Hydrocarbons in the Atmosphere. Public Health Service Publ No. 999-AP-33 (1967).

3/ Sharkey, A. G., Jr., J. L. Shultz, T. Kessler, and R. A. Friedel. High-Resolution Mass Spectrometric Investigation of Coal Derivatives. Ch. 1 in Spectrometry of Fuels, R. A. Friedel, ed., Plenum Press, 1970, pp. 1-14.

4/ Sharkey, A. G., Jr., J. L. Shultz, T. Kessler, and R. A. Friedel. Determining Organic Contaminants in Air and Water. Research/Development, Sept. 1969, pp. 30-32.

THE ANALYSIS OF THIN FILMS BY ION MICROPROBE MASS SPECTROMETRY

Charles A Evans, Jr. and J. Paul Pemsler

An ion microprobe mass spectrometer has been modified to provide a primary ion beam with a reproducible, homogeneous current density. The depth homogeneity has been found to be ± 20 Å at a depth of 1000 Å by visual observation of the color uniformity of craters sputtered in anodized Ta_2O_5 thin films. The technique has been used to study both isotopic and concentration gradients in metallic thin films and in thermal and anodized oxide layers. The technique and detailed results and discussion will be published in the July or August 1970 issue of Analytical Chemistry.

DIRECT IMAGING SPATIAL MASS SPECTROMETRIC ANALYSIS OF CANYON DIABLO METEORITE, PUEBLITO DE ALLENDE CHONDRITE AND APOLLO 11 RETURNED LUNAR MATERIAL. W. S. Updegrove and J. Oro´, Department of Biophysical Sciences, University of Houston, Houston, Texas 77004, and R. Lewis, Bell & Howell, Pasadena, California.

ABSTRACT

A Castaing/Slodzian type ion imaging mass analyzer has been used to study selected extraterrestrial material. The samples surveyed in this experiment are the Canyon Diablo meteorite, the Pueblito de Allende chondrite, and Apollo 11 returned lunar samples. Ion images show nuclide spatial distribution to a resolution of about 1 micron. Ion mass-to-charge spectra with a resolution, M/ΔM of 300 show gross chemical composition over a 150 micron diameter area. The search for carbon in the lunar sample, ionizable as negative C_2, shows the possible existence of the following phenomena in the different 150 micron diameter areas: (1) approximately uniform distribution, (2) spotty segregation on the 2-5 micron diameter scale, (3) more random segregation and in some cases, (4) the absence of this type of carbon. This study demonstrates the capabilities of the imaging mass analyzer that make it particularly suitable to the study of extraterrestrial material, e.g. minimum sample preparation, vacuum conditions simulating outer space, spatial and in-depth distribution of the elements present, and the ability to differentiate indigenous species from contaminants.

INTRODUCTION

Although it is repetitious to state the concern over contamination, laboratory induced alterations, and artifacts in data on extraterrestrial materials, it is nevertheless a prevailing problem. In the effort to minimize these factors sputter induced ionization combined with mass analyses is considered a good candidate technique for the investigation of returned lunar and other extraterrestrial materials. If, in the event this distinct type of nuclide analysis is not sufficient to justify the experiment, surely the additional feature of collecting data on the nuclide topography constitutes sufficient justification. This sputter technique peels-off & ionizes surface molecules from the solid samples under conditions which exclude subsequent contamination or the alteration of the secondary ion mixture composition prior to analysis in the mass spectrometer.

Using this technique it may be possible to obtain unambiguous data as to the elemental distribution and composition of the sample. To date only doped semiconductors and special metal alloys have been analyzed by this technique. Nevertheless it should be technically applicable to the study of extraterrestrial material also. The following samples were analyzed:

a) Pueblito de Allende Carbonaceous Chondrite
b) Canyon Diablo Iron Meteorite
c) Apollo 11 Returned Lunar Material

The prime objective was to observe carbon and determine what elements it is associated with in its indigenous state. Other elements were examined to correlate this with other techniques.

DESCRIPTION OF THE APPARATUS

The apparatus used is the outgrowth of studies in particle balistics by Castaing (1), Slodzian (2), and others (3). Originally the intent of these investigators was the improvement of electron microscopy, however, the relevance to heavier charged particles, i.e., ions, was obvious. The result of this work is the development of an instrument producing an ion image, a two dimensional replica of the object with a mass to charge filter in the middle. The ions of a selected m/e originating at a specific location in the source will appear at a corresponding location in the collector. The optic system really fills the function of a mass filter rather than a mass spectrometer. It is defined as having focussing free of: 1) distortion, along two axes, 2) field astigmatism, 3) aperture-aberrations, and 4) chromatic aberrations. In terms of mass spectrometry it is stigmatic focussing at the same point in both momentum and energy.

Ions are generated from a solid surface through sputtering induced by a beam of high energy primary ions. The source of the high energy primary ions is a dual plasmatron of the type described by Coggeshall (4).

Read-out utilizing the Daly ion to electron converter (5) is made on a three galvanometer recording oscillograph when total mass spectra are desired, while nuclide maps of the surface can be observed directly on the fluorescent screen or recorded on the 35 mm photographic film. Ions of the desired mass to charge ratio are selected by varying the magnetic field.

EXPERIMENTAL PROCEDURE

The sample specimen holder consists of a disc one inch in diameter. Several different methods of mounting the specimen in the holder were utilized, as follows:

1) Bismuth was melted on the face of the sample holder disc and powder from the Pueblito de Allende or the Moon was sprinkled on the bismuth as it solidified.

2) A 1/8 in. diameter hole was drilled through the disc and powder from the lunar material was pressed into the hole. A punch press and a tool steel packing plate were used to compact the powder.

3) Chips of the specimen were spring loaded into a cavity machined in the center of the sample holder with a flat side facing outward.

4) Chips of the specimen were potted in a cavity machined in the center of the sample holder with liquid bismuth, or a 95% tin/5% silver mixture.

5) The faces were smoothed on a wet lapidary wheel, when necessary, to produce a moderately flat surface.

Due to problems in electrical conductivity the chips were, in some cases, covered with a fine mesh silver gauze or with vapor deposited conductive coatings.

Once the sample mount was inserted in the outer roughing chamber, the pump-down and positioning sequence was automatic. An ion source pressure in the 10^{-8} torr range was achieved within a few minutes. Final movement and positioning of the sample was accomplished by remote control. After satisfactory sputtering has taken place on an area of interest, one or more of the data collecting options were exercised. Usually a survey was made observing the fluorescent screen while noting the magnet setting producing the most interesting patterns of ions. Then it was returned to the previously noted magnet settings and photographs were made on 35 mm films. In addition, mass spectra were recorded electrically. This same procedure is carried out for positive or negative secondary ions.

RESULTS AND CONCLUSIONS

The Canyon Diablo meteorite specimen was the best to work with because its high iron content made it easy to mount and polish and also made it quite conductive. A survey mass spectra of secondary positive ions using oxygen plus ions as the primary bombarding beam showed the relative concentration of sodium, magnesium isotopes, potassium, calcium, chromium and iron the strongest peak of all at mass 56. Several 125 micron in diameter images were collected. The Cr-42 images showed a one micron resolution and the fact that the chromium is very segregated in small spots. The Si-28 showed only three small spots and compared well with low silicone peaks in the survey spectra. To understand the C-12 image it has to be compared with the Mg-24, since it is possible to have doubly ionized Mg at m/e of 12, thus masking the carbon. It is obvious, however, from these two pictures that the m/e of 12 was not associated with the m/e of 24. Therefore, it is carbon not magnesium. Unfortunately, from this suite of pictures it is impossible to determine just what the carbon is associated with. Calcium appeared to be accumulated in a crevase which is conspicuously void of all other elements except oxygen.

The Pueblito de Allende chondrite images yielded good proof of segregated carbon on the 2-5 micron scale but did not reveal the associated species. Evidence of other distributions of carbon were negative. Chrondrules in the Pueblito were too non-conductive to permit the collection of good images, however nuclide assemblages were apparent in the other parts of the matrix, showing:

1) 10 micron diameter spots of chlorine
2) large backgrounds of sodium and magnesium
3) diffuse semi-segregated oxygen in some areas and well segregated in others
4) silica as SiO^+ more concentrated in certain regions
5) well segregated calcium
6) well segregated potassium

Since these results were obtained from the examination of only a very small region of one part of the matrix material of this chondrite, little can be said about the entire body or the relationship of this information to other data previously published.

The results on the lunar material are incomplete to say the least. Problems arose because of the irregularity and non-conductivity of the breccia analyzed here. Survey mass spectra indicate a general composition quite similar to that already published. The general isotopic relationships are confirmed as is the fact that most of the metals exist as oxides. The ions of the metals would mask the inert gases except for helium, which was not detected by this technique on the lunar breccia. Evidence for the presence of carbon was quite conclusive but a detailed examination of segregated carbon images does not rule out any of the following possibilities.

1) indigenous concentrations of carbon
2) surface geometry artifacts in place of real nuclide concentrations
3) contamination during the polishing of the sample

In general, this experiment provided more questions than answers. The newness of the technique contributed to the different problems. However the demonstrated potential of this technique should provide the stimulus for additional research in this area.

REFERENCES

1. R. Castaing, J. F. Hennequin, L. Henry and G. Slodzian In "Focusing of Charged Particles" (Ed. Albert Septier), Vol. I, p. 265, Academic, New York, 1967.

2. G. Slodzian and J. F. Hennequin, Comt. Rend. Acad. Sci., Paris, Series B, 263, 1246 (1966).

3. H. Liebl, J. Appl. Phys. 38, 5277 (1967).

4. N. Coggeshall , J. Appl. Phys. 18, 35 (1947).

5. N. R. Daly, Rev. Sci. Instr. 31, 264 (1960).

MASS SPECTROGRAPHIC ANALYSIS OF LUNAR MATERIALS BY PROBE TECHNIQUE*

by
A. J. Socha, Bell & Howell Company, Pasadena, California;
W. S. Updegrove and J. Oro, Department of Biophysical Sciences, University of Houston

ABSTRACT

Spark source mass spectrographic analyses of Apollo-11 lunar rock and powder were performed utilizing probe technique. Elements related to organic materials were of primary interest. The materials were handled in a dry nitrogen atmosphere before insertion into the high vacuum of the instrument. The powders were hydrostatically compacted at 60,000 psi without the use of additives, to minimize possible contamination from carbon, hydrogen and other low level impurities. Results indicate carbon concentration as low as 1 to 10 ppm in both the rock and powder.

1. INTRODUCTION

Six analyses of Apollo 11 lunar materials were conducted utilizing spark source mass spectrographic probe techniques.[1] These analyses were made of samples of fine powder and breccia rock. Although analyses for other elements were obtained, those elements related to organic materials were of primary interest. Obviously, the minimization of contamination was of prime importance. The rock presented no particular problems except for precautions against contamination. The powders, however, required special techniques due to the problem of compacting them into solid electrodes suitable for sparking. Initially, only one powder (unsieved) was analyzed to investigate the technique. This analysis was then followed by a second analysis of the same powder, a second powder (sieved) and three different locations of a small breccia rock.

2. HANDLING TECHNIQUES

All of the samples were received in containers filled with dry nitrogen. These containers were opened in a dry nitrogen-filled glove box.

The powders were prepared for analysis by the hydrostatic compacting of the materials into electrodes without the use of additives.[2]

A simple but efficient bagging facility was used for the hydrostatic pressing of the lunar powders.[2] A small latex bag is first cleaned by washing the outside with alcohol and by rinsing with de-ionized water. The bag is then turned outside-in and filled. It is sealed with a rubber stopper and evacuated through a hypodermic needle. After evacuation and sealing, the bag is tied off and inserted in a second bag. Hydrostatic pressing is then carried out at pressures of 60,000 psi. After pressing, the bags were returned to the glove box where they were cut open. Although great care was used in cleaning the bags for accepting the powders, the outer portions of each pressed sample were removed.

The three rock analyses were obtained from a single sample. The rock sample was approximately 1.5 X 1 X 0.5 cm in size and was cracked into pieces suitable for mounting in the sample holder. A multiple sample holder[3] was used so that many samples could be loaded with one pumpdown. Three separate loadings were made. The original unsieved powder was analyzed first to determine feasibility. Two weeks later the same sample was analyzed along with the sieved powder. This was then followed by the three rock analyses. For all analyses, ultra-pure gold foil was used extensively in the source of the mass spectrometer to reduce contamination from slits, holders, etc. The sample holder was removed from the glove box via a plastic glove bag. In Figure 1, the bag was filled with dry nitrogen, the holder placed inside, the bag tied off and carried to the mass spectrometer. After attaching the bag to the source, the source was rough-pumped and then backfilled with dry nitrogen. This was repeated three times before untying the bag and transferring the holder from the bag to the source.

3. ANALYTICAL TECHNIQUES

A. Gold Probe Technique. Gold probe techniques were used in the analysis of these

* Supported in part by the USAF under Contract No. F33615-68-C-1635 and by NASA under Contract No. NAS-9-8012.

lunar materials. Using these techniques, an important problem was eliminated--that of mixing additives with the powder. The technique permits the sparking of high resistivity materials such as these oxides which, using ordinary techniques, could not have been analyzed without mixing conductive additives to the powder. When viewed as a complete electric circuit power is developed over the high resistivity sample rather than the probe. The sample then becomes hotter than the gold counter electrode, and hence has the larger ion yield. In many samples it was found that the ions contributed to the mass spectrum from the probe were less than one percent[2] as was the case for these lunar samples. An analysis of the gold counter electrode material used is given in Table I. The maximum contribution of any of the gold impurities to the analysis was about two orders of magnitude lower than the values shown. The maximum exposure obtained for all samples was 1×10^{-7} coulombs. This exposure level was adequate for the analysis desired and provided nominal detection limits of approximately 0.1 to 0.3 ppm.

B. Instrument Background. The mass spectrometer used was a Bell & Howell/CEC 21-110 spark instrument which has a special high speed low background pumping system. Analyses for H, C, N, O and other gases can be seriously affected by residual gases in the source due to their contribution of ions to the mass spectrum. This is especially so for samples which show a marked increase in source pressure during sparking.[4] The instrument used is equipped with a 350 liter/sec ion pump connected to the source via a 5-inch manifold. This provides a system which has an effective pumping speed in the sparking area of 60 liter/sec pumping speed in the sparking area for water vapor and hydrocarbons. Utilizing this pumping system, the lowest concentrations found at a pressure of 5×10^{-8} torr during sparking are given in Table II. These values were obtained from hundreds of analyses of semiconductor materials. To provide good analytical results from gaseous materials such as these lunar oxide samples, high pumping speeds are essential.

C. Data Reduction. Mass spectra were accumulated using photographic plates and data reduction using an in-line analog computer.[5] Standardization was achieved by using factors obtained from a sample of Spex Mix 1000.[6] This is a standard comprised of mostly oxides and carbonates of 49 elements. Additional refinements were then made using analyses performed on a sample of Pueblito de Allende Meteorite.[6] Normalization was obtained by summing all metallic elements and assuming the oxygen content to be of their common oxide phases.

4. COMPOSITIONAL RESULTS

With the many elements present a number of interferences occurred. These were primarily multiply-charged species of very abundant elements which had undergone space charge broadening and occurred near an element of low concentration. This problem existed in the case of carbon at mass 12 because of the large concentration of Mg^{+2} at mass 12. These lines require a resolution of only 1 part in 1600, but the space charge broadening of Mg^{+2} affects the resolution. The samples were sparked slowly to reduce this effect. In addition, an adjustable object slit was used to control the number of ions in the ion beam. Figure 2 shows the lines of C^{+} and Mg^{+2}.

Table IV contains the analysis for H, C, N, F, and Cl. Note the carbon levels for the six analyses. The lowest carbon value was found for the cleaved inner surface of the rock at 2.7 ppm. The higher carbon concentration found for the second run of the unsieved fine is understandable because the specimen had been handled between analyses. The sieved material also had undergone some preparation before analysis. The rock, however, best exemplifies the carbon levels found. The low carbon levels found for the first analysis of the unsieved sample also is indicative of the low contamination received during preparation.

The hydrogen values being very low in all samples would indicate the water content in these samples to also be very low.

The major elements (excluding oxygen) are given in Table V. Silicon and iron are the major metallic elements. Note that magnesium is at a concentration of about 5%. Table VI contains the remaining 33 minor elements found. All of these data were found to be in good agreement with other analytical techniques.

Although other investigators have found large concentrations of inert gases, none

were found in these analyses. Suspicions are that these are trapped gases which escaped without ionization during the sparking process.

5. SUMMARY

The probe technique offers analyses which are not compounded with the necessity of using additives and hence reduces the probability of contamination. The analyses described required good handling techniques, high pumping speeds in the source of the mass spectrometer and standardized data reduction. The results, however, indicate this technique to have many advantages when analyzing for biological elements.

The authors would like to express their appreciation to E. M. Masumoto for the data reduction of the photographic plates and to J. R. Shirk for sample handling and operation of the mass spectrometer.

REFERENCES

1. A. J. Socha and M. H. Leipold, "Analysis of Nonconducting Ceramics," J. Amer. Ceramic Soc., Sept. 1965.

2. A. J. Socha, "Proceedings of the ASTM Committee E-14 Meeting on Mass Spectrometry," St. Louis, May 1965.

3. A. J. Socha and R. K. Willardson, Tech. Documentary Report ARL 68-0132, 9 July 1968.

4. A. J. Socha and R. K. Willardson, "Proceedings of the ASTM Committee E-14 Meeting on Mass Spectrometry," Dallas, May 1966.

5. A. J. Socha and R. K. Willardson, "Proceedings of the ASTM E-14 Meeting on Mass Spectrometry," San Francisco, May 1963.

6. A. J. Socha and E. M. Masumoto, "Proceedings of the ASTM Committee E-14 Meeting on Mass Spectrometry," Denver, May 1967.

7. E. A. King, Jr., E. Schonfield, K. A. Richardson and J. S. Eldridge, Science 163, 928, Feb. 1969.

TABLE I. IMPURITY CONCENTRATIONS IN COMINCO GOLD (ppma)

Element	Detection Limit	Shot Lot 32A	Element	Detection Limit	Shot Lot 32A
C	0.03	4.3	K	0.007	0.73
N	0.03	0.47	Ca	0.01	0.12
O	0.03	14	Cr	0.03	0.03
F	0.03	2.2	Mn	0.02	0.05
Na	0.003	7.1	Fe	0.05	0.84
Mg	0.03	0.19	Ni	0.02	0.39
Al	0.01	0.1	Cu	0.06	0.26
Si	0.04	0.43	Zn	0.2	0.2
S	0.03	0.22	Ag	0.05	0.2
Cl	0.03	0.71			

TABLE II. LOWEST DETECTABLE VALUE AT A SOURCE PRESSURE OF 1×10^{-8} TORR ($\sim 5 \times 10^{-8}$ TORR DURING SPARKING)

Element	ppma
O	0.4
N	0.01
C	0.01
H	0.01

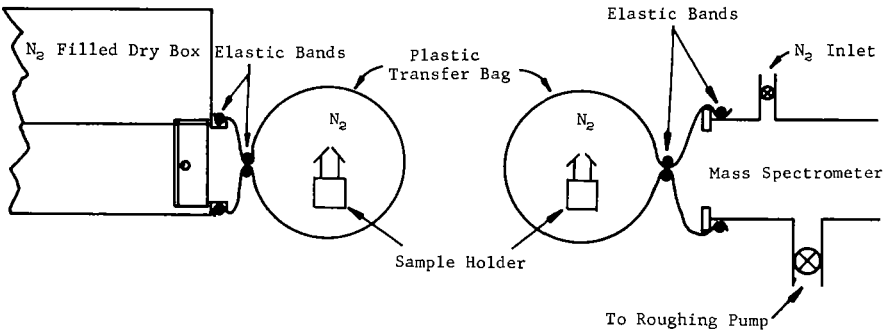

FIGURE 1. Plastic Bag Technique Used for Transferring Sample Holder from N_2 Filled Dry Box to N_2 Filled Mass Spectrometer Ionization Chamber

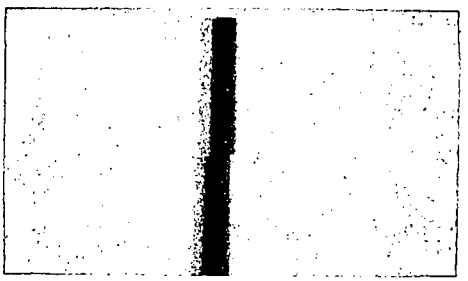

FIGURE 2.

C^+ 12.0000 Mg^{+2} 11.9925

TABLE III. MASS SPECTROGRAPHIC ANALYSIS OF APOLLO 11 LUNAR MATERIALS
(in ppm weight)

	Fines			Rock		
Element	Unsieved (1st Run)	Unsieved (2nd Run)	Sieved	Cleaved Surface	Outer Surface	White Spot
H	1.2	1.2	0.41	0.13	0.011	0.083
C	< 5-9	24	41	2.7	6.0	5.5
N	14	20	7	15	<10	<10
F	6.3	3.5	5.0	3.7	2.4	7.0
Cl	3.5	0.91	1.0	3.3	2.0	1.4

TABLE IV. MASS SPECTROGRAPHIC ANALYSIS OF APOLLO 11 LUNAR MATERIALS
Major Elements (in percent weight)

		Fines			Rock		
Element	Detection Limit	Unsieved (1st Run)	Unsieved (2nd Run)	Sieved	Cleaved Surface	Outer Surface	White Spot
Si	3	23	21	20	20	18	20
Fe	0.3	12	10.4	12	12	15	15
Ca	0.3	6.3	6.4	8.0	5.8	9.2	8.3
Mg	0.3	4.2	5.0	6.3	3.9	4.6	3.3
Al	1	4.0	5.2	6.2	4.4	7.9	6.2
Ti	2	3.8	5.6	2.4	5.3	3.8	5.2

TABLE V. MASS SPECTROGRAPHIC ANALYSIS OF APOLLO 11 LUNAR MATERIALS
Minor Elements (ppm weight)

		Fines			Rock		
Element	Detection Limit	Unsieved (1st Run)	Unsieved (2nd Run)	Sieved	Cleaved Surface	Outer Surface	White Spot
S	5	4200	590	960	2800	2100	1000
Na	0.07	2000	1660	1300	2600	340	780
Cr	0.1	1900	1700	1640	1800	2100	1300
Mn	0.1	1400	1650	1500	1000	2000	1300
K	0.07	600	1200	3600	1200	2300	1400
P	0.3	270	187	110	110	250	59
Ni	0.3	63	56	72	160	420	< 1
Ba	0.3	41	170	230	110	18	16
Sr	0.3	29	42	64	40	42	31
V	0.1	27	11	23	31	25	24
Zr	0.5	23	140	100	32	15	17
N	2	14	20	7	15	< 10	< 10
Zn	0.5	14	< 5	< 5	< 5.0	< 5.0	< 5.0
Rb	0.07	14	13	7.4	13	7.0	9.2
Cu	0.3	12	< 3	< 3	< 3.0	< 3.0	< 3.0
Li	0.03	9.2	4.9	3.5	4.1	3.7	2.6
C	1	< 5-9	24	41	2.7	6.0	5.5
Co	0.3	8.7	12	20	14	9.6	3.3
F	0.2	6.3	3.5	5.0	3.7	2.4	- 7.0
Ga	0.3	4.6	3.9	2.9	1.6	3.0	< 0.3
As	0.2	4.0	0.57	0.31	0.39	0.28	0.42
Ce	0.3	3.8	7.3	15	2.8	1.0	0.9
Cl	0.3	3.5	0.91	1.0	3.3	2.0	1.4
Nb	0.3	3.1	10	16	2.3	1.8	0.69
B	0.03	1.4	0.71	0.74	0.63	0.11	0.37
Y	0.3	1.4	11	9.3	1.4	1.3	0.74
H	0.03	1.2	1.2	0.41	0.13	0.11	0.083
Ge	0.3	1.0	1.3	0.38	0.45	1.3	0.83
Ag	0.4	0.91	3.9	0.44	1.0	3.0	3.0
Sn	0.5	0.5	< 1	< 1	< 1.0	< 1.0	< 1.0
La	0.3	0.3	0.67	1.0	0.73	0.34	0.9
Cs	0.1	0.19	0.24	0.16	0.22	0.89	1.2
Be	0.07	< 0.07	1.3	2.1	0.42	< 0.07	0.1

ON LINE ANALYSIS WITH A SPARK SOURCE MASS SPECTROMETER

R. A. Bingham, R. Brown and P. Powers
AEI Scientific Apparatus Limited
Manchester, England

INTRODUCTION

The provision of an electrical detection facility as an addition to the photographic plate detector has considerably increased the speed of survey analysis (1). As a logical step we in this laboratory have started to investigate ways to process the electrical output from the mass spectrometer. A small computer with a suitable interface has been put on line to acquire the data, and to carry out the usual interpretation procedures required to produce analytical information. The initial work has already been reported, (2) and so the purpose of this paper is to briefly summarise the principles and to describe the operation of the developed system in the analysis of a water pollution standard.

PRINCIPLES

The system we have used is based on the AEI MS702 and a PDP-8I computer with 4k core store and 64k disc backup store. The effects of spark fluctuation on the electrical output signal are minimised by the use of automatic spark control (2) and by the use of a ratiometer system as is shown diagrammatically in Figure 1.

The samples are loaded into the ion source of the spectrometer in the usual way and the discharge initiated. The 'Autospark' control is then used to maintain constant discharge conditions by automatically adjusting the electrode gap as required. The spectrometer is scanned by initiating an exponential decrease of the magnet current and the resulting mass spectrum is detected by an electron multiplier detector. A portion of the ion beam is intercepted by a monitor collector before mass separation takes place to provide a signal representative of the residual ion beam fluctuations. The multiplier and monitor signals are then divided, the one by the other, in a logarithmic ratio amplifier and the resultant logarithmic signal, free from fluctuations, is passed to a UV recorder and, via an antilog amplifier, to the data system.

The dynamic range of the ratio amplifier is 1000:1 and so this allows a concentration 'window' of about this range to be observed at any one time. Of course, the position of this 'window' in the concentration scale is determined only by the gain setting of the electron multiplier.

Two typical scan rates for this system are 3 and 9 minutes to cover the range from mass 210 to mass 7 and the precision on repeat runs is of the order of 35% standard deviation. (2,3).

The data system interface accepts the linear signal from the antilog amplifier and an analogue to digital converter digitises it at a frequency such that between 20 and 40 digital samples are taken across each peak of the spectrum. Peaks are detected by comparing these digital samples against an operator set threshold and those samples of a peak which are above threshold are processed to give a measure of the peak area and of the position of its centroid in time. This information is stored on the disc. Further processing converts these times to masses and finally an interpretation is carried out using reference data permanently stored on the disc.

The time to mass conversion takes place after the operator has identified up to 10 of the peaks from a peak time print out. The computer then calculates the masses of all other peaks by interpolation.

The interpretation process follows the procedure adopted by the chemist and is shown in Figure 2. Each element is looked for in turn by recognition of its characteristic isotope and its concentration is calculated by reference to the intensity of that isotope. The choice of characteristic isotope can be made at run time if need be for example: the characteristic isotope for nickel is ordinarily mass 58, but if iron is present in the spectrum, interference can occur at mass 58 and so mass 60 is preferable. The computer is therefore programmed to look at mass 57 first to see if iron is present or not and then to use mass 60 or mass 58 as appropriate.

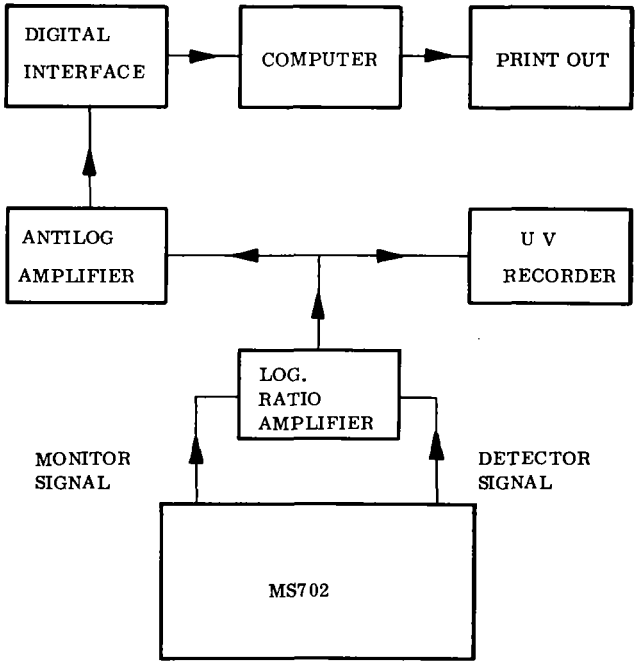

MS702 SPARK SOURCE DATA PROCESSING BLOCK SCHEMATIC

FIGURE 1

BASIC OPERATIONS.

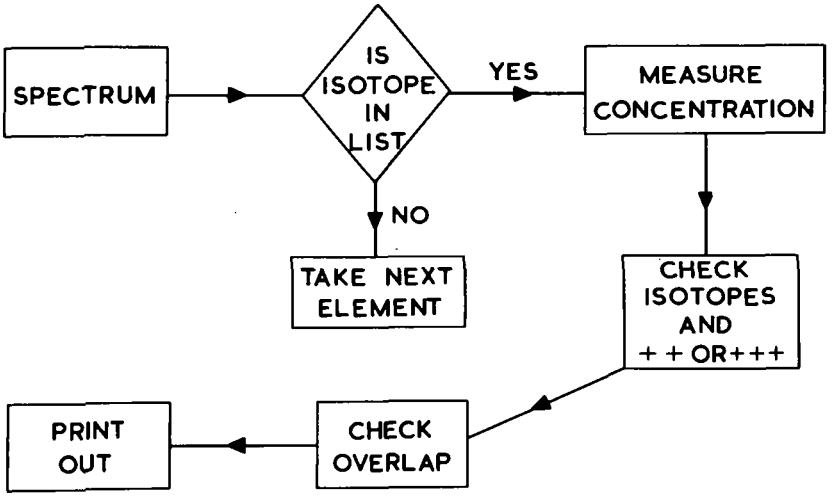

FIGURE 2

STDA

PEAK NUMBER	NO. OF SAMPLES	ABSOLUTE INTENSITY	TIME CENTROID
1	8	447	418.49
2	7	635	620.18
3	8	337	823.87
4	8	827	841.56
5	7	418	862.43
6	6	279	1001.43
7	9	515	1043.31
8	9	428	1064.74
9	10	1392	1085.12
10	8	712	1107.56
11	6	366	1129.56
12	8	342	1174.00
13	11	1691	1356.18
14	9	682	1669.24

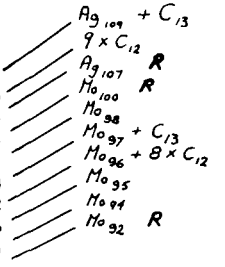

MS702 Data Processing Program

FIGURE 3

REFERENCES

PEAK	MASS
5	106.90
6	99.90
12	91.90
17	64.92
23	57.93
30	50.94
49	26.98
65	11.00

DUBIOUS MASSES

REFS	DUBIOUS
0 - 1	0
1 - 2	0
2 - 3	0
3 - 4	0
4 - 5	2
5 - 6	1
6 - 7	1
7 - 8	3
8 - 9	0

ACCEPT ? :Y

OUTPUT ? :Y

T(TY) P(TP) B(OTH) OR N(EITHER) ? :T

MS702 Data Processing Program

FIGURE 4

REFERENCES

PEAK	MASS
5	106.90
6	99.90
12	91.90
17	64.92
24	57.93
30	50.94
44	29.97
49	26.98
65	11.00

DUBIOUS MASSES

REFS	DUBIOUS
0 - 1	0
1 - 2	0
2 - 3	0
3 - 4	0
4 - 5	0
5 - 6	0
6 - 7	0
7 - 8	0
8 - 9	0
9 - 10	0

ACCEPT ? :Y

OUTPUT ? :Y

T(TY) P(TP) B(OTH) OR N(EITHER) ? :T

FIGURE 5

STDA

PEAK NUMBER	NORMALISED INTENSITY	ACCURATE MASS	
1	73	133.073	
2	104	120.409	
3	55	108.939	
4	136	108.001	
5	68	106.905	REF
6	45	99.907	REF
7	84	97.898	
8	70	96.887	
9	228	95.936	
10	117	94.901	
11	60	93.897	
12	56	91.906	REF
13	278	84.104	
14	112	72.112	

MS702 Data Processing Program

FIGURE 6

STDA

INTERPRETATION

SEARCH ELEMENTS : AG, MO, ZN, CU, NI, CO, FE, MN, CR, V, K, SI, AL, B,

MATRIX ELEMENTS : AG,

STANDARD ELEMENT: AG

CONCENTRATION FACTOR :5.0

FIGURE 7

ELEMENT	PPM ATOMIC	++? +++?	CONFIRM ISOTOPES	CHECK OVERLAP	COMPLEX IONS
SILVER	MATRIX(S)				
MOLYBDENUM	12.93	NO	YES		
ZINC	7.23	NO	YES		
COPPER	23.10	2+	YES		
NICKEL	24.34	NO	NO		
COBALT	29.52	2+	-		
IRON	28.07	3+	YES	108(54)	
MANGANESE	25.94	2+	-		
CHROMIUM	27.03	NO	NO		
VANADIUM	36.75	2+	-		
POTASSIUM	56.83	2+	NO		
SILICON	39.74	NO	NO	56(28)	
				84(28)	
ALUMINIUM	48.76	2+	-	54(27)	
BORON	4.43	NO	NO	33(11)	

END OF RUN

FIGURE 8

After the concentration has been calculated, several checks are made to establish a level of confidence in the value. Firstly, checks are made to see if either the doubly or triply charged specie is present in the spectrum, then checks are made for other isotopes of the element in question and if they are sufficiently intense a rough check of abundance will be made. Next, checks are made for interference both from multiply charged species of other elements, and from common complexes of the matrix with each of the isotopes of the element used during interpretation. The results of these checks are printed in a compact tabular form - see Figure 8.

OPERATION

There has been a growing need for a rapid and highly sensitive survey method for water samples. A useful feature of any technique is the ability to carry out analysis without the need for sample preconcentration. Consequently the choice of a water sample serves to check the usefulness of spark source mass spectrometry in pollution studies and also the viability of the computer program. The sample analysis reported here is on a water pollution standard prepared in our laboratory. The level of 10 micrograms per millilitre is much higher than the usual element levels in streams but the linearity of the method over a range of 10^5:1 allows accurate extrapolation down in concentration.

For this analysis, 1 millilitre of water was taken and deposited onto 100 milligrams of graphite. An internal standard of 5 micrograms of silver was added as silver nitrate in solution and the whole was wetted with 3 drops of pure ethyl alcohol to assist in achieving homogeneity. After evaporation of the liquid the remaining powder was ground in the agate vial in which it was prepared, and compressed as tips on a pure graphite substrate. The electrodes were mounted in the instrument source so that the sample tips formed the analysis gap.

The spectrum was scanned and a mass range from uranium down to lithium was covered in approximately 9 minutes. Data was acquired in the computer and at the same time a UV recording was made of the spectrum. Figure 3 shows the first stage after data acquisition where the list of peak times and intensities has been printed out.

The transformation of peak centroid times to mass numbers is accomplished using information typed in by the operator who must identify 5 or more peaks in the centroid time list. In this example the peaks corresponding to Ag107, Mo100 and Mo92 were the first three references chosen. Figure 4 shows the way in which these are entered in any order via the teletype. The peaks are identified by their serial number, their chemical symbol and isotopic mass. Although it is not shown in Figure 4, multiply charged peaks can be specified by typing '/n' after the isotopic mass where 'n' is the number of charges. Complete checks are made at type-in time to ensure that both the symbol and its isotopic mass are present in the disc resident file of all isotopes of the majority of elements.

When enough references have been typed in, the computer summarises the reference list and performs the mass measurement process. A print out of dubious masses is then produced so the operator can be sure he has identified all references correctly. This is a simple list of the number of measurements made in between each pair of reference peaks where the measured mass defect was outside the ordinarily expected range. Most inorganic ions have mass defects in the range 0.850-0.999, most doubly and triply charged ions therefore have mass defects in the range 0.425-0.500 and 0.283-0.333 respectively. Mass defects lying outside these ranges are either due to polyatomic species, to other impurities or are due to defective mass measurement. It is this class of measurements which are counted as dubious.

The unexpected occurrence of substantial numbers of dubious measurements can be caused by a wrong reference identification and the print out in Figure 4 shows this. No dubious measurements are found up to reference peaks 4 and 5 whereas after this point several are detected. The operator can choose to accept this result or not. If he does not the reference identification can be done again. If he does accept (as in this case) he may then print out the entire mass measurement list or go straight to the interpretation phase. In this example a further examination of the peak centroid time list revealed that in fact peak number 23 was not Ni58 but Co59 and therefore the entry should have specified peak 24 as Ni58. Figure 5 shows the revised dubious mass output when this correction is carried out.

As explained above, a print out of the exact mass measurements is possible and Figure 6 shows the format of it. Reference peaks are identified and intensities are normalised to a maximum of 10,000.

The final and main phase of the program is the interpretation. The operator first specifies the elements he wants the program to look for. He can specify all stored elements, merely some specified elements (as in Figure 7) or all the stored elements except selected ones. Next, specification of matrix, standard, and concentration of the standard are requested. Notice that the only reason for requesting the matrix element is to set up the process for searching for complexes of that element. There can be more than one and indeed it need not be the true matrix as is the case here. The true matrix of the pollution sample is carbon, of course, since the sample was graphite mounted.

Figure 8 and Table 1 show the results of the interpretation of the water pollution standard. Silver is marked as being both matrix and standard and the concentrations of other elements are determined relative to silver. The elements copper, molybdenum, nickel, cobalt, iron, manganese, chromium, vanadium and aluminium all give values well within a factor of 2 from the known concentration of 10 micrograms per millilitre. When one considers that no account was taken of the relative sensitivity coefficients of these elements in this instance, the agreement is excellent. Zinc shows a lower value than the rest of the elements and it is probable that there may have been some selective depletion of the element due to the very long sparking time to which the electrodes were subjected. We cannot at this time propose any reason why boron should show such a very low value, this element has been found to have about unit relative sensitivity in past experiments. A possible explanation is that double decomposition has occurred due to the complexity of the solutions.

Notice that although no interpretation was requested for carbon there is nevertheless a report made of its interference with iron ($9 \times {}^{12}C$) and silicon ($7 \times {}^{12}C$). Another point of interest is the fact that the nickel isotopes were not confirmed because carbon interferered with ^{60}Ni (used because iron was present) and this affected the apparent isotope ratios.

Standards for this method are very easily prepared and may be stored as dry powders, since essentially these are graphite standards.

The use of properly prepared standards should allow quantitative analysis of water samples down to the nanogram per millilitre level, without preconcentration. The use of preconcentration methods should allow limits of detection in the picogram per millilitre range.

TABLE 1
FOUND CONCENTRATIONS OF ELEMENTS IN WATER POLLUTION STANDARD

Values in μg/ml. Nominal value for all elements = 10μg/ml

Cu	13.6
Mo	11.5
Zn	4.4
Ni	13.2
Co	16.1
Fe	14.5
Mn	13.2
Cr	13.0
V	17.4
K	20.6
Al	12.2
B	0.4

CONCLUSION

The system is now operative and the first results are very encouraging. Scans can be processed in a time of about 15 minutes and the simplicity of operation and the concise report make the technique especially suitable for routine use by relatively inexperienced personnel.

REFERENCES

1. R. A. Bingham and P. Powers, 'Electrical Detection and Methods for Improving Quantitative Analysis Spark Source Mass Spectrometry', Sixteenth Annual Conference on Mass Spectrometry ASTM E-14, May 1968, Pittsburgh. Paper 111.

2. R. A. Bingham, P. Powers and W. A. Wolstenholme, 'Spark Source Mass Spectrometry using Autospark Sample Control and On Line Data Processing', Seventeenth Annual Conference on Mass Spectrometry ASTM E-14, May 1969, Dallas. Paper 86.

3. R. A. Bingham, P. Powers and W. A. Wolstenholme, 'Rapid Quantitative Impurity Analysis by Spark Source Mass Spectrometry using Electrical Detection, Automatic Spark Control and On Line Data Processing', Proceedings of the International Conference on Mass Spectrometry, Kyoto, Japan, September 1969.

ACKNOWLEDGMENT

The authors wish to thank Dr. J. D. Waldron, Managing Director, AEI Scientific Apparatus Limited, for permission to publish this paper.

A SPIRAL SPARKING SOURCE FOR SURFACE ANALYSIS

J6

by

R. A. Meyer

Science Center, North American Rockwell Corporation
Thousand Oaks, California

The subject of thin layer or surface analysis with a spiral sparking source for the RF spark source mass spectrometer is well documented by Clegg et al.(1)

SOURCE:

The JEOL-JMS 01B RF spark source mass spectrometer incorporates the very desirable feature of completely interchangeable source systems. Thus, by simply releasing the source vacuum, everything between the spark accelerating voltage contacts, and primary slit may be interchanged. Our spiral sparking source was designed to capitalize on this feature. Typical source turn-around time from breaking vacuum to sparking the new sample is ten minutes.

The source provides separate rotational and translational drive systems which, when operated simultaneously, cause the stationary counter electrode to trace a spiral path on the sample. In both cases the power originates in an external variable speed motor and is transmitted with an eccentric bellows type rotary feedthrough. Electro-craft type E-500 motors, which are variable in speed between 200 and 5000 rpm, were used for both drives. The rotational drive is transmitted by Pic gears and belt. Gear change coupled with the motor variation produces an ultimate sample rotation range between 3000 rpm and imperceptable movement. Translation movement is transmitted with anti-backlash gears and in its present configuration is variable between 0.4 and 94 mm per minute. Other ranges can be achieved by drive gear or motor interchange.

Figure 1 is a diagram of the mechanical system within the source vacuum. Our common samples are 1 to 2 inch diameter silicon wafers about 10 mils thick. These are mounted on the rotating copper pedestal with a ring clamp. The spring wires on the pedestal shaft engage slots in the ring. The copper pedestal is not removed for sample interchange, but provision is made for pedestal interchange. The alumina shaft is 1-7/8" long, 3/8" diameter and has two precision ground journals on either end of the pedestal thread. The thread is undersize and only holds the pedestal on the precision journals. This design allows interchange of sample pedestals and still limits runout at the edge of a 2" wafer to less than .001". Electrical contact is through two spring wire contacts riding in a groove in the lower part of the pedestal. The alumina shaft has two other journals on the lower end which accept dry MoS_2 lubricated ball bearings. Between the ball bearings, the shaft is grooved to accept the elastic belt drive. A single Bena N "0" ring has been used for several months without sign of impending failure. The elastic belt drive is required by the changes in position of the shaft during translation.

The shaft carriage is translated by anti-backlash bevel gears driving a 10-32-60° threaded lead screw. The carriage rides on two round ways. The selection of 304 stainless steel for the carriage and hardened 17-4 stainless steel for the ways reduced galling to a point where thorough burnishing with dry MoS_2 eliminated the problem. Each revolution of the drive shaft translates the sample 0.031". The translation system will move the sample over an inch thus allowing complete coverage of a 2" wafer.

The counter electrode consists of a simple clamp arm attached through bellows to an external micrometer. The system provides 3/16" of movement to compensate for electrode consumption during a run.

An unfortunate part of spiral geometry as developed by the technique we employed is non-constant surface velocity at the counter electrode. The coordinating control system shown in Figure 2 was developed to eliminate this problem and also provide for automatic termination of all operations after a preset number of .031" translation movements.

A micro switch operated by a cam on the translation drive shaft advances a stepping relay one contact for each .031" of X movement. The total number of steps may be preselected to limit sparking to a desired band. There are a total of 36 steps available while only 33 are necessary to cover an entire 2" diameter wafer. The pulse start switch and repetition rate circuits of the mass spectrometer have been connected to the control system. Reduction in surface velocity as the spiral proceeds toward the center requires a constant change in spark pulse repetition rate. This is accomplished with a second stepping relay which, operating in consort with the counting relay, changes condensers with each step. The condenser values were empirically determined to permit approximate constant pulse separation.

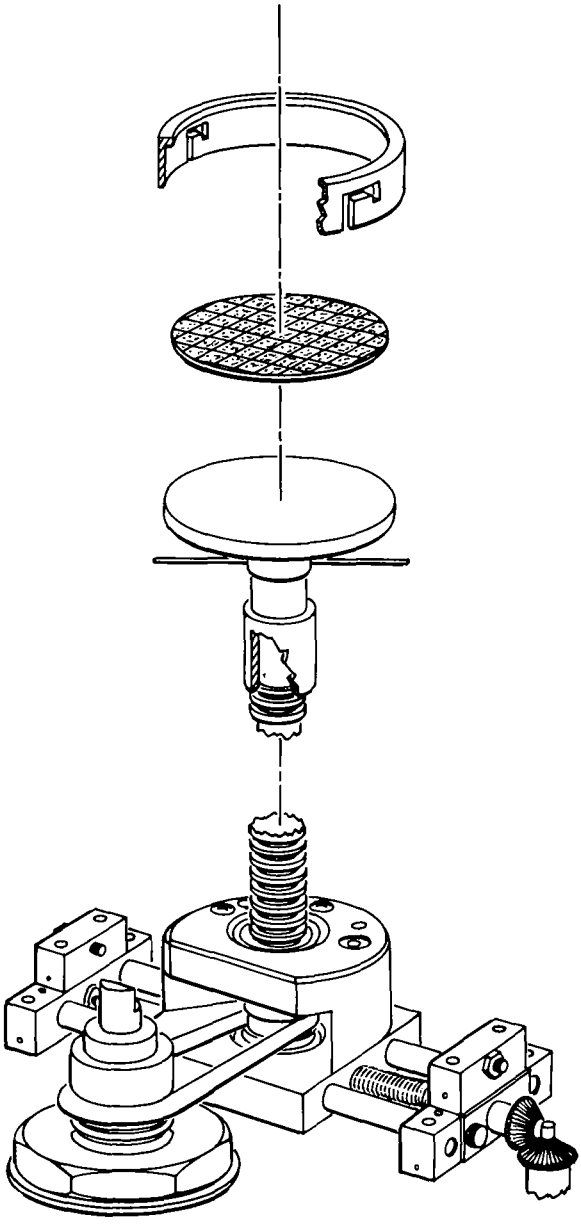

Fig. 1: Apparatus Diagram

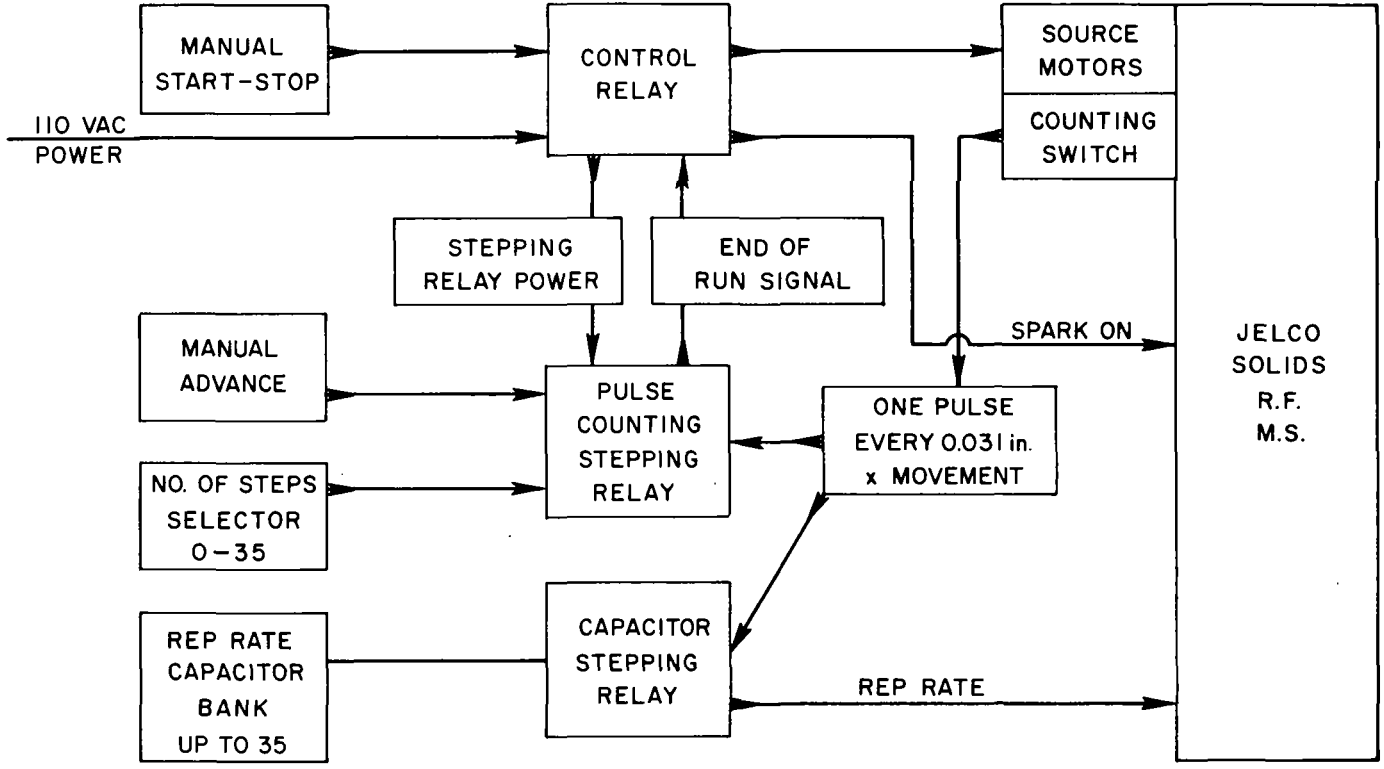

B237

Fig. 2: Control System

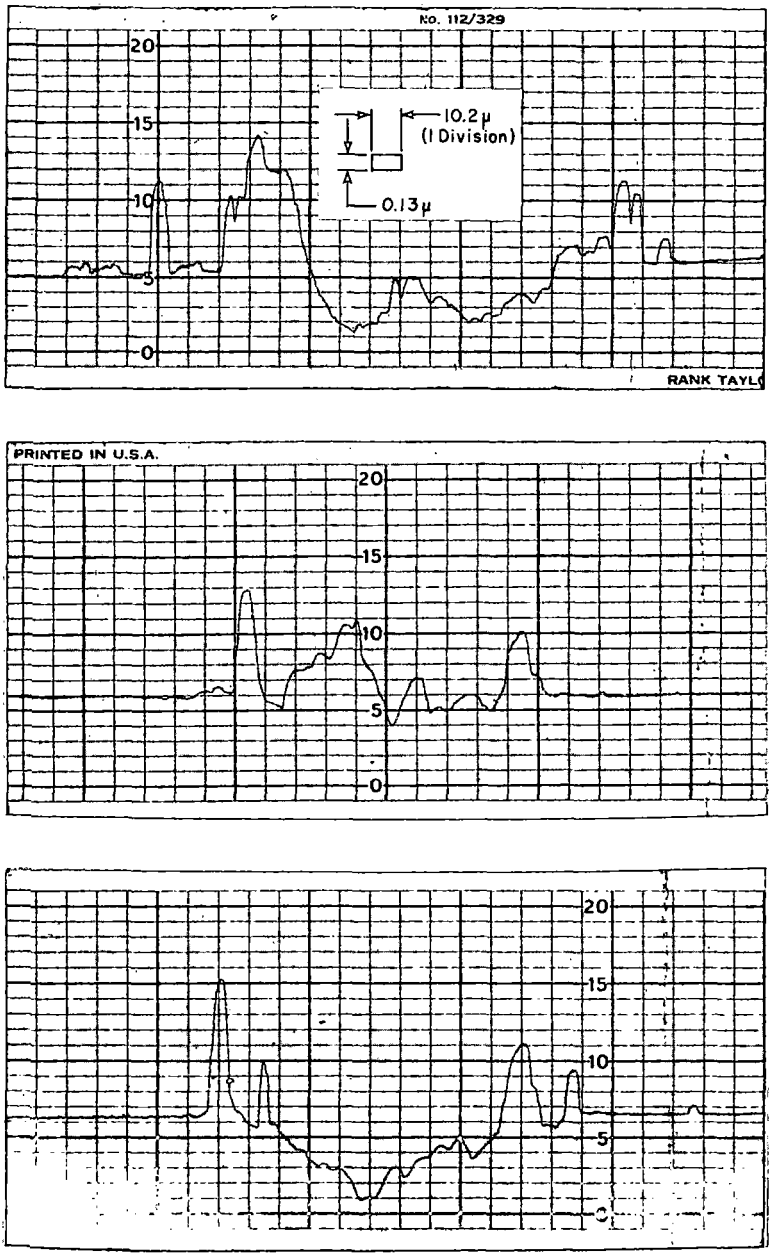

Fig. 3: Tallysarf Crater Tracings

The stepping relays may be pre-advanced to any step with a manual push button. When the operate button is depressed, a multi contact control relay is energized. This relay simultaneously energizes the rotational and translational motors, closes the pulse start switch, and energizes the micro switch operated stepping relay circuits. The sparking proceeds automatically (except for manual counter electrode movement); changing pulse repetition rate each .031" of radial movement until the preset number of steps have been completed. When the stepping relay reaches that particular contact, the holding circuit of the control relay is opened. This causes a cessation of all movement and sparking and the run is ended. A stop switch is provided to allow operator interruption of the run at any time.

OPERATIONAL EXPERIENCE:

Several counter electrode materials have been tried including gold, tungsten, and tantalium. Fine wires would be the natural choice, but the erosion rate of .002 to .006 inch diameter wires was too large for satisfactory spark gap maintenance. Thus, larger wire such as .025 inch gold has been pointed for use. The large wire appears to rapidly absorb the spark generated heat and protect the point from melting.

Many combinations of rotational and translational speeds have been used in an attempt to entirely cover the surface of the wafer. When speeds were selected to just overlap the spark craters in a continuous spiral pattern, the heat transferred to the wafer caused fractures in a large number of cases. At present the best compromise seems to be a rapidly rotating wafer (2000 rpm), an initial spark rate of 3 KHz, and a slow translation rate of 0.031"/minute. In this case, the entire wafer is covered with a random overlap of spark craters. The heat is well distributed and wafer breakage is minimal.

Calibration experiments present problems due to the extremely small quantities of material involved (10^{12} atoms Na = 4×10^{-11} grams). Experiments involving the doping of the surface of a wafer with radioactive sodium 22 show that 50 to 70% of the radioactivity is removed during a single sparking pass.

Calibration with surface deposited LiCl indicated a detection limit between 10^{11} and 10^{12} atoms. The lithium 7 line was well resolved from the silicon 28^{++++} and the nitrogen 14^{++}.

Many survey type runs have been made on silicon wafers with and without oxide coatings. Crater depths appear to be in the .7μ range on silicon surfaces and 2μ in silicon oxide surfaces.

Figure 3 shows Talysurf profilometer tracings of a series of 3 KV craters in silicon. It appears that the trace only covered the diameter of one crater, number 3. The volcano like ring reported by Clegg et al. is well evidenced. Weight loss experiments were thought to be meaningless due to deposition of counter electrode material on the surface of the wafer.

Exposures as high as 3×10^{-8} coulombs have routinely been achieved when sparking 2 inch wafers using the rapid rotation-slow translation technique.

Reference:

(1) J. B. Clegg, E. J. Millett, J. A. Roberts, Anal. Chem. 42, 713 (1970).

THE ANALYSIS OF NON-CONDUCTING SOLIDS BY SPARK SOURCE MASS SPECTROGRAPHY

by

Maynard H. Hunt

Hq Air Force Cambridge Research Laboratories
Solid State Sciences Laboratory
L. G. Hanscom Field, Bedford, Massachusetts 01730

The easiest and possibly the best way to analyze a non-conducting solid by spark source mass spectrography is to grind it into a fine powder, mix it with a pure, conductive powder in such proportions necessary to form a homogeneous mixture from which a pair of conducting rods may be pressed. These rods when sparked will yield a spectrum from which the impurity concentration in the solid may be inferred for all elements except those contained in the conductive powder at or above the concentration of that element in the solid. Thus the use of silver precludes the detection of Cl or S at less than a few parts per million since these are irreducible contaminant levels in the purest silver powder. Other available powders are graphite, copper, and gold. Copper is not available in the purity level of silver, and the best gold powder is not suitable for mixing. Reactor grade graphite is the purest conductive powder available, but the pressed rods are fragile, and the resulting spectra are extremely complicated because of carbon polymers and carbides. For a number of elements one must resort to the doubly or triply charged ion to identify the element and estimate its concentration. Quartz is an example; the faint line at $m/e = 52$ may be Cr or it may be SiC_2. Verification can only be made by looking at $m/e = 17\,1/3$ and the detection limit is increased by an order of magnitude.

The grinding of soft materials presents no problems. Such materials as magnesium oxide, lithium germanate, and calcium fluoride have all been reduced to fine powders in corundum, agate, or boron carbide mortars. Nor do these materials provide any memory problems in the mortar since they are easily dissolved, whereas the mortars are extremely resistant. But the materials discussed in this paper are among the hardest available to man. Quartz, ruby, and germanium oxide, 8, 9, and 9+ on the Mho scale cannot be ground in the aforementioned mortars, but must be crushed in a "soft" mortar, the Plattner mortar, available from most scientific supply houses. This consists of a steel plate with a cylindrical depression into which fits a cylindrical steel pestle. The hard materials may first be smashed and then ground to the desired fineness, after which it must be thoroughly leached with appropriate acids to remove all traces of the mortar and finally washed with high purity water. The desired degree of purity may not be attainable, since one may speculate on the chemisorption properties of as much as several hundred square centimeters of freshly exposed alumina or silica. There is some evidence that cations are strongly absorbed on such powders.

These are the reasons for not following the "easy" route and analyzing a powdered sample. A method first described by Ahearn[1] and modified by Stephani et. al.[2] has been adapted to the AFCRL instrument. Stephani used a pair of non-conducting electrodes married to conducting electrodes and obtained ions from sparks between the non conductors, but this arrangement was not found to produce a satisfactory ion beam at this laboratory. Instead, using Ahearn's method, a high purity gold rod was placed in one electrode holder along with the sample rod and positioned so that it made firm physical contact near the free end of the sample rod, and a second high purity gold rod was placed in the opposite electrode holder.

In order to initiate a spark, various tricks are sometimes necessary. As much as 80% of the available spark voltage may be used, although it is usually necessary to reduce this to 40-60% for stable operation. A film of gold evaporated onto the surface provides a conductive path. This film probably exists in the steady state anyway, and an initial coating by sparking the gold electrodes to each other merely establishes this condition. An extremely tough material such as ruby may be sparked at high voltage and a high duty cycle with little danger to the electrodes, but crystalline quartz will fracture from thermal shock if subjected to too great a heating rate.

The utility of this method to follow a laboratory preparation and purification of a ruby crystal is shown in Table I. Ruby powder #1 was prepared by dissolving aluminum and chromium alums in the desired proportions, evaporating to dryness and calcining to produce an intimate mixture of Al_2O_3 and Cr_2O_3. Ruby #1 was then grown by the Verneuil method, powder #1 being fed into a furnace thru an inverted H_2-O_2 flame onto a seed crystal. Ruby #3 was ruby #1 float zoned in an arc image

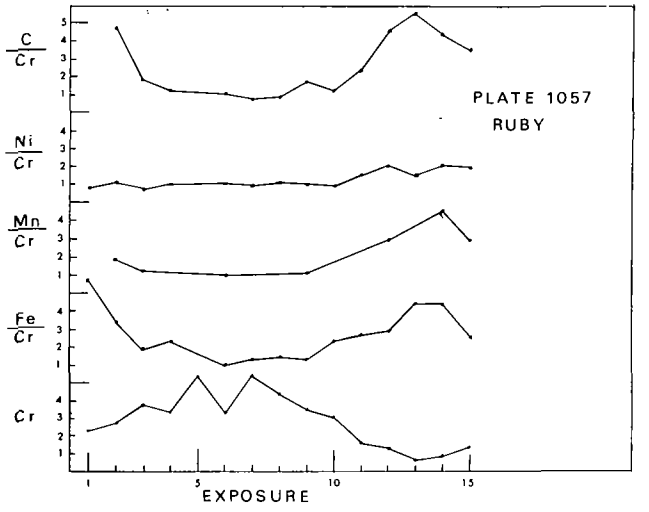

FIGURE 1. Variation of four elements in ruby relative to Cr and apparent Cr variation in concentration versus exposure number.

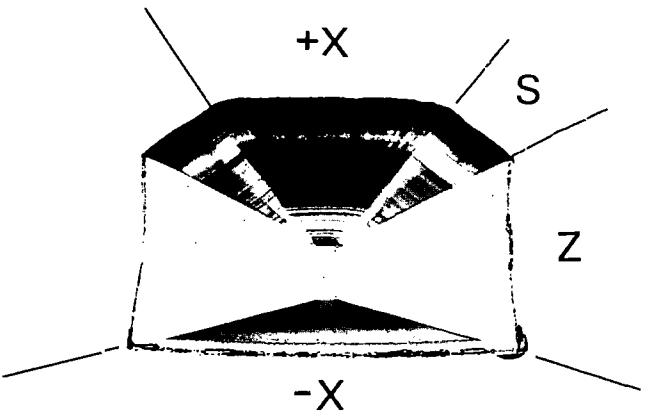

FIGURE 2. Section of Quartz Boule after irradiation, exposure 2 megarads ^{60}Co

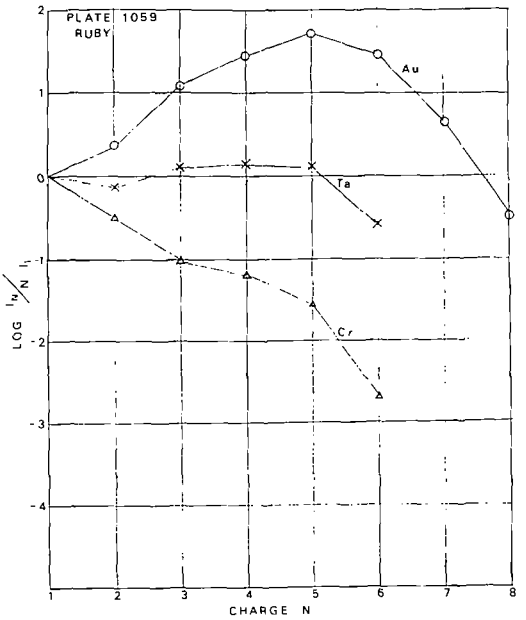

FIGURE 3. Relative abundance of ions from a ruby sample versus charge

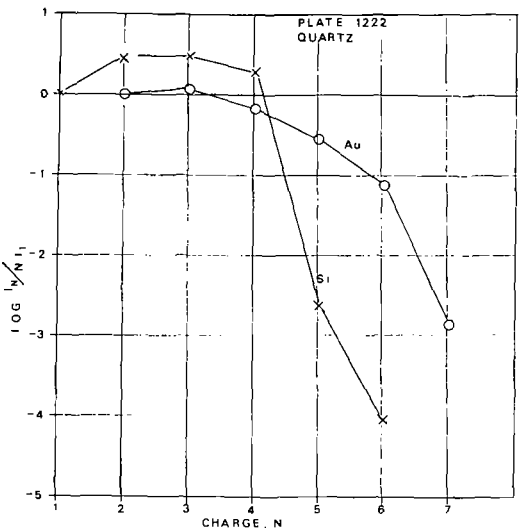

FIGURE 4. Relative abundance of ions from a quartz sample versus charge.

furnace in air. Of particular interest is nitrogen which presumably enters the ruby as a nitride of aluminum. Ruby # 3 was also ground in a Plattner mortar, leached, washed, and mined with silver powder. The analysis is comparable to the analysis of the solid rod except for Cl which, it is assumed, came from the leach since it is far in excess of its concentration in the silver powder.

Table I

ppm by wt.

Element	Ruby Powder #1	Ruby #1	Ruby # 3	Ruby # 3 + Silver Powder
N	3.3	4.7	61.	2.6
Mg	2.7	N.D.	N.D.	N.D.
Si	46.	3.3	27.	29.
S	110.	58.	12.	43.
Cl	62.	13.	30.	115.
K	120.	93.	25.	14.
Ca	34.	2.9	0.1	0.6
Cr*	1360.	800.	360.	360.
Fe	13.	6.2	5.0	6.7
Ni	0.5	5.8	N.D.	N.D.
Ga	53.	2.3	N.D.	N.D.

*Determined by neutron activation analysis.

In this kind of analysis using dissimilar electrode materials, there arises the question as to whether each contributes a constant proportion of ions to the beam. In the analysis of ruby this was avoided by employing the Cr as an internal standard. The Cr content was determined by neutron activation analysis, stated accuracy ± 10%. If we limit the useful exposure range of Q-2 plates to 100, any element can be determined relative to Cr if its apparent concentration is between .00045 and 84. times the Cr concentration. ^{54}Cr cannot be used because of possible interference by both Al_2 and ^{54}Fe.

This does not, however, guarantee an accurate analysis. Fig. 1 shows the result of an exposure by exposure determination of four elements relative to Cr as well as the apparent variation of Cr in the sample. The exposures were in the ratios of 1:3:10 repeated five times. The apparent variability of Cr, the standard, might well be attributed to varying contribution to the ion beam by the gold and ruby electrodes if it were not for the countervariant behavior of Fe, Mn and C. E. M. Dodson[3] has reported on a microcolorimetric determination of Cr and Fe in ruby sections a few microns thick perpendicular to the axis of the boule. She found periodic fluctuations as much as 30 in concentration for both Fe and Cr, and they were not in phase. So what is seen here may be a weak indication of this as the spark erodes through the ruby.

Fig. 2 shows a section perpendicular to the Y-axis of a quartz boule grown by Sawyers Research Products, Inc., of Eastlake, Ohio. This section, originally clear, has been subjected to 2 megarads from a ^{60}Co source. The visible striae are due to substitutional aluminum. It is quite apparent that the material is not homogeneous and the variations are known to be of a diurnal nature. Visible are the seed, the +X, S, Z and -X zones. Although the Z zone is clear, it also contains Al interstitially. This crystal was grown in a solution containing Li_2CO_3 and Na_2CO_3.

Table II

ppm by wt.

	C2-IU, X+			Emission	C2-IU, Z2			C2-IU, Z2(Plus Ag)	
	1155	1156	1157	Spectroscopy	1159	1160	1161	1181	1182
Li			19.	1.0			1.8	20.	17.
B						0.2	0.05	1.0	0.6
C		130.	61.			21.	180.		
F	31.		2.7		6.1	1.9	1.0	100.	80.
Na	130.	110.	84.	21.	66.	41.	130.	190.	210.
Al	60.	31.	80.	238.	7.1	20.	12.	17.	87.
P								6.	
S								10.	
Cl	380.	8.2	4.7		15.	9.8	3.6	305.	210.
K	2.6	0.8	.42		3.1	2.2	2.7	1.1	3.1
Ca	1.7	.32			1.0	0.8	15.	0.9	2.6
Cr	7.4				3.1	1.6	1.1		
Fe	5.2		11.		6.7	8.7	8.1		

Table II shows a series of analyses of the +X and Z zones of a similar quartz crystal. The repeatability of the analyses leaves much to be desired but as a quick survey of the approximate composition may be quite satisfactory. Note that Al in Z zone seems to be 25% what it is in the X zone. The Z material was also ground, leached, washed and mixed with Ag powder. The marked increase in F and Cl are again seen supporting the chemisorption hypothesis.

The variability of the results of the bulk analyses can be attributed to the inhomogeneity of the sample for three reasons. The first is the obvious one, the second is that the material, being frangible, tends to fracture along the weakest plane. Therefore, during sparking a thermal stress may produce spalling, revealing a new surface rich in impurities. The third is that the striae, being rich in impurities, may be favored as a conductive path for the spark. Therefore the analysis of a bulk sample has limited applicability as an analytical tool, but can be used as a survey method to determine the presence of impurities which may then be determined with greater accuracy by analysis of the powdered sample using the appropriate matrix.

This type of analysis has led to the observation of an interesting phenomenon which might be termed an inversion of the ion population produced by the spark. A similar phenomenon has also been observed with the refractory metals such as W and Ta, although not to such an extent.

Fig. 3 shows the relative abundances of the various charge states of the ions of Cr, Ta and Au produced while sparking ruby. The apparent abundance of each ion state was divided by the number of charges per ion as an approximate correction for the increase in plate sensitivity with ion energy. The correction is probably inadequate since the increase is less than linear at higher energies. While Cr behaves in the normal fashion, both Au and Ta exhibit a marked deviation from normal behavior. In Fig. 4 Si is seen to exhibit similar behavior until the M shell is depleted. The Au data from the same plate is relative to Au^{++} since Au^{+} was not on the photoplate.

The consequences of this phenomenon are that a large proportion of the ion current may be carried by multiply charged ions, not usually considered in photoplate evaluation, and that the phenomenon is not observed on every plate. It may be the explanation for the rather large spread in some of the data for quartz.

In conclusion, this method of analysis of bulk samples of non-conductors serves as a survey method to indicate the presence and approximate concentration of impurities, but more refined techniques are required for accurate analyses.

Acknowledgement

I wish to thank Mr. John J. Fitzgerald for his neutron activation analysis of the ruby samples for chromium, and for his emission spectrographic analyses of the quartz samples for Li, Na and Al. I also thank Dr. Stanley K. Dickinson for supplying the ruby samples and Mr. Richard N. Brown who supplied the quartz samples.

References

1. Ahearn, A.J., J. App. Phys. 32, 1195 (1961).
2. Stephani, R., Cornu, A., Bourguillot, R., Robin, Mlle A.M., Brun, J.C., Chimie Analytique, 48, 253 (1966).
3. Dodson, E.M., "The Measurement of Concentration Changes Across Growth Striae in Electronic Single Crystals", American Committee on Crystal Growth, Conference, NBS, Gaithersburg, Md., 11 - 13 August 1969.

RELATIVE SENSITIVITY COEFFICIENTS FOR ELEMENTS IN A SILICON MATRIX

DONALD LEE DUGGER

TEXAS INSTRUMENTS, INCORPORATED

ABSTRACT

A KNOWLEDGE OF RELATIVE SENSITIVITY COEFFICIENTS (RSC) IS IMPORTANT IF QUANTITATIVE INFORMATION IS DESIRED IN AN ANALYSIS PERFORMED ON A SPARK SOURCE MASS SPECTROMETER. TO DATE, LITTLE IF ANY INFORMATION IS AVAILABLE ON RSC FACTORS FOR ELEMENTS IN A SILICON MATRIX BECAUSE OF THE UNAVAILABILITY OF SUITABLE SILICON STANDARDS. THIS PAPER WILL DISCUSS THE USE OF SILICON STANDARDS TO DETERMINE EMPIRICAL RSC FACTORS FOR SEVERAL ELEMENTS IN SILICON. THE TECHNIQUE EMPLOYED AND ALL OPERATING PARAMETERS USED WILL BE PRESENTED AND DISCUSSED.

LITHIUM CONTENT DETERMINATION IN THE NANOGRAMME RANGE BY ISOTOPIC DILUTION

G. FREJAVILLE - R. BIR

Commissariat à l'Energie Atomique
Service de Spectrométrie de Masse
CEN.SACLAY - FRANCE

I - INTRODUCTION -

Lithium isotopes abundances are usually determined without big problems. The common practice is to use a pseudo multiple filament ion source. The evaporating surface is simply a nickel sheet put on a rod of the filament bead. A solution of Li nitrate is painted on the nickel flag and the heat radiated from the center filament produces evaporation of the sample. Li^+ ions are produced. At a temperature of 900 to 1000 °C and a sample size of 1 to 10 µg, currents of 10^{-10} to 10^{-9}A are readily produced.

The double collection techniques are specially easy to use for this low range of masses. The output of the mass spectrometer-something proportionnal to the isotopic ratio- remains well constant in spite of ion current evolution, at least in a wide range of current values. Using double collection involves comparative measurements. For the comparison to be achieved in the best conditions, it is obvious that all physical parameters of both measurements must be identical. More specifically, the value of the ion current at which the ratio is measured must be kept constant as strictly as possible. This reduces the mass discrimination and " intensity " effects (i.e.instrumental dependance between ion currents and measured ratio values).

As Li is a very abundant element, natural contamination possibilities must be always kept in mind. Contamination may come from chemicals, vessels, filaments, nickel frame, etc.. For instance, it is easy to produce an ion current as high as 10^{-9}A, from a bead without coating, if the filament temperature is raised at 1,200°C.

All these considerations suggest the specific problems arising if the sample size goes down the 10^{-8} to 10^{-9}g range.

1 - Although the ion current is anything but proportionnal to the sample size, it reduces greatly if the amount of product becomes very small. Moreover, the total electrical charge available for measurement becomes unsufficient. In addition, the maximum value of current is no longer reproductible and one cannot be sure to be able to take ratios at a constant output value. Altering the working temperature - i.e. increasing it - may be extremely dangerous for the value and the constancy of the contamination level. So the sensitivity must be actually increased, in such a way that the currents remain of the same order of magnitude in spite of sample size variation.

2 - Even if the sensitivity is made large enough, natural contamination will more or less occur. Even with specific precautions during all the analytical procedure, it may be shown that the minimum level of contamination is something in the neighbourhood of 2 ng. So a correction has to be made. But, as our purpose is to get a content value via isotopic dilution, it is possible to perform this correction in a very simple manner. This will be examined at first.

II - ISOTOPIC DILUTION WITH NATURAL POLLUTION -

The principle of isotopic dilution is well known. In the whole, it may be summarized as follows : let a mixture of several constituants differing only by the isotope abundance of a given isotope in the same element. If all quantities are known but the amount of one constituant, this unkown can be calculated from the isotope abundance of the mixture.

If N_i is the isotopic concentration of the i product

A_i a factor representing the relative amount of them :

$$(1) \qquad M = \frac{\sum A_i N_i}{\sum A_i}$$

where M is the isotope concentration in the mixture.

This equation can be written :

$$(2) \qquad \sum A_i (M - N_i) = 0$$

Let A_j be the quantity to be determined. So :

$$(3) \qquad A_j = \frac{\sum_{i \neq j} A_i (N_i - M)}{M - N_j}$$

In the specific case of isotopic dilution, if the subscript X reffers to the sample, equation (1) becomes :

$$(4) \qquad M = \frac{A_T N_T + A_X N_X}{A_T + A_X}$$

A_X may be calculated if all other quantities are known. More particularly, the isotope abundance of the sample (N_X) must be known. A special determination has to be performed, except if N_X is known a priori (natural value for instance).

Natural pollution will alter the background equations. Any product Y will be measured as:

$$(5) \qquad Y' = \frac{A_Y N_Y + A_0 N_0}{A_Y + A_0}$$

where N_0 is the natural isotopic concentration

A_0 is the pollution level.

The true value Y may be reached in to ways :

a - A_0 is known. This knowledge comes necessarily from special measurements.

b - A_0 is so that : $A_0 \ll A_Y$. Then : $Y' \neq Y$

Let us consider now the case of a mixture. The isotope abundance of the mixture is measured as :

$$(6) \qquad M = \frac{A_1 N_1 + A_2 N_2 + A_0 N_0}{A_1 + A_2 + A_0}$$

Suppose that N_1 has been run alone. We know the value of :

$$(7) \qquad N'_1 = \frac{A_1 N_1 + A_0 N_0}{A_1 + A_0}$$

So equation (6) can be changed to :

$$(8) \qquad M = \frac{(A_1 + A_0) N'_1 + A_2 N_2}{(A_1 + A_0) + A_2}$$

If the sum ($A_1 + A_0$) can be measured as a whole as $A'_1 = (A_1 + A_0)$, so :

$$(9) \qquad M = \frac{A'_1 N'_1 + A_2 N_2}{A'_1 + A_2}$$

and A_0 has no longer to be known or measured.

This applies immediatly to isotopic dilution. Sample-spike mixture will be measured as :

$$(10) \qquad M_X = \frac{A_T N_T + A_X N_X + A_0 N_0}{A_T + A_X + A_0}$$

the subscripts T, X and 0 refering to the spike, the sample and the pollution

Running the spike alone leads to :

$$(11) \qquad N'_T = \frac{A_T N_T + A_0 N_0}{A_T + A_0}$$

So equation (10) may be written :

$$(12) \qquad M_X = \frac{(A_T + A_0) N'_T + A_X N_X}{(A_T + A_0) + A_0}$$

To reach $(A_T + A_0)$, a calibration is necessary. A mixture of a standard solution (subscript E) with the spike gives a M_E value :

$$(13) \qquad M_E = \frac{(A_T + A_0) N'_T + A_E N_E}{(A_T + A_0) + A_E}$$

In this equation, $(A_T + A_0)$ is the only unknown. Let :

$$(14) \qquad A'_T = A_T + A_0$$

Equation (12) becomes :

$$(15) \qquad M_X = \frac{A'_T N'_T + A_X N_X}{A'_T + A_X}$$

A_X is now readily calculable if N_X is known.

N'_T and A'_T may be called " apparent " constants of the spike solution. Further uses of the constants require :

1 - A constant value for A_T : the amount of spike must be strictly the same for all analyses.

2 - A constant value for A_0 : the experimental procedure must be sufficiently identical that the absolute value of the pollution may be assumed constant. This involves the constancy of :

- amount and purity of all chemicals
- bead filaments materials
- working temperature of the filament
- analytical cycle of spectrometric determinations.

It may be pointed out that the conditions above can be tested in running several times the same sample. For instance the dispersion of successive N'_T and A'_T values during calibration includes the dispersion of pollution level. The table 1 shows the successive

values measured during a typical calibration run .

Table 1

SPIKE CALIBRATION

Isotopic (N'_T)	Li content (A'_T)
95.65 %	44.34 ng/g
95.66 %	44.35 ng/g
95.66 %	43.92 ng/g
95.59 %	44.02 ng/g
95.58 %	43.90 ng/g
95.60 %	44.36 ng/g
95.62 %	44.39 ng/g
95.57 %	43.98 ng/g
95.65 %	
95.68 %	
95.66 %	
95.62 %	
95.63 %	44.16 ng/g
Standard deviation : .03	Standard deviation : .07

Such values are constant enough to be used for actual measurements. Note that independent experiments permitted to evaluate the pollution level in the vicinity of 4 ng, that is very much greater than the A'_T standard deviation.

Working with " apparent " values for tracer constants requires that the isotope abundance of the samples are known. In the measurements described here, both the sample and the standard products had the natural composition.

III - INCREASING MASS SPECTROMETER SENSITIVITY -

The usual sizes of deposits lie somewhere between 1 to 10 μg.

To solve our problem we have to get about the same electrical charge with a deposit as low as . 01 μg and the same filament temperature.

Experiment showed that the two main parameters for increasing the sensitivity are :

1 - Chemical species of the Li to be deposited

2 - Width of the deposit.

It has been found that using Lithium acetate instead of nitrate leads to a gain of sensitivity as high as 100. On the other hand reducing the width of deposit to a maximum value of 1 mm instead of the usual value (5 mm) increases the sensitivity by a factor of 10. Both effects are cumulative, so that on the whole the gain in sensitivity compensates about the lost in material. The working procedure for mass spectrometric determinations remain unchanged.

IV - RESULTS -

The table 2 shows some typical results obtained with the working conditions described above.

TABLE 2

Lithium content in nanogrammes par gramme			
88.88	7.89	1.03	.167
88.86	7.89	1.03	.142
88.72	7.91	1.05	.154
88.60	7.92	1.03	.142
		1.06	.152
		1.03	.149
			.140
88.77	7.90	1.04	.149
Estimated standard deviations			
.12	.03	.02	.017

Each individual value was obtained within a one hour procedure. Intervals of several weeks separated the successive determinations of the same sample. From these figures the procedure appears to be very usable.

In addition to the reproducibility errors, systematical biases have to be considered. They come chiefly from the spike constants, i.e. the knowledge of the standard solution parameters. These errors are probably lower than .1 %.

In the particular case of lithium, another cause of systematic deviation may take place. It comes from the fact that the commercially available lithium compounds have very often a non-natural isotopic composition. This fact, in addition to the natural isotopic variations, produces an incertitude on the value of N_X to be put in the formulae. At the limit, even the isotopic composition of the natural pollution may become questionable.

V - CONCLUSION -

The procedure described here is very easy to perform. The mass spectrometer can be quite a conventional one. The lasting of determinations is very close to that of common practice.

However, the sensitivity is greatly improved. The detection limit can be evaluated as 3.10^{-11} g. In the 10^{-9} g range, the precision is about 3 %.

The actual lithium content of semi-conductor materials, where lithium was the main dopping product, has been determinad on numerous samples and related to their electrical properties.

The procedure is usuable for other lithium content measurements, on the same concentration range.

TRACE STUDIES WITH ION-MOLECULE REACTIONS IN THE PLASMA CHROMATOGRAPH - MASS SPECTROMETER INSTRUMENT

Francis W. Karasek, University of Waterloo, Waterloo Ontario
and
Martin J. Cohen, David I. Carroll, Franklin GNO Corporation,
West Palm Beach, Florida

Presented at the Eighteenth Annual Conference on Mass Spectrometry and Allied Topics - June 17, 1970. San Francisco, California.

ABSTRACT

Plasma Chromatography™ permits identification and analysis of trace constituents in gaseous mixtures. Functioning at atmospheric pressure, the instrumentation involves a positive and negative ion-molecule reactor coupled with an ion drift spectrometer, which produces a plasmagram of separated ion-molecule peaks from a sample mixture. Individual peaks of the plasmagram can be directed into a quadrupole mass spectrometer to identify the ion-molecules present.

This study explored the trace detection of the oxygenated compounds, 1-octanol and 1-nonanol, as preliminary work to the identification of more complex oxygenated compounds in air pollution studies. The positive ion plasmagrams and mass spectra were fairly complex and originated from a series of the type $(C_nH_{2n+2}O)_x(H_2O)_yH^+$. The less complex negative ion results showed a reactant ion corresponding to CO_4^- and resultant ion-molecules of the single species $(C_nH_{2n+2}O)O_2^-$, which were easily separated in the plasmagrams.

In contrast to fragmentation mass spectra obtained with an electron bombardment ion source, alcohol identification by this technique, coupled with mass spectral data, is quite easy.

INTRODUCTION

Plasma Chromatography™ is a technique whose characteristics permit the identification and analysis of trace constituents in a gaseous mixture. Functioning at atmospheric pressure, the instrumentation involves a positive and negative ion-molecule reactor coupled with an ion drift spectrometer, which produces a plasmagram of separated ion-molecule peaks from a sample mixture. Individual peaks of the plasmagram can be directed into a quadrupole mass spectrometer to identify the ion-molecules present.

After generation of ion-molecules in the reactor, they are then separated by a process of injection into a tube filled with a nonreactive gas through which they are drifted by a strong electric field. The ion-molecules arrive at a collector as ion peaks at times characteristic of their structure. The name of Plasma Chromatography (PC) arises because this entire separation process can be thought of in gas chromatographic terms. The drift time of different ion-molecules after sample injection is the result of their interaction with the gas and electric field through which they move, much as the retention time of molecules in gas chromatography is a result of their behavior as they move through a gas under the influence of the partitioning effect. The plasmagram resulting from a recording of detector output versus time resembles a chromatogram with a millisecond time scale. Like in a chromatogram, the peaks can be used in a qualitative and quantitative manner.

Basic features of this method have been described by Karasek (1). A further description and the considerations attendant to coupling a gas chromatograph to the system is the subject of a recent paper by Cohen (2). The great sensitivity of PC to trace compounds arises from the ion-molecule reaction occurring at atmospheric pressure, where many millions of collisions of reactant ions with the trace molecules are possible. This means the probability of detecting all the trace molecules present is very high. While the literature contains a great deal of information about such reactions, most of these studies have been made under low pressure (below 10 torr) conditions (3).

Fundamental to the sensitivity and selectivity of the technique are the specific characteristics of the ion-molecule reaction producing the detected species. Since these reactions have very high reaction rates and form stable ion-molecules for oxygenated compounds, this investigation was initiated to explore the trace detection of such compounds. The compounds used for this exploratory work were the alcohols; 1-octanol and 1-nonanol. Since other more complex oxygenated compounds are important species in studies of air pollution, this work was preliminary to determining suitability of the technique as an analytical method for such air pollution studies.

PRINCIPLES AND INSTRUMENTATION

A block diagram of the basic functions of the instrumentation is shown in Figure 1. The reactant gas and gaseous sample are introduced into the PC tube continuously. Formation of the plasma of reactant ions occurs in the ionizer region of the tube, through a series of steps that take place in less than a millisecond. These steps are initiated when radioactive nickel-63 emits electrons (with energies as high as 60 keV) that then create positive ions and low energy electrons in the reactant gas. The positive ions and electrons rapidly dissipate their initial energy to a thermal level through collisions with neutral molecules. In moist air the end product of these steps is creation of $(H_2O)_n O^-$ and $(H_2O)_n CO_4^-$ in the negative mode and $(H_2O)_n H^+$ ions in the positive mode; the value of n depends on water vapor concentration.[1] These hydrated ions react, in about a 10 millisecond interval, with the trace organic molecules from the sample to form stable ion-molecule entities that are separated and studied by the data contained in their plasmagrams and mass spectra.

Functions of the instrumentation to produce the plasmagram are illustrated in Figure 2. Ionization, reactant ion generation, and ion-molecule reaction processes are occurring continuously. To separate the ion-molecules produced, a discrete pulse of them is injected into the drift region of the PC tube by opening the shutter grid for 0.5 milliseconds. The ion-molecules drift down through the electric field and the gas present until they arrive at the collector; drift time of each ion-molecule depends on its interaction with the electric field and drift gas. The drifting step takes about 50 milliseconds, after which time the whole sequence is initiated again. The signal received by the collector produces a recorder tracing of a plasmagram.

Since the whole sequence of steps occurs in the millisecond time range, the plasmagram scan is produced by a moving gate technique. The gating grid in front of the collector opens for about a 0.2 millisecond interval to permit drifted ion-molecules to pass through to the collector. The gating grid opens at times delayed from the shutter grid operation varying from 0 to the entire 50 millisecond drift time. Typically, a 5 minute scan time is used. This means that after the sample is injected by the shutter grid, the delay of the gating grid function will slowly vary from 0 to 50 milliseconds in 5 minutes. A plasmagram results from the ion-molecules this moving gate allows through to the detector as it scans slowly across the range of drift times. This recording method is illustrated in Figure 3.

Many cycles of the injection and drift process have occurred during the scan. Observation of only one peak can be accomplished by permitting the grid delay time to remain fixed in the position corresponding to that ion; only that particular ion-molecule concentration and its related trace constituent can pass through to the detector and be measured. Ion intensity recorded at this peak is the sum of ion-molecules collected from about 6000 consecutive injections.

Drift time, much as retention time in gas chromatography, can be used to identify the trace molecule originating the peak in the plasmagram. However, by directing these ions into a mass spectrometer, a fairly complete identification can be obtained. This is done through an interfacing device with an aperture and ion focusing electrodes; this device reduces the pressure to the 10^{-5} torr required by the mass spectrometer and delivers the ion-molecules to the analyzer section of that instrument. Having charged particles that can be confined electrically permits the design of a more efficient interfacing device than those commonly used for interfacing gas chromatographic effluents into a mass spectrometer. These mass spectra, combined with the plasmagram, provide the information about the compounds under study. Either positive or negative ion-molecules can be studied.

EXPERIMENTAL PROCEDURE - ALCOHOLS

Samples of 1-octanol and 1-nonanol were obtained from a kit of gas chromatographic reference compounds. (Polyscience Corporation, Evanston, Illinois, cat. no. 120). Prior to introducing the sample alcohols, the drift cell and mass spectrometer tube were baked out overnight at 250°C under a vacuum of 10^{-6} torr or less.

The drift cell was operated with a drift field of 320 volts per centimeter at room ambient temperature and pressure. Bottled air at a flow rate of 100 cc/min was used as a carrier gas and nitrogen gas obtained from liquid nitrogen at a flow rate of 2.5 l/min was used as a drift gas. Both gases were passed through a molecular sieve trap and micron particle filter prior to use.

The sample alcohol was used to wet the barrel of a previously cleaned 5cc gas tight-syringe. The syringe was then back filled several times with dry nitrogen gas and allowed to come to equilibrium. The resulting nitrogen gas, saturated with sample vapor was injected into the carrier gas stream by means of a syringe pump at a rate of

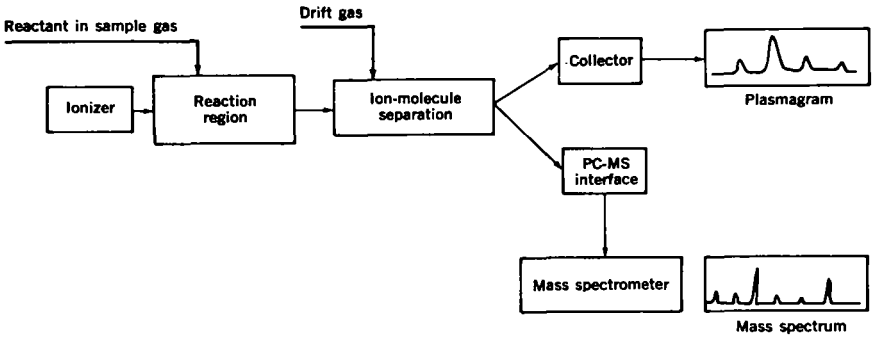

Fig. 1. Plasma Chromatography separation process. Sample gas containing organic compounds is ionized to convert each organic molecule to a very stable ion-molecule. Ion-molecules are separated by injection into a tube filled with a nonreactive gas; the ion-molecules are drifted through the gas by a strong electric field. They arrive at collector at times characteristic of their structure. Signal received by collector produces a recorder tracing of a plasmagram. When interface is used, ions of plasmagram peaks can be directed into mass spectrometer to provide positive mass identification of sample being studied.

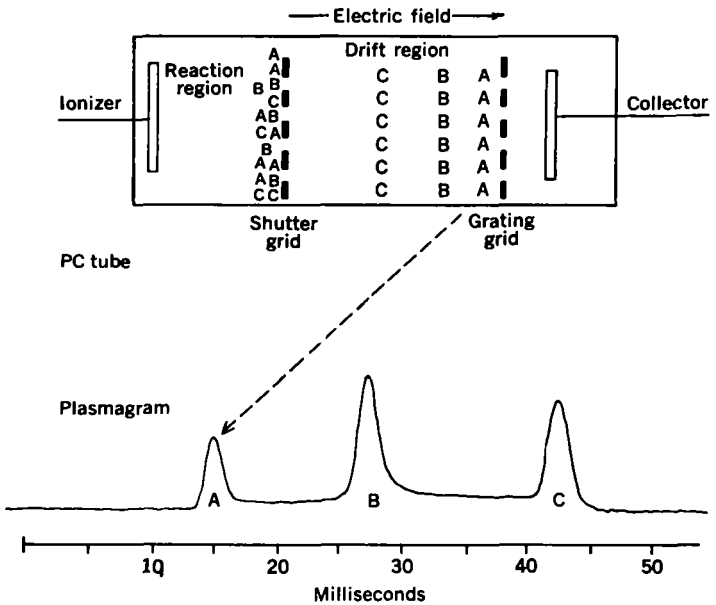

Fig. 2. Simplified diagram shows how plasmagram is produced.

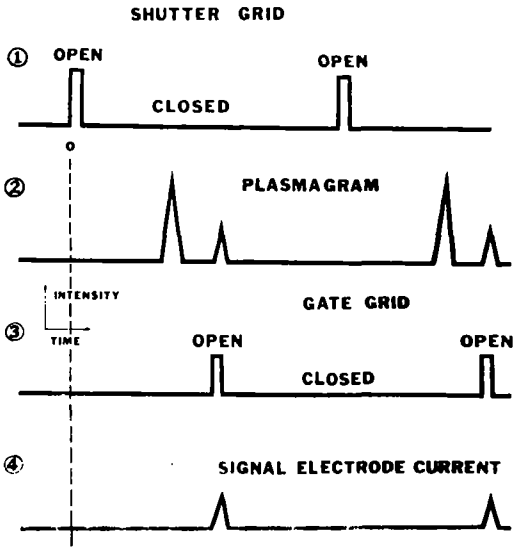

FIGURE 3 - PLASMAGRAM RECORDING USING A MOVING GATE TECHNIQUE

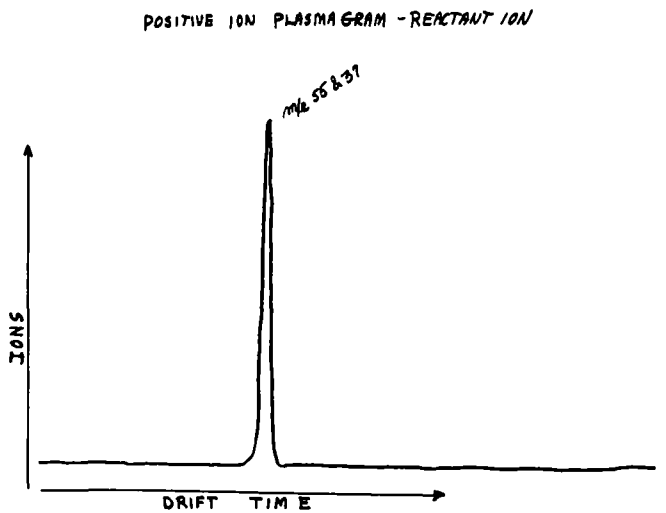

FIGURE 4

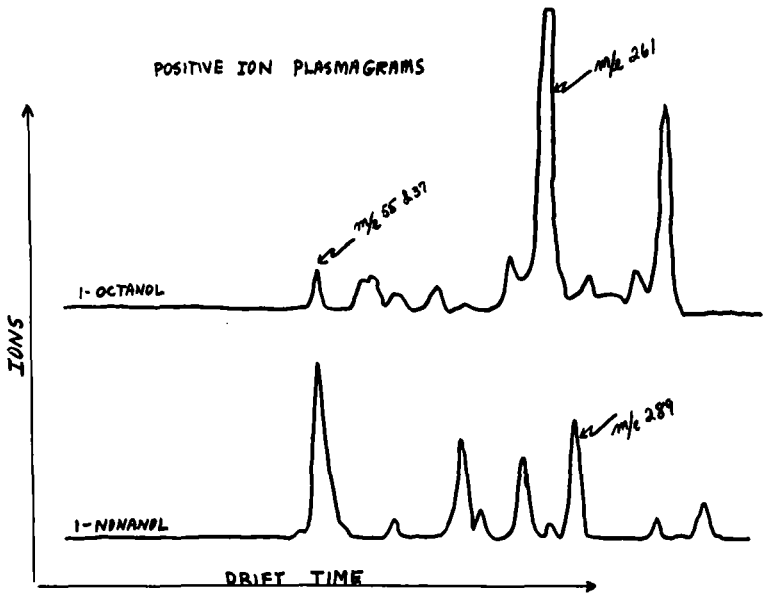

FIGURE 5 - POSITIVE ION PLASMAGRAMS OF 1-OCTANOL & 1-NONANOL

FIGURE 6 - POSITIVE ION MASS SPECTRA OF ALCOHOL PLASMAGRAMS

m/e	ION ABUNDANCE 1-OCTANOL	1-NONANOL
30	12	4
33	-	7
37	25	40
48	12	14
51	-	80
55	100	87
65	-	100
69	-	7
85	6	-
87	-	5
92	-	5
98	-	5
111	35	-
127	20	-
144	45	-
149	45	-
163	-	3
179	-	20
205	-	10
250	-	7
261	75	-
289	-	14

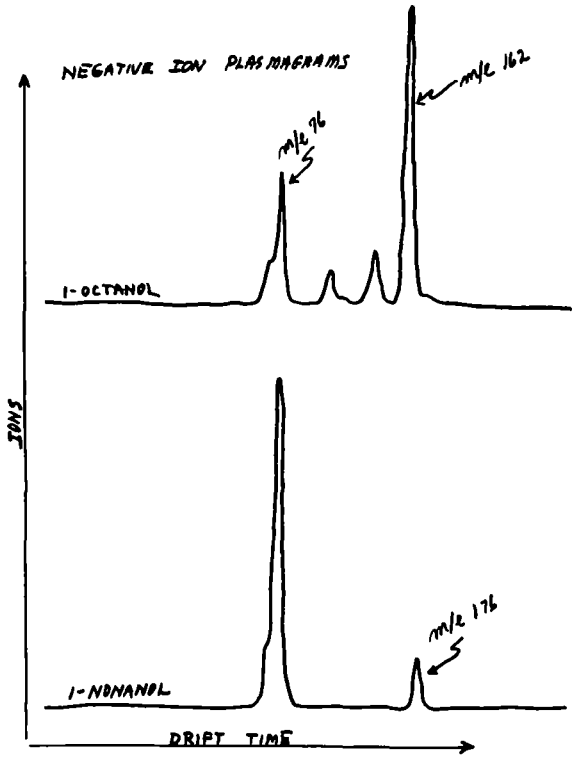

FIGURE 7 - NEGATIVE ION PLASMAGRAMS OF 1-OCTANOL & 1-NONANOL

FIGURE 8 - NEGATIVE ION MASS SPECTRA OF ALCOHOL PLASMAGRAMS

m/e	ION ABUNDANCE 1-OCTANOL	1-NONANOL
32	6	7
46	-	3
60	54	22
66	6	-
76	100	100
94	-	2
108	18	-
162	43	-
176	-	4

10 microliters/minute. This gave a sample concentration in the carrier gas of about 30 parts per billion.

Plasmagrams and mass spectra were taken of the resulting negative and positive ions.

The positive ion mass calibration was based upon the ion series $(H_2O)_nH+$ present in the initial control runs. This ion series has been identified previously based upon experiments with deuterium oxide and by spectrometer calibration with its standard electron bombardment ion source.

The negative ion calibration was obtained by adding several parts per million of sulphur hexafluoride to the drift gas. The resulting ions are SF^-_5 and SF^-_6 which serve as calibration points.

POSITIVE ION RESULTS

A plasmagram of the reactant ions before introduction of the alcohols is shown in Figure 4. The ions present in this peak were identified as $(H_2O)_2\ H^+$ and $(H_2O)_3H^+$ in equilibrium by the presence of ions of mass 37 and 55 in its mass spectrum. The mass spectrum also reveals the presence of small amounts of the ion $(H_2O)NO^+$, which as a minor constituent appears not to enter into the results found here.

A typical plasmagram obtained for each of the alcohols is shown in Figure 5 and the resultant mass spectra for these plasmagrams are tabulated in Figure 6. Because of the complexity of these positive data, and the simpler results shown for the negative ion case, only a partial identification of the ion-molecules present in the plasmagram peaks was determined. Those shown in Figures 5 and 6 suggest that ion clusters with structures corresponding to:

$$(C_nH_{2n+2}O)_x\ (H_2O)_y \cdot H^+$$

are being formed for both alcohols. The peak at mass 261 in the 1-octanol data is very possible $(C_8H_{18}O)H^+$, with a similar double cluster at mass 289 being observed for the 1-nonanol. The first large peak after the reactant ion in the 1-nonanol plasmagram of Figure 5 contains ion-molecules of m/e 163, 179, 205. The next peak contains ion-molecules of m/e 250.

The ion-molecules observed for 1-nonanol contained the series of masses 33,37,51, 55,65,69 and 87. This corresponds to the ion series expected for methyl alcohol water clusters of the form: $(CH_4O)_x(H_2O)_y \cdot H^+$ as illustrated below.

m/e	x	y
33	1	0
37	0	2
51	1	1
55	0	3
65	2	0
69	1	2
87	1	3

The fact that this series was only observed in the runs made with nonanol indicates it is a contaminant in the original sample and not due to experimental technique. In each case the same syringe and cleaning procedures were used and no trace of methyl alcohol was detected in the cleaned syringe when blanks were run.

Based upon the peak intensities and the vapor pressure ratios of methanol and nonanol, the contamination level is probably below 100 parts per million. Since samples were always poured from the original containers, and nothing ever introduced into the original container, it appears that this contaminant was most likely present in the original sample and not accidentally introduced at a later time. The detection of the minute trace of methyl alcohol contamination of the nonanol was an interesting outcome of these experiments and serves to illustrate the analytical scope of the ion-molecule reaction technique.

NEGATIVE ION RESULTS

The negative ion drift time and mass spectra are quite simple in comparison to the positive. Plasmagrams for the alcohols are shown in Figure 7 and the corresponding mass spectra are in Figure 8. The first peak in each plasmagram appears to be the reactant ion $(CO_2)O_2^-$ which transfers the charged oxygen to the alcohol molecule. It is not surprising to find the CO_4^- being present and assuming this role. Mohnen indicates that CO_4^- is a very stable ion found in mixtures of oxygen and carbon dioxide (4).

The major ion-molecule formed in each case appears to be the alcohol combined with a negatively charged oxygen molecule. These appear as the distinctive plasmagram peaks with different plasmagram times shown in Figure 7. The ions associated with the large plasmagram peaks are observed at m/e 162 and 176. The ion-molecules giving rise to the two smaller peaks in the 1-octanol plasmagram were not identified. A similar series with water in place of the alcohol; $(H_2O)_nO_2^-$ has been observed and verified using deuterium oxide. It is apparent that in the negative ion mode one can identify these alcohols from their characteristic plasmagrams and the presence of ion-molecules at m/e of 162 for 1-octanol and 176 for 1-nonanol.

CONCLUSIONS

Both positive and negative ion-molecules are formed with these alcohols. Under the conditions of this experiment the positive ion plasmagrams and mass spectra originated from a series of the type $(C_nH_{2n+2}O)_x(H_2O)_yH^+$. These positive plasmagrams and mass spectra were fairly complex. The negative ion results produced the simpler data. The plasmagrams showed a reactant ion corresponding to a CO_4^- ion and resultant ion-molecules of the single species $(C_nH_{2n+2}O)O_2^-$. These ion-molecules are easily separated in the plasmagrams which, coupled with mass spectral data, makes identification of the alcohols quite easy with this technique. By contrast, it is well known that these alcohols give no parent ions in their fragmentation mass spectra obtained with electron bombardment ion sources, which make identification difficult.

These results are encouraging. Being able to study both positive and negative ion-molecules and chose from a number of ion-molecule reactions to provide specific sensitivity and selectivity gives one a wide range of analytical possibilities. Applying these techniques to the identification of other oxygenated compounds appears quite feasible.

REFERENCES

(1) F.W. Karasek, Res./Dev., 21, No. 3, March 1970

(2) M.J. Cohen, "Plasma Chromatography: A New Dimension for Gas Chromatography and Mass Spectrometry" presented at the 6th International Symposium on Chromatography, Miami Beach, Florida, June 1-5, 1970

(3) E.W. McDaniels, "Collision Phenomena in Ionized Gases," John Wiley, New York,(1964) pages 426-524

(4) V.A. Mohnen, J. of Geo. Phys. Res., 75, No.9, 1717, 1970.

FIGURES

A COMPARATIVE STUDY BY GAS CHROMATOGRAPHY-MASS SPECTROMETRY OF ENVIRONMENTAL HYDROCARBONS FROM FOUR DIFFERENT LOCALITIES

J. ORO', J. GIBERT, D.W. NOONER*, and E.GELPI**

Department of Biophysical Sciences
University of Houston
Houston, Texas 77004

ABSTRACT

A number of air samples from Rochester, Montreal, Houston, the Sierra Nevada area, and water from Houston's Ship Channel, have been analyzed by combined gas chromatography-mass spectrometry for their alkane content. Environmental peculiarities of the zones where the samples were obtained indicate correlations between the patterns of the hydrocarbons found in each case and their likely sources.

The combination of high resolution capillary gas chromatography with the identification capability of mass spectrometry is considered one of the best techniques to perform analyses of such complex mixtures in which some individual components are present in very minute amounts.

INTRODUCTION

It is well known that hydrocarbons are widely distributed in nature (1). Alkanes are found, in addition to petroleum crudes (2), in animals, plants and their products (3,4); micro-organisms, e.g. algae (5) and bacteria (6); terrestrial and extraterrestrial samples, e.g. rocks, sediments (7), meteorites (8); air and air pollutants, e.g. dust (9), smoke, and exhausts; water, and in general in all those samples being exposed to the Earth's atmosphere and hydrosphere for some time.

In an attempt to get some complementary views on the overall distribution of hydrocarbons in air, we have undertaken a comparative study of the alkane fraction in air samples from four different localities: Montreal, Rochester, Houston and the Sierra Nevada. The aim of these studies is directed towards monitoring pollution on one hand and contamination control (of samples to be analyzed for hydrocarbons) on the other. The role played by contamination arising from environmental sources is quite critical in studying compounds present in the submicrogram level in samples which have been in our environment for certain periods of time. This situation is of particular concern in the analysis of extraterrestrial samples (meteorites and lunar soil) coming from high vacuum systems, a condition which consequently enhances the potential contamination by products of our biosphere (10).

In another aspect of this work we have studied the alkane fraction of the water from Houston's Ship Channel that connects Houston to the Galveston Bay system. We have attempted to correlate both quantitative and qualitative results to the environment peculiarities of the zones where the samples were obtained.

EXPERIMENTAL

a) Air Sampling

Air sampling was carried out by passing amounts of the order of 1500 m^3 of air through glass cloth filters in the case of Montreal and Rochester, and 3.5 m^3 of Houston's air through silica gel. Paper filters and a Staplex high-volume air sampler were used to sample 924 m^3 of Sierra Nevada's air.

b) Analytical Procedure

The filters and silica gel were Soxhlet extracted with a mixture of benzene/methanol (3:1). The extracts were fractionated on silica gel columns with pentane, benzene and methanol. The pentane fraction, which contained the alkanes, was studied

*Present address: Texaco Inc., Bellaire, Texas
**Present address: Space Sciences Laboratory, University of California, Berkeley, California

FIGURE 1

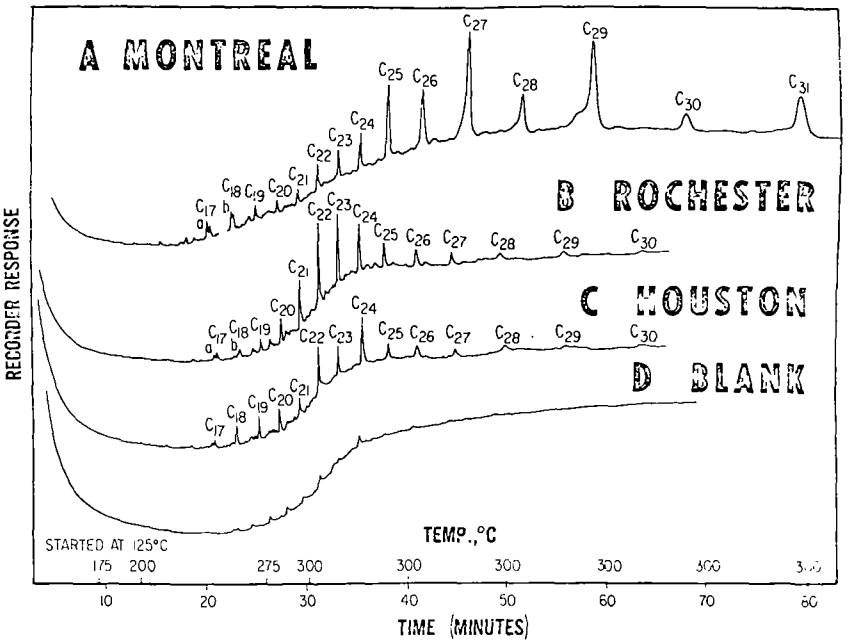

Gas chromatographic separation of alkanes from air on a, 30.5 m x 0.25 mm I.D., capillary column coated with Apiezon L.

FIGURE 2

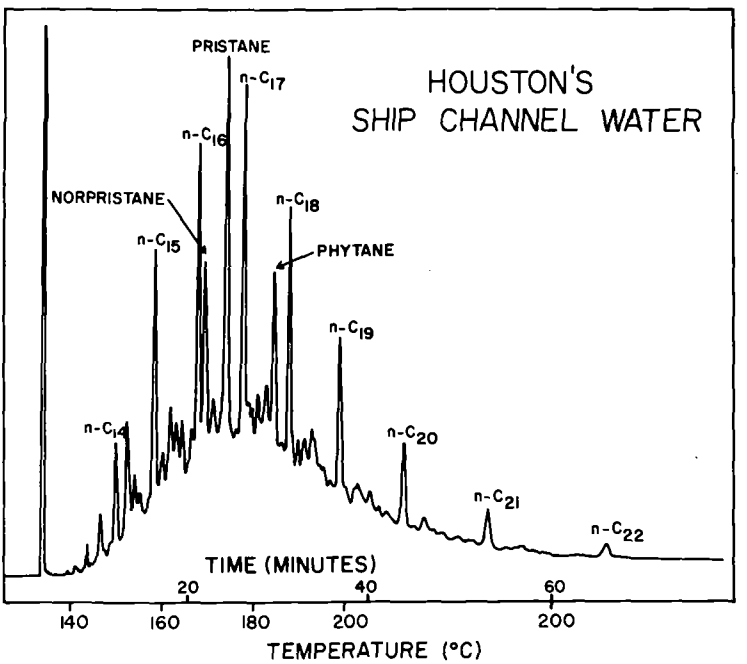

Gas chromatographic separation of alkanes from water on a, 154.0 m x 0.76 mm I.D., capillary column coated with Polysev.

by high-resolution capillary gas chromatography on 500 ft. x 0.02" columns coated with suitable phases (see Figures 1 and 2). Details on the procedure have been given elsewhere (8). The other fractions containing aromatics (benzene) and the polar compounds (methanol) will be the subject of later studies.

The effluent of the gas chromatographic column was introduced to an LKB 9000 GC-MS instrument that uses the Becker-Ryhage jet type separator. Mass spectra of the individual components emerging from the chromatographic column were recorded at 70eV.

RESULTS AND DISCUSSION

The preliminary results obtained in a survey of air samples undertaken some time ago are depicted in Figure 1 which shows the chromatograms of air from three different localities: Montreal, Rochester, and Houston. In the Montreal air, an odd over even carbon number predominance of alkanes can be observed. The air from Rochester shows a rather monomodal distribution, while Houston's air displays a slight even over odd predominance. Preliminary results on air samples from the Sierra Nevada (in the surroundings of Lake Tahoe) show in general less than 10^{-11} ppm of hydrocarbons which turned out to be insufficient to get a reliable chromatogram with the amounts of air sampled. Table I summarizes the amounts of alkanes in the air from the four localities studied.

TABLE I

Locality	Total ppm	Characteristics
Houston	1.7×10^{-6}	Even over odd predominance
Montreal	1.2×10^{-8}	Odd over even predominance
Rochester	7.2×10^{-9}	Monomodal distribution
Sierra Nevada	$<10^{-11}$	Trace amounts only

With the data presently available we cannot be too certain at the present time on the exact sources of these hydrocarbons. However, these patterns can be correlated to a certain extent to a biological or non-biological origin depending upon the predominance of the odd over even carbon number series of the alkanes. The odd over even predominance is commonly taken as an indication of biogenecity (4). Consequently, in this sense, one might assess a biological origin for the hydrocarbons detected in Montreal's air. It is interesting to note that the only even over odd predominance, which points to alkanes of industrial, or non-biological origin, is confined to the city with the heaviest concentration of petrochemical industry (Houston). This observation is also correct in a quantitative sense. Houston contains two orders of magnitude more than Rochester, three more than Montreal, and five more than the air from Sierra Nevada in the samples analyzed.

As indicated earlier we also studied for comparative purposes the water from the Houston Ship Channel. Figure 2 shows a rather complex distribution of hydrocarbons extracted from this water. The total amounts reach a value of 14.500 ppm, which can be compared with the 50.000 ppm obtained from an East Texas petroleum crude by application of the same method. Interestingly enough, on their tour of the Houston Ship Channel and Galveston Bay system, as recently reported (11), members of the President's advisory board for pollution control were appalled to see ships actually churning up oil from the two foot thick sludge from the bottom of the channel. This distribution resembles very much petroleum crudes of East Texas (usually characterized by a high content of isoprenoids, pristane and phytane), an observation which is in line with the above remarks.

CONCLUSIONS

Even though this work is only preliminary, the results presented here give an indication of what are the major sources of the hydrocarbons present in the samples studied. As far as air is concerned, not only the hydrocarbon distribution, but the total amounts found point in general, toward the predominance of determined sources of hydrocarbons over others which contribute to a lesser extent.

The water analyzed is a clear example of water polluted predominantly with petroleum-like hydrocarbons. The total amounts found are roughly 29% of the alkane fraction studied by application of the same procedure to an East Texas petroleum crude (12).

It should be made clear, however, that due to the interaction of other atmospheric phenomena, such as wind and rain, and to the different methods of sampling, there is an inherent difficulty in obtaining analyses of "representative" samples of air and water of any zone. Only continued studies can give a better correlation of the data resulting from this preliminary work.

ACKNOWLEDGEMENTS

We thank Dr. J.L. Monkman, Occupational Health Div., Environmental Health Centre, Tunney's Pasture, Ottawa 3, Ontario, Canada, who supplied us the filter samples of Montreal's and Rochester's air, and Dr. F.W. Went, Dessert Research Institute, University of Nevada, Reno, Nevada, who supplied us the filter samples of the Sierra Nevada air.

This work was supported in part by Grant NGR-44-005-002 from the National Aeronautics and Space Administration.

REFERENCES

1. R.C. Clark, Woods Hole Oceanographic Institution, Technical Report Ref. No. 66-34, Unpublished manuscript (1966).
2. W.G. Meinschein, Bull. Amer. Assoc. Petrol. Geol., 43, 925 (1959).
3. H.W. Gerarde and D.F. Gerarde, Ass. Food and Drug Officials, U.S. 25-26, 1 (1961).
4. J. Oro', D.W. Nooner and S.A. Wikström, Science, 147, 870 (1965).
5. E. Gelpi, H. Schneider, J. Mann and J. Oro', Phytochm., 9, 603 (1970).
6. T.G. Tornabene, E. Gelpi and J. Oro', J. Bacteriol., 94, 333 (1967).
7. J. Oro' and D.W. Nooner, Nature, 213, 1082 (1967).
8. D.W. Nooner and J. Oro', Geochim. Cosmochim. Acta, 31, 1359 (1967).
9. E. Gelpi, D.W. Nooner and J. Oro', Geochim. Cosmochim. Acta, 34, 421 (1970).
10. J.M. Gibert and J. Oro', J. Chromatog. Sci., 8, 295 (1970).
11. L.J. Carter, Science, 167, 1102 (1970).
12. D.W. Nooner, Ph.D. thesis, University of Houston (1966).

NOTE

This paper will be submitted for publication to Environmental Science and Technology.

K4

Mass Spectrometric Studies of the Reactions of Singlet Molecular Oxygen ($O_2\,^1\Delta_g$) and their Significance in Air Pollution*

John T. Herron and Robert E. Huie

National Bureau of Standards
Washington, D. C. 20234

The reactions of singlet molecular oxygen ($O_2\,^1\Delta_g$) with organic compounds have been studied in the gas phase using a flow system coupled to a mass spectrometer. The concentration of singlet oxygen was determined by titration with 2,5-dimethylfuran. Reaction mechanisms and rate constants were obtained for reactions with olefins and other organic compounds. The rates of these reactions are compared with those of the corresponding atomic oxygen reactions under atmospheric conditions.

* To be published in Environmental Science and Technology.

HIGH-TEMPERATURE HIGH-RESOLUTION MASS SPECTROMETRIC STUDIES OF APOLLO XI LUNAR FINES *

F. M. WACHI, D. E. GILMARTIN, W. K. STUCKEY and V. L. KNIGHT

Materials Sciences Laboratory
Aerospace Corporation, El Segundo, California

J. F. ORÓ and W. S. UPDEGROVE

Departments of Biophysical Sciences and Chemistry
University of Houston, Houston, Texas

ABSTRACT

The liquidus-solidus behavior of Apollo 11 lunar fines and the evolution characteristics of CO, N_2, He, Ne and Ar were investigated by the combined techniques of high vacuum differential thermal analysis (DTA) and mass spectrometry between 100° and 1500°C. The DTA thermogram has shown that the lunar fines undergo fractional melting over a broad range of temperature from about 915° and 1300°C, the iron-sulfide melt separates immiscibly from the silicate magma at about 1140°C, and the lunar material becomes a homogeneous melt at about 1300°C.

With the exception of a few surges of nitrogen gas below 1140°C, significant quantities of nitrogen gas are released between 1140°C and 1180°C. The source of nitrogen gas could be from decomposition of nitrides, nitrates and the sudden release of occluded nitrogen. Small amounts of CO are evolved continuously from about 580° to 1140°C. The rate of CO release increases sharply above 1140°C and reaches a maximum at about 1350°C indicating the existence of carbon in the lunar fines. Although the precise nature of the lunar carbon is still undefined, the source of CO could be from trapped CO, decomposition of carbonates and carbonyls, and reactions between the mineral oxides and carbides and the various allotropes of carbon (graphite, chaoite, lonsdaleite and diamond). The possibility of high temperature reactions of elemental carbon with the molten mineral matrix cannot be ruled out since all of these allotropic forms of carbon have been found in meteorites and the lunar soil from the Sea of Tranquility has been estimated to contain about 2% meteoritic material. The thermal evolution curves for the noble gases have indicated that these gases come from several sources with the principal sources being the solar wind, radiogenic decay reactions and spallation processes. Below about 1000°C the major source for the noble gases appears to be the solar wind. At higher temperatures the composition of the noble gases trends toward spallation and radiogenic decay type of noble gases.

The search for carbon-containing materials was performed with a special low hydrocarbon background vaporization apparatus that was coupled to the mass spectrometer. Comparison of the mass spectra from the blanks with the corresponding spectral data on the lunar fines has shown that the trace quantities of organic matter can be attributed to contaminants either from the exhaust of the lunar module or from terrestial handling of the lunar samples. All of the organogenic elements (H, C, N, O, S, P) have been observed mass spectrometrically, but the chemical nature of these species in the lunar material has not been identified.

---

* This work was supported under Air Force Contract No. FO 4701-69-C-0066 and NASA Contract NAS-9-8012

DECOMPOSITION OF FIRE RETARDANTS BY MASS SPECTROMETRIC THERMAL ANALYSIS

H. G. Langer and T. P. Brady

The Dow Chemical Company
Eastern Research Laboratory
Wayland, Massachusetts 01778

With the increased use of plastic materials in everyday items, the problem of flammability becomes acute. Up to now, the evaluation of fire retardant agents has been empirical. Thus, the need for methods and instrumentation to test fire retardants has never been greater. In this paper we shall describe a method which at least partially can fulfill this need.

In 1961 Friedman reported on the fire retardant properties of a number of bromine containing compounds (Fig. 1). An interesting conclusion may be drawn from this data: the total amount of bromine available in these compounds is apparently more important than the molecular structure of its carrier to inhibit burning. This, in turn, seems to indicate that indeed the smallest fragments such as bromine radicals, HBr or possibly Br_2 are the active species in the fire retarding process. If this is true it might only be necessary to study these low molecular weight species in the gas phase as a way of evaluating this type of fire retardant agent.

Obviously low molecular weight species cannot be incorporated into polymers or added to synthetic fibers without losses by diffusion or even chemical interaction. Thus a fundamental requirement for an additive fire retardant is a decomposition pattern producing such low molecular weight species at a time where a polymer also undergoes decomposition.

If the fire retardant agent is decomposed at temperatures below the decomposition range of the polymer, it might disappear before the flame starts. On the other hand, if the fire retardant agent is thermally much more stable than the polymer it might prevent the remaining char from burning but not the burning of the gaseous pyrolysis product from the polymer. Consequently, knowledge of the decomposition of fire retardant agents as a function of temperature and an identification of decomposition products must represent knowledge of fire retardant potential.

This is exactly the goal for the first phase of our studies on fire retardants by mass spectrometric thermal analysis, a method which we have previously described. (1) For this method intensities of ions observed in the mass spectrometer are plotted as a function of linearly increasing temperature. The sample itself is heated inside a time-of-flight mass spectrometer close to the ion source. Figure 2 shows the decomposition of pentabromochlorocyclohexane. The major ions are HCl^+, $C_6H_5^+$, $C_6H_5Cl^+$ and $C_6H_5Br^+$. In addition all ions formed by successive dehalogenation of the parent compound were detected although they are not plotted in this graph. What then is the information we can extract from these curves?

1. The decomposition starts slightly above 100°.
2. The major reaction product is benzene which shows up in part as the phenyl ion.
3. Negligible amounts of HBr were detected.
4. Surprisingly high concentrations of HCl and chlorobenzene are present.

The chemical reaction is summarized in Fig. 3.

Initiated by homolytic cleavage of a carbon-bromine bond the remaining radical becomes successively more stable with formation of double bonds after loss of a second halogen. Loss of HCl or HBr would explain the formation of bromobenzene and chlorobenzene. The large amount of HCl and chlorobenzene observed is explained by the presence of a considerable amount of dichlorotetrabromocyclohexane.

At this point it should be noted that field testing has shown that this brominated compound indeed has fire retardant properties as measured by several of the laboratory tests described under ASTM classifications. Empirically it has also been shown that this fire retardant does not alter

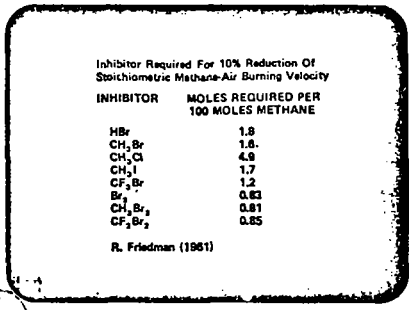

Figure 1

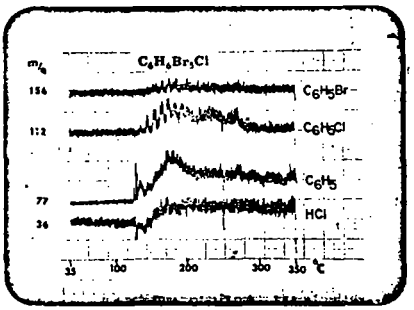

Figure 2

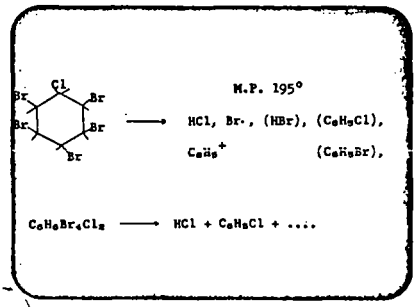

Figure 3

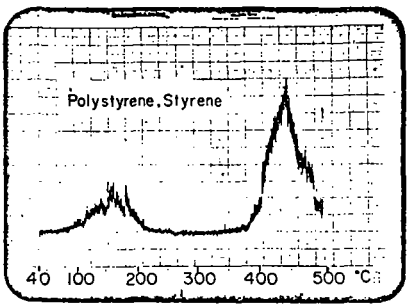

Figure 4

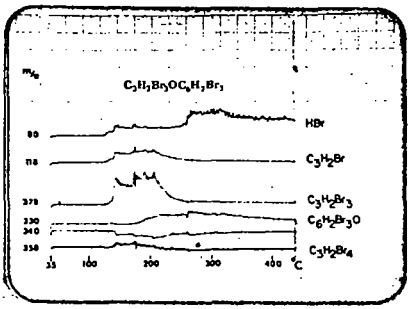

Figure 5

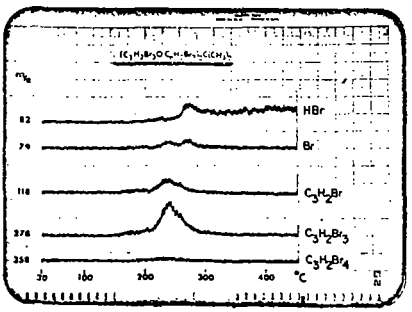

Figure 6

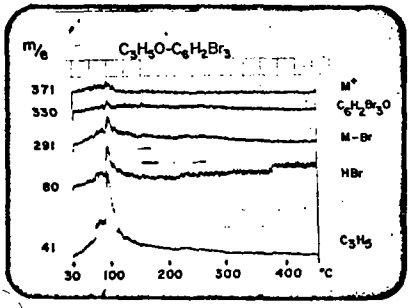

Figure 7

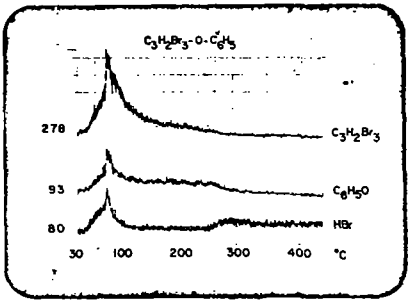

Figure 8

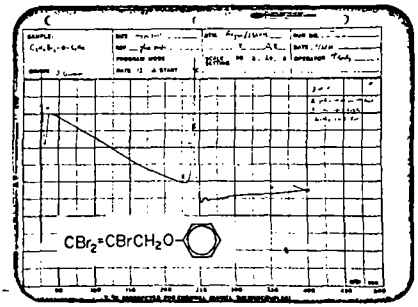

Figure 9

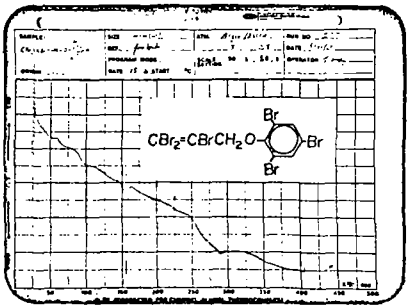

Figure 10

the properties of the polymer by chemical interaction so that we can classify this material as an additive FR agent. The effect of this agent then must be displayed in the flame front itself.

Looking at the decomposition of polystyrene, as shown in Fig. 4, which we have chosen as a model system because of the ease of handling the polymer in the laboratory, we find that the FR agent is decomposed slightly before the onset of polymer decomposition which is a prerequisite for fire retardancy.

Since different polymers do decompose at different temperatures, fire retardant agents should be available which will also decompose at different temperature ranges. One possibility is present in the structure of the fire retardant itself. Changing the location of the halogen on the carbon skeleton should have a definite effect on the onset of the reaction. On the other hand, physical properties of the FR agent can also become quite important. Both these phenomena are demonstrated with the following series of brominated allylphenyl ethers all of which have shown fire retardant properties. The decomposition of tribromoallyl-tribromophenyl ether (Fig. 5) similarily to the previous example also begins at approximately 150°. Here, however, the reaction proceeds in two steps with a number of reaction products appearing in the gas phase. Very significantly a fairly large amount of hydrogen bromide is liberated at low temperatures, more at the onset of the second reaction step, and continuing to temperatures of approximately 500°.

By linking two of these molecules at the phenyl groups to a dimethylmethane bridge (Fig. 6) the character of the decomposition is maintained. However, a relatively large amount of hydrogen bromide is liberated and the reaction is sustained, in fact, increased much more strongly with increasing temperature. The importance of physical properties is demonstrated with the following two examples, the allyltribromophenyl ether (Fig. 7) and the tribromoallylphenyl ether (Fig. 8). Both compounds vaporize readily, so that essentially no decomposition could be observed in the mass spectrometer. However, when the first of these two compounds was incorporated into a polystyrene matrix this molecule was not vaporized but styrene fragments and HBr was observed at about 350°. Where the ortho-position in this phenyl ring was not brominated (Fig. 9, 10) a sharp exothermic reaction was observed by differential thermal analysis, possibly indicating a Claisen rearrangement of a condensation reaction.

To summarize, molecular composition has an effect on the release of bromine within a given temperature range. If this temperature range is fairly low, one would expect this material to be very effective for a "flash fire". On the other hand, slower burning materials and those with high decomposition temperatures would require a fire retardant that shows a fairly high thermal stability.

We have shown that mass spectrometric thermal analysis is an excellent tool to study fire retardant potentials. At present, we are extending these investigations to detect possible interactions between polymers and fire retardants which would not only allow us to investigate the desired high temperature reaction but also detect undesirable reactions which might occur during the molding and processing operations on the polymer.

The question of synergism is also under investigation.

References

1. "Automated Mass Spectrometric Thermal Analysis". H. G. Langer and F. J. Karle, Reported at the 15th Annual Conference on Mass Spectrometry and Allied Topics. May 1967, Denver, Colorado.

MECHANISMS FOR TEMPERATURE EFFECTS IN MASS SPECTRA

BY

Fred P. Abramson
CEC/Analytical Instruments Division
Bell & Howell Co.
Monrovia, California 91017

This paper studies strong temperature effects in certain classes of compounds by varying instrumental parameters as well as comparing spectra obtained from field ionization with those obtained via electron impact. The purpose of these experiments was to evaluate the validity of comparative spectra run on different machines where some very large discrepancies were observed. Perhaps the largest discrepancy was observed by Spiteller-Friedmann, Eggers and Spiteller[1] who compared the spectrum of n-triacontane obtained from their Atlas CH-4 using direct inlet methods with one obtained from a CEC 21-103 using a batch inlet system[2a]. It was of interest to attempt a direct comparison using the same instrument in each case. Here a CEC 21-110C equipped with a heated all-glass inlet system and a direct introduction probe was used. The idea was to try to reproduce the API spectrum for a compound as closely as possible, and then to vary the experimental conditions and see if equally dramatic effects could be obtained. A sample of n-octacosane was chosen. It was introduced into the mass spectrometer first via the batch inlet system which was operated at 270° while the source temperature corresponded closely to that used for the API spectrum-270°. A comparison of the API[2b] and the present results are found in columns 1 and 2 in Table 1. Reasonable agreement is observed, especially for the very temperature sensitive molecular ion. Next, the ion source temperature was lowered to 115° while all other experimental parameters were held constant. The spectrum obtained appears in column 3. There is one large change which resulted from having lowered the source temperature-the molecular ion intensity increased by nearly a factor of 20. To complete this series of experiments, a sample of n-octacosane was introduced via the direct introduction probe with the source still at 115° and this spectrum is tabulated in column 4. There is some increase in the molecular ion intensity but the change of inlet method has only a small effect on the observed spectrum.

The explanation relates to the nature of thermal equilibrium in mass spectrometers. The thermal state in which a molecule finds itself just prior to ionization will reflect the last point in the system where some sort of thermal equilibrium occurred. In a "closed" ion source design like the 21-103 and 21-110, molecules spend a relatively long time in the ionization chamber and will thereby cause the molecules to ionize from a temperature represented by the ion source chamber. For thermally stable materials, such as the hydrocarbons studied here, the method of introduction will have little influence on the spectra; only the source temperature is an important parameter. It should also be noted that this increase in the molecular ion intensity is an absolute increase, not just a relative increase as in the case of low energy electron impact spectra.

The loss of small molecules from complex natural products is another way that spectra exhibit temperature effects. It is of interest to ascertain whether these losses occur in the act of vaporization or whether they are electron-impact induced. The comparison of field ionization and electron-impact ionization provides a potential method for deducing the dissociation reaction mechanism. These molecular losses are rearrangement reactions. It has been shown that, in general, rearrangement reactions are discriminated against in field ionization mass spectra[3]. However, there are examples of spectra where rearrangement processes produce the base peak in field ionization[4]. Therefore it was decided to investigate the effects of temperature on the FI and EB spectra to incorporate yet another physical parameter in the tests. The assumption is that strong temperature effects may be observed in EB spectra independent of whether the mechanism was pyrolytic or electron induced. However, since only the fastest rearrangement reactions may be observed in FI spectra and since the fast ones are those which already have sufficient energy, any increase in apparent dissociation in field ionization should represent the results of pyrolysis to produce a new molecular species which will then give its own FI spectrum superimposed on the spectrum of the original material.

Our own experience, as well as that of others[5], indicated that the residence time of a thermally unstable compound was yet another experimental parameter. In order to minimize the effects of residence time, 2 ug. samples were used for the follow-

TABLE 1

SPECTRUM OF N-OCTACOSANE

	API	PRESENT RESULTS				API	PRESENT RESULTS		
m/e	(a)	(b)	(c)	(d)	m/e	(a)	(b)	(c)	(d)
395	.3	.4	8.0	11.1	113	5.5	7.3	6.5	8.7
394	1.3	1.4	25.7	33.2	112	2.7	3.8	4.3	5.8
365	.3	.4	.9	1.1	111	3.1	4.6	5.8	6.3
351	.4	.6	1.1	1.4	99	8.7	11.5	10.4	12.5
337	.7	.9	1.5	1.9	98	4.0	4.6	5.6	7.2
323	.8	.9	1.8	2.2	97	7.5	8.9	10.6	12.5
309	.9	1.0	2.0	2.0	96	1.1	1.5	2.2	2.4
295	.9	1.0	1.8	2.2	86	2.6	3.3	3.5	3.1
281	1.0	1.0	1.8	2.	85	39.7	45.8	42.9	48.9
267	1.1	1.1	1.8	2.3	84	6.2	7.3	8.2	10.1
253	1.1	1.3	2.1	2.5	83	12.0	12.6	14.8	16.9
252	.5	.6	1.1	1.4	82	2.5	3.1	3.9	4.6
239	1.2	1.5	2.0	2.6	81	1.3	1.5	1.7	2.2
238	.5	.8	1.2	1.7	72	3.2	4.2	4.1	4.6
225	1.4	1.4	2.1	2.6	71	57.9	63.9	62.9	65.9
224	.6	.8	1.4	1.6	70	10.5	11.5	13.3	14.2
211	1.5	1.7	2.3	2.6	69	16.7	16.0	18.9	20.9
210	.7	.9	1.5	1.9	68	3.0	3.2	4.2	4.6
197	1.7	1.9	2.3	2.9	67	2.7	2.9	3.5	4.1
196	.9	1.3	1.7	2.2	58	4.4	4.4	4.4	4.4
183	1.9	2.2	2.6	3.1	57	100.	100.	100.	100.
182	1.0	1.3	2.1	2.4	56	15.6	14.5	17.4	16.9
169	1.9	2.4	2.9	3.1	55	31.1	26.5	30.0	30.3
168	1.0	1.7	2.4	2.9	54	3.2	2.8	3.8	3.9
155	2.3	2.9	3.0	4.3	53	1.4	1.5	1.8	1.7
154	1.2	1.8	2.7	3.4	44	3.5	3.2	3.3	3.4
141	2.9	3.7	3.1	4.6	43	105.0	75.9	84.3	75.0
140	1.6	2.4	3.2	4.1	42	10.8	8.3	9.1	8.7
127	3.9	5.1	4.8	6.0	41	37.2	27.7	30.0	27.0
126	2.0	2.9	3.5	4.3	39	3.6	3.2	3.5	3.4
125	1.3	1.9	2.0	2.6	29		15.6	17.7	14.4
					27		5.1	5.6	4.3

(a) cf. ref.2b, Inlet temp. 340° Source temp. 265°

(b) Inlet temp. 270°, Source temp. 270°

(c) Inlet temp. 270°, Source temp. 115°

(d) Inlet temp. 115°, Source temp. 115°

ing experiments and the mass spectrometer was repetetively scanned over a small mass range (from the molecular ion down to loss of acetic acid) every four seconds for the duration of the sample. Cholesterol was the first sample tested. Where the electron impact produced a M-H_2O peak which rose from 38% of the molecular ion at 200° to 64% at 295°, the field ionization produced peak at M-H_2O remained constant at 10%. It would appear that there is a temperature dependent fragmentation reaction for loss of water from cholesterol molecular ions but that this fragmentation doesn't occur under these conditions for cholesterol molecules. This is a similar result as previously noted[6].

Two acetates were studied next. Their behaviors were quite different from one another. Table 2 summarizes the results. The data for testosterone acetate points out nicely the discrimination for slow processes in field ionization and show, as did cholesterol, that temperature dependent electron impact induced eliminations are occuring but not from the neutral molecules. Androsterone acetate, on the other hand, shows a dominant loss of acetic acid under electron bombardment and also shows a considerable temperature dependent loss from field ionization. The rationalization here is that the rapid rise in the EB data reflects mostly an activation of the electron induced elimination while the FI data show that at 270° about half of the androsterone acetate is losing acetic acid prior to being ionized.

Experiments are continuing to evaluate the fragmentation mechanisms in cortisone which is a steroid with a high degree of thermal sensitivity[7].

REFERENCES

1 M.Spiteller-Friedmann, S. Eggers and G. Spiteller, Monatsh. Chem., 95,1740,(1964)

2 API Catalog of Mass Spectral Data: a) Serial No. 1316, b) Serial No. 886

3 H.D. Beckey, H. Hey, K. Levsen and G.Tenschert, Int. J. Mass Spectry. Ion Phys. 2, 101, (1969)

4 P. Schulze, W.J.Richter and A.L. Burlingame, Paper No. 168, 17th Annual Conference on Mass Spectrometry and Allied Topics, Dallas Texas, 1969

5 H.J.M. Fitches in "Advances in Mass Spectrometry", Vol. 2, R.M. Elliott, Editor,1963

6 J.N. Damico, R.P. Barron and J.A. Sphon, Int. J. Mass Spectry. Ion Phys.,2, 161,(1969)

7 M. Spiteller-Friedmann and G.Spiteller, Org. Mass Spectrom. 2, 901, (1969)

TABLE 2

FI/EB SPECTRA OF ACETATES

TESTOSTERONE ACETATE

	ELECTRON IMPACT			FIELD IONIZATION		
T	M	M-42	M-60	M	M-43	M-59
135°	100	51	13	100	21	4
200°	100	72	17	100	23	4
270	100	137	30	100	23	-

ANDROSTERONE ACETATE

	ELECTRON IMPACT		FIELD IONIZATION	
T	M	M-60	M	M-60
135°	100	440	100	20
200°	100	770	100	51
270°	100	1750	100	107

ANALYSIS OF COMPOSITE SPECTRA FROM MIXTURES SUBJECTED TO MICROMOLECULAR DISTILLATION IN A MASS SPECTROMETER

R. D. Grigsby, R. H. Cole, W. G. Fox, and G. M. Gable

Department of Biochemistry and Biophysics
Texas A&M University
College Station, Texas 77843

The technique to be described here could be classified as a special method in mass spectrometric thermal analysis.[1-5] However, we are choosing instead to call it "micromolecular distillation" because of its relationship to molecular distillation on a large-scale basis.[6-8]

Micromolecular distillation depends on the same principle of operation as the "integrated-ion current" method that has been described for quantitative analysis with a probe; i.e., the intensity of one or more masses is recorded while the sample is distilled completely to dryness.[9-13] However, micromoleculr distillation gives, in addition to the amounts of components present, their individual spectra also. The technique should find utility in the analysis of mixtures that are not sufficiently volatile for the GC-MS combination. An independent means of quantitative analysis by probe introduction has been described in the literature elsewhere.[14-15]

To subject a sample to micromolecular distillation a specially designed direct-introduction probe is used which can be temperature programmed linearly with time. The probe designed and constructed in our laboratory consists almost entirely of glass except for the heating element and thermocouple. It can be linearly programmed from room temperature to 300°C at greater than 20°C/min. and in a non-linear manner at more than 100°C/min. By employing a stream of nitrogen gas passed through a coil immersed in liquid nitrogen, the probe can be cooled at least to -50°C.[16] The apparatus is presently being used with a Bell & Howell Model 21-110B mass spectrometer.

The micromolecular distillation data are obtained by distilling the sample in the probe at a constant rate of temperature increase, which is normally 5-10°C/min. During the distillation multiple spectra are taken under fast scan conditions (0.4 octave/sec.) at recorded time increments. Plots are then made of peak intensity for given masses vs. time to give elimination curves similar to those obtained for macro-scale molecular distillation. In actuality the data are handled by a computer which uses a least squares technique to fit the points to an empirical equation:

$$I = a(t-b)^3 - ct^n$$

where I is intensity, t is time, and a, b, c, and n are constants determined by the least-squares fit.

A typical elimination curve for a single mass is shown in Figure 1. Note that the intensity increases rapidly with time until the component is distilled away, at which time the curve drops sharply to zero.

Three quantities of importance to the analysis of the data are obtained from the computer output. These are: t(Im), the time at which the curve "peaks out"; Im, the maximum intensity of the curve; and A, the area under the curve.

If elimination curves are plotted for several masses all of which arise from the same component, a family of curves results having the same t(Im) within experimental error. On the other hand, if curves are plotted for a number of masses originating from more than one component, separate families arise each corresponding to a single component. Thus, the number of components present in a mixture is determined by the number of families obtained in the analysis of the data. Experience has shown that two components can be separated if their t(Im)'s differ by more than 0.2 min. in the range of 0 to 10 min. total distillation time. Several curves for the two component system acetophenone azine-acetylalanine are shown in Figure 2.

The number of elimination curves that can be plotted for a mixture depends only on the number of peak intensities measured in the spectra. If automatic data acquisition equipment is available, curves can be plotted for all peaks above a certain minimum intensity. On the other hand, if intensities must be measured manually, curves will ordinarily be plotted only for the more significant spectral peaks.

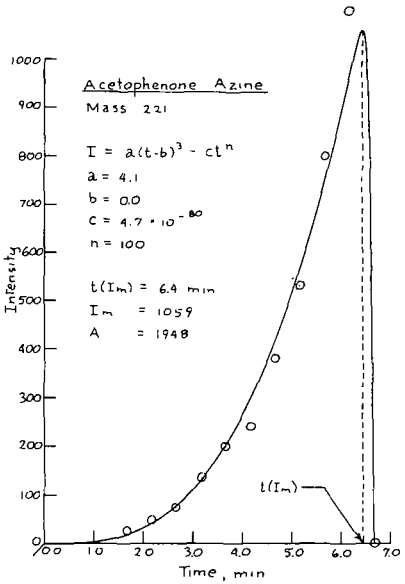

Figure 1. Elimination Curve for a Single Mass

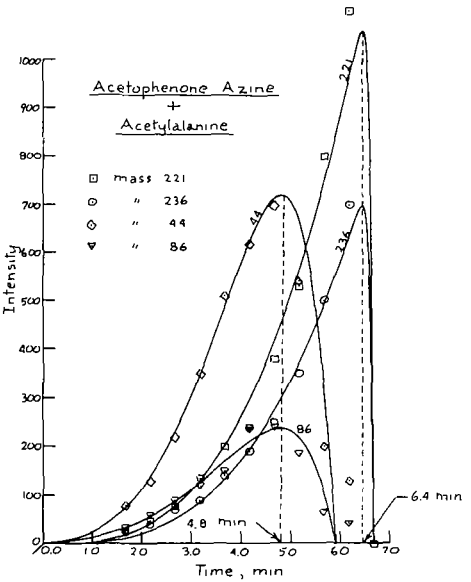

Figure 2. Elimination Curves for Masses Arising From Two Different Components

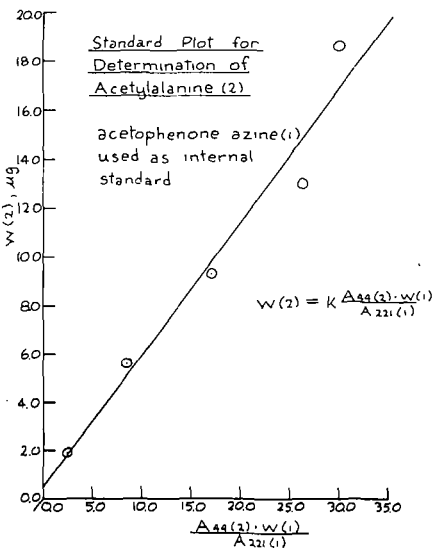

Figure 3. Quantitative Results for a Two-Component System

When an attempt is made to obtain the elimination curve for a mass arising from more than one component -- e.g., mass 43 in the spectra of a mixture of hydrocarbons -- the computer either rejects the data after a set number of iterations or else it produces a root mean square deviation which is abnormally high. In these cases, it is possible to use the constants determined for the different components present to plot a composite elimination curve from which the pertinent information for the origin of the mass can be obtained. Thus, t (Im), Im, and A can be approximately determined for each component adding to the intensity of the mass. This method is more or less successful depending on the nature of the individual data.

The results for eleven masses measured in the spectra of the acetophenone azine-acetylalanine mixture are given below.

Mixture of Acetophenone Azine + Acetylalanine

Mass	t(Im)	Im	A	Rel I (Im)	Rel I (A)	Rel I (Std)
			Acetophenone Azine			
236	6.4 min	697	1283	57.4	57.4	67.5
221	6.4	1059	1948	87.2	87.2	93.9
180	6.4	155	285	12.8	12.8	13.4
159	6.4	284	523	23.4	23.4	24.4
118	6.4	491	903	40.4	40.4	37.9
103	6.4	349	641	28.7	28.7	25.9
77	6.4	1214	2233	100.0	100.0	88.6
			Acetylalanine			
131	4.9	23	63	4.4	4.7	3.7
86	4.8	238	632	45.5	47.2	50.0
74	4.9	65	177	12.4	13.2	9.2
44	4.8	719	1807	137.6	134.9	138.0

$$\text{Rel I} = \frac{100n}{2} \cdot {}^{I_i}/_{\Sigma I_i}$$

n = no. of peaks

Note that the elimination curves obtained for acetophenone azine peak out at 6.4 min. and those for acetylalanine at 4.8-4.9 min. Relative intensities for the spectra of the components can be calculated either from Im or A. As seen from columns 5 and 6 these will be the same within error limits depending on the quality of the data. In column 7 are listed the relative intensities of the standard compounds run separately under isothermal and fast scan conditions. These are to be compared with the micromolecular distillation results in the two previous columns.

Mention should be included here on the method used to calculate relative intensities. These are actually given in percent ionization except that the results are multiplied by n/2 where n is the total number of masses used in the calculations. This method shares the advantage of %Σ in that the intensities are not relative to any one base peak and thus are not subject to the error inherent in the measurement of that peak. On the other hand, by multiplying the intensities by n/2 they are forced to fall in a range which generally runs from zero to 100 (or occasionally higher as seen for the acetylalanine data). Thus, the intensities can be read or visualized more conveniently than if they existed as small decimal fractions. This is particularly true for spectra containing a large number of peaks, in which case the %Σ numbers are generally very small. It should be noted, however, that the micromolecular distillation technique is not dependent on any one method of expressing intensities and that the calculations given here are primarily for the convenience of the authors.

The quantitative results for the two-component system are shown in Figure 3. Here, acetylalanine is considered the unknown and acetophenone azine an internal standard. The amount of acetylalanine present in a sample is determined from the equation

$$w(2) = K \frac{A_{44}(2) \cdot w(1)}{A_{221}(1)}$$

where w(2) is the weight of acetylalanine present, $A_{44}(2)$ is the area under the elimination curve for mass 44 in the spectrum of acetylalanine, $A_{221}(1)$ the corresponding area for mass 221 in the acetophenone azine spectrum, and w(1) the weight of

acetophenone azine added to the sample. The constant K is simply the ratio of the sensitivities for the two masses (area under the elimination curve ÷ the amount of component present). Note that K is independent of instrument operating conditions. The determinations would actually be more accurate if the sum of the areas under the curves were used in place of the areas determined for single peaks.

Theoretically, the line in Figure 3 should go through the origin. The finite value for the Y intercept occurs instead because the data were fit to an equation of the type Y = mx + b by the method of least squares. Thus, the effect of data scatter is enhanced for the purpose of testing the theory. In actual quantitative analysis calculations the line should probably be forced through zero.

Acknowledgements. The authors wish to express their appreciation to C. O. Hansen and D. G. Mannering for helping to program the mathematics of the least squares technique and to J. S. Bird for assistance in measuring the spectra.

REFERENCES

1. H. G. Langer, Seventeenth Annual Conference on Mass Spectrometry and Allied Topics, Dallas, May (1969) Paper No. 73.
2. B. B. Goshgarin, *Ibid.*, Paper No. 49.
3. H. L. Friedman, H. W. Goldstein, and George A. Griffith, Fifteenth Annual Conference on Mass Spectrometry and Allied Topics, Denver, May (1967) Paper No. 8.
4. W. W. Wendlandt, T. M. Southern, and J. R. Williams, Anal. Chim. Acta, *35*, 254 (1966).
5. H. G. Langer, R. S. Gohlke, and D. H. Smith, Anal. Chem., *37*, 433 (1965).
6. K. D. C. Hickman, Ind. Engr. Chem., *29*, 968 (1937).
7. N. D. Embree, *Ibid.*, p. 975.
8. K. D. C. Hickman, *Ibid.*, p. 1107.
9. M. G. Allcock, R. Belcher, J. R. Majer, and R. Perry, Anal. Chem., *42*, 776 (1970).
10. R. Belcher, J. R. Majer, R. Perry, and W. J. Stephen, Anal. Chim. Acta, *45*, 305 (1969).
11. *Ibid.*, *43*, 451 (1968).
12. B. R. Kowalski and T. L. Isenhour, Anal. Chem., *41*, 998 (1969).
13. A. E. Jenkins, and J. R. Majer, Talanta, *14*, 777 (1967).
14. J. M. Ruth, Anal. Chem., *40*, 747 (1968).
15. J. M. Ruth and J. N. Damico, Sixteenth Annual Conference on Mass Spectrometry and Allied Topics, Pittsburgh, May (1968) Paper No. 133.
16. W. F. Haddon, E. M. Chait, and F. W. McLafferty, Anal. Chem., *38*, 1968 (1966).

Gas Analysis in Films by Laser-Induced Flash Evaporation and Mass Spectrometry **K9**

Harold F. Winters and E. Kay

IBM Research Laboratory, San Jose, Calif. 95114

The presence of gases in thin films is known to significantly affect their physical properties. This is particularly important in sputtered films which are usually grown in a high pressure discharge.[1,2] A gas analysis technique, briefly described earlier,[1,2] has been perfected to systematically study the gas content of nitrogen and argon in sputtered films. This method involves laser induced flash evaporation of a small portion of the film followed by mass spectrometric analysis of the gas which has been released into a closed volume. In contrast to a related method, described by Guldner, the laser method evaporates less than 1 mm^2 per shot leaving most of the film undamaged. Moreover, mass spectrometric analysis allows concentrations smaller than 1 part per billion to be measured under ideal conditions.

This type of analysis is applicable for determining the noble gas or nitrogen concentrations in most film-substrate systems. Standards are not needed since the mass spectrometer is calibrated as a function of pressure using a Meleod and/or an ionization gauge. This method also has the advantage that it can be conducted in ultra high vacuum systems which are used for other purposes.

The fact that the area of the film from which the gas is released is closely approximated by the area which is visibly damaged by the laser beam has now been demonstrated for a variety of gas-film-substrate combinations. Hence a knowledge of the weight of the film, the damaged area, and the partial pressures of released gas allows calculations of the desired concentrations.

Whereas the technique has been shown to be exceedingly sensitive for such gases as nitrogen, argon and xenon, the accuracy of the present level of development is only good to ±25% at best. Similar sensitivity and accuracy is expected for the other noble gases. However, there are experimental questions which remain to be answered for some of the chemically active gases. The released oxygen, for example, appears mainly as CO and CO_2. It is possible that the partial pressures of these two gases may be a good indication of the oxygen content of the film. However, phenomena such as reversible CO adsorption on the vacuum system walls and the desorption of CO resulting from the presence of atomic and molecular oxygen must be investigated further before one can convincingly argue that the oxygen analysis is quantitative.

Most active gases will be adsorbed on the walls of the vacuum system if they are desorbed in the atomic form during flash evaporation.[4,5] In this case the pressure increase in a closed volume is not a reliable indication of the gas content. Hydrogen is expected to be desorbed to some extent as atoms[6] making quantitative analysis difficult.

Nevertheless, each evaporation produces a significant amount of H_2 which at worst places a lower limit on the concentration and at best is directly proportional to that concentration.

Temperature dependent affects such as the desorption of atoms have been detected in the following manner. The amount of energy in the laser pulse is changed by placing optical filters in the path of the laser beam. This changes the maximum temperature attained by the evaporated material. The presence of temperature sensitive phenomena is detected by showing that the measured concentration is a function of the energy in the laser pulse.

The gettering of devices such as the mass spectrometer and ion gauge can produce significant errors in this type of micro-analysis.[7] However, the affect of these devices can be minimized by using low work function emitters and by using very low emission currents.[1] For example, the partial pressure of CH_4 ($\sim 6 \times 10^{-6}$ Torr) will be reduced by a factor of two in 60 seconds if a standard ion gauge is operated at 1×10^{-3} amp emission, whereas, the pressure will be reduced by less than 2% during the same period if the emission is 1×10^{-7} amps. Results of a similar type have been observed for the mass spectrometer.

The affect of gettering by the laser evaporated material has been discussed in a previous paper.[7] In many instances there is no gettering. However, in cases where gettering occurs one can evaluate its significance by evaporating a relatively gas free film of the same thickness in the presence of partial pressure of the gas of interest. If gettering occurs the pressure will immediately decrease.

In conclusion, laser induced flash evaporation followed by mass spectrometry has been shown to give quantitative results for a number of gases and qualitative results for others. Methods of detection and prevention of several sources of error in this type of analysis have been discussed.

1. Harold F. Winters and Eric Kay, J. Appl. Phys. 38, 3928 (1967).
2. E. Kay and H. F. Winters, 1965 Transactions of the Third International Vacuum Congress, H. Adams, Ed. (Pergamon Press, Inc., New York, 1967), Vol. 2, pt. 2, p. 351.
3. W. G. Guldner, IEEE Trans. Component Parts CP-11 (1964).
4. H. F. Winters, D. E. Horne, and E. E. Donaldson, J. Chem. Phys. 41, 2766 (1964).
5. H. F. Winters, J. Chem. Phys. 44, 1472 (1966).
6. I. Langmuir, J. Am. Chem. Soc. 37, 417 (1915), and subsequent papers.
7. See for example, Harold F. Winters, J. Vac. Sci. & Tech. 7, 262 (1970).

GAS SAMPLING DEVICES FOR MASS SPECTROMETRIC ANALYSIS OF HERMETICALLY SEALED SYSTEMS

R. E. Witkowski and A. Pebler
Westinghouse Research Laboratories
Pittsburgh, Pennsylvania 15235

Several devices have been constructed and used in the laboratory to sample gases from encapsulated devices and hermetically sealed systems for mass spectrometric analysis. In addition to obtaining quantitative gas analysis, a means for establishing the pressure and quantity of gas within the sealed system has been incorporated in the sampling systems. Most sampling devices are integrated into the inlet system of the CEC 21-103 mass spectrometer and permit the analysis of hermetically sealed gas samples with the same rapidity as those stored in valved containers. The devices are capable of sampling sealed systems having pressures in the range of 10^{-6} - 10^{2} atm containing as little as 10^{-5} cc-atm of gas and can be used at temperatures as high as 400°C. The analyses are programmed in BASIC language using a remote terminal and provide information regarding evacuation, flushing and filling procedures, chemical reactions and the effectiveness of sorption or getter materials within the hermetically sealed device or systems. Several sampling devices will be described and their use illustrated.

L1

A Miniature Cold-Cathode Ion Source/Quadrupole Residual Gas Analyzer. F. L. TORNEY, Norton Research Corp., Cambridge, Mass. 02142.

A miniaturized version of the cold-cathode ion source residual gas analyzer reported previously[1] has been developed. The instrument, including all operating electronics is mounted in a cylindrical container 4½" o.d. x 12⅜" long. The unit weighs less than 5 lbs. and requires only 5.2 watts average power from a 28 volt dc source. The instrument mounts on a single UHV flange located at the ion source entrance. The mass range 1-50 amu is scanned automatically and a voltage analog of the mass number is provided. Peak width is nearly constant and is 1 amu or less (at 5% of height) over the entire mass range. The electronics utilizes integrated circuit operational amplifiers for high gain feedback control of the quadrupole parameters. A 6 decade logarithmic electrometer displays the full range of peak amplitudes on a 0 to 5 volt analog output. The minimum detectable nitrogen partial pressure is 10^{-10} Torr.

[1] F. L. Torney & P. Blum, 14th Annual Conference, Dallas, Texas, 1966.

This work was sponsored by NASA-Langley Research Center under Contract NAS1-5347, Task 14.

A COLD-ELECTRON SOURCE SUITABLE FOR MASS SPECTROMETRY

L2

J. F. Sprouse, K. M. Jackson, T. A. Raju, and M. K. Testerman

Department of Electronics and Instrumentation
University of Arkansas Graduate Institute of Technology
Little Rock 72203

A cold electron source which operates by a mechanism other than thermionic has been developed[1,2]. This source possesses the potential for use in instrumental applications and has been used in a mass spectrometer. It operates at approximately room temperature and produces non-collimated electron output currents of the order of 100-200 microamperes. A collimated output current of approximately 1 to 3 microamperes can also be obtained by making the emitted electrons traverse the inner diameter of a length of Vycor capillary tubing.

Figure 1 shows schematically the vapor-deposition apparatus used to deposit conductive tin oxide films along the inner diameter of a section of capillary tubing[3]. The capillary tubing is cut to length and cleaned with hot chromic acid and rinsed in distilled water. It is then sealed by means of an asbestos seal into one end of a section of delivery tubing. The opposite end of the delivery tubing is connected by means of tygon tubing to a flow-meter and then to an oxygen cylinder. The capillary tubing and delivery tube are extended into a furnace at 600°C. The system is allowed to reach thermal equilibrium; then approximately 0.2 milliliter of 0.2 molar $SnCl_4 \cdot 5H_2O$ is injected into the delivery tube by means of a hypodermic syringe. When the solution contacts the hot glass, hydrolysis occurs, producing vapor which is carried through the inner diameter of the capillary tubing. A conductive film of tin oxide is deposited along this diameter with oxygen acting as a carrier gas (F = 0.6 l/min) and oxidizing agent to the system.

Figure 2 shows the general structure of a typical capillary electron emitter after films have been deposited. Metal contacts are vacuum evaporated on to the end surfaces and extend approximately 5 millimeters from both ends along the outside of the tubing. The metal contacts also extend approximately 1 millimeter along the inner diameter of the tubing from both ends. This allows an electrical ohmic contact to be formed with the tin oxide film. The tin oxide film is electrically etched near one end of the capillary tubing[4]. This etch is made by using a tungsten or stainless steel probe and applying 50 to 150 volts on the probe relative

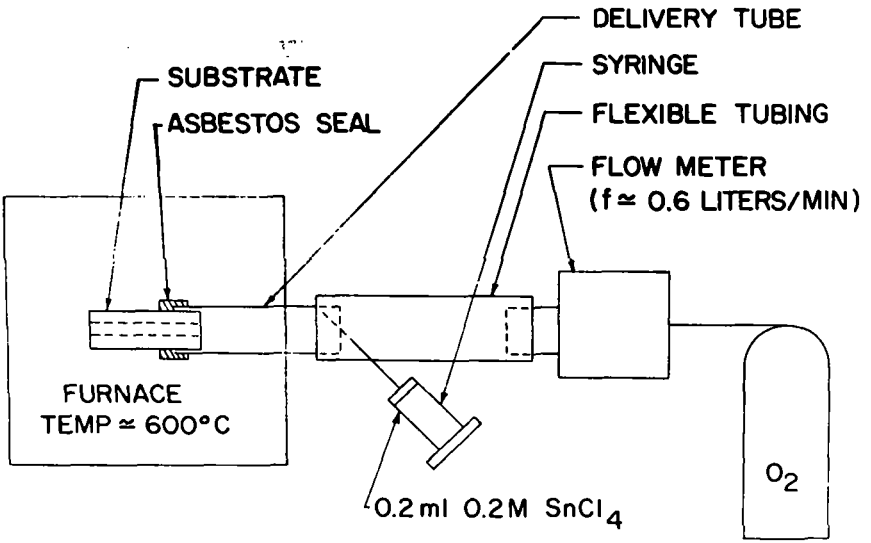

Figure 1. SnO_2 Vapor Deposition Apparatus

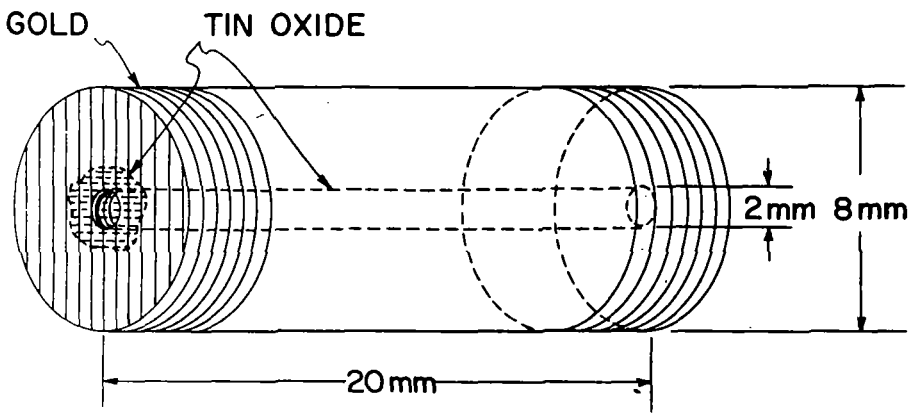

Figure 2. Capillary Electron Emitter

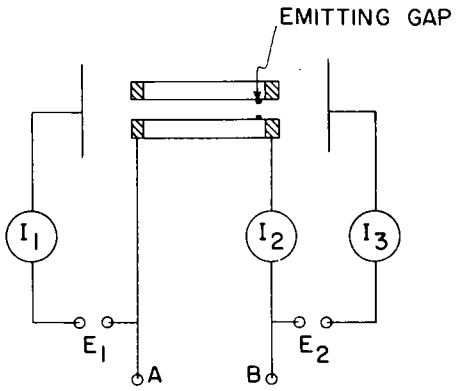

BIAS VOLTAGE	A	B	ELECTRON OUTPUT	ION OUTPUT
FORWARD	GROUND	+300V	NON-COLLIMATED	COLLIMATED
REVERSE	+300V	GROUND	COLLIMATED	NON-COLLIMATED

Figure 3. Capillary Emitter Testing Circuit

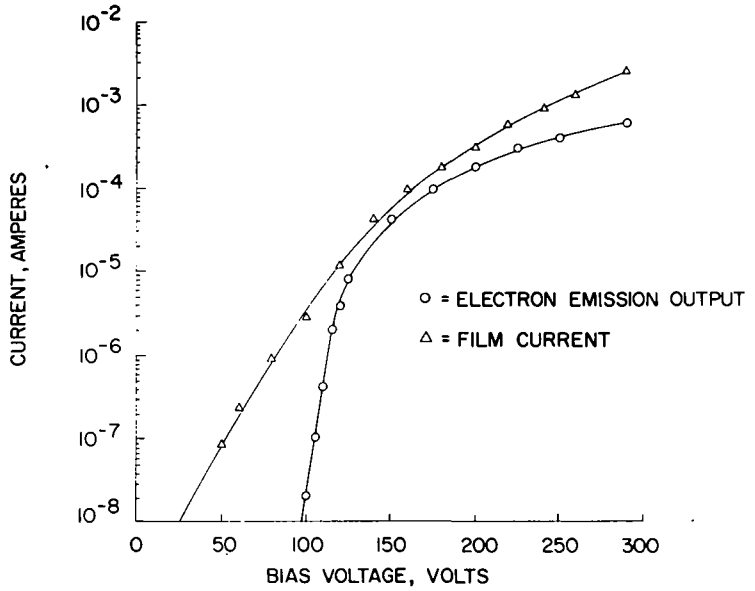

Figure 4. Voltage-Current Characteristic Curves for a Cold Electron Emitter

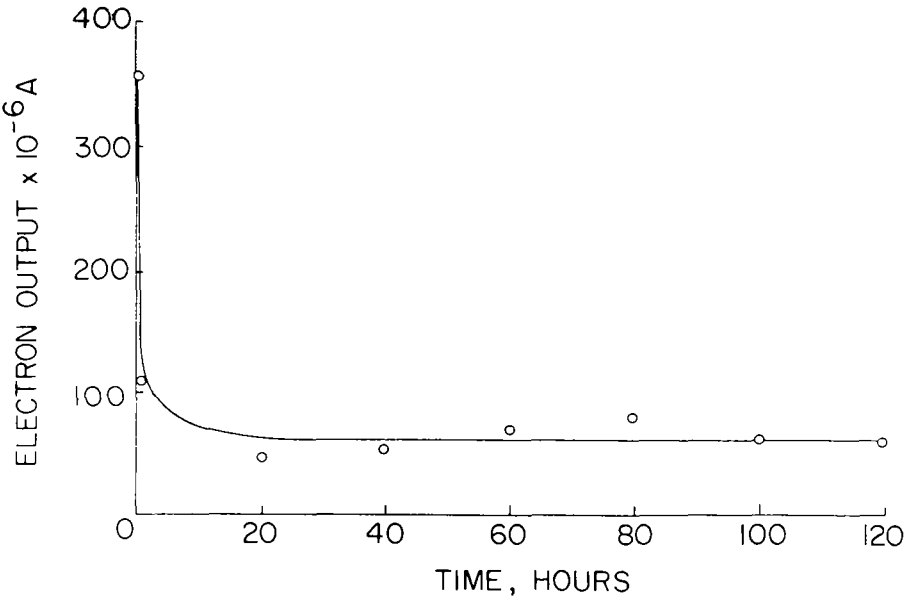

Figure 5. Electron Output Vs Time

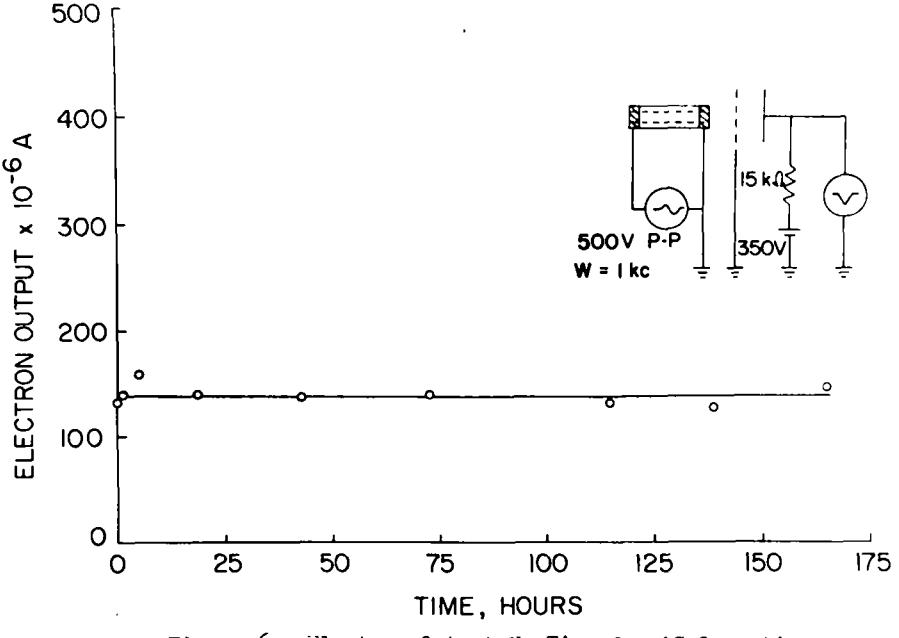

Figure 6. Electron Output Vs Time for AC Operation

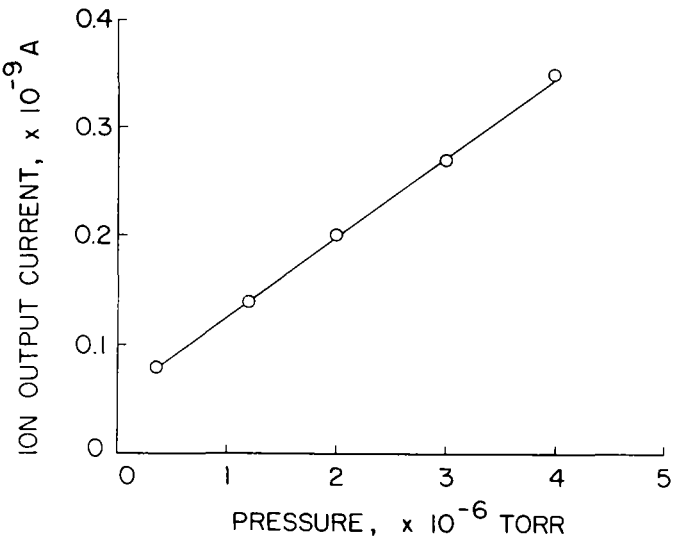

Figure 7. Ion Output Current Vs Pressure

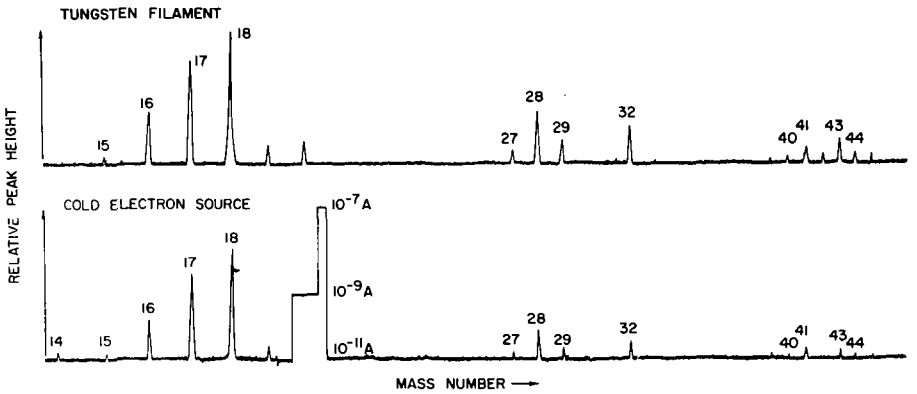

Figure 8. Spectra of Mass Spectrometer Background

to the capillary. The etch is usually made approximately 1 to 2 millimeters inside the inner diameter of the tubing. Before the etch, the electrical resistance from one end of the device to the other is approximately 1 kilohm. After etching, the resistance is increased to approximately 150 kilohms and the electron emission is acquired by applying 300 volts across the device (end to end).

Figure 3 shows a typical schematic diagram of a circuit which is used for activating and testing the emitter. The emitter is activated by placing 300 volts across the device for approximately 1 to 3 hours. The amount of time required for activation is determined by periodic checks of the output electron emission. The micron sized emitting region forms at the electrical etch and essentially all of the bias voltage is dropped across this region. After activation one of two modes of operation is used: (1) The forward bias position is with contact A at ground potential and contact B at +300 volts. This produces a non-collimated electron output since the emitting region is near to the end of the capillary with +300 volts applied. The electron output current is measured as I_3 and I_1 is the collimated ion beam output current. (2) The second mode is the reverse bias position with contact A having +300 volts applied to it and contact B is at ground potential. The electron output is now collimated and measured as I_1. The ion output is non-collimated and measured as I_3. I_2 is the film current passing through the emitting region and, when combined with the electron output current, can be used for determining electron emission efficiency in the forward bias mode.

Figure 4 shows the voltage-current characteristic curves for a cold emitter in the forward bias mode. The voltage-output current relationship appears to be exponential for small emitter electron output currents (1×10^{-6} amperes) and linear for outputs greater than 1×10^{-6} amperes up to the maximum electron output obtainable. After reaching maximum electron output the device tends to "saturate" with further increases in the bias voltage. The bias voltage-film current characteristics seem to follow essentially the same relationship as the output current-bias voltage. Under typical operation the film current will decrease to less than one milliampere after a short period of operating time. Initial electron emission is acquired at 40 to 80 bias volts depending upon the individual emitter.

Figure 5 shows the electron output current of a cold source for 120 continuous operating hours with 300V DC bias voltage applied. The output undergoes an exponential decay, becoming essentially constant after approximately 3 to 10 hours. Initial electron output is typically 100 to 300 microamperes and decays to a value

of approximately 50 microamperes. After operation the output electron current can be increased by placing the potentials on the device in the reverse bias mode for a short period of time. After return to forward bias again a sizeable initial output electron current is experienced and it undergoes an exponential decay as before.

Recent investigations into the behavior of the device under AC operation bias voltage have proven quite promising. Since the bias is reversed for a portion of the operating time cycle, the reactivation process of the device is utilized during actual operation. In contrast to the electron emitting behavior of the source in Figure 5, the same source after the 120 hour DC operation was operated using AC bias voltage. The electron emission current increased to 135 microamperes as shown in Figure 6 and remained essentially constant for 175 hours with no attempt at electron emission regulation. A 250 V peak, 1 kHz unregulated supply provided the AC bias voltage. The advantage of AC operation is readily apparent.

Figure 7 shows the ion current output generated by the emitter as a function of pressure in the 10^{-6} Torr pressure region. These data and others were obtained with the emitter operated in the forward bias condition and, thus, the device was generating a collimated beam of ions. At pressures less than 10^{-5} Torr a highly linear relationship exists between ion current and pressure. At pressures greater than 10^{-5} Torr the electron emission begins to decrease and; therefore, the ions generated per unit pressure decrease proportionately. However, the ratio of the ion current generated to the electron current emitted from the source remains constant. All of these data were obtained without any electron emission regulation.

Figure 8 presents a comparison of two background mass spectra obtained from a small magnetic sector single focusing mass spectrometer. The background in the analyzer tube was increased in both cases to 6×10^{-6} Torr by throttling the pumping speed of the diffusion pump. The top spectra was obtained while using a hairpin type tungsten thermionic filament as an ionizing electron source in a Nier type ion source. The tungsten filament was simply removed and the cold electron source placed in the same position. This source was reverse biased so that a collimated electron beam was generated which was aligned with the ion exiting slit of the Nier source. The bottom mass spectra was then obtained, all other factors remaining constant. As can be seen, there was no change in the resolution of the analyzer tube when the cold electron source was employed. It should be noted that the mass specta peaks are a logarithmic presentation.

The authors wish to express their sincere appreciation to Dr. John H. Hoffman at the University of Texas at Dallas for installing the cold source in his magnetic mass spectrometer and acquiring the spectra for this laboratory.

References

1. M. I. Elinson, A. G. Zhadan, G. A. Kudintseva, and M. E. Chugunova, Radioteknika i Elektronika 10 (8) 1500 (1965).

2. A. M. Soellner, J. F. Sprouse and T. A. Raju, J. Appl. Phys., 39; 1911 (1968).

3. L. Holland, "Vacuum Deposition of Thin Films", John Wiley and Sons, Inc. New York (1958) pp. 493-4

4. K. M. Jackson, "An Investigation of Methods to Improve Tin Oxide Thin Film Electron Emitters and Feasibility Study for Their Use as Ion Sources", M. S. Thesis, University of Arkansas (1970).

Routine isotopic analysis of solids for geological applications. L3

M.H. DODSON, D.R. DICKINSON and M.L. COLEMAN, Department of Earth Sciences, University of Leeds, England.

This paper outlines some modifications made to a commercial solid-source mass-spectrometer (A.E.I. MS5).[1] The developments were oriented towards the more efficient routine acquisition of geological data, including the precise measurement of isotopes of low abundance (e.g. ^{44}Ca or ^{204}Pb); they also had to be inexpensive and suitable for use by inexperienced operators. The two main changes were the adoption of peak-switching and digitisation of output.

Peak-switching, compared with continuous scanning of a mass spectrum, gives relevant data more rapidly. The system uses two circuits which are used to control the magnet current and accelerating voltage respectively. The former applies preset voltages to the basic magnet current power supply, for the selection of up to four peak positions. Although it is necessary to set up the switching routine in a cyclic pattern, and to keep to it; once the hysteresis loop has been set up for an element, it will remain stable over the period of a day's work, requiring very little adjustment. All peaks can be tuned to $\pm 1/30000$ in magnet field, or better, and the system has the advantage that drifts that may occur usually affect all peaks equally, and should not affect isotopic ratios. Stability is approximately 1/12000 in field, over a 20 minute run.

The other circuit is controlled by a three-position switch which produces small positive or negative increments to the normal value of the accelerating-voltage. This is used in two modes; to check tuning by peak centring, and to select positions away from the peaks for measurement of the baseline. In both these functions it has the advantage of not disturbing the hysteresis loop.

For the measurement of Calcium isotopes the large mass-differences involved made it difficult to set up a hysteresis loop. For this element a flux-integrating circuit controlling magnetic field (Dodson, in press), similar to Banner's mass marking system (Banner, 1968), has been used successfully. It has a response time of about 2 seconds, approximately three times better than the current control, and eliminates hysteresis effects.

The digitising system is similar in principle to that of Compston (Compston et al, 1965). A voltage-to-frequency converter (Hewlett-Packard) feeds a timer-counter (Advance); together they cost approximately half the price of the equivalent integrating-digital-voltmeter. With the large dynamic range of a 6 digit system, range-changing is avoided, even when measuring very low abundance isotopes. The integrating system gives objective averaging of a noisy signal during the gating period. A gate-time of 1 second or more is suitable for the output of the normal electrometer. The availability of gate-times of 2, 4 and 10 seconds extends the dynamic counting range for very small or noisy signals.

A parallel-entry printer was used alone initially, but for paper-tape output a serialising interface is necessary. Thus the output from the counter is fed to a serialiser, and from there to a serial-entry printer and tape-punch (both Addo, although a Westrex Teletype terminal might be more versatile). The gain in speed of magnetic tape is of no use in our application. Hence the choice of paper-tape, which gives a great saving in cost and is the standard input medium of the university computer. The capacity of the system, 1 reading per second, is quite adequate, in relation to the response of the ion detector and the magnet.

In use, the timing of the scanning program is controlled by the display time control set on the counter: the operator selects the next position as soon as the previous one has been counted. (An automatic peak selector is being built). The delay during the display time allows the magnetic field to achieve its new value. Delay times of 2 - 11 seconds are used as necessary, depending upon the response-time of the magnet or the

---

[1] To be submitted to J. Sci. Instrum.

time taken for depolarisation of the output resistor after passing a large signal.

Two main sorts of scanning routine are used. For rough work, the baseline values are averaged before and after a series of cyclic peak measurements. Alternatively, if the baseline is read once or more during each cycle, greater precision is obtained; standard errors within a run of 10 - 20 scans are 0.02 - 0.05‰, while between-run variation is sometimes as great as 0.1‰, possibly because of small-scale irregularity in the shape of the peak top.

Banner, A.E., 1968. 16th Conf. Mass Spectrometry, Pittsburgh, Paper 92.

Compston, W., Lovering, J.F. and Vernon, M.J. 1965. Geochim. Cosmochim. Acta 29, 1085.

Dodson, M.H., in press, J. Sci. Instrum.

Application of Sorption and Ion-Getter Pumping to the Sliding-Shaft Vacuum Lock*†

J. J. Stoffels

Pacific Northwest Laboratory, Battelle Memorial Institute
Richland, Washington 99352

A sliding-shaft vacuum lock made of sintered alumina was recently described[1]. Three stages of differential pumping were provided on the vacuum lock by two rotary pumps and a baffled oil diffusion pump. Experience revealed that, in the brief (15 sec) passage through the lock, samples were contaminated by backstreaming oil vapors from the pumps. It was decided to eliminate the source of contamination by use of a completely oil-free vacuum system. The use of sorption and ion-getter pumps to handle a dynamic gas load such as that associated with the sliding-shaft vacuum lock was untried. Calculations indicated, however, that a sorption pump could handle the quantity of gas involved in operating a vacuum lock for an 8-hour shift without becoming saturated.

Single sorption pumps containing 6.6 kg of molecular sieve material were connected through valves to the first and second pumping stages of the vacuum lock. A 25 ℓ/sec ion-getter pump was connected directly to the third pumping stage. The pressure attained against a constant leak from atmosphere is an order of magnitude lower (0.1 Torr) at the first pumping stage than the pressure attained with a 140 ℓ/min rotary pump. Other pressures are essentially as before.

Liquid nitrogen consumption for each sorption pump is about 1 ℓ/hr plus 5ℓ for initial chilldown. The sorption pumps are rejuvenated each night by allowing them to come to room temperature. A static O-ring seal at the atmosphere end of the vacuum lock permits rejuvenation of the sorption pumps without loss of vacuum.

---

* This work was supported by the United States Atomic Energy Commission

† Submitted for publication in full in the Journal of Vacuum Science and Technology

1 J. J. Stoffels and C. R. Lagergren, Rev. Sci. Instrum. 40, 1288 (1969)

A Stabilized Peak Switching System

P.C. Rankin ARS, USDA, Beltsville, Md. 20705
W.H. Craig and C.F. Hammer, Georgetown University, Washington, D.C. 20007

Under normal operating conditions the positive ion mass spectra of most compounds are complicated by the large number of fragment ions. Fortunately most compounds have characteristic ions in their mass spectra and if a mass spectrometer could be made to selectively detect these characteristic ions, mixtures could be analyzed. A useful application for a mass spectrometer which would selectively detect characteristic ions would be in isotopic kinetic studies. Non-deuterated and deuterated species of a compound are eluted from most g.l.c. columns with essentially the same retention times and if one was able to reduce these unresolved g.l.c. peaks, changes in the composition on non-deuterated/deuterated mixtures could be measured.

There are several ways of using the mass spectrometer as a selective detector for unresolved g.l.c. effluent analysis. An automated system was reported by Sweeley in 1966 (Anal.Chem,38,1549(1966). The basis of this system and the one reported in this paper is to alternately change the accelerating voltage in a square wave function so that pre-selected characteristic ions are alternately focussed at the detector.

One of the greatest problems encountered in trying to repeatedly refocus a mass spectrometer at a given m/e value is that of instrumental drift. Most instruments have short term stability but for extended work over longer periods of time instrumental parameters change so that constant adjustments have to be made to keep the ion beam focussed on the collector slit. There are several possible approaches to this problem with the most common being the use of wide slit settings to obtain broad flat-topped peaks. This is not a good practical approach as one is operating at low resolving power and for work extending over several hours a constant check on the ion beam focussing is still necessary. Our approach has been to automatically center and stabilize the ion peak during each voltage step of the high voltage switching. This results in minor retuning each time an ion peak is focussed on the detector.

The peak switching circuitry consists of four main sections. They are
(a) main logic and driver circuits
(b) high voltage switching circuits
(c) integrator circuits
(d) peak locking circuit

The main logic and driver circuits are all solid state and control the various switching procedures. The accelerating voltage switching circuitry enables us to switch to three different accelerating voltages. This number of channels was an arbitrary choice and could be extended if necessary. In our present system the switching time of the high voltage is limited by the response time of the 8 Kv. power supply. We have been operating at 1 cycle/second switching speed but planned modifications will enable us to increase this tenfold. We did try the approach of magnet current switching but hysteresis effects limited the switching speeds severely. There are three operational amplifier integrators; one for each channel. The integration data (taken during the time the particular ion is focussed on the detector) is read out on a digital voltmeter at the conclusion of a g.l.c. peak analysis. The locking circuit consists of a 5 KH$_z$ oscillator which provides a variable amplitude signal to modulate the accelerating voltage. When the accelerating voltage is adjusted so that the ion beam for a particular ion is focussed on the collector slit, the 5 KH$_z$ modulation slightly shifts the ion beam either side of the true focus at a 5 KH$_z$ rate. The result is a small AC signal superimposed on top of the DC ion intensity signal. A 5 KH$_z$ component filtered out of the detector signal has a phase shift relative to the original 5 KH$_z$ modulating frequency. This is caused by slight ion beam shifts about the true focus position. The recovered signal is synchronously rectified and filtered to produce a DC signal proportional to the deviation of the ion beam from the true focus position. The DC output from the phase detector is fed back to the high voltage supply as an error signal to correct for any instrumental

drift. This system enables the mass spectrometer to remain focussed on an ion peak for hours of switching time yet permits us to retain the resolving power capabilities of the mass spectrometer. We routinely operate at a resolving power of 2000 for g.l.c. peak analysis.

The maximum mass range of switching in the present design of the electronics is in the ratio of 1:2. However, the further apart the mass of the ions are the slower the switching speed possible. Also corrections for differences in ion beam energies would be necessary. The system has few operator controls and is a self-contained device requiring only a few minor modifications to the existing mass spectrometer. When the peak switching device is turned off the mass spectrometer operates normally.

Results on a number of non-deuterated/deuterated mixtures indicate an accuracy of better than 1%. This accuracy holds for wide ranges of d_0/d_1 ratios in the composition of the analyzed g.l.c. peak. Standardization procedures are necessary since some non-deuterated/deuterated mixtures either fractionate in the molecular separator or are selectively ionized. This latter occurs more predominantly at 20 ev than at 70 ev. For any given mixture only one standard sample need be analyzed and the constant factor so determined can be applied to the experimental data, as long as instrumental parameters are kept constant (e.g. slit width, band pass).

MASS SPECTROMETRIC SAMPLING OF SHOCK TUBE FLOWS

George Sanzone
Dept. of Chemistry, Virginia Polytechnic Institute, Blacksburg, Virginia 24061

R. Linn Belford
Dept. of Chemistry, University of Illinois, Urbana, Illinois, 61803

ABSTRACT

This paper reports recent theory and experiments involving the direct mass spectrometric sampling of shock tube flows. Experiments involving both steady orifice-nozzle flows and dynamic sampling of the reflected-shock region clearly demonstrate the importance of not only the geometry of the ion source but also the location and geometry of the free jet. It was found that the jet could be sampled independent of both static and dynamic background gas only at the orifice.

It is shown that the geometry of the jet boundary can be approximated, in the vicinity of the orifice, by the equation

$$y = 0.5D + 4.0\,x^2 \qquad (1)$$

where D is the diameter of the orifice or nozzle, y is the radial distance from the jet centerline to the jet boundary at a distance x from the nozzle throat.

The location of x_o, the virtual point source of the jet expansion, is given by the equation

$$x_o = \left\{0.20\,f - 0.56\right\} D, \qquad (2)$$

where x_o is the downstream distance from the orifice throat to the point-source expansion center of the underexpanded jet; f is the number of active degrees of freedom in the gas.

Glick and Hertzberg gave criteria for calculating the minimum start-up time of a nozzle. Application of these same criteria to the formation time of the free jet leads to the following equation.

$$\Delta t_{jet} = \frac{0.0152}{a_5 \tan A} \left\{\frac{5.43}{\gamma}\right\}^{5/2} \left\{\frac{X}{D}\right\}^{\frac{5(\gamma-1)}{2}} \qquad (3)$$

a_5 is the sound speed in the sampled reflected-shock region while A is the angle from the jet centerline to the widest diameter of the jet's Barrel Shock; Δt_{jet} is the jet-formation time at a distance x downstream of the nozzle throat while Y is the heat capacity ratio Cp/Cv. The validity of equation (3) is tested by comparison of its predictions with experimentally reported rise times.

This research was supported by National Science Foundation Grants GP-6986 and GP-17875 and by a Special Fellowship awarded to G. Sanzone by The National Committee for Air Pollution Control. Details of the work are reported in the Ph.D. thesis of G. Sanzone, University of Illinois, Urbana, 1969, and in publications to be submitted.

The Application of Field Ionization to GLC-MS Studies by J.N. Damico and R.P. Barron (Division of Food Chemistry and Technology, Bureau of Foods, Pesticides, and Product Safety, Food and Drug Administration, U.S. Department of Health, Education, and Welfare, Washington, D.C. 20204)

Introduction

Combined GLC-electron impact mass spectrometry for the analysis of GLC effluents is a widely used technique as evidenced by the excellent review articles and the references therein (1, 2). One of the most important bits of information obtainable from mass spectral data is the molecular weight of a compound. In electron impact ionization the relative intensity of the molecular ion for many compounds is very small and comprises a small percentage of the total ion yield. Components of interest in natural products are often present in the range of ppm or less. Accordingly, the total ion yield will be small and the molecular ion may be of low intensity and difficult to distinguish from column bleed and/or background. Field ionization (FI) was initially shown by Beckey (3) to be very effective in enhancing the relative intensity of molecular ions. For other examples (also see Table 1) and additional information on FI the reader is referred to a symposium on FI mass spectrometry (4). To the best of our knowledge no work has been published utilizing FI for the analysis of GLC effluents. The object of this report is to demonstrate that FI does have utility in combined GLC-mass spectrometry.

Experimental

All studies were made with an Atlas CH-4B mass spectrometer as supplied with a dual electron impact/field ionization source (EFO-4B). An exploded drawing of the GLC-MS system is shown in Fig. 1.

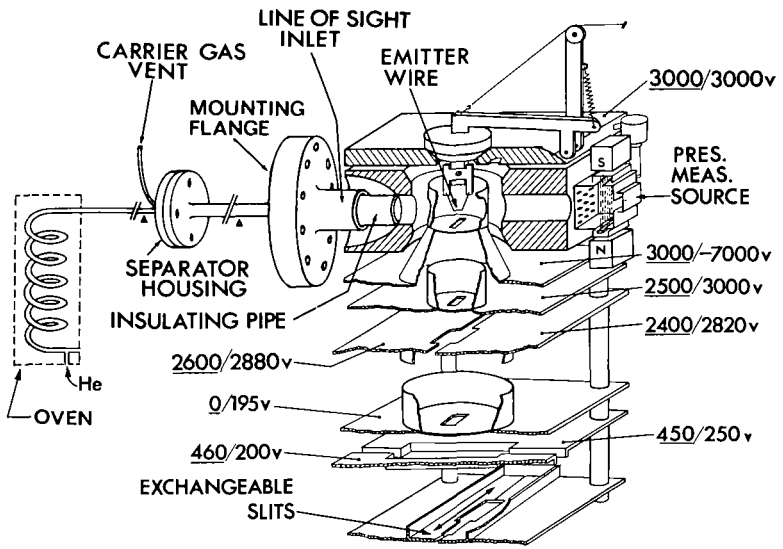

Figure 1. Exploded drawing of the GLC-MS system.

Instrumental Parameters. (1) Source exit and collector slits were 0.1 mm and 0.3 mm, respectively. The gain of the electron multiplier was usually 10^6. (2) The anodes employed were wires of 2.5 microns diameter, obtained commercially. They were activated as described previously (8) except that usually only 4 to 5 hours were required to approach maximum sensitivity. (3) The GLC detector was a pressure measuring source (PMS), an electron impact total ion collector. The electron energy was 20 ev and the trap current was 100 μa. The total ion monitor, widely used as the GLC detector for EI, is inadequate for FI because the total ion current is very small. For example, the maximum total ion current observed on the total ion monitor from FI of 2 μg of C_{10}Δlactone injected on the GLC column was about 10^{-14} amps, whereas the maximum response for the same amount of sample using the PMS was about 10^{-10} amps. (4) The column bath for the GLC was a Barber-Colman Model 5360 equipped with temperature programmer and controller. The bath also contained a flame ionization detector (FID); the effluent could be split to the FID and to the mass spectrometer. This made it possible to simultaneously monitor the effluent with the FID and the PMS. The column was a 6' x 1/4" O.D. glass coiled column packed with 10% diethylene glycol succinate on Gas Chrom Z, 100-120 mesh. (5) The GLC was

interfaced to the mass spectrometer with a permeable membrane separator (Varian, 5620). The membrane is a methyl silicone polymer layer 0.001" thick and has a surface area of 0.4 cm^2 exposed to the column effluent. Single-stage and double-stage membrane molecular separators in conjunction with 0.02 and 0.03" I.D. columns have been investigated by Black et al.(5). Insulated heating wire was used to heat the entire interface assembly which was mounted in line-of-sight to the ionization chamber. The carrier gas vent (see Fig. 1) for the effluent which does not permeate the membrane was sometimes monitored with a FID.

Results and Discussion

Although the sensitivity of FI is markedly less than EI, the FI spectra obtained from a 2 μg injection on the GLC column for $C_{10}\Delta$, $C_{12}\Delta$, and $C_{14}\Delta$lactones show molecular ion responses that have a greater S/N than is observed in the EI mode for these compounds (6).

Intense doubly charged ions were observed by FI but not by EI (6) for $C_8\Delta$, $C_{10}\alpha$, $C_{10}\Delta$, a lactones and for $C_{12}\alpha$, $C_{12}\Delta$, and $C_{14}\Delta$, b lactones. The lactones designated by a give abundant ions due to (M-0)++ which have relative intensities between 60-90%. In contrast the lactones designated by b give ions due to M++, but of about the same relative intensities as the (M-0)++.

During GLC-MS field ionization studies of food extracts containing carbonyl compounds, there were several instances when the response of the PMS and the molecular ion response were inconsistent. This suggested that some types of compounds might be more sensitive to FI than others. Accordingly, a FI sensitivity study was initiated. The system described in this paper offers a convenient way of doing this on a microscale. The results of this study are listed in Table 1. The maximum molecular ion response expressed in mv/μg is intended only for comparison purposes and does not imply that the sensitivity is linear. These results do show significant differences in sensitivity for various types of compounds. The ketones and lactones are the most sensitive of the group whereas the aldehydes and decyl acetate are the least sensitive. The experiments with decyl acetate were repeated at least ten times with comparable results.

In order to place credence in the sensitivity study (Table 1), the amount of sample which permeates the membrane must be known. The transmission of sample through the membrane was determined indirectly. The peak area response was obtained for a given sample injection with the column connected only to the FID in the column bath (C_{FID}), and again with the column connected directly to the membrane, the residual sample (RS_{FID}) being measured at the carrier gas vent with a FID. Percent transmission of sample through the membrane is equal to

$$\frac{\text{Peak Area Response } (C_{FID}) - \text{Peak Area Response } (RS_{FID})}{\text{Peak Area Response } (C_{FID})} \times 100$$

Table 2 shows that the aldehydes and decyl acetate permeate the membrane as well as the ketones and lactones. This indicates that the low sensitivity observed for these compounds (see Table 1) is in fact due to FI phenomena.

Although no data on alcohols are included in this report, a few were examined with very poor results. A 1 mg injection of decanol yielded only a very weak molecular ion peak (possibly M+1) (6). Similar results were observed with propanol. It appeared that the alcohols made the wire insensitive. Beckey (3) reported difficulty obtaining reproducible peak intensities for alcohols and suggested that this was caused by a monolayer of water on the surface of the wire anode produced by the alcohols. In addition to the decyl acetate studies, poor FI sensitivity was obtained for cis-9-tetradecen-1-ol acetate. These results indicate that esterification as acetates is not an effective means for enhancing the FI sensitivity of alcohols.

References

(1) W.S. Updegrove and P. Haug, Amer. Lab., pp. 8-30 (Feb. 1970).
(2) F.E. Saalfeld, Ind. Res., 11, 58 (1969).
(3) H.D. Beckey, "Field Ion Mass Spectra of Organic Molecules" in R.I. Reed (Ed.), "Mass Spectrometry," Academic Press, London and New York, 1965, pp. 93-127.
(4) Sixteenth Annual Conference on Mass Spectrometry and Allied Topics, ASTM Committee E-14, Pittsburgh, Pa., May 12-17, 1968. Papers numbered 9, 10, 11, 12, 21, 22, 23, and 24 (see also Int. J. Mass Spectrom. Ion Physics, 2, pp. 101-193).
(5) D.R. Black, R.A. Flath, and R. Teranishi, J. Chrom. Sci., 7, 284 (1969).
(6) Unpublished data from the authors' laboratory.
(7) ASTM Uncertified Mass Spectral Data File, No. 1809.
(8) Ibid., No. 1821.
(9) Ibid., No. 1822.
(10) Ibid., No. 1836.

Table 1. Field Ionization Sensitivity for the Molecular Ion of Some Carbonyl Compounds.

COMPOUND	AMOUNT INJECTED μg	MAXIMUM MOLECULAR ION RESPONSE mv/μg	RELATIVE INTENSITY OF MOLECULAR ION-% FI	EI	(Reference No.)
C_6 Δ LACTONE	50	45	100	6.6	(7)
$C_{10}\gamma$ LACTONE	30	100	100	0.3	(8)
$C_{10}\Delta$ LACTONE	30	250	100	3.5	(9)
$C_{12}\gamma$ LACTONE	30	88	100	0.1*	(6)
$C_{12}\Delta$ LACTONE	30	110	100	4.3	(10)
$C_{14}\Delta$ LACTONE	50	200	100	<0.1*	(6)
C_{10} ACID	250	12	100	4.0**	(6)
DECYL ACETATE	500	0.2	100	<0.3	(6)
C_{10} METHYL ESTER	40	62	100	3.6*	(6)
C_{12} METHYL ESTER	40	62	100	2.7	(11)
C_{14} METHYL ESTER	40	62	100	3.2	(12)
C_9 KETONE	50	70	100	4.9	(13)
C_{11} KETONE	50	200	100	2.5*	(6)
C_{15} KETONE	50	200	100	3.0***	(6)
C_8 ALDEHYDE	50	0.4	100	1.0	(14)
C_{10} ALDEHYDE	50	0.8	100	0.5	(14)
C_{12} ALDEHYDE	50	2	100	0.3	(14)

*Obtained with electron impact E-4B source using GLC-MS inlet.
**Obtained with electron impact E-4B source using direct probe.
***Obtained with EFO-4B source using GLC-MS inlet.

Table 2. Sample Transmission of Some Carbonyl Compounds Thru Polymer Membrane Separator.

COMPOUND	COLUMN TEMP. °C	MEMBRANE HOUSING °C	TRANSMISSION %
C_8 ALDEHYDE	80	30	43
C_9 KETONE	80	30	60
C_{11} KETONE	95	48	31
DECYL ACETATE	100	55	61
C_{10} ALDEHYDE	100	65	35
C_{10} METHYL ESTER	110	65	40
C_{12} METHYL ESTER	125	70	59
C_{12} ALDEHYDE	135	75	72
C_{15} KETONE	135	75	57
C_{14} METHYL ESTER	145	95	59
C_8 Δ LACTONE	155	80	29
$C_{10}\gamma$ LACTONE	170	85	48
$C_{10}\Delta$ LACTONE	180	85	46
$C_{12}\gamma$ LACTONE	195	92	62
$C_{12}\Delta$ LACTONE	205	100	54
$C_{14}\Delta$ LACTONE	225	100	72

References (contd)

(11) Ibid., No. 1081.
(12) Ibid., No. 1084.
(13) Ibid., No. 211.
(14) L.A. Gilpin and F.W. McLafferty, Anal. Chem., 29, 990 (1957).

Application of a High Resolution Double Beam GC-MS to Problems in Organic Chemistry.

L8

M.Barber, J.R.Chapman, B.N.Green, T.O.Merren and A.Riddoch.

A.E.I.Scientific Apparatus Ltd., Urmston, Manchester,England.

troduction.

ass spectral data suitable for mass measurement has usually been obtained at resolu-ons of the order of 10,000 or more. Campbell and Halliday (1) theoretically showed at electrically recorded mass measurement data obtained from a given amount of sample ould be just as accurate at reolutions lower than 10,000 and even as low as 1000 solution.

rthermore it can also be shown that by operating at low resolutions, mass measure-nts should be possible on smaller amounts of sample than at high resolution, albeit th less accuracy but nevertheless with sufficient accuracy to give useful information.

nfortunately, the inability of conventional instruments to separate the sample peaks om the reference peaks at low resolution has precluded carrying out mass measurements n this way except in a few limited cases. This objection is removed if the sample an be isolated from the reference by using a mass spectrometer in which there are two on beams on the same mass scale. Provided the mass scales in such a double beam nstrument can be precisely matched, one beam can be used to provide an accurate mass cale for the other, so enabling accurate mass data to be obtained on nanogram sample uantities. The high sensitivity achievable is an obvious advantagein the analysis of C eluents.. It is the aim of this paper to describe some work carried out on the MS30 ouble beam instrument at low resolution which shows that one beam can be used to eference the mass scale of the other beam with ppm accuracy.

Instrumental.

The essential features of the MS30 double beam mass spectrometer are shown in figure 1. Ions are produced by two independent ion sources in the usual way. These sources may be the same or different. For example both could be electron bombardment sources or one could be a electron bombardment source and the other a field ionization source. The same or different samples may be admitted to the two sources by a variety of inlet systems. After acceleration the ions pass out of the sources through two independently adjustable source slits. Immediately after leaving the source, each beam then passes through two sets of electrostatic deflection plates (not shown in the diagram) whose function is to bring the two beams closer together and direct them essentially parallel to one another into the electrostatic analyser. The two beams then pass side by side through the magnetic analyser, where they undergo mass separation in the usual way, and are refocused at two independently adjustable resolving slits. A separate electron multiplier and amplifier system for each beam allows the signals to be presented independently. Two total ion current collectors or monitors situated between the electrostatic and magnetic analysers enable either beam to be monitored. Essentially, therefore, the MS30 consists of two mass spectrometers which are independent with respect to sample introduction and data presentation but because the two beams share a common electrostatic and magnetic analyser, the spectra may be presented on the same mass scale. The two beams may be operated at the same or different resolutions.

Figure 2 illustrates a typical record obtained from the double beam instrument at 1000 resolution. The upper two traces show the parent region of 1-methyl naphthalene introduced into one source from the chromatograph and the lower trace shows the corresponding mass region of a reference compound, in this case perfluorokerosine (PFK), introduced into the other source. Since the peaks in the spectrum of PFK can be easily recognised, the masses of the peaks in the upper spectrum can be assigned. This spectrum was obtained by injecting 10 ngm of 1-methyl naphthalene onto the chromatograph column and scanning the mass spectrometer at 3 seconds per decade. During the time to scan from mass 200 to 10, about 3 ngm of sample were eluted from the column.

To show that one beam can be used to accurately mass reference the other beam, PFK was admitted to one source and hexachlorobutadiene (C_4Cl_6) was admitted to the other source. Both beams were set for 1000 resolution. Normally the two beams would be on the same mass scale in which case a two channel data system would be required. However, by displacing the mass scales in the spectrometer by an amount sufficient to ensure that sample and reference peaks occur separated in time when the instrument is scanned, a single channel data system may be used. The mass scale of the PFK reference was displaced relative to the C_4 Cl_6 sample by about 2000 ppm in mass. The two low resolution signals were then electronically combined in a simple adding circuit and the combined signal fed into the data acquisition and processing system (DS10) normally used for processing high resolution data. A series of 6, 10 second per decade scans were digitised at 12.5 KHz and the centroid of the peaks calculated by the computer.

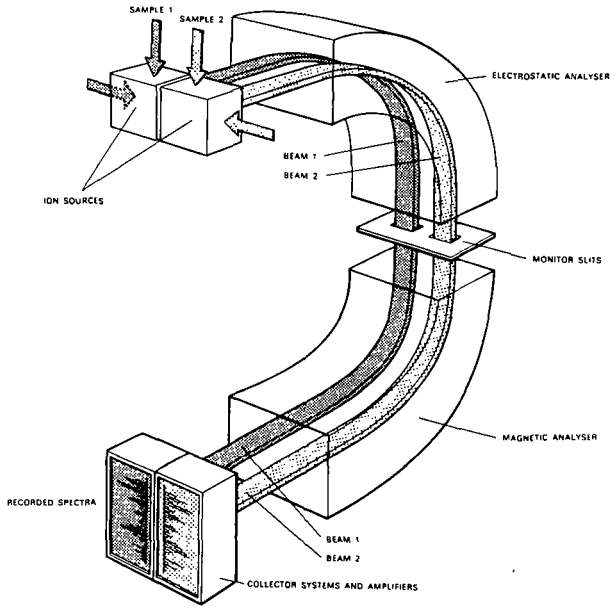

Figure 1. Principle of the MS30 double beam mass spectrometer

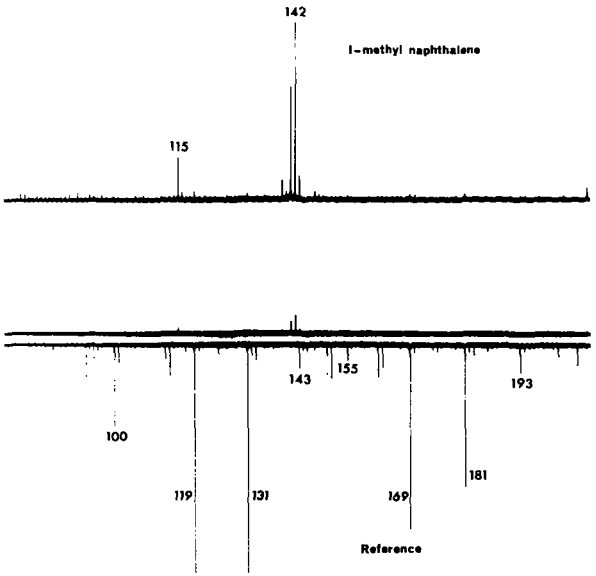

Figure 2. MS30: 10^{-8} g 1-methyl Naphthalene from G.C.

The masses of the peaks in the C_4Cl_6 spectrum were then calculated in the computer by the procedures normally used in high resolution single beam mass spectrometry using the PFK spectrum as the mass reference. The first and last of the six runs were used to calibrate the system, that is, measure the difference between the mass scales of the two beams. The results for the intermediate 4 runs calibrated in this way are given in table 1 below.

	Error (mmu)				
Mass	Run 1	Run 2	Run 3	Run 4	Mean
260	1.3	-0.2	3.1	-0.2	1.1
225	0.9	0.0	1.9	-1.6	0.3
188	-0.4	1.6	-0.3	1.4	0.6
153	1.9	1.7	-0.3	-1.7	0.4
118	-3.2	-0.6	0.8	0.6	-0.6
83	0.3	1.2	0.6	0.1	0.5
82	1.6	-0.5	-1.4	1.3	0.3
R.M.S	1.7	1.0	1.5	1.4	0.6

Table 1. Double beam mass measurement results at 1000 resolution.

It can be seen that all except two of the results are better than 2mmu and 68% are better than 1.5 mmu.

Discussion.

It has been shown that one beam of the MS30 double beam mass spectrometer can be used to reference the mass scale of the other beam with good accuracy. Furthermore the beams may be operated at resolutions as low as 1000. The accuracies which should be achievable with various amounts of sample are summarised in table 2.

Resolution	Sample Quantity (ngm)	Mass measurement Accuracy (ppm)	Intensity Range
10000	400	< 5	10:1
10000	200	< 5	10:1
1000	200	< 5-50	1000:1
1000	20	5-15	10:1
1000	2	15-50	10:1

Table 2. Variation of mass measurement accuracy with sample quantity at high and low resolution.

At 10,000, the usual resolution for mass measurement with the conventional single beam technique, a sample quantity of about 400 nanograms eluted from the chromatograph during the scan time would be needed to achieve accuracies better than 5 ppm. At 1000 resolution with the double beam technique, with 200 ngm injected on the column, mass measurements can be made over the same peak intensity range to the same accuracy as at 10,000 resolution. In addition, with this relatively large sample, the intensity range of peaks that can be detected at 1000 resolution is 100 times greater than at 10,000 resolution. Peaks down to 0.1% of the base peak can be observed and their masses at this level measured to an accuracy at least a factor 10 better than with the convential mass marker.

With only 20 ngm of sample injected on the column, mass measurements accurate to better than 15 ppm can be made. Actually on the more intense peaks, accuracies approaching 5 ppm should be achieved. It is worth noting that at 10,000 resolution with 40 ngm of sample, mass measurement data could be obtained only on the strongest peaks in the spectrum. Even with only 2 ngm of sample, the peaks can be detected and mass measured although the accuracies approach 50 ppm on the weakest peaks. Even so accuracies on the more intense peaks should approach 15 ppm.

Reference.

(1) Campbell, A.J., Halliday, J.S., 13th Annual Symposium on Mass Spectrometry, St Louis, 1965.

Improvements in Sensitivity in Ultra High Resolution Mass Spectrometry

S. Evans & B. Hallas

The performance of high resolution mass spectrometers has continued to improve year by year, in terms of the maximum useful resolution which can be achieved.[1] This improvement has been obtained by reducing instrumental aberrations, with until now little or no gain in sensitivity since Halliday [2] demonstrated that less than 100 nanograms of sample were required to obtain accurate mass measurements at 10,000 resolution. Such measurements could be achieved using a ten second/decade scan on the MS902 on peaks covering a considerable range of intensities. However, the amount of sample required for dynamic scans at higher resolution was considerably greater.

The limiting factor in obtaining high sensitivity at very high resolution was image curvature, originating from the passage of the ion beam through the inhomogeneous fringing fields of the magnetic sector.[3]

In the past, this effect was reduced by limiting the height of the beam in the z-direction, with the result that only a small fraction of the ions leaving the source actually reached the collector. By introducing hexapole image correctors, the principle of which was first suggested by Boerboom [4], image curvature distortion has been effectively eliminated in the MS902, thus enabling the beam height to be increased.

As a result of this the sample quantity now required for a 10,000 resolution, ten second/decade scan is reduced to 20 nanograms.

The effect of the hexapoles is most marked at higher resolution, however, and gives an effective increase in sensitivity of greater than a factor of 10 at 50,000. Under static conditions, the sensitivity now available at 40,000 resolution is roughly the same as that previously obtainable at a resolution of 10,000.

Setting up a mass spectrometer to obtain constant resolution over a wide mass range can be particularly difficult at very high resolution, as the effect of eddy currents and fringe field changes during a scan produces image defocussing. To overcome these effects, an ion lens was developed to enable the position of the image plane to be altered electrically and this was later improved so that the position could be continuously varied during a scan according to a predetermined law. By using this lens in conjunction with the hexapole, useful scans can now be obtained with a constant resolution of 40,000 at a scanning rate of 80 seconds/decade from about 1µg of sample.

Table 1 illustrates the performance which can now be obtained. The data shown was obtained using the early version of the ion lens from an 80 second/decade scan of perfluorotributylamine recorded on magnetic tape. Selected portions of this spectrum were played back at a reduced speed to a U.V. recorder, and the resolution measured from the chart. The resolution was a constant 50,000 up to mass 250 and the fall-off to 40,000 at the high mass end could now be avoided by using the facility now available for determining and correcting for the variation of focusing parameters with mass.

The sensitivity and intensity range available are well illustrated in figures 1 and 2, which show the parent and p-18 peaks from a spectrum of Streptovaricin A. This again was recorded on magnetic tape at 80 seconds/decade, the resolution being set to 40,000, as illustrated by the p-18 peak. The parent peak resolution of 65,000 is exaggerated by ion statistics, the peaks shown containing probably less than 20 ions. Obtaining a good parent peak from this material is particularly difficult as this peak represents only about 1 part in 10^4 of the total spectrum.

The ability to scan at very high resolution is particularly valuable for applications involving isotopic labelling, and an example of this has been described earlier in these Proceedings (Wolstenholme et al ·). During this work, ^{15}N labelled Gliotoxin was introduced via the direct insertion probe and, using perfluorokerosene as a reference, a 150 second/decade scan at 40,000 resolution was carried out on line to the DS10 data system. The scan speed was determined by the maximum digitisation rate available, and the requirement of 20 digital samples per peak. A portion of the elemental composition print out is shown in figure 3, the correct identification of each component being indicated by an asterisk. All the components of the multiplets shown were correctly identified, with very good mass measurement accuracy. The large apparent error of 0.97 mmu ($\sim$ 7ppm) for the C_9H_6NO peak at m/e 144 can be accounted for by the presence of the ^{13}C isotope of the large C_9H_5NO peak at m/e 143, which has not been resolved. The discrepancy introduced by the isotope peak is calculated to be between 0.7 and 0.8 mmu.

Figure 1

Parent Peak of Streptovaricin A. R.P. 65,000

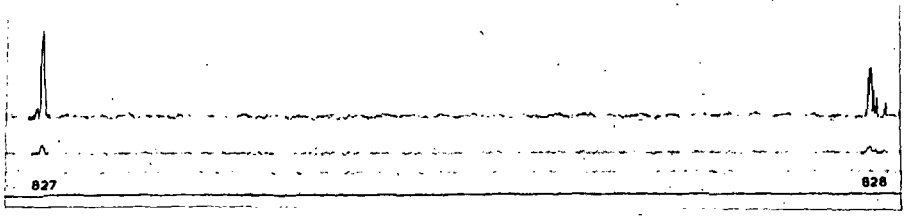

Figure 2

P-18 peaks of Streptovaricin A. R.P. 40,000

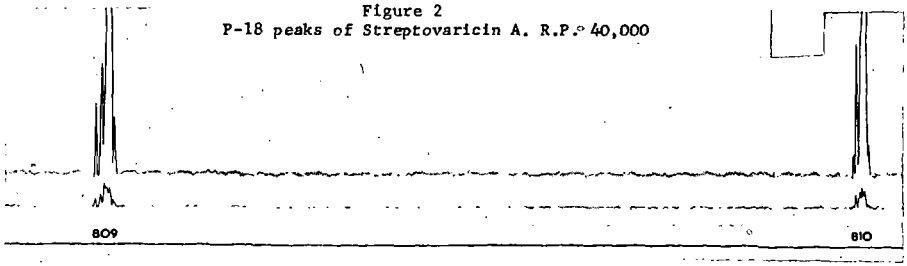

FIGURE 3

PART OF SCAN ON ^{15}N ENRICHED GLIOTOXIN (RP 40,000)

MEASURED MASS	ERR	C12/13	H	N	O	NX
145.0527	- .42	8/0	6	2	0	1
	.00	*9/0	7	1	1	0
145.0480	- .61	7/1	5	2	0	1
	- .18	*8/1	6	1	1	0
145.0418	- .06	*9/0	6	0	1	1
144.0439	-1.40	8/0	5	2	0	1
	- .97	*9/0	6	1	1	0
	1.28	5/0	7	1	3	1
144.0339	- .18	*9/0	5	0	1	1
143.0369	- .51	8/0	4	2	0	1
	- .12	*9/0	5	1	1	0

TABLE 1

HIGH RESOLUTION SCAN FROM A MODIFIED MS902

Sample:- Heptacosafluorotributylamine.
Magnet scan decrease rate 6. (80 second scan).
Recorded at 30 i.p.s.; playback 3$\frac{3}{4}$ i.p.s.
Feed-back resistor 10^9 ohm.

Measurements from the scan gave:-

m/e	Resolution
614	38,400
502	49,900
414	35,300
264	39,800
220	>50,000
219	46,400
131	>50,000
69	50,000

In this case, although the resolution was adequate to separate the two peaks at the 5% points, the valley between the peaks was above computer threshold. The r.m.s. error on the other five correctly identified peaks is 0.9 ppm.

The sample quantity required for a 40,000 resolution scan has been estimated from measurements of the base peak intensity for a given amount of Hexachlorobutadiene passing into the ion source. These measurements show that 400 ions would be obtained in the base peak for a sample consumption of 1.5 micrograms during the scan. This quantity would enable accurate mass measurements to be made over an intensity range of 20 to 1, the smallest peaks measured containing 20 ions. At this resolution, a 20 ion peak should be measurable to an accuracy of 1.1 ppm on the basis on ion statistics, compared with 4.4 ppm at a resolution of 10,000. For compounds in which the ions of a given species are concentrated, unlike hexachlorobutadiene, mainly into one isotopic peak, the same performance would be achieved on sample quantities two or three times smaller, i.e. less than 1 microgram.

Conclusions

It has been demonstrated that by using hexapole image correctors and an ion lens to provide dynamic control of the image position, the performance of the MS902 can be considerably improved. Dynamic scans at 40,000 resolution can now be achieved with a mass measurement accuracy from a single scan of less than 1 ppm, and from sample quantities of 1 microgram.

Ref.

1) Evans, S. Kemp T.R. Wolstenholme W.A.

Seventeenth Annual Conference on Mass Spectrometry & Allied Topics May 1969. Dallas. pp. 326-332.

2) Halliday, J.S.

Advances in Mass Spectrometry. Ed. E. Kendrick Inst. of Petroleum, London, 1968. pp. 239-254

3) Berry, C.E. R.S.I. Vol. 27. No. 10. pp. 849-853. Oct. 1956

4) Boerboom, A.J.H. Mass Spectrometry. Ed. R.I. Reed

Academic Press. London & New York. p.80. 1965

A NEW GC/MS-SYSTEM

C. Brunnée, L. Delgmann, K. Habfast
and S. Meier
VARIAN MAT GMBH, Bremen, Germany

Summary

A small low cost GC/MS-System is described consisting of gas chromatograph, separator and sector type mass spectrometer built into one unit. Mass range: 1000 (linear scale); resolution (10 % valley): 3500 maximum, 600 standard; sensitivity of the entire system: 0,2 µg injected sample gives an evaluable mass spectrum. An extra electron impact ionization detector allows simultaneous recording of gas chromatogram and mass spectrum without interference. The separator (variable slit type) accepts columns with flow rates between 1 and 100 ml/min. Typical results obtained with this system will be given.

1. Introduction

More than 90 percent of all the GC/MS analyses made during the last 10 years were performed with relatively expensive instrument combinations, i.e. with mass spectrometers priced between 30.000 and 60.000 Dollars. The experience gained during this time has meanwhile led to the conclusion that it should be possible to perform the majority of GC/MS analyses and, in particular, almost all routine analyses, with considerable smaller and simpler instruments. The question arises: What is expected from such a simple instrument?

According to our experience, a maximum molecular weight of 600 and a maximum GC temperature of about 300 °C will meet the requirements of more than 80 percent of all GC users. In respect to the sensitivity of the mass spectrometer, it seems to be sufficient when an injected sample amount of the order of 1 µg yields an evaluable mass spectrum. Another requirement is, of course, ease of operation. The numerous control knobs of larger mass spectrometers are provided with multipurpose applicability in mind and can therefore be omitted on a special GC/MS instrument.

Following up these considerations, we have built a special GC/MS system which is shown in fig. 1 and 2. In the following at first some information on the design and function of the three main elements - the gas chromatograph, the mass spectrometer and the separator - will be given and then some results obtained with the entire system will be reported.

FIGURE 1

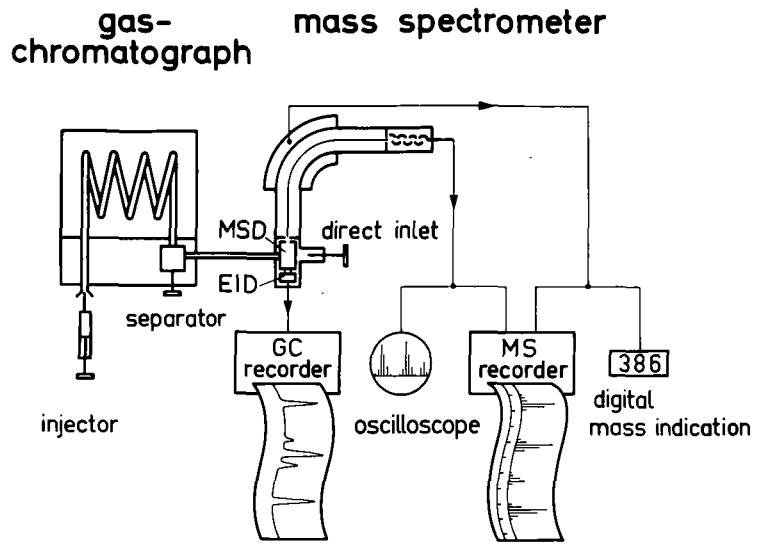
gas-
chromatograph
mass spectrometer
MSD
direct inlet
EID
separator
GC
recorder
MS
recorder
386
digital
mass indication
injector
oscilloscope

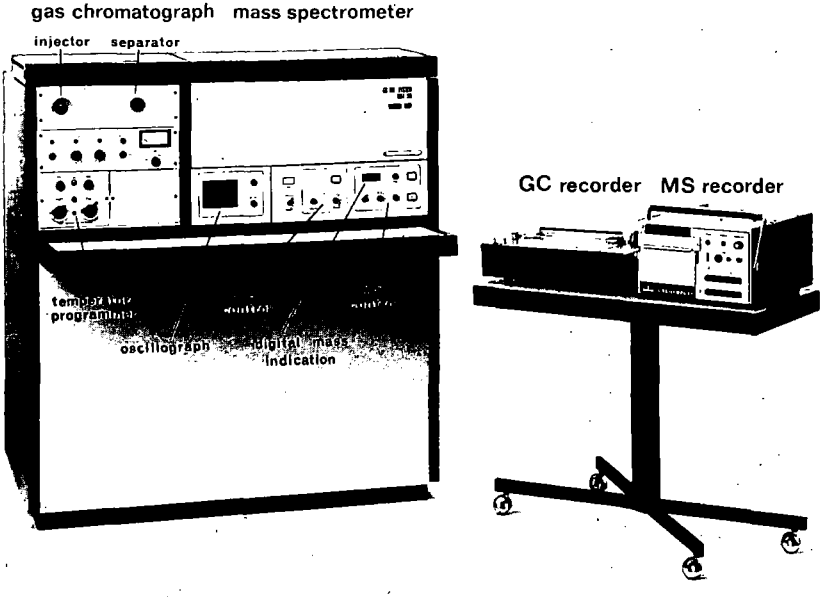
gas chromatograph
mass spectrometer
injector
separator
GC recorder
MS recorder
oscillograph
digital mass
indication

FIGURE 3

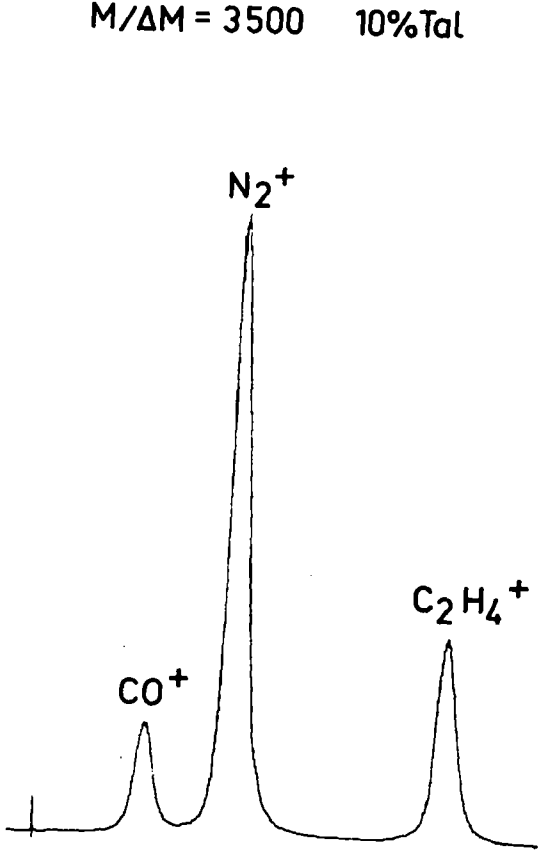

FIGURE 4

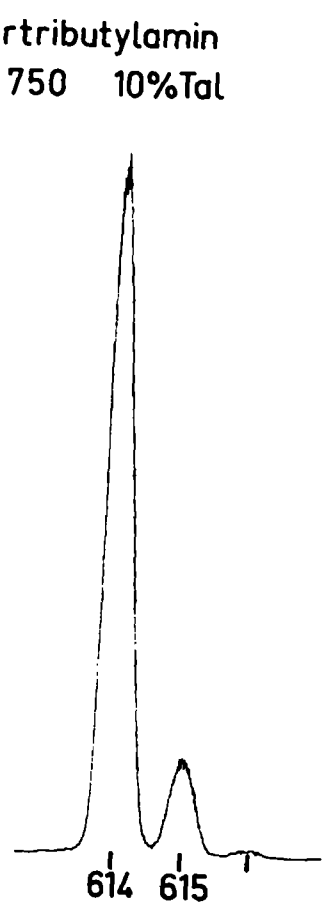

FIGURE 5

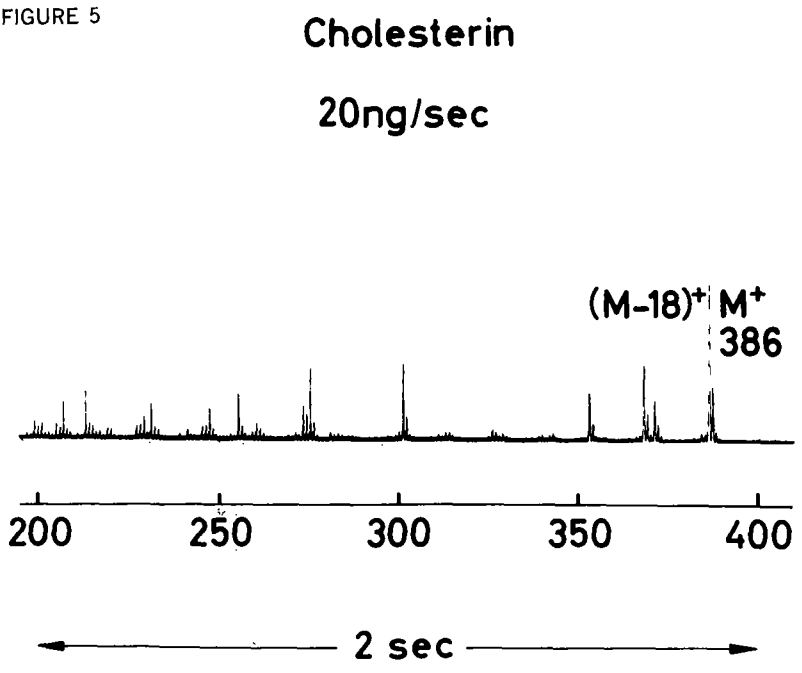

FIGURE 6

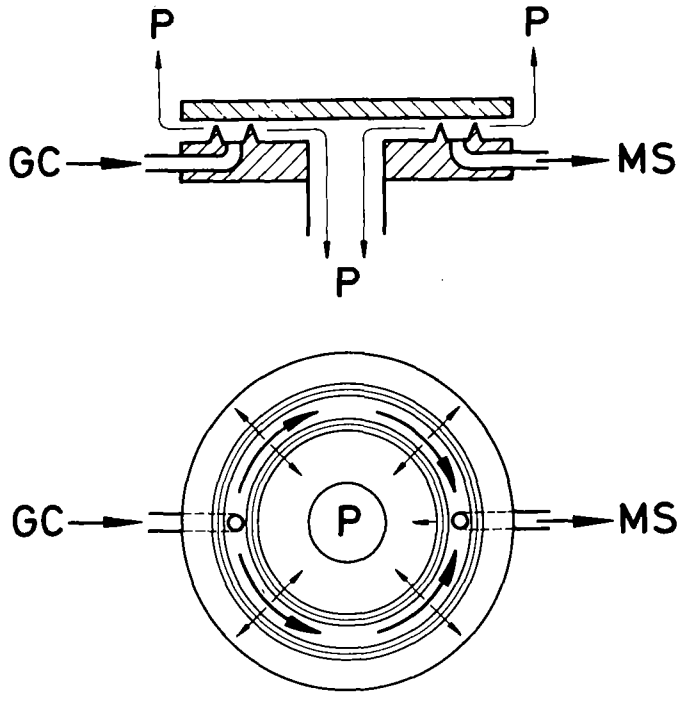

FIGURE 7

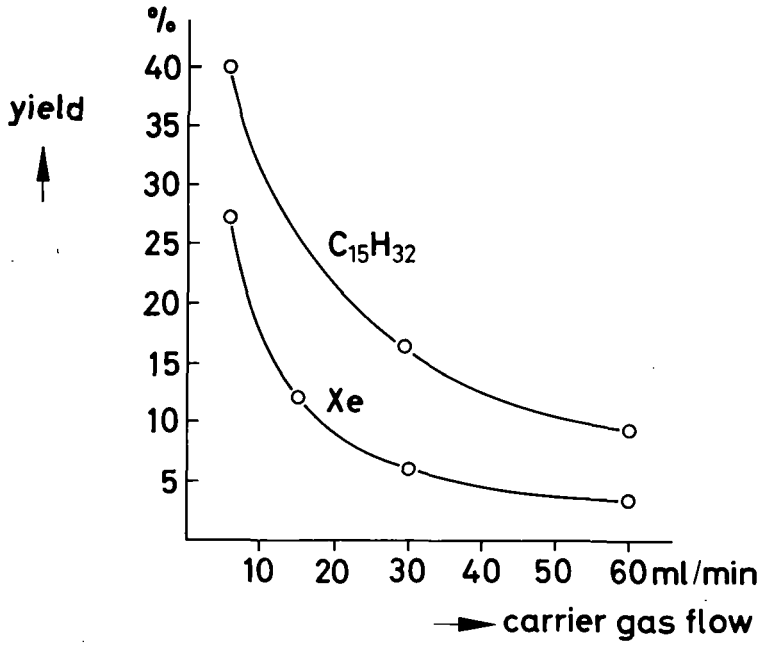

FIGURE 8

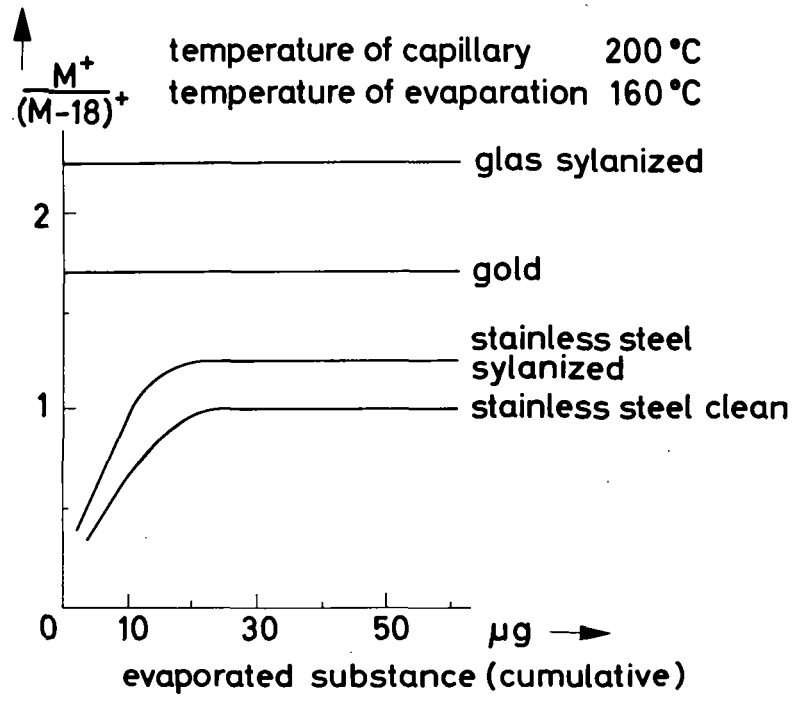

FIGURE 9

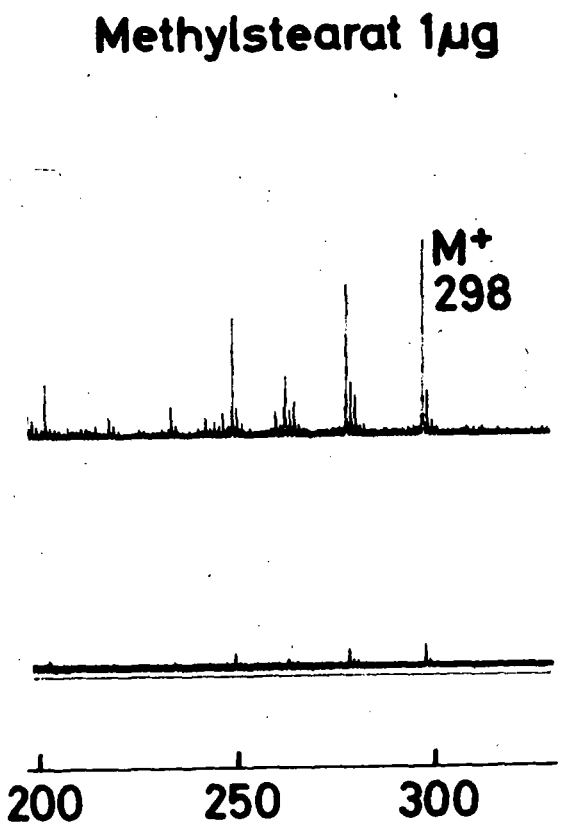

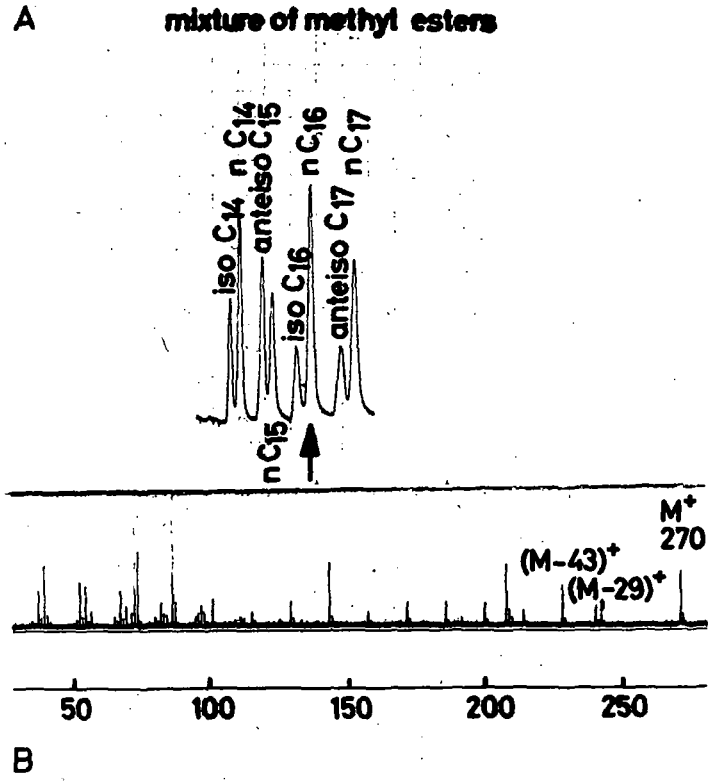

FIGURE 10

2. Gas chromatograph

A few words only on the gas chromatograph: Type Aerograph 1440 with linear temperature programmer for packed columns (metal or glass) and capillary columns. Two injection blocks can be mounted simultaneously.

3. Mass spectrometer

In respect to the mass spectrometer, we have been guided by the motto "what matters is the molecular peak" and have therefore given preference to the conventional sector field principle over the mass filter principle, in order to avoid the decrease in sensitivity and resolution in the upper mass range always observed with mass filters. The radius of the 90° sector field - 12 cm - is relatively large, for the following reason: the required specifications with respect to sensitivity and resolving power are to be obtained routinewise. The limit of resolution is at 3500, as can be seen in fig. 3 from the triplet at mass number 28. Hence, it is by a factor of 6 higher than the operating value of 600 to which the instrument is set normally, with accordingly larger slit widths. The standard resolution is shown in fig. 4, taking as an example the peaks 614 and 615 of perfluorotributylamine. At this resolution, the sensitivity is characterized as follows: for introduction of cholesterol via the direct inlet system at an evaporation rate of 1 ng/s, a molecular peak is obtained that is well above the noise, fig. 5. The spectrum in fig. 5 refers to an evaporation rate of 20 ng/s. The molecular peak is accordingly higher. The sensitivity data of the entire GC/MS system including column and separator will be given in section 5.

The sample flow from the column is let into a double ion source with two separate ionization chambers, fig. 1. The electron energy in the second chamber is 20 eV. As a result, the carrier gas, helium, is not ionized and the ion current produced from this part of the source gives the gas chromatogram. This part is called EID - electron impact ionization detector. In the first chamber we have the usual electron energy of 80 eV. This part, called MSD - mass spectrometer detector - produces the ions for the mass spectrometer. Both ion source parts, EID and MSD, are independent of each other, i.e. the gaschromatogram is recorded continuously without interruptions, no matter whether a mass spectrum is being recorded or not. The rising and falling of the peak heights of the mass spectrum can be observed on the oscilloscope using the cyclic mass scanning mode. In this mode the height of the largest peak is stored during each cycle and used to preselect automatically the apropriate sensitivity range for the subsequent recording of the next mass spectrum on the galvanometer recorder. The mass range is up to 1000; the mass scale is linear. By measuring the magnetic field the mass numbers can be marked on the strip chart with an

accuracy of 0.4 mass units and also displayed digitally.

4. Separator

For enrichment of the sample we use a separator of the variable slit type about which has been reported already on last year's meeting. The separator is operating on the effusion principle. However, in place of a frit we use a fine slit of about 10 µm width. In this slit the gas flow is molecular so that the carrier gas is pumped off preferentially, fig. 6. As in the case of the Biemann-Watson separator with frit the yield y of such a separator is given by

$$Y = N \cdot \frac{Q_{MS}}{Q_{GC}}$$

Y = yield
N = enrichment
Q_{MS} = carrier gas flow into the MS
Q_{GC} = carrier gas flow into the column

This means that the yield with separator is by a factor of N "better" than without separator, i.e. when using a simple split for which N = 1, the yield then only being given by the ratio of the gas flows. All separators with invariable effusion area, i.e. with invariable frit or slit area and working according to the effusion principle, give an optimum yield for only one value of the carrier gas flow. If the carrier gas flow is reduced below these optimum operating conditions, the yield decreases, because the separator pumps off more than required, and the sample amount entering the mass spectrometer is becoming smaller. If the carrier gas flow rate is increased beyond the optimum, i.e. maximum value, the mass spectrometer can tolerate the yield also decreases, because the ion source and the vacuum system cannot cope with such an amount of gas. This behavior very often requires the use of several separators, which have to be changed with different gas flow. This difficulty can be avoided by making the effusion area variable. In this way, one can obtain maximum results with every column and with every carrier gas flow rate from 1 to 100 ml/min. The variable effusion area used by us is designed as a circular slit formed by two knife edges and a glass plate lying above them. The distance can be varied between 0 and 100 µm by means of a drive.

Fig. 7 shows the dependence of the separator yield on the carrier gas flow, measured with xenon and n-C_{15}. In contrast to the frit separator, the yield does not decrease with decreasind gas flow, but even rises, provided the slit width is reduced accordingly in order to keep the gas flow into the mass spectrometer constant. The yield is, of course, highest when capillary columns are used; then it amounts to more than 50 percent.

Besides the yield, the effect to the separator on the separation of the column is of particular interest when using capillary columns. We have not found any difference in the number of theoretical plates between the direct vacuum-tight connection of the capillary column to the ion source which is known to give optimal results and the connection via the separator.

For packed columns we use a throttle to maintain atmospheric pressure at the column end so that the columns can be changed without the mass spectrometer. For changing columns, it is merely necessary to open the separator slit which is then acting as a bypass. Thus the amount of air still entering the mass spectrometer while the entrance of the separator is exposed to atmospheric pressure does not interrupt the operation of the instrument.

Of decisive influence on the efficiency of the coupling are the material and the surface treatment of the connecting lines. This influence is only noticed, however, when analizing very sensitive substances and, what is more important, when injecting only minute amounts of these. There are quite a number of papers published during the last few years reporting, for example, results obtained with cholesterol, where the ratio M/M-18 is taken as a standard for the efficiency of the coupling. These results do not mean much, unless the amounts injected are stated. Larger amounts can always be brought into the ion source because of the "deactivation" of the surface by the sample itself, provided there is enough of it. The results of some measurements made in this direction are shown in fig. 8. Very small amounts of cholesterol were introduced into the ion source via lines of different material and different surface treatment. The sample flow rate was of the order of 10 ng/s. As can be seen, when using steel, the sample reaches the ion source with acceptable decomposition only after some time, i.e. when the surface is sufficiently saturated. The behavior of glass or gold is much more favorable in this respect. As a consequence we use a gold line in order to make the system as rugged as possible mechanically.

5. Data of the entire system

The sensitivity of the entire system can be evaluated from the spectrum shown in fig. 9. Injected into the column was 1 µg of methyl stearate. The molecular peak is above the noise by a factor of about 100. 0.1 µg still yield an evaluable spectrum. Fig. 9a gives as example a gas chromatogram of a mixture of methyl ester recorded with the EID. In Fig. 9b the mass spectrum of one fraction, n-C_{16} Me-ester, is shown.

fig. 1 Block diagram of the GC/MS-system

fig. 2 GC/MS-system with electronic control and recorders

fig. 3 Maximum resolution

fig. 4 Standard resolution

fig. 5 Sensitivity of the MS. Sample: cholesterol (direct probe)

fig. 6 Variable slit separator (P - to rotary pump)

fig. 7 Yield of the separator

fig. 8 Influence of material and surface treatment of the connecting lines on the spectrum of cholesterol

fig. 9 Sensitivity of the entire system

fig. 10 a) Gas chromatogram recorded with the electron ionisation detector EID. b) mass spectrum of n-Me-ester.

ELECTRON MULTIPLIERS AND STATISTICS OF SECONDARY ELECTRON EMISSION

M1

L. A. Dietz
General Electric Company, Knolls Atomic Power Laboratory,*
Schenectady, New York 12301

ABSTRACT

Electron multipliers are extremely sensitive ion detectors which posses very high speeds of response, high detection efficiency and low noise. I will discuss the electron multiplier detector mainly as it is used in the pulse-counting mode and will point out some of its advantages and limitations. The secondary electron multiplication process will be described in terms of a Polya statistical model and its generality will be demonstrated by fitting it to a wide range of shapes of observed pulse-height distributions. The Polya model gives one considerable insight into the secondary electron multiplication processes in electron multipliers and in related pulse-counting detectors. For example, it shows how the target or conversion dynode dominates the statistical behavior of an entire detector. Using an Al_2O_3 target surface, we have made preliminary measurements of secondary electron yield as a function of ion mass, impact velocity and angle of entry. These results will be described. Also, practical considerations in using electron multipliers in either the dc or pulse-counting modes will be mentioned.

INTRODUCTION

Pulse-counting detectors offer the ultimate sensitivity and accuracy that is attainable for recording single atomic events such as the collision of an energetic ion, atom, electron or photon with a target surface. Detectors with this capability are gaining wide acceptance in mass spectrometry and in many physical measurements. This growing acceptance is fostered, on the one hand, by advances in theoretical understanding. For example, Parilis and Kishenevskii's theory[1] describes the kinetic ejection of secondary electrons from a metallic surface, whereas the low energy stopping power theory of Lindhard[2] and his co-workers describes the slowing-down process for atomic projectiles with keV energy. On the other hand, renewed interest in the detection process is being generated by the advent of the ion microprobe for surface studies and by the extension of spark source mass spectrometry to the accurate assay of elemental concentrations below the ppm level.

Throughout our investigations of ion detection we have found that the ion-converter dynode has by far the greatest effect on the pulse-counting response of a detector. Secondary electron response of the first stage shapes the output pulse-height distribution and fixes detection efficiency. Electron multiplying stages following the conversion dynode act merely as charge amplifiers and have little effect on the relative variance of a pulse-height distribution or on intrinsic detection efficiency. An especially valuable feature of the electron multiplier, when it is used in the pulse-counting mode, is that particle detection can be made virtually noiseless. For example, a monatomic ion with 20 keV impact energy releases about 15 secondary electrons from the ion-converter dynode in the KAPL electron multiplier. This allows the electronic discrimination threshold to be set high enough to bias out practically all pulses caused by thermionic electron emission -- even those from the first stage. Under these favorable conditions background counting rates can be reduced to less than 1 count/min. and detection efficiency is very close to 100%.

It is not my purpose this morning to recommend a particular type of electron multiplier to you, but rather to explore characteristic features which are common to different kinds of pulse-counting detectors. To do this we will describe a computational model for the secondary electron multiplication process in multistage detectors. The model applies to a wide variety of pulse-counting detectors. Secondly, we will apply the model to several detectors of interest: the electron multiplier, the scintillation detector, and the combination of a target dynode with a silicon semiconductor detector. Thirdly, we will review some of the macroscopic features of secondary electron emission from a thin film of aluminum oxide. Finally, we will mention some practical considerations and limitations of electron multipliers used for pulse counting. This approach is intended to help a potential user to decide for himself which detector arrangement is best suited to his needs. Areas which need further investigation will be pointed out as we proceed through this review paper and by other speakers this morning.

*Operated by the General Electric Company for the U. S. Atomic Energy Commission

COMPUTATIONAL MODEL FOR SECONDARY ELECTRON STATISTICS

The general method for computing the statistics of multistage pulse-counting detectors, presented at the ASMS meeting, has been submitted for publication in The International Journal of Mass Spectrometry and Ion Physics. A description of the computer program is included in the paper.

SECONDARY ELECTRON EMISSION FROM A THIN FILM OF Al_2O_3

Kaminsky[3], in his book Atomic and Ionic Impact Phenomena on Metal Surfaces cites the lack of systematic studies of the kinetic emission of secondary electrons for such practical applications as the secondary electron multiplier. We also note the scarcity of experimental measurements on secondary electron emission from thin oxide films used in ion-converter dynodes. Rarely are important factors such as chemical composition, surface cleanliness, crystal structure, surface roughness and film thickness carefully defined for published measurements.

We have constructed a high vacuum test apparatus to obtain preliminary measurements of ion-induced secondary electron emission from thin films of amorphous aluminum oxide. The apparatus is housed in a bell jar high vacuum system and is shown in Figure 1. The main purpose of these measurements is to gain sufficient experience to design and construct a more complex apparatus which will include mass analysis of the primary ion beam and energy analysis of the secondary electrons.

Ions are emitted from a surface ionization filament and are accelerated to energies up to 20 keV before they impinge on a flat target which is positioned several centimeters from the filament. The target can be rotated about an axis at right angles to the path of the ion beam. This arrangement allows one to measure secondary electron yield as a function of ion mass, impact energy and angle of entry into the target surface. Because there is no mass analysis in this device, we are limited to elements such as Li, Ca, K, Ba and Cs which emit pure ion beams.

An ion-converter dynode is prepared by evaporating about 3000 A of pure aluminum onto a section of glass microscope slide to which a thin-film electrical conductor has been attached. The glass surface is smooth to perhaps 10 or 20 A. Pressure during evaporation of aluminum is less than 10^{-6} Torr and during secondary electron measurement it is in the low 10^{-9} Torr range. Aluminum surfaces are oxidized in two ways: (1) by exposing the freshly deposited aluminum to pure oxygen and (2) by chemically anodizing the surface to an accurately known thickness of Al_2O_3. Oxide films formed by exposing the aluminum surface to oxygen are of the order of 10 A or less in thickness.

Typical results for Li are shown in Figure 2 and indicate that the secondary electron yield from a pure, freshly deposited aluminum surface or from an Al_2O_3 surface is approximately a linear function of ion velocity and has a definite threshold velocity below which no secondary electrons are released by kinetic ejection. We observe a velocity threshold of $(5\pm2) \times 10^5$ cm/sec for $^{40}Ca^+$, $^{39}K^+$, $^{138}Ba^+$ and $^{133}Cs^+$. The velocity threshold for Li is about twice as high. Our results for the heavy ions are in agreement with those of Schram[4] and his co-workers. For a BeCu dynode they observed a linear dependence of secondary electron yield with ion velocity for all the noble gases and a velocity threshold of 5.5×10^5 cm/sec. I should also mention that for 20 keV ions we observe little difference in secondary electron yield of monatomic ions over the mass range 6-238. Relative secondary electron yield of a monatomic ion correlates well with the electronic stopping power of that ion in an Al_2O_3 target surface. Stopping powers are computed with the aid of Lindhard's theory[2].

From simple considerations one would expect secondary electron yield at a given ion energy to be proportional to sec θ, where θ is the angle between the ion beam and the surface normal at the point of impact. This is shown in Figure 3. We observe that this relation generally holds to about 60°, but between 60 - 80° may be somewhat lower than that predicted by the secant relationship.

Another important parameter is the escape depth of internal secondary electrons formed below the target surface. To estimate this depth we successively anodized an aluminum thin film to 10, 20, and 30 A of Al_2O_3 in an electrochemical cell. Secondary electron yield at normal incidence was measured after each anodization. Because the yield of the metallic substrate is 5 - 10 times lower than that of Al_2O_3, internal secondary electrons formed in the substrate, near the Al-Al_2O_3 interface, cannot contribute significantly to observed secondary electron yield. Davies[5] and his co-workers at Chalk River have measured the ranges of heavy ions in amorphous Al_2O_3. From their results we infer that the range of 20 keV Li ions is much greater than 30 A, therefore

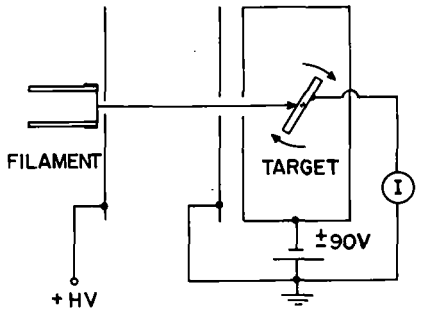

Fig. 1. Secondary electron emission test apparatus

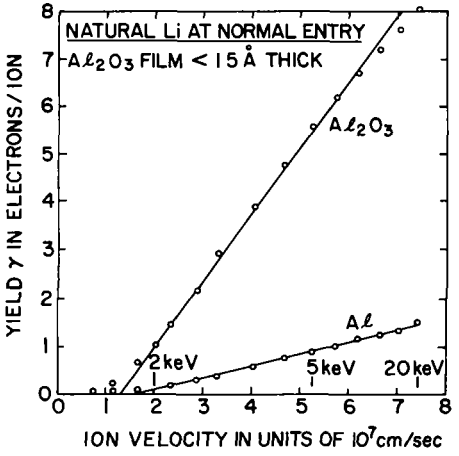

Fig. 2. Secondary electron yields from an aluminized surface before and after oxidation

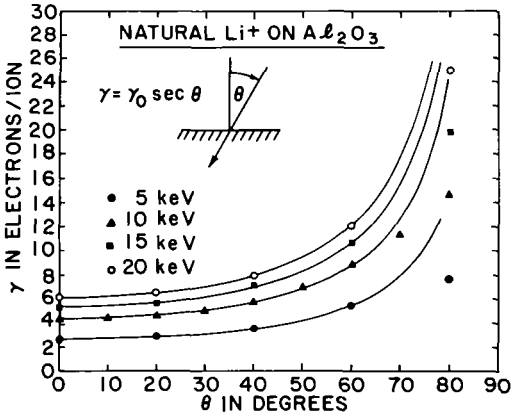

Fig. 3. Secondary electron yield as a function of impact energy and angle of incidence

any increase in secondary electron yield with oxide thickness would indicate a mean escape depth greater than 10 A. No such effect was observed and in fact the yield remained constant with increasing oxide thickness. From this we conclude that the attenuation length, or mean free path for escape from an amorphous Al_2O_3 film is less than 10 A. This is somewhat surprising and disappointing I might add. Nevertheless, the observed secondary electron yield is consistent with estimates made using Linhard's theory to compute the total electronic stopping power of the first 10 A of Al_2O_3. It also is consistent with a mean free path of 5 A in Al_2O_3 reported by Collins and Davies[6] for hot electron transport in Al-Al_2O_3-Al tunnel cathodes. More research needs to be done on ion-induced secondary electron yield.

PRACTICAL CONSIDERATIONS FOR ELECTRON MULTIPLIER DETECTION

In 1954 White and Collins[7] introduced pulse counting with electron multipliers to surface ionization mass spectrometry. Since then pulse counting has become a highly developed art for isotopic ratio measurements in the nuclear energy industry. It is apparent that no single electron multiplier design will serve all pulse-counting needs equally well. Physical size, gain, detection efficiency, speed of response and vacuum enviornment are important factors which must be considered when selecting an electron multiplier for a particular kind of measurement. For details of electron multiplier structures one is referred to a monograph by Sharpe[8] and to recent manufacturers literature. Our own electron multiplier detector is completely described in a KAPL report[9], which also includes details of fabrication and high temperature activation of the BeCu dynodes.

The importance of the ion-converter dynode must not be underestimated. It should be positioned close to the focal plane of a mass spectrometer, within 3 or 4 cm if possible. The entire multiplier should be shielded from stray magnetic fields. The z-aperture of the multiplier should be large enough and the dynodes long enough so that the entire height of the resolved ion beam strikes the ion-converter dynode. The oxide surface of the ion-converter should be at least 20 A thick but need not be more than several hundred A thick. Ideally it should be flat and smooth so that a constant angle of entry of the ion beam is maintained. A flat surface in the ion-converter is important for both the dc and pulse-counting modes. By inclining the target surface to the ion beam axis, secondary electron yield is increased according to the $\sec\theta$ relationship. This enhances detection efficiency and lowers background counting rate. It is very desirable that the ion converter be removable without disassembly of the electron multiplier, since occasionally one must detect radioactive atoms. They become imbedded in the target surface and can increase the background counting rate to unacceptable levels. The entire electron multiplier structure should be designed for use in ultra-high vacuum. It should be bakeable to at least several hundred degrees C and should be demountable for cleaning and reactivation. In linear focused structures, some form of beam alignment must be used to obtain maximum detection efficiency. This can be accomplished either by an electric deflecting field between the defining slit and multipler aperture or by lateral displacement of the first dynode by pivoting the multiplier about its base. We use both methods in our laboratory. Proper focusing of the secondary electrons in the first few stages is all-important, since the pulse-height distribution generated there will be passed on through succeeding stages. This is accomplished by focus rods located near the entrance aperture and between dynodes.

The operating characteristics of a particular electron multiplier depend on its total enviornment. For example, high vacuum is necessary to maintain a gain of 10^8, low noise and long life. We find that 10^{-8} Torr is sufficient for routine operation. Also, for fast electronic response it is desirable to connect the multiplier anode to a 50 ohm transmission line and thence into a 100 MHz solid state discriminator[10] which has a threshold of 5 mV or less. For continuous operation the anode current should not exceed a few μA, otherwise multiplier life will be reduced. At our operating gain of 1×10^8 this corresponds to a counting rate of approximately 2×10^5 cps. For short periods of time counting rates of several MHz can be used. I might add that one should not try to make the electron multiplier compete with dc detection for counting rates in excess of 1 MHz or 1.6×10^{-13} A. Precisions better than 0.1% can be attained at counting rates well below 10^5 cps, so there is no pressing need to pulse count in the MHz range, except in special circumstances. Some might regard this as a limitation of the electron multiplier.

I would like to conclude with a remark concerning the use of electron multipliers for pulse counting in spark source mass spectrometers. In surface ionization and ion-sputtering sources, the random rate of ion generation follows Poisson statistics and this allows one to make an accurate correction for coincidence losses in pulse counting. This is not the case at all with a spark source. Evans and Morrison[11] have studied

ion yield vs time in an rf spark discharge. Within a pulse of 100 μsec duration they find large variations in the rate of ion production over a time scale of a few μsec. In this case one should estimate the instantaneous ion current or counting rate, averaged over the duration of a pulse, not including the quiescent periods of milliseconds between pulses when no ions are formed. Also, one must always keep in mind that the thin oxide film of the ion converter is an electrical insulator and is limited in the number of secondary electrons/cm^2/sec it can deliver. It also is subject to a slow, steady erosion by ion sputtering. We have not measured the saturation yield current, but for an Al_2O_3 target in the KAPL multiplier, no detectable saturation is observed for a first stage gain of 15 secondary electrons/ion and a steady counting rate of 1MHz. Temporary loss of gain in the dynode chain is a more serious problem at very high counting rates. For example, if too intense an ion current even momentarily strikes the ion converter, both its secondary electron yield and the overall multiplier gain may be lowered during detection of a pulse. At high gain this will produce a non-linear multiplier response in either the pulse-counting or dc modes of detection - an effect analogous to reciprocity failure in ion-sensitive emulsions. Take a simple example. For a 1 ppm impurity a 30 sec exposure, approximately, is required to produce detectable blackening of an ion-sensitive plate, or about 10^4 ions. If, for this measurement, we use a pulse duration of 100 μsec and a repetition rate of 100 pulses/sec, then about 3 detectable ions are formed in each pulse. In this case, the instantaneous counting rate, averaged over a pulse, is 3/100 μsec or 0.3 MHz. For this rate, the expected coincidence loss correction in a 100 MHz pulse-counting system is 0.3%. But this is not the limiting consideration. The instantaneous pulse-counting rate really should be averaged over the time of actual spark breakdown. Suppose a spark breakdown occurs in 0.1 μsec and two detectable ions are formed in this interval. Then the instantaneous rate is 20 MHz and the counting loss correction is 20% if the counting system responds linearly. The point I wish to make is that even when only a few detectable ions are formed during each spark breakdown, coincidence losses will be high and the recorded number of pulses will require care in interpretation. The dynamic response of electron multipliers and other kinds of pulse-counting detectors need more investigation before many of the basic questions about their application to spark source mass spectrometry can be answered. Nevertheless, for the measurement of trace elements they offer improvements in detection sensitivity and accuracy that cannot be equalled by any other method.

ACKNOWLEDGMENT

I wish to thank J. C. Sheffield and J. H. Thomas for construction of the secondary emission apparatus and J. C. Sheffield for making the measurements of secondary electron yields.

REFERENCES

1. E. S. Parilis and L. M. Kishinevskii, Soviet Physics - Solid State, 3, 885 (1960).

2. J. Lindhard, M. Scharff and H. E. Schiøett, Mat. Fys. Medd., Dan. Vid. Selsk. 33, No. 14 (1963).

3. M. Kaminsky, Atomic and Ionic Impact Phenomena on Metal Surfaces, (Academic Press, 1965), p. 302.

4. B. L. Schram, A. J. H. Boerboom, W. Kleine and J. Kistemacker, Physica, 32, 749 (1966).

5. J. A. Davies, Atomic Energy of Canada Limited, Report No. AECL-2757, August (1967).

6. R. E. Collins and L. W. Davies, Solid State Electronics, (Pergamon Press, 1964), Vol. 7, p. 445.

7. F. A. White and T. L. Collins, Appl. Spectry. 8, No. 1, 17 (1954).

8. J. Sharpe, Nuclear Radiation Detectors, (Methuen, John Wiley, 1964) 2nd ed., Chap. V.

9. L. A. Dietz, A. B. Hance and L. R. Hanrahan, Knolls Atomic Power Laboratory Report No. KAPL-3352, June, 1967.

10. F. H. Sawada, IEEE Trans. Nucl. Sci. NS-12, No. 1, 374 (1965). See also A. B. Hance and L. R. Hanrahan, Knolls Atomic Power Laboratory Report No. KAPL-3122 (1966).

11. C. A. Evans and G. H. Morrison, Anal. Chem. 40, 2106 (1968).

SCINTILLATOR DETECTORS AND TECHNIQUES

M2

C. R. Lagergren
Battelle Memorial Institute
Pacific Northwest Laboratories
Richland, Washington 99352

The type of ion detector that I wish to discuss is one in which a scintillator is used as a high gain element. More specifically, I refer to the type of detector that converts ions to electrons, electrons to photons, and photons back to electrons. The use of the intermediate step involving photons is the process that characterizes this device. Neither of the names "Ion Converter Detector" or "Scintillation Type Ion Detector" seem to adequately describe it. Perhaps the name "Ion-Conversion Scintillation Detector" would be a good compromise. Before discussing its characteristics and some of the techniques involved in its operation, I would like to touch briefly on its origin and on the variety of forms in which it has been used.

HISTORICAL DEVELOPMENT

The detector was first introduced by Schütze and Bernhard[1] in 1956. They were apparently interested in developing a detector which had both high sensitivity and fast response for use on a sector mass spectrometer in which the mass spectra were to be displayed on an oscilloscope screen. Their main objection to the Allen detector[2], the "open" electron multiplier, which in principle satisfied their requirements, was that reactivation of the dynodes was necessary following each venting of the vacuum system in order to restore satisfactory gain. The other alternative open to them at that time was to use the "true" scintillation detector described by Richards and Hayes[3] in 1950. In their detector ions were post-accelerated by a -30 kev field directly into a scintillator which was viewed by a photomultiplier tube. The great advantage of this system is that the high gain element, the photomultiplier, is situated external to the mass spectrometer vacuum system and no dynode activation process is necessary. However, the effect of fatigue and permanent damage many scintillators suffer under ion bombardment presents a serious disadvantage. Bringing together the best features of the two previous detector concepts, namely the high sensitivity possible in an "open" electron multiplier and the freedom from bothersome activation procedures afforded by an external photomultiplier, Schütze and Bernhard produced a detector satisfying their needs.

A further development of this detector for the purpose of detecting individual ions appeared in 1961 by Bernhard, Krebs, and Rotter[4].

The principal changes lie in the ion and secondary-electron focusing system. Post acceleration of the ions occurs between curved electrodes in such a way as to focus the ions on a Ni target with an angle of incidence centered at 60°. The secondary electrons are focused onto the scintillator by the field penetrating the vertical cylindrical cavity of the target holder. This design operated excellently for voltages up to -24 kev.

In 1960 Daly[5] introduced another form of the detector. The basic difference of Daly's configuration is that the ions are deflected sideways into the target. This imposes a restriction on the relationship of target potentials and entrance ion energies that can be used for the particular geometry selected. For his flat target surface and a 1.2 cm. effective scintillator diameter, and for a target potential of -40 kev, ion entrance energies in the range 5 to 7 kev are required. This restriction is not

particularly disadvantageous unless one wishes to use electrostatic scanning over a wide mass range. A definite advantage is realized in that stray ions or ions which have lost more than 20% of their energy are automatically rejected. For the scintillator Daly used a 3 mm. thick plastic phosphor NE 102. The electron entrance side of the phosphor was coated with an aluminum film to maintain a ground potential at its surface and provide optical reflection of light toward the photomultiplier. The coating was thin enough so that the electrons in passing through it lost only about 1 kev of energy.

This form of the ion conversion scintillation detector has been the most widely used.

In 1963 Daly[6] modified his detector for the simultaneous measurement of two ion beams.

In this arrangement a thin metallic partition separates two independent detectors. The two ion beams are deflected in opposite directions to two targets each facing opposite sides of the partition. A magnetic field directed toward the axis of the incoming ion beams deflects the secondary electrons from the two targets into their corresponding scintillators. An obvious requirement for the success of any dual detector system is that the two detectors must have equal efficiencies or high stability so that adequate calibration can be made. The characteristically high efficiencies obtainable with this type of ion detector make them well suited for a dual system.

The description of an ion conversion scintillation detector having a large entrance aperature was given by Ridley[7] in 1961. This detector was developed for the detection of low energy recoil ions in beta-decay of gases and required a uniform sensitivity over an aperture of 4 cm. in diameter. The sensitivity of the detector proved to be uniform over the 4 cm. entrance aperture but displayed a few percent variation with ion energy due to a transmission effect of the screening grids.

Ion conversion scintillation detectors are not exclusively found in the domain of mass spectrometry. It should be mentioned that Stein and Leachman[8] in 1956 made use of the principle for the detection of fission fragments in the fission of U^{235}. In their arrangement, the secondary electrons, produced during the passage of the fission fragments through a thin Ni foil, were detected by a scintillation detector.

In 1960 Everhart and Thornley[9] applied the high gain and fast response possible in scintillation detectors to a scanning electron microscope. The secondary electrons released from the sample were accelerated into a plastic scintillator which,in turn, was optically coupled to a photomultiplier. This system proved superior to the "open" electron multiplier in mechanical flexibility.

BASIC PROCESSES

Let us now examine in some detail the basic steps in the operation of the ion-conversion scintillation detector.

The gain of the detector is the product of the three essential conversion factors and the multiplier gain.

1. The number of secondary electrons emitted from the target per positive ion,
2. the number of photons produced per secondary electron in the scintillator,
3. the number of photo-electrons released per photon, at the photocathode, and
4. the multiplier gain.

Three observations should be made at the outset.

1. Only the first factor is variable during operation (assuming saturation effects and non-linearities of the photomultiplier are avoided). The number of secondary electrons produced is, of course, dependent on the nature of the incident ion, its velocity and angle of incidence, and the

particular target used. The other three factors are "built in", so to speak, by design features and choice of operating parameters. This means that as a current gain device the response characteristics would be expected to be the same as those of the "open" multiplier but easier to maintain in a practical sense over a wide variety of environmental circumstances.

2. If the product of factors 2 and 3 is equal to the average gain per stage of the electron multiplier, the detector is essentially equivalent to the "open" multiplier except that a greater value for the first factor can be obtained due to the higher practical limit on the potential at which the conversion electrode can be operated.
3. If the product of factors 2 and 3 is large, the pulse height distribution of the detector output is determined primarily by the initial conversion process.

Factors 2 and 3 may be represented in greater detail as:

$$\left[\frac{E_e - E_a}{E_p} C_p\right]_2 \times \left[T_p \; Q_m\right]_3$$

where E_e = energy of electrons striking the scintillator
E_a = electron energy lost entering scintillator
E_p = average photon energy
C_p = conversion efficiency of energy into photons of energy E_p.
T_p = efficiency of the optical system
Q_m = quantum efficiency of the photocathode

$(E_e - E_a)$ represents the total electron energy transferred to the scintillator. E_a is the energy lost in penetrating any surface coating or inactive layers of scintillator surface material. It is a common practice when plastic scintillators are used, to evaporate a thin layer of aluminum onto the front surface in order to reflect light toward the photocathode. The optimum thickness for good reflectivity before noticeable energy is lost was found by Young[10] to be about 500Å. It should be noted also that any machining or polishing of the plastic front surface inevitably results in the deterioration of the scintillator efficiency. A new technique for forming scintillators so as to avoid machining and polishing was recently reported by Hatzakis[11]. His technique is to dissolve Pilot scintillator B material in scintillation and fluorometric grade toluene. The scintillator is then formed by applying the 5-10% solution a drop at a time on the end of a light pipe. After drying in a dry atmosphere free from air currents, the 10-20 micron thick scintillator thus formed is coated with aluminum in the usual way.

E_p is the average energy of the photons produced which for most scintillators is about 3 ev. C_p is the fraction of the net electron energy that is converted to photons. Values of C_p in the range .01 to .05 seem to be typical. It is apparent that for 30 kev electrons hundreds of photons are produced.

The second bracketed expression is factor 3 and is the product of T_p, the efficiency of the optical system and Q_m, the quantum efficiency of the photocathode of the photomultiplier. Quantum efficiencies are of course spectrally dependent and vary among commercial tube types. Values from around 7 to 30% are quoted for some of the commonly used photomultipliers. If one assumes a value of 0.5 for T_p and quantum

efficiency of 20%, one-tenth of the photons should result in the release of photoelectrons. Further, for a scintillator efficiency of 2%, 30 kev electrons incident on the scintillator would produce 20 photoelectrons.

In a study of the response of an anthracene scintillation counter to electrons in the 10-120 kev energy range, Johnston[12] found that for a bare crystal 0.060 in. thick, centered on the photocathode of an RCA 6199 photomultiplier, the release of one photoelectron required on the average 1.47 kev of incident electron energy. For 30 kev electrons this amounts to the generation of about 20 photoelectrons, which seems to give creditability to the approximations we assumed above.

PERFORMANCE

The overall performance of this type of this type of detector can be illustrated by an example of the output pulseheight distributions that can be obtained.

We have been using ion converter scintillation detectors in our laboratory at Battelle-Northwest since 1963. All of our detectors utilize the configuration introduced by Daly except for one minor difference. Instead of a flat target surface a spherical concave one is used, the center of curvature being located near the center of the scintillator. The focusing action that the concave surface exerts on the secondary electrons has the effect of increasing the entrance aperature of the detector without having to increase the size of the scintillator. Our targets are machined from a solid block of aluminum alloy and meticulously cleaned and polished so that they may be operated at potentials as high as 60 kev without high field emission or breakdown occurring. We use NE 102 scintillators made from 0.010 in. sheet material and cement them to 1/2 in. long lucite light pipes with Eastman 910 cement.

The pulse-height distribution we obtained for U^{238} ions of 12 kev energy entering one of our detectors is shown in the figure.

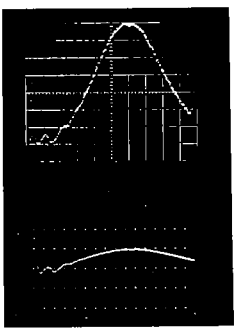

Pulse-Height Distribution for U^{238} ions

The target potential was -50 kev and an EMI 6097S photomultiplier, operated at 1600 V, was used. The ion conversion events leading to the release of one, two and perhaps three secondary electrons can be seen. Using these bumps to calibrate the pulse height scale, we estimate that the peak of the distribution lies at about seven electrons. With the discriminator set so as to accept most of the single electron peak, the detector background average count rate was about 1/2 count per second. Operated under these conditions and if one assumes that the secondary emission process can be described by a Poisson distribution, the detector is 99.9% efficient. Even if the single electron peak is excluded, about 99.5% of the distribution would be accepted. It is a little dangerous to claim such high detection efficiencies without taking into account the possibility that some other zero yield process, such as ion reflection, may be taking

place with substantial probability. With this provision these efficiencies are mentioned.

The need for a lower background and a higher ion count rate capability than we were able to achieve with the EMI 6097S led us to search for a more suitable photomultiplier. We have had our best and sustained success with the Amperex 56AVP. Background rates less than one count per minute, or less than 3×10^{-21} amp, can be maintained. The output pulses of the photomultiplier are about 10 nsec wide with an average amplitude of 1.5 v on a 50Ω load. Further amplification of the pulses is unnecessary so the multiplier output is cabled directly to a discriminator. With our discriminator deadtime adjusted to about 45 nsec, the response of our detector is linear, with deadtime corrections, to at least 2×10^{6} ion counts per second or 3×10^{-13} amp.

The performance characteristics of the ion conversion scintillation detector can be summarized as follows:

Dectection Efficiency--------Virtually 100%

Mass Discrimination----------None

Sensitivity------------------Limited only by background noise

Noise------------------------Less than 1 count per minute

Maximum Input Rate-----------2×10^{6} ions per second

Entrance Aperature-----------Several centimeters

Although there are undoubtedly some particular ion measurement situations where this detector would be usefully applied as a current gain device, its main value, I would say, lied with its use as an ion counting detector. The characteristics listed here refer to ion counting applications only.

With an average secondary electron yield in the ion conversion step equal to or greater than 5, the detector is virtually 100% efficient. For this reason there would be no mass discrimination.

The sensitivity is limited only by the level of background noise. This noise can be held to levels below one count per minute.

The maximum ion input rate that can be used depends on the photomultiplier output pulse characteristics and the precision with which the deadtime of the electronic circuitry can be determined For uncertainties in deadtime-corrected count rates no greater than 0.1%, input rates as high as 2×10^{6} ions per second can be measured. If greater uncertainties can be tolerated, the figure may be extended to 10^{7} ions per second. Finally, entrance aperatures as large as 4 cm have been successfully obtained through special design efforts; however, aperatures of 0.5 cm. can be realized without any difficulty.

REFERENCES

1. W. Schütze and F. Bernhard, Z. Phys. 145, 44 (1956).
2. J. S. Allen, Phys. Rev. 55, 966 (1939).
3. P. I. Richards and E. E. Hays, Rev. Sci. Inst. 21, 99 (1950).
4. F. Bernhard, K. H. Krebs and I. Rotter, Z. Phys. 161, 103 (1961).
5. N. R. Daly, Rev. Sci. Inst. 31, 264 (1960).
6. N. R. Daly, Rev. Sci. Inst. 34, 1116 (1963).
7. B. W. Ridley, Nucl. Inst. Meth. 14, 231 (1961).
8. W. E. Stein and R. B. Leachman, Rev. Sci. Inst. 27, 1049 (1956).
9. T. E. Everhart and R. F. M. Thornley, J. Sci. Inst. 37, 246 (1960).
10. J. R. Young, J. Appl. Phys. 27, 1 (1956).
11. M. Hatzakis, Rev. Sci. Inst. 41, 128 (1970).
12. L. W. Johnston, Et. al., Rev. Sci. Inst. 28, 765 (1957).

ION-SENSITIVE PLATE DETECTORS IN MASS SPECTROMETRY

J. M. McCrea
Applied Research Laboratory
United States Steel Corporation
Monroeville, Pennsylvania 15146

Extended Abstract

The ion-sensitive plate, as used in a contemporary mass spectrometer or mass spectrograph, becomes a graphic record summarizing events in the instrument over a series of exposure intervals. It must contend with ions with mass-to-charge ratios ranging in magnitude from 1 to over 1000, and with ion energies from about 5 to over 75 kev. The data recorded on a plate are available for subsequent recall, interpretation, and analysis in auxiliary equipment at the will of the investigator.

As this status review notes, mass spectrography with ion-sensitive plates and optical spectrography show many similarities in materials, associated techniques, and data handling. Despite formal similarities the processes of photographic exposure and ion interaction with the plates are different. The silver bromide grains of most photographic emulsions are seated deeply and display little sensitivity to 20 kev particles penetrating to depths of 0.2 microns or less. Emulsions designed for the 0.004 to 0.006 kev quanta of the strongly absorbed vacuum ultraviolet differ and have grain layers at or near the surface. Such emulsions are also rapidly exposed by ions. They include low-gelatin emulsions, emulsions with the gelatin surface removed, and high-gelatin centrifuged emulsions. A new detector with a vapor-deposited film of silver bromide has recently been developed with applications to ion detection more directly in mind.

In addition to detection based on the direct interaction of ions and silver bromide, conversion techniques with layers of ion sensitive materials have also been used. Fluorescent screens make a mass spectrum visible and subject to photography with any fast film. Conversion of ion energy to electrons has been applied to ion microscopes, and has received a preliminary investigation in mass spectrometry as an alternative to a fluorescent screen.

Instruments of the Mattauch-Herzog geometry dominate the use of ion-sensitive plates, and this use is very largely confined to the Type of Q-2 low-gelatin plate. The two widespread applications of this instrument-detector pair are organic structure studies by the electron-bombardment, high resolution method and elemental analysis of metals, inorganics, and surfaces by the spark-source method. It is in studies oriented towards these applications that a reviewer finds much of the data related to ion-sensitive plates, and it is largely against the Q-2 plate and these applications that new developments in the field stand for evaluation.

Bibliography

Listed in alphabetical order below are a number of recent or important papers dealing with ion sensitive plates. Each entry is classified according to subject matter as follows:

Small letter: t, theoretical; x, experimental; r, review.

Capital letter:

A, analysis	M, mass effect
B, background	P, properties
D, development	R, response
E, ion energy	S, sensitivity

1. N. W. H. Addink, Nature 211, 1168 (1966) (x, B)
2. A. J. Ahearn, "Homogeneity of Ion-Sensitive Emulsions and Precision of Ion Beam Measurements in Spark Source Mass Spectrometry" 16th Ann. Conf. on Mass Spectry. Allied Topics, Pittsburgh, Pa., May 12-17, 1968 (Paper 99) (x, P, S)
3. A. J. Ahearn, Kyoto Conference on Mass Spectry, Sept. 1969 (x,A,P,S)
4. A. J. Ahearn in "Trace Characterization Chemical and Physical W. W. Meinke and B. F. Scribner, eds, Nat. Bur. Stds. Monograph No 100, April 28, 1967. (r,A,B,C,M,R)
5. A. J. Ahearn and D. L. Malm, Appl. Spectry. 20, 411 (1966) (x,B)
6. C. A. Bailey, R. D. Carver, R. A. Thomas and R. J. Dapzyk, " A Computer-controlled System for Automatically Scanning and Interpreting Photographic Spectra." 16th Ann. Conf. Mass Spectry. Allied Topics, Pittsburgh, Pa., May 12-17, 1968 (Paper 47) (x,A)
7. M. L. Bazinet, C. Merritt, J. I. Masters, P. Vouros and J. P. Clune, "The Evaporated Silver Bromide Film as a Detector for Organic Ions," 15th Ann. Conf. Mass Spectry. Allied Topics, Denver, May 19-24 (1967) (x,P)
8. J. H. Beynon, "Mass Spectrometry and its Applications to Organic Chemistry," Elsevier, Publishing Company, Amsterdam, pp 58-61, 195-197 (r,A,R)
9. R. Brown, Kemisk Tedskrift 81, 22 (1969) (r,B,D,S)
10. E. Burlefinger and H. Ewald, Z. Naturforschg. 16a, 430 (1961) (x,M,R,S)
11. E. Burlefinger and H. Ewald, Z. Naturforschg. 18a, 1116 (1963) (x,t,E,R,S)
12. J. Capellen, R. J. Conzemius and H. J. Svec, "A Comparison of Electrical and Photographic Ion Detectors in the Assay of Trace Impurities with the Spark Source Mass Spectrograph." 13th Ann. Conf. Mass Spectry Allied Topics, St. Louis, May 16-23, 1965 (Paper No 15) (x,A,C,S)
13. A. Carnevale and A. J. Lincoln, Spectrochem Acta 24B, 313 (1969)(x,C)
14. A. Cavard in "Advances in Mass Spectrometry, Vol 4," E. Kendrick, ed. Institute of Petroleum (London) 1968, 419-428(x,t,B,D)
15. A. Cavard, Report CEA-R-3759 Commissariat a l'energie atomique (France) Aug. 1969 (x,r,t,B,D,E,M,P.R,S)
16. A. Cavard, R. Stefani and R. Bourguillot, Comptes Rendu (Paris), 263b, 928 (1966) (x,R,S)
17. P. Chastagner, Anal. Chem. 41, 796 (1969) (x,A,B,R)
18. P. Chastagner, "Variation of Photoplate Line Characteristics" 15th Ann. Conf. Mass Spectry. Allied Topics, Denver, May 19-24, 1967 (x,B)
19. J. R. Churchill, Ind Eng Chem. Anal Ed.16, 653 (1944) (r,C)
20. G. G. Cookson, W. Fletcher and R. Tushingham, "The Importance of Variations in Line Width and Emulsion Sensitivity in Spark Source Mass Spectrometry," 13th Ann. Conf. Mass Spectry. Allied Topics, St. Louis May 16-23, 1965 (Paper No 12) (x,A,C,P)

21. A. Cornu, in "Advances in Mass Spectrometry, Vol 4," E. Kendrick, ed., Institute of Petroleum, London, 1968, pp401-418 (r,A,B,D,S)
22. A. Cornu, "Analysis Application of Line Width Studies in a Spark Source Mass Spectrometer," 13th Ann. Conf. Mass Spectry. Allied Topics, St. Louis, May 16-21, 1965, Paper No 101 (x,C)
23. R. D. Craig, G. A. Enoch, and J. D. Waldron in "Advances in Mass Spectrometry," J. D. Waldron, ed., Pergamon Press, New York, 1959, pp 136-156 (particularly 142-146) (x,A,P,R)
24. G. Dearnaley, Proc. Rog. Soc. A311, 21 (1969) (t, E, S)
25. M. Desjardins and J. A. Moore, Appl. Spectry. 22, 713 (1968) (x,C)
26. M. Desjardins and J. Moore, "Computerized Celidometry in Spark Source Mass Spectrometry," 15th Ann. Conf. Mass Spectr. Allied Topics, Denver, May 14-19, 1967 Paper No 61. (x,C)
27. M. Desjardins, R. Stefani, R. Bourguillot and A. Cornu, in "Advances in Mass Spectrometry, Vol 3," W. L. Mead, ed., Institute of Petroleum, London, 1966, 131-142 (x,A,C,R)
28. E. Doernenburg and H. Hintenberger, Z. Naturforschg, 16a, 676 (1961) (x,M,R,S)
29. R. M. Elliott and P. Swift, "Techniques for Estimation of Detection Limits in Spark Source Mass Spectrometry," 13th Ann. Conf. Mass Spectry. Allied Topics, St. Louis, May 16-21, 1965 (x,t,A,C)
30. W. K. Fowler, W. A. Rense and W. R. Simmons, Appl. Optics 4, 1596 (1965) (x,B)
31. J. Franzen and E. Hebeda, Z. Naturforschg. 17a, 476 (1962) (x,P,R)
32. J. Franzen and H. Hintenberger, Z. Naturforschg. 18a, 397 (1963) (x,C,R,S)
33. J. Franzen, K. H. Maurer and K. D. Schuy, Z. Naturforschg. 21a, 37 (1966) (t,x,B,D,P,R,S)
34. J. Franzen and K. D. Schuy,"Theoretical Derivation of the Shape of the Tranparency Curve in the Region of Primary Blackening," Spring Meeting of the German Physical Society, Wuerzburg, 1965. (x,t,P,R,S)
35. J. Franzen and K. D. Schuy, Z. Naturforschg. 21a, 1479 (1969) (x,C,R)
36. K. I. Grais, Appl. Spectry. 23, 276 (1969) (x,R)
37. K. I. Grais, Appl. Spectry. 23, 607 (1969) (x,D,E,M,R)
38. K. I. Grais, Japan J. Appl. Phys. 8, 293 (1969) (x,E,R)
39. K. I. Grais, Japan J. Appl. Phys. 8, 953 (1969) (x,M,R)
40. K. I. Grais, Japan J. Appl. Phys. 8, 979 (1969) (x,D,R)
41. J. W. Guthrie, "Approaches to Mass Spectrometric Gas Analysis Using Photographic Plate Ion Detection," 10th Ann. Conf. Mass Spectry. Allied Topics, New Orleans, June 3-8, (1962) (x,A,C,R)
42. J. W. Guthrie, "Evaluation of a Modified Ilford Q2 Photographic Emusion for Mass Spectographic Uses" Sandia Report Nucl. Sci. Abstr.18, 21960 (1964) SC-DC-64-262
43. K. Habfast and K. H. Maurer, "Photographic versus Electrical Recording," 14th Ann. Conf. Mass Spectry. Allied Topics, Dallas, May 22-27, (1966) Paper No 59 (x,A,C)
44. J. S. Halliday, P.Swift and W. A. Wolstenholme in "Advances in Mass Spectrometry, Vol 3," W. L. Mead, ed., Institute of Petroleum, London, 1966, pp 143-161 (x,A,C)
45. K. Heinecke, "Automatic Evaluation of Photographically Registered Mass Spectrograms-Instrumentation, Physical and Technological Limitations." 14th Ann. Conf. Mass Spectry. Allied Topics, Dallas, May 22-27, 1966, Paper No 60. (x,C)

46. C. Hignite and K. Bieman, Org. Mass Spectry. 2, 115 (1969) (x,A,P.)
47. N. F. Hodgson, M. Desjardins and W. L. Baun, Anal. Chem. 35, 1112 (1963) (x,A,C)
48. R. E. Honig, J. R. Woodston and D. A. Kramer, "Gelatine-Free Ion-Sensitive Plates for Mass Spectrography," 14th Ann. Conf. Mass Spectry. Allied Topics, Dallas, May 22-27, 1966 (x,B,R,P,S)
49. R. E. Honig, J. R. Woolston and D. A. Kramer, Rev. Sci. Inst. 38, 1703 (1967) (x,B,R,P,S)
50. C. W. Hull, Int. J. Mass Spectry. Ion Phys. 3, 293 (1969) (x,B,S)
51. C. W. Hull, "Photographic Quantitative Analysis with a Solids Spark Mass Spectrograph," 10th Ann. Conf. Mass Spectry. Allied Topics, New Orleans, June 3-8, 1962 (x,t,C,R)
52. C. W. Hull and C. G. Blanchard, "Spark Source Mass Spectrograph Sensitivity Measurement, Experiment and Improvement," 13th Ann. Conf. Mass Spectry. Allied Topics, St. Louis, May 16-23, 1965, (Paper No. 14) (x,B,R)
53. M. H. Hunt, Anal. Chem. 38, 620 (1966) (x,A,B,P,R)
54. M. H. Hunt, "The Evaporated Silver Bromide Film as an Ion Detector," 14th Ann. Conf. Mass Spectry. Allied Topics, Dallas, May 22-27, 1966, Paper No. 58 (x,A,B,P,R)
55. Ilford Ltd., J. Sci. Inst. 12, 333 (1935) (x,P)
56. C. M. Judson and C. W. Hull, "Precision, Accuracy and Sensitivity in Spark Mass Spectrometry," 11th Ann. Conf. Mass Spectry. Allied Topics, San Francisco, May 19-24, (1963) (x,B,C,R,S)
57. O. Kammori, N. Yamaguchi, K. Soto and R. Suzaki, "Effects of Source Mass Spectrograph," Kyoto International Conference on Mass Spectroscopy, Sept. 8-12, 1969 (x,C,R)
58. P. R. Kennicott, "A computer Program for the Quantitative Interpretation of Mass Spectrograph Plates," 12th Ann. Conf. Mass. Spectry. Allied Topics," Montreal, June 7-12, 1964 Paper No 93 (x,C,R)
59. P. R. Kennicott, Anal. Chem. 37, 313 (1965) (x,B,D,R)
60. P. R. Kennicott, Anal. Chem. 38, 633 (1966) (x,B,D,R)
61. P. R. Kennicott, "An Internal Image Developer for Mass Spectrographic Plates," 13th Ann. Conf. Mass Spectry Allied Topics, St. Louis, May 16-21, 1965 Paper No 34 (x,B,D,R)
62. P. R. Kennicott, "A System for the Quantitative Evaluation of Mass Spectry. Allied Topics, Dallas, May 22-27, 1966, Paper No 61 (x,C,R)
63. L. G. Lewis and R. J. Hayden, Rev. Sci. Inst. 19, 599 (1948) (x,A,P)
64. J. Linhard, Proc. Roy. Soc. A311, 11 (1969) (t,E,S)
65. H. Mai in, "Advances in Mass Spectrometry, Vol 3," W. L. Mead, ed, Institute of Petroleum, London, 1966, pp 163-168 (x,B)
66. H. Mai, J. Sci. Inst. 42, 339 (1965) (x,B)
67. H. Mai and H. Wagner, J. Sci. Inst. 44, 833 (1967) (x,R,P)
68. M. Margoshes and S. D. Rasberry, Spectrochim. Acta 24B, 497 (1969) (x,C)
69. K. H. Maurer, J. Franzen and K. D. Schuy, "The Shape of the Transparency Curves Under Difference Developing Conditions," Spring Meeting, German Physical Society, Wuerzborg (1965) (x,t,D,R)
70. R. J. McClure, Rev. Sci. Inst. 36, 1246 (1965) (x,P,S)
71. J. M. McCrea, Anal. Chem.38, 1402 (1966) (t,R)
72. J. M. McCrea, Appl. Spectry. 19, 61 (1965) (x,D)
73. J. M. McCrea, Appl. Spectry. 20, 34 (1966) (x,D,P,R)

74. J. M. McCrea, Appl. Spectry. 20, 181 (1966) (x,D,P,R,S)
75. J. M. McCrea, Appl. Spectry. 21, 236 (1967) (t,B,C,P,R)
76. J. M. McCrea, Appl. Spectry. 21, 305 (1967) (x,D,P,R,S)
77. J. M. McCrea, Appl. Spectry. 23, 55 (1969) (x,A,B,C,R,S)
78. J. M. McCrea, "Characteristics of Ion-Sensitive Emulsions for Mass Spectry. Allied Topics, Montreal, June 7-12, 1964, Paper No 92 (x,D,P,R,S)
79. J. M. McCrea, "Characteristics of Ion-Sensitive Emulsions for Mass Spectrography II," 13th Ann. Conf. Mass Spectry. Allied Topics, St. Louis, May 16-21, 1965, Paper No 13 (x,D,P,R,S)
80. J. M. McCrea, "Detection Systems and Quantitative Aspects of Spark Source Mass Spectrometry," 3rd Nat. Meeting Soc. for Appl. Spectry. Cleveland, Ohio Sept 28-Oct 3, 1964 (r,A,B,D,P,R,S)
81. J. M. McCrea, in "Developments in Applied Spectroscopy, Vol. 4" E. N. Davis, ed., Plenum Press 1965 pp 501-516 (x,t,r,C,R)
82. J. M. McCrea, Int. J. Mass Spectry and Ion Phys. 3, 189 (1969) (x,R,S)
83. J. M. McCrea, J. Matls. 4, 210 (1969) (t,C)
84. J. M. McCrea, "Photographic Indexing Technique for Evaluating Emulsion Uniformity of Spectrographic Plates" 11th Ann. Conf. Mass Spectry Allied Topics San Francisco, May 19-24, 1963, Paper No 105 (x,D,P,R)
85. J. M. McCrea, "Propagation of Error from Densitometer Data to Spectrographic Results" 14th Ann. Conf. Mass Spectry. Allied Topics, Dallas, May 22-27, 1966, Paper No 62 (t,B,C,P,R)
86. J. M. McCrea, "Response of Photographic Emulsions to Photons and Kilovolt-Energy Charged Particles," 4th Nat. Mtg Soc. for Appl. Spectry, Denver, Col. Aug. 30-Sept. 2, 1965 (x,t,P,R)
87. J. M. McCrea, Spectrochim. Acta 21, 1014 (1965) (x,R)
88. R. J. McClure, Rev. Sci. Inst. 36, 1246 (1965) (x,P,R)
89. J. W. Mitchell, J. Phys. Chem. 66, 2359 (1962) (t,P)
90. E. B. Owens, Appl. Spectry. 16, 148 (1962) (x,E,M,S)
91. E. B. Owens, in "Mass Spectrometric Analysis of Solids, A. J. Ahearn, ed., Elsevier Publishing Co, Amsterdam, 1966 pp 56-110 (r,x,t,A,B,C,D,E,M,R,P,S)
92. E. B. Owens, "Photographic Emulsions as Ion Detectors in Quantitative Mass Spectrography" 12th Ann. Conf. Mass Spectry. Allied Topics, Montreal, June 5-12, 1964 Paper No 40 (r,A,C,D,P,R,S)
93. E. B. Owens, Rev. Sci. Inst. 32, 1420(1966) (x,D)
94. E. B. Owens, Rev. Sci. Inst. 41, 636 (1970) (x,A,C)
95. E. B. Owens and N. A. Giordino, Anal. Chem. 35, 1173 (1963) (x,t,A,B,C,M,R,S)
96. P. J. Paulsen and P. E. Branch, "Electronic Analog Computer for Measuring Intensity Areas on Mass Spectrographic Plates," 14th Ann. Conf. Mass Spectry Allied Topics, Dallas, May 22-27, 1966 Paper No 63 (x,C,R)
96. G. D. Perkins, "Plate Reader for Mass Spectrograph," 12th Ann. Conf. Mass Spectry. Allied Topics, Montreal, June 7-12, 1964 Paper No. 94 (x,C)
97. W. Reuter and J. C. Webber, "The Application of a Dual Emulsion Technique in Spark Source Mass Spectrography," 4th Nat. Mtg. Soc. for Appl. Spectry. Denver, Aug. 30-Sept 3, 1965 (x,B,P,R)

98. J. Roboz, "Introduction to Mass Spectrometry," Interscience Publishers, New York, 1968 pp 174-179, 340-342, 349-350, 389-399 (r,A,D,R)
99. W. Rudloff, Z. Naturforschg. 16a, 1263 (1961) (x,M,R)
100. W. Rudloff, Z. Naturforschg. 17a, 414 (1962) (x,D,E,M,R,S)
101. K. Sato, R. Suzuki, N. Yamaguchi and O. Kammori, Mass Spectroscopy, (Japan) 17 733 (1969) (x,C,R)
102. K. D. Schuy, J. Franzen and K. H. Maurer, "Ion Detection by Photographic Plates (Parts 3&4) Spring Meeting German Physical Society, Wuerzburg (1965) (x,r,B,C,D,S)
103. K. D. Schuy, K. H. Maurer and J. Franzen, "The Shape of the Transparency Curves, Spring Meeting German Physical Society Wuerzburg, (1965) (x,t,R,S)
104. R. K. Skogerboe, W. L. Harrington and G. H. Morrison, Anal. Chem. 38, 1408 (1966) (x,C,R)
105. J. Vastel, Mem. Sci. Rev. Metallurg. 66, 703 (1969) (x,r,A,C)
106. G. Vidal, P. Galmard and P. Lanusse, La Recher. Aerospatiale No 130, 29 (1969) (x,A,S)
107. G. Vidal, P. Galmard and P. Lanusse, Meth Phys Anal (GAMS) 5, 112 (1969) (t,x,E,M,P,S)
108. H. Wagner, Ann. Physik 7-13, 189 (1964) (x,E,M,R)
109. H. Wagner, J. Sci. Inst. 44, 883 (1967) (x,R,S)
110. H. Wagner, Some Aspects of the Physical Principles of the Quantitative Analysis of Mass Spectra with the Photoplate," Acta IMEKO 5, 526 Budapest 1961. (Inter. Messtechnik Konferenz) (see Nuclear Science Abstracts 18, 1998 (1964) (r,E,M,R,S)
111. H. Wagner and K. Bluether, Spring Meeting of German Physical Society, Wuerzburg, 1965 (x,P)
112. H. Wagner and H. Mai, Z. Naturforschg. 19a, 1624 (1964)(x,E,M,R)
113. H. Wagner and R. Hergt, Z. Naturforschg. 22a,1984 (1969) (x,t,B)
114. J. H. Webb, Phys. Rev. 74, 511 (1948) (r,t,T)
115. H. W. Werner, Philips Res. Repts, 21, 63 (1966) (x,E,M)
116. H. W. Werner and J. M. Niewenhuizen, Z. Naturforschg. 22a, 1035 (1969) (x,P)
117. J. R. Woolston, "Data Processing for the Mass Spectrographic Analysis of Solids," 13th Ann. Conf. Mass Spectry. Allied Topics, St. Louis, May 16-21 1965 Paper 17 (x,C,R)
118. J. K. Woolston, RCA Review 26, 539 (1965) (x,C,R)
119. J. R. Woolston and R. E. Honig, Rev. Sci Inst. 35, 69 (1964) (x,E)
120. J. R. Woolston, W. L. Harrington, R. E. Honig, E. M. Botnick and D. A. Kramer, "The Mass Response of Ion-Sensitive Plates Used in Mass Spectrography," 16th Ann. Conf. Mass Spectry Allied Topics, Pittsburgh, May 12-17, 1968, Paper No 100 (x,M,P,R,S)
121. J. R. Woolston, R. E. Honig and E. M. Botnick, "The Response of Ion-Sensitive Plates as a Function of Ion Energy," 14th Ann. Conf. Mass Spectry Allied Topics, Dallas, May 22-27, 1966 Paper No 98 (See Sci Inst.38) (x,E,P,R,S)
122. J. R. Woolston, R. E. Honig and E. M. Botnick, Rev. Sci. Inst. 38, 1708 (1967) (x,E,P,R,S)
123. N. Yamaguchi, R. Suzuki and O. Kammori, Japan Analyst 18, 3 (1969) (in Japanese)

PHOTOGRAPHIC VS. ELECTRICAL DETECTION FOR SPARK SOURCE INSTRUMENTS

F. D. Leipziger

Ledgemont Laboratory, Kennecott Copper Corp.
Lexington, Massachusetts

I. Introduction

As one reads the literature of spark source mass spectrography over the past ten years, it readily becomes apparent that workers in the field acknowledge analytical accuracy as the foremost problem of the method. As one reads further, it becomes clear that a major portion of the blame for problems in accuracy is placed on the ion sensitive photoplate which is the commonly used detector for these instruments.

The spark source instrument has been available commercially for about ten years and its raison d'etre is the analysis of traces in solids. The magnitude of the failure of this tool can be measured in the lack of quantitative data, the disagreements between laboratories running the same samples, and the number of papers in the literature attempting to revise raw data by means of corrections related to the photoplate. Only in a few specialized cases can the spark source be considered a successful analytical tool.

If we examine more carefully the causes for this failure, we find that present day instruments are essentially the same as the first instrument designed in 1947. The following is a description of a spectrograph:

> "A mass spectrograph for chemical analysis of solids has been developed. The Mattauch arrangement of $31^{\circ}50'$ electric deflection followed by a 90° deflection in a magnetic field is used in order to obtain a large mass range in focus on one plate.
>
> . . . During the introduction of the plate or insertion of new electrodes a gate valve is closed to isolate the spectrograph from the pumping system."

It applies to any of the modern day commercial instruments. Unfortunately, that was the description of the first solids instrument developed by Shaw and Rall at the Argonne National Laboratory in 1947[1]. These workers unhesitatingly chose the photographic detector. The erratic nature of the ion beam produced by the vacuum spark and electrical interference supposedly precluded the use of electron multiplier or Faraday cup detectors. It is rather a sad commentary that today's instruments have advanced so little in over 20 years.

The difficulties which are encountered in attempts to obtain quantitative information using the photoplate as an ion detector indicate that an extremely complex situation prevails. Experience with optical emission spectrographs and their excellent accuracy compared to poor results with the mass spectrograph confirms the presence of a problem. The need for standards for accurate chemical analysis was forseen by Shaw and Rall in 1947 and this is still true today.

Since most of the spark source instruments in use today are primarily used for chemical analysis, I will discuss the detector problem in this light.

II. Analysis using the Photoplate

Techniques for quantitative analysis using the photoplate have been described by many authors. A characteristic of all these techniques is that they are slow. Depending on the type of information the user requires, the lag between detection of the ion beam and reduction of the data will vary from a few hours to a day or more.

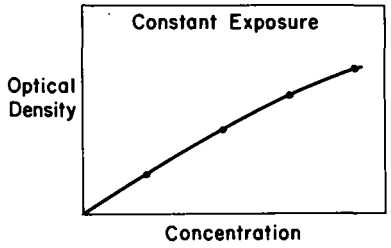

METHOD OF Kai AND MiKi

FIGURE 1

Block diagram of spark source log, ratio system

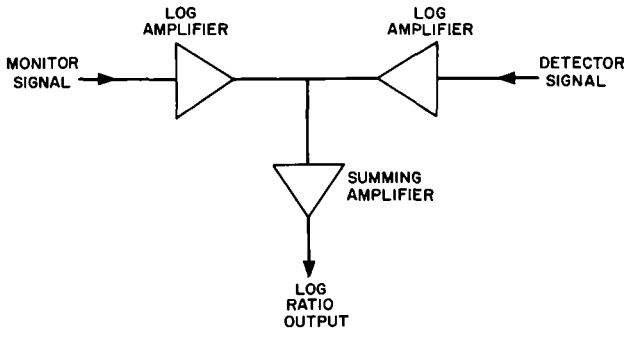

FIGURE 2

Tin and antimony region of ratio scan

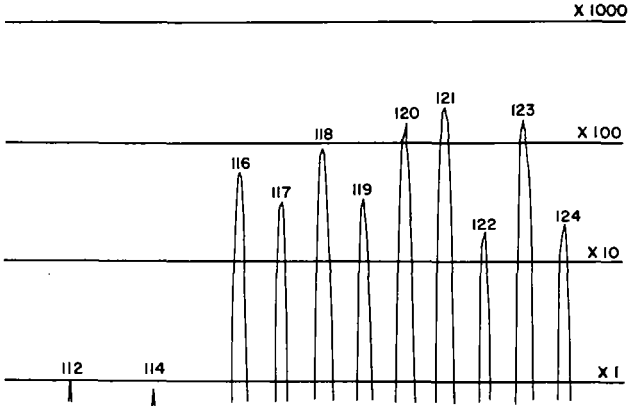

FIGURE 3

A typical procedure involves sparking samples to obtain a graded series of exposures to insure that several of the exposures are in the correct range for densitometry. Next the plate is removed from the spectrograph, developed, fixed and dried. Only then is the spectrographer ready to consider an emulsion calibration. These calibrations require a series of spectral lines of known relative exposure values, and from these the number of ions required to cause a specific degree of darkening may be calculated. The urgency and complexity of this problem may best be appreciated by considering the well known mass spectrographers whose names are associated with calibration techniques - Mattauch, Ewald, Hintenberger, and Dornenburg. The two line method of Churchill although originally developed for optical emission was adapted by Duke [2] and has found wide acceptance in mass spectrography.

The next step in this hypothetical procedure involves measurement of the actual relation between the impurity and the matrix. All of the photographic data treatment methods require careful densitometry and emulsion calibration. A common approach involves conversion of the line densities of the impurity and the matrix to relative beam intensities using the calibration curve. A number of corrections are then applied to this ratio and they are summarized in the following relation:

$$C_i = \frac{Es}{Ei} \cdot \frac{As}{Ai} \cdot \frac{Ss}{Si} \cdot \frac{Wi}{Ws} \cdot \frac{Mi}{Ms}$$

where the subscripts s and i refer to matrix and impurity and E is exposure, A is isotopic abundance, S is relative detector sensitivity, W is line width, and M is charge ratio when singly charged ions are not used.

Corrections for line width, background, the effects of ion mass and ion energy, and ion charge distribution are all on a sound theoretical basis and should be applied wherever possible.

It is unfortunate that this tedious, painful, and time consuming procedure does not work at all well. There is no guarantee that the final answer will bear any recognizable relationship to the true amount of an impurity in a solid.

When it is possible to use standards the situation will improve--but not to the point one might expect or hope. Several methods involving standards have been described by Kai and Miki [3].

If several standards for an element are available, a curve is constructed relating optical density, D, and concentration at a given exposure. A similar exposure is made with the unknown material and the concentration of the impurity may be read from the curve as shown in figure 1.

Alternatively, when only one standard is available, exposures are made which cover a wide range. The optical density of the lines of the known impurity are measured in all spectra. Then optical density is plotted against log X where X = CIE, with C = concentration, I = isotope abundance, E = exposure. Concentrations are then determined in the unknown by making use of the curve so constructed.

Experience in our laboratories with these methods has been disappointing. We have had occasion to work with a series of emission spectrographic copper standards which should have provided excellent results with either of the methods described above. The known impurities were all metallic in nature, at reasonable concentrations, and well characterized. Our results ranged from barely acceptable to abominable. This may be due, of course to technique problems, or to inhomogeneity or ion beam monitor difficulties.

Owens, [4] in a detailed discussion of photoplate procedures warns us that "the possibility of large errors must be considered in interpreting analytical results" The many ill defined or unknown parameters which contribute to these errors cannot be evaluated with any certainty using the photoplate because of its lack of speed and non-linear response.

Despite these difficulties several workers have shown excellent accuracy and precision in photoplate work. Franzen and Schuy[5] have obtained data which is at least as good as electrical detection data, using a pulsed dc source which apparently is insensitive to electrode positioning.

III. Electrical Detection

Electrical detection has been the normal mode of operation for mass spectroscopists in most fields. Gas analysis, high resolution organic analysis, Knudsen cell studies and thermal instruments have all made use of the electron multiplier with a good deal of success. The exception which concerns us is in the field of solids analysis.

An early and strongly held view insisted that the erratic nature of the vacuum spark and attendant problems of electrical interference would make electrical detection for solids instruments impossible. However, as long ago as 1941, Strauss[6] successfully attempted the electrical detection of nickel ions from a spark source. Ten years after that, Gorman Jones and Hipple [7] made another successful attempt and at the same time introduced the ion beam monitor. These and other early attempts were of an exploratory nature and the first valid demonstration of trace analysis is by Conzemius, Capellen, and Svec[8]. The efforts of these workers were shortly followed by those of Bingham, Brown, and Powers, [9] and Socha, Baker, and Masumoto, [10] and Evans, Guidoboni, and Leipziger[11].

The aspect which all workers in this field stress is the speed with which data is available for inspection or manipulation. The reasons for this are twofold--first there is no time lost in plate development, densitometry, etc. and second, sensitivity is increased. A given exposure is obtained in less instrument time than with photographic detection. For example, an impurity which requires a 0.1 nanocoulomb exposure is detectable and analyzed electrically within seconds while at least an hour would be needed with the photoplate.

Hull [12] has discussed the time advantage which may be gained by using electrical detection. Obviously the level of the impurity and the number of impurities to be surveyed will enter into the time advantage. A large number of impurities at high levels (1 ppm) is most advantageous to the photoplate and the time saving with electrical detection is as small as a factor of two. The most favorable case for electrical detection involves analysis of ten to twenty elements at the part per billion level. The time factor here may be in excess of one hundred.

I would like to describe briefly the paths some of the early workers have taken when assembling electrical detection systems.

The system developed by Conzemius, Capellen, and Svec contains three essential features--facilities for evaluating the ratio of the impurity and total ion beams, automatic step scanning of the electrostatic or magnetic fields, and the availability of an internal standard. Components have been chosen to ensure ease of computer interfacing.

An important aspect of the Iowa State set up is that the step scanning circuit is activated only after a preset number of counts accumulate in the denominator (total ion beam) of the ratio recorder. In this manner scanning is avoided when the spark

is not operating. This is an elegant way around the problem of the erratic ion beam produced by the vacuum spark.

The performance of this system has been excellent. Conzemius and Svec have obtained results on a series of steels certified by the Bureau of Standards for homogeneity. Using a large sample as recommended by the Bureau they obtained an average precision of ± 6% with over 60% of the total elements having precision appreciably better than 6%.

The second system I would like to discuss is that of the AEI workers, Bingham, Brown and Powers. This particular system is in most ways similar to the one at our Laboratory.

The AEI approach is twofold. One mode of operation involves continuous magnetic scanning and ratiometry to obtain rapid semiquantitative data. The second mode uses electrostatic peak switching to obtain accurate and precise analytical data.

Magnetic scanning has proved to be an excellent rapid survey method where semiquantitative results are acceptable. In this mode of operation the magnet is scanned to sweep the peaks over the collector. Figure 2 shows the amplifier arrangement used to correct for fluctuations in the ion current while the peak is on the collector. The double logarthmic amplifier obtains a ratio of the impurity ion current to the total ion beam. This ratio may then be displayed on a recorder--such a spectrum is shown in Figure 3. A dynamic range of 1000 to 1 can be displayed with this arrangement. For example, if the line marked "x1" can be set to a value of 2 ppm then the values at the other lines are 20, 200, and 2000 ppm. The region over which this range is used can be easily changed.

Table I shows the type of results which can be obtained with peak scanning. The precision and accuracy are better than ± 30% in most cases and the speed of the scan (110 seconds per decade) is orders of magnitude faster than any photoplate procedure.

Table I
Reproducibility of Nine Repeat Analysis on Copper
Standard CA2 with Ratio Scanning

	Found	True
Bi	44 ± 14	40
Pb	36 ± 15	30
Sb	68 ± 24	60
Sn	57 ± 21	65
Ga	79 ± 30	75
Cr	83 ± 31	70

The second mode of operation of this system, peak switching, is used where the highest analytical precision is required. It is necessary to spend longer times on the peaks of interest to obtain the required precision and this necessitates the use of a device to insure beam stability.

This problem has been solved with the aid of an external vibrator. This device is attached to one of the manipulators and the resultant motion of that electrode is sufficient to ensure continuity of the spark.

The peak switching mode of operation involves electrostatic voltage changes. The peaks of interest are preset by ascertaining the voltages necessary to center them on the multiplier slit. Quantitative analyses are then performed by integrating the

collector current for the impurity of interest while a particular charge is collected by the ion beam monitor. For results to be truly quantitative, standards are required.

The procedure when standards are available in quite straight forward--the response of the multiplier to a known amount of the impurity element is determined. Next the unknown is sparked and the concentrations are then in the ratio of the collector currents. The results which may be obtained with this type of system have been published by several workers and Table II shows some work from our laboratory on NBS steels. The excellent precision and accuracy are typical of electrical detection when standards are available.

Table II

Analysis of NBS Steels for Molybdenum using Electrical Detection

NBS #	Mass Spec.	w/o	NBS Value
461	0.38		0.36
462	0.94		0.94
463	1.13		1.15
465	0.0024		0.002
466	0.0075		0.007
467	0.47		0.47

However, we have found it necessary to develop a rather meticulous sample handling procedure to obtain these results routinely, and we feel that the speed of the detector was of paramount importance in developing the required procedure. Positioning of the sample was found to be a key aspect of the routine analysis of metals.

The next slide illustrates the changes which appear when the electrodes are sparked at varying positions relative to the first plate.

Table III

Variations Caused by Electrode Placement

Increasing Distance from Accelerating Plate	Cu^{+1}/Cu^{+2}
↓	12.30
	4.98
	5.49
	5.97
	4.43

It immediately is apparent that a standardized mounting procedure must be used to minimize these large variations in ion current. The procedure we have adopted involves a mounting jig which reproducibly sets the distance of the sample from the accelerating plate. A microscope is used to align the electrodes with the extraction orifice. These steps are apparently sufficient to reduce the error in mounting to less than ± 5%. The following data indicates the reproducibility obtained in the analysis of silver in the Johnson-Matthey copper standards.

Table IV

Repetitive Sample Loadings

(Integrated Multiplier Current)

Ag in JM CA6

Run	1	2	3	4	5	6	7
Counts	1172	1125	1166	1197	1156	1158	1180
% RSD	2.9	2.4	1.4	4.4	3.2	1.6	3.0
Avg. of Avg's.	1165 ± 1.9%						

These electrode pairs were remounted in the source for each run and the precision of the entire procedure speaks for itself. Once the samples were mounted the time for a single set of data (ten determinations) was approximately ten minutes.

Summary

The contrast between electrical and photographic detection is most striking in the areas of speed and accuracy. Whether one operates in the peak switching mode with standards for highest accuracy or in a magnetic scanning mode for survey analysis the electrical system is faster than the photoplate by factors of two to one hundred.

This speed of presentation allows the operator a much greater latitude for ascertaining the effects of spark parameters and sample positioning. In these cases the data is available within minutes as opposed to hours with the photoplate.

It should also be obvious that the output of an electron multiplier is easily interfaced with a computer to obtain an automated system. The only automation possible with the photoplate involves plate scanners which remove the tedium associated with manual densitometry. The time lag between sparking of the sample and availability of the data is essentially unchanged.

When one considers other analytical tools of the same era such as atomic absorption and flame emission spectroscopy, electron microanalysis, and scanning electron microscopy, the lack of growth of spark source instruments is painfully apparent. The acceptance of these other tools is universal. They have satisfied a need--the need still exists for ultra trace analysis and it is still unsatisfied.

In conclusion, I feel strongly that if the spark source mass spectrograph is ever to become a routine and accurate tool it must do so with electrical detection.

References

1. A. E. Shaw, and W. Rall, Rev. Sci. Inst. 18 5, 278 (1947).
2. J. F. Duke, and M. S. Brooks, and J. K. Kennedy, (Eds.) "Ultrapurification of Semiconductor Materials", Macmillan, New York, 1962, P. 294.
3. J. Kai, and M. Miki, Mitsub. Denki Lab. Rept. 5 175 (1964).
4. E. B. Owens, in A. J. Ahearn (Ed.) "Mass Spectrometric Analysis of Solids", Elsevier, New York 1966, Chap. III.
5. J. Franzen, and K. Schuy, Z. Anal. Chem. 225-2 295 (1967).
6. H. A. Strauss, Phys. Rev., 59, 430 (1941).
7. J. G. Gorman, J. A. Hipple, and E. J. Jones, Anal. Chem., 23, 438 (1951).
8. R. J. Conzemius, J. Capellen and H. J. Svec, Thirteenth Annual Conference on Mass Spectrometry and Allied Topics, St. Louis (1965).
9. R. A. Bingham, R. Brown, and P. Powers, Pittsburgh Conference on Analytical Chemistry and Applied Spectroscopy, Cleveland (1968).
10. A. Socha, C. W. Baker, and E. M. Masumoto, Seventeenth Annual Conference on Mass Spectrometry and Allied Topics, Dallas (1969).
11. C. A. Evans, Jr., R. J. Guidoboni, F. D. Leipziger, Appl. Spec., 24 85 (1970).
12. C. W. Hull, Int. J. Mass Spectrom. Ion Phys. 3 293 (1969).

SOLID STATE AND SPECIALIZED DETECTOR METHODS

F. A. White

Department of Nuclear Science
Rensselaer Polytechnic Institute
Troy, N. Y.-12181

INTRODUCTION

I have been asked to comment on the possible use of solid state and specialized detectors that might be utilized in monitoring ion beams in mass spectrometry. The remarks which follow are presented in the spirit of the conference; namely to discuss potential applications of new detectors with the understanding that these detectors are not at the stage of development that is comparable to ion detection methods which have been presented in the previous papers. Nevertheless, one of the schemes which I shall mention appears to have substantial merit, especially since it may ultimately replace (for restricted applications) the photographic plate, which possesses the advantage of monitoring ion beam currents simultaneously over an extended mass scale.

THE P-N JUNCTION AS AN ION DETECTOR

The use of reversed bias p-n junctions for the detection of high energy nuclear particles has been important for nearly a decade. These junction counters are able to provide an energy resolution for alpha particles, beta particles, and even gamma rays. The first application of solid state diodes to mass spectrometry was reported in 1961.[1] In this early application the ion detection efficiency was exceedingly poor. However, the basic concept was to allow the incident ion to strike a "converter" in order to produce secondary electrons.[2] These secondary electrons were then accelerated and focused into the "depletion region" of the junction, and the kinetic energy of the electron was converted (in part) to the generation of electron-hole pairs. Basically the reverse bias junction acts as a solid state ionization chamber with approximately 1 electron-hole pair being formed per 3.5 ev of energy expended in a silicon crystal.

A major difficulty in adapting a p-n junction for direct ion detection is the very restricted range of charged atoms in matter. Only very light ions of high energy (>30 keV) have a sufficient range to penetrate the silicon junction "dead layer", expend a large fraction of their energy in the "depletion region", and thereby generate a large amount of ionization. Post-acceleration of mass-resolved ion beams is possible, but very high voltages (>100 kv) would be required for the direct detection of heavy ions. The alternative of letting the primary ions strike a "converter" plate that will generate secondary electrons and accelerate these secondaries into the junction, appears quite practical. As in the case of the scintillation counter for ion detection, there is the further advantage of charge amplification in the secondary electron process itself.

A silicon p-n junction, operating under conditions of reverse bias, functions as an exceedingly shallow ionization chamber for the detection of secondary electrons. The "depth" of this silicon ionization chamber, or "depletion zone", can be derived from Poisson's equation, the

current continuity equation, and various parameters of the material. The results, however, can be expressed simply as:[3]

$$x = 3.2 \times 10^{-5} (\rho V)^{\frac{1}{2}} cm \quad \text{(p-type)}$$

$$x = 5.3 \times 10^{-5} (\rho V)^{\frac{1}{2}} cm \quad \text{(n-type)}$$

where x is the depletion depth, V is the reverse bias (in volts) applied to the p-n junction, and ρ is the resistivity of the silicon expressed in ohm-cm. For high resistivity silicon (3000 ohm-cm), and a reverse bias of only 50 V, the effective depth of the depletion zone would be approximately 200 microns. This depth is greater than the range of a 100 kev electron.

Figure 1 is a schematic of the apparatus for detecting ions, using a secondary electron converter. Positive ions are focused onto a high-voltage anodized aluminum electrode (30 kV, negative) and secondary electrons are accelerated onto a surface-barrier junction. The interesting results are shown in Figure 2. The graph clearly shows 18 quantized peaks as displayed in a multichannel analyzer. The spectrum indicates the relative number of secondary electrons released by primary ion impact.[4] The first peak is caused by ions that generate only a single secondary electron with the subsequent production of electron-hole pairs in the junction after this electron has acquired 30 kev). Successive peaks indicate ionization energies in the junction region of 60, 90, ----, 540 kev, corresponding to the "ionization" in the junction due to two, three, -----, eighteen (30-keV) electrons that arrive simultaneously.

I am extremely optimistic about the ultimate use of such junctions in mass spectrometry. Because of their small physical size, a large number of diodes can be adapted to read-out an entire mass spectrum simultaneously. If this is ultimately achieved, such a method would possess the sensitivity of an electron multiplier; it would also have the integrating capability of an extended photographic plate.

POTENTIAL USE OF BEAM FOIL SPECTROSCOPY

I should now like to comment on a possible detection scheme for ions which, at present, is far from practical. I believe this mechanism for ion detection merits mention simply because it is a unique means by which ion beams, in principle, can be detected and monitored. I refer to a recent development in the field of beam foil spectroscopy. Consider an ion to be incident upon an exceedingly thin film ($\sim$200 angstroms). Assume also that the kinetic energy of an incident ion is sufficiently high to completely penetrate the thin foil. If the ions are positive ions, many of these incident atoms will become neutralized during their penetration through the foil and a large number will emerge in various excited states. We can expect that such atoms would de-excite at times depending upon the energy level of the emerging atom, and the atom will radiate photons which correspond to differences between the energy level of the excited state and the ground state.

Indeed, workers in Stockholm have recently reported[5] not only the detection of the photon spectrum of lithium atoms (56 kev) emerging through a thin ($10 \mu g/cm^2$) foil but they have published results which indicate the lifetimes of such excited levels. The beam of excited atoms was analyzed slightly downstream from the thin foil with a low dispersion Jarrell-Ash scanning monochromator equipped with a photo multiplier detector[6]. Thus, it is appropriate to ask whether single atoms can be detected and whether this new technique could be utilized on mass spectrometry. I cannot answer this question with any degree of confidence. However, there are reasons for assuming that the fractional number of atoms emerging from such a thin foil would be a constant, and it is simply a question of advanced technology to pick up the optical spectra from ions which are passing by a suitable photo tube sensor and have these signals amplified and registered with output circuitry. Let me restate that I do not consider this technique to be a practical one, but I was invited to suggest new "solid state" devices that might be applicable in some specialized situations.

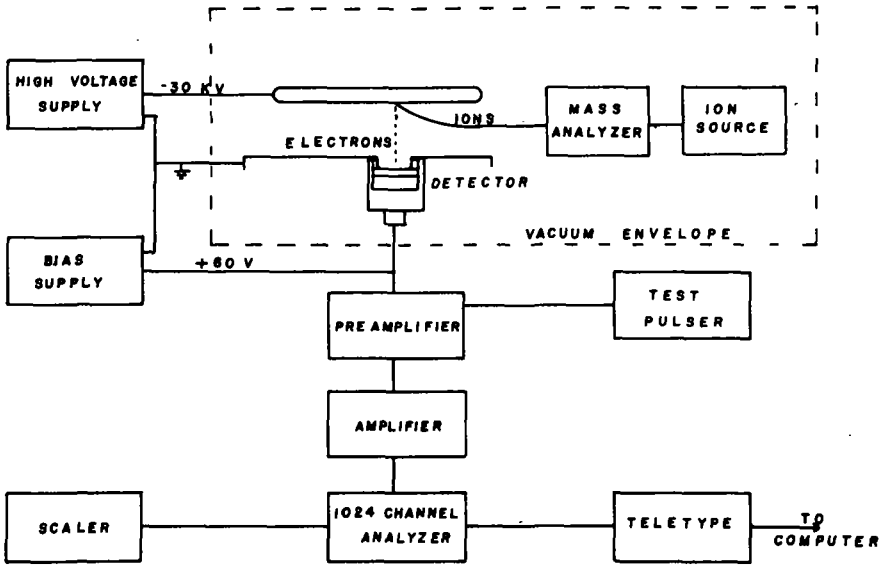

BLOCK DIAGRAM OF DETECTOR

Figure 1

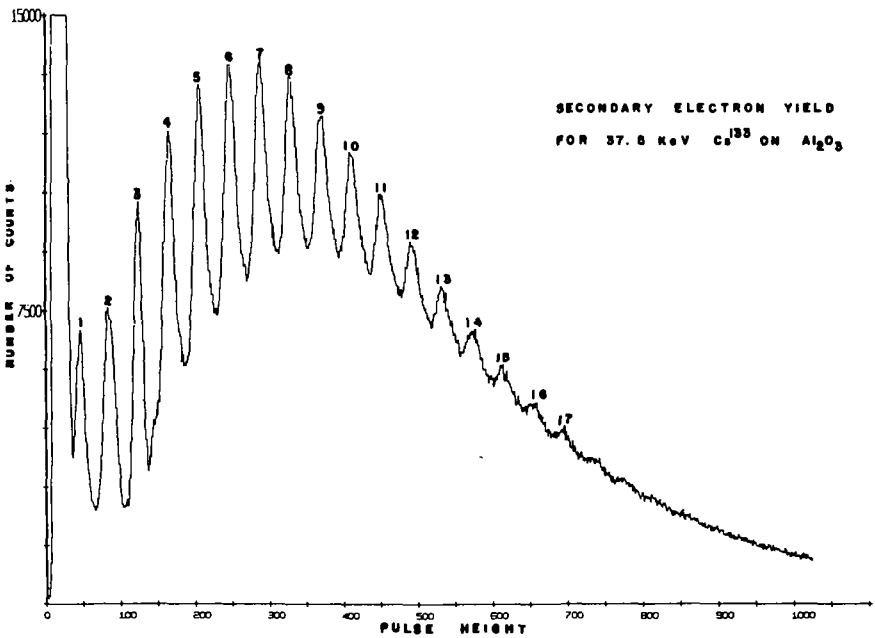

Figure 2

CONCLUSION

There is little doubt that the photographic plate and a variety of electron multipliers will continue to be the basic detectors in mass spectrometry for the next decade. However, there is substantial evidence to indicate that reversed bias p-n junctions, with improved circuitry, may offer significant advantages. When we realize that the communications industry has already adapted solid state devices in which hundreds of thousands of diodes (within a few cm^2) comprise a photo-sensing element, it is not unreasonable to assume that at least hundreds of p-n junctions can be built into a sophisticated mass analyzing system. The inherent advantages of having a simultaneous readout of all the chemical elements, or being able to monitor isotopic spectra on a time-dependent basis, suggests that solid state devices must be regarded quite seriously for future use.

REFERENCES

1. F.A.White, J.C. Sheffield and J.W.Mayer Electronics 34, 74, (1961)

2. F.A. White, Mass Spectrometry in Science & Technology, John Wiley, N. Y. 1968, p.106.

3. G.Dearnaley and D.C.Northrop, Semiconductor Counters for Nuclear Radiations, Wiley, New York (1966) p.128.

4. J.D.Stein and F.A.White (to be published).

5. W.S.Bickel, I. Bergstrom, R.Buchta, L.Lundin, and I.Martinson. Phys. Rev. 178, 118, (1969.

6. IBID

Comparisons between Ionic Collision Processes in Gaseous Water and Gaseous Ammonia *

K. R. Ryan, C.S.I.R.O., Camden, N.S.W. 2570 Australia

Rate coefficients for reactions resulting from collisions of H_2O^+ and OH^+ with H_2O and of NH_3^+ and NH_2^+ with NH_3 have been measured as a function of primary ion translational energy over the energy range of 0 to 8.0 eV. The experiments were performed using the techniques of single-source high pressure mass spectrometry.

A great similarity exists between the results of collisions of H_2O^+ with H_2O and of NH_3^+ with NH_3. In both cases the measured rate coefficient drops sharply with increasing energy from thermal energies to about 1 eV. maximum translational energy (K.E.). Above 3 eV. K.E. an essentially constant value for the rate coefficient is obtained. For the water system this constant value is within 5% of that predicted by the theory of Giomousis and Stevenson (G. and S.) while in the case of ammonia the value obtained is about 60% of the value predicted by the theory of G. and S.

It is shown that both OH^+ and NH_2^+ react with high rate coefficients over the K.E. range examined. The fraction of reacting OH^+ which proceeds by proton transfer is shown to fall rapidly from about unity at thermal ion energies to a negligible value for ions with energy above 1 eV. K.E. Electron transfer or ion-atom interchange continues to occur with high rate coefficient. The behaviour of NH_2^+ collisions with NH_3 is quite similar to the analogous process in water at ion energies below 3 eV. K.E. Once again ion-atom interchange or electron transfer processes dominate the collision reactions as the ion energy is increased from near thermal values. However NH_4^+ production appears to have a new onset between 2 and 3 eV. K.E. It is suggested that this new production of NH_4^+ proceeds via the endoergic reaction in which the neutral products are N + H and not NH_2 as is supposed for the proton transfer process at lower ion energies.

* A complete description of this work is expected to appear in forthcoming issues of the Journal of Chemical Physics.

KINETIC ENERGY DEPENDENCE OF THE REACTIONS OF O^+ WITH CO_2*

N2

by

M. Mosesman and W. T. Huntress, Jr.

Jet Propulsion Laboratory
California Institute of Technology
Pasadena, California 91103

The previous work of Schildcrout and Franklin[1] on the reaction of O^+ with CO_2 suggested that charge transfer from O^+ to CO_2 competes with O atom abstraction when the O^+ ion has sufficient kinetic energy to overcome the 0.20 eV endothermicity of the charge transfer reaction, viz.

$$O^+ + CO_2 \begin{cases} \xrightarrow{k_1} O_2^+ + CO & -1.61 \text{ eV} \\ \xrightarrow{k_2} CO_2^+ + O & 0.20 \text{ eV} \end{cases}$$

In this work, the existence of these two channels is proven using a triple resonance experiment in an ion cyclotron mass spectrometer. This technique involves a unique combination of pulsed ion ejection and cyclotron irradiation of O^+ permitting observation of both reaction channels as a function of kinetic energy.[2] The kinetic energy scale in this experiment is undetermined.

In order to determine the O^+ kinetic energy scale, experiments similar to those pioneered by L. R. Anders[3] were performed. These experiments were conducted in the following manner. The gas is first ionized by a 150 μsec pulse of 50 V electrons. The O^+ ion is irradiated at its cyclotron frequency for 150 μsec shortly after termination of the ion production pulse and before reaction can occur. This sequence is repeated at a rate of 200 Hz. From the magnitude of the rf field and its pulse duration, the kinetic energy of the O^+ ion can be calculated. The dependence of the relative rate for channel 1 on O^+ kinetic energy was obtained by monitoring the O_2^+ ion intensity with a marginal oscillator whose output is amplified and measured with a boxcar integrator. The large CO_2^+ signal from primary ionization of CO_2 prevented observation of channel 2 with this technique. However, by comparison of the kinetic energy experiment with the triple resonance data, the charge transfer channel could be simultaneously plotted. The results are given in Fig. 1. In order to increase the signal/noise for channel 1, the primary ion current of O^+ was increased by continuous cyclotron ejection of primary CO_2^+ ion which permits the electron emission current to be raised.

*This paper presents the results of one phase of research carried out at the Jet Propulsion Laboratory, California Institute of Technology, under Contract No. NAS 7-100, sponsored by the National Aeronautics and Space Administration.

REFERENCES

1. S. M. Schildcrout and J. L. Franklin, J. Chem. Phys., 51, 4055 (1969).

2. M. Mosesman and W. T. Huntress, J. Chem. Phys., in press.

3. L. R. Anders, J. Phys. Chem., 73, 469 (1969).

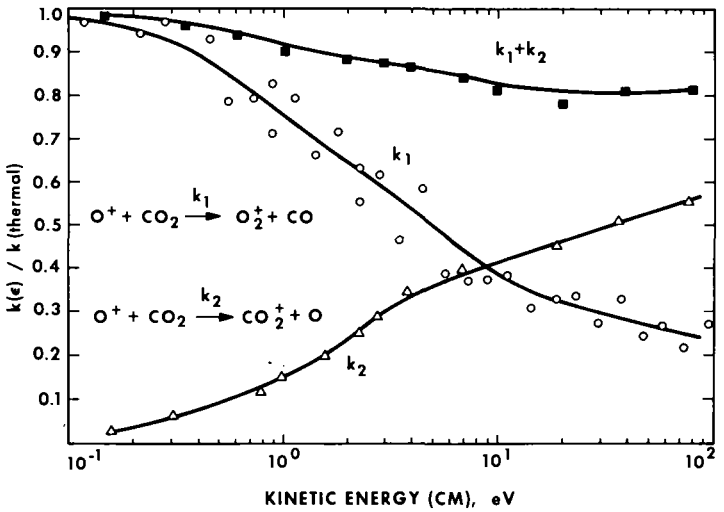

Fig. 1

Kinetic energy dependence of the relative rate constants for the channels available in the reaction of O^+ with CO_2.

High Pressure Photoionization Mass Spectrometry. III. Reactions of $NO^+(X'\Sigma^+)$ with C_3 through C_7 Hydrocarbons at Thermal Kinetic Energies.*

Stuart K. Searles† and Wayne Sieck
National Bureau of Standards
Washington, D. C. 20234

Introduction

The reactions of $NO^+(X'\Sigma)$ with alkanes and cycloalkanes (RH_2) has been investigated using 10.0 eV (123.6 nm) photons supplied by a Kr resonance lamp. The use of such a lamp as an ionizing source greatly simplified the interpretation of these experiments since only the NO component in NO-RH_2 mixtures was ionized for most RH_2 combinations. The advantages of the photoionization technique over electron impact are discussed in some detail.

Experimental

A detailed description of the experimental apparatus has been published.[1,2] In brief, it consists of a field free reaction chamber (photoionization source) equipped with windows to admit ionizing radiation from a rare gas line source or lamp monochromator combination. The resulting primary and product ions at any given source pressure may pass out of the reaction chamber through a pinhole leak coupled with a quadrupole mass analyzer. The fabrication and operational characteristics of static Xe, Kr, Ar, Ne and He resonance lamps used as ionizing sources have been described by Gorden, Rebbert and Ausloos.[3] Power for these low pressure lamps is provided by a microwave generator, and the useful output is usually concentrated in the manifold of lowest excited states of the rare gas atoms. The available wavelengths and corresponding energies are listed in Table I.

---

*This work was supported in part by the United States Atomic Energy Commission.

†NRC-NBS Research Associate.

TABLE I

Low Pressure Rare Gas Lamp Emission

Gas	Wavelength(Å)	Energy (e.V.)	Window
He	584.3	21.22	Al
Ne	735.8	16.85	Al
Ar	1048.2 1066.7	11.83 11.62	LiF
Kr	1164.9 1235.8	10.64 10.03	Lif Lif or CaF_2
Xe	1295.6 1469.6	9.57 8.44	Lif or CaF_2

The energy spread in each line is of the order of 0.01 eV, and tnc output of each lamp is $\sim 10^{14}$ quanta/sec, corresponding to an electron beam current of ~10μA. Perhaps the principal advantage of tnese lamps is the low energy of the emitted photons (relative to $\geq$ 70 eV electrons which are more commonly used in mass spectrometry) which results in a simplified primary mass spectrum. This feature of the photoionization technique has great potential in the field of mass spectral identification of unknowns, and is also helpful in the investigation of ion-molecule reaction kinetics. For example, it is often possible to ionize just one component in a mixture. Furthermore, this ionization may lead only to the parent molecular ion if tne ionization potential of the parent is close to tne photon energy. Information on fragment ions may be obtained by using a lamp which emits higner energy photons. There are also several instrumental advantages associated with photoionization, including the fact that tne lamp does not heat the reaction chamber (ion source) as is usually the case with tne heated filament associated with electron impact ionization. In addition, the use of windows on the reaction chamber rather than an open slit reduces the rate of gas flow out of the chamber, and permits higher total pressures in the ionization region.

Results

The vapor phase reaction of $NO^+(X'\Sigma^+)$ with C_3 through C_6 normal, branched, or cyclic alkanes was found to proceed exclusively via an H^- transfer mechanism:

$$NO^+(X'\Sigma^+) + RH_2 \rightarrow RH^+ + HNO \qquad (I)$$

In addition to (I), $C_4H_9^+$ was also formed by a second order process in the reaction with 3-methylhexane. Absolute rate constants were determined for all systems at thermal kinetic energies. Isomers containing tertiary

H atoms were found to be the most reactive, exhibiting rate constants on the order of 10^{-9} cm^3/molecule-second. The rate constants found for n-alkanes and non-substituted cycloalkanes fall in the range 10^{-12} to 10^{-10} cm^3/molecule-second. The results on reaction I suggest that NO may be a good candidate for chemical ionization analysis. An article describing these results will appear in the near future.[4]

References

1. L. W. Sieck, S. K. Searles and P. Ausloos, J. Am. Chem. Soc. 91, 7627, (1969).
2. L. W. Sieck and S. K. Searles, J. Am. Chem. Soc. 92, 2937 (1970).
3. R. Gorden, Jr., R. E. Rebbert and P. Ausloos, Natl. Bur. Std. Tech. Note 496, October 1969.
4. S.K. Searles and L. W. Sieck, J. Chem. Phys.,scheduled for July 15, 1970.

Molecular Beam Studies of Short Lived Molecules and Ions

J. Gray and R. H. Tomlinson

McMaster University, Hamilton, Ontario.

Molecular beam techniques have been used to investigate the existence of short lived molecules and ions. The apparatus used is essentially a tandem mass spectrometer employing a charge transfer and reionization unit in the region between the mass analysers. Ion beams are produced from a radio-frequency source, mass analysed and passed through a charge-transfer canal containing lithium vapour. The resulting neutrals are allowed to continue undeflected while the remaining ions are removed in an electrostatic field. On emerging from this field, a fraction of the neutrals are reionized by electron bombardment from a hot filament. The resulting ions are then mass analysed and detected in a Faraday cup. The geometry of the apparatus is such that only molecules which were neutral for the time of flight through the electrostatic field may become available for reionization and subsequently be focused in the second mass analyser.

The apparatus was calibrated using beams of H^+, D^+, H_2^+, and HD^+ ions. The results obtained with these beams showed that it was feasible to neutralize and reionize a fraction of the beam, and still detect the final products as relatively sharp and identifiable peaks in the mass spectrum.

Fig. 1a shows the spectrum obtained after final mass analysis of the mass 8 primary beam obtained from a helium discharge. With charges up to 5000 volts on the deflector plates and introduction of lithium vapour into the neutralizer, the spectrum shown in Fig. 1b was obtained on mass analysis of the reionized fraction of the neutrals. The two peaks are identified as He_2^+ and He^+ ions. The presence of the peak corresponding to He_2^+ ions is consistent with the assumed existence of neutral He_2 and molecules having lifetimes long in relation to the 10^{-8} seconds necessary for their detection in this apparatus.

The He_2^+ ions in the primary beam would be largely in the $^2\Sigma u^+$ ground state on entering the charge transfer cell since approximately 10^{-4} seconds elapse between production of the ions and subsequent neutralization. The singlet states of the He_2 molecule are unstable with respect to the ground $^1\Sigma g^+$ state and would be expected to lead to the production of two He atoms. Some of the triplet states however are bonding, and would rapidly decay to the $^3\Sigma u^+$ state, which is metastable to the non-bonded singlet ground state. There would be essentially no decay of the $^3\Sigma u^+$ state of the He_2 molecule in the time between formation of the molecule and subsequent reionization (10^{-7} seconds).

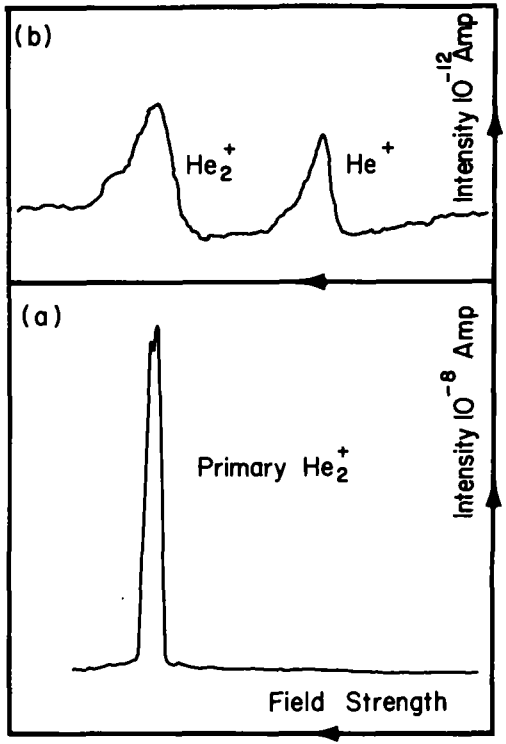

Figure 1

Primary and secondary spectra

from a beam of He_2^+ ions

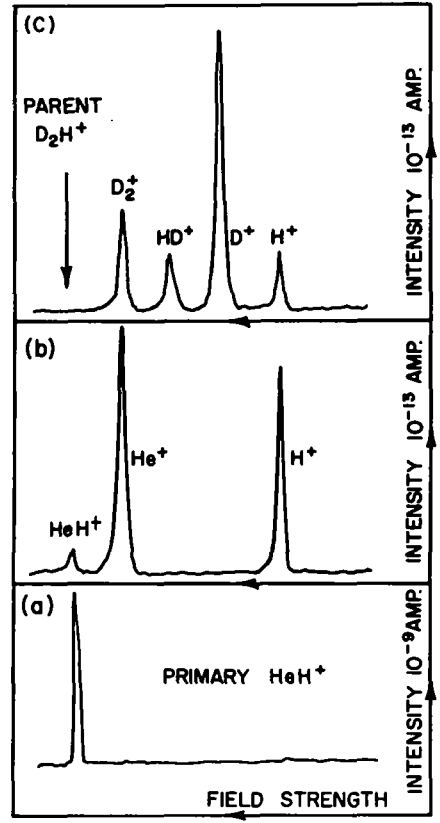

Figure 2 a and b: Primary and secondary spectra from a beam of HeH^+ ions

c: Secondary spectrum from a beam of D_2H^+ ions

Similar procedures have been applied to the HeH^+ and HeD^+ systems. Fig. 2a shows the spectrum obtained in the second mass analyser of the mass 5 primary beam corresponding to 5000 ev. HeH^+ ions obtained from a mixture of H_2 and He in the rf source. Fig. 2b shows the secondary spectrum obtained on neutralization. The peak positions correspond to 5000 ev HeH molecules, 4000 ev He and 1000 ev H atoms. The appearance of a mass 5 peak in the secondary spectrum indicates the existence of HeH molecules with lifetimes of the order of 10^{-8} seconds. Similar results were obtained with HeD^+ beams.

To preclude possible interference from D_2H^+ and D_3^+ ions, it was necessary to investigate these systems separately. Fig. 2c shows the secondary spectrum obtained from a beam of D_2H^+ ions. The position of the primary beam is shown. Similar spectra were obtained with D_3^+ ions and in neither case was it possible to detect a signal corresponding to D_2H or D_3 neutral molecules. Spectra obtained on H_3 itself are complicated by the presence of HD in natural abundance which yields a peak at mass 3. Investigation of the HD system has shown that the natural abundance of D_2 in H_2 could account for the signal intensity observed in the H_3 experiment.

The results of these experiments are interpreted as follows:

1 HeH and HeD systems

$HeH^+ (^1\Sigma) + e(Li) \rightarrow HeH$ (excited doublet states)

$HeH^+ (^1\Sigma) + e(Li) \rightarrow HeH$ (dissociative recombination)

The states in which the HeH molecules are formed depend upon the energy defect of t the charge transfer process.[1] Lithium (I.P. 5.36 ev) was chosen to increase the probability of populating the excited states of the HeH molecule[2]. The results are consistent with the assumed existence of neutral HeH molecules in excited bound doublet states having lifetimes as long as 10^{-8} seconds or approximately 10^5 vibrations. Since the mean lifetime of a molecule in an excited state, having an allowed transition to the ground state, is often of this order of magnitude, the existence of HeH and HeD in this apparatus seems reasonable.

2 H_3, D_2H and D_3 systems

No evidence was found for the existence of these molecules with lifetimes as long as 10^{-8} seconds, however, the existence of bound excited states of H_3 remains a possibility.

The existence of the He_3^+ molecular ion in a low temperature helium discharge was investigated using a similar procedure to that described. Collisional dissociation in the charge transfer cell was used to distinguish between He_3^+ and C^+ ions present in the

beam. He_3^+ ions, on dissociating would be expected to produce peaks in the spectrum corresponding to masses 4(He^+) and 12(He_3^+) in contrast to mass 12 only, in the C^+ system. The spectra obtained demonstrated that at liquid nitrogen temperatures a fraction of the mass 12 beam did consist of He_3^+ ions. Low intensities of the beam, however, precluded investigation of the neutral He_3 molecule.

REFERENCES:

1. H. S. W. Massey, Rept. Progr. Phys., 12 (1949), 248.

2. H. H. Michels and F. E. Harris, J. Chem. Phys., 39 (1963), 6.

This paper is to be published in J. Chem. Phys.

Ion-Molecule Reactions of H_3^+ and D_3^+ with Ethylene Oxide and Acetaldehyde*

by

Michael T. Bowers and Paul A. Kemper

Department of Chemistry, University of California,
Santa Barbara, California 93106

The ion-chemistry generated by the reaction of H_3^+ with ethylene oxide and acetaldehyde is quite rich. The principle reactions are

$$H_3^+ + C_2H_4O \rightarrow \begin{cases} C_2H_3O^+ + 2H_2 & A \\ HCO^+ + H_2 + CH_4 & B \\ C_2H_3^+ + H_2 + H_2O & C \\ H_3O^+ + H_2 + C_2H_2 & D \end{cases}$$

with approximate product distributions given in Table I. These product distributions are

Table I. Product Distributions for Reactions A-D

Product Ion	$\triangle^O$	CH_3CHO
$C_2H_3O^+$	0.27	0.17
HCO^+	0.30	0.44
$C_2H_3^+$	0.33	0.17
H_3O^+	0.10	0.22

averages over the H_2-pressure range of 1×10^{-5} to 1×10^{-3} torr. C_2H_4O pressures were typically 5×10^{-7} torr. The pressure dependence is due to the variation in internal energy of the H_3^+ ion with pressure, as previously suggested by Leventhal and Friedman[1] and Bowers and Elleman,[2] and to collisional stabilization of the internal energy in the $C_2H_5O^+$ intermediate. In addition to reactions A-D, charge exchange is observed at lowest pressures and complete stabilization of the $C_2H_5O^+$ complex at higher pressures. Reactions of D_3^+ with ethylene oxide and acetaldehyde give the results in Table II. It is clear

Table II. Product Distributions for D_3^+ Reactions

Product Ions	$\triangle^O$	CH_3CHO	*Random*
$C_2H_2OD^+$	7.0	~1.3	1.5
$C_2H_2OH^+$	1.0	1.0	1.0
DCO^+	0.05	0.16	0.25
HCO^+	1.0	1.0	1.0
$C_2H_2D^+$	~0.25	~0.3	1.5
$C_2H_3^+$	1	1	1
H_2DO^+	1.0	1.0	1.0
H_3O^+	0.1	~0	0.66

* Supported by a grant from the National Science Foundation.

that most of the eliminations are quite specific and that there is no particular relationship to the random distributions. The results for the elimination of H_2O (reaction C) and the formation of $(H,D)_3O^+$ (reaction D) indicate that the proton (or deuteron) from H_3^+ (or D_3^+) is initially transfered to the oxygen and remains on the oxygen until decomposition occurs. This result is consistent with the earlier work on the mass 45 ion in a medium pressure mass spectrometer.[3] The large discrepancy in isotope effect between ethylene oxide and acetaldehyde for reaction A indicates a distinctly different mechanism is operating for this reaction in the two systems. In particular, H_2 is apparently lost from the oxirane ring before it has a chance to open up to the protonated aldehyde structure. In reaction B, a CH_3^- moiety may be selectively abstracted from acetaldehyde. This methide ion abstraction reaction has been observed for reactions of H_3^+ with ethanol.[4] The prefered loss of CH_3D in reaction B in ethylene oxide is attributed to an elimination of the type

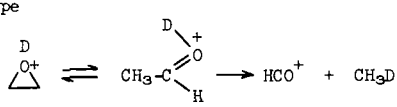

rather than a CH_3^- abstraction reaction. Further studies with selectively deuterated acetaldehyde and ethylene oxide are proceeding in our laboratories.

References

1. J. J. Leventhal and L. Friedman, J. Chem. Phys., 49, 1974 (1968); ibid., 50, 2928 (1969).
2. M. T. Bowers and D. D. Elleman, J. Amer. Chem. Soc. (in press).
3. D. Van Raalte and A. G. Harrison, Can. J. Chem., 41, 3118 (1963).
4. J. L. Beauchamp, private communication. The CH_3^- abstraction from ethanol has also been observed in our laboratories.

The Reaction $H^+ + H_2 \longrightarrow H_2 + H^+$

N7

M. G. Holliday, J. T. Muckerman and L. Friedman

Chemistry Department, Brookhaven National Laboratory, Upton, N. Y. 11973

The atomic-ion-molecule systems of protons or deuterons and isotopic hydrogen molecules have been the subject of an experimental study designed to provide data to be compared with recently reported classical trajectory calculations on an ab initio potential energy surface.[1] Absolute cross sections (accurate to within an estimated error of ±20%) for the following atomic-ion exchange reactions

$$D^+ + H_2 \longrightarrow HD + H^+ \qquad (1)$$

$$H^+ + D_2 \longrightarrow HD + D^+ \qquad (2)$$

$$D^+ + HD \longrightarrow D_2 + H^+ \qquad (3)$$

have been investigated in a tandem mass spectrometer system, with carefully calibrated geometry, as a function of collision energy. Endothermic charge-transfer processes

$$D^+ + H_2 \longrightarrow HD^+ + H \qquad (4)$$

$$D^+ + D_2 \longrightarrow D_2^+ + D \qquad (5)$$

$$D^+ + HD \longrightarrow HD^+ + D \qquad (6)$$

$$\longrightarrow D_2^+ + H \qquad (7)$$

$$H^+ + H_2 \longrightarrow H_2^+ + H \qquad (8)$$

$$H^+ + D_2 \longrightarrow HD^+ + D \qquad (9)$$

$$\longrightarrow D_2^+ + H \qquad (10)$$

have been observed and their cross sections were determined as a function of collision energy. Energy distributions of the ionic species participating in these reactions were measured by application of appropriate retarding fields. The experimental results for atomic-ion exchange reactions [(1), (2), (3)] are not easily compared with theoretical cross sections because the latter were calculated above energy thresholds for endothermic charge-transfer reactions [reactions (4) to (10)]. These processes were not considered in the theoretical treatment, though our results show that, where energetically possible, they indeed dominate the reactive collisions. Relatively good agreement between experimental atomic-ion exchange cross sections and theoretical values are obtained if the latter are extrapolated to energies below the charge transfer threshold. The extent of the observed endothermic charge transfer was unexpected, but can be rationalized by noting that very efficient translational to internal energy

conversion occurs, followed by radiationless transition to a weakly bound or repulsive excited electronic state of H_3^+. This state has been identified and its energy characterized by a simple Hückel calculation. Comparison of energy distributions of product and reactant ions superficially indicate "complex formation" at relatively low collision energies and "spectator stripping" at higher energies for atomic-ion exchange reactions [(1), (2), (3)]. The efficient transfer of kinetic to internal energy in the endothermic charge-transfer processes suggests complex formation mechanisms. This idea is further supported by observed energy distributions of molecular-ion products and isotopic abundance data. Although the energy distributions of atomic-ion exchange products above the endothermic charge transfer threshold are consistent with a direct, or stripping, mechanism, it should be noted that the relative yield of atomic-ion products compared to molecular-ion products is small in this energy range. This is in no way inconsistent with trajectory studies and may indeed be present at lower energies where it would be effectively concealed. The absolute characterization of mechanism as "stripping" or "complex formation" does not appear in the trajectory calculations nor is it suggested in our experiments.

The work described above has been submitted for publication in the Journal of Chemical Physics. Research was performed under the auspices of the U.S. Atomic Energy Commission.

[1]I. G. Csizmadia, J. C. Polyani, A. C. Roach, and W. H. Wong, Can. J. Chem. 47, 4097 (1969).

Product Ion Deflection Measurements as an Indication of the Mechanisms of Low-Energy Ion-Molecule Reactions

Thomas O. Tiernan and B. Mason Hughes

Aerospace Research Laboratories
Chemistry Research Laboratory
Wright-Patterson Air Force Base
Ohio 45433, U.S.A.

For some time our laboratory has been engaged in the study of ion-neutral collisions at low ion energies using a double mass spectrometer[1]. Recently, attempts have been made to measure rate constants with this instrument for various ion-molecule reactions for which well-established kinetic data is available from other sources. It was expected that such comparison would provide insight into instrumental factors such as discrimination or collection efficiency which might be inherent to our techniques. In general, it was found that for reactant ions of 0.3 eV kinetic energy, the rate constants derived with our instrument by referencing to a standard reaction agree quite well with the corresponding values reported from other laboratories in which a variety of techniques were employed. Table I gives representative data for various reactions from our laboratory and other sources.

---

* A more detailed account of this work will be submitted for publication in the International Journal of Mass Spectrometry.

Table I. Comparison of Rate Constants Measured in the ARL Tandem Mass Spectrometer with Values from Other Sources

	$k(10^{-9}cm^3\ molecule^{-1}sec^{-1})$	
	This Laboratory	Other
$N_2^+ + O_2 \rightarrow O_2^+ + N_2$	0.043	0.047[a]
$N^+ + O_2 \rightarrow O_2^+ + N$	0.32	0.6[a]
$O^+(^4S) + O_2 \rightarrow O_2^+ + O$	0.0057	0.02[a]
$CH_4^+ + CH_4 \rightarrow CH_5^+ + CH_3$	1.2*	1.2*[c]
$H_2^+ + H_2 \rightarrow H_3^+ + H$	2.2	1.9[b]
$H_2O^+ + H_2O \rightarrow H_3O^+ + OH$	1.02	1.6[c]

* Reference Reaction

a. E. E. Ferguson, et. al., Planet. Space Sci., 12, 1169 (1964); E. E. Ferguson, et. al., J. Chem. Phys. 44, 4095 (1966).

b. B. G. Reuben and L. Friedman, J. Chem. Phys. 37, 1636 (1962).

c. S. K. Gupta, et. al., Can. J. Chem. 45 (1967).

The reactions studied encompass a variety of reaction types including charge transfer, proton transfer, hydrogen atom transfer, and condensation processes which presumably involve complex intermediates. Since the good agreement obtained was somewhat unexpected for this broad category of reactions using an instrument such as ours, which can only sample products scattered within a rather narrow angle about the incident beam, the present experiments were undertaken in an effort to rationalize our low-energy rate data. It was expected that this study would also provide some general information regarding discrimination factors in fixed-angle scattering instruments.

Consider a crossed beam experiment in which A^+ ions are reacted with BH molecules. If a direct or spectator stripping mechanism is operative, then a hydrogen atom abstraction product, AH^+, would have essentially the same momentum as the A^+ projectile while a charge transfer product, BH^+, would have approximately the initial BH momentum. In a crossed beam experiment, such a mechanism can be readily verified if the reactant beams are intersecting at an angle of 90^o. However,

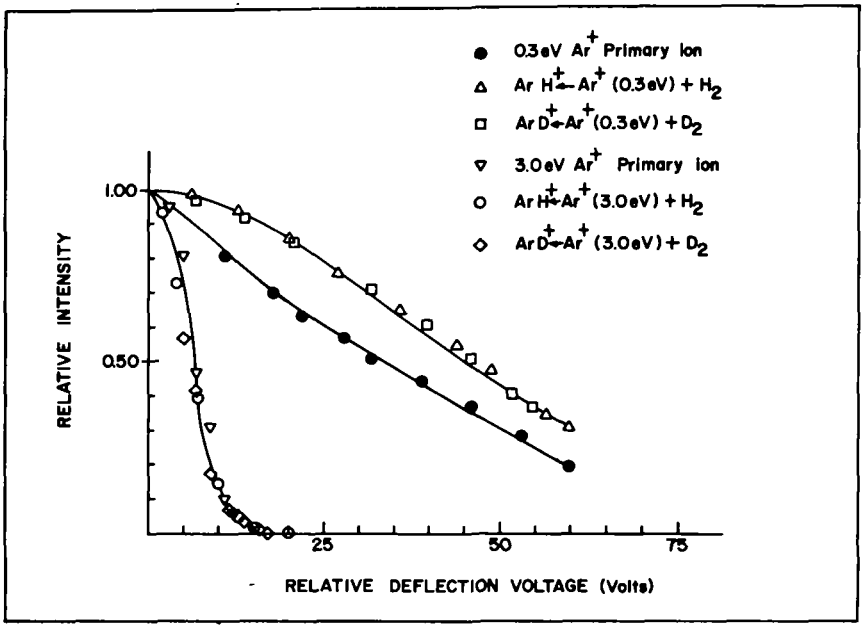

Figure 1. Ar^+, ArH^+ and ArD^+ ion profiles for Ar^+ translational energies of 0.3 and 3.0 eV.

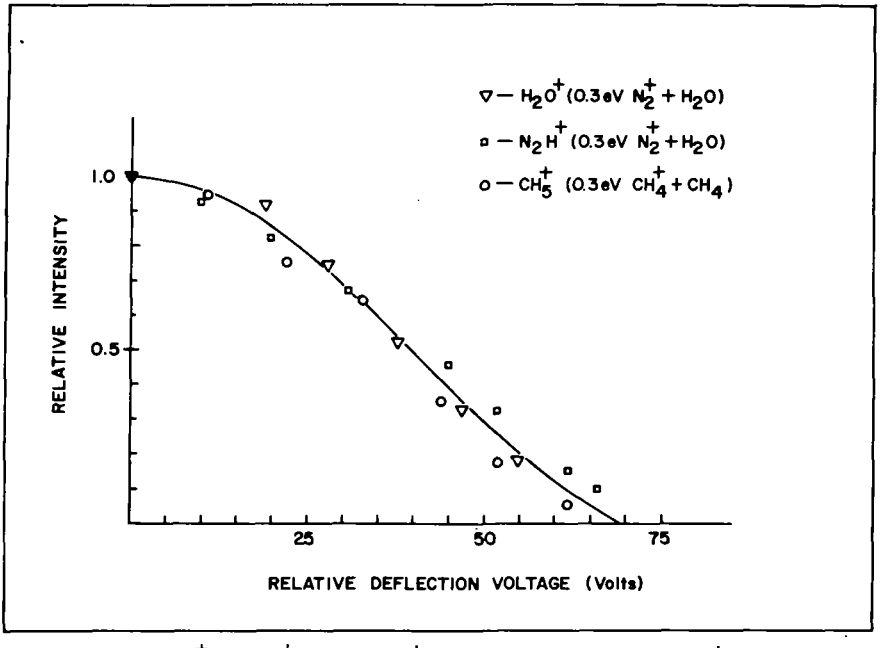

Figure 2. N_2^+, N_2H^+ and H_2O^+ ion profiles for N_2^+ energies of 0.3 eV.

in the ARL tandem mass spectrometer, as in all instruments utilizing a collision chamber, the collision region is not precisely defined. The neutral target in such a case is diffuse and is characterized by a velocity distribution. On the other hand, the ion beam in our case is well defined and has an energy spread of only $\pm$ 0.3 eV. These factors lead to considerable uncertainties in the angular dependences of the various ion-neutral processes observed. This is further compounded by the fixed collection angle in our instrument which is not precisely known, since ions emerging from the collision chamber are refocused prior to entering the analyzer. Also, since there is no extraction field in the interaction region of our tandem instrument, only products which diffuse out into the accelerating field of the analyzing spectrometer are collected. Obviously, products having forward momentum will be preferentially collected with our in-line geometry. Nevertheless, primary ions undergo only one collision at pressures and path lengths typical of our experiments, and the angular dependence of product ions is therefore dependent only on the kinematics of the ion-neutral collision.

Berry and Durup and Durup[2] have employed a deflection technique to study the momentum profile of ions emerging from an ion source. With this technique, as adapted to our tandem mass spectrometer, the voltage on one of the split focusing elements immediately following the source is biased, permitting the ion beam to be progressively swept across the comparatively narrow object slit of the analyzing mass spectrometer. A plot of product ion intensity as a function of deflection voltage thus gives a measure of the profile of the emerging beam.

Figure 1 shows typical ion profiles for the Ar^+/H_2 and Ar^+/D_2 reactions for 0.3 eV and 3.0 eV Ar^+ ion energies. The ArH^+ and ArD^+ products formed from 3.0 eV Ar^+ ions exhibit a profile identical to that of the projectile ion. However, for the low energy reaction, the ArH^+ and ArD^+ products show a considerably broader profile than the 3 eV results. These effects can be interpreted as being consistent with a modified stripping mechanism as has been suggested by Herman and Wolfgang[3]. Such a model predicts that the low energy ion-neutral interaction is perturbed by the induced dipole of the neutral species.

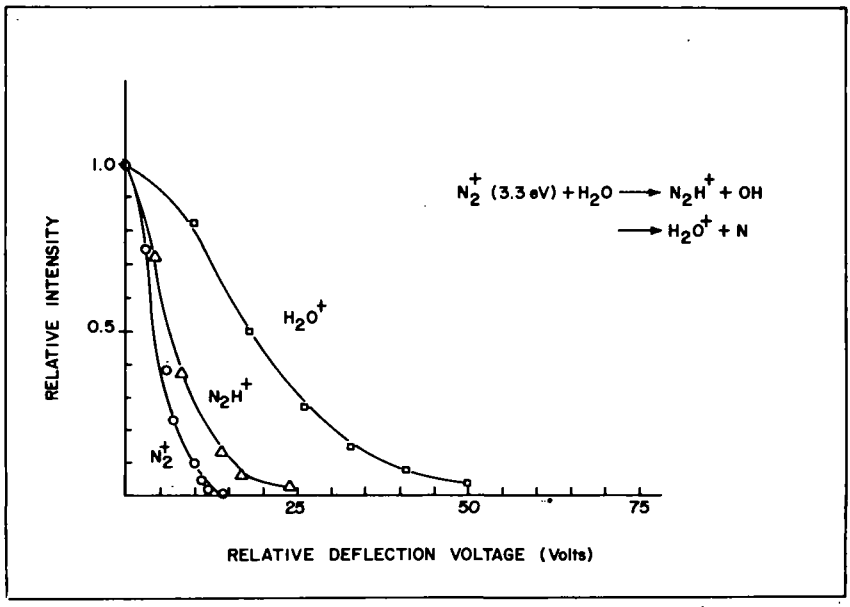

Figure 3. N_2^+, N_2H^+ and H_2O^+ ion profiles for N_2^+ energies of 3.3 eV.

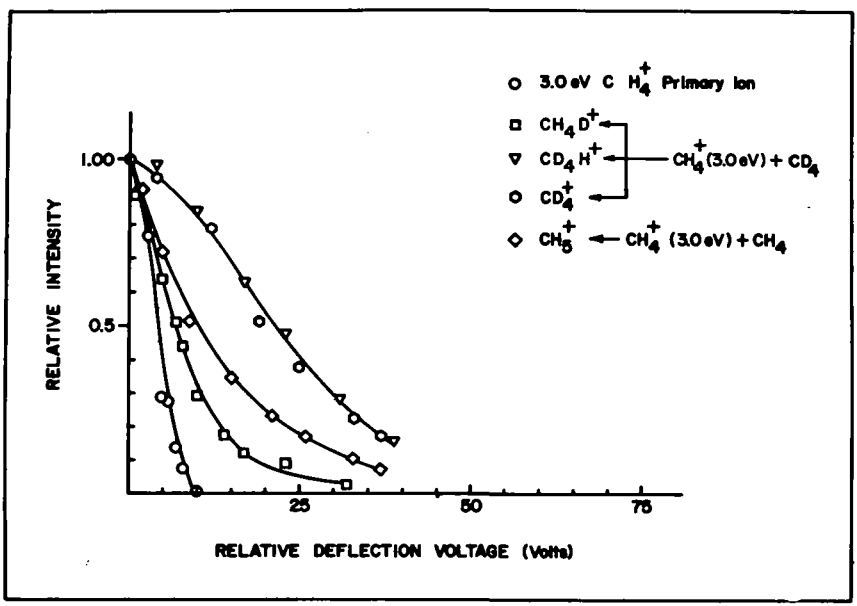

Figure 4. CH_4^+, CD_4^+, CH_4D^+, CD_4H^+ ion profiles for 3.0 eV CH_4^+ collisions with CD_4.

Ion profiles were also measured for products from the N_2^+/H_2O reaction. This interaction involves both hydrogen atom abstraction and charge transfer as reaction paths. Figure 2 shows the profiles for the 0.3 eV N_2^+ projectile ion and the N_2H^+ and H_2O^+ products. As was the case for the Ar^+/H_2 and Ar^+/D_2 reactions, the secondary products at 0.3 eV kinetic energy have broad profiles compared to the N_2^+ primary ions. The profiles observed from 3.3 eV N_2^+ ions reacting with H_2O are shown in Figure 3. Again, the hydrogen atom abstraction product has a profile very nearly identical to that of the primary ion. The charge transfer product, however, has a broader profile than either the N_2H^+ or N_2^+ products. Profiles for the H_2O^+ charge transfer product were determined at reactant energies from 0.3 to 38.7 eV. At energies of 3.3 eV and above, the profiles are all superposable, while the 0.3 eV profile is again much broader. This suggests that there is essentially no momentum transfer to the H_2O^+ product over the energy range, 3.3 to 38.7 eV. The broadening of the H_2O^+ produced by 0.3 eV N_2^+ ions on the other hand presumably indicates that momentum transfer occurs in charge transfer reactions of these very low energy ions.

As a third study, product profiles for the reaction of CH_4^+ with CD_4 were measured. Herman and Wolfgang[3] demonstrated that the angular dependence of the CH_5^+ product formed in the CH_4^+/CH_4 reaction could be explained by a modified stripping mechanism. The profile of the products formed from reacting 0.3 eV CH_4^+ ions with CD_4, (CH_4D^+,CD_4H^+ and an additional product, CD_4^+) were found to be identical to those shown in Figure 2 for the N_2^+/H_2O reaction. Profiles of the products from the 3.0 eV CH_4^+ reaction are shown in Figure 4. In this case, the CH_4D^+ product has nearly the momentum of the primary CH_4^+ ion, while the CD_4H^+ and CD_4^+ products have profiles corresponding to that of the neutral species (as deduced for H_2O from the N_2^+/H_2O reaction shown above). A third profile is shown for the 3.0 eV CH_4^+/CH_4 reaction. In this case, it is evident that one might misinterpret the latter reaction on the basis of this evidence alone since the proton transfer and hydrogen atom transfer products cannot be separately distinguished.

Conclusions: Some positive conclusions regarding collection efficiencies can be drawn from a comparison of the ion profiles for the products of various reactions involving different mechanisms. For 0.3 eV

ion-neutral collisions, there seems to be essentially uniform collection efficiency for all reactions observed in our instrument. For energies of 3.0 eV and larger, our in-line geometry favors detection of forward scattered products and the observed intensities must be corrected to give a reliable basis for comparing competing reaction channels. Discrimination effects for charge transfer products are apparently essentially constant over the energy range from 0.3 to ~40 eV, while hydrogen atom abstraction products are subject to larger discrimination at higher energies.

References

1. J. H. Futrell and C. D. Miller, Rev. Sci. Instr. 37 1521 (1966).
2. C. E. Berry, Phys. Rev. 78, 597 (1950); J. Durup and M. Durup, J. Chim. Phys. 64 386 (1967).
3. Z. Herman, et. al., Disc. Faraday Soc. 44, 123 (1967); Z. Herman, et. al., J. Chem. Phys. 48, 4319 (1968).

Negative-Ion Electron-Transfer Reactions[+]

C. Lifshitz[*] and T. O. Tiernan

Aerospace Research Laboratories
Chemistry Research Laboratory
Wright-Patterson Air Force Base
Ohio 45433, U.S.A.

INTRODUCTION

Our interest in electron transfer reactions of negative ions was prompted by observations in low pressure mass spectrometric studies[1], of reactions of molecular metastable ions such as SF_6^- with small molecules, (e.g. NO_2), which do not yield parent negative ions by electron capture. During the course of this work it was realized that most molecular electron affinities are not accurately known. In the following report, we describe work in which the ARL tandem mass spectrometer[2] was employed to determine the energy dependences of exothermic and endothermic negative-ion charge-transfer reactions. Energy thresholds for endothermic charge transfer from halide ions[2] were measured in an effort to determine molecular electron affinities.

Results and Discussion

The following rate constants were obtained for reactions with NO_2 of 0.3 eV ions (laboratory energy) relative to $\kappa(O^- + NO_2 \rightarrow O + NO_2^-) = 1$: SH^-, 0.65; SF_6^-, 0.02; Cl^-; $<2 \times 10^{-4}$; SF_5^-; $<2 \times 10^{-6}$. The first two reactions have energy dependences characteristic of exothermic reactions[2]. Since the electron affinity of the SH radical is 2.32 eV[3], this indicates that the electron affinity of NO_2 is higher than 2.3 eV. The slow rate of the SF_6^- reaction, despite its exothermicity, is apparently related to the complexity of the donor negative ion. The reactions of Cl^-, (Fig 1), and SF_5^- both show

---

[*] Ohio State University Research Foundation Visiting Research Associate under Contract F3361567C1758; from The Hebrew University of Jerusalem, Israel.

[+] A more detailed account of this work will be submitted for publication in the Journal of Chemical Physics.

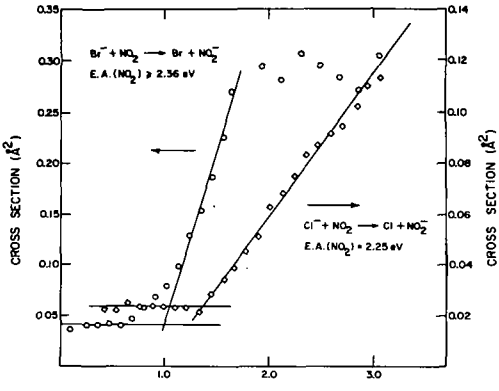

Figure 1. Cross sections for the electron transfer reactions of Cl^- and Br^- with NO_2 as a function of translational energy.

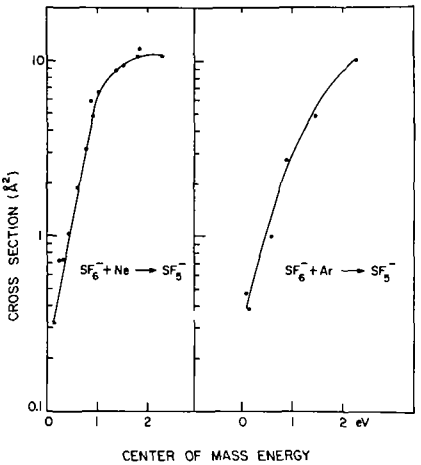

Figure 2. Cross sections for the rare gas collision induced dissociation of SF_6^- as a function of translational energy.

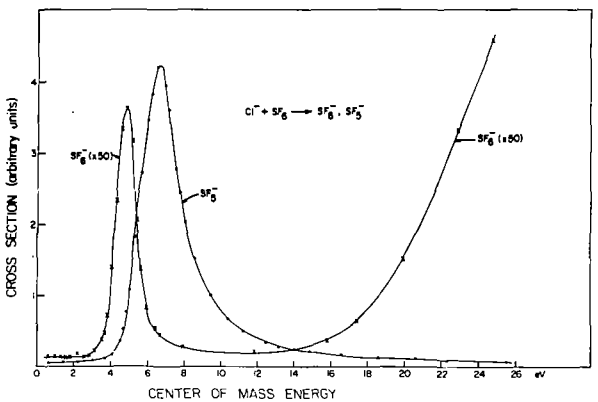

Figure 3. Energy dependence of the cross section for formation of SF_6^- and SF_5^- from the reaction of Cl^- with SF_6.

characteristic endothermic dependence. A linear dependence of the reaction cross section upon energy in the region above threshold, as expected from theory, was observed for most endothermic electron transfer reactions over a limited energy range. For the cases in which the halide ions were employed as reactant ions, the measured threshold energies (C.M.) were subtracted from the well known electron affinities of the halogen atoms[4] to estimate lower limits of molecular electron affinities. Some of the electron affinity values obtained in this manner are Cl_2, 2.6 eV; I_2, 2.6 eV; NO_2, 2.3 eV; O_2, 1.0 eV; SF_6, 0.4 eV; SO_2, 0.5 eV.

The following rate constants for reactions with SF_6 for 0.3 eV ions, (Laboratory energy) relative to $k(O^- + NO_2 \rightarrow O + NO_2^-) = 1$, were obtained: NO^-, 0.126; O_2^-, 0.03; D^-, 0.13; O^-, 2×10^{-4}; SF_6^-, not observed, ($<1 \times 10^{-3}$). These observations establish that the electron affinity of SF_6 is greater than 0.75 eV but lower than 1.47 eV[4]. Furthermore, since no electron transfer was observed from SF_6^-, this establishes that energetic criteria are not the sole determining factors for negative ion charge transfer reactions. Franck-Condon factors must also be an important consideration.

The tail observed in the threshold region for endothermic charge transfer to polyatomic molecules is not yet understood. It may result in part from "hot bands", although poor transition probabilities to the lowest vibrational levels of the molecular negative ions of these species seem to be a more likely explanation.

The collision induced dissociation of SF_6^- observed from impact on rare gases, (Fig 2), indicates a large internal energy content of the "metastable" ions. Finally, the energy dependence for products from the reaction of Cl^- with SF_6, (partly shown in Fig 3) indicates that both SF_6^- and SF_5^- are formed at low energies while at higher energies, F^- and ClF^- are formed as well. The production of SF_6^- at high center of mass energies (>15 eV), was observed to exhibit a second order pressure dependence. This can be ascribed to the following consecutive reactions: $Cl^- + SF_6 \rightarrow Cl + e^- + SF_6$; $e^- + SF_6 \rightarrow SF_6^-$.

References

1. C. Lifshitz and R. Grajower, Int J. Mass Spectrom. Ion Phys. 3 Appl. 5-8 (1969)
2. T. O. Tiernan and B. M. Hughes, "Translational Energy Effects for Negative Ion-Molecule Reactions", 16th Annual Conference on Mass Spectrometry and Allied Topics, Pittsburgh, Pennsylvania (1968).
3. L. M. Branscomb, Phys. Rev. 148, 11 (1966).
4. R. S. Berry, C. W. Reimann, and G. N. Spokes, J. Chem. Phys. 37, 2278 (1962).

Causes of Inaccurate Line Position Measurements on Photoplates

01

J. Franzen and W. Riepe
Institut für Spektrochemie, Dortmund, Germany

High resolution mass spectra of organic compounds on photoplates, taken with a Varian MAT SM1, show small-range distortions of the mass scale. The distortions are very reproducible from spectrum to spectrum, but vary strongly over periods of weeks. These irregularities of the mass scale prevent precise and accurate measurements of the ion masses and, therefore, hinder current element mapping.

To investigate this effect, we measured the line positions on 25o perfluorokerosene spectra with an automatic line comparator[+] (Leitz-Varian MAT) in connection with a computer program which calculated the centers of gravity. The reproducibility of the measuring system including the computer calculations is below O,1 µm standard deviation and thus has negligible effects on our results.

During exposure and developing of the photoplates, we changed numerous conditions. The following conditions showed no significant effect: ion current density; resolution of the mass spectrograph; switching off and resetting the magnet field to its initial value; gelatine shrinking effects caused by washing in running or still water, by rapid (blower) or slow drying, or by rapid fixing or stabilizing.

The only effect which could be changed reproducibly by varying experimental conditions was induced by the position of our photoplate holder. In extreme positions, i.e. if spectra were taken very near to the edges of the photoplates, the spectra exhibited long-range distortions of the mass scale.

The small-range distortions did not respond to variations of the experimental conditions. Nevertheless, the reason for these irregularities could be elucidated. Charged dust particles between the pole pieces deflect the ion beams passing nearby. The dust is introduced by the photoplates and catapulted into the magnet gap. Cleaning of the pole pieces eliminates the distortions of the mass scale.

Fig. 1 demonstrates the reproducibility of the distortions of the mass scale. The mass scale is represented by the 'slope curves' which are formed by the differential slopes between a pre-given set of PFK calibration lines. Fig. 2 outlines schematically the effect of two dust particles in different positions in the gap. Particle 'A' is lying near the entrance slit of the magnetic region, and, therefore, deflects a lot

[+]Acknowledgement. The authors would like to thank Dr. W. Schäfer, München, for his generous permission to use the comparator of the MPI für Biochemie, and his helpful support.

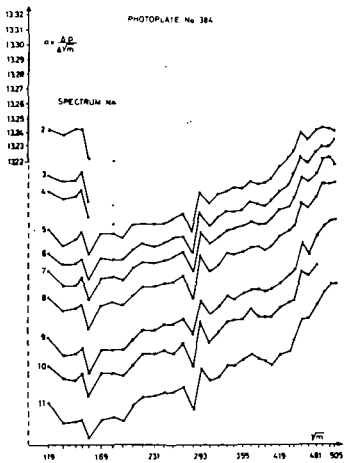

Fig. 1

Reproducibility of small range distortions of the mass scale ('slope curves')

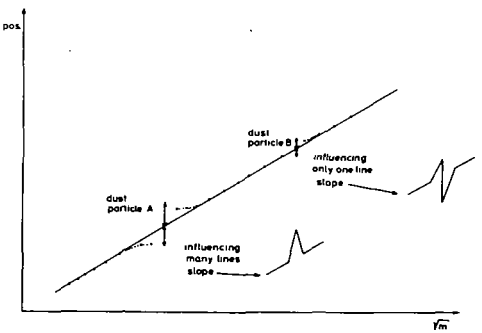

Fig. 2

Mechanism of distorting the mass scale by charged dust particles

of ion beams in the vicinity, because the different ion paths are still very close. The mass scale, represented as a straight line in the graph of position vs. the square root of mass, is distorted into a step function, and a single peak appears in the slope curve. In contrast, particle 'B' lies close to the photoplate and deflects essentially only one of the calibration lines. In this case, a zigzag deflection of the slope curve results.

In fig.3, the points are the measured, greatly enlarged deviations of the positions from the theoretical mass scale. They form a smooth, parabola-like curve. Only one point in the center of the parabola does not fit the curve, it is shifted from its expected place by about 3 µm. This point corresponds to a strong zigzag deflection of the respective slope curve. Fig. 4 shows a microphotograph of this special line and its vicinity.

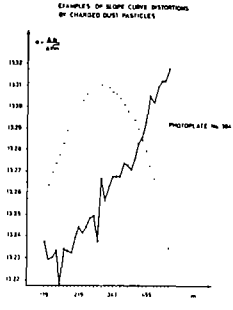

Fig. 3

Example of slope curve distortion. The points represent deviations of the calibration lines from the ideal mass scale

Fig. 4

Lines shifted by charged dust particles

The Selective Response of Photographic Emulsions to Ion Structure

Paul Vouros, D. M. Desiderio, J. V. M. Leferink and James A. McCloskey

Institute for Lipid Research

Baylor College of Medicine

Houston, Texas 77025

Introduction and Experimental

The dependence of emulsion response to ion structure and size has been investigated. The results of our experiments reported here provide the first direct experimental evidence that for quantitative organic mass spectrography a new parameter--i.e. ion structure--significantly influences the emulsion darkening, in addition to ion mass and ion energy.

Special care was taken to control the experimental conditions both during exposure and development. For example, to avoid effects due to mass discrimination or plate inhomogeneity (1) ions of similar nominal mass were compared, and thereby their developed images were separated by not more than one or two millimeters on the photoplate. The CEC-110B high resolution mass spectrometer was connected to two independent inlet systems, one of which was equipped with a fixed leak and the second with a variable leak, and the two compounds under investigation were introduced into their respective reservoirs. The partial pressures of the two compounds were adjusted until the relative intensities of the two molecular ions were equalized as indicated by repeated oscillographic recordings obtained using the peak matching circuit. It was thus possible to make a number of simultaneous exposures of the two ions covering a wide dynamic range (in some cases as many as three orders of magnitude). All exposures were made under the normal operating conditions of high resolution mass spectrometry (Accelerating voltage 8KV, Resolution in the range of 15,000 to 27,000). Studies were conducted with three types of photoplates, Ilford-Q2, Kodak-SWR and Tech/Ops evaporated AgBr. They were developed in undiluted Microdol-X (20°) for fifteen minutes, undiluted Kodak-HRP (20°) for three min. and

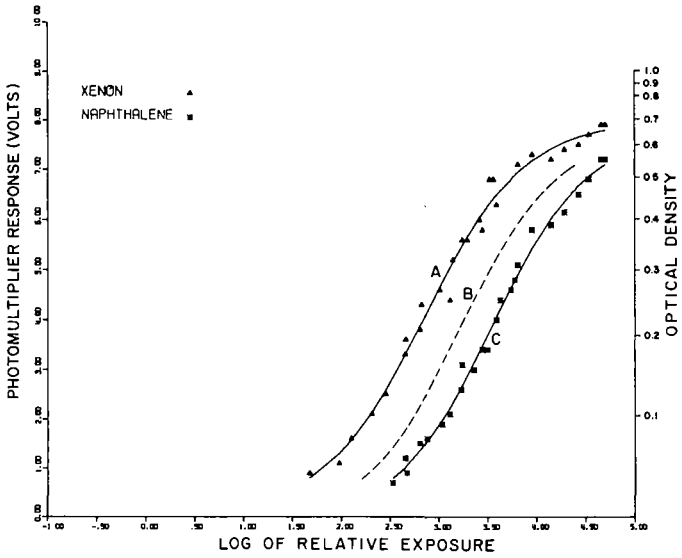

Figure 1

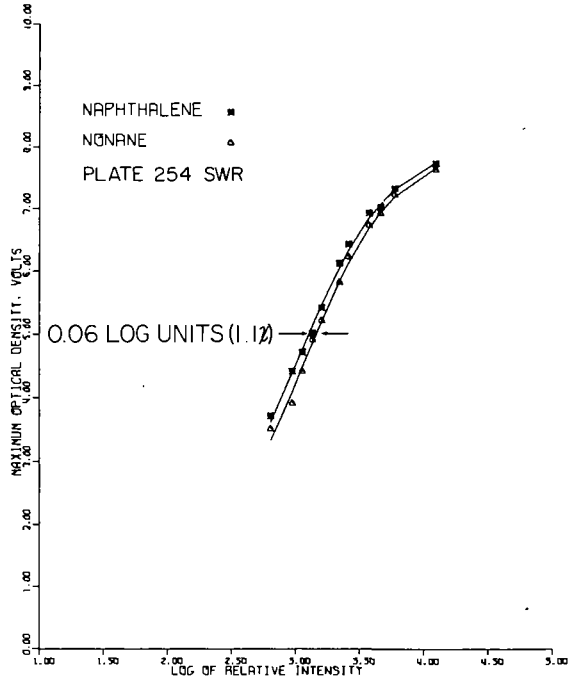

Figure 2

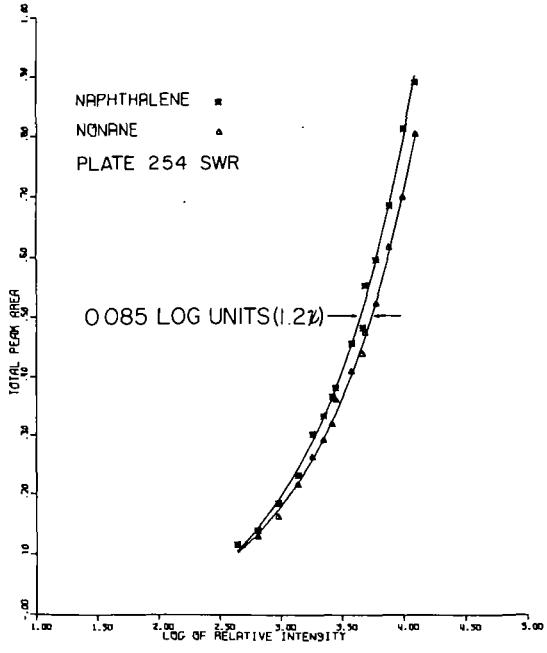

Figure 3

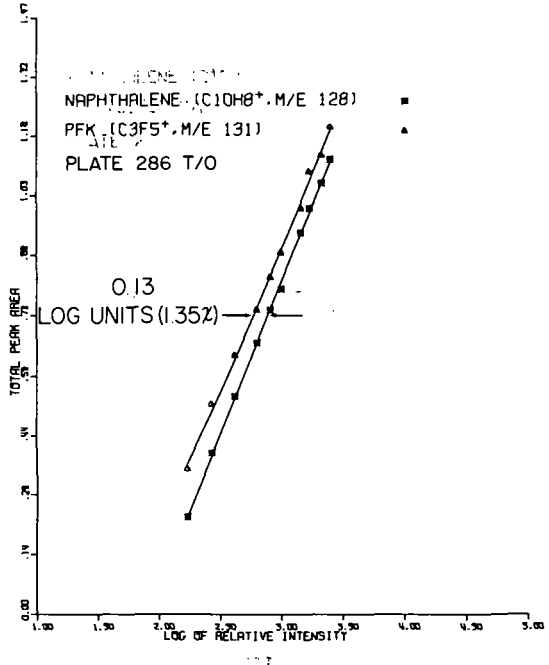

Figure 4

same amount of darkening in the photographic emulsion. If, however, the higher response of the electron multiplier to naphthalene over xenon ions--determined with the Faraday cup--is taken into consideration, the actual emulsion discrimination in favor of xenon is still 2.50 fold and the naphthalene curve is shifted 0.325 log units to the position indicated by the dotted line (curve B). When the total areas rather than the maximum densities were compared a 2.7-fold difference between xenon and naphthalene was found. Hayes (2) has also recently reported that emulsion sensitivity toward Xe followed the relation $(m/e)^{-0.5}$ while for fluorocarbon ions the relation was $(m/e)^{-1.5}$. This variation was attributed to possible differences in emulsion response to polyatomic *vs* monoatomic species. The following comparisons indicate that such emulsion response differences even exist for polyatomic species of different structure.

Naphthalene - Quinoline. A comparison of emulsion response to these two substantially similar in "size" and "shape" ions showed no apparent differences.

Naphthalene - Nonane. The molecular ions of these two compounds were compared in order to ascertain the difference in emulsion response between an ion of rigid structure (naphthalene) and one which is conformationally mobile (nonane). As is shown in Figure 2 a maximum O.D. plot obtained from Kodak SWR exposures shows that 1.1 more nonane than naphthalene ions are needed to produce the same amount of emulsion darkening. An area plot of the same plate (Fig. 3) shows an almost equal (1.2-fold) difference in emulsion response between the two ions.

Naphthalene - $C_3F_5^+$. Comparison of these two ions using an Ilford-Q2 emulsion indicated that the $C_3F_5^+$ ion gave a darker image than naphthalene. It was found that for the gelatinous emulsion 1.7 - 1.6 more naphthalene than $C_3F_5^+$ ions were needed to produce an image of the same density, whereas with the evaporated AgBr Tech/Ops photoplate the discrimination in favor of the smaller $C_3F_5^+$ ion was somewhat less (1.35X). It is significant to note the linear relationship of area *vs* log E obtained for the Tech/Ops photoplate (Fig. 4) which is probably due to the contiguous grains of AgBr in the film and the resulting latteral image development.

the Tech/Ops developer (18°) respectively. Optical density profiles were obtained with a Gaertner (Model M-1205C)-Datex microdensitometer system. The total ion current for each exposure was recorded with an Infotronics integrator coupled to the ion beam monitor.

The emulsion response to the following pairs of ions is reported here:

Naphthalene ($C_{10}H_8$, m/e 128.063) vs ^{129}Xe (m/e 128.905);

Naphthalene ($C_{10}H_8$, m/e 128.063) vs quinoline (C_9H_7N, m/e 129.058);

Naphthalene ($C_{10}H_8$, m/e 128.063) vs n-nonane (C_9H_{18}, m/e 128.141);

Naphthalene ($C_{10}H_8$, m/e 128.063) vs PFK (C_3F_5, m/e 130.990).

Characteristic response curves for each ion (shown in Figures 1-4) were obtained by plotting the logarithm of relative exposure vs the maximum optical density (expressed in photomultiplier output in volts) or the area under the densitometric profile. It is interesting to note that the differences in emulsion response were essentially constant ($<10\%$) as a function of either maximum optical density or area in the four cases considered. On the other hand precision was increased when areas above half height rather than total areas were plotted. This may be attributed to errors introduced due to variations of the background level (particularly on Q2 plates) or contribution of adjacent and not entirely resolved peaks when the total areas are calculated.

Results and Discussion

Naphthalene - Xenon. This pair of compounds was selected in order to determine the difference in photoplate response between a monoatomic and a polyatomic ion of the same mass. The intensity of the molecular ion of naphthalene (m/e 128) was equalized on the electron multiplier to that of $^{129}Xe^+$, by proper adjustment of the partial pressures of the gases, and several photoplate exposures were made. A plot of the maximum optical density (photomultiplier output in volts) vs log of relative exposure for the above pair of ions is shown in Figure 1. A difference of 0.73 log units between the two curves at their linear portion (4.0V) indicates that ~ 5.3 more naphthalene than xenon ions are needed to produce the

The results obtained thus far suggest a definite dependence of photographic emulsion response to ion structure. They may be summarized as follows:

(a) Monoatomic ions produce a stronger image than polyatomic ions of the same mass.

(b) Where organic ions are involved, the more compact ion produces a more intense image.

(c) Ions of similar size, shape and mass produce very similar images.

[Submitted for publication to the Journal of Analytical Chemistry.]

References

1. A. J. Ahearn, Homogeneity of Ion Sensitive Emulsions and Precision of Ion Beam Measurements in Spark Source Mass Spectrometry., 16th Annual Conference on Mass Spectrometry and Allied Topics, Pittsburgh, May 1966.

2. J. M. Hayes, Anal. Chem., 41, 1966 (1969) and references therein.

The Performance and Utilization of Evaporated Silver Bromide Plates for Recording High Resolution Mass Spectra

C. E. Hignite, N. R. Mancuso, and K. Biemann

Department of Chemistry
Massachusetts Institute of Technology
Cambridge, Massachusetts 02139

Over the past year the performance of photographic plates produced on an experimental basis by Technical Operations, Inc. (Burlington, Mass.) (1) has been tested and evaluated (for leading references on previous evaluation of these plates see reference 2). Initial difficulties with the plates, which employ a thin layer of pure silver bromide rather than a conventional emulsion, have included irreproducibility of sensitivity, line broadening and concomitant loss of resolution, and background smears. Changes in the developing procedure and improvements in the manufacturing process have minimized these undesirable characteristics so that plates of high photographic quality are now obtained. The most dramatic improvement in plate quality was obtained by adding sufficient sodium bicarbonate to the developing chemicals to lower the pH from 11.0 to 10.5. The low fog level, lack of background grain, and sensitivity to ions of high mass are attractive features, and this photoplate is now in routine use in our laboratory (3).

Two parameters in the developing procedure which were found to have dramatic effects on the quality of the processed photoplates are temperature and pH of the developing chemicals. The temperatures of the fixer and water wash were found to have little effect on plate quality, but a temperature of 20°C $\pm$ 2°C is required for the developer solution. The use of developer temperatures greater than 22 °C resulted in increased grain size and subsequent loss of resolution on the plates. The use of temperatures lower than 18 °C caused a noticable decrease in sensitivity. The pH of the developing chemicals was adjusted with sodium bicarbonate and optimized at 10.5, a value 0.5 pH units lower than the initial value of 11.0 for the original developing chemicals provided by Tech/Ops. Increasing the pH to values greater than 10.5 caused a corresponding increase in grain size and background smears, and the use of lower pH values resulted in a substantial decrease in sensitivity.

The Tech/Ops photoplates are 10 inches in length and most plate holders used in mass spectrometers employing photoplate detection are 12 inches in length or longer. There are therefore many possibilities for positioning the plate in the plate holders. The two extreme positions would involve placing the plate to record either as low a mass as possible or as high a mass as possible. A graph which allows one to predict the mass range which will be recorded on the Tech/Ops plates using a CEC-21-110B instrument at various magnetic

field and accelerating voltage values is shown in Figure 1. The area between the two dotted lines (-----) represents the mass range covered at various magnetic field settings by the Tech/Ops plate when it is placed as far as possible to the high mass end of the plate holder. For example the mass range covered at 10 kilogauss magnetic field and 7 kilovolt accelerating potential is shown by the solid horizontal line. Reading down to the 7 kilovolt axis it can be seen that the first line recorded on the plate would be at approximately mass 100 and the last line at mass 625. If a spectrum were recorded at 3.5 kilovolts the range covered at the same magnetic field setting would be from mass 200 to mass 1250. The lower lines (—-—-) indicate the range covered when the plate is placed as far as possible to the low mass end of the plate holder. The area where the hash marks overlap in the center of the graph represents the mass range covered regardless of the position of the plate in the holder.

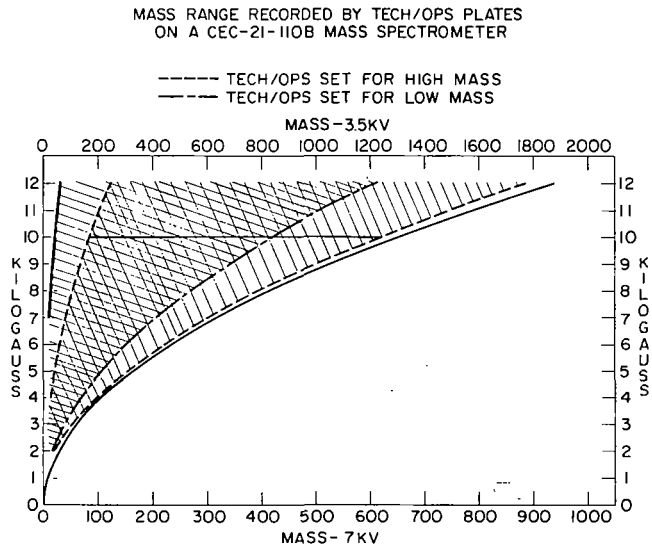

Figure 1.

Several characteristics of the plates obtained using the improved developing procedure have been evaluated. An indication of the high sensitivity of the plates was obtained by recording the spectrum of methyl myristate, the C14 straight chain fatty acid having molecular weight 242, at various exposure levels. An exposure level corresponding to less than 0.5 ug sample was sufficiently intense to record all ions down to 0.5% of the base peak at mass 74 (CEC-21-110B mass spectrometer, 200 microamperes anode current, 8 kilovolt accelerating potential, 1:15,000 resolution). It should be noted that the apparent sensitivity of the plates is increased by their low fog level. This, combined with an automatic microdensitometer-comparator operated on-line with a computer (4), allows the threshhold for ion detection by the computer to be set very close to the background level of the plate so that very weak lines may be detected.

An indication of the dynamic range of ion detection, the ratio of weakest to strongest lines for which accurate mass measurements can be made, was obtained by recording the spectrum of perfluorocyclohexane at increasing exposure levels until the accuracy of mass measurements was decreased for the more abundant lines. Exposure levels sufficiently high to include ions at m/e 230.9 and m/e 301.9, the former line being 8100 times more abundant than the latter, were

recorded with no apparent decrease in the accuracy of mass measurements (Table I). With respect to mass measurements, the dynamic range is therefore at least 8100 and probably exceeds 10,000.

Table I.

DYNAMIC RANGE OF ION DETECTION USING

TECH/OPS EVAPORATED AgBr PLATES

(SAMPLE = C_6F_{12})

ION	MASS	ERROR(MMU.)	REL. ABUND.
C_5F_9	230.98564	0.42	8095
$C_4{}^{13}CF_9$	231.98899	0.00	450
$C_3{}^{13}C_2F_9$	232.99235	1.30	10
C_6F_{12}	299.98098	-1.32	538
$C_5{}^{13}CF_{12}$	300.98433	-1.68	36
$C_4{}^{13}C_2F_{12}$	301.98769	-1.52	1

The resolving power of the plates was examined by recording 1:20,000 and 1:30,000 doublets. A photograph and optical density plots of the commonly used 30,000 doublet in the spectra of methylnaphthalene and dimethylnaphthalene at mass 142 are shown in Figure 2. The computer plot of the doublet represents optical density along the y-axis and distance along the x-axis. The x's along the curve denote positions along the plate or doublet 0.5 micron apart where distance and optical density values were recorded. The curve obtained represents a 3-5% valley in actual intensities, and therefore attributes to the plate a resolving power greater than 30,000.

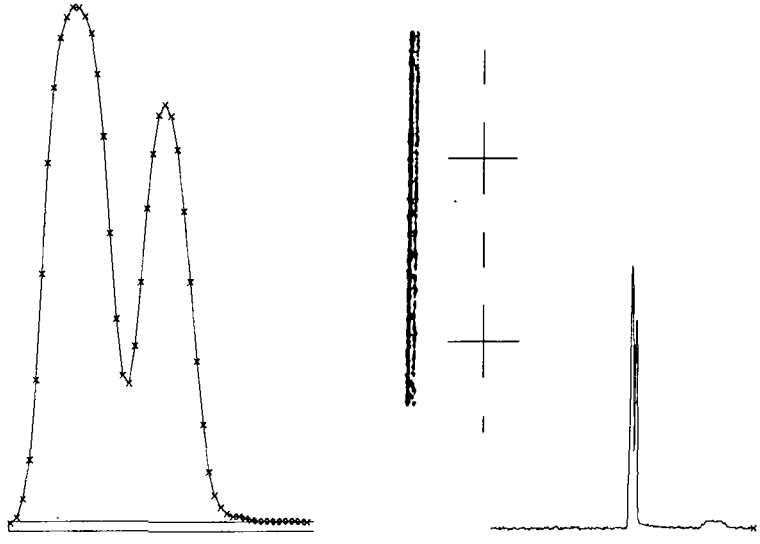

Figure 2.

The accuracy of mass measurements obtained using the Tech/Ops plates was evaluated by surveying data procured in a variety of research problems encountered in this laboratory. The errors resulting were less than 5 ppm, and examples of mass measurement values in the spectra of two compounds are provided. The first, shown in Figure 3, is a metabolite of monensin (5). The compound was thought to be the sodium salt of the carboxyl group and was also thought to contain a six-carbon sugar moiety attached to one of the hydroxyls. These predictions were confirmed by recording ions corresponding to the molecular ion M and the loss of water 18 mass units lower with errors less than 2 millimass units or 2.5 ppm.

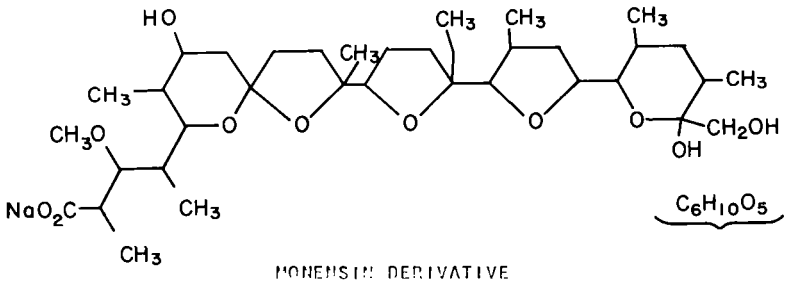

MONENSIN DERIVATIVE

Ion	Elemental Composition	Calculated Mass	Found Mass	Error mmass
M	C42H71O16Na	854.4640	854.4623	-1.7
M-H2O	C42H69O15Na	836.4534	836.4523	-1.1

Figure 3.

A second compound investigated was nygromycin, a trisaccharide antibiotic having the structure shown in Figure 4. Molecular weight confirmation was necessary for the identification of this compound, and again detection of the high mass ions was possible with good accuracy. Ions corresponding to the molecular ion M and M minus the elements of one and two molecules of acetic acid, respectively, were detected with errors less than 4 ppm.

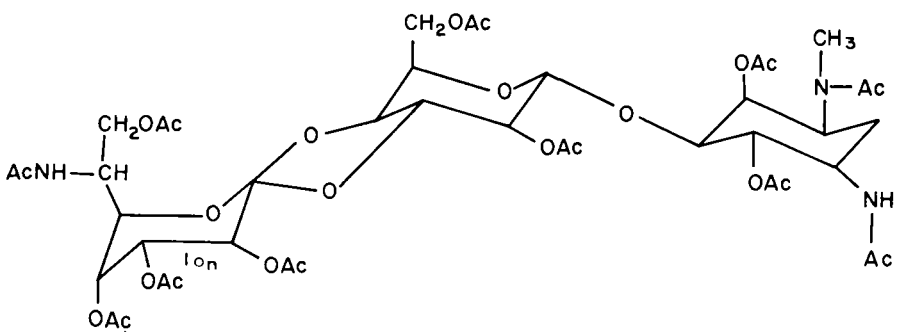

NYGROMYCIN

Ion	Elemental Composition	Calculated Mass	Found Mass	Error mmass
M	C42H59N3O24	989.3488	989.3520	3.19
M-HOAc	C40H55N3O22	929.3277	929.3295	1.81
M-2HOAc	C38H51N3O20	869.3066	869.3099	3.34

Figure 4.

A few observations should be made concerning physical properties of the Tech/Ops plates before and after developement. The evaporated silver bromide layer is hard and therefore before developement the plates are more difficult to scratch or damage by handling than plates employing emulsions. After developement, however, the lines on the plates are quite fragile and can be damaged or erased if accidentally touched or scraped. Developed plates should therefore be handled with care and stored in an appropriate manner.

The plates, as previously stated, are very sensitive to ions, but are also characterized by low sensitivity to photons, this property being at least partially responsible for their low background fog level. The plates have been briefly exposed to weak light sources with only a slight increase in background. Finally the Tech/Ops plates require a shorter time to pump down to operating pressures than plates employing emulsions. A pumping time of 30 minutes or less has been sufficient to lower the pressure into the operating region.

Briefly summarizing we can say that the evaporated silver bromide photoplates produced on an experimental basis by Tech/Ops and developed according to the revised procedure are of good photographic quality. The plates possess the desirable characteristics of high sensitivity, especially at high mass, large dynamic range, good resolution, low fog level, and line quality conducive to accurate mass measurement.

References

1. A. Shepp, R. E. Whitney, and J. I. Masters, Photographic Science and Engineering, 11, 322 (1967).

2. M. H. Hunt, Anal. Chem., 38, 620 (1966); M. H. Hunt, J. I. Masters, and J. P. Clune, 14th Annual Conference on Mass Spectrometry and Allied Topics, Dallas, Texas, May 1966; J. R. Woolston, W. L. Harrington, R. E. Honig, E. M. Botnick, and D. A. Kramer, 16th Annual Conference on Mass Spectrometry and Allied Topics, Pittsburgh, Pa., May 1968. J. I. Masters, Nature, 233, 5206 (1969).

3. C. E. Hignite and K. Biemann, Org. Mass Spectrom, 2, 1215 1969.

4. C. Cone, P. V. Fennessey, R. A. Hites, N. R. Mancuso, and K. Biemann, 15th Annual Conference on Mass Spectrometry and Allied Topics, Denver, Colorado, May 1967.

5. J. W. Chamberlin and A. Agtarap, Org. Mass Spectrom., 3, 271 (1970). A. Agtarap, J. W. Chamberlin, M. Pinkerton, and L. Steinrauf, J. Am. Chem. Soc., 89, 5737 (1967).

Acknowledgements

The authors are grateful to Dr. Guy Arsenault for his interest and many helpful suggestions concerning this work. The authors also appreciate the close collaboration of Mr. Masters of Technical Operations, Inc. We thank Mr. Pierre Schaub and Mrs. Shirley Sze for their excellent assistance in this work. This work was supported by National Institutes of Health Research Grant No. RR00317 from the Division of Research Resources.

Discrimination at an Electron Multiplier for 24 mass-analyzed atomic Ions. ROBERT C. LAO, Environmental Health Center, Department of National Health and Welfare, Ottawa 3, Canada, and R.F. POTTIE, Division of Chemistry, National Research Council of Canada, Ottawa 2, Canada.

Despite the widespread use of electron multipliers as ion detectors in mass spectrometry, very few systematic studies have been made of multiplier discrimination as a function of the nature of the impinging ion. In many cases, such as high temperature chemistry, knowledge of multiplier yields is required to obtain vapor pressure calibration. This work was undertaken to provide a set of multiplier gains for atomic ions, referred to an internal standard, for comparison with results of previous workers and to test some of the assumptions usually made regarding multiplier discrimination for atomic and polyatomic ions.

Measurements were made with an ATLAS CH4 mass spectrometer, that was equipped with an electron multiplier and a movable Faraday cup collector. The multiplier was a 17 stage Cu-Be type, and was magnetically shielded. To obtain the atomic ion of interest, appropriate compounds were admitted to the mass spectrometer via the gas inlet, and complete mass spectra were taken to ensure non-interference at the atomic ion mass from higher fragments. The multiplier yield was obtained from the ratio of the ion signals at the multiplier vs Faraday cup, referred to that for argon, which was admitted before and after the sample. The total ion energy was 5.1 KeV, and the ionizing voltage was 70 eV. The results, arranged according to groups as in the Periodic table, are shown in Table I. Within each group, maximum yields are found for the series $B^{11} \rightarrow Ne^{20}$, with decreasing values at higher atomic ion masses.

There is no apparent overall correlation with the $1/\sqrt{M}$ dependence of atomic yields that has been widely accepted, except within groups for M>40. Presumably the electronic structure is of comparable importance to the mass effect as a source of variation in ion yields. Results have also been obtained for many diatomic ions. Comparison of the atomic ion yields reported here with previous experimental values, reveals surprisingly good agreement despite the use of various types of multipliers and a wide range of ion energies. These and other details will be published in "The International Journal of Mass Spectrometry and Ion Physics".

We conclude that multiplier yields for atomic ions can be obtained with good reproducibility by a relatively uncomplicated technique, and that the results are in good agreement with those of other workers. Thus, relative multiplier yields can be transferred from one experimental system to another, since they are not particularly sensitive to the type of multiplier nor to the ion energy in the normal mass spectrometric range of values (4-7 KeV).

TABLE I. Relative multiplier yields for atomic ions at ion energies of 5.1 KeV. Yields are for positive ions at the indicated isotopic mass, referred to that for argon.

IVA	VA	VIA	VIIA	RARE GASES
			H^{1}	He^{4}
			0.669	0.997
C^{12}	N^{14}	O^{16}	F^{19}	Ne^{20}
1.036	1.164	1.224	1.083	1.226
Si^{28}	P^{31}	S^{32}	Cl^{35}	Ar^{40}
0.909	0.940	0.926	0.951	1.000
Ge^{72}	As^{75}	Se^{76}	Br^{79}	Kr^{84}
0.590	0.578	0.675	0.626	0.733
Sn^{116}	Sb^{121}		I^{127}	Xe^{129}
0.524	0.494		0.567	0.650
Pb^{206}				
0.400				

Others: B^{11} = 0.779, Hg^{202} = 0.429

AN IMPROVED TECHNIQUE FOR MULTIPLIER CALIBRATION & NOISE REDUCTION

BY

Bert E. Evans and William Kneen
ELECTRONIC ASSOCIATES, INC.
Palo Alto, California 94303

ABSTRACT

A metallic electrode asymmetrically located on the axis of a quadrupole mass filter such that it blocks any optical path between the ionizer and first dynode, but never-the-less permits optimal asymmetric first dynode field penetration to the exit aperture has been tested. It is found to give a factor of 25 increase in useful gain of venetian blind multipliers with no consequent deterioration in high mass sensitivity, and to act as an efficient Faraday collector.

INTRODUCTION

Noise of various kinds has been observed on the output signal when a quadrupole mass filter is used with an electron multiplier detector. There is first of all dark noise which is that caused by the multiplier alone. This can be due to high voltage vacuum breakdown phenomena in the high field regions around the multiplier or to surface breakdown along insulators. These effects can be minimized by multiplier modification incorporating asperity-free electrodes, and high quality ceramic insulators.

Another source of noise, the subject of this paper, occurs when the electron multiplier is operated on a direct optical path with the ionizer. The basic causes of this noise are uncertain, but the noise is dependent on both pressure and emission current. It appears to be due to either photons or excited neutrals passing directly from the ionizer to the first dynode without being influenced by the quadrupole field. Since both the photons and excited neutrals have no charge, they follow straight line paths, and an off axis technique would suffice to lower the noise to signal ratio.

It is also known that multiplier gain gradually decays with exposure to gases. A simple means for calibrating the multiplier is therefore essential. These problems can be simultaneously solved by the use of an intermediate asymmetric optical baffle, which also functions as a Faraday collector.

APPARATUS

The apparatus used as a standard EAI QUAD® 250B mass filter with two filament ionizer, a 5 inch rod structure, a 1 inch drift tube, and a venetian blind multiplier. The venetian blind multiplier was chosen over the box and grid because the necessary structural modifications were simplier and the dynodes can be independently changed. It also permits an axial mounting because of the larger dynode surface area. The apparatus is schematically illustrated in Figure 1.

Noise was measured with a Tektronix 556 oscilloscope and a high bandpass type 1A7 plugin amplifier. The multiplier anode was connected to the amplifier input through 5 feet of RG 62 cable. The noise was measured by photographing a single scan of long enough duration that it contained a large number of pulses and counting the pulses.

EXPERIMENT

The first attempt at an optical block was a 7/16 inch diameter disk on the axis 1 inch from the filter exit aperture and 1/8 inch from the first dynode. The disk electrode was provided with a separately shielded lead to the outside of the vacuum system. It could thus be used as a Faraday collector when the multiplier was off and grounded when the multiplier was in use. The measurements obtained in this way were compared with those obtained when the optical baffle was removed. This first disk shaped device

reduced the noise from 900 counts/second to less than 50 counts/second, but gave rise to mass discrimination against the high masses.

Since a static field cannot discriminate between masses, this means that there is not a proper penetration by the first dynode field into the region of the exit aperture and a mass dependent fraction of the ions are lost in the exit fringe field. The discrimination encountered when a symmetric disk is used can be understood when one considers that the electric field component along the axis and normal to the axis is zero. Hence, the transverse forces due to the first dynode field are weakest near the axis where most of the ions are emerging. In order to get an idea of the fields necessary to draw the ions off from their filter determined trajectories, and through the fringe field, some knowledge of the energy distribution of ions emerging from the filter is needed.

Idealized theory based on maximum transverse momentum an ion can have in the filter suggests that an emerging ion can have an energy $Ve=0.7V_{RF}e$ electron volts where e is the electron charge and V_{RF} is the peak RF voltage. Preliminary observations indicated that most of the ions come out at much lower energies. In order to find the actual energy distribution of emerging ions, a Faraday collector was installed at the filter exit as illustrated in Figure 2. Using perflourotributylamine as the test gas, spectra were taken as the retarding collector potential was increased in steps. The normalized peak heights of four principal peaks are shown in Figure 2 as a function of collector voltage. The peaks are normalized to their value at zero collector voltage. From differentiation of this plot an energy distribution curve was made as shown in Figure 3. The significant aspect of this curve is that there is a narrow energy spread around the 6 volt ionizer energy. Secondly, mass discrimination effects are observable. As the mass increases the energy spread is broader and the peak in the distribution is shifted to slightly higher energies. The conclusion that can be drawn is that it should be very easy to get sufficient field penetration to extract the ions if an asymmetric extraction field is used. An optical baffle was then constructed from a flat plate cut for optimal asymmetric first dynode field penetration and such that the first dynode could only see about an inch of the exit end of the rod structure.

RESULTS

The multiplier was calibrated at 5×10^5 gain throughout the experiment in order to maintain constant average noise pulse amplitude. The pulse amplitudes varied from 0.2 to 2 millivolts across 10^6 ohm. The noise with the ionizer off was less than a pulse/second at 10^{-7} Torr. Increasing the pressure to 5×10^{-6} Torr increased the dark noise to about 2 counts/second.

With the ionizer on and no optical block the noise was approximately 900 pulses/second. Introduction of the asymmetrical optical block reduced the noise to less than 30 pulses/second. Thus, the optical block reduces the ionizer noise by about a factor of 30 and gives a corresponding increase in useful multiplier gain.

In the test for mass discrimination, perflourotributylamine was introduced and the spectrometer set for baseline resolution from mass 69 through 503 with no optical baffle. The spectra were chart recorded. Without further adjustment, the optical baffle was introduced and a second spectra taken. There were no observable changes in the spectral distribution.

The method thus provides an effective optical block to ionizer noise with no consequent mass discrimination. From the standpoint of head and vacuum system simplicity the asymmetric optical block provides a desirable alternative to right angle mounting of the detector.

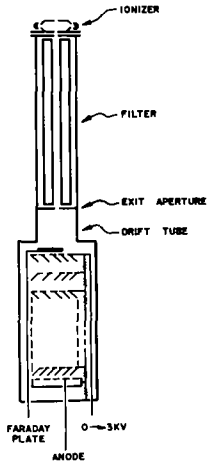

FIG. 1
SCHEMATIC ILLUSTRATION OF APPARATUS

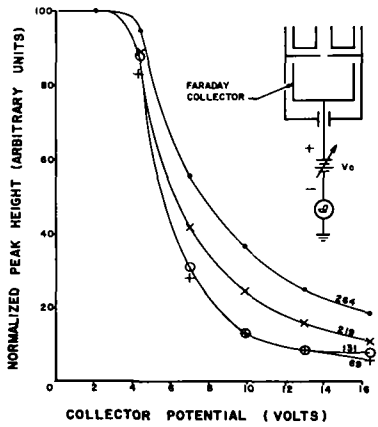

FIG. 2
PEAK HEIGHTS NORMALIZED TO THEIR AMPLITUDE AT $V_c = 0$. (IONIZER CAGE POTENTIAL 6 VOLTS)

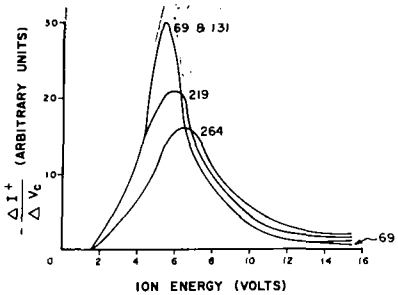

FIG. 3
ENERGY DISTRIBUTION OF MAJOR FC 43 IONS

A Stable, High S/N Ratio Ion Counting Detector For Ultra-High Vacuum RGA's.

F. L. TORNEY, Norton Research Corp., Cambridge, Mass. 02142.

The electron multiplier ion detector used in quadrupole residual gas analyzers is not characterized by a high degree of stability. In ultra-high vacuum applications the detector's sensitivity is difficult to measure because of the small ion currents involved. Ion counting techniques suggest a solution to these problems. The present work, shows that a more stable ion counting detector can be devised if a high gain, low noise multiplier is utilized with appropriate counting circuitry. For example, a gain loss of 70 in the multiplier results in an average reduction of counting sensitivity of only 11.4% for ions in a 1-50 amu range. Moreover, the detector design has improved the S/N ratio of the instrument at very low partial pressures. The improved detector is used in conjunction with a cold-cathode ion source/quadrupole analyzer described previously.[1]

[1]F. L. Torney & P. Blum, 14th Annual Conference, Dallas, Texas, 1966.

This work was sponsored by NASA-Langley Research Center under Contract NAS1-5347, Task 16.

ICR Mass Spectrometry of Some Simple Unsaturated Systems. GILLIAN C. GOODE, REBECCA M. O'MALLEY, A.J. FERRER-CORREIA, R.I. MASSEY and K.R. JENNINGS, Dept. of Chemistry, The University, Sheffield, England.

The purpose of this paper is to establish conditions under which quantitative data on relative rate constants can be derived from measurements made using an ion cyclotron resonance mass spectrometer. Observations were made using a Varian V-5900 instrument fitted with a "flat" three-section cell, with a drift plate separation of 1.1 cm. Total ion currents were measured using a Keithley 602 electrometer and were typically $3 - 6 \times 10^{-12}$A so that space-charge effects would be small: under these conditions, the total ion current was constant during a scan of the magnetic field. In all cases, conversions were kept low so that a simplified form of the integrated rate equation could be used.

Three different types of spectra were obtained: (a) ICR spectra in which the power absorption A of different ions is measured by scanning the magnetic field. For such spectra, the amplitude of the r.f. oscillator was kept as low as possible so that relatively few ions were lost by "sweep-out" effects and the total ion current remained approximately constant; (b) TIC spectra obtained at r.f. levels sufficiently high to sweep-out completely ions which absorb energy during a scan of the magnetic field, causing a reduction R in the total ion current; (c) TIC spectra obtained in a similar manner but at a fixed magnetic field strength by sweeping the frequency of the r.f. oscillator, leading to a reduction R' in the total ion current. If allowance is made for the mass dependence of power absorption and for the variation of drift velocity in magnetic field scans, the relative rate constants for the two reactions

$$P^+ + M \rightarrow S_1^+ + N_1 \qquad (1)$$

$$\rightarrow S_2^+ + N_2 \qquad (2)$$

can be derived from the following three expressions, assuming that the secondary ions undergo no further reaction:

$$\frac{k_1}{k_2} = \frac{A_1 m_2^2}{A_2 m_1^2} = \frac{R_1 m_2}{R_2 m_1} = \frac{R_1'}{R_2'}$$

The three expressions have been tested using the reactions

$$C_2H_4^{+\cdot} + C_2H_4 \rightarrow C_3H_5^+ + CH_3\cdot \qquad (3)$$

$$\rightarrow C_4H_7^+ + H\cdot \qquad (4)$$

and have led to values of k_3/k_4 of 9.5, 10.3 and 9.3 respectively, giving an average value of 9.7. The good internal agreement between the three values together with good agreement with literature values confirms the validity of the expressions. In the propylene system, the relative rate constants for the formation of the four products arising from the reaction

$$C_3H_6^{+\cdot} + C_3H_6 \rightarrow \text{Products}$$

are given in the table and are compared with the zero-field results obtained by Harrison and Herod[1]:

	$C_3H_7^+$	$C_4H_7^+$	$C_4H_8^{+\cdot}$	$C_5H_9^+$
Zero Field	0.21	0.11	0.42	0.26
ICR B scan	0.22	0.12	0.41	0.26
TIC B scan	0.18	0.12	0.43	0.27

Again, good agreement is found between the results obtained by different methods. A more complete account of this work will be submitted to the International Journal of Mass Spectrometry and Ion Physics.

[1] A.A. Herod, A.G. Harrison, R.M. O'Malley, A.J. Ferrer-Correia and K.R. Jennings, J. Phys. Chem., in Press.

P2

Information Concerning Reactive and Nonreactive Collision Processes from an Analysis of Ion Cyclotron Resonance Lineshapes*

D. P. Ridge, T. B. McMahon,† and J. L. Beauchamp‡

Arthur Amos Noyes Laboratory of Chemical Physics,
California Institute of Technology,
Pasadena, California 91109

A study of the collision broadening of ion cyclotron resonance absorption spectra has been initiated in order to better understand factors that influence ion-neutral collision phenomena. Under the conditions of a typical ion cyclotron resonance experiment, only unreactive ions are observed above a pressure of about 10^{-4} torr in most systems. At higher pressures the widths of the resonances of the remaining ions increase as a result of collision broadening. Since the broadening is induced by collisions, information about the nature of ion neutral interactions is available from linewidth measurements.

An appropriate velocity damping term can be added to the equation of motion for an average ion in the ion cyclotron resonance apparatus to account for the effect of collisions. When the equation is solved and an expression for the power absorption obtained, the linewidth (half-width at half-height) is found to be equal to a collision frequency, ξ, given by the expression[1]

$$\xi = n \frac{M}{m+M} \langle \sigma_d(v)\, v \rangle \qquad (1)$$

Here n is the neutral number density, M the mass of the neutral, m the mass of the ion, $\sigma_d(v)$ the velocity dependent diffusion cross section, and v the relative ion neutral velocity. The brackets indicate an average over the ion and neutral velocity distributions. The nature of the ion neutral interaction determines the diffusion cross section and therefore the linewidth.

If only the polarization interaction is considered, the ion molecule interaction is represented by

$$V(r) = -\frac{\alpha e^2}{2r^4} \qquad (2)$$

where α is the angle-average polarizability of the neutral, e the electronic charge, and r the distance between the ion and the neutral. The diffusion cross section can be calculated for this potential[2] and the result gives for the collision frequency

$$\xi/n = 2.210\, \pi e \frac{\mu^{\frac{1}{2}}}{m} \alpha^{\frac{1}{2}} \qquad (3)$$

where μ is the reduced mass of the ion-neutral pair. The reduced collision frequency, ξ/n, is proportional to the ratio of the linewidth to the pressure and according to Eq. 3 is independent of temperature and ion energy. For a series of ions in the same gas Eq. 3 predicts that the reduced collision frequencies will vary as $\mu^{\frac{1}{2}}/m$.

For the ions CH_5^+, $C_2H_5^+$, $C_3H_7^+$, and $C_4H_9^+$ in methane the measured reduced collision frequencies increase with $\mu^{\frac{1}{2}}/m$ but are 15 to 20% larger than the polarization limit. The collision frequencies were measured by determining the slopes of plots of linewidth versus pressure which were all found to be linear within about 1%. The collision frequencies were found to be independent of ion energy up to an energy of approximately 0.2 eV (lab.). Similar measurements were made on a series of ions in hydrogen. The results for the ions $C_3H_7^+$, N_2H^+, $C_2H_5^+$, H_9O^+, and CH_5^+ agree within a few percent with the simple theory (Eq. 3). Disagreement is obtained only in the case of H_3^+ which again is approximately 20% larger than predicted by Eq. 3. Although $C_2H_5^+$ and N_2H^+ have the same mass, they have measureably different collision frequencies, that of $C_2H_5^+$ being larger by 5%.

The simple theory can be crudely extended to treat polar molecules by including an ion-dipole interaction in the potential so that

$$V(r) = -\frac{\alpha e^2}{2r^4} - \frac{\mu_D e}{r^2} \cos\theta$$

where μ_D is the dipole moment of the neutral and θ the angle between the intermolecular vector and the dipole. Using the locked dipole approximation ($\cos\theta = 1$) and using the capture cross section of the resulting potential[3] to estimate the diffusion cross section yields a collision frequency

$$\xi/n = 2\pi e\,[\alpha^{\frac{1}{2}} + \mu_D(\tfrac{2}{\pi KT})^{\frac{1}{2}}]\mu^{\frac{1}{2}}/m \qquad (4)$$

which should represent an upper limit to the actual collision frequency.

Measured collision frequencies for the two ions CH_2OH^+ and $(CH_2O)_2H^+$ in formaldehyde exhibit the predicted variation with $\mu^{\frac{1}{2}}/m$ with absolute magnitude midway between the locked dipole limit and the polarization limit.

Information derived from an analysis of collision broadened ion cyclotron resonance lineshapes has numerous applications. First, and most important, it provides a fairly sensitive means of probing the nature of the ion neutral interaction potential. Terms which may be important in the interaction potential in addition to the ion induced dipole attraction include attractive ion-induced quadrupole and dispersion interactions as well as short range interactions. The balance of these attractive and repulsive interactions at thermal ion energies is fairly critical in determining whether the collision frequencies are greater or less than the values predicted by Eq. 3. At thermal ion energies the increased importance of attractive interactions has the general effect of increasing the collision frequencies. The general effect of increasing the ionic "radius" (which is determined by the repulsive interaction) is to cause a decrease in the collision frequencies with increasing ion energy up to approximately 0.5 eV, beyond which the collision frequency generally increases with increasing ion energy.[4] Thus the results for ions in methane and H_3^+ in hydrogen indicate that attractive forces in addition to the polarization interaction are important in determining momentum transfer collision frequencies at thermal ion energies. The above factors may nearly balance in the case of the heavier ions in hydrogen to give fortuitous agreement with the predictions of Eq. 3 at thermal ion energies. The results for ions in formaldehyde indicate the usefulness of linewidth data in determining quantitative effects of permanent dipole moments on ion neutral interactions.

A second application of the data is in the determination of ion mobilities and diffusion cross sections. Ion mobilities are inversely proportional to collision frequencies for momentum transfer.[5] The results of the experiments described above can be directly employed to give a more complete description of the motion of ions in chemical ionization experiments involving methane or hydrogen as chemical ionization reagents.

A third application of linewidth data is in the determination of the lifetimes of intermediate species in ion molecule reactions. If an ion-molecule reaction proceeds via an intermediate that can either fall apart or be collisionally stabilized, an analysis of the variation of relative ion abundances with pressure yields the ratio of the rate of stabilization to the rate of decomposition. The collision frequency determined from linewidth measurements sets an upper limit on the rate of stabilization and therefore a lower limit on the lifetime of the intermediate.

A more complete account of this work has been submitted for publication to the Journal of Chemical Physics.

---

*Research supported in part by the Atomic Energy Commision Grant No. AT(04-3)767-8.

†NRC Predoctoral Fellow.

‡Alfred P. Sloan Fellow, 1968-1970.

[1]J. L. Beauchamp, J. Chem. Phys., 46, 1231 (1967).

[2]A. Dalgarno, M. R. C. McDowell, and A. Williams, Phil. Trans. Roy. Soc. (London), A-250, 411 (1958).

[3]John V. Dugan, Jr., and John L. Magee, J. Chem. Phys., 47, 3103 (1967).

[4]Edward A. Mason and Homer W. Schamp, Jr., Ann. Phys. (New York), 4, 233 (1958).

[5]Darol Wobschall, John R. Graham, Jr., and Dennis P. Malone.

Nucleophilic Displacement Reactions in the Gas Phase Studied by Ion Cyclotron Resonance Spectroscopy*†

David Holtz and J. L. Beauchamp

Arthur Amos Noyes Laboratory of Chemical Physics
California Institute of Technology,
Pasadena, California 91109

Nucleophilic displacement reactions of the type illustrated in reaction 1 have been found to be a general gas phase reaction. For example,

$$Y + RX^+ \longrightarrow RY^+ + X \qquad (1)$$

at 10^{-4} torr in a 2.4:1 mixture of HCl and CH_3F subjected to electron impact, CH_3FH^+ forms and is observed to react with HCl yielding CH_3ClH^+ with HF being displaced (reaction 2).

$$HCl + CH_3FH^+ \longrightarrow CH_3ClH^+ + HF \qquad (2)$$

Nucleophilic displacements have been found to occur whenever the reaction process is exothermic, provided that proton transfer from the substrate undergoing substitution to the entering nucleophile is not exothermic. With the above criteria a relative ordering of nucleophilicity toward CH_3^+ may be calculated to be $NH_3 > CO > H_2S > CH_2O > HI > H_2O > HBr > HCl > N_2 > HF$.

The nucleophilic displacement process generalized in reaction 1 may be conveniently used for the gas phase synthesis of organic ions. Two of the most interesting results obtained in the experimental verification of the nucleophilic ordering given above are the use of N_2 and CO as nucleophiles in conjunction with CH_3F as substrate to generate the species methyl diazonium ion, $CH_3N_2^+$, and acyl cation, CH_3CO^+ (reactions 3 and 4).

$$N_2 + CH_3FH^+ \longrightarrow CH_3N_2^+ + HF \qquad (3)$$

$$CO + CH_3FH^+ \longrightarrow CH_3CO^+ + HF \qquad (4)$$

Reaction 3 is a novel means of nitrogen fixation in which N_2 reacts with an organic ion in the gas phase forming a new stable organic ion that has incorporated molecular nitrogen.

Rare gas atoms may also be used as nucleophiles in reaction 1. Thus, xenon has been found to undergo reaction 5 generating the methyl xenonium ion, CH_3Xe^+.

* Research supported by the U.S. Atomic Energy Commission under Grant AT(04-3)767-8.

† Submitted for publication, J. Amer. Chem. Soc.

$$Xe + CH_3FH^+ \longrightarrow CH_3Xe^+ + HF \qquad (5)$$

The occurrence of reaction 5 allows the estimation of a lower limit of 32 kcal/mole for the C— Xe bond energy in CH_3Xe^+.

The present findings have important implications for many other studies dealing with ionization phenomena. For example, species such as NH_3, H_2S, H_2O and CH_4 are frequently utilized as ionic scavengers or ionization agents in photolysis, radiolysis or chemical ionization experiments. Clearly, in understanding the chemical activity of these additives, it is necessary to recognize the possible occurrence of processes such as generalized in reaction 1.

P5

ION-CYCLOTRON RESONANCE STUDY OF ION-MOLECULE REACTION RATES*

Stephen Wisniewski, Roger Clow, David Smith and Jean H. Futrell
Department of Chemistry, University of Utah, Salt Lake City, Utah 84112

The ion cyclotron resonance (ICR) mass spectrometer is ideally suited to the determination of ion-molecule reaction mechanisms at thermal and higher energies. Quantitative rate constants can, however, be obtained only if the reaction time is known accurately. The reaction time or ion residence time can be calculated for the ICR mass spectrometer assuming the drift plates to have infinite area.[1] Using a modified Varian Associates Syrotron[2] ICR mass spectrometer, we have developed a method to measure directly the ion residence time. A short pulse of electrons (100 μs) produces a packet of ions which drift down the cell. In normal operation, these ions are detected on the total ion current collector at some time, τ, later. If a short negative pulse (10 μs) is applied to one trapping plate at some time τ' where $\tau > \tau'$, the packet of ions will be attracted to a trapping plate and will never reach the total ion current collector. A plot of total ion current versus τ' gives the ion residence time directly. With drift voltages and magnetic field set such that an ion residence time of 1.83 ms is calculated, the actual residence time was measured to be 1.18 ms, 1.65 ms and 2.45 ms corresponding to trapping voltages of 1.30 V, 0.80 V and 0.40 V. This strong dependence of ion residence time on trapping voltage is striking since the theoretical calculation assumes that ion residence time is independent of trapping voltage.

The effect of electron current on ion residence time was determined in another experiment. Using a 10% pulse duty cycle on the electron beam modulation unit, the ion residence time was found to increase by about 10% as the electron current is decreased from 0.10 μa to 0.02 μa. A study of ion residence time as a function of magnetic field indicates that it does not increase as rapidly as would be predicted from theory. At 4 KG, the measured value is about 90% of the calculated while at 14 KG it is only 67%. From this work it is clear that a quantitative rate constant can be measured only if the ion residence time is measured directly.

Thermal energy rate constants have been measured for the reactions given in Table I. The method of determination consists of monitoring the reactant ion intensity while increasing the concentration of neutral. Since the reaction time is known accurately, the greatest uncertainty in the rate constant determination lies in the pressure measurement. In this work, an ionization gauge is used to measure the pressure which is corrected for the ionization cross section.

The O^+ reactant ions in reactions 1-3 are obtained from electron impact of CO_2. Little work has been done previously on the reactions of H_2^+ with CO_2 and CO_2^+ with H_2 because both reactions lead to large amounts of CO_2H^+, and it is impossible to determine the relative importance of the two reaction channels in the conventional mass spectrometer. One of the unique features of the ICR mass spectrometer lies in the ability to selectively eliminate reactant ions from the cell by applying an oscillating electric field of the proper frequency to the trapping plate. Table I shows that the rates for reactions 8 and 9 are considerably lower than those predicted on the basis of the ion-induced dipole model. Using the heats of formation given in a recent compilation,[3] these reactions are about 0.8 eV endothermic for ground state CO_2^+ ions. From this it is clear that after 10^{-3} seconds, many CO_2^+ ions formed by impacting 50 eV electrons on CO_2 still have at least 0.8 eV excitation energy.

It is also surprising to observe charge-transfer (reactions 6 and 8) actively competing with proton transfer (reactions 7 and 9) at thermal energies. This result indicates that the recombination energy of at least some of the H_2^+ ions is very near the ionization energy of CO_2.

In the future we plan to look further into the question of isotope effects as well as the competition between charge-transfer and ion-molecule reactions at thermal energies. Preliminary results indicate that CO^+, COH^+ and H_2O^+ are minor products in the H_2/CO_2 system. Efforts are being directed at quantitatively substantiating these observations.

References.

1. J.L. Beauchamp, L.R. Anders and J.D. Baldeschwieler, J. Am. Chem. Soc., 89, 4569 (1967).

2. Varian Associates, Palo Alto, California.

3. J.L. Franklin, J.G. Dillard, H.M. Rosenstock, J.T. Herron and K. Draxl, "Ionization Potentials, Appearance Potentials and Heats of Formation of Gaseous Positive Ions," NSRDS-NBS 26 (1969).

*Research sponsored by the Aerospace Research Laboratories, Office of Aerospace Research, Contract F33615-68-C-1022.

TABLE I. Thermal Energy Ion-Molecule Reaction Rates.

		Theory $k(cm^3\ mol^{-1}\ sec^{-1} \times 10^9)$	Experimental $k(cm^3\ mol^{-1}\ sec^{-1} \times 10^9)$
(1)	$O^+ + H_2 \rightarrow$ Products	1.6	0.7
(2)	$O^+ + D_2 \rightarrow$ Products	1.1	0.7
(3)	$O^+ + CO_2 \rightarrow$ Products	1.1	0.9
(4)	$H_2^+ + CO_2 \rightarrow CO_2^+ + H_2$	2.8	0.7
(5)	$H_2^+ + CO_2 \rightarrow CO_2H^+ + H$		2.0
(6)	$D_2^+ + CO_2 \rightarrow CO_2^+ + D_2$	1.9	0.5
(7)	$D_2^+ + CO_2 \rightarrow CO_2D^+ + D$		2.3
(8)	$CO_2^+ + H_2 \rightarrow CO_2H^+ + H$	1.5	0.5
(9)	$CO_2^+ + D_2 \rightarrow CO_2D^+ + D$	1.0	0.4

TIME HISTORY PLOTS AND COMPUTER-MADE MOVIES OF ION-POLAR MOLECULE COLLISIONS OF INTEREST IN MASS SPECTROMETRY*

by John V. Dugan, Jr., NASA-Lewis Research Center, Cleveland, Ohio
and John L. Magee, University of Notre Dame, Notre Dame, Indiana

INTRODUCTION

Capture cross sections have been calculated for ion-polar molecule collisions; the interaction potential consists of classical ion-dipole plus ion-induced dipole (polarizability) terms. These capture cross sections set a rough upper limit to the reaction cross section. The ion-dipole energy transfer and formation of ion-molecule collision complexes have been studied using computer-plotter techniques. Mutual orbiting of the ion-molecule pair and hindered rotation of the dipole have also been studied via computer-made motion pictures. The latter is of interest for ion-molecule reactions since preferred dipole orientation favors certain reactions. This paper reports on results obtained for ion-molecule systems of particular interest in mass spectrometry.

COLLISION TARGETS

The polar targets studied were chosen mainly because they have been studied in the mass spectrometer. Ion-molecule reactions involving CH_3CN have been studied by Moran and Hamill.[1] The good agreement between theory and mass spectrometer experimental values have been reported.[2] Large cross sections for CH_3OH targets were reported in refs. 3 and 4 for low ion energies. Negative ion-molecule cross sections reported for H_2O targets are roughly 10^{-13} cm^2.[5]

ION MOLECULE INTERACTION

The ion-molecule interaction consists of the ion-permanent dipole and ion-induced dipole (polarizability) terms. The first term $= -\mu e \cos\gamma / r^2$ where μ is the permanent dipole moment; e is the electronic charge, γ is the ion-dipole orientation angle and r is the ion-molecule separation. The Langevin term is $-\alpha e^2/2r^4$ where is the spherically symmetric molecular polarizability. The separate cross section contributions are the Langevin cross section

$$\sigma_L \equiv \pi b_L^2 = \pi \left(2\alpha e^2/\epsilon\right)^{1/2} \quad ,(1)$$ and the ion-dipole cross section $$\sigma_D \equiv \pi b_D^2 = \pi \mu e / \epsilon \quad ,(2)$$

Assuming favorable orientation of the dipole, i.e., $\gamma = 0$, the cross section

$$\sigma_M \equiv \pi b_M^2 = \sigma_L + \sigma_D \qquad (3)$$

is somewhat of a maximum.[6] In equations (1) thru (3), ϵ is the relative translational energy. The ion and molecule are reflected off a hard-core potential at $r = r_c$ for lifetime studies.

COMPUTER APPROACH

Collision quantities such as ion velocity and dipole rotational energy are plotted using values obtained by numerical integration. The time history plots are done in the coordinate system where the polar molecule is fixed.[7] The differential equations of motion are integrated using the variable step-length Runge-Kutta scheme of Ref. 6. Solutions of the equations include the coordinates for movie models of the colliding partners. The initial conditions and successful steps (for variables and time derivatives) are stored in a plotting array for both computer-made time history plots and movies.[8]

MOVIE MODEL

The coordinate solutions are used to draw projections of the ion and polar molecule models in the center-of-mass system. A sample movie frame consists of simple ion and dipole models with a clock.[9] Each frame is traced on a cathode-ray-tube and photographed using the IBM 360-67 computer with the CDC DD280 plotter. The clock measures real time and moves at different rates during a collision since a variable step-size integration routine is used.

INITIAL CONDITIONS

The initial conditions on the dependent variables and their first time derivatives are obtained using a random number generator. Trajectories were studied for ion velocities of 5×10^4, 10^5, and 2×10^5 cm sec^{-1}. Target rotators were chosen from a heat bath at rotational temperature T_R = 500 K. The assigned reflection distances for the collision complex studies were 2, 2.5, and 3.0 Å for CO, HCl, and CH_3CN, respectively, whereas 2Å was used as a capture distance in all cross section calculations.

DISCUSSION AND RESULTS

In all numerical calculations the energy equation and behavior of trajectories with time reversal were used as checks on the accuracy of the integration routine.

Capture cross sections. - For each impact parameter 36 to 50 trajectories were calculated for the capture cross section; these trajectories were truncated once $r \leq 2$ Å.

Unlike Langevin collisions there is no all-or-nothing answer to the question of capture in ion-permanent dipole collisions for fixed initial impact parameter. For fixed values of energy and impact parameter there is a probability that the system will arrive at an ion-molecule separation corresponding to capture. The fraction of collisions resulting in such a prescribed "minimum" separation we call the capture ratio C_R. Such a fraction can be correlated with the reaction probability.

The capture cross section is[2]

$$\sigma_c \equiv \pi \int_0^{b_0} C_R(b)\, d(b^2) \tag{4}$$

Numerical capture cross sections σ_c have been calculated for four ion-molecule pairs. The σ_c values for $CH_3CN^+ + CH_3CN$ and $C_6D_{12}^+ + CH_3CN$ are considerably larger than σ_L but vary from two-thirds to one-half σ_M values. Both σ_c values have approximately $\epsilon_1^{-.65}$ dependence on ion energy ϵ_1. The integrated Q_c (over ϵ_1 values) is within 20% of the reaction cross section Q_R for all ϵ_m values (ϵ_m = experimental ion exit energy) for $CH_3CN^+ + CH_3CN$. The Q_c values are within 20% to 50% of Q_R for $C_6D_{12}^+ + CH_3CN$ over the range of ϵ_m from 0.2 to 2.0 eV.

The $HCl^+ + HCl$ capture cross section has very nearly a Langevin $\epsilon_1^{-1/2}$ dependence although the σ_c values are uniformly 15% larger than σ_L. There is no satisfactory mass spectrometric data available for this reaction cross section.

The $CH_3OH^+ + CH_3OH$ σ_c values have an $\epsilon_1^{-.7}$ dependence on ion energy. The Q_c values are within factors of 2 to 3 of the observed reaction cross section from 0.1 to 1.0 eV.

The σ_c for $H^- + H_2O$ was calculated only for $\epsilon_1 = 0.2$ eV; this σ_c value is 130 Å^2. The maximum cross section σ_M is 250 Å^2 whereas the measured reaction cross section is 5×10^{-13} cm^2 (5000 Å^2).

The agreement between theory and experiment appears satisfactory except for the large discrepancy in the case of the $H^- + H_2O$ reaction.

Collision Lifetime and Hindered Rotation. - Trajectories have been investigated by computer-plotter techniques. Collision orbits and ion-molecule interaction behavior are studied for a range of collision parameters. The interaction potential consists of a hard-sphere term plus the attractive polarization and ion-dipole terms. Multiple reflections off the hard-core barrier at small ion-molecule separations occur only in collisions with permanent dipoles. Multiple reflection times τ_c are 10 to 500 times longer than the corresponding values for single reflections. The average number of reflections is 2 to 5 for CO whereas it is nearly 20 to 30 for CH_3CN targets. The fraction of these collisions varies from about 0.1 for CO to roughly 0.5 for CH_3CN. There are few multiple reflection collisions for HCl but the average number of reflections is large.

Plots are made of relative velocity, rotational energy, projections of the ion and dipole angle coordinates and the ion-dipole orientation angle γ. The plot of γ decreasing with decreasing r suggests that the dipole is hindered by the incident ion.

Motion pictures of the ion-dipole collisions have also been made with the computer-plotter system. Computer-made movies furnish a convenient visual means for observing the relative motion of the ion-molecule pair, as well as hindering of the dipole by the incident ion. The degree of hindering is best described by a parameter which depends on the dipole moment, rotational energy and impact parameter. Leger and Meisels[10] and Leger[11] et al. have investigated the relative reaction probabilities in $CH_3OH^+ + CH_3OH$ and $CH_3OH^+ + CH_3CHO$ collisions. They point out that their results are consistent with the hypothesis that hydrogen abstraction from electromegative sites in the polar molecule is formed for collisions in which the ion is able to orient the dipole attractively. The numerical results indicate that this is very probable.

The extension of computer-made plots and movies to a description of vibrating targets is already in progress. Studies of chemical reactions will be more difficult since the construction of accurate potentials is not straightforward.

REFERENCES

1. T. F. Moran and W. H. Hamill, J. Chem. Phys. 39, 1413 (1963).
2. J. V. Dugan, Jr., and J. L. Magee, J. Chem. Phys. 47, 3103 (1967).
3. Private Communication, D. P. Stevenson to W. H. Hamill.
4. L. P. Theard and W. H. Hamill, Am. Chem. Soc. J. 84, 1134 (1962).
5. J. A. D. Stockdale, R. N. Compton and P. W. Reinhardt, Phys. Rev. 184, 81 (1969).
6. J. V. Dugan, Jr., J. H. Rice, and J. L. Magee, NASA TM X-1586 (1968).
7. J. V. Dugan, Jr., J. H. Rice and J. L. Magee, Chem. Phys. Letters, 3, 323 (1969).
8. J. V. Dugan, Jr., and J. H. Rice, NASA TN D-5407 (1969).
9. J. V. Dugan, Jr., R. B. Canright, Jr., R. W. Palmer and J. L. Magee, NASA TM X-52662 (1969); paper presented at VI ICPEAC, Cambridge; MIT Press, July 1969, pp. 333-340.
10. L. J. Leger and G. G. Meisels, Chem. Phys. Letters 1 (1968) 661.
11. L. J. Leger, G. G. Meisels and T. O. Tiernan, paper at 17th Mass Spect. Mtg., Dallas, Texas, May 1969.

☆ The unpublished results of this paper will be submitted to The Journal of Chemical Physics.

COLLISION-INDUCED DECOMPOSITION OF $H^+(H_2O)_n$ AND $NO_3^-(H_2O)_n$*

Rudolf R. Burke

AeroChem Research Laboratories, Inc.
Sybron Corporation
Princeton, New Jersey

A technique was developed for the measurement of the kinetics of cluster decomposition. In the present application a room-temperature Ar stream at 5 Torr containing small smounts of H_3O^+ and NO_3^- produced in an atomic O/atomic N/C_2H_2 reaction is expanded through a Mach 3 nozzle. This reduces the pressure to 0.2 Torr, cools the gas mixture to 85 K, and causes extensive hydration of the ions in the free jet to form $H_3O^+(H_2O)_n$ and $NO_3^-(H_2O)_n$ ($n = 0$ to ≈ 15). The supersonic jet impinges upon a blunt-faced sampling system, thus forming a detached shock wave. In the shock layer the pressure recovers to 1.5 Torr and the temperature to 270 K inducing decomposition of the cluster ions. Mass spectrometric profiles of the ion composition are taken through the subsonic region behind the shock by adjusting the shock front-to-sampling orifice distance.

The $H^+(H_2O)_n$ concentration profiles are analyzed in terms of a series of reactions which successively strip H_2O molecules from the ions;

$$H^+(H_2O)_n + Ar \rightarrow H^+(H_2O)_{n-1} + H_2O + Ar$$

The rate constants (k_n) obtained are (molecule^{-1} ml sec^{-1}): $k_{11} = k_{10} = 1.3 \times 10^{-11}$; $k_9 = 1.2 \times 10^{-11}$; $k_8 = 7.8 \times 10^{-12}$; $k_7 = 6.6 \times 10^{-12}$; $k_6 = 5.4 \times 10^{-12}$; $k_5 = 4.4 \times 10^{-12}$. The values obtained can be correlated with the k_2 to k_5 values obtained by Good, Durden and Kebarle,[1,2] using their pulsed electron beam mass spectrometer. The influence of $H^+(H_2O)_n$ vibrational relaxation on the rate constants k_5 and k_6 is discussed.

The $NO_3^-(H_2O)_n$ concentration profiles are also interpreted in terms of consecutive ion decomposition reactions;

$$NO_3^-(H_2O)_n + Ar \rightarrow NO_3^-(H_2O)_{n-1} + H_2O + Ar$$

The rate constants (k_n) obtained are (molecule^{-1} ml sec^{-1}): $k_{11} = k_{10} = 1.5 \times 10^{-11}$; $k_9 = 1.2 \times 10^{-11}$; $k_8 = 1.0 \times 10^{-11}$; $k_7 = 8.7 \times 10^{-12}$; $k_6 = 6.3 \times 10^{-12}$. The first hydration reaction of NO_3^- is discussed.

This paper will be submitted for publication to the Journal of Chemical Physics.

1. Good, A., Durden, D.A. and Kebarle, P., "Ion-Molecule Reactions in Pure Nitrogen and Nitrogen Containing Traces of Water at Total Pressures 0.5-4 Torr. Kinetics of Clustering Reactions Forming $H^+(H_2O)_n$," J. Chem. Phys. 52, 212 (1970).

2. Good, A., Durden, D.A. and Kebarle, P., "Mechanism and Rate Constants of Ion-Molecule Reactions Leading to Formation of $H^+(H_2O)_n$ in Moist Oxygen and Air," J. Chem. Phys. 52, 222 (1970).

* This research was sponsored by the Air Force Cambridge Research Laboratories under Contract No. F19628-67-C-0325. Funding for this research was supplied by DASA under Subtask No. 11BHAX504(07.504).

Abstract

Photoelectron spectroscopy of small molecules.

Jacques E.COLLIN, Jacques DELWICHE and Paul NATALIS

Laboratoire des Etats Ionisés, Université de Liège
Sart-Tilman, 4000 Liège, Belgique(*)

Photoelectron spectra of some diatomic and triatomic molecules have been obtained, using various types of energy analyzers. The energy resolution was of the order of 30 mV in the best cases. Various light sources and pressure conditions were used as to study the influence of the photon energy on the relative transition probabilities and the possible occurrence of collision-induced photoelectron emission. Vibronic sequences are identified. In cases like O_2, N_2, CO and NO, the influence of autoionization of the relative transition probabilities is considerable. The complex photoelectron spectrum of NO is considered. In some cases, notably N_2O, pressure-sensitive photoelectron bands are observed at high pressures. Their possible origin, notably from induced preionization, will be discussed.

(*) Full papers published or due to appear in Journal of Mass Spectrometry and Ion Physics, and in Chemical Physics Letters.

Abstract

Electron impact excitation of N_2, CO, C_2H_4 and C_6H_6 by the SF_6 method.

Marie-Jeanne HUBIN-FRANSKIN and Jacques E.COLLIN

Laboratoire des Etats Ionisés, Université de Liège
Sart-Tilman, 4000 Liège, Belgique (*)

The SF_6 scavenger technique has been applied to a study of the electron impact excitation at threshold energy of some molecules. Improvement of resolution has been obtained by the use of a deconvolution method. Below the ionization limit, many transitions have been observed in N_2, CO, C_2H_4 and C_6H_6. A number of those transitions are optically-forbidden and important differences in transition probabilities are found, as compared to other published data, and will be discussed. In this respect, the so-called "mystery band" of ethylene has been observed. In the four molecules studied, the technique allows the observation of compound-state molecular negative ions. Some evidence for preionization above the first ionization limit has also been obtained.

(*) The full papers will appear in one 1970 issue of the Journal of Mass Spectrometry & Ion Physics.

Q3

A Coincidence Time-of-Flight Mass-Spectrometer

by

A. Harvey, (Mrs) M-de-L.F. Monteiro, and R.I. Reed

The Chemistry Department,

The University of Glasgow, Glasgow W.2.

A coincidence time-of-flight mass-spectrometer has been developed in which ionization is effected by the 584 Å helium line; considered to give a beam of monoenergetic-photons. The ionization process yields a positive ion and an electron. The latter is accelerated to a box-and-grid electron multiplier followed by a cathode follower, a high gain amplifier, thence through a time delay line to a "coincidence" unit followed by a scaler. In a comparable way the ion first traverses a known potential gradient, strikes the first dynode of a "venetian-blind" multiplier and continues as the electron;there is no delay line.

When impulses from the electron and ion multipliers arrive at the coincidence unit simultaneously (or substantially so) a signal is counted upon the scaler. Thus by plotting the counting rate vs the electron delay time one may plot out the mass-spectrum of the material under examination.

In our prototype instrument the resolution is rather low, but it may readily be improved by:-

i) lengthening the flight-tube to increase the ion transit time,

ii) modifying the potential gradient through which the ion falls, and

iii) increasing the "sharpness" of response of the coincidence unit.

The second of these is valid for only rather small alterations in the potential for such adjustments have a deleterious effect upon the focusing of the ion beam.

In spite of these obvious improvements some major problems connected with the resolving power remain. In general ions are formed with kinetic-energy so that two ions may be formed successively at the same point one moving directly towards the ion-accelerator, the other directly away from it. The transit times of these two particles will differ by the turn round time of the latter. Moreover, the photon beam is of a finite width

and thus ions may be formed in a finite volume within the ion source. A combination of these two effects may speed the overall transit times significantly. Nevertheless serviceable spectra have been obtained and this instrument has the further advantage of being an "absolute" mass-spectrometer.

To be published in the Journal of Mass Spectrometry and Ion Physics

Photoelectron Spectra and Ionization Potentials of H_2, HD, D_2 and the Halogens

Q4

A.B. Cornford, D.C. Frost, C.A. McDowell, J.L. Ragle* & I.A. Stenhouse

Department of Chemistry, University of British Columbia
Vancouver 8, B.C. Canada

Abstract:

The photoelectron spectra of H_2, HD, D_2 and the halogens have been obtained using a high resolution spectrometer with the 584 Å helium resonance line as the radiation source. The spectrometer is a 180 degree electrostatic spherical analyzer. The spectra of H_2, HD, and D_2 allow ω_e and $\omega_e X_e$ for their ground state molecular ions to be calculated. The ionization bands obtained for the halogens (F_2, Cl_2, Br_2, and I_2) are correlated with molecular orbital theories. A discussion of vibrational frequencies, hot bands, bond lengths and spin-orbit couplings is included for these latter compounds.

Introduction

The photoelectron spectra were obtained using a double focusing hemispherical electrostatic analyzer operating at a nominal resolution of .03 eV. The instrument is essentially the same as previously described[1]. The entrance lens to the analyzer and electrostatic deflectors leading to the multiplier have been removed giving a subsequent rise in intensity without sacrificing resolution. The entrance and exit slits to the analyzer are maintained at ground potential and the electrostatic monachrometer adjusted to focus ~ 2er electrons with the aid of Helmholtz coils.

The Hydrogen Molecule Ion & Deuterium Derivatives.

The 584 Å photoelectron spectrum of H_2^+, HD^+ and D_2^+ allow the vibrational intervals in the $^2\Sigma g^+$ states of the ions to be measured. The vibrational constants ω_e and $\omega_e x_e$ are calculated and compared with previous theoretical energy values of Hunter and Pritchard[2]. In addition the Morse function is shown to be a satisfactory description of the potential curves[3].

The Halogen Positive Ions (F_2^+, Cl_2^+, Br_2^+, & I_2^+).

Previous electron impact and low resolution photoelectron spectroscopic work has been summarized by Frost et al[4]. We report here a summary of recent photoelectron data[5] yielding more complete and detailed information on the nature and properties of the lowest lying few states of the halogen positive ions. A summary of photoelectron spectroscopic data for the halogens appears in Table 1. The results of calculations of spin-orbit couplings, vibration intervals and changes in bond lengths derived from observation of hot bands appear in Table 2, and are briefly described below.

Hot bands were resolved on the low energy edge of the first I.P.'s of Cl_2^+ and Br_2^+ (occurring in transitions from the $^1\Sigma q_g^+$ state of the neutral to the $^2\Pi g$ state of the ion). The distribution of the intensities was used to calculate the values for Δr_e (see table 2).

* On leave from the Department of Chemistry, University of Massachusetts, Amherst, Massachusetts 1969-1970.

TABLE I SUMMARY OF PHOTOELECTRON DATA

Compound	State of Ion	Ionization Potential		ζ (cm^{-1})	$\omega_e(cm^{-1})$[a]
Fluorine	$^2\pi_g$	15.70[b]	-	337±40	1050±40
	$^2\pi_u$	18.4[c]	(18.98)[d]	-	-
	(?)$^2\Sigma_{g,u}$		(? 21)[d]	-	-
Chlorine	$^2\pi_g$	11.49[b]	-	645±40	645±40
	$^2\pi_u$	14.0[c]	(14.43)[d]	-	-
	$^2\Sigma_g^+$	15.8[c]	(16.10)[d]	-	-
Bromine	$^2\pi_g$	10.51[b]		2820±40	360±40
	$^2\pi_u$	12.5[c]	(13.08)[d,e]	∿2000 - 2200	-
	$^2\Sigma_g^+$	14.3[c]	(14.60)[d]	-	-
Iodine	$^2\pi_g$	-	(9.34, 9.97)[d]	5125±40	∿ 220
	$^2\pi_u$	10.8[c] 11.6[c]	(11.03, 11.82)[d]	∿6400	-
	$^2\Sigma_g^+$	12.7[c]	(12.95)[d]	-	-

a apparent ω_e, any anharmonicity being smaller than precision of measurement.

b resolved 0-0 band.

c onset value.

d band maximum.

e see Figure 1.

TABLE 2

Quantity	F_2	F_2^+	Cl_2	Cl_2^+	Br_2	Br_2^+	I_2	I_2^+
			$^2\pi_{3/2}$	$^2\pi_{1/2}$	$^2\pi_{3/2}$	$^2\pi_{1/2}$		
r_e (Å)	1.326[11.]		1.892[12]	1.891[12]	-			
ω_e (cm^{-1})	10.54.5[11.]	1050±40	645.6[12]	644.8[12]	-	376.0[12]		~220
$\omega_e x_e$	∿9.1		3.0[12]	3.0[12]	-	1.25[12]		
ζ	—	337±40		645±40		2820±40		5125±40
Δr_e (Å)		~0.11[11]		0.106		∿(-)0.095		-
r_e (Å)	-		2.28[10]	2.30[10]				
ω_e (cm^{-1})	498.6[11]		572.3[10]	564.8[10]	190.0[12]	152.0[12]		
$\omega_e x_e$	~7.3[11]		5.32[10]	4.13[10]	1.0[12]	0.35[12]		
ζ						2000-2200		~6400
r_e (Å)	1.435[10]		1.988[10]		2.283[10]		2.666[10]	
ω_e (cm^{-1})	892.1[10]		564.9[10]		323.2[10]		214.6[10]	
$\omega_e x_e$			4.0[10]		1.1[10]		0.6[10]	

The P.E. spectra yield the spin-orbit splittings between the $^2\pi$ states of all the halogens studied, these transitions being unavailable from u-v spectra. Sample calculations employing single "hole" occupancy of the four available spin orbitals, neglecting differential overlap and other two-centre integrals, produces a multiplet splitting

$\zeta = 2\beta e^2 < Z_E^{eff}/r_F^3 >$, the expectation value varying approximately as the fourth power of the effective nuclear charge. The small upward shifts of ζ observed for the positive ions (as compared to the atomic values tabulated) may be best accommodated by a small increase in this charge.

A more complete analysis of this work will appear in articles to be published in the Journal of Chemical Physics.

References.

1. G.R. Branton, D.C. Frost, T. Makita, C.A. McDowell & I.A. Stenhouse J. Chem. Phys. 52, 802 (1970).
2. G. Hunter and H.O.Pritchard, J. Chem. Phys. 46, 2153 (1967).
3. A.B. Cornford, D.C. Frost, C.A. McDowell, J.L. Ragle, & I.A. Stenhouse To Be Published.
4. D. C. Frost, C.A. McDowell & D.A. Vroom, J. Chem. Phys. 46, 4255 (1967).
5. A.B. Cornford, D.C. Frost, C.A. McDowell, J.L. Ragle & I.A. Stenhouse To Be Published.
6. P.E. Cade (Private Communication).
7. Gilbert & Wahl. (Unpublished Results).
8. P. Venkateswarlu, Can. Jour. Phys. 47, 2525 (1969).
9. P. Venkateswarlu, Can. Jour. Phys. 48, 1055 (1970).
10. G. Herzberg "Spectra of Diatomic Molecules" D. Van Nostrand Co. Inc. Princeton N.J. 2nd Ed. 1950.
11. T.L. Porter, J. Chem. Phys. 48, 2071 (1968).
12. F.D. Huberman, J. Mol. Spec. 20 29 (1966).

PHOTOIONIZATION MASS SPECTROSCOPY USING SYNCHROTRON RADIATION

James W. Taylor, James A. Kinsinger, and William L. Stebbings
Department of Chemistry, University of Wisconsin
Madison, Wisconsin 53706

The high intensity light which is radiated from electrons accelerated to relativistic velocities in a synchrotron is continuous from the soft x-ray region to the infrared and is devoid of fine structure. This light source is, therefore, ideal for use in photoionization mass spectrometry and for photoelectron spectroscopy. This paper describes some of the preliminary results and progress made in the determination of the ionization potentials, appearance potentials and in observing vibrational fine structure in ions produced by photon impact using this light source.

The experimental arrangement at the Wisconsin Physical Sciences Laboratory consists of a 50 MeV injector machine followed by a storage ring. In the holding ring the electron energy is raised to the operating value of 240-250 MeV. Moving on an average radius of 1.5 meters at approximately 32 M hz, the speed of the electrons circulating is 99.999% the speed of light. At a beam pulse intensity of 10 ma and at 10^{-9} torr, the half-life is about 20 minutes.

There are presently three ports on the holding ring. Two are identical, and the light originates from a section of the tangent after focusing by the quadrupole magnets and has a peak intensity at 200 Å. One port which is used for photoionization measurements observes the light originating near injection and after a straight section. Its peak maximum occurs at 600 Å, but in the region from 500 Å - 1400 Å (24.8 - 8.9 eV) the intensity is fairly constant. The intensity can be decreased by a factor of about 2.5 by changing the beam energy. This feature is useful in order sorting when the mass spectrometer is operated windowless below the lithium fluoride cut off at 1050 Å. Using a McPherson one-meter vacuum ultraviolet monochromator with MgF_2 overcoated grating, the available photon flux is approximately 5×10^7 photons/sec Å ma of beam current. Because operating currents are in the 5 - 10 ma range, a flux of approximately 10^8 photons/sec Å is available.

A combination mass spectrometer and photoelectron spectrometer has been constructed to permit mass spectral measurement and also kinetic energy analysis of the ejected electrons, but initial experiments use only the mass spectrometer portion, which is a modified Finnigan 1015 quadrupole unit. The first compound described was benzene which was used for calibration. The IP obtained was 9.23 eV. Other literature values are: 9.247 [1] (spectroscopic); 9.24_2 [2] (photoionization); 9.25_0 [3] (photoelectron spectroscopy). All the observed fine structure from PES measurements was observed by photoionization in

the region 1350 - 1290 Å.

Other compounds studied were methanol, 2-pentanone-d_5, 3-hexanone, and 3-hexanone-d_4. Vibrational fine structure, ionization potential and appearance potential data were obtained on the molecular and selected fragment ions. Some correlations with infrared and Raman frequencies were presented for methanol m/e 32 and m/e 31 ions. For the ketones, the M-28 ion from McLafferty rearrangement appeared at a higher energy (shorter wavelength) than did the M-29 ion from simple cleavage of an ethyl group. Contributions from vibrationally excited species (hot bands) were considered in making the vibrational assignments and ionization onsets. The curves for the cleavage and rearrangement reactions appear to show structure ascribed to autoionization about 0.5 eV above the onset for ionization.

References

1. P. G. Wilkinson, J. Chem. Phys., 24, 917 (1956); Can. J. Phys., 34, 596 (1956).

2. V. H. Dibeler and R. M. Reese, J. Res. Nat. Bur. Std., 68A, 409 (1964).

3. A. D. Baker, C. R. Brundle, and D. W. Turner, Intern. J. Mass Spectry. Ion Phys., 1, 443 (1968).

Acknowledgment

This research is supported by the Air Force Office of Scientific Research and the Wisconsin Alumni Research Foundation.

To be submitted to J. Am. Chem. Soc.

Q6

Effects of Vibrational Hot Bands on Threshold Measurements of Halogen Molecules

Vernon H. Dibeler and James A. Walker

National Bureau of Standards
Washington, D. C. 20234

Photoionization yield curves with energy resolution of about 0.01eV are obtained for fluorine, chlorine, bromine and iodine from threshold to 600Å by means of a combined vacuum uv monochromator and mass spectrometer. In the threshold regions, the curves show the anticipated effects of hot bands due to the ionization of molecules in the first, or higher, vibrationally excited states. Although thresholds for the 0,0 transition can be designated with some confidence for fluorine and chlorine, it is apparent that cooled-gas measurements are necessary in order to reduce the ambiguity due to hot-bands for the heavier halogens.

Accordingly, molecular ionization threshold measurements were made on fluorine, chlorine, and bromine at room temperature and at temperatures sufficiently low to eliminate or to significantly reduce hot band contributions. Experiments on iodine were limited by the low vapor pressure of the molecule.

The table summarizes the present results and previously reported values obtained by other authors and by other methods. It is apparent that the effects of hot band on threshold measurements are difficult to predict in the case of electron impact measurements. This is possibly the result of partial compensation for the unfavorable threshold law by the presence of hot-bands. On the other hand, both photoelectron spectroscopy and photoionization techniques tend to give too low a value for the (0,0) transition when the hot band is not resolved or correctly identified.

The recent high-resolution measurements of Rydberg series in the vacuum ultraviolet spectrum of bromine observe five series converging to a limit approximately 0.05eV above the threshold identified in the present work as the 0,0 transition. From cooled and heated gas measurements, it is apparent that the present photoionization results correctly identify the ground-state transition whereas the spectroscopic limit relates to the first vibrationally excited state of the ion.

Table I. Molecular Ionization Thresholds for the Homonuclear Halogens

	Method	Threshold (eV)	Reference
F_2 :			
	VUV Spectrum	15.7	1
	Elect. Impact	15.83 ± 0.05	2
	Photoelect. Spectrosc.	15.63 ± 0.01	3
	Photoion. MS	15.69 ± 0.01	4
Cl_2:			
	VUV Spectrum	11.47	5
	Elect. Impact	11.64 ± 0.05 11.63 ± 0.04	2 6
	Photoelect. Spectrosc.	11.50 ± 0.01	3
	Photoion.	11.48 ± 0.01	7
	Photoion. MS	11.48 ± 0.01	This Work
Br_2:			
	VUV Spectrum	10.56 ± 0.01	8
	Elect. Impact	10.58 ± 0.08 10.69 ± 0.03	2 6
	Photoelect. Spectrosc.	10.51 ± 0.01	3
	Photoion.	10.55 ± 0.02	7
	Photoion. MS	10.51 ± 0.01	This Work

Table I (continued)

	Method	Threshold (eV)	Reference
I_2 :			
	VUV Spectrum	9.400 ± 0.001	9
	Elect. Impact	9.35 ± 0.03	6
	Photoelect Spectrosc.	9.33 ± 0.01	3
	Photoion.	9.28 ± 0.02	7
	Photoion. MS	9.3 ± 0.1	10

References for the Table

1. R. P. Iczkowski and J. L. Margrave, J. Chem. Phys. 30, 403 (1959).
2. J. T. Herron and V. H. Dibeler, J. Chem. Phys. 32, 1884 (1960).
3. D. C. Frost, C. A. McDowell, and D. A. Vroom, J. Chem. Phys. 46, 4255 (1967).
4. V. H. Dibeler, J. A. Walker, and K. E. McCulloh, J. Chem. Phys. 51, 4230 (1969).
5. R. P. Iczkowski, J. L. Margrave, and J. W. Green, J. Chem. Phys. 33, 1261 (1960).
6. D. C. Frost and C. A. McDowell, Can. J. Chem. 38, 407 (1960).
7. K. Watanabe, T. Nakayama, and J. Mottl, J. Quant. Spectrosc. Radiat. Transfer 2, 369 (1962).
8. P. Venkateswarlu, Can. J. Phys. 47, 2525 (1969).
9. P. Venkateswarlu, Can. J. Phys. 48, 1055 (1970).
10. J. D. Morrison, H. Hurzeler, M. G. Inghram, and H. E. Stanton, J. Chem. Phys. 33, 821 (1960).

Q7

Photoionization of Carbon Monoxide

Kenneth E. McCulloh

National Bureau of Standards
Washington, D. C. 20234

The photoionization of carbon monoxide has been studied with spectral resolution of 0.12 and 0.25 Å, using a near-normal-incidence grating monochromator combined with a mass spectrometer. The molecular ion yield curve shows a wealth of autoionization structure which is compared with published absorption spectra and discussed in terms of Rydberg series and electronically excited states of the ion. A value of 14.00 eV is proposed for the lowest ionization potential of this molecule.

ELECTRON IMPACT EXCITATION EFFICIENCY CURVES FOR THE FORMATION OF NEUTRAL METASTABLE SPECIES*

R1

Amos S. Newton and G. E. Thomas

Lawrence Radiation Laboratory
University of California
Berkeley, California 94720

For some years now, a group at the Lawrence Radiation Laboratory at Berkeley has been engaged in making measurements of the excitation efficiency curves for the formation of neutral electronically metastable species.[1,2] Basically, an electron beam from an RPD gun has been crossed with an atomic or molecular beam. The metastable neutrals can be detected via their ability to eject electrons from a metal surface. In this work, the metal surface is the Cu-Be first dynode of an EMI type 9603 electron multiplier.

A difficulty encountered in making these measurements in this way is that U.V. photons produced in the collision chamber are also detected by the multiplier. However, the photons can be separated from the metastables by taking advantage of their flight time from the collision region to the detector. If excitation is effected by a short pulse of electrons, photons are observed to arrive at the detector during the pulse. The metastables arrive at later times.[2]

In attempting to extend the earlier work,[1,2] we have developed a method of making RPD measurements on the time-resolved species. The pulsing scheme used is shown in Fig. 1. A master clock pulse triggers an ∿1 kHz pulse train from a time-based

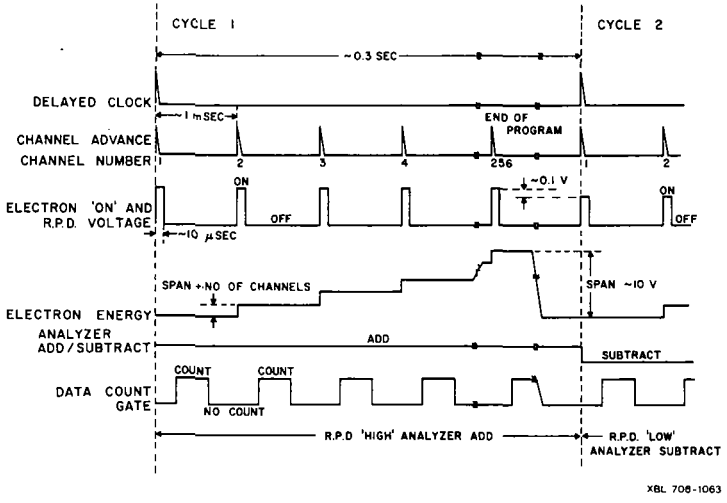

Fig. 1. Pulsing scheme for time-resolved RPD measurements.

*This work was performed under the auspices of the U. S. Atomic Energy Commission.

oscillator. These time-base oscillator pulses are used to trigger the channel advance of a Hewlett-Packard 5400 A multichannel analyzer used in the multiscale mode. An ∿10 μsec pulse, triggered by the time-base oscillator is applied to the RPD grid of a 5-electrode RPD gun. The voltage applied during the pulse is exactly that to allow a truncated electron distribution to pass through the collision chamber. The voltage of the collision chamber is set to give the desired initial electron energy. A data count gate is opened after a preset delay. The width and delay of the count gate is variable. This allows counts to be registered in the multichannel analyzer only during a specified time slot after the electron pulse. After ∿1 msec, a second time-base oscillator pulse advances the channel number and advances the electron energy (derived from the X-output of the multi channel analyzer) by one step. After scanning 256 channels in this fashion, the multichannel analyzer produces an end-of-program pulse which stops the sequence. On receipt of the second clock pulse, the entire sequence is repeated, except that the electron 'on' voltage is lowered by ∿0.1 V, and the analyzer is automatically reset to operate in the subtract mode. This produces an RPD scan of the time-resolved species. Multiple RPD scans are always accumulated in the analyzer.

Figure 2 shows an example of the application of this scheme to N_2. The upper

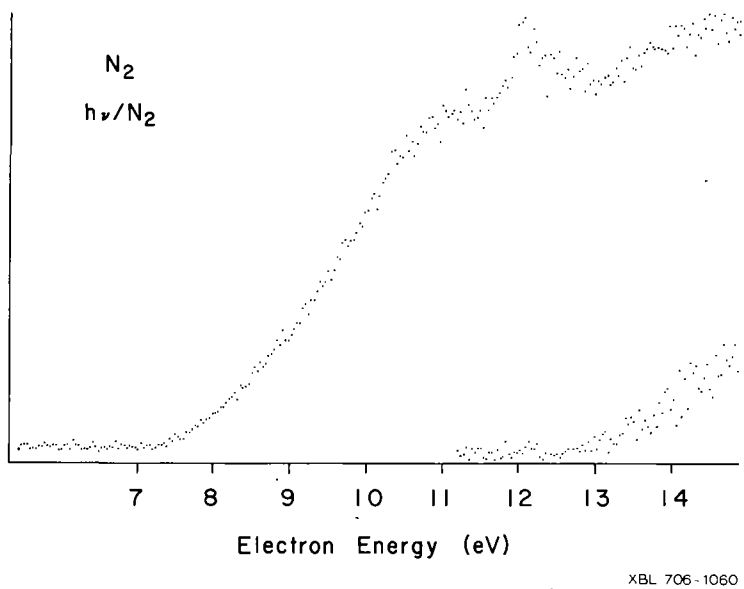

Fig. 2. Excitation efficiency curves for metastables and photons from N_2.

curve in Fig. 2 shows the formation of metastables in N_2. This species has been examined and discussed in detail by, e.g., Olmsted,[3] Lichten,[4] and Freund.[5] In the present study, the $E^3\Sigma_g^+$ state near 12 eV shows up clearly. The lower curve of Fig. 2 shows the photon signal observed in N_2. The appearance potential of the photons coupled with the knowledge

that they are sufficiently energetic to eject an electron from the multiplier strongly suggests that the Birge-Hopfield System is the source of the light.

In the studies of the rare gases Ne, Ar, and Kr, the metastable excitation efficiency curves agree very well with those of Olmsted, Newton, and Street.[1] In all cases, the photon appearance potential was equal, within experimental error, to that of the metastable. In Ar and Kr, a break in the photon curve was observed near the energy of the np^5nd configurations.

A time-of-flight survey of a variety of gases has revealed that there are species with a flight time shorter than that expected for the molecular metastable (but with a flight time longer than the fast photon signal) in O_2 and in CS_2. No excitation efficiency curves for the latter species are available.

References

1. John Olmsted III, Amos S. Newton, and K. Street, Jr., J. Chem. Phys. 42, 2321 (1965).
2. R. Clampitt and Amos S. Newton, J. Chem. Phys. 50, 1997 (1969).
3. J. Olmsted III, Radiation Res. 31, 191 (1967).
4. William Lichten, J. Chem. Phys. 26, 306 (1957).
5. Robert S. Freund, J. Chem. Phys. 50, 3734 (1969).

SOME NEW WAYS OF STUDYING METASTABLE ION DECOMPOSITIONS: ION KINETIC ENERGY SPECTROSCOPY

by R. M. Caprioli, J. H. Beynon, W. E. Baitinger, and J. W. Amy

Department of Chemistry, Purdue University, Lafayette, Indiana

The new technique of ion kinetic energy (IKE) spectroscopy has been used to study metastable ions without interference from the stable ions which make up the normal mass spectrum. By this method, the voltage applied to the electric sector of a double-focusing mass spectrometer is varied at fixed accelerating voltage. A singly-charged ion which undergoes a metastable decomposition in front of the electric sector with ejection of a neutral fragment will share the kinetic energy between the charged and neutral fragments formed in proportion to their masses. If the electric sector voltage is reduced from the normal value at which the main beam of ions having normal accelerating energy is transmitted, the main ion beam will strike the wall of the electric sector, but the low energy ions may be transmitted. If a detector is placed behind the energy resolving slit (the β-slit), a spectrum can be produced of ion abundance vs. kinetic energy and is called an ion kinetic energy spectrum. Use of an electron multiplier behind the β-slit achieves high sensitivity.

There are many advantages to being able to study the product ions of metastable decompositions at high sensitivity. These transitions represent a filtering out of the fragmentation processes occurring with only a small amount of energy in excess of the minimum required for a reaction. Thus, small differences in structure can be studied with greater sensitivity than when only ions formed via fast high energy reactions are studied. Also, because these decompositions represent single steps in a complicated reaction path, knowledge concerning the fragments involved is valuable in determining the structures of unknown chemical species.

Just as the position of a "metastable peak" in a normal mass spectrum can be used to determine the masses m_1 and m_2 of the precursor and daughter ions of the transition, so can the position of a peak in the ion kinetic energy spectrum since it occurs at a fraction F of the sector voltage at which the main ion beam is transmitted. This fraction is equal to the ratio m_2/m_1, usually permitting m_2 and m_1 to be determined uniquely.

The high sensitivity of the IKES technique can be used to make measurements which have not previously been possible in mass spectrometry. For example, the percentage deuteration of isotopically enriched chemical compounds has been determined by this method. Suppose that a metastable decomposition occurs in which a hydrogen atom or a deuterium atom is lost from the molecular ion. The abundance of the "metastable peaks" due to these two transitions is proportional to the amounts of deuterated and undeuterated species present. The proportionality factors can be determined by an isotopic dilution experiment in which measurements are also made on a sample diluted with a known amount of the unlabeled compound. The very high sensitivity of the IKES technique makes such measurements possible in a large number of cases.

The energy spread of the ion beam issuing from the ionization chamber can be very simply determined by scanning the voltage on the electric sector over a small range around its normal value and observing the current on the detector behind the β-slit. It has been found that in the Hitachi RMH-2 mass spectrometer that for a 5KV ion beam, the main ion beam has a width of only 1.5 volts at half-height. The dispersion of the beam at the β-slit is 5 mm for a 1% change in ion energy. As the β-slit is narrowed, higher energy resolution can be obtained. In most metastable transitions involving singly-charged ions there is a release of kinetic energy often of the order 0.1eV. This can result in a spread of kinetic energies in the m_2 ions of around 5eV. The resultant spreading in the width of the peak due to the m_2 in the IKE spectrum often limits the achievable resolution. The energy resolution is improved as the accelerating voltage of the mass spectrometer is made as high as possible. Thus the spread in energies of m_2 ions becomes a smaller fraction of the kinetic energy. This effect will be illustrated in the lecture.

Occasionally very narrow peaks are observed in IKE spectra corresponding to transitions in which very small amounts of kinetic energy are released. Compounds in which very narrow IKE peaks have been seen include pyrazine, pyrimidine, pyridazine.

The voltage across the electric sector can be increased from its normal value and an energy spectrum obtained of ions which have more energy than ions making up the main beam. Peaks in this region can appear in several ways. For example, any doubly-charged ions in the mass spectrum will acquire during acceleration twice the energy acquired by singly-charged ions. However, they will be transmitted through the electric sector at the normal voltage because the force on such ions is doubled by the presence of the two charges. If a collision gas is introduced into the field-free

region preceding the electric sector, the doubly-charged ions can undergo charge-exchange reactions without losing any appreciable kinetic energy. They will then be passed by the electric sector at double the normal voltage irrespective of their mass. Introduction of a collision gas and examination of the ion beam transmitted through the electric sector at double the normal voltage has enabled mass spectra of all doubly-charged ions to be obtained on the final detector of the mass spectrometer without interference from singly-charged ions. In order to do this, the detector located behind the β-slit must be moved laterally so as to allow the ion beam to pass into the magnetic sector. These spectra are important in structure elucidation.

When the collision gas is removed, doubly-charged ions can still undergo unimolecular decomposition in the field-free region preceding the electric sector. Such decompositions are accompanied by the release of a large amount of kinetic energy due to the separation of the charges. If this energy is measured, information can be obtained about intercharge distance in the doubly-charged ion. One of the fragment ions released will carry more than half the energy of the doubly-charged ion. The transition can thus be observed by increasing the electric sector voltage to an appropriate value. The IKE peak can be observed at high sensitivity without interference from the normal peaks in the mass spectrum. Many new transitions have been discovered with these techniques. For example, measurements have been made of intercharge distances in compounds containing 2 heteroatoms and has given information concerning localization of charges on such atoms and also on rearrangements which take place in such compounds before the ions have separated.

Detection of "Fast Metastable" Ions in a Double Focusing Field Ionization Mass Spectrometer

A. L. Burlingame, A. M. Falick, G. W. Wood,
Peter Schultze* and W. J. Richter†

Space Sciences Laboratory
University of California
Berkeley, Calif. 94720

There has recently been a considerable amount of interest in the study of "fast metastables" in field ionization (FI) mass spectrometry. A fast metastable fragment is an ion which results from a decomposition occurring within a field ionization source, but sufficiently long after ionization that its kinetic energy is measurably less than that of the molecular ion. Ion decomposition processes which occur in the range of about 10^{-13} to 10^{-8} sec after ionization may produce fast metastable fragments.

In a single focusing instrument these ions are detected as a shifting and/or tailing of a fragment ion peak toward lower mass. In a double focusing instrument only a portion of the fast metastable peak will be detectable, as is shown in Figure 1. Two possible peak shapes which might be observed in a single focusing instrument are shown. Curve A would result from a more rapid decomposition process than curve B. If we assume that the electrostatic analyzer of a double-focusing spectrometer has an energy bandpass of 2%, i.e. allows only those ions to pass whose energy differs from the desired value by $\pm$1% or less, then the double focusing machine will detect only those ions between the dashed lines. These ions will then be refocused to give a sharp peak at m, the true fragment mass.

It is possible to observe the lower mass (i.e. lower energy) portions of these peaks by means of either of two defocusing techniques.[2,3,4,7] The FI emitter voltage (which also provides the acceleration) may be held constant and the electrostatic sector voltage varied, or the emitter voltage can be varied while the electrostatic sector voltage remains unchanged. The latter method was used to obtain most of the results described below. The most obvious advantage of the method of changing the blade voltage is that the mass scale calibration is unchanged because the kinetic energy of the ions entering the magnetic analyzer is always the same. The method has a possible disadvantage in that the field strength in the ionization region near the emitter does not remain constant, a condition which could conceivably cause changes in the rates of the processes under observation. This effect was probably not significant in the experiments reported here for the following reasons: 1) The blade voltage was changed over a range of 10% at most of the total voltage, usually less. 2) Beckey and Metzinger[5] found that the effective field strength in the emitting region for conditioned emitters was nearly independent of the applied voltage. This is explained by the fact that the total emitting area of the less sharp protrusions on the emitter surface is much greater than that

*Current address: Varian MAT, Bremen, Germany

†Current address: J. R. Geigy A.G., Basel, Switzerland

of the sharper ones. As the applied voltage is increased the bulk of the emission is shifted from the sharper whiskers to the blunter ones, thus continuing to produce a majority of ions under nearly the same field conditions. Of course, as the applied voltage is increased the acceleration of the ions will still be increased proportionately because the foregoing considerations apply only in the region very near the blade surface, and the average field will increase as expected. 3) We have performed several experiments using the method of changing the electrostatic sector voltage and have found essentially the same results as with the complementary method.

Field ionization spectra of a number of compounds, mostly simple esters, have been measured. The most striking feature of these spectra is a very intense peak, often the base peak, which is due to an apparent rearrangement reaction. A typical example is the spectrum of n-butyl acetate which is shown in Figure 2. The base peak at 56 appears to indicate a hydrogen rearrangement in which a hydrogen migrates from the alcohol side to the acid side of the molecule and cleavage occurs at the alcohol O-C bond. Deuterium labelling experiments showed that the hydrogen which is shifted comes from the β-position, to the extent of at least 90%.

Figure 3 shows the effect of changing the emitter voltage on the intensities of several peaks in the n-butyl acetate spectrum. If an appropriate function for the potential distribution in front of the blade is assumed, it is possible to calculate the time elapsed between ionization and fragmentation[1] as a function of the emitter voltage at which a given range of ions is detected. Since the elapsed time vs. voltage relationship is a function of the fragment ion mass, each of the curves in Figure 3 will be based on a somewhat different time scale. For curve D, for example, the peak occurs at 3×10^{-12} sec (7400V) and at 7500 V the delay time is about 1.5×10^{-11} sec. The other curves will have time scales which are not greatly different. The widths of curves G and H correspond to the resolving power of the electric sector, about 1.6%.

The results for the mass 56 ion show that a sizeable fraction of these ions was formed in 10^{-11} to 10^{-12} sec after ionization and at distances of several thousand Å from the emitter surface. It has been suggested[6] that this kind of result can be explained as a rearrangement reaction occurring on the emitter surface, followed by desorption, ionization and then cleavage in the gas phase. However, the results of the labeling experiments show that the initial hydrogen abstraction is highly specific, an unexpected event if the rearrangement were indeed occurring on the surface. There is no apparent reason to expect that the β-hydrogens would be preferentially extracted in a surface process.

In addition, the fact that the rate of formation of m/e=56 ions appears to be significantly slower than the rates for the simple cleavage ions of mass 29 and 43 suggests that the rate-determining step in forming m/e 56 ions may be of a different character than simple cleavage.

The technique described above permits studies of the kinetics of unimolecular decomposition reactions over a wide range of times. The information thus obtained can be a valuable aid in the understanding of the fragmentation mechanisms in FI and may provide further understanding of electron impact fragmentation processes as well.

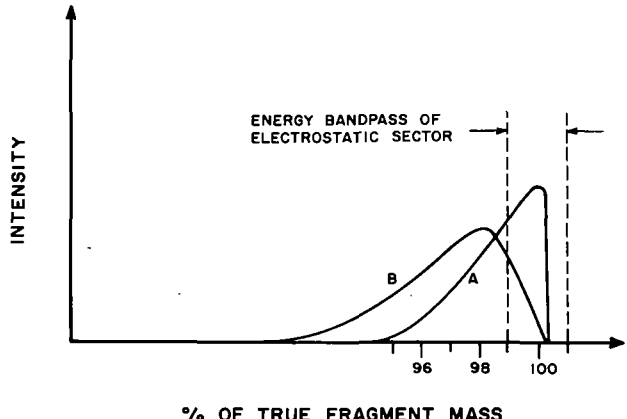

Fig.1. Fraction of fast metastable fragments observable in a double focusing mass spectrometer

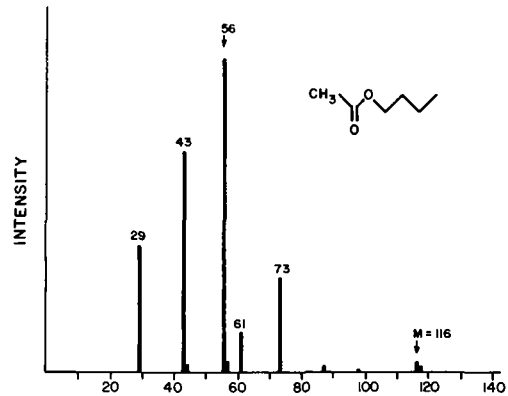

Fig. 2

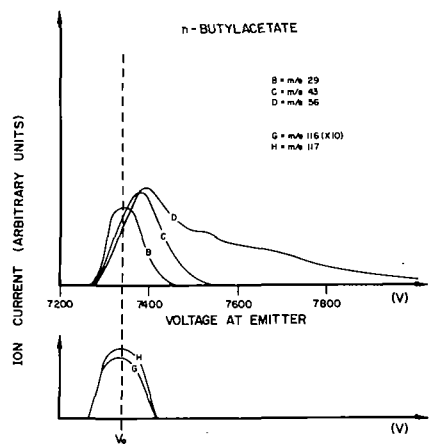

Fig. 3 Ion current as a function of emitter voltage for several peaks in the n-butyl acetate spectrum.

REFERENCES

1. H. D. Beckey, H. Hey, K. Levsen and G. Tenschert, Int. J. Mass Spec. & Ion Phys., 2, 101 (1969).

2. M. Barber and R. M. Elliott, ASTM 4-14 Committee, 12th Annual Conf. on Mass Spectrometry & Allied Topics, Montreal, Canada, May 1964.

3. P. Schultze and A. L. Burlingame, J. Chem. Phys., 49, 4870 (1968).

4. T. W. Schannon, T. E. Mead, C. G. Warner and F. W. McLafferty, Anal. Chem., 39, 1748 (1967).

5. H. G. Metzinger and H. D. Beckey, Z. Phys. Chem. NF, 52, 27 (1967).

6. E. M. Chait and F. G. Kitson, Org. Mass Spec., 3, 533 (1970).

7. K. R. Jennings, Chem. Commun., 1966, 283.

ION KINETIC ENERGY SPECTROSCOPY

E. M. Chait and W. B. Askew
Contribution No. 1722 Central Research Department,
E. I. du Pont de Nemours and Company, Wilmington, Delaware 19898

Preliminary results indicate the value of ion kinetic energy (IKE) spectra in adding a new dimension to structural information obtained by mass spectrometry. These spectra are especially useful in the distinction of some isomer pairs. Energy spectra provide a summary of gaseous ion chemistry occuring as metastable transitions in the first-field free-drift region of the double-focusing (Mattauch-Herzog geometry) mass spectrometer and are produced by scanning the electrostatic sector voltage while recording the ions transmitted by the sector with the beam monitor electrometer.

The technique of defocusing the double-focusing mass spectrometer for the sensitive observation of metastable ions and assignment of metastable transitions is well established[1,2] and has been discussed specifically for mass spectrometers of the Mattauch-Herzog geometry[3,4]. A variation of this technique produces a unique spectrum for the metastable transitions observed for a particular compound. Production of these ion kinetic energy (IKE) spectra was first demonstrated by Beynon[5,6] using double-focusing instruments of the Nier-Johnson geometry. In this report, results obtained using an instrument of the Mattauch-Herzog geometry are summarized.

In defocused metastable experiments described previously, the daughter ions from the precursor decompositions are observed by variation of the magnetic field to focus the mass m_2 or m^* as allowed by the appropriate accelerating or electrostatic sector voltage. If, however, only kinetic energy of the daughter ions is considered, a spectrum may be recorded of the metastable transitions of a particular sample without consideration of the mass.

In many cases it is impossible to distinguish isomer pairs by mass spectroscopy because of similarity of fragmentation patterns. The use of metastable peaks to distinguish hydrocarbon isomers has been demonstrated.[7] Camphor and its isomer, trans-8-methylhydrindan-2-one, give almost identical fragmentation patterns[8]; however, their IKE spectra are radically different (Figure 1) and are unique fingerprints for the respective isomers. For example the 289.70 volt peak in the IKE spectrum of camphor assigned to the loss of ketene from the molecular ion is not present in the IKE spectrum of the isomeric ketone.

In this report IKE spectra have been obtained for the first time using a double-focusing instrument of the Mattauch-Herzog geometry. Previous workers have used instruments of the Nier-Johnson geometry having an intermediate point of β focus. The resolution of IKE spectrs from our instrument could be improved by addition of an adjustable β stop to the mass spectrometer. Sensitivity could be improved 1000-fold by the use of an electron multiplier as a detector for the daughter ion beams.

* In the Mattauch-Herzog spectrometer used (CEC 21-110B) the electrostatic sector voltage is 5% of the ion accelerating voltage.

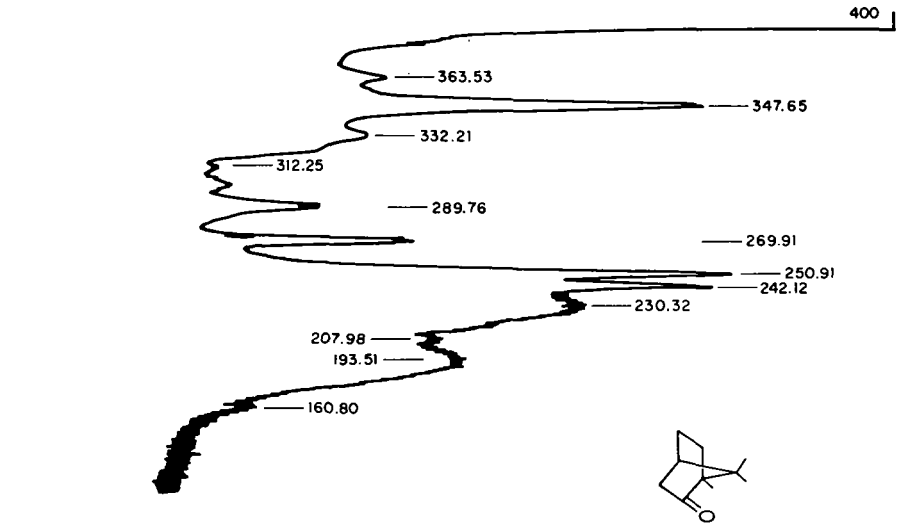
400
363.53
347.65
332.21
312.25
289.76
269.91
250.91
242.12
230.32
207.98
193.51
160.80
O

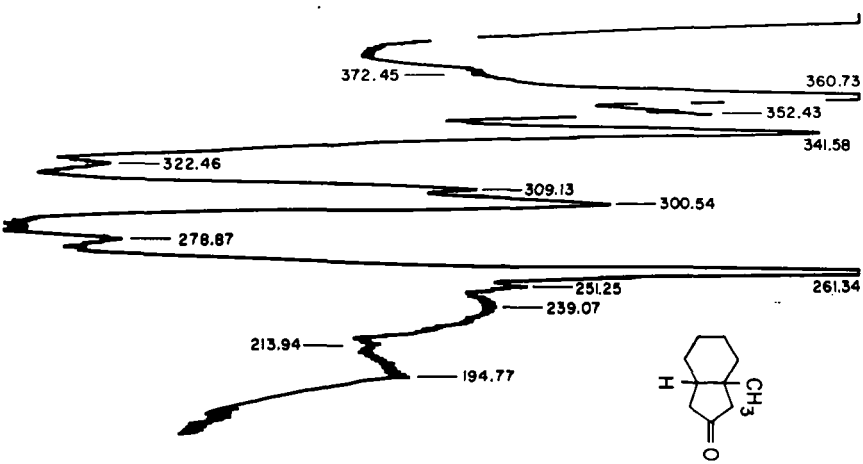
372.45
360.73
352.43
341.58
322.46
309.13
300.54
278.87
261.34
251.25
239.07
213.94
194.77
H
CH3
O

FIG. 1

IKE spectra are useful from a fundamental standpoint in summarizing gaseous ion chemistry of metastable decompositions which can be applied to structural problems. To be used effectively computer processing of the large amounts of data from IKE is necessary and could be used to produce metastable maps.

A most fascinating aspect of IKE spectra is their use in resolving mass spectra ambiguities of isomers and compounds with similar fragmentation patterns. Beynon has applied this to quantitative analysis of deuterated toluences.[9] Since the IKE spectrum in most cases is a unique fingerprint of a compound, it is a useful tool to determine if two compounds with similar mass spectra are isomers. If the IKE spectra are different, the two compounds must have different structures.

IKE spectroscopy is in an early stage of development and few compounds have been investigated. Even so it is easy to envision an IKE spectrometer consisting of an ion source, electrostatic sector, and detector which would find use in organic structure determination and as a potential method for gas chromatographic peak identification.

REFERENCES

1. M. Barber and R. M. Elliot, "Comparison of Metastable Spectra from Single and Double-Focusing Mass Spectrometers", 12th Annual Meeting, ASTM Committee E-14 on Mass Spectrometry, Montreal, Canada, June 7-14, 1964.

2. J. H. Beynon, R. A. Sanders, and A. E. Williams, Nature 204, 67 (1964).

3. T. W. Shannon, F. W. McLafferty and C. R. McKinney, Chem. Commun., 1966, 478.

4. P. Schultze and A. L. Burlingame, J. Chem. Phys. 49, 483 (1968).

5. J. H. Beynon, J. W. Amy, and W. E. Baitinger, Chem. Commun., 1969, 723.

6. A. H. Struck and H. W. Major, "Enhanced Metastable Ion Measurement by Defocused Operation of Double Focusing Mass Spectrometers", 17th Annual Meeting, ASTM Committee E-14 on Mass Spectrometry, Dallas, Texas, May 18-23, 1969.

7. F. W. McLafferty and T. A. Bryce, Chem. Commun., 1967, 1215.

8. H. Budzikiewiz, C. Djerassi, and D. H. Williams, Mass Spectrometry of Organic Compounds, Holden Day, San Francisco, 1967, p. 150.

9. J. H. Beynon, J. E. Corn, W. E. Baitinger, J. W. Amy and R. A. Brewster, Org. Mass Spec., 3, 191 (1970).

GAS CHROMATOGRAPHY - CHEMICAL IONIZATION MASS SPECTROMETRY

G. P. Arsenault and J. J. Dolhun

Department of Chemistry
Massachusetts Institute of Technology
Cambridge, Massachusetts 02139

This paper describes a gas chromatograph-mass spectrometer (GC-MS) combination in which the carrier gas from the gas chromatographic (GC) column is deliberately and completely passed through the ion source of the mass spectrometer (MS) where it is used as the reactant gas for chemical ionization (CI).

Chemical ionization mass spectrometry (CIMS), first described by Munson and Field (1) and since proved useful in organic structure elucidation (2,3), requires the presence in the ion source of about 1 torr of a reactant gas which, by a combination of electron impact ionization (EI) and ion-molecule reactions, gives rise to the reactant ions used for CI. GC effluents are ideally suited as input to CI sources provided the carrier gas and the reactant gas are the same. In that case there is no need for splitters or separators which are customarily used for gas chromatography-electron impact ionization mass spectrometry (GC-EIMS).

The QUAD 300 quadrupole mass spectrometer was selected as the MS component of the gas chromatography-chemical ionization mass spectrometry (GC-CIMS) system because the quadrupole mass filter has two distinct advantages over a magnetic deflection analyzer for CIMS. The first is that it requires much lower ion energy, in the neighborhood of 10V. The second is that it can operate at much higher pressure. These advantages are not absolute in the sense that magnetic deflection instruments can not be used for the same purpose. Indeed the first (1) as well as most of the existing CI sources (4) are being used in magnetic deflection mass spectrometers. Nevertheless the quadrupole mass filter has relative advantages for CIMS which weighed heavily in its favor when the choice of instrument was made.

The trial carrier-reactant gas selected for GC-CIMS was methane because it had already been used extensively for CIMS (1-4). In separate experiments with a GC equipped with a thermal conductivity detector, methane was shown, with mixtures of hydrocarbons and of methyl esters of fatty acids, to give separations and retention times identical for practical purposes to those obtained when helium was used as the carrier gas. This in effect means there is no need to use methane while working out the detailed conditions of the gas chromatographic separation of a mixture. The conditions may be worked out using helium and a flame ionization detector. A shift to methane is then made when the GC and the CIMS are used in combination.

The GC used is a Varian Aerograph Series 1200 equipped with a flame ionization detector and a standard 1/8" injector as well as a capillary injector. When the GC is to be used in combination with the MS, the outlet of the GC column is disconnected from the flame ionization detector and connected to a hollow tube which leads, via an on/off valve, directly into the CI source. None of the conventional detectors is used at the outlet of the column. When the GC-CIMS combination is in use, the CIMS in effect becomes the GC detector. This mode of detection was decided upon because there are a number of potential carrier-reactant gases which could be used interchangeably as the need arises. Independently of the carrier-reactant gas in use, a high sensitivity of detection of the order of one picogram per second was required.

Detection of the GC effluent by the quadrupole mass spectrometer may be divided into three component steps which are the same whether the instrument is used in the EI mode or the CI mode. First, the GC effluent is ionized in the ion source of the mass spectrometer. Second, the total ion beam thus produced is allowed to enter the quadrupole mass filter which is operated with the DC voltage off and the RF voltage set at a pre-selected value. Finally, the partial,

unresolved ion beam which emerges from the quadrupole mass filter is detected by means of the electron multiplier. The electron multiplier signal is conditioned and recorded with a pen and ink recorder. The equivalent of a gas chromatogram, with recorder response as the ordinate and time as the abscissa is thus obtained from the GC-MS combination. There are two advantages to this mode of detection. The first is that it is highly sensitive because the DC voltage is off and the electron multiplier is used. The ion transmission by the quadrupole mass filter operated in the DC off mode approaches 100%. The second is that it is selective since the ions transmitted through the quadrupole mass filter depend on the value at which the RF voltage is set. This is particularly useful with the CI source since the unresolved ion beam which emerges from this source is made up mainly of unreacted reactant ions which would interfere with the detection of the compound ions should they still be present at the detector. Thus, with methane as reactant gas and a source pressure of 1 torr, the principal reactant ions are CH_5^+, $C_2H_5^+$ and $C_3H_5^+$ (5), and their passage through the quadrupole mass filter may be prevented by setting the RF voltage such that the transmission for all ions below m/e 50 is zero.

A scientific communication which includes data obtained with the GC-CIMS system described above operated both as a gas chromatographic detector and as a mass spectrometer has been accepted for publication (6). GC-CIMS shows promise as a useful variation of GC-MS which has so far been confined to EIMS. Since CI sources are de facto EI sources if they are operated at low pressure, the possibility now exists for doing GC-EIMS and GC-CIMS runs on successive injections using the same GC-MS system. Since electron impact and chemical ionization mass spectral data are complementary, a combination of the data obtained using the GC-MS system operated in the EI and CI modes should prove useful in examining complex mixtures such as those encountered in nature.

Acknowledgement: The authors are indebted to J. Burden, R. Supple and B. Evans of Electronic Associates, Inc., for their cooperation in the course of this work, to members of the M.I.T. Mass Spectrometry Laboratory directed by Professor K. Biemann for their enthusiastic support and to the National Institutes of Health for financial support (Division of Research Resources Grant No. RR 00317) and for a traineeship to J.J.D. (Training Grant No. GM 01523).

REFERENCES

1. M.S.B. Munson and F.H. Field, J. Am. Chem. Soc., 88, 2621 (1966).

2. G.P. Arsenault, J.R. Althaus and P.V. Divekar, Chem. Communications, 1414 (1969).

3. H.M. Fales, G.W.A. Milne and M.L. Vestal, J. Am. Chem. Soc., 91, 3682 (1969).

4. See, for example, G.P. Arsenault, Seventeenth Annual Conference on Mass Spectrometry, Dallas, Texas, May 1969, p.372.

5. F.H. Field and M.S.B. Munson, J. Am. Chem. Soc., 87, 3289 (1965).

6. G.P. Arsenault, J.J. Dolhun and K. Biemann, Chem. Communications, In press, (1970).

APPLICATION OF CHEMICAL IONIZATION MASS SPECTROSCOPY TO THE AMINO TERMINAL SEQUENCE OF PROTEINS

William R. Gray
Department of Biology, California Institute of Technology, Pasadena, California 91109
and
Leonard H. Wojcik and Jean H. Futrell
Department of Chemistry, University of Utah, Salt Lake City, Utah 84112

We wish to report the results of our efforts in the field of peptide sequencing by chemical ionization. Wet chemical methods of peptide sequencing involve derivatization, cleavage and chromatographic analysis of the fragments to determine the amino acids present. Such techniques — dansylation (formation of phenylthiohydantoin derivatives), or the more sensitive fluorescent dye technique — suffer from the fact that a rather large amount of sample is required for identification (3 - 5 micrograms/residue). Peptide sequencing has met with some success[1] by high resolution electron impact instruments, but again suffers from the low volatility of the sample, and rather complicated spectra, requiring computer analysis. We wish to report here a combination of chemical and mass spectral treatment that relieves some of these difficulties.

The peptides are n-terminal acetylated with an equimolar mixture of acetic anhydride and perdeutireo acetic anhydride, then cleaved enzymatically and permethylated,[2,3,4] which produces a tagged n-terminal peptide derivative easily separable from the water soluble cofragments. Cleavage before acetylation results in a mixture that can be separated by thin-layer chromatography and analyzed. Peptides containing arginine or sulfur must be pretreated — arginine is hydrolized and acetylated; sulfur-containing residues are treated with raney nickel. Peptides so treated have residues of unique nominal mass with the exception of leucine and isoleucine.

The chemical ionization spectra were run in the instrument described previously[5,6] with the following source conditions: pressure 0.5 Torr, repeller voltage 1.25 volts, anode voltage 0, temperature 200°C.

A teflon probe tip was constructed so that sample temperature can be controlled independent of source temperature. Chemical ionization of the derivatized peptides produces quite clean spectra with about 90% of cleavage at the peptide bonds. Cleavage apparently produces the acylium ions almost exclusively, and thus the doublet showing presence of the n-terminal residue (deuterium label) occurs in nearly all peaks. Thus the integral mass difference between doublets represents the individual residue, and the sequence is defined by the presence of the terminal residue in each successive fragment. The sensitivity of the chemical ionization system allows us to work with considerably smaller samples than other techniques. Usable spectra have been obtained with 0.7 micrograms of the peptide tetra-alanine. A number of peptides have been run, and the results appear promising at this point. The advantages of the combined derivatization/chemical ionization treatment are increased volatility of sample, making it possible to run larger peptides, specific cleavage, sensitivity of the technique, and ability for rapid sample throughout due to lack of residual contamination of the chemical ionization source. A complete report of this work will appear in the Journal of the American Chemical Society.

References

1. F.W. McLafferty, R. Venkataraghavan and P. Irving, Biochem. Biophys. Res. Commun., 39, 274 (1970).
2. S.I. Hakamor, Biochem. J., 55, 20 (1964).
3. D.W. Thomas, B.C. Das, S.D. Gero and E. Lederer, Biochem. Biophys. Res. Commun., 32, 199 (1968).
4. W.R. Gray and E. del Valle Ursino, Biochemistry (in press, 1970).
5. J.H. Futrell and L.H. Wojcik, 17th Annual E-14 A.S.M.S. Meeting, Dallas, Texas, 1969.
6. J.H. Futrell and L.H. Wojcik, Rev. Sci. Instr. (in press, 1970).

ISOTOPE EFFECTS IN THE DECOMPOSITION OF METHANOL BY ELECTRON IMPACT

S.M. Gordon and G.J. Krige

Chemistry Division, Atomic Energy Board, Pelindaba, South Africa

Introduction

We have recently obtained experimental results for the ionization and dissociation of methanol by electron impact[1]. Ionization efficiency curves for the parent ion and several fragments were measured over a wide energy range using the retarding potential difference (RPD) technique. The data were used to construct a breakdown curve for methanol which showed good agreement with that obtained by charge exchange.

In the present investigation, a study of the deuterated molecule CD_3OH has been undertaken. This has enabled us to measure the appearance potentials of those ions which could not be distinguished from one another in CH_3OH. In addition, an H-D isotope effect has been investigated in terms of the quasi-equilibrium theory (QET) of mass spectra[2]. The results suggest that the assumption of a large number of energy level crossings to ensure energy randomization may not be satisfied in the case of methanol.

Experimental

A single-focussing Nuclide 12-inch 90-degree mass spectrometer, equipped with a 5-electrode RPD gun, was employed[3]. Ionization efficiency curves were obtained using a multichannel analyzer in the multiscaling mode to accumulate RPD data automatically[4].

The CD_3OH was obtained from Merck, Sharp and Dohme Ltd. of Canada. It had a stated isotopic purity of 99 atom % D, and was used without further purification.

Results

A reasonable set of primary and secondary reactions for the dissociation of CD_3OH^+ is given in Fig. 1. This scheme is based on that proposed by Friedman et al.[5] and the experimental data of Beynon et al.[6]. Approximate values for the activation energies E_{act} for the primary reactions P1 to P6 and the secondary reactions S1, S2, S4 and S7 were obtained by taking the difference between the measured appearance potentials of the product ions and the ionization potential of CD_3OH^+(10.98 ± 0.07 eV). Other values for E_{act} were estimated from thermochemical considerations.

Typical ionization efficiency curves obtained in the present study are shown in Fig. 2. The electron energy scale was calibrated using krypton. The slope of the parent ion curve for CD_3OH^+, like that for CH_3OH^+, decreases above about 14.5 eV[1]. This indicates some deviation from the ideal threshold law. The curve for $CDOH^+$ has been corrected for the presence of an isotopic impurity.

Lifshitz et al.[7] have also used the RPD technique to measure the appearance potentials of CD_3OH^+, CD_2OH^+ and CDO^+ from CD_3OH^+. Their results are in good agreement with ours.

Second derivatives of all the ionization efficiency curves were used to construct the histogram-like breakdown scheme shown in Fig. 3.

Discussion

According to Fig. 3, the loss of a methyl-D from CD_3OH^+ occurs far more rapidly than the loss of the hydroxyl-H. This observation is supported

by the...../2

		REACTION	E_{act} (eV)
P1	CD_3OH^+	$\longrightarrow$ CD_2O^+H + D	0.06
P2		$\longrightarrow$ CD_3O^+ + H	1.52
P3		$\longrightarrow$ CDO^+H + D_2	1.92
P4		$\longrightarrow$ CD_2O^+ + HD	1.32
P5		$\longrightarrow$ CD_3^+ + OH	3.26
P6		$\longrightarrow$ CD_2^+ + HDO	3.99
S1	CD_2O^+H	$\longrightarrow$ CDO^+ + HD	3.0
S2		$\longrightarrow$ CO^+H + D_2	3.4
S3		$\longrightarrow$ CD_2O^+ + H	5.4
S4	CD_3O^+	$\longrightarrow$ CDO^+ + D_2	3.0
S5		$\longrightarrow$ CD_2O^+ + D	5.4
S6	CDO^+H	$\longrightarrow$ CDO^+ + H	3.4
S7		$\longrightarrow$ CO^+H + D	3.4
S8	CD_2O^+	$\longrightarrow$ CDO^+ + D	2.7

Fig. 1 Reaction mechanism and activation energies for the unimolecular decomposition of CD_3OH^+ ions.

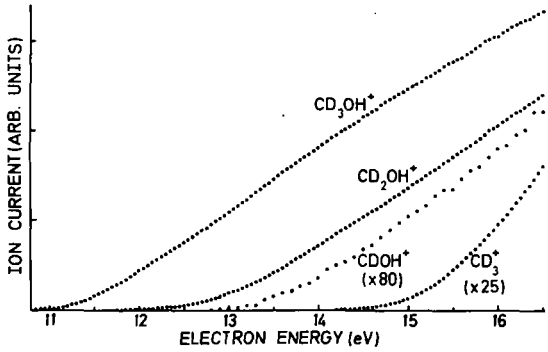

Fig. 2 RPD ionization efficiency curves for ions from CD_3OH.

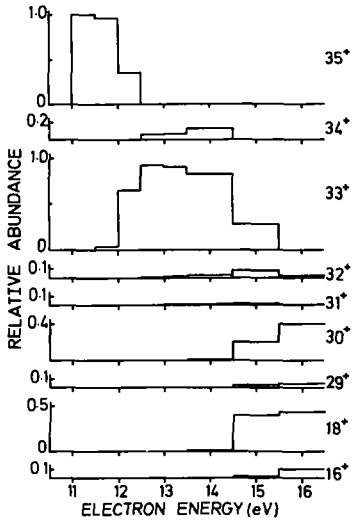

Fig. 3 Experimental breakdown curve for CD_3OH.

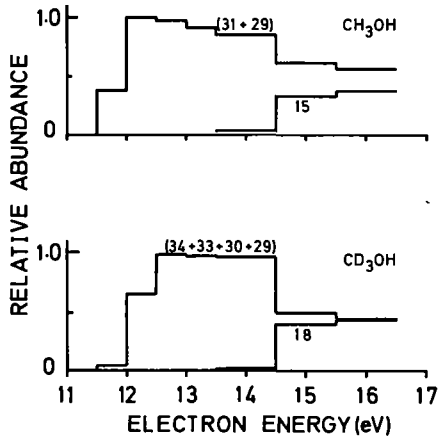

Fig. 4 Composite breakdown curves for masses (31 and 29) and 15 in CH_3OH, and masses (34, 33, 30 and 29) and 18 in CD_3OH.

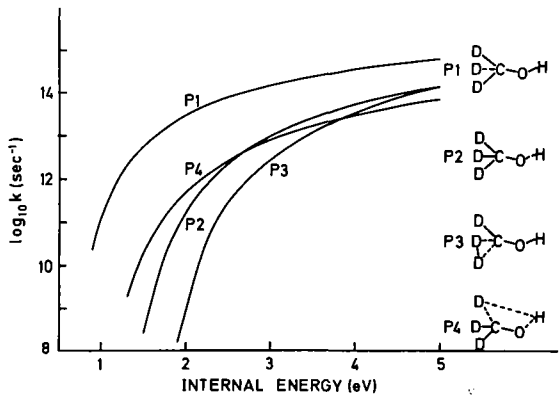

Fig. 5 Schematic activated complex configurations, and the calculated rates as a function of internal energy, for the primary reactions P1 to P4 (cf. Fig. 1)

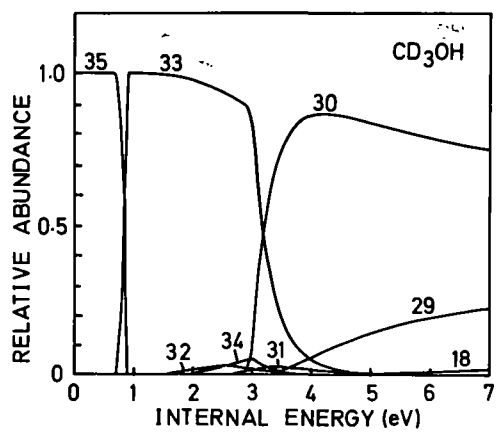

Fig. 6 Calculated breakdown curve for CD_3OH.

by the 70 eV mass spectrum of CD_3OH[6], in which the CD_3O^+/CD_2OH^+ ratio is about 0.03. Consequently, we may reasonably assume that mass 31 in CH_3OH consists of CH_2OH^+ ions.

In terms of the QET, which assumes that fragment ions are formed after energy randomization by competitive unimolecular decompositions from the ground electronic state of the parent ion, reactions in which H is lost are faster than the corresponding reactions in which D is lost[8]. As a result the relative amount of CH_2OH^+ from CH_3OH^+ should be significantly larger than that of CD_2OH^+ from the deuterated molecule, whereas the amount of CD_3^+ from CD_3OH^+ should correspondingly exceed that of CH_3^+ from CH_3OH^+.

Before we can test this prediction in practice, allowance must be made for subsequent dissociations of the CD_2OH^+ and CD_3O^+ ions. This was done as follows: (1) According to the reaction scheme (Fig.1), CD_2OH^+ yields CDO^+, COH^+ and CD_2O^+ by reactions S1, S2 and S3, respectively. On the basis of the activation energies and the assumptions of the QET, CD_2OH^+ mainly forms CDO^+ and COH^+. Similarly, CD_3O^+ mainly forms CDO^+ by reaction S4. (2) Since reaction S6 yields very little COH^+ (Fig.3), it follows in the same way that reaction S7 forms a negligible amount of CDO^+. (3) The shapes of the breakdown curves for masses 32 and 30 suggest that reaction S8 forms very little CDO^+ in this region.

In view of the above considerations, we may assume that CDO^+ and COH^+ are formed exclusively by reactions S1, S2 and S4. Consequently, we have added our breakdown curves in Fig.3 for CD_3O^+ and CD_2OH^+ (analogous to mass 31 in CH_3OH), and CDO^+ and COH^+ (analogous to mass 29 in CH_3OH) to give the composite curves for CD_3OH^+ and CH_3OH^+ in Fig.4.

Fig.4 shows that the total relative abundance of CH_2OH^+ from CH_3OH^+ is roughly the same as that of CD_2OH^+ from CD_3OH^+. Similarly, the abundances of CH_3^+ and CD_3^+ are approximately equal. This result is at variance with the prediction made earlier on the basis of the QET.

To place these results on a sounder footing we have used the QET to calculate a breakdown pattern for CD_3OH^+. The assumed reaction scheme (Fig.1) is more comprehensive than those previously employed[5,9] because consecutive competing reactions have been included. Rate constants for the various decomposition processes in this scheme have been calculated from the equations developed by Haarhoff[10] for the accurate enumeration of the density of states. Activated complex configurations for each primary reaction were chosen by changing the frequencies of the parent molecule ion (assumed identical to those of the neutral molecule[11]) so as to reflect the loose, semi-rigid or rigid character of the complex[12]. Schematic diagrams of the configurations used for reactions P1 to P4, and the corresponding rates as a function of internal energy are given in Fig.5. Thus, it may be seen for example that although reactions P2 and P3 have higher activation energies than reaction P4, their rates overtake that of reaction P4 since they proceed via looser complexes, and they become dominant at higher energies.

The relative intensities of all the ions given in Fig.1, 10^{-6} seconds after ionization, are shown in Fig.6 as a function of the internal energy

...../3

of the molecular ion. This result agrees essentially with that given by Davis and Long[9] for CH_3OH^+, whose calculations were based on the simpler reaction scheme originally proposed by Friedman et al.[5]. On the whole, qualitative features are reproduced quite accurately by the calculated curves but two striking differences between the theoretical and experimental intensities should be noted[9].

In the first place, despite the choice of an extremely loose complex for the formation of CD_3^+ by reaction P5, the theoretical curve is about two orders of magnitude smaller than the experimental curve. This result provides additional evidence that CD_3^+ is not formed by a competitive unimolecular process from the ground state of the CD_3OH^+ ion. In a molecule of this size, it may well be that the number of energy level crossings is insufficient to ensure complete energy randomization.

The second noteworthy point concerns the secondary decomposition of CD_2OH^+ to form CDO^+. According to the theoretical calculations, the abundance of mass 30 rises very rapidly between 3 and 4 eV of internal energy and is one to two orders of magnitude larger than the observed abundance. At higher values the discrepancy reduces to about a factor of two. Since CD_2OH^+ is formed along with a neutral D atom from the parent with no excess energy, all of the excess internal energy in the system is available to CD_2OH^+ for further decomposition. Thus, within the framework of the QET the curve for mass 33 should rapidly decrease to zero at the onset for mass 30. The fact that our experimental curves do not exhibit this behaviour again suggests that the randomization of energy in the CD_2OH^+ ion is incomplete.

We wish to thank Dr. D.M. Kemp and Dr. P.C. Haarhoff for their interest and advice, and Miss J.F. Brown for technical assistance.

References

1. G.J. Krige and S.M. Gordon, Paper presented at the International Conference on Mass Spectroscopy, Kyoto, Japan, 8-12 September, 1969.
2. H.M. Rosenstock and M. Krauss, "Mass Spectrometry of Organic Ions", edited by F.W. McLafferty, Academic Press, London, 1963, p. 1.
3. S.M. Gordon, G.J. Krige and P.C. Haarhoff, Intern. J. Mass Spectry. Ion Physics, 3, 13, 1969.
4. P.J. Chantry, Rev. Sci. Instrum., 40, 884, 1969.
5. L. Friedman, F.A. Long and M. Wolfsberg, J. Chem. Phys., 27, 613, 1957.
6. J.H. Beynon, A.E. Fontaine and G.R. Lester, Intern. J. Mass Spectry. Ion Physics, 1, 1, 1968.
7. C. Lifshitz, M. Shapiro and R. Sternberg, Israel J. Chem., 7, 391, 1969.
8. P.C. Haarhoff, Mol. Phys., 8, 49, 1964.
9. G.G. Davis and F.A. Long, unpublished work.
10. P.C. Haarhoff, Mol. Phys., 7, 101, 1963.
11. M. Falk and E. Whalley, J. Chem. Phys., 34, 1554, 1961.
12. M. Vestal, "Fundamental Processes in Radiation Chemistry", edited by P. Ausloos, Interscience, New York, 1968, Chapter 2.

ON THE IMPROVEMENT OF APPEARANCE POTENTIAL MEASUREMENTS BY NUMERICAL ANALYSIS[1]

by

B. G. Giessner[2] and G. G. Meisels
Chemical Physics Program
Department of Chemistry
University of Houston
Houston, Texas 77004

ABSTRACT

The deconvolution of hypothetical and experimental ionization efficiency curves by the energy distribution difference (EDD) technique and by Fourier Transforms was examined. The EDD method was found to be capable of removing the contribution from the high energy tail of the electron energy distribution, but did not lead to appreciable improvement in the resolution of fine structure for conventional electron guns which also suffer from energy broadening factors other than filament temperature.

The Fourier Transform approach was found to be relatively insensitive to the details of the electron energy distribution, but highly dependent on noise. A simple smoothing procedure based on a three-point least squares polynomial was found to make possible the recovery of fine structure. Deconvolution of the experimental Xenon ionization efficiency curve could be achieved with a nominal width at half height of the quasi-electron energy distribution of ca. 0.17 eV as judged from the width of the line corresponding to the 6d autoionizing level.

INTRODUCTION

Ionization efficiency curves determined experimentally by the use of conventional electron guns lend themselves to the extraction of ionization and appearance potentials only with difficulty because of the super position of the broad electron energy distribution, typically with a width at half height of about 1 eV, on the ionization cross section function[3]. Precise knowledge of ionization and appearance potentials can be achieved experimentally by employing photoionization[4,5] or energy selected electrons[6]. The adaptations of these methods to conventional mass spectrometers requires considerable expertise and is sometimes forbidding when the instrument must serve a multiplicity of purposes. It is therefore desirable to remove some of the electron energy spread by electronic or numerical-mathematical analysis of ionization efficiency data when modified commercial instruments are employed for appearance potential determinations.

We have recently described a method by which the first and second differential ionization efficiencies of molecules can be measured easily.[7] At the same time, electron energy distributions were measured and shown to have a width at half height of approximately 0.6 eV[8]. Both determinations were made without mechanical modifications or entry into the ion source regions. While these techniques permitted the unique assessment of appearance potentials, the broad energy distribution made onset and structure in the ionization efficiency difficult to assess. We have therefore examined analytical methods to affect better energy resolution.

Two methods have been proposed to achieve the removal of the electron energy distribution from the observed ionization efficiency curve. Historically, the first is that of Morrison[9] who used a Fourier Transform method and estimated electron energy distributions. The second, proposed by Winters, Collins and Courchene[10], is based on an analysis of energy distribution of the ionizing electron beam, which is assumed to be of the simple quasi-Maxwell-Boltzman type[11]. This method is similar to an interpretation by Marmet[12] of the retarding potential difference (RPD) method of Fox et. al.[13].

The first method has been employed only sparingly in the past[14], even though it achieved a considerable improvement in a nominal resolution, about comparable to velocity selected electrons[5]. The second method has been used more frequently, but has led to discrepancies in the assignment of transition probabilities of acetylene[15] and to ionization efficiency curves not in agreement with known spectroscopic levels[16].

It appears at this time that the Fourier Transform method, which is clearly superior in principle, has not found wide acceptance while the simpler Energy Distribution Difference (EDD) method[10] is suspect because of possible oversimplication. We have therefore compared these deconvolution techniques using two approaches. The first consisted of the synthesis of simulated ionization efficiency curves from an assumed cross section function and assumed electron energy distributions both of which were of the types one might find experimentally. This was followed by deconvoluting the first derivative of these curves by both techniques. At the same time, noise and the effects of deconvolution by distribution functions of incorrect shape or width were assessed. The second approach applied the two techniques to the experimental derivative ionization

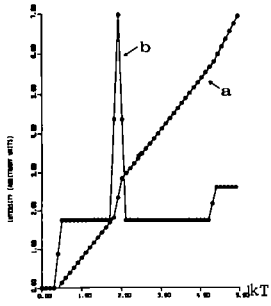

(1) assumed ionization efficiency curve (a) and its first derivative (b)

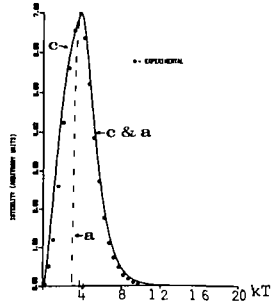

(2) electron energy distrib'ns. (a) quasi-Boltzman, (b) (points) experimental, (c)&(a) 4 kT potential drop

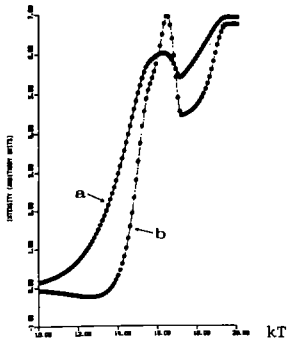

(3) derivative curves from (a) folding 1b and 2a, (b) after EDD on 3a

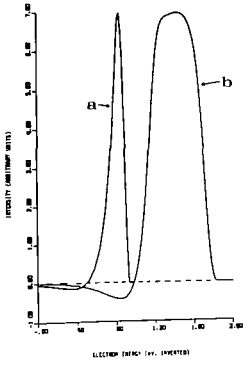

(4) Pseudo-electron energy distrib'ns from application of EDD to (a) curve 2a and (b) curve 2c

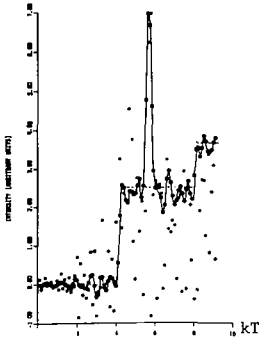

(5) Effect of noise on FT deconvolution. • input data smoothing only; connected points, special smoothing (see text)

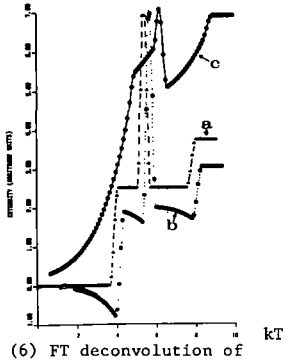

(6) FT deconvolution of curve 3a by (a) correct distribution (b) 20% too wide & (c) 40% too narrow. Curves offset for clarity.

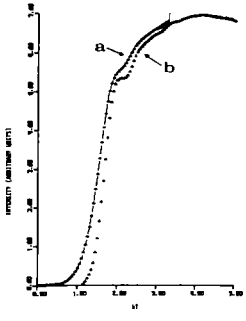

(7) First differential ionization efficiencies of xenon: (a) experimental (b) after application of EDD method

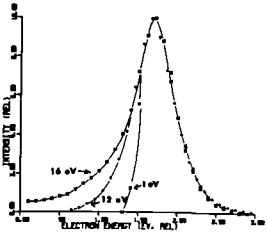

(8) Experimental electron energy distributions

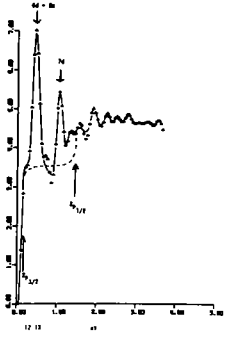

(9) Deconvoluted experimental differential ionization efficiency curve of xenon using 13eV electron energy distribution

efficiency curve of Xenon. The first derivative was chosen because it displays structure more clearly.

EXPERIMENTAL

The first differential ionization efficiency curve of Xenon was determined directly using modulation of the electron energy at 20 Hz with an amplitude of 70 millivolts, and synchronous detection of the ion current as described elsewhere[7]. The electron energy distribution was measured similarly by modulation of the electron energy and synchronous detection of the trap current, using a retarding potential between electron collector and ionization chamber[8].

RESULTS

1. Hypothetical Case.

a. Idealized ionization efficiency curve. The assumed ionization efficiency curve and its derivative are shown in Figure 1. The energy scale is expressed in units of kT because this unit automatically allows an assessment of energy resolution as a function of filament temperature. The idealized curve has a linear threshold (representative of direct ionization) followed by a step (autoionization) at 1.5 kT above[9] a second linear portion begins 4.0 kT above threshold, with a slope of 1.5 that of the preceding linear section. The first derivative of this function was obtained by a numerical method which calculates the derivative of x_i of the Lagrangian interpolation polynomial of degree 2 relative to the three successive points i-1, i, and i+1. It shows two steps of relative heights 1.0 and 0.5, and a delta function centered at 1.5 kT units above the first step. At a typical filament temperature of 1730°K, one kT unit corresponds to ca. 0.15 eV, so that the spacing for such conditions would be 0.22 eV between onset and the step function, and 0.60 eV between onset and the second linear portion. The differentiation procedure introduces a slight amount of smoothing and therefore broadening, increasing width at half height from 0.1 kT to 0.2 kT units.

b. Electron energy distribution. The EDD approach is based on a mathematical analysis of the quasi-Boltzman distribution of the form E exp(-E/kT) (Figure 2). However, this function is a poor approximation of the experimentally measured distribution (points of Figure 2), largely as a result of potential drop across the filament[17]. It is readily possible to improve the approximation by allowing for this effect. An acceptable fit is obtained when broadening is taken to be the result of a uniform 4 kT potential drop (Figure 2, Curve b). Both distributions were used in the calculations.

The hypothetical ionization efficiency curve and the electron energy distribution were folded into each other by a point-to-point numerical multiplication and summation technique at 0.1 kT intervals. The first differential of this curve was again taken numerically as above.

c. Deconvolution by the Energy Distribution Difference (EDD) method. The EDD method employs a simple subtraction of a fraction b of the ion current observed at an electron energy higher by a constant increment than that at which subtraction occurs. For a synthetic curve using the pure quasi-Boltzman distribution, 0.67 kT (ca. 0.1 eV at 1730°) was used as the constant increment while the factor b was varied until the optimum fine structure was obtained. As predicted by the simple analysis of Winters, Collins, and Courchene[10], the value of b best suitable for this purpose was found to be 0.67 and the resultant curve is shown in Figure 3, curve b. The existence of the delta function in the first derivative at 1.5 kT above threshold is discernible, but it is not completely resolved from the first step function. The second step function is clearly visible. The delta function can be resolved entirely when the energy spacings between the processes are increased, and shows a width of kT at half height.

The capability of the method can be assessed more directly by using it to deconvolute the electron energy distribution itself, that is, by calculating the quasi-distribution which is achieved by this technique[15]. This approach also yields a pseudo-distribution of width kT at half height, and with essentially no high energy tail (Figure 4.). However, when the EDD method is applied to a broadened electron energy distribution (curve c, Figure 2) which represents our experimental distribution more realistically, a pseudo-distribution results (Figure 4) which is improved only by ca. 10%, but has its high energy tail removed. Application of the EDD method to an experimental ionization efficiency curve will therefore usually reduce the tailing of the ionization efficiency curve and make the initial break more easily visible, but will not permit an assessment of fine structure in the curve. Since the EDD method appears incapable of producing a major improvement in energy resolution under most circumstances, the effect of incorporating noise on the hypothetical function was not investigated.

d. Deconvolution by Fourier Transform (FT) methods. The use of Fourier Transform for the removal of instrument functions was explored by Stokes[18], and its applicability to the deconvolution of ionization efficiency curves has been demonstrated by Morrison[14]. It was also employed by Moore[14]. It is based on the representation of the ionization efficiency curve and the electron energy distribution by transforms whose meaningful

numbers of real and imaginary terms are equal to those available in the original functions. The descriptions are exact when the numerical methods are handled properly, and the inverse transforms recover the original curves without error. When FT methodology[19] is employed for deconvolution, small numerical errors are introduced by the division of two small numbers, as pointed out by Morrison[9]; this is a serious complication only for the higher terms of the expansion, and following Morrison's suggestion we have compared the normalized moduli and reduced the values for the first derivative ionization efficiency function to those of the instrument function where the former was greater. When the inverse transform corresponding to the deconvoluted curve is obtained, the result is considered to be in error when the imaginary part exceeds 10^{-9} of the real one; this condition was always fulfilled in our calculations. When the correct functions are employed for deconvolution, the original hypothetical ionization efficiency curve is recovered exactly and without artifacts, and is indistinguishable from Figure 1b. It is immaterial whether the quasi-Boltzman distribution on the broadened quasi-experimental function is employed.

The addition of rectangular, random noise of 0.5% peak to peak intensity to the hypothetical first derivative ionization efficiency curve made the deconvoluted results extremely noisy (Figure 5, open circles). However, integration produced an ionization efficiency curve in which the structure was considerably sharpened over the original.

A vast improvement in the appearance of the deconvoluted derivative curve could be obtained by the following technique. The noise first derivative curve convoluted with the instrument function is smoothed by evaluating y_i at x_i as the least squares polynomial of degree one relevant to the three successive points, i-1, i, and i+1. The smoothed curve is deconvoluted, the result is integrated and smoothed again by the same method. The differential of this function is also shown in Figure 5 (filled circles) and it is clear that the original structure is well recovered and the noise reduced to a level no longer forbidding the use of the first derivative. This smoothing procedure introduces some broadening and therefore loss of resolution as demonstrated by its application to a noiseless function (Figure 6, curve a), which increases the width at half height of the delta function from 0.2 to somewhat more than 0.3 kT. This unremovable broadening, which corresponds to ca. 0.05 eV under typical operating conditions, can be reduced by a high point density but is only a small sacrifice for the improvement.

When deconvolution of curve a in Figure 3 is attempted by a quasi-Maxwellian distribution arbitrarily cut off by linear extrapolation of the steeply descending high energy portion, only minor oscillation about the horizontal portions, not exceeding 10% of their values, are observed. When noise is also added the truncation of the higher energy terms becomes totally lost and the result is indistinguishable from curve b of Figure 5. When a distribution of correct shape (i.e. quasi-Boltzman) but with excessive width is employed, the location of the delta function is not affected (Figure 6, curve b) but the steps of the first derivative ionization efficiency curve show appreciable negative curvature. When a quasi-Boltzman distribution of reduced width at half height (corresponding to a lower temperature) is employed, significant upward curvature of the sections which should be horizontal results. However, even an underestimate of the width by 60% does not obscure structure and still permits the assessment of thresholds.

The combined effects of incorrect function shape and noise were also investigated. The scatter resulting from the noise substantially obscures the effect of using the incorrect function even when the width of the latter is underestimated by as much as 25%.

2. Deconvolution of the Experimental Xenon Curve.

a. By the EDD method. The experimental first differential ionization efficiency curve of Xenon (Figure 8) shows sharpening of a step-function when the EDD technique is applied. In the integral form (ionization efficiency curve), this would correspond to a "break" at ca. 0.6 eV above threshold. In view of the multiplicity of autoionizing states between onsets of the $^2P_{3/2}$ and $^2P_{1/2}$ states of Xenon[21] such a simplicity of behavior is suspect of being an artifact. Experimental evaluations using velocity selected electrons do not show such behavior, but indicate the presence of autoionization at energies approximately corresponding to known states[22]. This observation confirms the earlier comment that, for a real electron energy distribution, the EDD method serves primarily to reduce the high energy tail of the quasi-distribution.

b. By the Fourier Transform method. One difficulty in the application of the FT method is the choice of the instrument function. Whereas the method is not particularly sensitive to the form of the electron energy distribution, the improvement in resolution deteriorates substantially when incorrect instrument functions are employed. This is a rather critical factor for Xenon since the energy separation of the onset of direct ionization and the first autoionizing state is small, and the higher autoionizing states become denser and eventually converge on the onset of the $^2P_{1/2}$ state. Previous investigators have used either an assumed function[9], or taken the axis-reversed second differential ionization efficiency of helium to be representative of the electron energy distribution[9,14]. Unfortunately, the electron energy distribution in most conventional instruments is dependent on the nominal electron energy[8]. We have therefore made experimental measurements of the distribution at several electron energies (typical examples are shown

in Figure 8), and used those at nominal energies of 12,13, and 14 eV for deconvolution.

Considerable structure in the first derivative curve is apparent no matter which distribution function is employed, and the delta functions at approximately 0.3V and 0.7V above the steepest portion of the initial rise are easily recognizable. The result of a deconvolution using the 13 eV distribution is shown in Figure 9. The positions of some of the known states are drawn in for comparison. The first peak ascribable to the 6d autoionizing state is resolved from the intital stepfunction increase only by a small and almost indiscernible shoulder. It is not present when the deconvolution employs the other electron energy distributions, which also do not lead to the essentially horizontal portion at the highest energies. The effective width at half height of the quasi-distribution achievable by FT analysis can be assessed from the shape of the line coinciding with the spacing of the 6d autoionizing level, and is approximately 0.17 eV. This resolution is about equivalent to that obtainable by the RPD method and that of the EDD method when temperature is the only factor causing electron energy broadening. The Fourier Transform deconvolution is considerably superior and less equivocal than the EDD approach for conventional instruments where the simple quasi-Boltzman distribution does not suffice to describe the instrument function.

ACKNOWLEDGMENTS

The authors are greatly indebted to Prof. J. D. Morrison for his invaluable assistance and encouragement, and his guidance in the recreation of his computer program. A number of enlightening discussions with Dr. F. P. Lossing and his transmittal of unpublished data were most helpful. We are sincerely grateful to the Robert A. Welch foundation for partial support of this research. The computer facilities employed were those of the Common Research Computer Facility, Texas Medical Center, which is supported in part by U.S.P.H.S. grant No. FR-00254.

LITERATURE CITED

1. From the dissertation of B. G. Giessner, submitted to the Graduate School of the University of Houston (1970)
2. Present address: Department of Chemistry, Cornell University, Ithaca, New York
3. J.D. Morrison, J. Chem. Phys. 21, 1767 (1953)
4. W.A. Chupka and J. Berkowitz, J. Chem. Phys. 47, 2921 (1967)
5. R. Botter, V.H. Dibeler, J.A. Walker and H.M. Rosenstock, J. Chem. Phys. 44, 1271 (1966)
6. F.P. Lossing and G.P. Semeluk, Int. J. Mass Spectrom. Ion Phys. 2, 408 (1969)
7. G.G. Meisels, J.Y. Park and B.G. Giessner, J. Am. Chem. Soc. 92, 254 (1970)
8. B.G. Giessner and G.G. Meisels, Int. J. Mass Spectrom. Ion Phys. 4, 84 (1970)
9. J.D. Morrison, J. Chem. Phys. 39, 200 (1963)
10. R.E. Winters, J.H. Collins and W.L. Courchene. J. Chem. Phys. 45, 1931 (1966)
11. R.E. Honig, J. Chem. Phys. 16, 105 (1948)
12. P. Marmet, Can. J. Phys. 42, 2102 (1964)
13. R.E. Fox, W.M. Hickman, T. Kjeldaas and D.J. Grove, Rev. Sci. Instr. 26, 1101 (1955)
14. L. Moore, Brit. J. Appl. Phys. Ser. 2, 1, 237 (1968)
15. J.H. Collins, R.E. Winters and G.G. Engerholm, J. Chem. Phys. 49, 2469 (1968)
16. I.P. Fisher and E. Henderson, Trans Faraday Soc. 63, 1342 (1967)
17. W.A. Chupka and M. Kaminsky, J. Chem. Phys. 35, 1991 (1961)
18. A.R. Stokes, Proc. Phys. Soc. 61, 382 (1948)
19. IBM SHARE library routine
20. The original program written with the aid of Prof. Morrison required 300 seconds of execution time to deconvolute 240 points by 110 points. Its use was discontinued because the revised program based on ref. 19 required only 5 seconds for deconvolution of 256 points by 256. Main program and necessary subroutines are available from the authors, or in the dissertation.
21. R.E. Huffman, Y. Tanaka and J.C. Larrabee, J. Chem. Phys. 39, 902 (1963)
22. F.P. Lossing, private communication

"Threshold Electron Impact Excitation of CO, Ar, Kr and Xe"

C.E. Brion and L.A.R. Olsen

Department of Chemistry,

University of British Columbia,

Vancouver 8, B.C., Canada.

The work described in this paper has now been published (1,2,3).

(1) C.E. Brion and L.A.R. Olsen, Phys. Rev. 187, 111 (1969).

(2) C.E. Brion and L.A.R. Olsen, J. Chem. Phys. 52, 2163 (1970).

(3) C.E. Brion and L.A.R. Olsen, in press, J. Physics (B), (Proc. Phys. Soc.) (1970).

ELECTRON ATTACHMENT TO MOLECULES

F. C. Fehsenfeld and D. B. Dunkin
Environmental Science Services Administration
Aeronomy Laboratory
Boulder, Colorado 80302

The flowing afterglow technique is being used to study the attachment of low energy electrons to a variety of molecules. The present research is concerned with effective electron scavengers, molecules which rapidly attach electrons in a quasi-binary fashion to form negative ions which are stable against detachment. Apart from the practical aspects, this research provides new information concerning low energy electron interactions with various molecular structures. The experimental arrangement used to study these processes will be described and several attachment rates including that of electrons to SF_6, C_4F_8, CF_3I, C_2F_5Cl, NO_2, and O_3 will be reported. Also the temperature dependence of these rates, the temperature dependence of the attachment channels and the pressure dependence of the reactions will be discussed. For example it is found that electrons attach to SF_6 with a rate constant of 2.2×10^{-7} cm^3/sec. This rate is independent of pressure and temperature in the range studied. At 273° the principal negative ion is SF_6^- with the relative concentration of SF_5^- less than one part in 10^4 while at $473^\circ K$ the SF_5^- signal has increased to four parts in one hundred of the SF_6^- signal.

THERMODYNAMICS OF NEGATIVE IONS USING A FLAME ION SOURCE*

Rudolf R. Burke, David E. Jensen and William J. Miller

AeroChem Research Laboratories, Inc.
Sybron Corporation
Princeton, New Jersey

This paper summarizes the results of a series of negative ion studies which have led to the determination of the electron affinities of a number of metallic oxides and hydroxides stable at high temperatures. Specifically, the negative ions formed upon the addition to K-seeded $H_2/O_2/N_2$ flames, of boron,[1,2] molybdenum,[3] tungsten,[4,5] chromium and vanadium compounds have been examined and equilibrium constants derived in those cases for which the necessary supplementary thermodynamics of neutral species are available. This information is not presently available for chromium and vanadium; therefore, the complete interpretation of the data obtained for these additives is impossible.

The flames employed in this study are fuel rich $H_2/O_2/N_2$ flames having temperatures between 1815 and 2475 K. These flames have been extensively studied over a period of years and are now very well characterized. The burner is shown in Fig. 1. It provides for an annular shield flame surrounding the inner test flame. Both parts of the flame are fed the same fuel gas mixture, producing a well-defined, high temperature, isothermal test stream with no cool boundaries. Ionization in these flames is provided by the addition of alkali metal salts from an atomizer. This apparatus can also be used to supply the metals being studied in the form of water soluble salts; more commonly, however, the metallic additives are introduced into the unburned gas stream as volatile fluorides or carbonyls.

Electron concentrations are measured via a microwave resonant cavity technique; the cavity surrounds the flame as indicated in Fig. 1. Details of this technique are given in Ref. 6. Other experimental procedures include mass spectrometry for ion identification and relative ion concentration determination, electrostatic probes for absolute ion concentration determinations,[1] and optical spectroscopic methods (both absorption and emission) for measurements of neutral metal atom concentrations.

The mass spectrometric apparatus is shown in Fig. 2. Ions are sampled through a 0.05 mm diameter hole in the tip of a stainless steel cone mounted on a water-cooled plate. When sampling metal-containing flames, it is necessary to allow the tip of the sampling cone to become hot enough to preclude condensation of refractory oxides. The cones were therefore made of stainless steel (a poor conductor) and angles chosen such that a compromise was achieved between the smallest possible outside angle (to minimize flame disturbance) and the largest possible inside angle (to maximize pumping) consistent with the heating requirements described above. Typical successfully employed cones had internal and external cone half-angles of 42° and 47°, respectively.

In order to illustrate the experimental techniques and data interpretation, the negative ion results obtained for molybdenum additives are here summarized; a full account of this work is given in Ref. 3. Typical effects of addition of molybdenum to flames containing potassium are illustrated in Fig. 3. Clearly both electron attachment and potassium-molybdenum compound formation are occurring. Plots of $[n_-]$ vs. $[Mo]_c$ ($[n_-] \equiv$ total negative ion concentration, $[Mo]_c \equiv$ total molybdenum in all forms in the flame) are straight lines of gradient 1.0, as are similar plots of individual negative ions. Two groups of negative ions were observed at masses 140-148 and 157-165 and were identified as MoO_3^- and $HMoO_4^-$, respectively. The hydrogen content of the ions was further confirmed by substituting D_2 for H_2 as fuel.

From available neutral species thermochemistry[7] it was computed that the dominant Mo-containing species is H_2MoO_4. It is therefore reasonable to conclude that

* Work sponsored by the Office of Naval Research under Contract Nonr 3809(00).

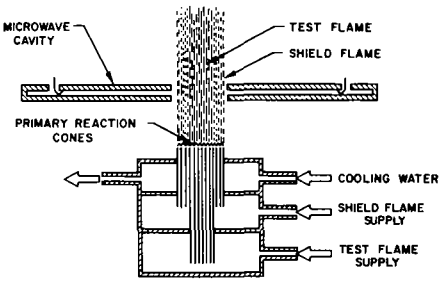

FIG. 1 BURNER AND MICROWAVE CAVITY

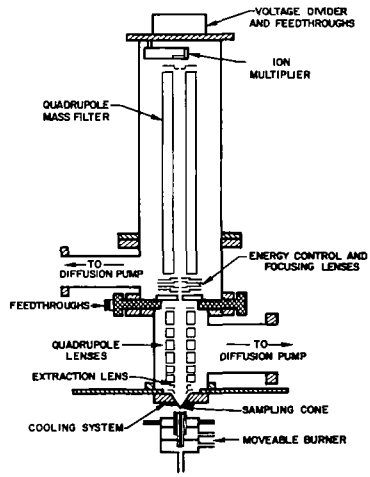

FIG. 2 FLAME ION MASS SPECTROMETER

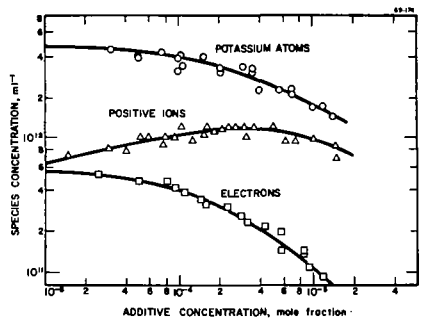

FIG. 3 EFFECTS OF Mo-CONTAINING ADDITIVES IN A K-SEEDED $H_2/O_2/N_2$ FLAME AT 2250 K.

attachment takes place via

$$e^- + H_2MoO_4 \rightleftarrows HMoO_4^- + H \quad (1)$$

followed by

$$HMoO_4^- + H \rightleftarrows MoO_3^- + H_2O \quad (2)$$

Whether or not these are the dominant elementary reactions, there is sufficient data to demonstrate that these reactions are equilibrated. From the measured ratios of ion concentrations and known flame gas compositions one may calculate equilibrium constants (K_i) for reactions (1) and (2). These in turn, combined with thermochemical data for the neutral molybdenum species permit calculation of the electron affinities for the ions observed. These calculations are performed using both 2nd and 3rd Law assumptions; one test of the postulated reaction mechanisms and the assumption of equilibrium is a comparison of the 2nd and 3rd Law values obtained. An alternative procedure involves adding chlorine to the flame simultaneously with molybdenum. Then, by comparing the relative concentrations of Cl^- and Mo-containing ions, K_1 and K_2 may be derived by comparison with the known equilibrium constant for Cl^- formation.

Analogous studies of the other metals cited above have produced thermochemical data for the electron attachment and ion-molecule reactions listed in Table I. Derived electron affinities are given in Table II. The values of the equilibrium constants governing formation of BO_2^-, MoO_3^-, WO_3^-, $HMoO_4^-$, and HWO_4^- illustrate the high stabilities of these ions; boron, molybdenum and tungsten are all more electrophilic in these flames than chlorine. Comparison of equilibrium constants for compound formation shows that these additives also form compounds with potassium more stable than KCl under flame conditions.

Further confirmation of the quantitative interpretation of these results and improvement of the precision of the recommended enthalpy changes must await accurate determination of the molecular parameters of the species involved. It should also be noted that at this time the interpretation of the chromium and vanadium results is extremely uncertain. The reactions for these two metals have therefore not been included in Table I. There is not yet sufficient thermochemical data available on the neutral species involved even to identify with certainty the oxides and hydroxides present in these flames or the reactions responsible for negative ion formation. The ions observed include CrO_2^-, CrO_3^-, and $HCrO_3^-$ in the case of chromium and HVO_3^- and $H_2VO_4^-$ from vanadium. The extent of electron attachment is much smaller for these two metals than for chlorine or any of the metals cited in Table I.

TABLE I. EQUILIBRIUM CONSTANTS AND ENTHALPY CHANGES FOR FORMATION OF NEGATIVE IONS AND COMPOUNDS

Reaction	Equilibrium Constant	ΔH_0° (kJ mole^{-1})	Reference
$HCl + e^- \rightleftarrows Cl^- + H$	180 exp(-7600/T)	+74	8
$HBO_2 + e^- \rightleftarrows BO_2^- + H$	1500 exp(-10000/T)	+94 ±20	1
$H_2MoO_4 + e^- \rightleftarrows HMoO_4^- + H$	24 exp(500/T)	+50 ±40	3
$H_2WO_4 + e^- \rightleftarrows HWO_4^- + H$	25 exp(1300/T)	+40 ±40	4
$HMoO_4^- + H \rightleftarrows MoO_3^- + H_2O$	0.85 exp(10400/T)	-60 ±40	3
$HWO_4^- + H \rightleftarrows WO_3^- + H_2O$	0.87 exp(5700/T)	-22 ±40	4
$K + HCl \rightleftarrows KCl + H$	10.3 exp(-2100/T)	+ 6	8
$K + HBO_2 \rightleftarrows KBO_2 + H$	37 exp(-2500/T)	+ 8 ±20	1
$K + H_2MoO_4 \rightleftarrows KHMoO_4 + H$	3.6 exp(3500/T)	-46 ±40	3
$K + H_2WO_4 \rightleftarrows KHWO_4 + H$	4.0 exp(2900/T)	-40 ±40	4

ΔH_0° is the standard enthalpy change at 0 K. Reactions of chlorine-containing species are included for purposes of comparison.

TABLE II. ELECTRON AFFINITIES

Ion	Electron Affinity ($kJ\ mole^{-1}$)	Reference
Cl^-	280	8
BO_2^-	393 ± 20	1,2
BO^-	≥ 240	2
$HMoO_4^-$	410*	3
MoO_3^-	249 ± 50	3
HWO_4^-	400*	4
WO_3^-	304 ± 50	4

* Error limits not given due to uncertainties in H—O bond dissociation values.

REFERENCES

1. Jensen, D.E., "Electron Attachment and Compound Formation in Flames. I. Electron Affinity of BO_2 and Heats of Formation of Alkali Metal Metaborates," Trans. Faraday Soc. 65, 2123-2132 (1969).

2. Jensen, D.E., "Electron Attachment and Compound Formation in Flames. II. Mass Spectrometry of Boron-Containing Flames," J. Chem. Phys. 52, 3305-3306 (1970).

3. Jensen, D.E. and Miller, W.J., "Electron Attachment and Compound Formation in Flames. IV. Negative Ion and Compound Formation in Flames Containing Potassium and Molybdenum," February 1970; (prepared for submission to 13th Combustion Symposium).

4. Jensen, D.E. and Miller, W.J., "Electron Attachment and Compound Formation in Flames. III. Negative Ion and Compound Formation in Flames Containing Potassium and Tungsten," October 1969; (prepared for submission to J. Chem. Phys.).

5. Jensen, D.E. and Miller, W.J., "Thermodynamic Studies in Metal-Containing Flames," DDC AD 698 559, October 1969.

6. Padley, P.J. and Sugden, T.M., "Some Observations on the Production and Recombination of Ions and Electrons from Metallic Additives in Hydrogen and Hydrocarbon Flames," Eighth Symposium (International) on Combustion (Williams & Wilkins Co., Baltimore, 1962) pp. 164-179.

7. Belton, G.R. and Jordan, A.S., "The Volatilization of Molybdenum in the Presence of Water Vapor," J. Phys. Chem. 69, 2065-2071 (1965).

Electron Attachment in Substituted Aromatic Hydrocarbons† ‡

W. T. Naff* and R. N. Compton
Oak Ridge National Laboratory, Oak Ridge, Tennessee 37830
and
C. D. Cooper
University of Georgia, Athens, Georgia 30601

Attachment of slow (0 - 5 ev) electrons to a number of aromatic species has been studied in a TOF mass spectrometer using an automatic R.P.D. electron beam with resolutions of $\sim$ 0.1 eV. Autodetachment lifetimes were measured for parent ions formed by two-body attachment of thermal ($\sim$ 0.03 eV) electrons to the following molecules (lifetimes in μsec are given in parentheses): C_6F_5Cl (17.6), C_6F_5Br (21), C_6F_5CN (17), C_6F_5CHO (36), C_6H_5CN ($\sim$ 5), $C_6H_5NO_2$ (17.5), $C_6D_5NO_2$ (22), m-$C_6H_5ClNO_2$ (47), and perfluoronapthalene (123). The highly fluorinated ions had lifetimes exhibiting a systematic increase with the number of vibrational degrees of freedom consistent with the trend observed in our previous study of cyclic fluorocarbons. The value of 17.5 μsec for the nitrobenzene lifetime is a correction of a previously reported value of 40 μsec. Stabalization effects are presumed responsible for the previous erroneous measurement. The measured increase of lifetime with deuteration is in qualitative agreement with the theory of long-lived negative ion lifetimes [1]. The vibrational density of states of the ion is expected to be increased by deuteration since heavier vibrators have more closely spaced vibrational levels.

Cl^-, Br^-, and I^- were formed from C_6F_5X (X = Cl, Br, I) along with $C_6F_5^-$ at incident electron energies below 0.1 eV. Current ratios for X^- to $C_6F_5^-$ were found to be approximately 100/1, 3/1, and 1/30 respectively. No nondissociative attachment was observed for C_6F_5I. Parent and fragment ion production in C_6F_5Cl and C_6F_5Br overlapped in the energy region around 0.05 eV within the limits of our resolution with parent currents having $\sim$ 1/20th the intensity of fragment current. A thorough investigation showed that measurable dissociation occurred in < 1 μsec. Parent ions living more than one microsecond decayed only through autodetachment. These results indicated that either dissociation occurs from a resonant state different from the long-lived state, or that autodetachment with a long lifetime occurs when the incident electron energy is below the threshold for dissociation. The former possibility requires that the long-lived state does not have the correct assymptotic form for dissociation. The latter assumption would indicate that dissociation occurred with a dominating rate when energetically allowed, with our apparatus unable to differentiate between energies for which dissociation was allowed and those for which autodetachment was the only open channel.

Mono-chlorination of nitrobenzene essentially doubled the autodetachment lifetime and added a new mode of dissociation. Cl^- and NO_2^- ion currents from m-chloronitrobenzene showed almost identical energy dependences with peaks at $\sim$ 1 eV and $\sim$ 3.5 eV corresponding closely to the energy dependence of NO_2^- dissociation from nitrobenzene. This was taken as evidence that the Cl^- and NO_2^- ion currents result from unimolecular dissociation of the same intermediate negative ion state with the incident electron in a π-electronic orbital. Iodine substitution in nitrobenzene had the effect of elimination of long-lived parent ion formation with dissociative attachment producing I^- dominating at thermal electron energy.

[1] R. N. Compton et al., J. Chem. Phys. 45, 4634 (1966).

†Research sponsored by the U.S. Atomic Energy Commission under contract with Union Carbide Corporation.

‡A manuscript on the above work is in preparation to be submitted to the Journal of Chemical Physics.

*Oak Ridge Graduate Fellow, University of Georgia, under appointment from the Oak Ridge Associated Universities.

Mass Identification of Negative Ions Formed in Electron Swarm Experiments†‡

R. N. Compton, D. R. Nelson and P. W. Reinhardt

Health Physics Division, Oak Ridge National Laboratory
Oak Ridge, Tennessee 37830

An apparatus has been constructed to mass-identify negative ions formed in high pressure (~ 1 torr) electron swarm experiments. Electrons are produced at a plane parallel cathode by photoemission from a palladium film. The photoelectrons make many collisions with the gas as they drift toward a positively biased anode located a few centimeters from the cathode. The negative ions formed from primary attachment or secondary collisions (stabilization of virtual ions, ion-molecule reactions, etc.) are mass analyzed with a quadrupole mass spectrometer after they exit through a 5 mil hole bored in the anode. A study of negative ions formed in pure SF_6 showed SF_6^- to be the dominate ion at low values of the electric field to pressure ratio, E/P. The SF_6^- ion signal decreases with increasing E/P as expected for an attachment cross section which increases with decreasing electron energy. The SF_5^- ion is observed to have a peak coincident with the SF_6^- ion at thermal energies and at room temperature SF_5^- is approximately 4% as intense as the primary SF_6^- ion. This is in good agreement with the recent temperature dependence studies of Chen and Chantry [1] where production of SF_5^- at thermal energies is shown to be due to dissociative attachment to vibrationally excited SF_6. The current of SF_5^- exhibits a second more intense peak at E/P ~ 100 v/cm/torr where SF_5^- and SF_6^- are approximately equally abundant. F^- first appears at an E/P of ~ 40 v/cm/torr and increases rapidly with increasing E/P and becomes the dominate ion for E/P > 500 v/cm/torr. Under pre-ionization and actual discharge conditions the SF_7^- ion is observed to be of comparable intensity to that of SF_6^- and SF_5^-. Part, or all, of this current may result from the clustering of SF_6 to F^- ions. Beginning at an E/P of ~ 400 v/cm/torr weak signals of F_2^- and SF_4^- are found to appear.

Studies of attachment of electrons to SF_6 using CO_2 as a carrier gas (CO_2 plus 1 ppm SF_6) show that SF_6^- increases with decreasing E/P and is about 25 times more abundant than SF_5^-. The SF_6^- signal is approximately constant below E/P = 1 v/cm/torr and decreases rapidly to about one fifth this constant value at E/P = 3 v/cm/torr. An analysis of the dependence of the SF_6^- current with E/P, together with knowledge of the electron energy distributions in CO_2, indicate that the energy half-width of the SF_6^- cross section is less than 0.025 eV.

Reference

[1] C. L. Chen and P. J. Chantry, Temperature Dependence of SF_6^-, SF_5^- and F^- Production from SF_6, Book of Abstracts, 22nd Gaseous Electronics Conference, p. 39.

†Research sponsored by the U.S. Atomic Energy Commission under contract with Union Carbide Corporation.

‡A manuscript on the above work is in preparation to be submitted to the Journal of Chemical Physics.

COMPUTERIZED PHOTOPLATE DATA REDUCTION

By

G. Lauer, R. A. Meyer and R. S. Carpenter

Science Center, North American Rockwell Corporation
Thousand Oaks, California

We have designed a system to automatically locate and integrate the lines on a spark source mass spectrometer photoplate.

The major criterion for this development was the reduction of operator time to a minimum consistent with a fiscal limitation to equipment at hand. We selected the concept of continuous incremental density recording on magnetic tape followed by subsequent computer processing.

DATA ACQUISITION

We continuously translate the photoplate and take 150,000 incremental densities from the 15 inch plate in 75 seconds. Our resolution is 2.5μ which seems adequate for spark source work.

The output from the photomultiplier of the microdensitometer is fed into an operational amplifier for impedance matching and then over 40 feet of coaxial cable to the sample and hold amplifier of the PDP/8 computer system.

The PDP/8 has 4K of core, a 32K disk, and a 12.5 ips magnetic tape. A Tektronix 611 storage display unit and normal input-output hardware complete the system.

During the continuous translation of the photoplate, a clock within the computer generates an interrupt signal every 450μsec. This causes the instantaneous analog voltage, which is a measure of photoplate transmission, to be sampled, digitized, and stored sequentially in one of two 512 word buffers in core memory. When one buffer is full, its contents are written onto the tape. During the writing the other buffer is being filled with incoming data. When the particular exposure or desired portion has been completely scanned, the operator manually signals the computer. This function may also be performed by a preset limit switch. An end of file mark is then written on the tape and the typewriter outputs the amount of unused magnetic tape left. Thus, each exposure becomes one of several files on the tape. A roll of tape holds 6 complete 15 inch scans and requires 7½ minutes of operator time. The software allows prior identification of each file through alphanumeric information input as a header. The typing of an E in response to the question "OPTION" causes entry into the second phase of operation.

DATA REDUCTION

Without further attention, the tape rewinds and the 20 lightest and the 20 darkest readings in each file are located, averaged, stored, and output as baseline and saturation values. Again the tape rewinds and each file is searched for lines or peaks that fit a set of previously input parameters. Output at this point may be directed to the typewriter, scope, and/or paper tape punch. The data from the paper tape is re-entered for mass identification, ion intensity determination, and analytical calculation. This last phase will be the subject of another presentation.

Once the incremental densities are recorded on magnetic tape, the operator has two programs available. Normal usage is to continue in the automatic mode; type "Y" when asked "do you want to reduce this data?" and then leave the typewriter to do other work for about 45 minutes. After this period of time, all lines have been located, their positions have been determined with respect to start of the scan, they have been integrated above baseline, and their maximum density and line width have been determined and recorded. Alternately, the operator may watch the scope and see each selected peak displayed. He may interrupt the program at any point to make changes, mark anomalous peaks, change parameters, etc. However, typical operation is in the latter unattended mode.

An alternate program developed during the evolution of the automatic system allows much greater operator control. With this program a 25,000 data point window is read from the tape to the disk. Any 512 successive points may be displayed on the scope, including a pointer which provides a running reference within the entire file of a particular exposure. The display may be expanded, integrated, or each transmission value may be listed. Thus, one is given an opportunity to optimize parameters for automatic peak location. The entire window may be displayed block by block and the window moved to any

place on the tape. This mode is used mostly for demonstration purposes.

The automatic mode starts with location and storage of the lightest and darkest portions of the file or scan. The tape is rewound and a 25,000 point window read onto the disk. Header information is output and peak is searching initiated. The entire peak location algorithm is based on the arithmatic difference between one incremental density data point and its immediate successor. This difference we choose to call SLOPE. Thus, if SLOPE is large and positive, we are on the upslope part of a peak; if small, we are in an area of constant intensity; and if large and negative, the line is moving off the densitometer slit. In the search mode, each successive SLOPE value is compared to a parameter called forward slope. This is the minimum slope consistent with start of a normal peak. If the SLOPE is greater than forward slope, an upslope counter is started. A preset number of such successive SLOPE causes branching into the upslope mode. Any single SLOPE not meeting the forward SLOPE test during the counting causes the counter to reset the counter to zero. When the upslope test has been satisfied, the location of the peak start is stored and the program branches to upslope. Here each successive slope is now compared in two ways: is it zero or negative or is it positive and less than shoulder slope. This allows the algorithm to differentiate between the top of a peak and a shoulder or incompletely resolved line. Identification of n SLOPES meeting the shoulder parameters causes a flag to be set and resumption of the rapid upward path indicated by slope greater than forward slope triggers peak end. The "peak" is intergrated above baseline, its centroid determined, maximum density and width determined. Then the integral is compared to the minimum peak integral parameter, its height is compared to minimum height above running background and its width is compared to the maximum unsaturated width. If the peak passes all these tests, its values are output and it is displayed on the oscilloscope. The integration limits are indicated by dotted lines and the centroid by a solid line. Running background is displayed as a horizontal line. 100 points are displayed on each side of the peak. The location of n SLOPES less than shoulder slope, trigger the peak end routine and causes output subject to the same peak end tests. The upslope mode may also be terminated by n SLOPES having a greater negative value than the downslope parameter. Analogous shoulder tests are applied in the downslope mode. Downslope is terminated by location of n SLOPES having a less negative value than end slope and exits to peak end mode. From peak end the program re-enters the search mode. During search mode, the last 25 point window is continuously averaged and called running background. This value is used in the peak end mode to define acceptable peaks.

Advantages and Disadvantages of High Resolution Data Reduction with the Projectina.
PAT HAUG*, DAVID BONNELL, BILL PHILLIPS, JACK RUNYAN and CHUCK BECKER, Department of Chemistry, Rice University, Houston, Texas 77001

With the acquisition of a Consolidated Electrodynamics Corporation 21-110B high resolution mass spectrometer, the department has been faced with the problem of efficiently reducing the high resolution data obtained. Without the financial capability of acquiring an automated microdensitomer and hoping for the interim development of an on-line, real-time computer system (capable of accurate intensity measurement as well as mass measurement), we have devoted considerable effort to the development of a routine system for obtaining complete high resolution mass spectra. The relative advantages and advances in automated microdensitomer systems and suitable computer acquisition and reduction systems have already been discussed at considerable length. Peak matching, although accurate, appeared to be too time consuming and tedious; more significantly it involved tying up the instrument for considerable periods of time, particularly if a substantial number of fragments were of interest.

We, therefore, purchased a Bell and Howell projectina. Originally, W. Richter conceived of the idea of modifying a microscope designed for quality control of yarns. The instrument is basically a microscope (with x 10 or x 50 magnification) with a large viewing screen which has a vertical hairline. A 14 inch stage has been attached which can be moved by a lend screw accurate to 2 μ. Unfortunately this only travels 30 mm before it is necessary to reset it using a calibration line. This does introduce a certain potential error into large distance measurements which is not present with a longer lead screw. For high precision measurements it is necessary to measure all lines by proceeding in the same direction, in other words one cannot go past a line and then go back to it without recalibrating, as a consequence of screw slack. Another minor disadvantage is that the viewing area is only half the width of the plate. Only half of the lines may, therefore, be viewed at any one time. This also means that lines 1-15 will have distance increasing with increasing mass and lines 15-30 will have distance decreasing with increasing mass.

Bell and Howell provide a mass table with the projectina listing masses, compositions and R.D. values for combinations of C, H, N, and O from mass 69-500. Values are based on the fact that

$$\frac{\sqrt{m_x} - \sqrt{m_1}}{\sqrt{m_2} - \sqrt{m_1}} = \frac{d_x - d_1}{d_2 - d_1}$$

$$\frac{d_x - d_1}{d_2 - d_1} = \text{R.D.}$$

which reduces to one simple division if d_1 is chosen as O. Note that this assumes that d_2 is larger than d_1 so that for half of the lines on the plate, an additional substraction is required. We have found that this table was useful for only half of the compounds we were interested in studying. In several cases (10%) we required data from m/e 40 - 69; we had several compounds (20%) in excess of m/e 500 and several compounds (20%) with elements other than C, H, N and O.

Two programs have been written compatible with the Rice Burroughs 5500 for reducing data from the projectina, which are modifications of the Baylor Medical High Resolution system. These are available on request from the author* either in written form or on IBM cards. The first of these RD/KOMP requires that the distance measurements be punched out on IBM cards. There is a slot for intensity which, however, must be estimated by the operator. This program generates a data deck and print out with all the accurate masses. Sometimes the masses are so obviously off at this point that the student can correct his choice of calibration lines. The accurate masses are then fed to the second program ELCOMP/ELDRIV which computes the empirical compositions of the measured masses, the calculated masses, and the error involved.

It is necessary for the calibration masses to be identified and inserted manually. (The computer cannot do this since visual relative intensity measurements are not really accurate enough so that the computer could select the calibration lines.)

About ten freshman were utilized in this study with a mortality rate of approximately 50%. The first spectrum measured by a student usually required about 25 hours for reading a plate from mass 40 to mass 600. One might assume that the reset procedure required considerable time, but this averaged only one and one-half minutes/reset with approximately ten required. The second plate usually required only about 10 hours, since by then students could find their way around the spectrum. About three hours were required to punch the 600 data cards and another six hours to get them run through the two programs. Altogether twenty complete spectra were measured. The average deviations of mass measurement varied from .01 mass units to .003 mass units depending on the operator. Three of the same plates were run on the Baylor automated microdensitomer and gave an accuracy of .003 mass units. However, only about 50% of the lines were detected by the thresholding device. Many of the remaining plates were fogged and could not be run on the automated system. In summary, the advantages of the projectina over peak matching are:

1) There is a permanent record retained which may be referred back to at any time. We have found it instructive to allow freshman students to determine the empirical composition of particular ions in some of the high resolution spectra in an experimental chemistry experiment.
2) The instrument is only tied up during the running of the plate rather than while the peaks are being matched.

However, it is not felt that the overall time involved in obtaining the measurements is necessarily shorter.

Advantages of projectina over automated microdensitomer are:

1) Frequently one can work with plates which are cloudy due to poor developing.
2) It is possible to determine accurate masses for very weak (below threshold) lines which automated systems frequently do not record.

It should be emphasized that one major conclusion, after all of the work of modifying a program for data reduction, is that the projectina is not really desirable for complete spectra reduction. Far greater accuracies are possible with far less frustration if only the dozen or two dozen lines of interest are measured rather than all lines. The time required for such determinations is not disproportionately less and accuracy is usually satisfactory.

ACKNOWLEDGEMENT - The mass spectrometer was provided through grants from N.I.H. and N.S.F. Research was supported by the Petroleum Research Corporation.

A Computerized Fully Automatic Analytical Mass Spectrometer*

R. W. Crawford, J. W. Frazer and R. K. Stump

Our gas analytical mass spectrometer at the Lawrence Radiation Laboratory is used to quantitatively analyze a great number of gas samples. In order to save manpower and increase accuracy, we decided to fully automate the mass spectrometer by interfacing it to an 18-bit digital computer. I would like to emphasize that this is not just another data logger, but is a system for taking gas samples, introducing them at known pressure, analyzing them and putting out data for computation. This sequence of operations is under computer control and functions completely unattended.

A completely new inlet system was designed and built to replace the original inlet furnished with the spectrometer. Contained in the inlet are valves and connectors for running automatically 8 samples and 18 attached standards. There are 2 complete vacuum systems, plus the necessary vacuum gauges and power supplies.

The entire inlet vacuum system is constructed of stainless steel tubing and valves and is either welded together or connected with high vacuum flanges. All inlet valves are pneumatically operated and can be used in two ways, manually controlled by pushbutton or by relays driven by the computer.

An inexpensive pressure transducer is used to monitor the pressure of the sample in the inlet and give the computer data so it can decide how to expand the gas into the sample reservoir. An accurate capacitance type pressure transducer is connected to the sample reservoir and its output read into the computer to give an accurate measure of the final sample pressure.

Eighteen of the most commonly needed pure gas standards are permanently attached to the inlet system. Each standard is contained in a stainless steel sphere with a manual bellows valve. This standard bulb is attached to an air operated bellows valve with a small variable leak in between the standard and the pneumatic valve. All standard assemblies are connected to a common manifold.

The electronics of the original instrument have been replaced with the exception of the ion source control. Some of the new electronics are commercial such as the electrometer and the accelerating voltage power supply. Others were designed and built at the laboratory. The magnet regulator presented the greatest design problem because of the high impedance of the magnet coils. A regulator was built that would select or scan fields by computer control. The accelerating voltage control was built to select or sweep voltages on computer command.

During each run the computer reads several signals from the mass spectrometer. The signals we provide are ion current, accelerating voltage, magnetic field, sample line pressure and sample reservoir pressure.

The output of the ion current electrometer is transmitted to the computer's analog bay. Here it is fed into a differential amplifier with high common mode rejection and then through a low pass filter. To obtain the required dynamic range the signal is conditioned by both a X1 and X8 amplifier.

As the spectrum is scanned, peak tops are located and measured, mass calculated and the mass and peak height immediately typed out on a teletype next to the mass spectrometer. This information is also written on magnetic tape, along with the spectrum serial number and pressure. When the days run is complete, the magnetic tape is taken to the large computation center for off-line processing. Quantitative results are calculated using a modification of the stepwise regression program of Tunnicliff and Wadsworth.

To control the mass spectrometer we use a medium sized 18-bit digital data processor in a time-shared mode. There are 7 instruments using the computer at the same time. The control program is written in a form of assembly language.

This form of programming is necessary to conserve computer memory space, and time, since all programs are memory contained and operate in real time.

It is planned to submit this work to Analytical Chemistry for publication.

* Work performed under the auspices of the U. S. Atomic Energy Commission.

ACQUISITION AND REDUCTION OF HIGH RESOLUTION MASS SPECTRAL DATA WITH A MULTI-USER TIME-SHARING COMPUTER SYSTEM

William F. Haddon, D. R. Black, and R. H. Elsken

Western Regional Research Laboratory, Agricultural Research Service,
U.S. Department of Agriculture, Albany, California 94710

High resolution mass spectral data acquisition and processing is accomplished in our laboratory by a direct, real-time interface between a 21-110 spectrometer and an IBM 1800 process control computer with 32 K of core storage. The computer controls and acquires data from an X-ray diffraction, an infrared, and two Raman spectrometers in addition to the mass spectrometer. We have utilized the computer's interrupt and priority structure to permit simultaneous and asynchronous operation of the mass spectrometer, the X-ray diffraction unit, and one of the IR or Raman spectrometers. The laboratory automation system is also time-shared with off-line batch processing operations and thus the 1800 serves as a general-purpose computer for our staff of about 200 scientists. The maximum data acquisition rate for the mass spectrometer is 18.5 KHz and is limited by the IBM analog input system. All mass spectral data processing is done on the 1800. Incremental magnetic tape is used to store raw and processed data.

Our choice to digitize the electron multiplier output of the 21-110 was motivated by the demonstrated superior mass-measuring accuracy for magnetic scans over alternative photoplate procedures (1) (2) and by the exciting possibility for obtaining high resolution mass spectral information before removing the sample from the instrument. These advantages more than compensate for the possible loss in sensitivity for electrically detected mass spectra compared to photoplate recording (3).

Figure 1 is a diagram of the computer-spectrometer interface. The control console is of our own design and is similar to consoles in the X-ray, IR/Raman, NMR, and EPR laboratories. Particular program options are initiated by number using a 16-bit digital input group of toggle switches in conjunction with a "control entry" interrupt. The same toggle switches are used to enter data using a separate "data entry" interrupt. General programming details published for the IR/Raman system (4) are similar to those used for the mass spectrometer. The primary communication device is a Tektronix R564B storage oscilloscope which can be used to write messages at up to 250 characters per second or to plot spectra. The CRT driver subroutines are supplied by IBM. A programmable audible alarm is used to alert the operator to problems detected by the programs or to signal the end of a mass spectral scan. An intercom permits direct voice communication with the computer operator. The data acquisition system can also be operated at the computer, and mass spectrometer programs which require use of the line printer are usually called from the computer room to avoid interleaving printed data with that of off-line users. All the mass spectrometer programs are stored on disk. One of the two tape units on the 1800 is available to the mass spectrometer greater than 90% of the time for recording or processing data.

The only two changes required on the 21-110 were the addition of an electronic computer-controlled scanner and a solid-state FET electrometer amplifier (Keithley Instruments Co. Model 301). An exponential scan from mass 750 to 22 at 100 seconds per decade has been used for most work at 10 - 20,000 resolution. An Anadex Model CF-611R crystal clock drives the ADC and thus establishes the time base for the spectrum.

The data acquisition program operates as shown in Figure 2 using IBM cycle-stealing subroutines for transferring the digitized data into core and for writing the thresholded data to magnetic tape. The time scale is assigned by the thresholding program and is based on the position of the data in the input tables and the sequential number of the input table being processed. All arithmetic is in integer mode and the coding is IBM symbolic assembler language. Between 15 and 20 tape records are written for a spectrum containing 250 peaks at 15,000 resolution. Data acquisition and control functions for the other spectrometers operate from different areas of core so that asynchronous operation is achieved without loss of mass spectrometer data. After recording a mass spectrum the peak centers can be calculated by a separate program which then feeds back information on the number of valid peaks recorded over different mass ranges, and the number of peaks which exceeded the dynamic range of the ADC. For a spectrum of 100 peaks this information is available less than 10 seconds after termination of the magnet scan, thus allowing adjustment of the spectrometer gain in real time. The internal mass standard (PFK) is usually admitted after obtaining a satisfactory preliminary scan unless the sample size is limited.

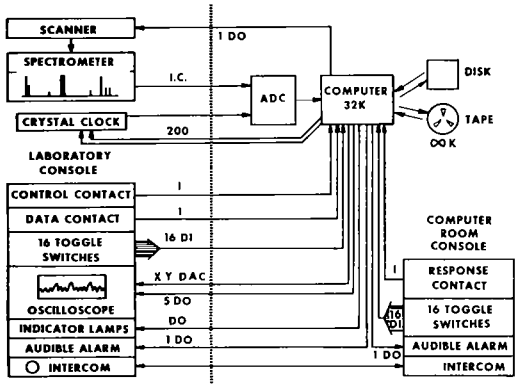

Figure 1. Computer-Mass Spectrometer Interface. I = Interrupt. DI, DO = Digital input, output.

M.S.-1800 DATA ACQUISITION PROGRAM

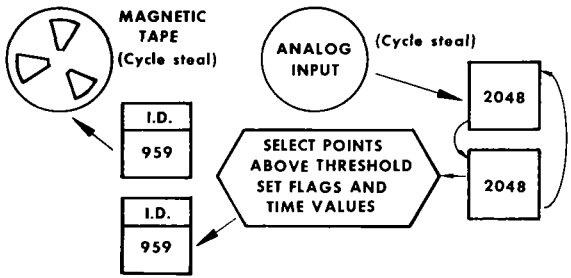

Figure 2. Data Acquisition Program.

ON-LINE PROGRAM OPTIONS

NUMBER	FUNCTION	FEED BACK
0,15	Go On, Off Line	Console Lights
1	Scan M.S. w/o D.A.	Alarm
2	Initiliazation	Scope
3	Data Acquisition	Alarm
5	Calc. Peak Centers	Scope
6	Calc. M/E Values	Scope
4,7,8,11	Mag. Tape Manipulation	--
10	Analog Noise Meas.	Scope
9,13,14	Unused	--

Figure 3. Mass Spectrometer Program Options.

CH N-BUTYL HEXANOATE

UNSAT	0	0	0	0	0	0	0	1	1	1		
MWT	0 9	2 3	3 7	5 1	6 5	7 9	9 3	0 7	2 1	3 5		
R+DB											SUM I	ADD
2.0											1.05	3
1.5											15.35	4
1.0											21.98	5
0.5											32.05	6
C NUM	1	2	3	4	5	6	7	8	9	10		

$C_5H_{11}^+$

Figure 4. Element Map for C-H Ions in Spectrum of n-Butylhexanoate.

Figure 3 lists the disk-resident programs which can be initiated from the mass spectrometer console. Any of these programs can be modified without disrupting on-line operation of the computer. Option 6, which calculates m/e values, is based on PFK and $CHCl_3$ as internal mass standards. The standard masses are taken six at a time and fitted using IBM polynomial regression routines. The algorithm which identifies the first 6 peaks is based on the time differences between them (constant to about 1 part in 2500 over several months) and on their intensities (peak areas).

Programs requiring use of the line printer are initiated from the computer room. The program for calculating elemental compositions is conversational and allows heteroatom limits to be set and changed during execution. We use the line printer for element mapping and an example of the output is shown in Figure 4 for the carbon-hydrogen peaks of n-butyl hexanoate. Peak intensities, represented by asterisks, are plotted against carbon number to produce a series of mass spectra for each rings-plus-double bond value and elemental combination. Rearrangement peaks are thus clearly separated from even electron ions and particular ion series are easily identified. The sum of intensities for each ion series is also given to indicate the relative importance of the series. The molecular weight of a particular peak can be calculated by adding the numbers at the top and right-hand edge of the element map.

Operation of the NMR and EPR spectrometers will also require the analog input system of the 1800 so that asynchronous operation of these instruments with the mass spectrometer is not feasible with our current system. We plan to acquire a separate ADC and mini-computer for the mass spectrometer to digitize and threshold the data before transferring it to the 1800.

Reference to a company or product name does not imply approval or recommendation of the product by the U.S. Department of Agriculture to the exclusion of others that may be suitable.

References

1. A. L. Burlingame, D. H. Smith and R. W. Olsen, Anal. Chem. 40, 13 (1968).

2. A. L. Burlingame, D. H. Smith, T. O. Merron and R. W. Olsen, 16th Annual Conference on Mass Spectrometry and Allied Topics, May 12-17, 1968, Pittsburgh, Pa.

3. K. E. Habfast and K. H. Maurer, 14th Annual Conference on Mass Spectrometry and Allied Topics, May 22-27, 1966, Dallas, Texas.

4. J. R. Scherer and Saima Kint, Applied Optics, in press.

A COMPUTER PROGRAM FOR THE IDENTIFICATION OF LOW RESOLUTION MASS SPECTRA

Stanley L. Grotch

Jet Propulsion Laboratory, California Institute of Technology
Pasadena, California 91103

A computer program aiding in the identification of low resolution mass spectra has been developed and successfully tested. The only spectral information required for each unknown is the absence or presence of a peak above a specified threshold (typically, 1% of the base peak) at each nominal mass over the a.m.u. range 12-200.

A one-bit encoding of peak height (i.e., only peak or no peak information) results in two significant computational advantages: (1) essentially parallel computation becomes possible in the matching process, (2) binary packing permits highly efficient use of core storage. These two factors result in extremely rapid library search rates (several thousand comparisons/sec).

Each unknown binary spectrum, X, is compared against all individual members, L_i, of a similarly encoded library of approximately 7000 compounds. A criterion of mismatch, C, is calculated for each comparison:

$$C = XOR(X, L_i) - N*(AND(X,L_i)-NPK) \qquad (1)$$

where:

$XOR(X,L_i)$ = logical "exclusive or" operation (the total number of channels which disagree in the comparison of X with L_i).

$AND(X,L_i)$ = logical "and" operation (the total number of channels in which spectrum X and spectrum L_i both have a "1" present).

N = a constant weighting factor (typically 2-5)

NPK = number of peaks ("1"s) in unknown spectrum, X.

As the library search proceeds, a record is maintained for each unknown of the ten library members yielding the minimum values of C. In essence, the search locates the ten compounds in the library which have binary spectra with the least number of weighted disagreements minus agreements with the unknown.

The term, NPK, is not essential for the calculation. It is an offset value which assures that C=0 for a perfect match. The constant weighting factor, N, was found to produce the "best" separations when equal to 2-5.

Extensive calculations (1) have shown that a binary mass spectrum is a unique pattern for identification purposes. Tests have also been performed with the identi-

fication program using mass spectral data from three texts (2-4) and data measured in our laboratory (5) as "unknowns." Of a total of 168 compounds present in the library, 156 were correctly identified among the top ten. Even when the compound was not among the top ten, valuable insights were provided by the program as to the unknown's identity.

Preliminary tests of the program with mixtures of two compounds have proven very encouraging. In one test, 134 "unknown" spectra were synthesized by combining two pure compound spectra from the library such that each "unknown" had a peak present at a given mass if and only if at least one of the pure spectra had a peak (essentially a 50-50 mixture). In 2/3 of the cases, both compounds were correctly identified in the top ten, and in only 3 cases was neither compound in the top ten.

It is planned to publish a more complete account of this work in Analytical Chemistry.

REFERENCES

1. "The Matching of Mass Spectra When Peak Height is Encoded to One Bit," S. L. Grotch, submitted to Analytical Chemistry.
2. "Interpretation of Mass Spectra, an Introduction," F. W. McLafferty, W. A. Benjamin, New York, 1967.
3. "More Spectroscopic Problems in Organic Chemistry," A. J. Baker, G. Eglinton, F. J. Preston, T. Cairns, Heydon & Son Ltd., London, 1967.
4. "Spectrometric Identification of Organic Compounds," R. M. Silverstein, G. C. Bassler, Wiley and Sons, New York, 1967.
5. H. G. Boettger, personal communication, May 1970.

SMALL COMPUTER DATA SYSTEM FOR A PORTABLE QUADRUPOLE MASS FILTER*/

N. A. Jones, R. D. Friesen, and J. W. Pyper

Lawrence Radiation Laboratory, University of California
Livermore, California 94550

INTRODUCTION

A small, inexpensive computer data system has been constructed and evaluated for a portable pulsed-beam quadrupole mass filter. This system is composed of a conventional stereo audio tape deck interfaced to the detector of the mass filter which records the digitized mass spectra on audio tape. These tapes are processed on an identical tape deck interfaced to a 4 K word memory-12 bit PDP-8 computer.

Some practical constraints were placed on the development of this data system. Because of future specialized uses, the entire mass filter system was built on a portable vacuum cart. Consequently, the data system hardware had to be easily portable so we couldn't connect it directly to the computer. The second constraint was a very tight budget. By using conventional stereo tape decks rather than computer-compatible units, we greatly reduced the cost of the system.

INSTRUMENTATION

The pulsed-molecular-beam quadrupole mass filter is described in detail in reference 1. The first component of the mass filter-to-tape-deck interface was a Vidar voltage-to-frequency converter which digitized the signal from the synchronous detector. A 12 bit binary counter collected that data for 24 milliseconds. Then the counter was gated off, and the data word transferred to a shift register. Twelve shift pulses moved the data word to a Viking 433 tape deck which recorded the word serially on one track of the tape. On the other track the 12 shift pulses were recorded to be used for synchronization later. While data from one channel were being shifted out, the next channel's data were being collected. Channels were collected until a channel counter reached a preset number. At that time, a sweep counter was incremented, a 1 second record gap left on the tape, and the whole process repeated until a preset number of sweeps was collected. A digital-to-analog converter connected in parallel with the channel counter created a synchronous voltage ramp to sweep the mass filter. The data, collected at a rate of 42 Hz, were recorded at a tape speed of 3 3/4 inches per second. The computer's tape deck played it back at twice that speed.

A tape deck identical to the one on the mass filter transferred the data from the tape into the computer. It loaded the data serially into a shift register using the sync track for shift pulses. After 12 pulses, the data were transferred in parallel to a holding buffer and the computer interrupted. The computer had 12 milliseconds to service the interrupt before the next channel of data was loaded. Half a second gap in the data indicated the end of a scan.

COMPUTER PROGRAM

The first part of the data reduction program read the data tape, rejected any bad records, added sweeps together into one spectrum, and displayed the summed spectrum as data were read in. Since the tape's format was so simple, we used software flags and counters combined with 2 timing loops to organize the data channels. The oscilloscope display was done during these loops. The first timing loop, which was between 12 milliseconds and half a second, finished only when the end of a sweep had been found. The program then checked the channel counter; if it didn't agree with the preset number of channels, the sweep just collected was rejected. Otherwise, it was added to the previous summed sweeps.

The second loop, longer than 1/2 a second, finished only when the last sweep had been collected. Once this loop was done, the program went on the second part of the reduction program. A complete summed spectrum was now stored in the computer's memory to be reduced in any convenient way. For our particular needs, we wrote a program to strip a spectrum of up to seven masses and store and output the peak masses and net intensities. The computer found the top of each peak and subtracted from it the average of the lowest points on either side. The program printed out and stored this net peak height along with the appropriate mass number and gross height. If the operator wished, the program outputted the raw spectrum.

DISCUSSION

The evaluation of the data system was carried out by re-examining the extensively studied hydrogen-deuterium self exchange in water vapor.[2,3] The equilibrium constant for hydrogen-deuterium exchange in water determined from many spectra taken on our new data system was compared with the constants calculated from spectra taken on a chart recorder and reduced by hand. We averaged seven successive chart recorded sweeps together, which is roughly equivalent in time to 119 summed tape sweeps. We also summed tape sweeps of 10, 25, 50, 75, and 100 sweeps. Except for 10 sweeps, the summed tape records agreed fairly well with the chart record. Averaging only 10 sweeps together apparently wasn't sufficient to overcome the sources of error in this system, namely peak pressure decay and noise from the phase-sensitive detector. After about 20 to 25 sweeps were summed, these errors were smoothed out. For the chart record, peak pressure decay was corrected for by hand, and the recorder's time constant and the slower scan rate smoothes out the detector's noise. By using several deuterium concentrations, we checked to see if there was any trend in equilibrium constants with deuterium concentration, but we didn't find any.

We also compared the constants with previously published values. Table I shows that comparison and the agreement is excellent. It's interesting that each constant shown was measured on a different type of spectrometer with a different ion source; Friedman and Shiner used a steady-molecular-beam ion source on a single-stage magnetic spectrometer; Pyper, Newbury, and Barton used a pulsed-molecular-beam source on a double focusing magnetic-electrostatic spectrometer; and the present work used a pulsed-beam quadrupole mass filter.

TABLE I COMPARISON OF RESULTS

	Temp.	% D Range	No. of Analyses	K
Friedman and Shiner[3]	25°C	25-75%	2500	3.76 ± 0.02
Pyper, Newbury, and Barton[2]	24.8 ± 0.5	23-70%	38 of 30 sweeps each	3.74 ± 0.07[4]
Present work	22.7 ± 0.5	23-65%	37 of 100 sweeps each	3.76 ± 0.07[4]

We conclude, then, that this computer data system for the quadrupole mass filter gives data of equivalent quality to previous data from the same instrument and to data from our double focusing instrument.

* This work was performed under the auspices of the United States Atomic Energy Commission.

† To be submitted to the Review of Scientific Instruments.

1 - J. W. Pyper and R. S. Newbury, J. Chem. Phys. 52, 1966 (1970).

2 - J. W. Pyper, R. S. Newbury, and G. W. Barton, Jr., J. Chem. Phys. 46, 2253 (1967).

3 - L. Friedman and V. J. Shiner, J. Chem. Phys. 44, 4639 (1966).

4 - The standard deviation listed is that of a single measurement. The standard deviation of the mean in each case would be ± 0.01.

An Automated Signal Averaging Data Acquisition System for Ionization Studies *†

C. Herndon Williams and Arthur W. Lynch
Sandia Laboratories
Albuquerque, N. M. 87115

An automated signal averaging data acquisition system was developed for some electron impact ionization studies performed in the ion source of a Bendix 3015 TOF mass spectrometer. The atoms and molecules studied included both condensible (Ag(v) and C_n(v), where n = 1...5) and non-condensible (Xe(g) and SF_6(g)) species. It was desired to form the ion yield, $I^{\pm}/e^{-}$, i.e. the ion current per unit ionizing electron current, from the measured analog signals in such a way that the ion yield is proportional to the ionization cross section, and thereby exhibits its energy dependence. Once formed the ion yield was signal averaged to achieve (1) higher S/N and better reproducibility on the low level $C_n^{\pm}$ signals, (2) subtraction of the residual gas background contributions to condensible species ion yields (3) relative freedom from slow temperature drift of the Knudsen furnace, and (4) less manual reduction and more convenience in treating the output ion yield curves.

The system was built around a Nuclear Data Model 800 "Enhancetron" signal averager, whose time base sweep drives the electron energy power supply, and whose 1024 channels accumulate, digitize, and average the quantity $I^{\pm}/e^{-}$. The ion current $I^{\pm}$ was the analog electrometer output of the mass spectrometer; the electron current e^{-} was collected on ion source electrodes (trap anode and trap shield) and measured on another electrometer. The ion yield was formed by dividing $I^{\pm}$ by e^{-} in an Intronic M602 operational amplifier divider. The averaging process could be monitored on an oscilloscope and the averaged ion yields vs. EE were plotted on an X-Y recorder.

A manual molecular beam shutter was used to interrupt the condensible species beam. With the condensible beam shuttered, the ND-800 could be operated in a SUBTRACT mode to remove residual gas contributions. This proved to be especially necessary in the case of the fragmentation contribution of CO to C^+ and in all ion yields that were measured out to 100 eV. The ion yields for Xe^+ and Ag^+ were compared to total ionization cross sections measured by others[1,2] through 30 eV and were found to accurately (± 5%) reproduce their energy dependence. The S/N was sufficiently good to resolve several elements of fine structure (appearance potentials) in the ion yield curves of Xe^+, Ag^+ and C_n^+. One concrete result of this data acquisition system was the ability to measure the ion yields of the very low level C_4^+ and C_5^+ species.

---

* This work was supported by the United States Atomic Energy Commission.

† This material is being prepared for submission to the Review of Scientific Instruments.

1. D. Rapp and P. Englander-Golden, J. Chem. Phys. 43, 1464 (1965).
2. S. I. Pavlov et.al., Sov. Phys. JETP (Eng. Trans.) 25, 12 (1967).

ON-LINE QUANTITATIVE ANALYSES WITH MASS SPECTROMETER AND COMPUTER

H. E. Lumpkin and J. H. Harding

Analytical Research Laboratory
Esso Research and Engineering Company
Baytown, Texas 77520

The use of computers to handle mass spectral data was almost forced on spectroscopists by the sheer volume of data available from high resolution instruments. As early as 1964, Biemann and co-workers(1) used measurements from a photoplate as input to a computer and calculated masses, assigned molecular formulas, and printed an element map as an aid in pure compound structure determination. Automatic data acquisition systems followed(2,3) with data being collected and sometimes partially processed in real time. More recently a technique for quantitative high resolution-low voltage analyses of very complex mixtures was described by our group(4). This method was developed in these laboratories(5) but has been expanded and computerized.

The availability of a medium size computer (IBM 1802), acquired primarily to handle high resolution data, has led to its use for on-line data acquisition and computations of spectra from a low resolution mass spectrometer. Our aims were to reduce the time and cost of established procedures and to cut out human errors. These aims have been achieved using the equipment and programs described in this paper.

An overall view of the data flow is shown in the figure below. A Consolidated Model 21-103C has been modified by replacing the entire ion current amplifier system with an Analog Devices Model 301 solid state operational amplifier. It has a fast response time and no drift. Communications between the instrument and the computer are provided by interfacing equipment.

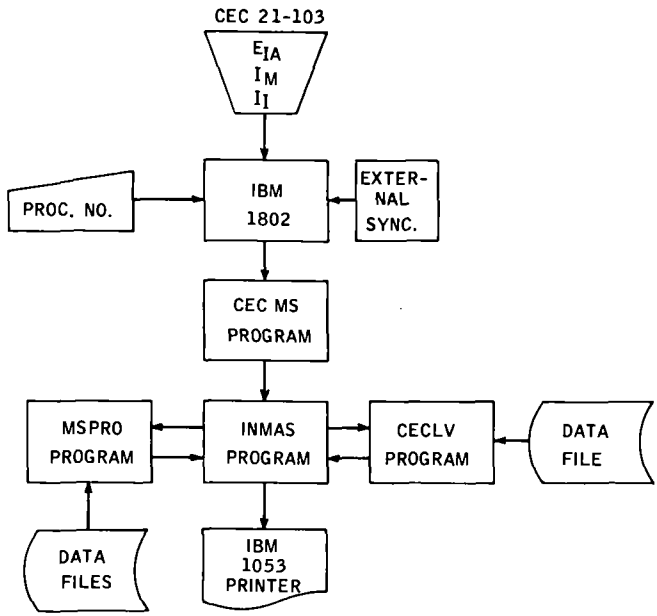

INTERFACE

The interface establishes a triangle of communications between the MS, the MS operator, and the computer. The interface performs control functions and signal conditioning.

Control functions are passed to the computer by means of a single pushbutton and four toggle switches. The pushbutton creates an interrupt for the computer which, upon successive occurrences, is interpreted as a request for computer service, a command to start a scan, and a command to stop a scan. Toggle switches are interrogated at the end of a scan to determine which analysis is to be performed on the data. Control functions generated by the computer activate status lights on the MS operator's console and provide start-stop control for MS scans.

Signal conditioning is required for the three analog signals monitored by the computer: Magnet current, accelerating voltage, and ion intensity. Redcor amplifiers, Model 391030, are used for this purpose.

Magnet current is sampled prior to and after a run, and the average value is used in mass calculations. Accelerating voltage and ion intensity are each sampled 250 times per second for a MS scan rate of 1 mass decade/minute. Analog to digital (A/D) conversion rates are controlled by using the external synchronization feature of the IBM 1800.

LOGIC OF PROGRAMS

CECMS

This is a mainline program. Its function is to control status lights on the MS, start and stop MS scans, and branch to other programs which perform specific tasks.

If the MS operator does not start a scan within 18 seconds after the computer activates a ready light on the MS console, this program branches to a mass number calibration routine named CECMI. CECMI is discussed later.

If the MS operator initiates a scan, this program causes the scan to start and branches to the subroutine ONFLY for detecting peaks in real time. CECMS then calculates mass and saves an array of peak heights and mass.

At the completion of a scan CECMS interrogates four toggle switches and either prints the spectrum obtained and exits or chains to INMAS.

ONFLY

This subroutine receives ion current signals from the MS in real time. An average baseline is determined at the start of a run and this is assumed to be constant throughout the run. The program detects peaks and saves their maximum intensity and corresponding accelerating voltage. Peak heights are used rather than peak areas in order to save computer time. The routine has worked successfully at A/D conversion rates up to 1 KC.

CECMI

This subroutine is used for mass number calibration. A signal proportional to accelerating voltage, monitored by the computer, is adjusted while the MS is focused on a known peak until the mass number calculated by the computer is correct. The current value of mass number, ion intensity, magnet current, and accelerating voltage are printed on a typewriter located at the MS.

INMAS

This mainline program gets the number of peaks in the spectrum and arrays of mass number and peak height from CECMS. It compares mass spacing and peak height of four peaks at a time and rejects noise spikes, metastable ions, and half masses. A running delta for difference between calculated mass and integral mass compensates for drift in magnetic field and nonrepeatability of the voltage decay scan. The peak height array is re-indexed to correspond to integer mass. For example, the peak height for mass 69 is entered into a PKHTA array as PKHTA(69). We refer to this peak height array indexed to integer mass as the integral spectrum. The peak heights of missing masses are set to zero.

INMAS then prints an integral spectrum at a typewriter in the MS laboratory, turns to the next page and chains to MSPRO or CECLV as determined by the setting on the toggle switches.

MSPRO

This mainline program receives the integral spectrum from INMAS, reads fixed data from a selected disk data file, sums the peak heights for specified masses, does matrix multiplication, and prints analyses at the typewriter. The contents of a data file and the space requirements for a 12 component analysis are shown below:

Item	No. Words
Title of procedure	25
No. of rows, columns, components	3
Inverted matrix of calibration data	288
Names of components	96
No. of peaks in summation	12
Mass numbers used	80
	504

On an IBM 1810 disk storage unit, one sector corresponds to 320 words; therefore, only 2 sectors are required for this data file.

MSPRO prints the sums of peak heights and both un-normalized and normalized analyses in a fixed format for each procedure.

CECLV

Peak heights of specified masses are divided by calibration coefficients to give an aromatics low voltage analysis. A compound type and carbon number distribution analysis from C_nH_{2n-6} through C_nH_{2n-18} covering a range of n=6 to n=22 is printed in a rectangular array. Appropriate mass series and carbon numbers are given as row and column headings.

APPLICATION

We have used the computer for data acquisition resulting in what we call a raw spectrum for almost two years. The raw spectrum consists of peak height and approximate mass and is used primarily for experimental scans. The programs yielding completed analyses have been in use for over a year. The following procedures are currently on-line:

Procedure	No. of Components
Raw spectrum only	-
Integral spectrum only	-
Naphtha-Petroleum	11
Gas Oil Saturates	7
Gas Oil Aromatics	12
Aromatic Low Voltage	89
Naphtha-Coal Liquefaction	16
Gas	22

Recently we replaced the four toggle switches, which allowed up to 16 procedures to be selected, with two decade digital switches, providing 100 different selections. As the requirements for established procedures change, we have the capability of developing new methods and putting them on-line.

We plan to submit an expanded version of this paper to Analytical Chemistry.

(1) D. Desiderio, P. Bommer, and K. Biemann, Tetrahedron Lett., 1964, 1725.
(2) W. J. McMurray, B. N.Greene, and S. R. Lipsky, Anal. Chem., 48, 1194(1966).
(3) R. A. Hites and K. Biemann, ibid., 40, 1217(1968).
(4) T. Aczel, D. E. Allan, J. H. Harding, and E. A. Knipp, ibid., 42, 341(1970).
(5) H. E. Lumpkin, ibid., 36, 2399(1964).
(6) S. H. Hastings, B. H. Johnson, and H. E. Lumpkin, ibid., 28, 1243(1956).